V-2

Behaviour of Horizontal Connections for Precast Concrete Load-bearing Shear Wall Panels Subjected to Large Reversed Cyclic Deformations

by

Khaled A. Soudki

A Dissertation
Submitted to the Faculty of Graduate Studies
in Partial Fulfilment of the
Requirements for the Degree of

DOCTOR OF PHILOSOPHY

Structural Engineering Division
Department of Civil & Geological Engineering
University of Manitoba
Winnipeg, Manitoba

© April, 1994

BEHAVIOUR OF HORIZONTAL CONNECTIONS FOR PRECAST CONCRETE LOAD-BEARING SHEAR WALL PANELS SUBJECTED TO LARGE REVERSED CYCLIC DEFORMATIONS

BY

KHALED A. SOUDKI

A Thesis submitted to the Faculty of Graduate Studies of the University of Manitoba in partial fulfillment of the requirements for the degree of

DOCTOR OF PHILOSOPHY

© 1994

Permission has been granted to the LIBRARY OF THE UNIVERSITY OF MANITOBA to lend or sell copies of this thesis, to the NATIONAL LIBRARY OF CANADA to microfilm this thesis and to lend or sell copies of the film, and UNIVERSITY MICROFILMS to publish an abstract of this thesis.

The author reserves other publications rights, and neither the thesis nor extensive extracts from it may be printed or otherwise reproduced without the author's permission.

CHAPTER 5

COMBINED FLEXURE/SHEAR TEST RESULTS

5.1 GENERAL

Eleven specimens were tested in combined flexure and shear: three specimens under monotonic loading and eight specimens subjected to reversed cyclic loading conditions. Results for all the flexure/shear specimens are presented and analyzed in this chapter. The test results of the various specimens are compared and discussed in detail in Chapter 6. The behaviour of the specimens tested under monotonic loading conditions is presented in section 5.2. The cyclic specimens were divided into two groups: connections with mild steel reinforcement and connections with post-tensioned reinforcement. The results for the cyclic specimens with mild steel reinforcement are presented in section 5.3, while the post-tensioned specimens are reported in section 5.4. Because of the enormous amount of data collected, the results are presented in graphical form and numerical values are given only for selected significant parameters.

Behaviour of the connection is presented in terms of the following measured quantities sketched in Figure 5.1(a):

(a) The applied horizontal load, P, at the top of the upper panel at 1800 mm above the connection region. The location of the load was selected to produce a moment-to-shear ratio of 1.5 for the given connection length, as discussed in section 3.12.

(b) The total horizontal displacement at the top of the upper panel, D, which is the net displacement of the top panel with respect to the bottom panel close to the joint region. The top panel displacement is at the location of the applied load.

c) The slippage, D_s, of the connection is the horizontal shear slip of the top panel relative to the bottom panel at the connection interface. The slip was measured at two stations located at the connection interface.

d) The flexural deformation, D_r, is the horizontal deformation due to rocking and is expressed as the difference of the total deformation and the slip deformation.

(e) The gap, D_v, is the vertical rocking in terms of opening and closing of the connection interface. The gap was measured at seven stations across the length on both sides of the connection.

(e) The rotation, θ, which represents flexural rocking is expressed as the ratio of the absolute summation of the measured gaps at the connection extreme ends to the connection length. The computation of the rotation, θ, from the gap measurements is described in Figure 5.1(b).

(f) Strains, ε, of the continuity reinforcement at the connection region and several locations along the length of the bar above the connection region.

The general format used in this thesis to present the results of each test includes the following:

1. Description of the specimen configuration and an overview of the response.
2. Behaviour of the specimen during elastic, first-yield and post-yield stages.
3. Rocking mechanism including distribution of the vertical gap measurements.
4. Slip characteristic in terms of shear force-slip at the interface.
5. Behaviour of steel continuity reinforcement using electric resistance strain gauges.

5.2 SPECIMENS SUBJECTED TO MONOTONIC LOAD

This section provides a summary of the experimental results for the monotonic flexural/shear test specimens. Three specimens (RS-S, PTB-S, and PTS-S) were tested under static loading conditions to determine the monotonic behaviour of three different types of continuity reinforcement across the joint, namely: mild-steel reinforcing bars, post-tensioned strands and post-tensioned bars. Companion cyclic specimens were tested for each continuity reinforcement type and their results are presented in sections 5.3 and 5.4. Each of the cyclic specimens was identical to its companion static specimen in terms of connection configuration, reinforcement layout, and material specification.

For all monotonic specimens, prior to application of the in-plane horizontal load, a nominal axial stress of 2 MPa was applied on the connection. The normal load, which is independent of the lateral in-plane motion, was maintained constant for the entire test duration. The specimen was loaded monotonically in plane in the push direction. The orientation of applied load caused gap opening at the push end and crushing at the pull end. The push end is the one closest to the loading actuator and the pull end is the other extreme end. At first, loading was applied using load increments of 25 kN until yielding of the continuity reinforcement at the joint region. Subsequently, testing continued using displacement control. The specimen was subjected to displacement levels of 1Dy, 2Dy, 3Dy,... up to failure, where Dy is D at the initial yield of the reinforcement. The onset of failure was defined when the load-carrying capacity of the connection dropped below 80% of the maximum measured load. Post-failure response was also monitored to determine the connection residual strength.

5.2.1 Specimen RS-S

Specimen RS-S was identical to specimen RS. The connection consisted of a plain-surface drypacked region. Continuity was provided by two 25.4 mm diameter mild steel reinforcing bars spaced at 900 mm on centres. The bars were mechanically spliced with an NMB splice sleeve. Details of the configuration was given in section 3.3. This specimen was tested to study the monotonic flexural/shear behaviour of the connection with mild steel continuity bars.

Overview

The overall response of the connection is given by the load versus displacement relationship shown in Figure 5.2. As is evident from Figure 5.2, the connection exhibited a very ductile stable behaviour until failure, which occurred by pull-out of the continuity reinforcement from the splice sleeve and crushing of the drypack at a ductility ratio 9. The measured yield displacement was 4 mm and the ultimate displacement was 36 mm. Local deformations at the connection region are given by the horizontal slip, shown in Figure 5.3, and rocking through gap opening and closing presented in terms of joint rotation, as shown in Figure 5.4. A summary of specific connection response quantities at different ductility levels is given in Table 5.1. Specimen performance during the different stages of loading is discussed in detail in the following sections.

Overall Behaviour

Initially, the behaviour of the connection was slightly nonlinear for the load-control increments up to a load of 200 kN as shown in Figure 5.5, which is an enlargement of the initial portion of Figure 5.2. Breaking of the bond between the drypack and the

upper wall panel appears to have occurred at an applied load of approximately 75 kN, as opening (uplift) was measured by gap #7, at the connection tension zone end. This compares with the predicted load of 85 kN needed to cause tensile stress at the connection corner equal to the bond strength. However, it should be noted that there were no visible cracks in the connection region or in the wall panel near the joint at this level.

The specimen was loaded until yielding of the reinforcement bar at the push end of the connection, station mark STRW1, occurred at an applied horizontal load of 220 kN, as shown in Figure 5.6. The corresponding top displacement was 4 mm, as is evident in Figure 5.5. At this stage, the measured slip and gap opening were still very small, in the order of 0.2 and 0.9 mm, respectively. After yield, the specimen was loaded in the push direction in displacement increments as multiples of the yield displacement. Horizontal slip was in the same direction as the applied load. No damage was visible in the drypack or the surrounding wall panel edges at the connection region, up to 3Dy. The measured horizontal slip at 3Dy was 1 mm and the maximum gap opening at the connection edge was 4.2 mm. The condition of the connection at the initial stages is shown in Figure 5.7(a).

At 4Dy and 5Dy, only minor damage to the drypack was noted in the form of vertical cracks. A few hairline cracks were observed in the panel near the joint region. Condition of the joint region at 5Dy is shown in Figure 5.7(b). Further widening of the gap opening to 7.5 mm and increase in slip to 2.2 mm were measured at 5Dy. The measured connection resistance, i.e., the applied horizontal load, reached a maximum of 285 kN at this ductility level. Crushing and spalling of the drypack

grout and concrete in the lower panel near the connection edge were observed at 6Dy and 7Dy. A gap opening of 11 mm and slip of 3.5 mm were measured at 7Dy. Continued crushing and spalling of drypack and concrete, spreading along the compression zone, were observed at 8Dy and 9Dy. A horizontal slip of 5 mm, a gap opening of 15 mm at one end and gap crushing of 4 mm at the other end were measured at 9Dy. The measured connection resistance remained close to the maximum load of 285 kN during displacement increments from 5Dy to 9Dy. Failure of the connection, defined as a 20% reduction in the load carrying capacity, occurred as the specimen was loaded to 10Dy, 12Dy, and 14Dy. During these displacement increments, the load gradually dropped to 200 kN, at 14Dy, which is 70% of the previously measured maximum as shown in Figure 5.2. Failure was mainly due to pull-out of reinforcement bar from the splice sleeve at the push end coupled with crushing of drypack at the other end as shown in Figure 5.7(c) which represents the condition of the connection at 10Dy. At this stage, the bulk of the drypack inside the compression zone was still intact, while the drypack at the outer edges had spalled off. Condition of the connection during post-failure at 15Dy is shown in Figure 5.7(d). The drypack was still intact at this stage. Since beyond 9Dy the connection was not able to sustain additional load; therefore, the displacement ductility of the connection was taken as 9.

Rocking Behaviour

Figure 5.8 represents the rocking behaviour throughout the duration of the test as it gives the distribution of measured vertical gap deformations across the length of the connection at various loading increments. Initially, the rocking at the joint region was nonlinear as shown in Figure 5.8(a), which gives the gap distributions at 50 kN, 100

kN, 150 kN and 1Dy loading cycles. The initial nonlinearity in the distribution of the measured gap readings across the joint could be attributed to the nonlinearity of the drypack material at a low stress level or the accuracy of the instrumentation, since the measured deformation was very small. The gap distribution across the connection at 1Dy, 3Dy, 5Dy, 7Dy and 11Dy loading cycles is shown in Figure 5.8(b). The rocking response during these cycles was linear. Figures 5.8(a) and (b) demonstrate how the neutral axis position migrated within the connection length as the bending moment at the connection section was increased. The behaviour went from an almost compression gradient at the 50 kN load cycles to rocking about 2/3 the connection length (2/3L) at the 150 kN load cycles. At 1Dy, the neutral axis moved towards the compression ends and the compression zone reduced to about L/3 as shown in Figure 5.8(a). As the applied displacement ductility was increased from 1Dy to 11Dy, hinging of the connection occurred and the depth of the compression zone remained almost constant at L/5 with a slight reduction in the compression zone due to crushing of the drypack. Hinging of the connection is evident in Figure 5.8(b).

Slip Behaviour

The second relative displacement measured at the joint region was the horizontal slippage between the top and bottom panels at the connection drypack-to-concrete interface. At early stages of loading, up to a displacement of 1Dy, the slip mechanism had a very limited effect on the system behaviour. The slip accounted for less than 5% of the overall displacement response, as shown in Figure 5.3. The connection response was governed mainly by the rocking mechanism at this initial stage. A displacement increment of 1Dy represented the onset of slip. As the specimen was loaded from 2Dy to 9Dy, the slip contribution to the overall response increased to

about 14% at 9Dy. This was a result of drypack crushing in the compression zone and the propagation of rebar plastification above the connection region which caused radial cracking around the reinforcing bar and increase the bar link length over which the horizontal shear is transferred. Because the drypack in the compression zone was still intact, slippage was still resisted by friction at the panel-to-drypack interface.

Continuity Bar Reinforcement

Behaviour of the mild steel reinforcement bar was monitored by means of electric resistance strain gauges. Strain gauges were placed at three locations along the length of the bar with gauge #1 inside the 20 mm connection region, gauge #2 at 300 mm and gauge #3 at 600 mm above the connection region inside the upper wall panel. The complete response of gauge #1 at the tension and compression bars is presented first since gauge #1 reflects the connection local response. Subsequently, the relative performance of gauges #1, #2 and #3 and the degree of plastification along the bar length is given.

The load versus bar strain relationship at the connection region, gauge #1, is shown in Figures 5.9. Yielding of gauge #1 was used to define the first yield of the connection, as discussed earlier. Figure 5.9 reveals that the behaviour was not symmetrical in tension and compression. For the same load level, the measured tension bar strain was much higher than the compression strain since the response of compression bar was influenced by the drypack compressive resistance. However, the behaviour of both the tension and compression bars was similar to that of a bar in uniaxial tension, with linear response up to yielding followed by strain hardening, as seen in Figure 5.9. From measured strains in the continuity bars, the resistance of

each component of the connection could be determined based on material properties of the bars and the drypack, using force equilibrium and strain compatibility relations.

A comparison of the measured gauge #1 strain at the tension bar in the push end and the average drypack strain at the location of the bar is given in Figure 5.10(a). The average drypack strain was determined based on the measured vertical gap station at the bar location and a gauge length of 152 mm over which the LVDT was mounted. A very good correlation is evident in Figure 5.10(a) between the measured bar strain and the average drypack strain, suggesting that the bar was completely bonded to the drypack. Above 2Dy, the strain data from the bar strain were lost due to debonding of the strain gauge from the bar and thus further comparison can not be made. It should be noted, also, that the drypack strain at ultimate agrees well with the ultimate strain obtained from typical tension tests on reinforcing bars coupled by the same splice sleeve assembly used for the connection. A comparison plot for the strains across the joint at the compression bar in the pull end of the connection is given in Figure 5.10(b). Again good initial correlation is clear between the measured reinforcing bar strain and the average drypack strain at the bar location. However, Figure 5.10(b) suggests that beyond a ductility level of 3Dy, the bond between the bar and drypack was broken due to deterioration of drypack in the compression zone. Also, the higher measured bar strains suggested a redistribution of the compressive stresses whereby the compression bar resisted more of the compression force as the drypack deteriorates in the compression zone. This behaviour differed from conventional monolithic concrete where tests have shown that strains in the compression steel remain of the same order of magnitude as those in the concrete up to failure.

The relative performance of gauges #1, #2, and #3 at different ductility levels is shown in Figure 5.11. Figure 5.11(a) represents the performance of the tension bar at the push end and Figure 5.11(b) gives the response of the compression bar at the pull end. The data in Figure 5.11 represent peak strain values at different ductility levels. As noted above, gauge #1 data for the push-end bar were lost beyond 2Dy due to the debonding of the gauge from the bar. Gauges #2 and #3 functioned well up to failure of the specimen, since neither reached strain magnitudes similar to those of gauge #1. Again, it is clear from Figure 5.11 that the behaviour in tension and compression was not symmetrical. This was because the concrete/drypack contribution to the compression resistance was much more than its contribution in tension, if any. Figure 5.11 also reveals that the values for gauges #2 and #3 were significantly lower than those for gauge #1, as expected. The three gauges showed a trend similar to the strain distribution in pull-out tests.

The degree of plastification above the connection region was measured by the extent of yielding of the tension bar. The yield length was determined graphically and was defined as the length over which the bar strain was greater than 0.0025. This strain corresponds to yielding of a bar in uniaxial tension from material tests. The extent of plastification for the tension bar of specimen RS-S is shown in Figure 5.12 which gives the strain data at gauges #1, #2 and #3, for 1Dy, 2Dy and 9Dy ductility levels. At 9Dy, gauge #1 strain data was lost and was replaced by the drypack strain at gauge #1 location because there was very good correlation between the drypack strain and the bar strain at the connection level up to 2Dy as seen in Figure 5.10(a).

Figure 5.12 demonstrates the progression of yielding along the length of the

tension bar at the different ductility levels. At 1Dy, a plastic hinge length of 40 mm was measured as seen in Figure 5.12. The strain distribution along the bar at 1Dy gives a bar development length of about 550 mm. This development length measured at 1Dy agreed very well with the basic development length of 580 mm calculated using existing code equations and given material properties. After first yield, the strain distribution around the joint region became very nonlinear as the load was increased from 1Dy to 9Dy. At 2Dy, a very high strain value was measured in the connection region at gauge #1 while the strain dropped significantly at gauge #2. Between gauges #2 and #3 the strain appeared to be linear. Thus the strain distribution along the bar could be divided into two regions an elastic region up to yield with linear strain distribution and a plastic region with nonlinear strain distribution beyond yield. The exact distribution of strain in the plastic region is unknown; however, a parabolic function could be used to approximate the distribution of strain between the yield and the maximum strains at the critical section (Park and Paulay 1975). The strain distribution in the elastic region is linear and extends a distance equivalent to the development length of the bar in tension. Similarly, the strain distribution at 9Dy is divided into a linear elastic region up to yield and a plastic region between the yield point and the critical section at the connection region as seen in Figure 5.12.

5.2.2 Specimen PTB-S

Specimen PTB-S was identical to specimen PTB. The connection consisted of a plain surface drypacked joint region post-tensioned using two 5/8" (15 mm) diameter dywidag high strength bars, spaced at 900 mm on centres. The specimen was tested under static loading conditions to study the monotonic behaviour of the connection post-tensioned with prestressing bars.

Overview

The overall connection response during the test is given by the load versus displacement relationship shown in Figure 5.13. The horizontal slip behaviour is shown in Figure 5.14. Figure 5.15 presents the vertical rocking behaviour in terms of joint rotation. Table 5.2 gives a summary of specific response quantities at different ductility levels. In general, specimen PTB-S showed very ductile and stable behaviour until rupture of the post-tensioning bar at the push end occurred with crushing of drypack in compression zone of the pull end at a ductility ratio of 11. The measured yield displacement was 4 mm and the ultimate displacement, 44 mm. The performance of the specimen during different stages of loading is discussed in the following sections.

Overall Behaviour

Initially, the behaviour of the connection was nonlinear during the load-control increments up to a load of 180 kN, as shown in Figure 5.16. The bond between the drypack and the upper wall panel broke at an applied load of about 60 kN, as measured by opening of gap #7 at the tension zone in the push end. However, it should be noted that no cracks were observed at the connection region or in the wall

panel near the joint at this stage.

As the specimen was loaded to 200 kN, a sudden jump occurred in the measured strain increment in the tension bar from 0.00244 to 0.004. Since the prestressing bar had an initial pretension strain of 0.003 due to initial prestressing to 59% of the tensile strength of the bar, 0.59fpu, the total bar strain at 200 kN would have jumped from 0.00544 to 0.0065 as shown in Figure 5.17. From material tension tests, the post-tensioned bar yielded at a strain of about 0.65% (0.0065). Thus a load level of 200 kN represents the connection first yield as the bar had yielded in tension. The corresponding top displacement was 4 mm as shown in Figure 5.16. At this stage, the measured slip was only +0.14 mm. Gap opening and gap crushing were very small, in the order of +1 and -0.54 mm, respectively. No visible damage was noted in the drypack at the connection region or in the wall panel near the joint. Figure 5.18(a) shows the condition of the connection before any observed damage had occurred.

After yield, the specimen was loaded in increments of the yield displacement. No damage was observed in the drypack or the surrounding concrete panel edges near the connection region up to a displacement of 3Dy. Minor drypack crushing at the extreme edge and cracking and spalling of concrete outer shell in the lower panel occurred at around a ductility level of 3Dy. The connection strength reached 220 kN at 3Dy. The measured horizontal slip was 1.22 mm. Gap opening at the connection edge was 4.3 mm and gap crushing was -2.1 mm. At 4Dy, 5Dy, and 6Dy, drypack crushing continued at the joint extreme end. Drypack spalling was observed at the connection edge. Some vertical cracks were observed in the top panel near the joint

region and minor spalling of the cracked concrete in the lower panel occurred. The condition of the connection at 4Dy is shown in Figure 5.18(b). Further widening of the gap opening to 8.70 mm, gap crushing to -4.25 mm, and increase of slip to 3.44 mm were measured at 6Dy. The connection resistance maintained around 230 kN at these ductility levels. Crushing and spalling of the drypack grout continued and progressed along the compression zone at 7Dy and 8Dy. Spalling of the cracked concrete shell at the upper and lower panels near the connection edge continued. A gap opening of 11.71 mm and a slip of 3.5 mm were measured at 8Dy. The connection resistance reached a maximum of 240 kN at 8Dy. The condition of the connection at 8Dy is shown in Figure 5.18(c).

Continued crushing and spalling of the drypack were observed at 9Dy and 10Dy. Cracking and spalling of the upper and lower panel concrete at the joint end stabilized. Horizontal slip was measured as 6.9 mm. A gap opening of 14.62 mm at one end and gap crushing of 6.71 mm at the other end were measured at 10Dy. The measured connection resistance remained around 230 kN during displacement levels from 3Dy to 10Dy. As the specimen was loaded to 11Dy, the post-tensioning bar ruptured and the load suddenly dropped to about 130 kN, as shown in Figure 5.13. This load is less than 80% of the maximum load of 240 kN measured during the test. Therefore, failure of the connection, defined as a 20% reduction in the load-carrying capacity, occurred at this ductility level. Failure was due mainly to rupture of the prestressing bar at the push end coupled with crushing of the drypack at the other end. At this stage, the bulk of the drypack inside the compression zone was still intact, while the drypack at the outer edges was spalled off. The condition of the connection at failure, 11Dy, outside the loading frame is shown in Figure 5.18(d).

Rocking Behaviour

The rocking behaviour of specimen PTB-S was similar to that of specimen RS-S. Two stages of the rocking behaviour are identified in Figure 5.19, which represents the distribution of measured vertical gap deformations across the length of the connection at various loading increments. Figure 5.19(a) gives the rocking behaviour at 50kN, 100, 150 kN and 1Dy loading levels. At these initial stages, the behaviour was slightly nonlinear. The rocking behaviour at 1Dy, 3Dy, 5Dy, 7Dy and 11Dy loading increments is shown in Figure 5.19(b). The response during these increments was almost linear. Figure 5.19 demonstrates how the neutral axis moved within the connection length as the bending moment was increased. The behaviour ranged from pure compression at 50 kN to rocking about the centre line of the connection (L/2) at 150 kN. At 1Dy, the compression zone moved towards the connection ends and reduced to L/3 as shown in Figure 5.19(a). As the applied displacement increment was increased from 1Dy to 11Dy, hinging of the connection occurs and the compression zone depth remained constant at about L/3, while the compression area slightly reduced by crushing. Hinging is evident in Figure 5.19(b).

Slip Behaviour

The slip behaviour of specimen PTB-S was similar to that of specimen RS-S. At early stages of loading, up to displacement increment of 1Dy, the slip mechanism had very limited effect on the system behaviour. The slip accounted for less than 5% of the overall response. As the specimen was loaded from 1Dy to 11Dy, the slip contribution to overall response increased to about 17% at 11Dy. This increase was a result of drypack crushing in the compression zone and the inherent flexibility of the post-tensioning bar provided no resistance to the horizontal shear.

Post-tensioned Bar Response

The behaviour of the post-tensioning bar was monitored by means of electric resistance strain gauges. Each bar was instrumented with two gauges at the inner and outer surfaces of the bar within the 20 mm connection region. The bars were initially post-tensioned to 0.6fpu which produced an initial pretension strain of 0.0032 in each bar. Prestress losses were about 4%, as the average initial bar strain at the time of testing was measured to be 0.0031. During the test, the measured strain was the strain increment excluding the initial prestrain. The strain in the bar at any loading stage was obtained as summation of the strain increment and the initial prestrain. Figures 5.20(a) and (b) show the load versus bar-strain relationship for the bars at the push end and pull end, respectively. Data were given for the two gauges, inside and outside gauge, on each bar. Due to the orientation of loading, the push-end bar was in tension and the pull-end bar was in compression. Looking at Figure 5.20(a), which represents the bar strain at the push-end, it is seen that the outside gauge ceased to function at load level around 200 kN, while the inner gauge remained functional until just prior to rupture of the bar. At the initial stages, the measured strain at the inside and outside gauges were in excellent agreement, suggesting that the inner gauge alone was reliable to give the behaviour of the push-end bar. The load-bar strain relationship in Figure 5.20(a) showed similar trend to that of the behaviour of a bar in uniaxial tension: linearly elastic up to yielding of the bar, followed by strain hardening, softening and rupture. The yield strain and rupture strain values agreed well with those obtained in the material tension test of a prestressing bar with the same properties. The load-strain relationship of the compression bar at the push end, as given in Figure 5.20(b), shows very similar behaviour to that of the tension bar at the pull end.

Comparisons of the measured strain increments, excluding the initial prestrain, in the prestressing bar and the average drypack strain of the measured vertical gap station at the bar location are given in Figure 5.21(a) and 5.21(b) for the push bar and pull bar, respectively. The drypack strain is defined as the ratio of the measured vertical gap divided by the average gauge length of 152 mm over which the instrumentation was mounted. Very good agreement is evident in Figure 5.21 between the measured bar strain and the average drypack strain at the initial stages of loading suggesting that the bars were initially bonded to the drypack. However, compatibility of the strains no longer exited beyond a ductility ratio of 1 for the tension bar and a ductility ratio of 2 for the compression bar. Above 1Dy, the tension bar strain was lower than the drypack strain, as shown in Figure 5.21(a), which implied possible loss of bond between the bar and the grout in the post-tensioning duct in the joint region. Above 2Dy, the compression bar strain was higher than the average drypack strain as shown in Figure 5.21(b). The compression strain behaviour suggested that the bond between the compression bar and drypack was also broken due to deterioration of the drypack in compression zone. The higher bar strains indicated a redistribution of the compressive stresses with the compression bar resisting more of the compression force as the drypack deteriorated in the compression zone. It is worth noting that the percent difference between the bar strain and the drypack strain at the compression end was higher than that at the tension end.

5.2.3 Specimen PTS-S

Specimen PTS-S was identical to specimen PTS. The connection consisted of a plain surface drypacked joint region post-tensioned using two 1/2" (12.7 mm) diameter strands spaced at 900 mm on centres. The specimen was tested under static loading conditions to study the monotonic behaviour of the connection post-tensioned with prestressing strands.

Overview

Figure 5.22 gives the overall connection response over the test duration in terms of load versus displacement relationship. The horizontal slip behaviour is shown in Figure 5.23 and the rocking behaviour is shown in Figure 5.24. A summary of specific response quantities at different ductility levels are given in Table 5.3. The specimen showed very stable behaviour with limited slip. Rupture of the tension prestressing strand at the push end and some drypack crushing at the compression zone in the pull end occurred at a ductility level of 7. The yield displacement was 4 mm and the ultimate displacement was 28 mm. The performance of the specimen during the different stages of loading follows.

Overall Behaviour

Initially, the behaviour of the connection was nonlinear elastic for the load control increments until yielding occurred at around a load of 225 kN as shown in Figure 5.25. Breaking of the bond between the drypack and the upper wall panel appears to have occurred at around a load of 80 kN due to the measured opening by gap #7. However, no damage was noted at the connection region or in the wall panel near the joint at this stage.

A sudden jump was observed in the measured top displacement from 4.60 mm to 7.60 mm as the specimen was loaded to a load increment of 225 kN. The gap station, mark G2, at the location of the tension strand in the push end also showed a sudden jump from 1.20 to 3.2 mm. As a result, the drypack strain jumped from 0.008 to 0.022. The drypack strain was calculated as the ratio of the measured vertical gap at the location of the strand to an average gauge length of 152 mm over which the LVDT instrumentation was mounted. No strain gauges were placed on the prestressing strands and thus the strain increment in the strand could only be estimated from the measured drypack strain using a bar/drypack strain correlation factor of 0.67 which was determined for specimen PTB-S. The bar/drypack strain correlation was the slope of the bar strain versus drypack strain relationship at different loading stages. Using the correlation factor and the measured gap, the strain in the strand can be estimated. The jump in the strain increment of the strand corresponding to the jump in the vertical gap would be from 0.0053 to 0.0146. The prestressing strand had an initial pretension strain of 0.005, due to initial prestressing to 0.6fpu. The total tension strain in the strand would have gone from 0.0103 to 0.0196 at load level of 225 kN as shown in Figure 5.26. But based on material tension tests, the post-tensioned strand yields at a strain of about .9% (0.009). Thus the connection first yield should have occurred at a slightly lower load (displacement) level. Therefore, instead of the measured displacement of 4.60 mm, the yield displacement was chosen as 4.0 mm since this displacement of 4.0 mm corresponds to the first yield of specimen PTB-S, as presented in the previous section. At this stage, the measured slip was +0.16 mm. Gap opening and crushing were very small in the order of +1.4 and -0.45 mm, respectively. No damage was observed in the drypack at the connection region or in the wall panels near the joint. Figure 5.27(a) shows the condition of the connection

before any observed damage has occurred.

After yield, the specimen was loaded in displacement increments of the yield displacement. Up to a displacement increment of 3Dy, very minor damage was observed in the drypack and in the surrounding concrete panel edges near the connection region in the form of vertical cracks. Minor drypack crushing and spalling occurred at the extreme panel edge at 4Dy. The connection strength reached 236 kN. The measured horizontal slip was only 0.86 mm. Gap opening at the connection push-end was 8.24 mm and gap crushing at the other end was -1.57 mm. At ductility ratios of 5Dy and 6Dy, drypack crushing continued at the joint extreme end. More drypack spalling was observed at the connection end region. However, drypack crushing did not progress along the compression depth as observed in specimen PTB-S. Also, minor vertical compression cracks were observed in the top and lower panel near the joint. At 6Dy, further widening of the gap opening to +12.17 mm and gap crushing to -2.61 mm. The measured slip increased to +1.55 mm. The connection resistance reached a maximum of 243 at 5Dy and dropped to 230 at 6Dy. As the specimen was loaded to 7Dy, the load suddenly dropped to 124 kN as shown in Figure 5.22 due to rupture of the post-tensioning strand. This load is about 50% of the maximum load of 243 kN measured during the test. Therefore, failure of the connection, defined as reduction in the load carrying capacity below 80% of the maximum, occurred at this ductility level. Failure was mainly due to rupture of the prestressing strand at the pull-end coupled with some crushing of drypack at the other extreme end of the connection as shown in Figure 5.27(b) which represents the condition of the connection at 7.5Dy. At this stage, the drypack inside the compression zone was still intact. The damage observed for the monotonic specimen PTS-S was much less severe than that observed

for specimen PTB-S. Furthermore, the degree of damage was not nearly as severe as in the case of the companion cyclic specimen; the connection was not subjected to progressive deterioration. The condition of the connection at failure outside the loading frame is shown in Figure 5.27(c).

Rocking Behaviour

The rocking behaviour of specimen PTS-S was similar to that of PTB-S connection. Again due to the nature of the monotonic loading, severe drypack deterioration along the connection length did not occur and crushing concentrated over the extreme edge of the connection pull-end region. The rocking behaviour throughout the duration of the test is given in Figures 5.28(a) and (b) which show the distribution of measured vertical gap deformations across the length of the connection at various loading increments. Initially, the rocking at the joint region was nonlinear as shown in Figure 5.28(a) which gives the gap distributions at 50 kN, 100 kN, 150 kN and 200 kN loading increments. The nonlinearity in the distribution of the measured gap across the joint could be attributed to the initial nonlinearity or accuracy of the instrumentation. The gap distribution across the connection at 1Dy, 3Dy, 5Dy and 7Dy loading increments is shown in Figure 5.28(b). The rocking response during these cycles is almost linear. Figures 5.28 demonstrates how the neutral axis position ranged form pure compression at 50 kN to rocking about the centre line of the connection (L/2) at 150 kN to rocking about L/3 at 1Dy. As the applied displacement ductility was increased from 1Dy to 4Dy, the compression zone depth moves from L/3 to L/6. From 4Dy to 7Dy, hinging of the connection occurs with the depth of the compression zone constant around L/6 while the compression area is slightly reducing by drypack crushing at the extreme end. Hinging is evident in Figure 5.28(b).

Slip Behaviour

The slip plane was between the top panel and the drypack interface. However, the slip behaviour of specimen PTS-S was different from that of specimen PTB-S and specimen RS-S. Slip had a very limited effect on the system behaviour and the connection response was mainly governed by the rocking mechanism. Since the rocking behaviour exhibited hinging at about L/6 in comparison to hinging at L/3 for specimen PTB-S, higher shear stress resistance developed at the drypack to panel interface and hence significantly lower horizontal slip was measured. The slip for specimen PTS-S accounted for less than 5% of the overall response.

5.3 MILD STEEL SPECIMENS SUBJECTED TO CYCLIC LOAD

The test results of specimens with mild steel continuity bars under cyclic loading are presented in this section. Five specimens with reinforcing continuity bars (RS, RSK, RSU, RW, and RT) were tested under reversed cyclic flexure and shear loading. The specimen nomenclature was explained earlier in section 4.2.1. All the mild steel specimens, with the exception of specimen RSK, had a plain surface joint. The experimental variables included: connections with plain surface (RS) versus shear keys (RSK); connections with reinforcement spliced by a sleeve (RS), welding (RW) or bolted to a tube section (RT) and connections with bonded reinforcement (RS) versus partially unbonded reinforcement (RSU).

As in the specimens tested under static conditions, each cyclic specimen was initially loaded to an axial stress of 2 MPa normal to the connection which was kept constant throughout the test. The specimen was then subjected to a two-phase cyclic loading history with load control cycles in the initial stage followed by displacement control cycles up to failure. The cyclic loading history was explained in section 3.8.2 and is briefly presented here. Initially, the specimen was subjected to load control cycles with three cycles at each level load increment up to the yield displacement of the connection, Dy. After yield, the specimen was loaded in displacement control. Three cycles of displacement increments were used at each multiple of the yield displacement with a lower service-level cycle in between these increments. The displacement increment was increased as the test progressed up to failure. Failure was defined by inability of the connection to sustain any additional loads when the resistance dropped below 80% of the maximum measured.

5.3.1 Specimen RS

Specimen RS was connected by mild steel reinforcing bars mechanically spliced by NMB splice sleeve. The connection consisted of a plain surface "drypack" grouted region and two vertical mild steel reinforcing bars 25.4 mm in diameter spaced at 900 mm on centres. A description of the splice sleeve is given in section 3.3.

Overview

The overall response of the RS connection is given by the load versus displacement hysteresis relationship for the entire test duration as shown in Figure 5.29(a). The load-displacement hysteresis loops up to 6Dy cycles are magnified and given in Figure 5.29(b). The specimen exhibited "stable hysteresis" behaviour and maintained the strength up to the first cycle to 5Dy. Pull-out of the reinforcement bar from the splice sleeve, followed by extensive crushing of the drypack, occurred at the third cycle to 5Dy. The measured yield displacement, Dy, was 4.25 mm. The measured ultimate displacement was five times the yield displacement. Horizontal slip behaviour at the joint between the top to bottom panel is shown in Figure 5.30. The rocking deformation measured by gap opening and closing at the joint is shown in Figure 5.31. Specific measured values of the force, displacement, slip, and gap quantities at critical stages of the connection response are summarized in Table 5.4. Observations of the specimen performance over the duration of the test and examination of damage at failure provide invaluable information that supplements measured instrumental data. The observed specimen performance and progression of damage is given in the following paragraphs.

Overall Specimen Behaviour

The behaviour of the connection during the first loading phase, which was controlled by load, was almost linearly elastic without significant loss in stiffness as shown in Figure 5.32. This behaviour was maintained for 15 cycles up to 200 kN load level. Figure 5.32 indicates a rather gradual nonlinear behaviour of the drypack as the connection stiffness, given by the slope of the load-displacement plot, slightly degrades during cycles to load levels between 150 and 175 kN. The initial crack due to breaking of the bond is evident in the load versus gap relationship, as shown in Figure 5.33, by the change in slope (stiffness) around a load of 80 kN at which the gap station reads positive indicating uplift. The measured onset of cracking agreed well with the predicted value of 85 kN based on measured material properties. However, it should be noted that no cracks were observed in the connection region at this stage.

The specimen was then loaded in single cycles until yielding of the east bar reinforcement, strain gauge mark STRE1, at a load of -220 kN in the pull direction as shown in Figure 5.34. Yielding of the continuity bar corresponded to displacement of 3.6 mm as seen in Figure 5.35. Yielding of the west bar reinforcement, strain gauge mark STRW1, occurred at load of +230 kN in the push direction as seen in Figure 5.34. The corresponding displacement at yield was 4.9 mm as given in Figure 5.35. A yield displacement of 4.25 mm was used in this test based on the average of the yield displacements measured in the two directions of the loading. Figure 5.34 also reveals the significant variation in stiffness as the load direction is reversed reflecting the contribution of the different connection components to the behaviour. The applied compression stresses were resisted by both the drypack and the

reinforcement while the tensile stresses were resisted by the reinforcement only followed by breaking of the bond between the drypack and the top panel at the connection zone. This behaviour is evident by the measured stiffness of the tensile stresses zone being in the same order of magnitude as the young's modulus of elasticity of continuity reinforcement as shown in Figure 5.34. At this stage the slip and gap measurements were small in the order of 0.15 mm and 0.8 mm, respectively. No visible damage was recorded. Minor damage to the drypack in the form of vertical cracks at the connection edges was observed.

After first yield, the specimen was loaded in displacement control by 3 cycles of displacement increments as multiples of the yield displacement, i.e., 1Dy, 2Dy, 3Dy, ... up to failure. In general, it is observed that the behaviour of the connection after yielding was nonlinear and inelastic for all post-yield loading cycles. A slight degradation in the measured strength was observed between the 1st and 2nd cycle to a displacement ductility level. The magnitude of the strength reduction was always less than 10%. In some instances no reduction was measured between the 1st and 2nd cycle. The response stabilized during the 3rd cycle to the same ductility level as no or minimal degradation was measured.

At 1Dy, no damage was observed. The connection strength maintained around +200 kN and -235 kN for the push and pull 1/2-cycles, respectively. The slip and gap measurements were small in the order of 0.15 and 0.85 mm, respectively. At 2Dy, damage was concentrated at the connection end corners: minor crushing and spalling of the drypack grout and flexural cracks in the concrete panel at the connection region were observed as shown in Figure 5.36(b). The condition of the connection at the

beginning of the test is shown in Figure 5.36(a). The measured vertical gap opening between the top panel and the top surface of the drypack at the joint ends was approximately 2.2 mm. The average horizontal slip was less than 1 mm at 2Dy. Continued crushing and spalling of the drypack in the joint at the extreme ends of the connection was observed at 3Dy. Further widening of the gap opening to about 3.5 mm and average slip of 1.2 mm was measured at the 3rd cycle of 3Dy. During these two ductility levels, the drypack remained intact with minor spalling and vertical cracks at the two ends of the connection. The average drypack crushing at the connection edges was of the order of 0.2 mm. The maximum connection resistance in the push (forward) direction was reached at the 1st cycle to 2Dy with a measured horizontal load of +266 kN as seen in Figure 5.29. The measured connection resistance in the pull (reverse) cycles reached a maximum of -280 kN during the 1st cycle to -3Dy as shown in Figure 5.29. The slight difference, less than 5%, in the connection resistance between the push and pull cycles was possibly due to the progressive damage from cyclic loading between the push and pull loading directions.

At 4Dy, the drypack grout continued crushing and spalling off. Crushing and spalling of concrete at the extreme ends was observed. Spreading of deterioration along the connection length occurred. Gap opening of 4.3 mm and average slip of about 2.0 mm were measured at the 3rd cycle to 4Dy. Average drypack crushing at the connection ends of 0.40 mm was measured. Up to this stage, the behaviour was fairly consistent with nearly stable hysteresis loops as can be seen in Figure 5.29.

Additional crushing and spalling of drypack and the concrete at the two ends of the connection with closing and widening of the gap across the length of the joint

was observed during the cycles to displacement increment of 5Dy. Strength degradation was measured in the pull direction among the three cycles to 5Dy as shown in Figure 5.29(b) which implies that failure was imminent. The load dropped from -250 kN at the 1st cycle to -175 kN at the 3rd cycle which is about 65% of the average measured maximum strength in the pull-direction. This reduction in the connection resistance during the 1/2-cycles in the pull-direction was caused by the gradual pull-out of the east bar from the splice sleeve. The east-bar pullout, which implies lower tension force in the east bar during the pull 1/2-cycle, is evident by the measured drop in measured strain gauge mark STRE2 located on the east bar 300 mm above the connection region as shown in Figure 5.37. As a result of the reduction in the connection strength in the pull 1/2-cycle and the reduced tension force in the east bar, the drypack compression force in the compression zone at the west end drops to maintain equilibrium of forces. The resistance to interface shear slip, which was in proportion with the compressive force was reduced and therefore the connection slipped more towards the pull-direction. This behaviour is clear in the load-slip behaviour during the cycles to 5Dy as shown in Figure 5.38. At the 3rd cycle to 5Dy, the measured gap opening/closing was of the order of 6.7 mm and the horizontal slip range was 4.3 mm. The permanent drypack crushing at the connection ends was on average about 1 mm. The drypack at the connection ends at the 3rd cycle to 5Dy was severely deteriorated as shown in Figure 5.36(c).

Significant degradation in the strength and stiffness were measured as the connection was loaded to displacement increment of 6Dy. The load-carrying capacity of the connection dropped to about +/-180 kN which is about 65% of the previously measured maximum. This reduction in strength was mainly due to pullout of

continuity bar from the splice sleeve at the east end coupled with extensive drypack and concrete crushing at the west end. The drypack was literally ground to dust at the connection ends. The measured extreme gap opening/closing was 8.5 mm. The slip range was 5.3 mm and permanently shifted towards the west direction due to gradual pullout of the east bar from the sleeve at 5Dy. The combined effect of extensive crushing, rebar pullout and slip caused slightly pinched hysteresis loop at 6Dy. Strength degradation continued as the connection was loaded in single cycles to 7Dy and 8Dy as shown in Figure 5.29. The residual connection resistance during these cycles was provided mainly by the applied axial load normal to the connection which remained constant as the displacement was increased. The condition of the connection at 8Dy outside the frame is shown in Figure 5.36(d). Failure of the connection occurred around the third cycle to 5Dy as this level corresponded to the onset of significant reduction of strength and rigidity of the connection with nearly unrestrained deformations. Since failure occurred at the third cycle to displacement increment 5Dy, the ductility of this type of connection was taken as 5.

Since all inelastic deformations and damage were concentrated at the connection region, deformations across the connection could be characterized by a combination of rocking and slip motion. Rocking was associated with the vertical opening of the drypack gap region at one extreme end while pivoting about the opposite end of the region. Horizontal shear slip was at the interface of the panel to the drypack. The following paragraphs give a discussion on the two basic response mechanisms: rocking and slip and their contributions to the overall behaviour of the connection.

Rocking Mechanism

The rocking mechanism throughout the duration of the test is given in Figure 5.39 which show the distribution of the measured vertical gap deformation at seven stations across the length of the connection for various loading increments. Figure 5.39(a) gives the rocking response in the push-direction and Figure 5.39(b) represents the rocking in the pull-direction. In general, the vertical gap distribution along the connection length was almost linear. Also, the rocking behaviour at the joint region was almost symmetrical as the load alternates. The gap distributions in Figure 5.39 clearly showed how the drypacked joint region opens and closes alternately as the top wall panel displaces right and left. It was clear that uplift never completely returns to zero; crushing of the joint drypack and rebar pull-out from sleeve caused gradual deterioration of the joint thickness at the connection ends. Figure 5.39 gives the rocking behaviour during cycles to .5Dy, 1Dy, 3Dy and 5Dy. It is evident from Figures 5.39 that the neutral axis moved within the compression zone as the bending moment at the connection section was increased. The behaviour went from pure compression at 50 kN load cycles to hinging about the centre line of the connection at 150 kN load cycle. As the applied displacement ductility was increased above 1Dy, hinging of the connection took place as the depth of the compression zone moved towards the connection ends as shown in Figure 5.39(a) for the push-direction. The depth of the compression zone remained the same as the loading increased from 1Dy to 3Dy while the compression area was reduced due to crushing of the drypack. As soon as significant drypack crushing occurred, the neutral axis shifted back closer to the centre line of the connection as seen in Figure 5.39(a). Very similar rocking response was observed for the pull-direction of loading as shown in Figure 5.39(b). The average drypack crushing along the connection length at onset of failure,

displacement increment to 5Dy, was less than 1 mm as seen in Figure 5.39. This represented a 5% decrease in the initial joint thickness of 20 mm.

Slip Mechanism

The second relative deformation measured at the joint region is the horizontal slippage between the drypack and the panel concrete at the connection interface. The load-slip hysteretic relationship was given in Figure 5.30. It can be seen from Figure 5.30 that at early stages of loading, up to a displacement increment of 1Dy, the slip mechanism had a very limited effect on the system behaviour. The slip accounted for less than 5% of the overall response in terms of displacement as shown in Figure 5.14. At this initial stage, the connection response was mainly governed by the rocking mechanism. Displacement ductility of 1Dy represents the onset of slip. As specimen was loaded from 1Dy to 4Dy, the shear slip contribution to the overall response increased to about 8% at 4Dy as a result of drypack crushing in the compression zone and the propagation of continuity bar plastification above the connection region which caused radial cracking around the continuity bar and an increase in the bar link length over which the horizontal shear was transferred. In general, sliding in one end was in phase with uplift at the other end of the connection. Peak slip displacements were in proportional to the amount of uplift. The load-slip hysteresis loops were almost symmetrical in the push and pull direction up to a displacement increment of 4Dy as shown in Figure 5.30. At failure however, average sliding tended to be more in the pull-direction as shown in Figure 5.30. This permanent offset in the cyclic horizontal slip behaviour was probably due to the reinforcement pullout from sleeve and extensive crushing of drypack and concrete at 5Dy. At failure, sliding contributed about 13% of the total displacement.

Continuity Bar Reinforcement

As in the static specimen, the behaviour of the reinforcement bar was monitored by means of electric resistance strain gauges. The bar was instrumented with gauges at three locations: within the 20 mm connection region, gauge #1, at 300 mm above the connection, gauge #2, and at 600 mm above the connection, gauge #3, inside the upper wall panel. Gauge #1 clearly reflects the connection local response.

The complete load versus strain gauge #1 hysteresis loops are given in Figure 5.40(a) and 5.40(b) for the west bar and east bar at the connection push-end and pull-end, respectively. As discussed earlier the connection first yield was determined by the yielding of gauge #1 for the east and west bar. Figure 5.40 indicates that the load-strain behaviour in tension had similar trend to the that of a bar in uniaxial tension. The response; however, was not symmetrical as the load is reversed. The behaviour of the bar in compression was influenced by the drypack/concrete compression resistance at the joint. The Bauschinger effect also influenced the nonlinear response in compression following loading in tension. Similar to the monotonic specimen, the measured strain at gauge #1 in the bar could be used to evaluate the force in the bar and consequently the contribution of the different components to the connection resistance could be identified by equilibrium and compatibility.

Comparison of the measured bar strain at gauge #1 and the average drypack strain of the measured vertical gap station at the bar location is given in Figures 5.41(a) and 5.41(b) for the west bar and east bar, respectively. The drypack strain was determined from the measured vertical gap and a gauge length of 152 mm, over which the LVDT instrumentation was mounted. A very good agreement is evident in Figures

5.41(a) and 5.41(b) between the measured bar strain and the average drypack strain at the initial stages of loading suggesting that the bar was initially bonded to drypack. At 2Dy compatibility of the strains became no longer valid for the west bar as shown in Figure 5.41(a). In this figure, the tension bar strain was about 50% higher than the drypack strain which might imply possible loss of bond between the bar and drypack at the connection region. The compression strain, following the tension 1/2-cycle, in the bar was almost half the compression drypack strain. This could be due to the Bauschinger effect in steel following stress reversal. Above 2Dy, the bar strain was lost as gauge #1 was debonded from the surface of the bar. The comparison of the east bar and drypack strain at +2Dy, was not possible since as seen in Figure 5.41(b), gauge #1 on the east bar debonded prior to reaching the 2Dy level. The behaviour at -2Dy revealed excellent correlation between the bar and drypack strain suggesting that the east bar was still bonded to the drypack at this stage. Beyond 2Dy the bar strain data were lost and further comparison could not be made.

The relative performance of gauges #1, #2, and #3 at different ductility levels are compared in Figure 5.42. Figures 5.42(a) and 5.42(b) give the response for the west bar at the push end and the east bar at the pull end, respectively. The data in Figures 5.42 represent peak strain values corresponding to different ductility levels. Figure 5.42(a) revealed that the strain data for gauge #1 at the west bar were lost beyond 2Dy due to the debonding of the gauge from the bar. While gauges #2 and #3 functioned well up to failure of the specimen, since the measured strain for both gauges did not reach similar magnitudes as gauge #1. The measured strain values for gauges #2 and #3 were significantly lower than gauge #1 as expected. Figure 5.42(a) indicates also that the behaviour in tension and compression was not symmetrical.

This could be due to the higher contribution of the concrete/drypack to the compression resistance as opposed to its contribution in tension, if any. The response of the east bar at the pull end was very similar to that of the west bar as shown in Figure 5.42(b). The symmetry in the response was expected due to the symmetry in the reversed loading scheme between the push and pull directions. However, gauge #1 at the east bar seems to have pealed off before 2Dy as clear from Figure 5.41(b). The behaviour of gauges #2 and #3 at the east bar were symmetrical to that of gauges #2 and #3 at the west bar as seen in Figure 5.42(b). For both bars, the relative values of the three strain gauges at any given ductility level seem to follow a similar trend as the strain distribution in tension pull-out tests.

As in the monotonic specimen, the degree of plastification above the connection region was measured graphically by the extent of yielding of the tension bar and was defined as the length over which the strain was greater than 0.0025. This strain corresponded to yielding of a bar in uniaxial tension from material tests. The extent of yielding for the west bar at the push-end is shown in Figure 5.43 which gives the strain data at gauges #1, #2 and #3, for 1Dy, 2Dy and 5Dy ductility levels. Figure 5.43 demonstrates the progression of yielding in tension along the length of the bar at the different ductility levels. The behaviour at 1Dy was very similar to that of the tension bar in the monotonic specimen. The strain distribution along the bar gave a development length of about 550 mm. This development length agrees very well with the basic development length of 580 mm obtained using existing code equations. A plastic hinge length of 50 mm was measured at 1Dy as seen in Figure 5.43. The strain distribution around the joint region became very nonlinear after first yield as loading was increased from 2Dy to 5Dy, similar to the static specimen. At 2Dy, a

very high strain value was measured at gauge #1 while the strain dropped significantly at gauge #2. Between gauges #2 and #3 the strain gradient was very small. Thus the strain distribution along the bar could be divided into two regions: an elastic region up to first yield and a plastic region above yield close to the connection region. Again as in the static specimen, a parabolic function was used to approximate the distribution of strain between gauges #1 and #2. While the strain distribution between gauges #2 and 3 was assumed linear. Beyond 2Dy, the strain data at gauge #1 were lost due to debonding of the gauge from the bar. At 5Dy, gauge #1 strain data was replaced by the drypack strain at the bar location because there was very good correlation between the drypack strain and the bar strain at the connection level up to 2Dy as seen in Figure 5.41. Again the strain distribution at 5Dy exhibited a linear elastic region up to yield and a plastic region between the yield point and the critical section at the connection region as seen in Figure 5.43. However, unlike the case of the monotonic specimen, the reversed cyclic loading limited the bar strain at ultimate. The measured strain at the location of the bar at 5Dy for the cyclic specimen RS was only 50% of that in the companion static specimen RS-S. The extent of yielding of the east bar at the pull end was similar to the behaviour of the west bar.

5.3.2 Specimen RSK

Specimen RSK was the only flexure/shear specimen with a multiple shear key configuration. The connection consisted of five shear keys across the joint interface, grouted with drypack. Two vertical 25.4 mm diameter mild steel reinforcing bars crossed the joint region at 900 mm on centre. Similar to specimen RS, the reinforcing bars in specimen RSK were mechanically spliced with an NMB splice sleeve located in the lower panel of the specimen. Details of the splice sleeve and the shear keys used were given in section 3.3.

Overview

The behaviour of specimen RSK was slightly different from that of the RS configuration. The presence of the multiple shear keys across the joint interface enhanced the shear resistance and provided a limited slip mechanism for the entire duration of the test. The connection response was governed mainly by the rocking mechanism. The overall response of specimen RSK is given by the load versus displacement hysteresis relationship as shown in Figure 5.44. The response was characterized by "stable" hysteretic and strength behaviour up to 4Dy. Bar pull-out from the splice sleeve and extensive crushing of the drypack occurred at the 1st cycle to 5Dy. The yield displacement was 4.5 mm and the ultimate displacement ductility was 4. The horizontal slip at the joint is given in Figure 5.45. The rocking deformation is represented by joint rotation as shown in Figure 5.46. Table 5.5 gives a summary of the test results at critical stages of the response. Before identifying the contribution of the different mechanisms to the overall response, a detailed description of the observed specimen performance and examination of the progressive damage up to failure is given.

Overall Specimen Behaviour

Initially, prior to the application of the horizontal load, specimen RSK exhibited a rather nonuniform drypack compression from one end of the connection to the other due to the applied vertical normal load. This variation in response could be attributed to the variability in packing from one end to the other end of the connection or to the accuracy of the instrumentation. The initial measured compression strain across the drypack was about twice that measured for the plain surface connection. The presence of a large volume of drypack grout in the RSK within the shear keys in comparison to the plain surface connection seemed to have affected the initial deformability of the joint. Also, the measured compressive bar strains for specimen RSK were initially higher in comparison with those of specimen RS and thus confirmed the higher initial flexibility of the RSK relative to the RS connection.

Similar to the RS connection, the behaviour of the RSK connection during the load control cycles was almost linearly elastic without significant loss in stiffness as shown in Figure 5.47. This behaviour was maintained for 15 elastic cycles at load increments of about 50 kN with three cycles at each level up to a maximum load of 200 kN. The apparent slight change in stiffness at around zero load between the push (positive) and the pull (negative) load cycles could be attributed to the characteristics of the drypack material. The breaking of the bond between the drypack and the concrete panel interface is evident in the change in the slope (stiffness) of the load versus gap #1 plot, shown in Figure 5.48, at around a load of 80 kN at which the gap station reads positive which indicates uplift. Figure 5.48 also shows the load versus gap #7 behaviour at the pull-end. Gap #7 reads positive or uplift at around -85 kN which imply breaking of the bond at about that load. The onset of cracking based on

given material properties is 85 kN. This agreed well with the measured values. No visible cracks were observed in the connection region at this stage. The local deformations measured at the joint interface were small in the order of +/- 0.16 mm and +0.8/-0.5 mm for the slip and gap stations.

The specimen was then loaded in single cycles to determine the connection yield. Yielding in tension of the west continuity reinforcement, strain gauge mark STRW1, at the connection push end occurred at a load of +225 kN in the push direction as shown in Figure 5.49. The corresponding displacement at the top of the upper panel was 4.6 mm as seen in Figure 5.50. Figure 5.49 also shows that the west bar at gauge STRW1 had previously yielded in compression at -175 kN load level which would activate the "Bauschinger" effect. It should be noted that gauge STRW1 had a slightly higher initial electrical resistance which would imply that the gauge would respond in its nonlinear range and thus measured data from that gauge should only be relied on with caution. On the other hand strain gauge, mark STRE2, on the east bar at the pull end seemed to be working within its linear range of response as its electrical resistance was normal. Yielding of the east bar, strain gauge mark STRE1, commenced at a load of -230 kN and a displacement of 4.5 mm in the pull-direction. Yielding of east bar is evident in Figure 5.49. A yield displacement of 4.5 mm was used in this test based on the two yield displacements measured in the two reversed directions of the loading. The condition of the connection at the beginning of the test is shown in Figure 5.51(a).

At cycles to 1Dy and 2Dy, very minor damage to the drypack in the form of vertical cracks at the connection edges was observed. The connection resistance

increased from +/-225 at 1Dy to +277/-262 kN at 2Dy, where +ve or -ve indicates loading in the push or pull-direction, respectively. At 3Dy, minor crushing and spalling of drypack was noted as shown in Figure 5.51(b). The measured rocking through vertical gap opening and crushing of the drypack between the top panel and the drypack interface at the joint ends was approximately +5.6 and -1.5 mm, respectively. The crushing concentrated at the connection ends. The average horizontal slip was less than 1 mm. The connection resistance reached a maximum of +285 in the push and -271 in the pull direction. The slight difference, less than 5%, in the resistance between the push and pull cycles was mainly due to the nature of the drypack material between the two extreme ends of the connection.

Continued crushing and spalling of the drypack in the joint at the extreme ends of the connection was observed at 4Dy. Drypack crushing extended over 1/6 the connection length from either end. The measured widening and crushing of the drypack at the joint end region was about +7 mm uplift and -5 mm crushing. The measured slip was about 1.25 mm at the 3rd cycle of 4Dy. Minor vertical cracking in the top panel south-east face at the push-end and a diagonal crack in the lower panel north-east face at the connection pull-end were observed. No cracks were observed in all the shear keys which remained intact. The measured connection resistance in the push and pull direction was maintained around +285 kN and -271 kN, respectively. Up to this stage, the behaviour of the connection was fairly consistent with nearly stable hysteresis loops as can be seen in Figure 5.44(b).

As the specimen was loaded in push to +5Dy, a significant drop in the strength to +225 kN, which is about 75% of the maximum resistance, was measured. This

reduction in strength was mainly due to pull-out of west bar from sleeve at the push end of the connection. In the reverse direction to pull -5Dy, no degradation in the response was observed as the connection maintained the strength of -260 kN. During the 2nd and 3rd cycle to 5Dy, the connection resistance dropped to and maintained +175 kN in push while gradually reducing to -200 kN in the pull direction. This strength reduction indicated pullout of east bar from the sleeve at the pull end of the connection. The response at 5Dy is clear in the magnified load versus displacement hysteresis shown in Figure 5.44(b). Failure of the connection occurred during the cycles to 5Dy since the strength dropped and maintained below 80% of the measured maximum. The condition of the drypack joint at 5Dy is shown in Figure 5.51(c). To collect post-failure information, the specimen was subjected to additional single cycles at 6Dy, 7Dy and 8Dy. The response of the connection during these cycles could be seen in the load versus displacement relation given in Figure 5.44. The severe pinched response and significant stiffness degradation is rather obvious. Condition of the connection at 8Dy outside the loading frame is shown in Figure 5.51(d). The onset of failure was taken at 5Dy since reduction in the strength was measured in the two directions of loading. Therefore, the ductility of this type of connection was 4.

Rocking Mechanism

The rocking behaviour of specimen RSK was slightly different from that of the RS connection. Since the shear keys within the connection remained intact during the test, overall drypack crushing along the connection length did not occur and crushing concentrated over the connection end regions. The presence of the shear keys seemed to have prevented the severe drypack deterioration due to cyclic shear deformations. No thickness reduction was measured. The rocking throughout the duration of the test

is given in Figures 5.52(a) and (b) for the push and the pull directions, respectively. Figures 5.52 give the distribution of measured vertical gap deformations for seven stations across the length of the connection at 0.2Dy (50 kN) 0.5Dy (150 kN), 1Dy, 3Dy and 5Dy. The response during these cycles was almost linear and symmetrical. Figure 5.52 demonstrates how the neutral axis position moved within the connection length as the applied ductility level was increased. The behaviour went from a compression gradient at 50 kN (0.2Dy) load cycles to hinging about the centre line of the connection at 150 kN (0.5Dy) load cycles. At 1Dy, the depth of the compression zone moved towards the connection ends. The compression zone depth continued to move towards the end region as the displacement ductility was increased from 1Dy to 3Dy. As soon as severe drypack crushing occurred at the pull-end, the neutral axis shifted back slightly closer to the centre line of the connection as seen in Figure 5.52(b) at loading increment of 5Dy. The behaviour in the push direction during cycles to 4 and 5Dy was different than as no severe crushing was observed at the pull-end and the neutral axis position continued to move towards the connection end corner as evident in Figure 5.52(a).

Slip Mechanism

The shear slip behaviour of specimen RSK was significantly different from that of the RS connection. The multiple shear keys across the interface provided a limited slip mechanism for the entire duration of the test as shown in Figure 5.45. This limited slip behaviour could be attributed to the higher shear resistance provided by the keys relative to that of a plain surface connection. Looking closely at Figure 5.45, it could be seen that unlike specimen RS which had fat slip hysteresis loops, specimen RSK exhibited narrow slip hysteresis. The slip behaviour was nonlinear elastic as the

measured slip for an applied ductility ratio was almost fully recovered when the load returned to zero. Also, a full slip-interface plane did not occur along the joint length as the drypack within the keys remained intact. Instead the slip mechanism was triggered by the rocking response with the intact drypack inside the keys riding along the inclined drypack-panel bearing surfaces. Thus the connection strength could be determine by its flexural resistance from the rocking response alone. The flexural strength was much smaller than the shear resistance provided by the shear keys and thus slip was limited. The slip accounted for less than 7% of the overall response at all ductility levels.

Continuity Bar Reinforcement

Similar to specimen RS, each reinforcement bar in specimen RSK was instrumented with gauges at three locations: within the 20 mm connection region, gauge #1, at 300 mm above the connection, gauge #2, and at 600 mm above the connection, gauge #3, inside the upper wall panel. The behaviour of gauge #1 is given by load versus strain hysteresis loops in Figures 5.53(a) and 5.53(b) for the west bar and east bar at the connection push end and pull end, respectively. Figure 5.53 indicates that the behaviour of both bars was very similar to specimen RS. The response was not symmetrical in tension and compression. The presence of the drypack influenced the compression resistance. Since the loading was reversed cyclic compression-tension, the Bauschinger effect also influenced the response. The envelope of load-strain had a very similar trend as the behaviour of a bar in uniaxial tension.

Comparison of the measured bar strain at gauge #1 and the average drypack strain of the measured vertical gap station at the bar location is given in Figures

5.54(a) and 5.54(b) for the west bar and east bar, respectively. The drypack strain was defined as the ratio of the measured vertical gap divided by the gauge length of 152 mm, over which the LVDT instrumentation was mounted. As in specimen RS, good agreement is evident in Figures 5.54(a) for the west bar between the measured bar strain and the average drypack strain suggesting complete bond. Prior to 2Dy, gauge #1 was pealed off and no further comparison was possible. The comparison of the east bar and drypack strain in Figure 5.54(b) revealed a discrepancy between the measured bar strain and the drypack strain at the initial stages. Consequently, the bar strain was consistently higher than the drypack strain up to 2Dy which could be due possibly to the bar being unbonded. Beyond 2Dy, the bar strain data were lost and further comparison could not be made. The comparisons showed similar trends as in the case in specimen RS.

The relative performance of gauges #1, #2, and #3 at different ductility levels are compared in Figure 5.55. Figures 5.55(a) and 5.55(b) give the response for the west bar at the push end and the east bar at the pull end, respectively. The response of the two bars was rather symmetrical. The performance of the three gauges was very similar to that observed in specimen RS. Figures 5.55 indicate again that the behaviour in tension and compression was not symmetrical. For both bars, the relative values of strain gauges seemed to follow a similar trend as the strain distribution in pull-out tests. The extent of yielding of the tension bar was determined graphically and was defined as the length over which the strain was greater than 0.0025. This strain corresponded to yielding of a bar in uniaxial tension from material tests. The extent of yielding for the west bar at the push-end is shown in Figure 5.56 which gives the strain data at gauges #1, #2 and #3, for 1Dy, 2Dy and 5Dy ductility levels. As in

specimen RS, Figure 5.56 demonstrates the progression of yielding in tension along the length of the bar at the different ductility levels. The behaviour of the bar was nearly identical to that observed in specimen RS. Two stages are identified in Figure 5.56: an elastic region up to first yield and a plastic region above yield close to the connection region. Again a parabolic function was used to approximate the distribution of strain between gauges #1 and #2. While the strain distribution between gauges #2 and #3 was assumed linear. The ultimate cyclic strain for the bar in specimen RSK as measured in terms of the drypack strain was 0.038 in comparison to 0.032 measured for cyclic specimen RS and 0.090 for static specimen RS-S. The reversed cyclic loading, the severe drypack deterioration and the Bauschinger effect limited the tension bar strain at ultimate. On the other hand, the extent of yielding of the east bar at the pull end was very similar to the behaviour of the west bar at the push end.

5.3.3 Specimen RSU

Specimen RSU was similar to specimen RS which consisted of a plain surface drypack grouted joint with two 25.4 mm diameter mild steel reinforcing bars mechanically spliced with NMB splice sleeves. The only difference between the two configurations was that in specimen RSU the continuity reinforcement was unbonded for a 600 mm distance in the upper wall panel above the drypack grout region.

Overview

In general, the behaviour of specimen RSU was similar to that of specimen RS. However, because of the partially unbonded bars, specimen RSU had a higher deformability capacity than specimen RS; therefore, more severe damage to the connection region was observed. The overall response of specimen RSU is presented by hysteresis loops of load versus displacement relationship as shown in Figure 5.57(a). Figures 5.57(b) through 5.57(d) show the hysteresis loops for selected ductility levels. The specimen exhibited very stable hysteresis behaviour up to the 3rd cycle to 6Dy. Bar pull-out from the splice sleeve occurred at the 1st cycle to 7Dy. Thickness reduction through crushing of the drypack occurred over displacement increments from 4Dy to 6Dy. The measured yield displacement, Dy, was 6.5 mm and the ultimate displacement was 39 mm. This deformation capacity was almost double (1.8 times) that of specimen RS with fully bonded reinforcement. The local horizontal slip deformation is shown in Figure 5.58(a). Figures 5.58(b) through (d) give the slip hysteresis at selected ductility levels. The local vertical rocking deformation is given in Figure 5.59. Table 5.6 summarizes selected response values at critical stages. The following paragraphs discuss the observed performance of the specimen and the various response mechanisms.

Observed Specimen Behaviour

The behaviour of the connection before yielding of the continuity bars and during the reversed load control cycles was almost linear elastic without significant loss in stiffness as shown in Figure 5.60. This behaviour was maintained for 16 cycles, one startup cycle at 25 kN and 3 cycles at load increments of 50 kN, up to a maximum load of 200 kN. Figure 5.60 indicates a rather gradual cracking of bond between the drypack and concrete wall panels as the connection stiffness, given by the slope of the load-displacement plot, slightly degrades at load levels between 100 and 150 kN. This gradual stiffness degradation could be also attributed to nonlinear behaviour of the drypack material. The initial crack due to breaking of the bond at the push-end is evident in the load versus gap #1 as shown in Figure 5.61 around a load of 80 kN at which the gap station reads positive which indicates uplift. The onset of breaking of bond at the pull-end is also evident in Figure 5.61 by opening of gap #7 at -80 kN in the pull-direction. The measured onset of cracking agrees well with the predicted value of 85 kN based on measured material properties. At this stage, no visible cracks were observed in the connection region. The local deformations measured at the joint interface were small in the order of +/- 0.25 mm and +1.3/-0.8 mm for the slip and gap stations.

The full unbonded length, 600 mm, of the continuity bar in the upper panel yielded as could be seen in the strain distribution along the length of the bar shown in Figure 5.62. Yielding of the continuity bar, strain gauge mark STRW1, near the push end occurred at a load of +230 kN as shown in Figure 5.63. The corresponding displacement at bar yield was 6.6 mm as given in Figure 5.64. Yielding of the east continuity reinforcement, gauge STRE1, commenced in the pull direction at a load of -

230 kN and displacement of 6.4 mm as the load was reversed. The extent of yielding along the unbonded length of the east bar is clearly shown in Figure 5.62. The local yielding of the east bar at gauge mark STRE1 is evident in Figure 5.63. Figure 6.63 also reveals the contribution of the drypack and reinforcing bars to the connection resistance in the compression and tension zones which results in less compression strain in comparison to tension strain at same level. The higher stiffness in the compression zone reflects the additional contribution of the drypack to the resistance as opposed to no contribution in the tension zone. A yield displacement of 6.5 mm was used based on the two yield displacements measured in the two directions of the loading. At this stage, the slip and gap measurements were small in the order of 0.35 mm and +2.6/-1.2 mm, respectively. No visible damage was recorded. The condition of the connection at the beginning of the test is shown in Figure 5.65(a).

After first yield, the specimen was loaded by displacement control. At each displacement increment three cycles were used for each multiple of the yield displacement (Dy) up to failure.

At 1Dy only minor damage to the drypack in the form of vertical cracks at the connection edges was observed. At 2Dy, damage was concentrated at the extreme end corners with minor crushing and spalling of the drypack grout. Flexural cracks in the concrete panel and minor spalling of the concrete cover in the lower panel edge in the connection were observed at the push end, south east, as shown in Figure 5.65(b). Moderate crushing was observed over 1/6 of the connection length from the two ends. The measured rocking through vertical gap opening and closing between the top panel and the top surface of the drypack at the joint ends was approximately +5.0 and -2.5

mm, respectively. The horizontal slip was less than 1 mm. Continued crushing and spalling of the drypack in the joint at the extreme ends of the connection was observed at 3Dy. At this stage, the drypack crushing extended over 1/3 the connection length from either end. A compressive diagonal crack was observed at the top panel in the push end. The gap opening increased to +7 mm, gap crushing at the extreme end to -5 mm and slip to 1.4 mm at the 3rd cycle of 3Dy. During these two ductility levels, the drypack remained intact with average drypack crushing across the connection of the order of 0.3 mm. The measured connection resistance in the push and pull direction was maintained around +225 kN and -240 kN, respectively. The slight difference in the connection resistance, less than 6%, between the push and pull cycles could be attributed to the difference in the characteristic of the drypack material and/or experimental setup.

At 4Dy, major crushing and spalling of the drypack grout occurred with deterioration spreading towards the centre line of the connection. Crushing and spalling of concrete cover at both extreme ends was also observed. The condition of the connection at 4Dy is shown in Figure 5.65(c). Gap opening of 9 mm, gap crushing at the extreme end of -7 mm and slip of about +/- 2.0 mm were measured at the 3rd cycle of 4Dy. Average drypack crushing along the connection length was about 1.0 mm. Up to this stage, the behaviour of the connection was fairly consistent with nearly stable hysteresis loops as can be seen in Figure 5.57. Similar to specimen RS, slight strength degradation was measured between the 1st and 2nd cycle of a ductility level. The magnitude of the reduction was always less than 10%. The response stabilized during the 3rd cycle with no or minimal degradation.

Additional crushing and spalling of drypack and concrete at the two ends of the connection with closing and widening of the gap across the length of the joint was observed during cycles to displacement increment of 5Dy. Concrete crushing seems to be concentrated at the one face and progresses within the connection width to the other face. No stiffness and strength degradation was observed between the three cycles to 5Dy in terms of as shown in Figure 5.57(c). However, the loops were fat in the centre and pinched at higher loads with a very sharp pointy "banana"-like shape possibly due to local slip and/or unbonding of the reinforcing bars. The connection resistance maintained well up to +225 kN in push and -243 kN in pull direction. At the 3rd cycle to 5Dy, the measured gap opening and closing at the extreme ends was of the order of 8 and -12 mm, respectively. The horizontal slip was 1.80 mm in push and -6.6 mm in pull direction. The measured overall crushing along the connection length was 3.0 mm which represents a 15% reduction in the thickness to 17 mm from the original 20 mm. Kinking or buckling of the continuity bar occurred at this ductility level. As a result of combined extensive crushing and buckling of the joint rebar, the measured horizontal slip across the interface was permanently shifted towards the compression zone in the pull direction of loading. This behaviour is clear in the hysteresis loops of load-slip at 5Dy as shown in Figure 5.58(c).

No significant change in the crack pattern was observed at 6Dy as concrete crushing stabilized and only drypack crushing occurred. The average drypack crushing along the connection length was 7 mm which amounts to 35% reduction of the initial drypack thickness of 20 mm. At this stage, the drypack was severely deteriorated along the full length of the connection. This level of deterioration was not observed for specimen RS as the connection failed at a lower ultimate displacement of 21 mm

compared to ultimate deformation of 39 mm in this case. No strength degradation was observed among the three cycles to 6Dy as shown in Figure 5.57(d). The hysteresis loops were perfectly symmetrical. The connection resistance maintained well about 250 kN in the push and pull directions. However, the slip across the connection was more towards the compression zone in the pull direction (push end) as can be seen in the hysteresis loops of load-slip relationship at 6Dy as given in Figure 5.58(d). This shift in the slip behaviour was possibly caused by the significant deterioration of the drypack and local kinking deformation of the bar at the joint region. At the 3rd cycle to 6Dy, the slip range was 12 mm with a measured slip of +2 mm and -10 mm in the push and pull cycles, respectively. The gap opening and crushing at the extreme end of the connection were about +7 mm and -14 mm. The condition of the connection after the 3rd cycle to 6Dy is given in Figure 5.65(d).

As the specimen was loaded in push to 7Dy, a significant drop in the strength to 175 kN, which is 70% of the maximum resistance, was measured. This reduction in strength was mainly due to pull-out of the west bar from the splice sleeve at the connection push end. In the reverse pull direction to -7Dy, no degradation in the response was observed and the connection maintained the strength. The specimen was then subjected to one additional cycle to 8Dy. Again the lower strength in the push direction was noted indicating bar pull-out from the sleeve. In the pull loading direction, however, the connection still resisted the applied load without any loss. The response of the connection during the cycles to 7Dy and 8Dy can be seen in Figure 5.57(d). The condition of the connection at 8Dy is shown in Figure 5.65(e). The onset of failure was taken at 7Dy as reduction in the strength was measured in one direction of loading at that level. The displacement ductility of this type of connection

was taken as more than 6Dy. In comparing the bonded to unbonded response: specimen RSU, with unbonded reinforcement, had almost twice (1.8xtimes) the deformation capacity of specimen RS with bonded bars. Therefore, the nonlinear ductility of specimen RSU, relative to specimen RS, was $1.8 \times 6 = 11$.

Rocking Behaviour

The rocking behaviour of specimen RSU was similar to that of specimen RS. The main difference lies in the severe nature of the degradation observed for specimen RSU which resulted in considerable thickness reduction of the drypack along the connection length. The rocking behaviour throughout the duration of the test is given in Figures 5.66 which show the distribution of the measured vertical gap deformations at seven stations across the length of the connection at various loading increments. Figure 5.66(a) represents the thickness reduction at various ductility increments measured at the zero displacement. Very small thickness reduction, up to 5%, was measured up to 4Dy. At 5Dy, the overall crushing of the drypack caused a 15% reduction in the thickness. The severe deterioration continued at 6Dy with a 35% reduction in the thickness. This behaviour altered the shear-slip mechanism and caused a permanent shift in the slip response. Figure 5.66(b) shows the rocking behaviour in the push direction to 50 kN (0.2Dy), 150 kN (.6Dy), 1Dy, 4Dy and 6Dy. It is evident from Figure 5.66(b) that the compression depth moved as the loading was increased. The behaviour went from a compression gradient at 50 kN load cycles to hinging about the centre line of the connection at 150 kN load cycle. As the applied displacement ductility was increased to 1Dy, the depth of the compression zone moved towards the connection ends. The compression zone depth remained almost constant as the loading increased from 1Dy to 2Dy while the compression area was reduced by

drypack crushing. As soon as some drypack crushing occurred, the neutral axis shifted back closer to the centre line of the connection for loading increment at 4Dy. Further increase in the displacement increment caused severe deterioration of the drypack. An average 35% reduction in the initial drypack joint thickness was measured at the 3rd cycle to 6Dy. Due to the severe deterioration of the drypack, hinging was transferred over the thin drypack layer to the concrete panel edges and the depth of the compression zone shifted slightly away from the centre line towards the ends of the connection as shown in Figure 5.66(b). Rocking was symmetrical as the load was reversed. The response was very similar in the pull direction of loading as seen in Figure 5.66(c).

Slip Behaviour

The contribution of slip to the overall mechanism was similar to that of the RS connection. The slip plane was between the top panel and the drypack interface. However, the severe deterioration of the drypack in the connection region caused a permanent shift in the slip due to shear kinking mechanism of the bar. The shear resistance was provided by the shear friction mechanism based on the compressive force of the drypack. At early stages of loading, up to displacement increment of 1Dy, the slip mechanism had a very limited effect on the system behaviour. The slip accounted for less than 5% of the overall response in terms of displacement as shown in Figure 5.58(b). As specimen was loaded from 1Dy to 4Dy, the shear slip contribution to the overall response increased to about 9% at 4Dy as a result of drypack crushing in the compression zone. In general, sliding in one end was in phase with uplift at the other end of the connection and peak slip displacements were in proportional to the amount of uplift. Slip magnitude was almost symmetrical as the

direction of load was reversed up to 4Dy as shown in Figure 5.58(b) and (c). At 5Dy, the slip tended to be more towards the push end, i.e., the compression zone in the pull direction, as shown in Figure 5.58(c). This permanent offset in the cyclic slip behaviour was probably caused by the severe deterioration of the drypack in the joint region coupled with shear kinking deformation of the reinforcement. The shift in slip was again measured at 6Dy cycles as seen in Figure 5.58(d). At failure, sliding contributed about 15% of the total displacement.

Continuity Bar Reinforcement

The behaviour of the continuity reinforcement was rather unique as extensive bar straining did not concentrate only at the connection section, as was case in the other specimens with bonded mild steel reinforcement. Bar straining was distributed uniformly over the full unbonded length. This phenomenon was clearly demonstrated in Figure 5.64, which represents the extent of bar yielding at 1Dy. Each bar was instrumented with strain gauges at 4 locations: gauge #1 within the 20 mm drypacked connection, gauge #2 at 300 mm, gauge #3 at 600 mm and gauge #4 at 900 mm above the connection region inside the upper wall panel.

The behaviour of the continuity reinforcement at gauge #1 is given by hysteresis loops of load-strain in Figures 5.67(a) and 5.67(b) for the west bar and east bar at the connection push end and pull end, respectively. Figure 5.67 indicates that the response was not symmetrical in tension and compression. The presence of drypack influenced the compression resistance. Since loading was fully reversed compression-tension, the Bauschinger effect also influenced the response. Furthermore, gauge #1 was functional up to 3Dy as seen in Figure 5.67. Also, evident

in Figure 5.67 was that the envelope of the load-strain had very similar trend as the behaviour of a bar in uniaxial tension. The bar strain at gauge #1 was compared to the drypack strain as shown in Figures 5.68(a) and 5.68(b) for the west and east bar, respectively. The drypack strain was determined as the ratio of the measured vertical gap at the bar location to the unbonded length of 600 mm of the bar. Excellent agreement is evident in Figures 5.68(a) for the west bar between the measured bar strain and the drypack strain up to 3Dy. The agreement validated the assumption that bar straining occurred over the full unbonded length. At 3Dy, the bar strain in compression was slightly higher than the drypack strain possibly due to redistribution of stress caused by the crushing of the drypack at that level. Beyond 3Dy, gauge #1 was pealed off and no further comparison was possible. The comparison of the east bar and drypack strain in Figure 5.68(b) was similar to that at the west bar. Again very good agreement is observed up to 3Dy. At 3Dy, the measured bar strain in compression was higher than the average drypack strain. Beyond 3Dy, bar strain data were lost and further comparison could not be made. The drypack-bar strain comparisons were similar to that of specimen RS.

The relative performance of gauges #1, #2, #3 and #4 at the various ductility levels are compared in Figure 5.69. Figures 5.69(a) and 5.69 (b) give the response for the west bar at the push-end and the east bar at the pull end, respectively. The response of the two bars was rather symmetrical. The performance of the four gauges was different from that observed in specimen RS due to the debonding effect. Figure 5.69 indicates that bar strains were uniform along the unbonded length at gauges #1, #2, and #3. The measured strain at gauge #4, embedded in the concrete was significantly lower than the other gauges. It should be noted that the behaviour in

tension and compression was not symmetrical. The extent of yielding of the tension bar was determined graphically and was defined as the length over which the strain was greater than 0.0022. The extent of yielding for the west bar at the push end was shown in Figure 5.70(a) which gives the strain data at gauges #1 through #4 for ductility increments from 1Dy to 4Dy. As in specimen RS, Figure 5.70 demonstrated the progression of yielding in tension along the length of the bar at the different ductility levels. Since the continuity bar was unbonded over a 600 mm length above the connection region, the full unbonded length yielded at 1Dy. The strain gauge readings at 2Dy were also uniform along the unbonded length of the bar. At 3Dy the bar exhibited some tension softening at gauge #4 possibly due to the Bauschinger effect after yielding in compression or due to the crushing of the drypack at the connection region which caused redistribution of the strains along the length of bar. Similarly, at 4Dy, strain softening was measured. A parabolic function could be used to approximate the distribution of strain between gauges #3 and #4. The ultimate cyclic bar strain for specimen RSU as measured in terms of the drypack strain was 0.028 in comparison to 0.032 measured for specimen RS. On the other hand, the extent of yielding of the east bar at the pull end was symmetrical to the behaviour of the west bar and is seen in Figure 5.70(b).

5.3.4 Specimen RW

The configuration of the connection in specimen RW was similar to that of specimen RS which consists of a plain surface drypack grouted joint and two vertical 25.4 mm diameter mild steel continuity reinforcement spaced at 900 mm o/c. However, the reinforcing bars in specimen RW were spliced by welding the continuity bars from the upper wall panel to an iron angle anchored in the lower panel of the specimen. The welded splice detail used was typical of current practice and a description of the detail is given in section 3.3.

Overview:

Specimen RW was the first specimen tested in this experimental program. Before discussing the behaviour, general comments on the testing stages is given. Being the pilot specimen, RW was subjected to a slightly different loading history than all other specimens. The same pattern of load cycles was used up to yielding of the continuity bars. During displacement increments from 1Dy to 3Dy, the specimen was subjected to additional intermediate displacement increments of 0.5Dy, i.e. 1Dy, 1.5Dy, 2Dy, 2.5Dy, 3Dy, followed by full multiples of the yield displacement, Dy, up till failure. Also, specimen RW had only 5 gap stations along the connection length in comparison to the 7 stations used for all the other specimens. It is worth noting also that close to the end of the elastic load cycles, specimen RW experienced overall movement of the bottom panel relative to the floor at around the cycle to 200 kN load level, prior to 1st yield in the continuity reinforcement, due to improper anchorage of the abutments which fixed the lower panel to the floor. The problem was corrected by properly jacking the abutments to the floor and the test was resumed. During subsequent loading cycles, the measured lower panel movement was minimal, if any. All

measurement stations were laid out so that the connection behaviour was monitored. The overall motion was determined in terms of relative panel to panel displacement given as the difference between top panel motion at the location of the applied load and the lower panel movement close to the joint region.

Specimen Observed Response

The overall response of specimen RW is given by the load-displacement hysteresis relationship as shown in Figure 5.71(a) using the same scale as the other specimens. Figure 5.71(b) is a magnified version with a smaller scale. The specimen exhibited stable hysteretic behaviour until extensive crushing of the drypack occurred during displacement cycles to 5Dy followed by buckling of the continuity reinforcement at the 3rd cycle to 5Dy which resulted in a slightly pinched hysteresis loop. Drypack crushing stabilized during the displacement cycles to 6Dy. The specimen was able to sustain 3 "stable" 6Dy cycles without loss of strength until the 3rd cycle to -6Dy in the pull direction, when the east bar at the pull-end ruptured and the strength dropped significantly. The measured yield displacement, Dy, was 5 mm. The measured ultimate displacement was 6 times the yield displacement. Local deformations at the connection region are given in terms of horizontal shear slip and vertical rocking. The horizontal slip behaviour is shown in Figure 5.72(a). For clarification, the slip hysteresis at the various ductility levels are shown in Figures 5.72(b) thorough (d). The rocking behaviour in terms of rotation of the connection is shown in Figure 5.73. Specific measured values of the force, displacement, slip, and rocking response quantities at critical stages of the connection response are summarized in Table 5.7. The following paragraphs detail the observed specimen performance and behavioral mechanisms over the duration of the test.

During the load control cycles, the behaviour of the connection was linear elastic without significant loss in stiffness as shown in Figure 5.74. This behaviour was maintained for 21 cycles up to a maximum load of 200 kN. The initial crack due to breaking of the bond between the drypack and the upper wall panel appears to have occurred at around a load level of 60 kN. The onset of cracking of bond is evident in the load versus gap #5 by the abrupt change in stiffness at around a load of +60 kN at which gap opening was measured as can be shown in Figure 5.75. The same behaviour was also observed for gap #1 at a load of -70 kN in the pull-direction as shown in Figure 5.75. At this stage, the local deformations measured at the joint interface were very small in the order of +/- 0.2 mm and +/-0.6 mm for the slip and gap stations. No visible cracks were observed in the connection region, few hairline cracks were noted in the panels near the joint.

The specimen was loaded in the push direction until yielding occurred at the west bar reinforcement, strain gauge mark STRW1, near the push end at a load of +210 kN as shown in Figure 5.76. The displacement corresponding to bar yield was 4.8 mm as shown in Figure 5.77. Yielding of the east bar reinforcement at strain gauge mark STRE1 commenced at -230 kN in the pull-direction and a displacement of -5.6 mm as the load was reversed. Yielding of STRE1 is evident in Figure 5.76. A yield displacement of 5 mm was used in this test, based on the average of the two yield displacements measured in the two directions.

At 1Dy cycles, no drypack crushing was observed and the connection strength maintained around +194 kN and -210 kN for the push and pull cycles, respectively. The slip and gap measurements were small in the order of 0.24 mm and 0.7 mm, respectively. At 2Dy, very minor crushing of the drypack grout at the joint corners was observed as shown in Figure 5.78(a). The measured rocking through vertical gap

opening between the top panel and the top surface of the drypack at the joint end was approximately 2 mm. Gap crushing at the other end was of the order of 1 mm. The horizontal slip was less than 1 mm. The connection strength reached +220 kN and -256 kN in the push and pull directions. The difference in the connection resistance between the push and pull cycles, less than 15%, could be attributed to the progressive deterioration due to reversed cyclic in the push and pull directions. At 3Dy, minor spalling and crushing of the drypack in the joint and the concrete panels at the extreme ends of the connection was observed. Further widening of the gap opening to about 4 mm and the slip to 1.5 mm was measured at the 3rd cycle to 3Dy. Up to this ductility level, the drypack remained intact with minor vertical cracks at the two ends of the connection. The average crushing along the connection length was less than 1 mm. Additional crushing and spalling of drypack grout and panel concrete at the extreme ends was observed at 4Dy. Flexural shear cracks were also observed in the top panel. The condition of the connection at 4Dy is shown in Figure 5.78(b). At the 3rd cycle to 4Dy, the gap opening was 5.2 mm and slip was 3 mm. An average drypack crushing of 2 mm was measured across the joint length at this ductility level. The behaviour of the connection, up to this stage, was fairly consistent with nearly stable hysteresis loops as can be shown in Figure 5.71(a). The connection strength in the push and pull directions maintained well around 215 kN and -225 kN, respectively.

Continued crushing and spalling of drypack and the concrete at the two ends of the connection across the length of the joint was observed. The measured thickness reduction progressed from 3.75 to 6.0 mm during the first 2 cycles to displacement increment of 5Dy. The connection strength dropped slightly to + 200 and -215 kN.

At the 3rd cycle to 5Dy, major drypack crushing occurred resulting in a thickness reduction of the order of 10 mm which is a 50% reduction from the initial 20 mm value. The load carrying capacity of the connection dropped to +190 in push and -186 kN in pull cycle which is about 79% of the average measured maximum. Average horizontal slip of about +/- 10 mm was also measured. The combined effect of extensive crushing, buckling of continuity bar and extensive slip caused a slightly pinched hysteresis loop at the 3rd cycle to 5Dy as shown in Figure 5.71(c).

No significant change in the crack pattern was observed at 6Dy as the drypack crushing stabilized. Additional crushing and widening of the opening in the joint region at the two ends of the connection was observed. An average crushing of 12 mm in the drypack was measured. At this stage the drypack was severely deteriorated along the connection length and the resistance to compression forces transferred over the thin drypack layer to the edges of the concrete wall panels. The connection resistance during the first 2 cycles to 6Dy increased to and maintained about 210 and -240 kN. Due to buckling of the reinforcement, the slip response was permanently shifted towards the compression zone in the pull direction (push end). Average slip values of -4 and -14 mm were measured as load was reversed. At the end of the 3rd cycle to - 6Dy, a significant reduction in the shear force from -240 kN to -120 kN was measured as shown in Figure 5.71(d). This was mainly due to rupture of the east bar at the pull end coupled with further extensive drypack and concrete crushing at the other end. The drypack was literally ground to dust and the gap was almost completely closed. The condition of the connection at failure is shown in Figure 5.78(c). Buckling of the continuity reinforcement is evident in Figure 5.78(d). Failure of the connection, defined as a reduction in the load carrying capacity under increasing

deformation, occurred at this ductility level as significant reduction of strength and rigidity of the connection occurred. Attempting to load the panel in the forward direction, to +7Dy, the maximum load that could be measured was only 150 kN which is 60% of the previously measured maximum at 250 kN. It was obvious that at this stage, the restoring force of the rocking mechanism was only provided by the applied axial load normal to the connection which remain constant as the displacement was increased. Since failure of the connection occurred at the 3rd cycle of displacement increment 6Dy, the ductility of this type of connection was 6.

Rocking Mechanism

The rocking behaviour of specimen RW was similar to that of specimen RSU as severe drypack crushing was observed at failure. The rocking mechanism is given in Figures 5.79(a) through (c) which show the distribution of the measured vertical gap deformations at five stations across the connection length for various loading levels. Figure 5.79(a) represents thickness reduction through overall drypack crushing along the connection length at different ductility increments. As shown in this figure, 3Dy represented the onset of crushing and 5Dy corresponded to severe drypack deterioration. The thickness of the drypack joint reduced from an initial value of 20 mm to 18, 10 and 8 mm at the end of ductility levels, 4Dy, 5Dy and 6Dy, respectively. Figures 5.79(b) and (c) show the rocking deformation in the push and pull directions, respectively. It is clear from Figure 5.79(b) that the neutral axis moved as the loading was increased. Before severe deterioration of the drypack, the behaviour was similar to specimen RS: pure compression at 50 kN to rocking about the connection centre line at 100 kN to hinging towards the connection ends at 1Dy. The compression zone depth remained almost constant during cycles to 1Dy and 2Dy.

As soon as there was appreciable drypack crushing, the compression depth moved back towards the centre line of the connection as seen in Figure 5.79(b) for displacement cycles to 1Dy, 3Dy and 5Dy. The rocking response was symmetrical as the load was reversed as seen in Figure 5.79(c).

Slip Mechanism

The second relative deformation measured at the joint region was the horizontal slippage between the drypack and the panel concrete at the connection interface. The shear-slip hysteresis loops are given in Figure 5.72(a). At early stages of loading up to displacement increments of 1Dy, the slip mechanism had a limited effect on the system behaviour. The slip accounted for less than 4% of the measured overall displacement. As the specimen was loaded from 1Dy to 4Dy, the slip contribution to the overall response increased to about 8% as seen in Figure 5.72(b). However, shear slip contribution to the overall response increased to about 35% at the 3rd cycle to 5Dy as a result of extensive drypack crushing and buckling of the reinforcement across the joint. The major slip at the 3rd cycle to 5Dy was accompanied by low stiffness and pinching of the hysteresis loop as can be seen in Figure 5.72(c). Up to this stage, the slip response was symmetrical as the load was reversed. Also, sliding in one end was in phase with uplift at the other end of the connection and peak slip displacements were in proportional to the amount of uplift. At failure however, sliding tended to be more towards the push end. This permanent offset in the slip behaviour was probably due to the orientation of buckling of joint reinforcement bars and the extensive crushing of drypack. This is clearly shown in Figure 5.72(d) that gives the load-slip hysteresis loops at 6Dy cycles.

Continuity Bar Reinforcement

The reinforcement bar was instrumented by one gauge within the 20 mm connection region, gauge #1. The behaviour of the bar at gauge #1 is given by load versus strain hysteresis loops in Figures 5.80(a) and 5.80(b) for the west bar and east bar at the connection push-end and pull-end, respectively. Figure 5.80 indicates that the behaviour of both bars was very similar to that of specimen RS. The response was not symmetrical in tension and compression. The presence of the drypack influenced the compression resistance. The Bauschinger effect also influenced the response since the loading was reversed compression-tension. The envelope of load-strain had a similar trend as the behaviour of a bar in uniaxial tension.

Comparison of the measured bar strain at gauge #1 and the drypack strain is given in Figures 5.81(a) and 5.81(b) for the west bar and east bar, respectively. The drypack strain was determined as the ratio of the measured vertical gap at the bar location to a gauge length of 152 mm, over which the LVDT instrumentation was mounted. Good agreement is evident in Figures 5.81(a) for the west bar between the measured bar strain and the average drypack strain up to 1Dy. At 1Dy, the bar strain was consistently higher than the drypack strain which could be due possibly to the bar being unbonded. At 1.5Dy, the strain gauge was pealed off and no further comparison was possible. The comparison of the bar and drypack strain at the pull end (east end) in Figure 5.81(b) revealed excellent agreement the measured bar strain and the drypack strain up to 2Dy. Beyond 2Dy, the bar strain data were lost and further comparison can not be made. The comparisons showed similar trends as in the case in specimen RS.

5.3.5 Specimen RT

Specimen RT consisted of a drypack grouted joint with mild steel continuity reinforcement connected mechanically by bolting to a Hollow Structural Steel (HSS) tube section. The HSS-tube section was located in a rectangular pocket within the connection region. The detail of the tube section was given in section 3.3.

Overview

The behaviour of specimen RT was different from specimen RS. As anticipated, the strength and deformation capacity of the connection was controlled by that of the HSS tube section. The tube was envisioned to enhance the energy dissipation through local flexural deformations of the tube walls. However, while the tube was fairly strong in resisting tension forces, its compressive resistance was limited by local buckling of its vertical walls. Also, as oriented in the specimen with its hollow face parallel to the joint interface and its vertical walls perpendicular to the joint interface which was needed for ease of assembly and drypacking, the tube resistance to shear forces was very poor. The tube resistance to shear and compression forces was enhanced by the drypack grout packed inside the tube section and inside the pocket around the tube. Initially, the drypacked grout confined the deformations of the tube section. However, as soon as major crushing occurred in the drypack within the tube section, failure was imminent and was much more severe than specimen RS.

Figure 5.82(a) gives the overall response of specimen RT in terms of the load versus displacement hysteresis relationship. Figure 5.82(b) is a magnified plot of the load displacement cycles up to 6Dy. Looking at Figure 5.82, the specimen exhibited almost stable hysteretic behaviour without significant loss of strength until the first

cycle to 5Dy when the load-carrying capacity dropped below 80% of the maximum measured value. Major crushing and spalling of the drypack within the tube and extensive local deformation of the vertical walls of the tube occurred during the cycles to 5Dy. The yield displacement was 4.5 mm and the ultimate displacement was 18 mm. Figure 5.83(a) represents the horizontal shear-slip mechanism over the duration of the test. Figure 5.83(b) is a magnification of slip hysteresis cycles up to 5Dy. The rocking response is given in Figure 5.84 based on the joint rotation. Table 5.8 gives specific measured values of force, displacement, slip and rocking quantities at critical stages of the connection response. A detailed description of the observed specimen performance and examination of the progressive damage up to failure is given in the following paragraphs.

Observed Specimen Response

Initially, during the reversed load control cycles, the behaviour of specimen RT was similar to the RS connection: almost linear elastic without significant loss in stiffness as shown in Figure 5.85. This behaviour was maintained for a total of 9 elastic cycles at load increments of 50, 100 and 150 kN with 3 cycles at each level. The bond between the drypack and the concrete panel interface at the connection ends appears to be first broken around a load of +40 in push and -60 kN in pull at which the gap stations read positive indicating uplift as evident in the load versus gaps plot of Figure 5.86. This load level represented the onset of rocking as the applied uniform axial normal compression across the connection was being overcome by the tensile stresses. At the 3rd cycle to 150 kN, hairline cracks were observed in the drypack pocket at the west end. No cracks were observed in the drypacked connection region or in the wall panels. Measured local deformations at the joint interface were small in the order of

+/- 0.2 mm and +0.95/-0.5 mm for the slip and gap stations, respectively. All four strain gauges applied to the tube section were still below the yield.

As the specimen was loaded to +175 kN, the load - displacement relationship became nonlinear and yielding of the top horizontal plate of the tube at the push end occurred. Yielding of the horizontal wall, as evident in Figure 5.87(a), was measured by means of two strain gauges, mark StrNW and StrFW, applied at the center line of the top horizontal plate. The measured corresponding displacement was 4.50 mm. Yielding of the horizontal plate of the other tube commenced during the pull cycle to -175 kN as shown in Figure 5.87(b) by yielding of gauges StrNE and StrFE which were located at the center of the top horizontal plate. Yield of the tube at the pull end corresponds to a displacement of 3.50 mm as shown in Figure 5.88. The average displacement at the first cycle to 175 kN, first yield, is 4.0 mm. The specimen was subsequently subjected to two more cycles of 175 kN. The average displacement during the subsequent two cycles of 175 kN was 4.5 kN. Therefore, based on the above, a yield displacement of 4.5 mm was selected. Minor crushing and no spalling was observed at 1Dy. However, only hairline horizontal cracking occurred in the drypacked pocket at around the location of the horizontal plate of the tube. The measured slip was very small in the order of 0.30 mm. The rocking through vertical gap opening and crushing was about +1.5 and -0.5 mm, respectively.

At 2Dy cycles, widening of existing horizontal cracks in the drypacked pocket at the location of the top and bottom horizontal plates of the tube at the push end occurred. Similar cracking pattern was noted in the tube pocket at the pull end with only one horizontal crack above the connection region. Minor damage to the drypack

and cracking to the panel concrete at the edges of the connection end corners was also observed with the exception of one vertical compression crack in the top panel at the east end. The condition of the connection at the 3rd cycle to 2Dy is shown in Figure 5.89(b). The condition of the connection at the beginning of the test is shown in Figure 5.89(a). The connection resistance reached its maximum value of +208 kN in the push and -200 kN in the pull direction at the 1st cycle of 2Dy. At this stage, the measured slip was about 1 mm. The rocking through vertical gap opening and crushing was in the order of +1.2 and -0.5 mm. At 3Dy, more crushing and some spalling of the drypack in the tube pockets occurred. Crushing concentrated at the connection ends. The drypack at the connection ends was severely crushed and spalled off. The drypack within the tube section was still intact with horizontal cracks and minor spalling. The cracking pattern in the east and west-end tube pockets was identical with two horizontal cracks at the location of the horizontal plate of the tube. The concrete at the corners of the joint in the lower panel was severely crushed and spalled off. Widening of existing vertical compression crack in the top panel at the east end also occurred. The rocking measured as opening/crushing was approximately +5.6 and -1.5 mm, respectively. The measured horizontal slip was on average about 1.70 mm. The connection resistance maintained well around +195 in push and -175 kN in pull.

Continued crushing and spalling of the drypack and concrete at the connection extreme end corners was observed at 4Dy. At the pull end, the drypack in the tube pocket was crushed and partially spalled off with the tube section walls exposed. The vertical compression crack in the top panel progressed along the height of the panel. The drypack crushing and cracking in the west-end pocket was identical. However, the instrumentation prevented the cracked drypack piece inside the tube section from

spalling off. The drypack inside the tube section was still intact. The measured widening/crushing of the drypack at the joint end region was about +7.2 mm uplift and -3.0 mm crushing. The average drypack crushing along the connection length was only 0.2 mm. The slip was about 2.35 mm at the 3rd cycle of 4Dy. The connection resistance in the push and pull 1/2-cycles dropped on average from about +/-180 kN at the 1st cycle to +/-164 kN at the 3rd cycle of 4Dy (which is about 80% of the maximum load). Up to this stage, the behaviour of the connection was fairly consistent with stable hysteresis loops as can be seen in Figure 5.82(b).

At the 1st cycle of + 5Dy, the connection strength maintained an average of +/- 160 kN between the push and pull 1/2-cycles which is about 78% of the maximum measured load. During the 2nd and 3rd cycles of 5Dy, the connection resistance dropped to an average of +/-130 kN which is about 60% of the maximum load as shown in Figure 5.82(b). Failure of the connection occurred during the cycles of 5Dy since the strength dropped and maintained below 80% of the measured maximum. The condition of the drypack joint at 5Dy is shown in Figure 5.89(c). Severe crushing of the drypack within the tube section and in the tube pocket occurred. The drypack inside the tube section was partially spalled off. Crushing of the concrete panel end corners stabilized and no additional cracking was noted in the panels. The existing vertical compression crack in the top panel was progressed. The compression resistance at the connection end corner was mainly provided by the tube section alone as the drypack inside the tube was cracked and crushed. Hence reduced connection strength was measured. The drypack at the connection ends was severely crushed to almost powder. However, the overall thickness reduction was limited to 0.35 at the 1st cycle and 0.75 mm at the 3rd cycle of 5Dy. The rocking was 7.7 mm uplift and -

4.8 mm crushing. The measured slip was about 3.30 mm.

To collect post-failure information, the specimen was subjected to additional single cycles at 6Dy, 7Dy and 8Dy. No additional concrete panel cracking was noted and only the severe crushing of the drypack continued. At 8Dy cycle, the drypack within the tube was completely spalled off. Condition of the connection at 8Dy outside the loading frame is shown in Figure 5.89(d). The connection resistance dropped to and stabilized to about +/-120 kN which is 60% of the maximum. The response of the connection during these cycles can be seen in the load versus displacement relationship given in Figure 5.82. The fat hysteresis loops were mainly due to the unconfined slip mechanism that has occurred following the complete spalling of drypack within the tube at 7Dy. Since the reduction in connection strength was first measured at the cycles of 5Dy, the onset of failure was taken at 5Dy. Therefore, the displacement ductility of this type of connection was 4.

Rocking mechanism

The presence of the tube pockets seemed to have prevented overall thickness reduction of the drypack due to cyclic shear deformations. The overall crushing of the drypack along the connection length did not occur and crushing concentrated over the connection end region. The thickness reduction was less than 1 mm at 5Dy, onset of failure. This represented less than 5% decrease in the initial joint thickness of 20 mm. The rocking mechanism through gap opening and closing is presented in Figure 5.90(a) and 5.90(b) for the push and pull direction, respectively. The rocking characteristic was similar to that of specimen RS. Figure 5.90 gives the distribution of the measured vertical gap deformations. In general, the vertical gap distribution

along the connection length was almost linear. The behaviour was symmetrical as the load alternates. Figure 5.90(a) gives the rocking behaviour during cycles to 0.1Dy, 0.6Dy, 1Dy, 3Dy and 5Dy in the push direction. It is evident from Figures 5.90(a) how the neutral axis position moved within the compression zone from a compression gradient at 50 kN load (0.1Dy) to hinging about the center line of the connection at 150 kN load cycle (0.6Dy). As the applied displacement ductility was increased above 1Dy, hinging of the connection took place as the depth of the compression zone moved towards the connection ends. The depth of the compression zone remained the same as the loading increased from 1Dy to 3Dy while the compression area was reduced due to crushing of the drypack. As soon as significant drypack crushing occurred, the neutral axis shifted back closer to the centre line of the connection at 5Dy as seen in Figure 5.90(a). Very similar rocking response was observed for the pull direction of loading as shown in Figure 5.90(b). However, in the pull direction hinging between 1Dy to 3Dy did not occur. The compression zone depth shifted continually towards the center line of the connection during 1Dy to 5Dy loading increments as seen in Figure 5.90(b).

Slip Mechanism

The complete load-slip hysteretic relationship was given in Figure 5.83(a). The slip characteristic was similar to that of specimen RS. Figure 5.83(b) is a magnified plot of the slip behaviour and included cycles from 1Dy to 5Dy only. It is evident from Figure 5.83(b) that the slip response was symmetrical in the push and pull direction at all ductility increments. At early stages of loading, up to 1Dy increment, the slip mechanism had a very limited effect on the system behaviour and accounted for less than 4% of the overall response. As the specimen was loaded from 1Dy to 4Dy, the

slip contribution to the overall response increased to about 17% at 4Dy as a result of drypack crushing in the compression zone and local buckling of the tube in shear. At failure, sliding contributed about 19% of the total displacement.

Reinforcing bar/Tube response

The connection response was controlled by the behaviour of the bar/tube detail used to connect the reinforcement from the top panel to that of the bottom panel at the joint region. The behaviour of the bar/tube detail was monitored by electric resistance strain gauges. Five strain gauges were placed in the locations as indicated in Figure 5.91. One gauge was applied on the reinforcing bar at 200 mm above the connection region within the top panel. The tube section was instrumented by four gauges as follows: two gauges were mounted on the centre line of the exterior and interior vertical walls and two gauges were mounted on the top horizontal plate in the location of maximum moment at the center line of the plate on either side of the oversized hole. The strain gauges were installed on the HSS tube to determine the flexural deformations (stresses) of the horizontal plate and to examine the load distribution among the vertical walls. The reinforcing bar was gauged to examine the transfer of force from the tube to the bar. The behaviour of each bar/tube detail could be summarized as follows:

1. Reinforcing bar remained elastic well below the yield at all ductility levels.
2. Vertical walls: no yielding in uplift tension rather yielding was through local buckling of the walls.
3. Horizontal plate: yields in tension followed by large flexural deformations.
4. Failure occurred by local buckling of the vertical walls due to combined compression/shear deformations after significant deterioration of the drypack.

The behaviour of the reinforcing bar was monitored by a strain gauge placed at 200 mm above the drypack grout region. Figure 5.92(a) and (b) show the hysteresis loops of load versus bar strain for the west bar at the push end and east bar at the pull-end, respectively. The bar strain remained elastic and well below the yield at all ductility levels as can be seen in Figure 5.92. At onset of failure, 5Dy, the bar strain was less than 50% of the measured yield strain in material tension tests. Thus confirming that most of the deformation occurred within the tube section. Also, the "double nuts/stiff washer plates" system used proved to be very effective in preventing pullout of the bar from the oversized hole in the top horizontal plate despite the large deformations that occurred to the top and bottom horizontal plates during the test. The double nuts and stiff washer plates were used in lieu of conventional ring-shaped washers to connect the threaded end protruding bars from the top panel to the tube plate.

The behaviour of the interior and exterior vertical walls of each tube were monitored by means of a strain gauge placed at the center line of the each wall. Figure 5.93(a) represents the complete hysteretic strain behaviour of the interior and exterior walls of the west tube. Figure 5.93(b) is the envelope of the strain versus ductility behaviour for the west tube walls. The west tube was subjected to tension/shear forces in the push direction and to compression/shear forces in the pull direction of loading. It is evident from Figure 5.93 that the vertical walls did not reach yield in uplift tension in the push direction. Also, as expected, the exterior wall had slightly higher tension strain than the interior wall. The ratio of the tension strain in the exterior and interior wall was slightly greater than 1. The increase in tension strain was almost constant at the various ductility increments up to 3Dy. At 3Dy, the

strain reached a maximum of 0.1% which was less than 50% of the measured yield strain at 0.25% from material tension tests. Beyond 3Dy, both gauges at the interior and exterior walls measure compressive strain during the tension cycle in the push direction. This could be due to local shear deformation of the wall at the connection region where the gauge was located or it could be caused by ill-function in the gauge. At this level, the degree of spalling of the drypack in the tube section was rather moderate. At 4Dy in push, the gauges definitely became out of order as clear in Figure 5.93(b). In the pull loading direction, the tube was primarily subjected to compression and shear stresses. As a result, the vertical walls experience local buckling which could induce tension or compression strains at the wall center line, where the gauge was located, depending on the orientation of buckling. Looking at Figure 5.93, it is clear that buckling of the exterior and interior walls occurred in the direction away from the tube center line as evidenced by tension strains measured at both walls. The interior wall experienced higher tensile strains than the exterior wall as seen in Figure 5.93(b). The local compression/shear buckling of the tube walls corresponded to severe crushing and spalling of the drypack grout inside the tube section. The response of the vertical walls in the east tube were similar to that of the west tube. Figure 5.94(a) and (b) give respectively the complete strain hysteretic behaviour and the envelope of the strain behaviour for the vertical walls in the east tube at various ductility increments. In addition to the shear force, the east tube was subjected to compression in the push direction and to tension in the pull direction. The maximum measured tension strain in the pull direction was 0.09% which is less than 50% of the material yield strain. The ratio of the tension strain in the exterior and interior walls was about 1 up to 2Dy. Beyond 2Dy, the interior wall maintained a tension strain about twice that of the exterior wall as can be seen in Figure 5.94(b).

At 5Dy, the gauges became out of order. In the pull loading direction, the gauge at the interior wall measured tension while the gauge at the exterior wall measured compression. This could reflect the orientation of the local buckling of the walls in the tube: the interior wall may have buckled away from the tube center line producing tension strain at the center line of the wall and the exterior wall buckling towards the center line of the tube causing compression strain at the wall center line. Again buckling of the walls was accompanied by severe crushing and spalling of the drypack within the tube.

The behaviour of the top horizontal plates of each HSS tube was monitored by means of two gauges placed at the center line of the plate on either side of the oversized hole. The response of the west tube horizontal plate at the push end is shown in Figure 5.95(a). Only one of the two gauges on the plate was functional. As seen in Figure 5.95(a), the load-strain behaviour in tension had similar trends to the uniaxial tension coupon test of mild steel with an elastic portion, a yield plateau and strain hardening. The early change in slope in the curve could be attributed to the cracking of the drypack in the tension zone which caused an increase in the strain. The response; however, was not symmetrical in tension and compression. The load-strain curve revealed a stiffer response in compression than in tension. This was mainly due to the contribution of the drypack grout to the compressive resistance. Further, the flexural deformations of the horizontal plate and the cracking of the drypack in tension at the plate location caused a shift in the measured strain and produced a permanent residual tension plastic strain following a tension loading increment as seen in Figure 5.95(a) between the elastic and 1Dy cycles. At 2Dy, the gauge data were lost due to debonding of the gauge from the surface of the tube as

seen in Figure 5.95(a) and thus no further analysis was possible.

The strain behaviour of horizontal plate of the tube at the pull end is given in Figure 5.95(b). The two strain gauges on the horizontal plate of the tube at the pull end were functional up to 2Dy cycles. The measured data from the two gauges were almost identical as would be expected and are given in Figure 5.95(b). Comparing Figures 5.95(a) and (b), it is rather obvious that the performance of the horizontal plate of the tube at the pull end was very similar that of the tube at the push end as expected due to the symmetry in the reversed loading. Again it was clear that the load-strain behaviour in tension has similar trends to a uniaxial tension coupon test. Also, the response was not symmetrical in tension and compression. Following a higher tension loading increment, the strain did not return to the previous compressive value, rather there was a permanent tension plastic strain as the loading was increased from 0.5Dy to 1Dy to 2Dy. This was a result of the flexural deformations in the horizontal plate and cracking of the drypack grout at the location of the plate. Beyond 2Dy, the gauges pealed off and no further strain was recorded. However, the observed crack pattern after 2Dy, with horizontal cracks at the location of the top and bottom horizontal plates, revealed significant flexural deformations of the horizontal plate in the tube. The significant deformation was coupled with severe cracking and spalling of the drypack within the tube section. This was accompanied by local compression/shear buckling of the vertical walls as discussed previously.

Comparison of the measured strain at the center line of the top horizontal plate and the drypack strain from the vertical gap station located at the center line of the tube is given in Figures 5.96(a) and 5.96(b) for the tubes at the push and pull ends,

respectively. The drypack strain was defined as the ratio of the measured vertical gap divided by the gauge length of 405 mm, over which the LVDT instrumentation was mounted. A good agreement is evident in Figures 5.96(a) at the west tube between the horizontal plate strain and the drypack strain in the push direction to a tension loading. In the pull direction, the tube was subjected to compression loading and the strains were incompatible. While compressive strains were measured for the drypack region, residual tension strains were measured at the horizontal plate following tension loading as previously discussed. At 2Dy, no further comparison was possible as the strain gauge became unbonded from the horizontal plate.

The comparison between the horizontal plate strain and the drypack strain at the east tube is given in Figure 5.96(b). Good correlation was observed at the initial elastic load cycles. At 1Dy and 2Dy, the measured horizontal plate tension strain was twice that of the drypack strain during tension loading in the pull direction as seen in Figure 5.96(b). This suggested complete loss of bond between the plate and the drypack. No correlation between the horizontal plate strain and the drypack strain was evident during the compression loading in the push direction. The response during the compression loading was similar to that observed for the horizontal plate of the tube at the push end: residual tension strain was recorded for the horizontal plate while compression strain was measured for the drypack. Beyond 2Dy the horizontal plate strain data were lost and further comparison could not be made.

5.4 PRESTRESSED SPECIMEN SUBJECTED TO REVERSED CYCLIC LOAD

This section presents the results of the specimens connected by prestressed reinforcement and subjected to cyclic loading. Three prestressed specimens (PTS, PTB and PTBU) were tested under cyclic combined flexure and shear loading. The specimen nomenclature was explained earlier in section 3.3. All the prestressed specimens had a plain surface joint. The experimental variables included: connections with fully bonded prestressing strands (PTS) versus fully bonded prestressing bars (PTB); and connections with fully bonded prestressing reinforcement (PTB) versus fully unbonded reinforcement (PTBU). The totally bonded and totally unbonded prestressed reinforcement was achieved by fully grouted and not grouting the prestressing ducts, respectively.

Each prestressed specimen was loaded to an axial stress of 2 MPa normal to the connection which was kept constant throughout the test. The specimen was then subjected to a two-phase reversed cyclic loading history as explained in section 4.2.3. Briefly, loading was typically as follows: initially, the specimen was subjected to load control cycles with three cycles at increasing increments of load up to yielding of the prestressed reinforcement. After yield, the specimen was loaded by displacement control in multiples of the yield displacement with three cycles at each displacement increment and one lower service level cycle between these increments. The displacement increment was increased as the test progressed up to failure. Failure was defined by inability of the connection to sustain any additional loads more than 80% of the maximum measured.

5.4.1 Specimen PTS

The configuration of specimen PTS was identical to specimen PTS-S tested under monotonic loading. Specimen PTS consisted of a plain surface drypacked joint region post-tensioned using two 1/2" (12.7 mm) diameter strands spaced at 900 mm o/c. Each prestressing strand was prestressed to an effective stress of 0.6fpu to produce an equivalent prestress load of 1.2 MPa on the connection.

Overview

The overall connection response is given in Figure 5.97(a) in terms of load versus displacement hysteresis relationship over the duration of the test. Figure 5.97(b) is a magnified plot of Figure 5.97(a) and included the hysteresis loops up to 7Dy cycles. The specimen showed very stable hysteretic behaviour. Rupture of the post-tensioning strand in the push end occurred at the 2nd cycle of 8Dy. Severe drypack crushing and spalling at the other extreme end accompanied the rupture of the strand. The measured yield displacement was 4 mm and the measured ultimate ductility of the specimen was 6. The connection local response was measured by the horizontal slip behaviour as shown in Figure 5.98 and by the vertical rocking behaviour given in Figure 5.99. The vertical rocking was very similar to the overall response. The horizontal slip constituted a small portion of the overall displacement and thus had a limited effect on the connection overall response. A summary of specific response quantities at different ductility levels are given in Table 5.9. The performance of the specimen during the different stages of loading follows.

Overall Behaviour

Initially, the behaviour of the connection in load control was linear elastic without any

stiffness loss for 12 cycles up to a load of 175 kN as shown in Figure 5.100. Breaking of the bond between the drypack and the upper wall panel appears to have occurred at a load of +160 kN and -125 kN as opening (uplift) was measured by gaps #1 and #7 at the connection push and pull end, respectively. The gap openings are evident in Figure 5.101 which gives the load versus gap#1 and load versus gap#7 hysteresis loops. However, no damage was noted at the connection region or in the wall panels near the joint at this stage.

As the specimen was loaded to the 200 kN load cycle, a sudden jump was measured in the vertical gaps at the location of the strands. Since no strain gauges were placed on the prestressing strands, the strain increment in each strand could only be estimated from the drypack strain. The drypack strain was determined as the ratio of the measured vertical gap at the strand location to a gauge length of 152 mm over which the LVDT instrumentation was mounted. The total strain in the strand was determined as the summation of the strain increment (drypack strain) and the initial pretension strain of 0.005 due to initial prestressing to 0.6fpu. Figure 5.102 gives the load versus strain behaviour at the location of the push and pull end strands. The jump in the strain at +/-200 kN load is evident. At +200 kN, the strain at the push end strand was 0.0105 and at -200 kN the strain at the pull end strand was 0.0102. Based on material tension tests, the post-tensioned strand yields at a strain of 1% (0.01). Thus the connection first yield occurred at the first cycle to 200 kN load level. Yielding of the push end strand corresponded to a displacement of +3.75 mm while the pull end strand yielded at a displacement of -4.25 mm as seen in Figure 5.103. A yield displacement of 4.0 mm was used in the test based on the average of the two yield displacements. Figure 5.102 also revealed unsymmetric response in tension and

compression. This was because the compression force was resisted by the drypack and the strand while the tension force was resisted by the strand only. Following first yield, the specimen was subjected to two more cycles at 200 kN load which were taken as the cycles to 1Dy. At this stage, no visible damage was observed in the drypack or in the wall panels at the connection region. The measured slip was +/-0.12 mm. Gap opening and crushing were small at +1.0 and -0.85 mm, respectively. Figure 5.104(a) shows the condition of the connection prior to any damage.

After yield, the specimen was loaded in three cycles at multiple increments of the yield displacement. As in the case of the specimens with mild steel reinforcement, the post-yield response of specimen PTS was nonlinear inelastic. The hysteresis loops; however, were narrower and the residual plastic displacement was lower.

Up to a displacement increment of 4Dy, minor damage was observed in the drypack and the wall panel edges at the connection region. The drypack remained intact with some crushing and spalling at the two end corners. Limited compression cracking was noted in the wall panels at the joint. The connection resistance maintained around an average of +/-225 kN for the 2Dy to 4Dy cycles. This value was the average of the peak resistances in the push and pull directions among all nine cycles from 2Dy to 4Dy. The maximum resistance reached was +235 kN at 3Dy in the push direction and -240 kN at 4Dy in the pull direction as seen in Figure 5.97(b). The horizontal slip was less than 1 mm at 4Dy. The vertical gap opening and crushing at the joint ends were approximately +7.5 mm and -2.50 mm, respectively. The condition of the connection at 4Dy is shown in Figure 5.104(b). Continued crushing and spalling of the drypack at the connection extreme ends was observed at

5Dy. Concrete cracks occurred at the lower wall panel push and pull extreme ends. Further widening of the gap opening to about +9 mm and gap crushing at extreme ends of the connection to about -4.5 mm was measured at the 3rd cycle to 5Dy. The slip was about +/-1.3 mm. The connection strength dropped from an average of 225 kN at the 1st cycle to 196 kN at the 3rd cycle to 5Dy.

At cycles to 6Dy, the drypack grout continued crushing and spalling off. The drypack was literally ground to powder at the connection ends. The drypack deterioration progressed to about 1/3 the connection length from the joint extreme ends. A big piece of cracked concrete cover in the lower panel at the west end corner spalled off as shown in Figure 5.104(c) which gives the condition of the connection at 6Dy. Gap widening to +10 mm and gap crushing to -7.5 mm was recorded at the 3rd cycle to 6Dy. The horizontal slip increased to 2.5 mm at the 1st cycle to 6Dy. At the 2nd cycle to 6Dy, no horizontal slip was measured as the slip stations were lost. The average thickness reduction through overall drypack crushing was about 0.60 mm. The strength reduction among the three cycles to 6Dy was about 8% from an average of 192 kN at the 1st cycle to an average of 176 kN at the 3rd cycle. The latter value was 78% of the average connection strength of 225 kN measured from 2Dy to 4Dy cycles. Strength reduction could be caused by the prestress loss in the strand due to some permanent reduction in thickness which occurred between 5Dy and 6Dy.

At 7Dy, panel concrete cracking stabilized and only drypack crushing and spalling occurred. The crushing progressed further towards the center line of the connection. The average permanent crushing along the connection length was about -

1 mm at the 3rd cycle to 7Dy. Gap opening was 11.5 mm and gap crushing was -9.66 mm at the extreme edges. Slip could not be measured as the slip stations were lost. The strength degradation among the cycles to 7Dy was less than 4%. The connection resistance maintained an average of 178 at the 1st cycle and 171 kN at the 3rd cycle. The connection strength was on average of 176 kN at the 1st cycle to 8Dy. However, as the specimen was loaded to 8Dy in push, the strand at the push end ruptured and the load dropped to 100 kN as seen in Figure 5.97. The condition of the connection at 8Dy is shown in Figure 5.104(d), which also shows the ruptured strand. Failure was taken as the point when the load carrying capacity dropped and maintained below 80% of the average maximum strength. Failure was probably caused by loss of prestressing due to extensive crushing of the drypack which occurred during the cycles from 5Dy to 7Dy. During the three cycles to 7Dy, the connection strength maintained at 76% of average connection strength. Thus the ductility of this type of connection was 6.

Rocking Behaviour

As in the specimens with mild steel reinforcement, the rocking mechanism for specimen PTS was monitored by seven vertical gap stations along the connection length. The distribution of gap stations represented the rocking response. Figure 5.105(a) and (b) gives the rocking behaviour in the push and pull direction of loading, respectively. These figures include rocking at 0.5Dy, 1Dy, 3Dy and 6Dy level. The rocking response during these cycles was almost linear. Figure 5.105 also showed the movement of the compression zone as loading was increased. The rocking response was similar to that observed in the specimens with mild steel reinforcement. Initially, the connection was under uniform compression. As the bending moment at the

connection region was increased, the behaviour moved from a compression gradient at 0.1Dy (50 kN) to rocking about the connection center line at 0.48Dy (150 kN) to hinging about L/3 from the end corner at 1Dy to hinging about L/4 at 3Dy. The compression zone depth was about the same during cycles from 2Dy to 4Dy. Hinging was accompanied by crushing and spalling of the drypack at the connection ends. As soon as significant deterioration to the drypack occurred the neutral axis shifted back closer to the connection center line at 6Dy as seen in Figure 5.105(a). Rocking behaviour was symmetrical as the load was reversed. This was clear from comparing the rocking response in the pull direction in Figure 5.105(b) to that for the push direction given in Figure 5.105(a). The thickness reduction in terms of overall drypack crushing along the connection length at 6Dy was less than 1 mm which is about 4% of the initial drypack thickness.

Slip Behaviour

The slip was the horizontal movement of the top panel relative to the bottom panel at the connection region. The horizontal slip response was given in Figure 5.98. The load versus slip response was almost symmetrical in push and pull direction but was slightly shifted towards the push end. The slip plane was between the bottom panel and drypack interface. It is evident in Figure 5.98 that initially, up to 1Dy, the slip had very narrow hysteresis loops and small contribution to the system behaviour. At 1Dy, the slip was less than 4% of the total displacement. As the specimen was loaded from 1Dy to 6Dy, the slip increased to almost 11% of the total displacement with a rather fat hysteresis loop at the 1st cycle to 6Dy. This was caused by the crushing and spalling of the drypack in the compression zone. Beyond 6Dy, the slip behaviour was not recorded since the slip stations were lost.

5.4.2 Specimen PTB

Specimen PTB was identical to specimen PTB-S consisting of a plain surface drypacked joint region post-tensioned using two 5/8" (15 mm) diameter Dywidag high strength bars, spaced at 900 mm o/c. The bars were fully bonded though an expensive grout injected in the ducts. Each bar was stressed to an effective prestress of 0.6fpu. The configuration was detailed in section 3.3.

Overview

The connection overall response is given in terms of load versus displacement relationship and the local response is given in terms of horizontal slip and vertical rocking. Figure 5.106(a) shows the load versus displacement hysteresis relationship over the test duration. Figure 5.106(b) is a magnification of the load-displacement hysteresis plot. The horizontal slip versus load behaviour is shown in Figure 5.107(a). Figure 5.107(b) gives the horizontal slip versus ductility behaviour. Figure 5.108 presents the vertical rocking behaviour. Table 5.10 gives a summary of specific response quantities at different ductility levels. In general, specimen PTB showed ductile and stable behaviour. Between cycles of 3Dy and 4Dy, the strength gradually reduced due to gradual reduction in the connection thickness. At 5Dy, a further drop in the strength was measured possibly because of the loss in prestress caused by thickness reduction. Between 5Dy and 6Dy, the strength maintained at the same lower load level. At 7Dy, the strength picked up to the same load level measured in cycles of 3Dy and drypack crushing stabilized. During the 3rd cycle to 7Dy in the pull direction, the load dropped suddenly as the prestressing bar at the pull end ruptured. Rupture of the bar was coupled with more crushing of the drypack at the push end. The measured yield displacement was 4 mm and the ductility was 6. The observed

overall performance at different loading stages follows.

Overall Behaviour

In the initial load control cycles, the behaviour of the connection was linear elastic without any stiffness loss. This was maintained for 16 cycles up to a load of 200 kN as shown in Figure 5.109. The bond between the drypack and the upper wall panel appears to break at a load of +/-60 kN as evident in Figure 5.110 for gaps #1 and #7 at the connection push and pull end, respectively. At this stage, no visible damage was observed at the connection region or in the wall panels near the joint.

As the specimen was loaded to a load increment of 200 kN, the strain increment at push-end bar in the push end jumped from 0.0015 to 0.0036 and the strain increment at the pull-end bar in the pull end jumped from 0.0015 to 0.0045. The prestressing bar had an initial pretension strain of 0.003, due to initial prestressing to 0.6fpu. Thus the bar strain at 200 kN jumped from 0.0045 to 0.0066 for the push-end bar and jumped from 0.0045 to 0.0075 for the east bar. The strain behaviour for the push and pull end bars is evident in Figure 5.111. Based on material tension tests, the prestressing bar yields at a strain of about 0.65% (0.0065). The 200 kN load level represents the connection first yield at which the bar yielded in tension. A displacement of 4.20 mm corresponded to yielding of push end bar and a displacement of 3.60 mm corresponded to yielding of pull-end bar as shown in Figure 5.112. A yield displacement of 4.0 mm was selected based on the two directions of loading.

At 1Dy cycles, the connection strength maintained an average of 198 kN between the push and pull directions. The horizontal slip was only +/-0.15 mm. The

vertical gap opening and crushing were small in the order of +1.5 and -0.75 mm, respectively. Few vertical hairline cracks were noted in the drypack and no cracks were observed in the wall panel edges at the connection region. The condition of the connection before any observed damage is shown in Figure 5.113(a).

The observed damage at 2Dy was very minor with limited crushing and spalling of the drypack at the extreme edges. Some vertical cracks were observed in the concrete upper and lower panels at the connection ends. The connection reached its maximum strength at +/-225 kN during the 1st cycle to 2Dy. The slip increased to 0.46 mm. The gap opening increased to +3.5 mm and the gap crushing at the extreme connection end was -1.30 mm. At 3Dy, crushing of the drypack progressed to about 1/3 the connection length. Vertical cracks were noted in the wall panels at the location of the prestressing bars. The cracked concrete in the lower wall panel at the connection ends crushed and spalled off at this stage. The connection strength maintained an average of 198 kN between the push and pull direction. The slip was about +/-1 mm and the gap increased to an opening of +4.75 mm and crushing of -3 mm. Up to 3Dy, the drypack at the connection ends remained fairly intact and overall thickness reduction was less than 0.3 mm. Condition of the connection at 3Dy is shown in Figure 5.113(b).

At 4Dy, no significant change occurred to the cracking patterns. Crushing and spalling of the drypack continued. The extent of crushing remained at about 1/3 the connection length. Widening of existing cracks occurred. A large concrete cover piece in the lower panel cracked. The panel cracking was limited to surface cracks which did not propagate within the thickness of the wall. The overall crushing along

connection length was -0.85 mm. The connection strength dropped to 177 kN at the 3rd cycle of 4Dy. The strength reduction could be due to the prestress loss in the bar which was caused by permanent thickness reduction. The vertical gap opening and crushing at the connection ends were approximately +5.90 mm and -5.90 mm, respectively. The horizontal slip was shifted towards the push end. The slip ranged from -0.31 mm in push to -1.74 mm in pull direction at 3rd cycle to 4Dy. The shifted slip behaviour could be due to the orientation of buckling of the prestressing bar or due to the loading system. Thus ductility ratio of 4 represented onset of strength reduction, onset of thickness reduction and onset of buckling of bar.

At 5Dy, the drypack at the connection extreme ends continued to crush and spall off. Severe crushing was observed at the connection ends. Drypack crushing propagated towards the center line of the connection. The overall crushing along the connection length increased to 1.6 mm which represented 8% thickness reduction. The large concrete cover piece in the lower panel at the west end corner, which cracked at 4Dy, spalled off as shown in Figure 5.113(c) which gives the condition of the connection at 5Dy. The gap opening increased to about +6.0 mm and gap crushing increased to about -8.0 mm at the 3rd cycle to 5Dy. The measured slip remained permanently shifted and was -0.17 mm in push and -2.40 mm in pull. The connection strength dropped from an average of 171 kN at the 1st cycle to 160 kN at the 3rd cycle to 5Dy. This value represents 78% of the average strength of 205 kN during cycles to 1Dy, 2Dy and 3Dy, prior to any significant strength reduction.

At 6Dy, concrete cracking and crushing stabilized while the drypack grout continued to crush and spall off. The drypack was literally ground to powder at the

connection ends. The deterioration through thickness reduction increased to about 3 mm at the 3rd cycle to 6Dy. Gap widening to +7.2 mm and gap crushing at the connection extreme end to -11 mm was recorded at the 3rd cycle to 6Dy. The horizontal slip ranged from 0 mm in push and -2.74 mm in pull. The connection strength slightly increased to an average of 172 kN which is 84% of the average strength of 205 kN. The three cycles to 6Dy were almost identical without any strength degradation.

At 7Dy, further concrete cracking did not occur and only drypack crushing and spalling continued. The drypack in the connection region was reduced to a very thin layer. The connection resistance increased and maintained at an average of 186 kN during the first 2 cycles to 7Dy. The resistance was transferred from the top panel through the thin drypack layer to the concrete in the bottom panel. At the 3rd cycle to 7Dy, as the specimen was loaded in the pull direction, the load suddenly dropped to 110 kN. This drop in the load was caused by rupture of the prestressing bar. At this stage, gap opening was +7.5 mm and gap crushing was -13.2 mm at the extreme edges. Slip was still permanently shifted towards the push end and ranged from -1.0 mm to -5.30 mm in the push and pull directions, respectively. It was suggested earlier that the slip orientation was a consequence of the orientation of the local shear deformation of the bar in dowel action. The deformation of the bar is evident in Figure 5.113(d) which shows how the bar was deformed towards the pull direction. Figure 5.113(d) represents the condition of the connection at the 3rd cycle of 7Dy. The thickness reduction along the connection length at the 3rd cycle of 7Dy increased to about 5 mm which was a 25% reduction from the initial 20 mm thickness. Failure was probably caused by loss of prestressing due to the extensive crushing of the

drypack which occurred during the cycles from 4Dy to 7Dy. The connection strength dropped below 80% of the average strength only for the 3rd cycle to 5Dy. This was possibly due to the loss of prestressing at the onset of drypack crushing which occurred at 4Dy. The resistance increased back to 84% during the cycles to 6Dy and to 90% during the two cycles to 7Dy. This increase in the load was probably because of the strain hardening effect of the prestressing bar. However, since the bar ruptured at the 3rd cycle to 7Dy, the ductility of this type of connection was taken as 6.

Rocking Behaviour

Again, the rocking behaviour for specimen PTB was monitored by seven vertical gap stations along the connection length. Figures 5.114(a) and (b) give the rocking behaviour in the push and pull direction of loading, respectively. These figures include rocking at 0.5Dy, 1Dy, 3Dy and 6Dy level. Figure 5.114(c) gives the overall thickness reduction of the connection due to crushing of the drypack at various ductility increments. Figures 5.114(a) and (b) show the movement of the compression zone as loading was increased. Initially, the connection was under uniform compression. As the bending moment at the connection region was increased, the behaviour moved from a pure compression at 0.1Dy (50 kN) to rocking about the connection center line at 0.48Dy (150 kN) to hinging about L/3 from the end corner at 1Dy and 2Dy. Crushing and spalling of the drypack during cycles from 3Dy to 6Dy caused the neutral axis to move back towards the center line of the connection. This is clear in Figure 5.114(a) for movement from 1Dy to 3Dy to 5Dy. As soon as drypack at the extreme ends of the compression zone was completely crushed, the compression zone depth moved back towards the connection ends as seen in Figure 5.114(b) between 5Dy and 7Dy. The rocking behaviour was symmetrical when the

load was reversed as clear by comparing Figure 5.114(b), which gives rocking in the pull direction, to Figure 5.114(a), which represented rocking in the push direction. The thickness reduction due to overall drypack crushing along the connection length is given in Figure 5.114(c). It is evident from figure 5.114(c) that cycles to 4Dy represented the onset of thickness reduction. At failure, the reduction was 25% of the initial thickness of 20 mm.

Slip Behaviour

The horizontal slip behaviour of specimen PTB was similar to that of specimen RS. Up to displacement increment of 1Dy, the slip mechanism had very limited effect on the system behaviour and the connection response was mainly governed by the rocking mechanism. The slip accounted for less than 3% of the overall response at 1Dy. As the specimen was loaded from 1Dy to 3Dy, the slip contribution to the overall response increased to about 10% at 3Dy as a result of drypack crushing in the compression zone and the flexibility of the prestressing bar. The slip response was almost symmetrical up to this level. At 4Dy, the slip became unsymmetrical and tended to be more towards the push end as clear in Figure 5.107(a). This shift in the slip response could be due to a permanent compression/shear deformation of the prestressing bar towards the push end. Thus cycles to 4Dy represented the onset of in-plane buckling of the prestressing bar. The slip response continued to be unsymmetric and permanently shifted towards the pull end during cycles to 5Dy, 6Dy and 7Dy. At failure, displacement increment 7Dy, sliding contributed about 17% of the displacement in the pull direction.

Post-tensioned Bar Response

Each prestressing bar was instrumented by means of two electric resistance strain gauges mounted at the inner and outer surfaces of the bar within the 20 mm connection region. No gauges were placed along the length of the bar. The bars were initially post-tensioned to 0.6fpu. This produced an initial pre-tension strain of 0.0032 in each bar. At the time of testing, the average bar strain was 0.0030 which means that the prestress losses were in the order of 6%. During testing, the strain increment, which did not include the initial pre-strain, was measured. At any loading stage, the strain in the bar was determined as summation of the measured strain increment and the initial prestrain of 0.003. Figures 5.115(a) and (b) give the load versus bar strain relationship for the bars at the connection push and pull end, respectively. These figures include the data for the inner and outer gauges on each bar. In the push loading direction, the push end bar was the tension bar and the pull end bar was the compression bar. As the load was reversed, in the pull direction, the push-end bar became the compression bar and the pull-end bar became the tension bar. Looking at Figure 5.115(a), which represents the bar strain at the push-end, it is seen that at the initial stages, the measured strain at the inner and outer gauge were in excellent agreement. As loading was increased, the outer gauge measured more tension strain than the inner gauge. Both gauges became out of order at the 1st cycle to 2Dy. The load-bar strain relationship in Figure 5.115(a) showed similar trend to the behaviour of a prestressing bar in uniaxial tension. Also, the measured yield strain, including the initial pre-strain, agreed well with those measured in material tension test of prestressing bar. The load versus bar strain relationship at the pull end in Figure 5.115(b) shows very similar behaviour to the push-end bar. As evident in Figure 5.115(b), the outer gauge remained functional at the cycles to 2Dy thus capturing the

response of the bar into the strain hardening zone. Beyond 2Dy, the gauge data were lost.

Comparison of the measured bar strain increment, excluding initial pre-strain, and the drypack strain at the bar location is given in Figure 5.116(a) and 5.116(b) for the push and pull end, respectively. The drypack strain was determined as the ratio of the measured vertical gap at the bar location divided by a gauge length of 152 mm, over which the instrumentation was mounted. Looking at Figures 5.116(a) and (b), it was obvious that initially, up to 0.5Dy, the drypack strain and bar strain were almost identical suggesting that the bars were bonded to the drypack at this stage. Compatibility of the strains became no longer valid beyond 1Dy. Specifically, the strains in the compression zone became incompatible possibly due to unbonding of the bar. The compression strain in the drypack was consistently higher than that measured in the bar possibly because of the residual tension strain in the bar following loading in tension. The permanent shift in the bar strain due to plastic deformations during loading in tension is clearly shown in Figures 5.116(a) and (b). Such a phenomena was not observed for the drypack strain. On the other hand, there was a very good agreement between the drypack and the bar strain in the tension zone at different ductility increments as clear in Figure 5.116(b) during the pull loading direction. The strain gauge on the bar at the push end became out of order at 2Dy as seen in Figure 5.116(a) while the gauge on the bar at the pull end remained functional during the cycles to 2Dy as seen in Figure 5.116(b). Beyond 2Dy, the gauge on the bars became out of order and further comparison was no possible.

5.4.3 Specimen PTBU

The configuration of specimen PTBU was similar to that of specimen PTB which consisted of a drypacked plain surface connection post-tensioned using two 5/8" (15 mm) diameter prestressing bars spaced at 900 mm o/c. The major difference between the two specimens was that the prestressing bars in this specimen, PTBU, were fully unbonded and the ducts were not grouted. As in specimen PTB, the prestressing bars were each stressed to an effective prestress of 0.6fpu to produce an average stress of 1.2 MPa on the connection region.

Overview

Because of the fully unbonded prestressing bars, the behaviour of specimen PTBU was different from specimen PTB. Specimen PTBU deformed significantly higher than specimen PTB and therefore more damage was observed at the connection region. The overall specimen response is given in Figure 5.117(a) which represents the load versus displacement hysteresis relationship over the test duration. Figures 5.117(b) through (e) presents the hysteresis loops at selected ductility levels. Splitting the hysteresis loops of Figure 5.117(a) into four subsequent graphs was essential to examine the cyclic hysteretic behaviour which could not possibly otherwise from Figure 5.117(a) alone due to congestion of the loops. Figures 5.117(b) through (e) will be used to explain the different stages observed for the tested specimen. The local connection response was measured in terms of horizontal slip and vertical rocking. The complete horizontal slip versus load behaviour is shown in Figure 5.118(a). The slip hysteresis at selected ductility levels is presented in Figure 5.118(b) and (c). Figure 5.118(d) gives the slip versus ductility behaviour. The vertical rocking behaviour is quantified in terms of joint rotation as shown in Figure 5.119.

Summary of the response quantities at different ductility levels are given in Table 5.11. Since the bar was unbonded, the strain along the entire length of the bars was uniform and no localized yielding could occur at the connection region. Therefore, the applied yield displacement was 4 mm based on the measured localized yield displacement of specimens PTB and PTS which were connected with fully bonded prestressing bars and strands, respectively. The measured ultimate displacement was 56 mm and the ultimate ductility was 14. Throughout the duration of the test, the specimen showed very ductile and stable hysteretic behaviour. Severely pinched and narrow hysteresis loops characterized the response. Rupture of the bar did not occur and failure was caused by significant crushing and spalling of the drypack grout and the concrete wall panels at the connection region. Failure was accompanied by significant reduction in the thickness of the drypacked connection. The observed overall performance at different loading stages are described below.

Overall Behaviour

The behaviour of the connection in the load control cycles up to 100 kN was linear elastic without any stiffness loss. At load level of 150 kN, the response showed slight nonlinear behaviour with slight stiffness loss at load ranging between 100 kN and 150 kN increments as shown in Figure 5.120. The response was also unsymmetric between the push and pull loading directions. This nonlinearity and unsymmetry could be attributed to the nonlinear characteristic of the drypack material from one end of the connection to the other. Breaking of the bond between the drypack and the upper wall panel appears to have occurred at a load of +30 and -80 kN as evident in Figure 5.121 based on the measured vertical gaps #1 and #7 at the push end and pull end, respectively. No observed damage at the connection region or in the wall panels near

the joint was noted at this stage.

At load cycles of 175 kN increment, the load-displacement loops exhibited pronounced nonlinear behaviour during the 3rd cycle in the push direction as the displacement jumped from 6 mm to 9 mm. This behaviour was accompanied by minor crushing of the drypack grout at the extreme connection corner. At this stage, however, the strain in the prestressing bars, including the initial pre-tension strain, were only 0.35% which was well below the yield strain of the bar at 0.7% based on material tests. Since the prestressing bars were fully unbonded, bar yielding was unlikely to occur as evident in Figure 5.122 which gives the strain behaviour of the prestressing bars for displacement increments up to +/- 12 mm. The complete bar strain behaviour, which will be discussed later, over the duration of the test confirmed that the bars remained linear elastic below yielding. Thus the definition of connection yielding based on the yielding of the bars could not be used for specimen PTBU. Since the onset of nonlinear behaviour occurred at load cycles of 175 kN, this level will be used as a guide to verify the equivalent-yield displacement selected. The average displacement between the push and pull loading direction for the three cycles to 175 kN was 4.56 mm. While the measured yield displacement for the post-tensioned specimens with bonded prestressing bars (specimen PTB) and strands (specimen PTS) was 4 mm. This displacement of 4 mm was very close to the average displacement of 4.56 mm for the 175 kN load cycles. Therefore, it was decided to apply an equivalent-to-yield displacement of 4 mm to be consistent with specimens PTB and PTS and for ease of comparing the relative behaviour of the various prestressed specimens.

Similar to the other specimens, specimen PTBU was loaded in displacement control at multiple increments of the selected equivalent-to-yield displacement with three cycles at each increment. Among the three cycles to a ductility increment, the behaviour was similar to what have been observed for other specimens: about 10% strength degradation between the 1st and 2nd cycle and no degradation between the 2nd and the 3rd cycle. The hysteresis loops; however, were narrower and more pinched possibly because of the fully unbonded bars.

Up to cycles of 3Dy, minor crushing and some spalling occurred to the drypack at the connection ends. Crushing of the drypack spread over 150 mm from the connection ends. Minor cracking and spalling of a concrete cover piece occurred in the lower panel at the pull end and a vertical compression crack was noted in the upper panel at the push end. The strength maintained an average of 172 kN in the push and pull direction at cycles to 3Dy. The horizontal slip was small at +/-0.6 mm. Gap opening and crushing at the connection extreme ends were 4.90 mm and -3.0 mm, respectively. The drypack at the connection ends remained fairly intact and overall thickness reduction was less than 0.45 mm. The condition of the connection at third cycle of 3Dy is shown in Figure 5.123(b). The condition of the connection at the beginning of the test is given in Figure 5.123(a).

At cycles to 4Dy and 5Dy, further crushing and spalling of the drypack occurred. Crushing of the drypack progressed towards the center line of the connection. The drypack was still intact at the center line of the connection but was severely crushed at the extreme ends. Concrete cracking occurred along the edges of the lower panel at the pull end. A concrete cover piece in the upper wall panel

cracked and spalled off at the pull end. Concrete cracking at the push end did not change with one vertical compression crack at the top panel. The connection strength slightly increased to an average of 178 kN. The slip was symmetrical and increased to +/-0.85 mm. The gap opening increased to +7.7 mm and the gap crushing was -6 mm. The thickness reduction through overall crushing along the connection length increased to 1.5 mm at the 3rd cycle to 5Dy. The hysteresis load-displacement loops during cycles from 1Dy to 5Dy exhibited very stable response as seen in Figure 5.117(b). The loops were narrow and slightly pinched. The envelope of the load-deformation during these ductility increments conformed to an elasto-plastic behaviour. Condition of connection at 5Dy is shown in Figure 5.123(c).

At 7Dy, no significant change occurred to the cracking patterns in the concrete wall panels. However, severe crushing and spalling of the drypack continued along the connection length. The resistance was transferred from the crushed drypack to the concrete panels at the connection region and the strength increased to about 190 kN. The gap opening increased further to +9.70 mm and gap crushing to -10.5 mm at the 3rd cycle to 7Dy. The connection thickness was reduced by 4 mm which was 20% of the initial 20 mm thickness. The slip at the 1st cycle to 7Dy was almost symmetrical at +1.40 and -1.87 mm between the push and pull direction. At the 3rd cycle to 7Dy, the slip was permanently shifted towards the push direction with range of +0.45 mm and -1.90 mm in the push and pull direction, respectively. This shifted slip behaviour was possible due to permanent shear deformation in the bar through dowel action at 7Dy.

Further crushing and spalling of the drypack grout within the connection region

occurred during cycles from 8Dy to 10Dy ductility increments. The drypack in the connection region reduced to a very thin layer and the resistance transferred to the concrete wall panel edges at the connection ends. Compression cracking in the concrete of the upper and lower panels at connection corners increased. Significant thickness reduction occurred during ductility increments from 8Dy to 10Dy. At 10Dy, the connection thickness reduced by 7.5 mm. Gap opening increased to +10 mm and gap crushing was -17 mm. The slip was permanently shifted towards the push end and ranged from -1.72 to -4.52 mm in the push and pull direction. The connection resistance reached and maintained a maximum of 200 kN during ductility increments from 8Dy to 10Dy. The hysteresis loops were very narrow and severely pinched possibly because of the fully unbonded bars, as evident in Figure 5.117(c) for ductility increments from 6 to 10Dy. Condition of the connection at 10Dy is shown in Figure 5.123(d).

During ductility increments from 11Dy to 14Dy, the drypack was completely crushed and ground to powder. Significant crushing and some spalling of the concrete wall panels at the connection end corners occurred. The condition of the connection at 14Dy is shown in Figure 5.123(e). At 14Dy, gap opening increased to 20 mm and gap crushing increased to -25 mm at the connection ends. Since the connection thickness was initially 20 mm, gap crushing of 25 mm implied a 5 mm crushing in the concrete wall panels has occurred. The overall reduction in the connection thickness was 11.5 mm. The slip continued to be shifted towards the pull direction and ranged from -4.25 to -7.22 mm in the push and pull direction. The resistance dropped from 190 kN at 11Dy increment to 164 kN at 14Dy which represents 82% of the measured maximum of 200 kN. At 12Dy, the limit of the stroke of the actuator was reached in

the pull direction. Thus beyond 12Dy, testing continued by applying an unsymmetric loading pattern with ductility increments larger than 12Dy possible in the push direction while loading in the pull direction was limited by the actuator's stroke to -12Dy. The unsymmetric loading is very obvious in the load-displacement loops of Figure 5.117(d) for increments from 11Dy to 15Dy. The characteristic of the hysteretic response throughout the test could be identified by comparing the load-displacement loops at selected ductility increments to 1Dy, 5Dy, 10Dy and 14Dy as shown in Figure 5.117(e). It is evident from the figure that at all ductility levels, the hysteresis loops were very narrow and pinched. Figure 5.117(e) also reveals the significant stiffness degradation as ductility level was increased.

At 15Dy cycles, the limit of the actuator's stroke in the push direction was also reached and further testing was not possible. At this stage, 15Dy, the resistance dropped to 140 kN which is 70% of the maximum measured load. The resistance had gradually dropped from 190 kN at 11Dy to 164 kN at 14Dy, which is 82% of the maximum load, as evident from Figure 5.117(d). Failure, reduction of the resistance below 80%, was characterized by more severe crushing and spalling of the panel concrete at the connection end corner. Since onset of failure was at 14Dy, the ultimate ductility of this type of connection was 14. The condition of the connection outside the loading frame at 15Dy is shown in Figure 5.123(f).

Rocking Behaviour

The rocking behaviour at ductility increments of 0.5Dy, 1Dy, 7Dy and 14Dy is given in Figures 5.124 (a) and (b) for the push and pull loading directions, respectively. The rocking was monitored by seven vertical gap stations along the connection length.

Figures 5.124 (a) and (b) illustrate the movement of the compression zone within the connection length as loading was increased. The behaviour moved from a compression gradient at 0.1Dy (50 kN), which was not shown in the figure since the measured gap deformations were very small, to rocking about the connection centre line (L/2) at 0.5Dy (150 kN) to hinging about L/3 from the end corner at all other ductility levels. The severe crushing and spalling of the drypack during cycles from 3Dy to 14Dy caused permanent reduction in the connection thickness while the neutral axis remained constant at about 1/3 the connection length. This was clear in Figure 5.124(a) for the push direction and was repeated in Figure 5.124(b) for the pull direction of loading. The rocking behaviour was symmetrical when the load was reversed as clear by comparing Figures 5.124(a) and Figure 5.124(b). The thickness reduction due to overall drypack crushing along the connection length is given in Figure 5.124(c). It is evident from Figure 5.124(c) that 4Dy represent onset of thickness reduction. At failure, the reduction was 60% of the initial 20 mm thickness.

Slip Behaviour

The horizontal slip behaviour of specimen PTBU was similar to that of specimen PTB. However, due to the larger deformability and more severe damage at the connection, the shear deformation of the bar was much more pronounced than that observed in specimen PTB. Up to a displacement increment of 7Dy, the connection response was mainly governed by the rocking mechanism and the slip had very limited effect on the behaviour accounting for about 6% of the overall response at the 1st cycle of 7Dy. The slip response was almost symmetrical up to this level. At the 3rd cycle of 7Dy, the slip became unsymmetrical and tended to be more towards the pull end as clear in Figure 5.118(b). This shift in the slip response could be due to a permanent

compression/shear local deformation of the prestressing bar towards the pull end which was in phase with the more severe damage that occurred in the pull end as opposed to the push end. Thus cycles to 7Dy represented the onset of in-plane local shear deformation of the prestressing bar through dowel action. The slip response continued to be permanently shifted towards the pull end during cycles from 8Dy to 14Dy as seen in Figure 5.118(c). The slip range; however, remained constant. At failure, ductility increment of 14Dy, sliding contributed about 14% of the displacement in the pull direction.

Post-tensioned Bar Response

As in specimen PTB, the prestressing bars were each instrumented by means of two electric resistance strain gauges mounted at the inner and outer surfaces of the bar within the connection region. The bars were initially post-tensioned to 0.6fpu which produced an initial pretension strain of 0.3% in each bar after prestress losses. During testing the strain increment was measured. The strain increment did not include the initial prestrain. The total strain in the bar was determined as summation of the measured strain increment and the initial prestrain of 0.003. The load versus bar strain relationship for the bars at the connection push and pull end are given in Figures 5.125(a) and (b), respectively. These figures included the data for the inner and outer gauges on each bar and represented the total strain in the bar including the initial pretension strain. Figure 5.125(a) represents the bar strain at the push-end, clearly indicates that the strain behaviour was stiffer during compression loading versus tension loading. The stiffer response in a compression loading cycle was expected since the compression stresses were resisted by the drypack/concrete and not by the continuity bars. Also, at initial stages, the strain at the inner and outer gauges were

in excellent agreement. As loading was increased, the outer gauge measures more tension strain than the inner gauge. The strain behaviour at the inner gauge indicated that the bar response was still linear and below yielding of the bar. At 10Dy, the measured strain at the inner gauge was 0.6% while the yield strain from material tests was at 0.7%.

The outer gauge; however, seemed to have exceeded the material yield of the bar at an applied ductility increment of 10Dy. Unless the local shear deformation in the bar occurred at the location of the outer gauge in an orientation to produce such high tension strains. Such a drastic change in the strain across the thickness of the bar is impossible and thus one of the two gauges should be neglected. The behaviour of the outer gauge could possibly be due to nonlinearity in the gauge. To see if there was any repetitive trend in the bar behaviour, the strains at the inner and outer gauges on the pull end bar were compared. Figure 5.125(b) gives the load versus strain relationship for the inner and outer gauges at the pull end. The agreement between the inner and outer gauge data was excellent. The response was similar to that of the inner gauge for the bar at the push end: linear elastic in tension and well below the yield strain. This confirmed that the measured strains of the outer gauge at the push end bar could be neglected. Both inner and outer gauges remained functional beyond the cycles to 10Dy.

Comparison of the measured bar strain increment, excluding initial pre-strain, and the average drypack strain at the bar location is given in Figure 5.126(a) and 5.126(b) for the push and pull end, respectively. The average drypack strain was determined as the ratio of the measured vertical gap at the bar location divided by a

gauge length of 2600 mm, over which the bar was unbonded, to account for the unbonding effect. This average drypack strain did not; however, reflect the actual strain in the drypack at the connection region. The comparisons for the bar versus drypack strains at the push and pull ends were very similar. Prior to significant crushing of the drypack, there was excellent correlation between the bar strain and the average drypack strain. After crushing of the drypack, the agreement remains excellent between the bar strain and the average drypack strain in tension at different ductility increments as clear in Figures 5.126(a) and (b). The compression strain in the drypack was consistently higher than that measured in the bar, as would be expected since the compression resistance was provided mainly by the drypack and concrete. The strains in the compression zone were incompatible possibly due to the unbonded bar.

Table 5.1 Summary of measured response quantities for specimen RS-S

Ductility ratio	Load P (kN)	Displacemen D (mm)	Slip Ds (mm)	Rotation θ (x1E-3)	c (mm)
0.0	0	0.05	0.00	0.05	1200
0.1	54	0.46	0.02	0.20	1000
0.3	100	1.03	0.04	0.39	1038
0.5	151	1.81	0.08	0.61	769
0.9	201	3.50	0.17	1.04	557
1	226	4.22	0.20	1.24	496
2	261	8.22	0.52	2.85	303
3	270	12.02	1.01	4.44	257
4	278	15.85	1.61	6.11	250
5	283	20.01	2.17	7.98	247
6	286	23.98	2.84	9.80	248
7	286	27.76	3.49	11.49	252
8	285	31.87	4.35	13.47	263
9	280	35.73	4.91	15.29	258

P = applied horizontal load
D = total displacement at location of load
Ds = slip deformation
θ = rotation at the connection
c = depth of compression zone

Table 5.2 Summary of measured response quantities for specimen PTB-S

Ductility ratio	Load P (kN)	Disp D (mm)	Slip Ds (mm)	Rotation θ (x1E-3)	c (mm)
-0.0	-2	-0.16	-0.00	0.02	1200
0.1	51	0.33	0.00	0.06	1000
0.2	101	0.93	0.01	0.15	823
0.5	150	2.05	0.01	0.42	560
1.0	200	4.14	0.14	1.27	429
2	216	8.31	0.58	3.25	406
3	221	12.51	1.22	5.40	402
4	224	16.16	1.91	7.14	405
5	227	19.74	2.56	8.81	407
6	234	24.42	3.44	10.88	403
7	235	28.21	4.35	12.54	401
8	238	32.19	5.19	14.40	389
9	234	36.12	6.10	16.15	387
10	229	40.02	6.89	17.90	386
11	124	44.00	7.67	20.29	361

P = applied horizontal load
D = total displacement at location of load
Ds= slip deformation
θ = rotation at the connection
c = depth of compression zone

Table 5.3 Summary of measured response quantities for specimen PTS-S

Ductility ratio	Load P (kN)	Disp D (mm)	Slip Ds (mm)	Rotation θ (x1E-3)	c c (mm)
0.0	0	0.03	0.00	0.03	1200
0.1	51	0.35	0.01	0.07	1000
0.2	100	0.98	0.03	0.20	860
0.4	151	1.90	0.05	0.48	440
0.9	201	3.77	0.14	1.20	360
1	216	4.30	0.16	1.43	350
2	226	8.27	0.38	3.41	233
3	236	12.23	0.63	5.58	222
4	235	16.83	0.86	8.13	209
5	243	20.77	1.04	10.30	203
6	230	26.14	1.55	12.85	199
7	224	28.20	1.69	13.89	203

P = applied horizontal load
D = total displacement at location of load
Ds= slip deformation
θ = rotation at the connection
c = depth of compression zone

Table 5.4 Summary of post-yield test results for specimen RS

Stage	Cycle	Load P (kN)	Displ. D (mm)	Slip Ds (mm)	Rocking Behavior θ *1E-3	c (mm)	δtg (mm)
1Dy	+1	201	+4.29	0.21	+0.89	403	
	-1	-244	-4.27	-0.09	-1.02	350	
	+3	193	+4.30	0.21	+0.92	417	
	-3	-233	-4.29	-0.08	-1.03	357	0.09
2Dy	+1	265	+8.67	0.71	+2.50	305	
	-1	-261	-8.64	-0.63	-2.74	280	
	+3	240	+8.82	0.75	+2.64	376	
	-3	-252	-8.54	-0.44	-2.85	353	0.09
3Dy	+1	256	12.87	1.38	+4.37	347	
	-1	-272	-13.04	-1.04	-4.82	322	
	+3	237	12.85	1.46	+4.39	432	
	-3	-257	-12.78	-0.81	-4.86	393	0.13
4Dy	+1	247	17.12	2.31	+6.17	423	
	-1	-268	-17.37	-1.52	-6.98	379	
	+3	221	17.48	2.31	+6.47	570	
	-3	-261	-17.29	-1.28	-7.11	486	0.26
5Dy	+1	229	21.36	2.60	+8.45	568	
	-1	-249	-21.32	-2.42	-8.92	492	
	+3	198	21.27	0.14	+9.95	616	
	-3	-174	-23.29	-4.15	-9.86	549	0.7
6Dy	+1	182	25.61	0.51	12.62	600	
	-1	-179	-25.70	-4.69	-10.94	577	1

P = applied horizontal load
D = total displacement at load
Ds = slip deformation

θ = rotation at the connection
c = depth of compression zone
δtg = crushed thickness of drypack

Table 5.5 Summary of post-yield test results for specimen RSK

Stage	Cycle	Load P (kN)	Displ. D (mm)	Slip Ds (mm)	Rocking Behavior θ *1E-3	c (mm)	δtg (mm)
1Dy	+1	220	4.55	0.24	1.35	364	0.22
	-1	-213	-4.55	-0.18	-1.06		0.22
	+3	221	4.64	0.24	1.36	352	0.23
	-3	-218	-4.70	-0.18	-1.08	489	0.22
2Dy	+1	277	9.10	0.45	3.25	255	0.18
	-1	-262	-9.02	-0.47	-2.72	291	0.14
	+3	266	9.13	0.55	3.43	262	0.08
	-3	-251	-9.11	-0.46	-2.73	341	0.08
3Dy	+1	284	13.55	0.73	5.68	214	0.07
	-1	-271	-13.75	-0.77	-4.84	268	-0.00
	+3	278	13.53	0.87	5.58	236	-0.07
	-3	-261	-13.62	-0.81	-4.86	307	-0.06
4Dy	+1	285	18.12	1.13	8.03	203	-0.08
	-1	-271	-18.18	-1.10	-7.13	295	-0.12
	+3	266	18.01	1.26	8.11	208	-0.06
	-3	-250	-18.35	-1.23	-7.23	330	-0.04
5Dy	+1	203	22.80	1.46	11.49	176	0.05
	-1	-252	-22.62	-1.39	-9.63	328	0.00
	+3	177	22.87	1.47	11.63	168	0.12
	-3	-200	-23.18	-1.41	-10.68	358	0.10

P = applied horizontal load
D = total displacement at load
Ds = slip deformation

θ = rotation at the connection
c = depth of compression zone
δtg = crushed thickness of drypack

Table 5.6 Summary of post-yield test results for specimen RSU

Stage	Cycle	Load P (kN)	Displ. D (mm)	Slip Ds (mm)	Rocking Behavior θ *1E-3	c (mm)	δtg (mm)
1Dy	+1	235	6.52	0.45	2.57	264	0.23
	-1	-230	-6.64	-0.20	-2.69	267	0.22
	+3	220	6.56	0.42	2.61	280	0.23
	-3	-224	-6.56	-0.16	-2.72	298	0.23
2Dy	+1	236	13.09	1.34	5.72	244	0.21
	-1	-249	-13.12	-0.84	-5.82	307	0.17
	+3	218	13.02	0.98	6.13	317	0.22
	-3	-235	-13.25	-0.61	-6.26	364	0.22
3Dy	+1	235	19.82	2.46	8.92	334	0.23
	-1	-249	-19.17	-1.61	-8.91	388	0.22
	+3	217	19.76	1.43	9.67	457	0.32
	-3	-224	-19.66	-1.46	-9.39	498	0.36
4Dy	+1	223	26.42	3.25	12.37	462	0.48
	-1	-238	-26.20	-2.63	-12.31	506	0.50
	+3	210	26.37	0.97	13.95	505	0.78
	-3	-226	-26.32	-2.77	-12.76	558	0.97
5Dy	+1	224	32.52	3.14	16.18	492	1.62
	-1	-245	-32.60	-5.30	-14.74	532	1.93
	+3	226	32.61	1.74	16.57	504	3.32
	-3	-246	-32.26	-6.57	-13.76	544	3.82
6Dy	+1	249	38.42	3.97	18.68	466	4.74
	-1	-268	-39.09	-8.37	-16.86	478	5.12
	+3	240	39.07	1.69	20.19	448	6.53
	-3	-264	-40.14	-10.21	-16.28	464	6.88
7Dy	+1	178	45.20	-0.92	25.64	347	7.62
	-1	-275	-45.27	-11.44	-18.66	408	7.81

P = applied horizontal load
D = total displacement at load
Ds = slip deformation
θ = rotation at the connection
c = depth of compression zone
δtg = crushed thickness of drypack

Table 5.7 Summary of post-yield test results for specimen RW

Stage	Cycle	Load P (kN)	Displ. D (mm)	Slip Ds (mm)	Rocking Behavior θ *1E-3	c (mm)	δtg (mm)
1Dy	+1	191	5.07	0.34	0.93	373	
	-1	-211	-4.99	-0.07	-0.95	433	0.12
	+3	192	5.14	0.31	0.94	373	
	-3	-209	-5.00	-0.08	-0.98	433	0.12
2Dy	+1	219	10.20	0.83	2.99	375	
	-1	-256	-10.06	-0.66	-2.86	368	0.14
	+3	219	10.04	0.27	2.92	468	
	-3	-247	-10.09	-0.42	-3.11	417	0.14
3Dy	+1	214	15.18	1.91	5.22	560	
	-1	-242	-15.06	-0.87	-5.66	505	0.55
	+3	203	15.07	0.60	5.45	516	
	-3	-231	-15.00	-0.46	-5.88	442	0.70
4Dy	+1	215	20.20	2.06	7.42	500	
	-1	-236	-19.28	-1.16	-8.35	440	1.36
	+3	196	20.12	1.61	7.74	546	
	-3	-220	-20.36	-1.77	-8.47	509	2.09
5Dy	+1	203	24.78	6.30	9.17	620	
	-1	-214	-25.01	-4.40	-9.71	578	3.75
	+3	190	24.63	9.08	7.78	640	
	-3	-186	-25.09	-12.12	-6.27	591	10.50
6Dy	+1	213	30.08	4.08	13.87	487	
	-1	-242	-30.28	-11.80	-9.93	411	11
	+3	183	30.15	-4.52	14.33	511	
	-3	-116	-24.47	-15.80	-10.25	474	12

P = applied horizontal load
D = total displacement at load
Ds = slip deformation
θ = rotation at the connection
c = depth of compression zone
δtg = crushed thickness of drypack

Table 5.8 Summary of post-yield test results for specimen RT

Stage	Cycle	Load P (kN)	Displ. D (mm)	Slip Ds (mm)	Rocking Behavior θ *1E-3	c (mm)	δtg (mm)
1Dy	+1	175	4.47	0.30	1.89	386	
	-1	-175	-4.42	-0.33	-1.45	391	0.05
	+3	172	4.66	0.29	2.03	399	
	-3	-156	-4.41	-0.35	-1.42	435	0.06
2Dy	+1	208	9.12	0.72	4.07	269	
	-1	-200	-9.06	-1.00	-3.21	305	0.11
	+3	193	9.09	0.88	4.01	285	
	-3	-182	-9.00	-1.21	-3.11	391	0.11
3Dy	+1	204	13.73	1.37	6.16	253	
	-1	-191	-13.50	-2.64	-4.83	440	0.14
	+3	180	13.73	0.79	6.90	312	
	-3	-165	-13.63	-1.73	-5.05	443	0.14
4Dy	+1	189	18.06	1.56	9.32	284	
	-1	-170	-18.12	-3.23	-6.11	420	0.20
	+3	166	18.10	1.58	10.78	338	
	-3	-153	-21.25	-3.68	-6.46	407	0.20
5Dy	+1	164	22.18	3.08	12.80	360	
	-1	-153	-22.48	-2.86	-6.73	373	0.35
	+3	139	22.29	3.58	14.39	382	
	-3	-121	-23.28	-3.28	-6.97	515	0.75

P = applied horizontal load
D = total displacement at load
Ds = slip deformation

θ = rotation at the connection
c = depth of compression zone
δtg = crushed thickness of drypack

Table 5.9 Summary of post-yield test results for specimen PTS

Stage	Cycle	Load P (kN)	Displ. D (mm)	Slip Ds (mm)	Rocking Behavior θ *1E-3	c (mm)	δtg (mm)
1Dy	+1	200	3.95	0.06	1.05	358	
	-1	-201	-4.28	-0.18	-1.55	476	0.18
	+3	200	4.14	0.04	1.14	357	
	-3	-200	-4.62	-0.20	-1.75	445	0.18
2Dy	+1	226	8.00	0.24	3.10	267	
	-1	-219	-8.01	-0.26	-3.53	271	0.10
	+3	222	7.97	0.26	3.03	299	
	-3	-220	-8.01	-0.28	-3.62	288	0.14
3Dy	+1	235	11.93	0.50	5.10	239	
	-1	-232	-12.02	-0.42	-5.67	228	0.11
	+3	224	12.00	0.53	5.17	239	
	-3	-229	-12.15	-0.41	-5.76	245	0.19
4Dy	+1	228	16.02	0.79	7.26	227	
	-1	-240	-15.98	-0.55	-7.83	214	0.19
	+3	209	16.14	0.83	7.43	273	
	-3	-232	-16.29	-0.51	-8.05	230	0.22
5Dy	+1	212	19.87	1.19	8.70	281	
	-1	-234	-20.25	-0.60	-9.63	239	0.22
	+3	186	20.26	1.51	8.93	386	
	-3	-206	-20.59	-1.12	-7.99	370	0.31
6Dy	+1	185	24.09	2.48	12.02	431	
	-1	-199	-24.21	-1.72	-12.08	425	0.44
	+3	168	24.37		13.41	471	
	-3	-184	-24.44		-12.07	470	0.61
7Dy	+1	169	28.41		15.51	483	
	-1	-186	-27.70		-13.74	466	0.77

P = applied horizontal load
D = total displacement at load
Ds = slip deformation
θ = rotation at the connection
c = depth of compression zone
δtg = crushed thickness of drypack

Table 5.10 Summary of post-yield test results for specimen PTB

Stage	Cycle	Load P (kN)	Displ. D (mm)	Slip Ds (mm)	Rocking Behavior θ *1E-3	c (mm)	δtg (mm)
1Dy	+1	205	4.60	0.17	1.69	295	
	-1	-205	-4.20	-0.17	-1.61	345	0.07
	+3	186	4.01	0.09	1.49	316	
	-3	-188	-4.07	-0.20	-1.54	345	0.10
2Dy	+1	223	8.04	0.44	3.63	274	
	-1	-228	-8.14	-0.61	-3.51	285	0.07
	+3	200	8.01	0.31	3.69	374	
	-3	-205	-8.02	-0.49	-3.65	346	0.11
3Dy	+1	207	12.08	0.94	5.70	374	
	-1	-212	-12.06	-1.00	-5.59	353	0.14
	+3	184	12.01	0.13	6.30	463	
	-3	-188	-12.28	-1.25	-5.75	440	0.31
4Dy	+1	180	16.06	0.68	8.31	475	
	-1	-195	-16.17	-1.90	-7.61	452	0.44
	+3	159	16.37	-0.31	9.11	532	
	-3	-173	-16.00	-1.76	-7.63	470	0.83
5Dy	+1	160	20.26	0.48	10.47	539	
	-1	-183	-20.11	-2.15	-10.00	468	1.22
	+3	152	20.56	-0.17	11.03	552	
	-3	-168	-20.88	-2.40	-10.44	520	1.74
6Dy	+1	163	24.02	0.41	13.07	542	
	-1	-181	-24.33	-2.77	-11.63	488	2.36
	+3	170	25.76	0.04	14.24	537	
	-3	-172	-23.17	-2.72	-11.55	503	3.32
7Dy	+1	191	28.55	0.40	15.39	511	
	-1	-181	-28.01	-4.01	-13.48	482	3.88
	+3	195	28.08	-1.06	15.79	506	
	-3	-110	-29.09	-5.27	-13.53	470	4.65

P = applied horizontal load
D = total displacement at load
Ds = slip deformation
θ = rotation at the connection
c = depth of compression zone
δtg = crushed thickness of drypack

Table 5.11 Summary of post-yield test results for specimen PTBU

Stage	Cycle	Load P (kN)	Displ. D (mm)	Slip Ds (mm)	Rocking Behavior θ *1E-3	Rocking Behavior c (mm)	Rocking Behavior δtg (mm)
1Dy	+1	176	5.73	0.24	2.36	309	
	-1	-176	-3.01	-0.04	-1.26	288	0.14
	+3	176	6.52	0.34	2.79	331	
	-3	-176	-2.99	0.21	-1.37	310	0.16
3Dy	+1	174	12.02	0.43	6.10	390	
	-1	-179	-11.98	-0.78	-6.09	394	0.31
	+3	167	12.36	0.09	6.49	429	
	-3	-169	-12.57	-0.80	-6.52	419	0.51
6Dy	+1	182	23.95	1.38	12.38	421	
	-1	-191	-24.08	-1.13	-12.97	436	1.89
	+3	176	24.48	0.80	13.00	433	
	-3	-184	-24.49	-1.25	-13.23	438	2.65
9Dy	+1	197	36.11	0.47	20.26	372	
	-1	-207	-36.28	-3.48	-19.21	423	5.94
	+3	187	36.06	-0.73	21.04	384	
	-3	-189	-36.34	-3.68	-18.85	417	6.66
12Dy	+1	178	49.15	-1.88	29.16	379	
	-1	-199	-47.37	-5.41	-25.04	400	9.18
	+3	162	48.07	-2.82	29.37	391	
	-3	-184	-47.63	-5.99	-24.79	411	9.53
14Dy	+1	152	56.88	-3.91	35.59	393	
	-1	-181	-47.53	-6.95	-24.29	387	10.59
	+3	140	56.30	-4.24	35.17	398	
	-3	-178	-47.63	-7.22	-24.34	387	11.18

P = applied horizontal load
D = total displacement at load
Ds = slip deformation
θ = rotation at the connection
c = depth of compression zone
δtg = crushed thickness of drypack

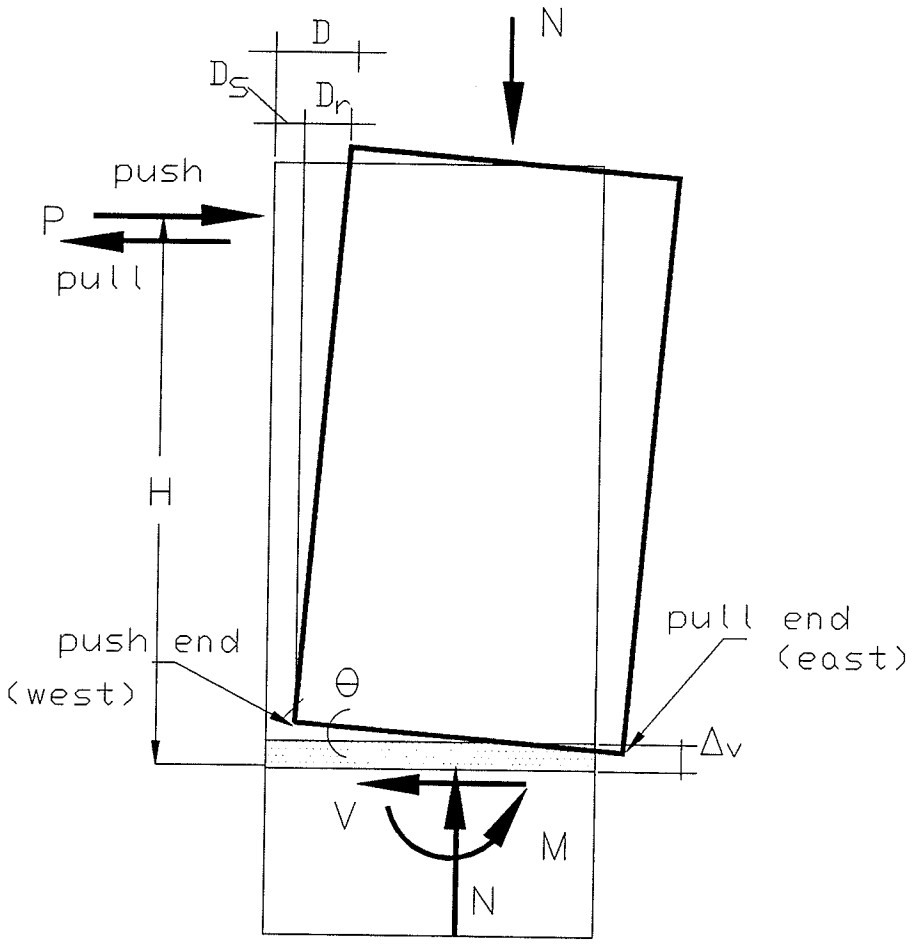

Figure 5.1 (a) Connection response quantities

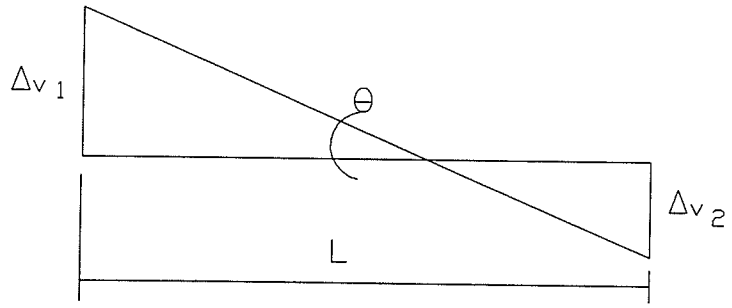

$$\theta = \frac{|\Delta_{v1}| + |\Delta_{v2}|}{L}$$

Figure 5.1(b) Computation of rotation from Gaps

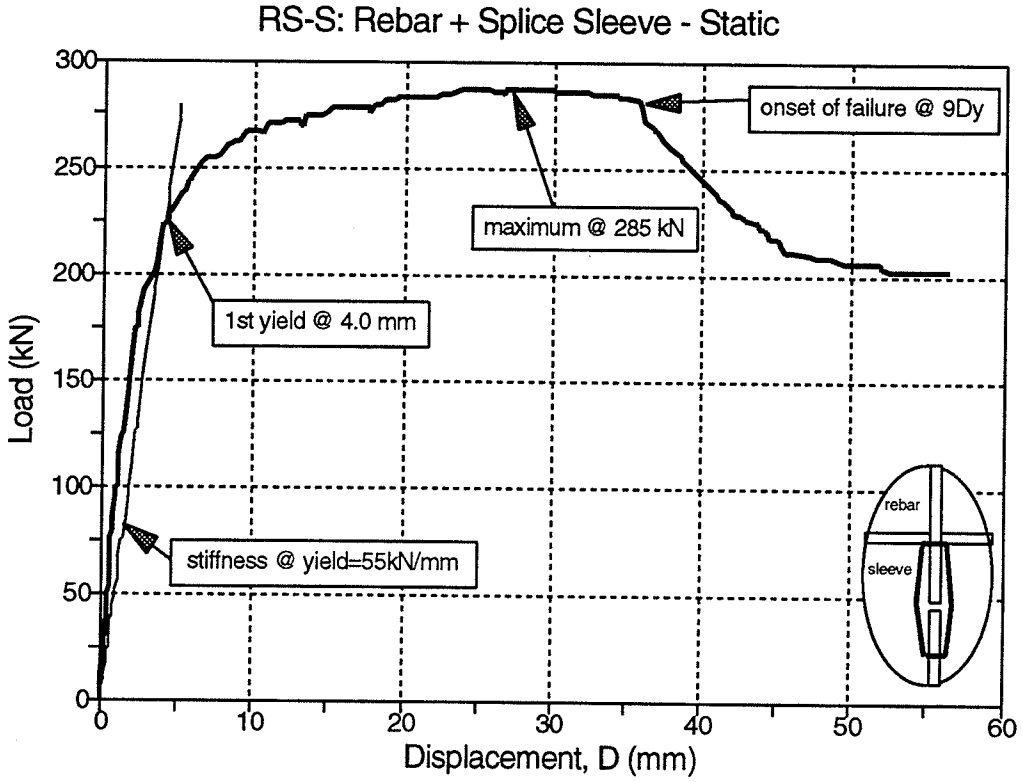

Figure 5.2 Load versus displacement relationship for specimen RS-S

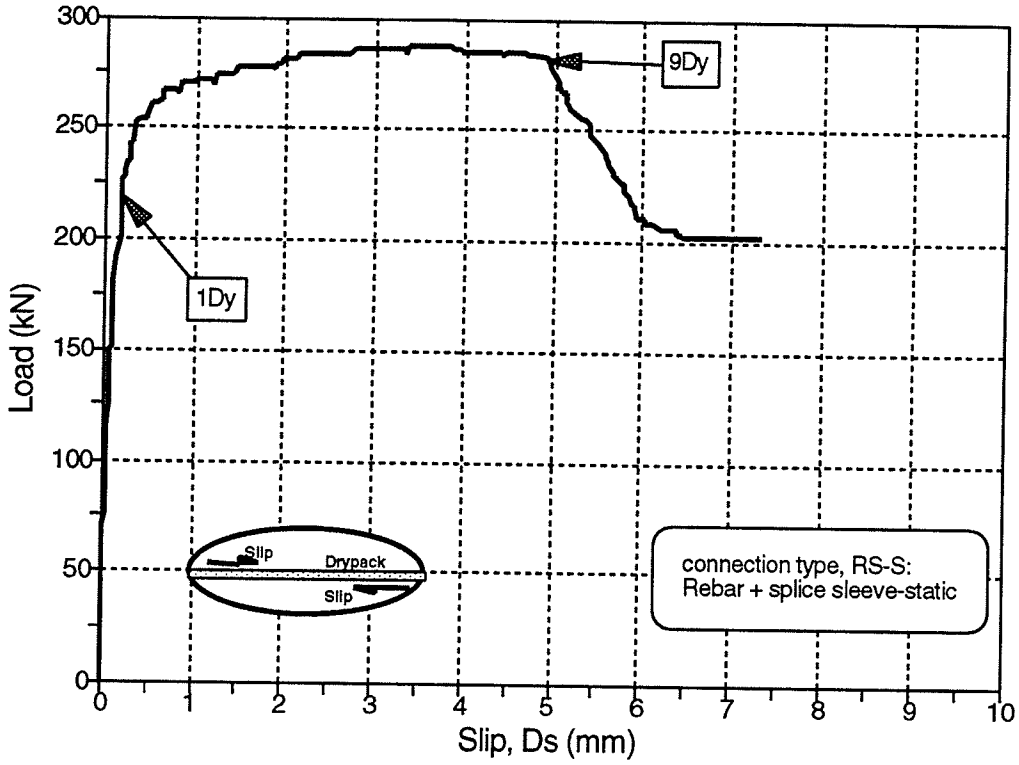

Figure 5.3 Load versus horizontal slip behaviour for specimen RS-S

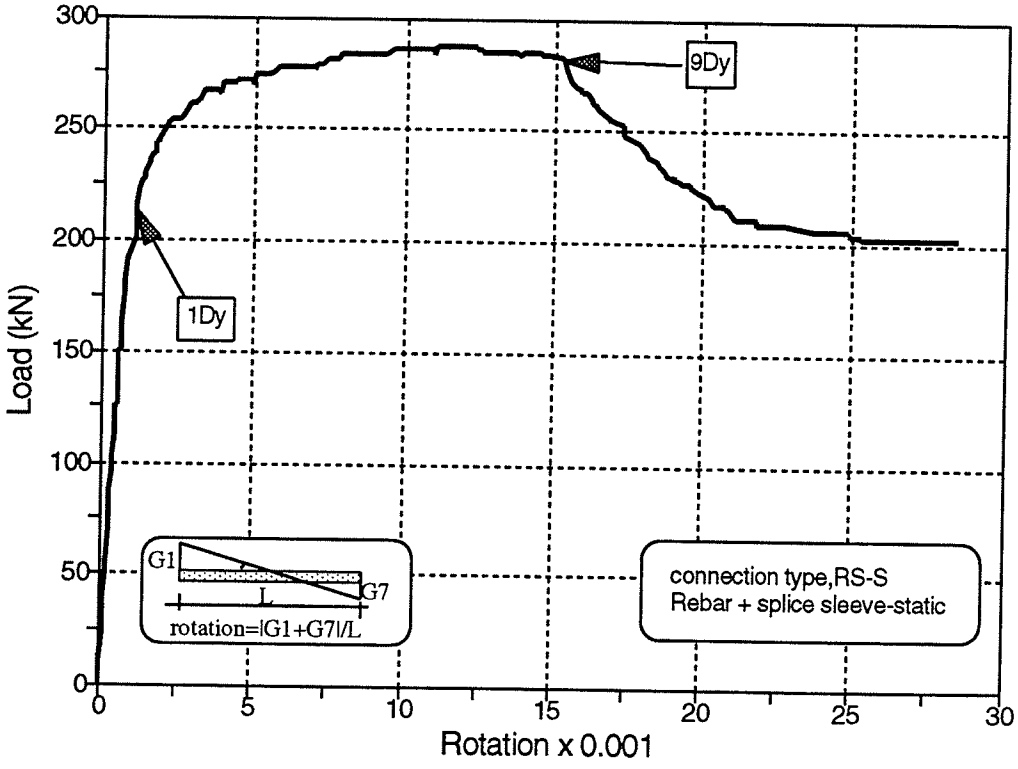

Figure 5.4 Load versus rotation relationship for specimen RS-S

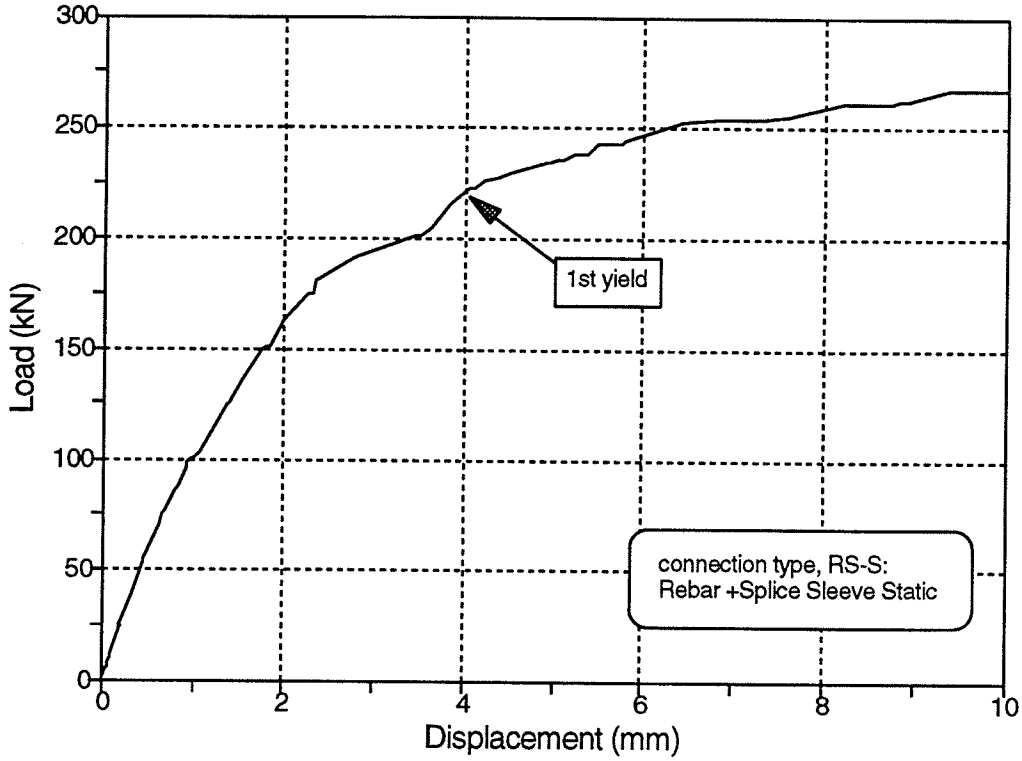

Figure 5.5 First yield response per load vs. displacement relationship for specimen RS-S

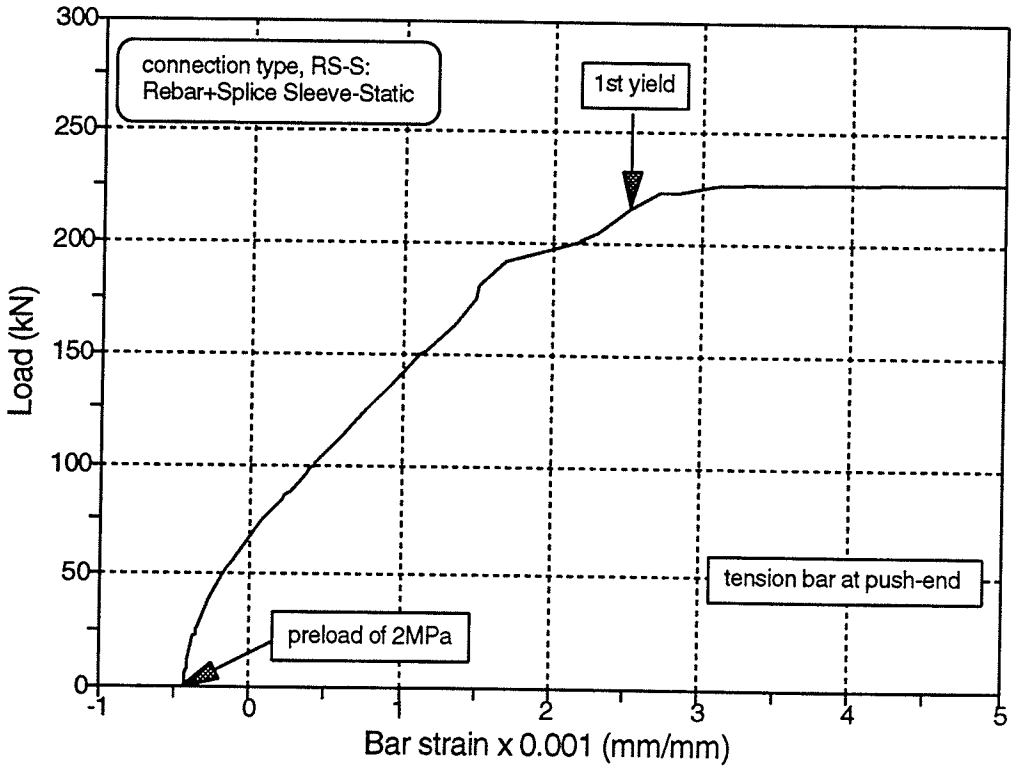

Figure 5.6 First yield response per load vs. tension bar strain for specimen RS-S

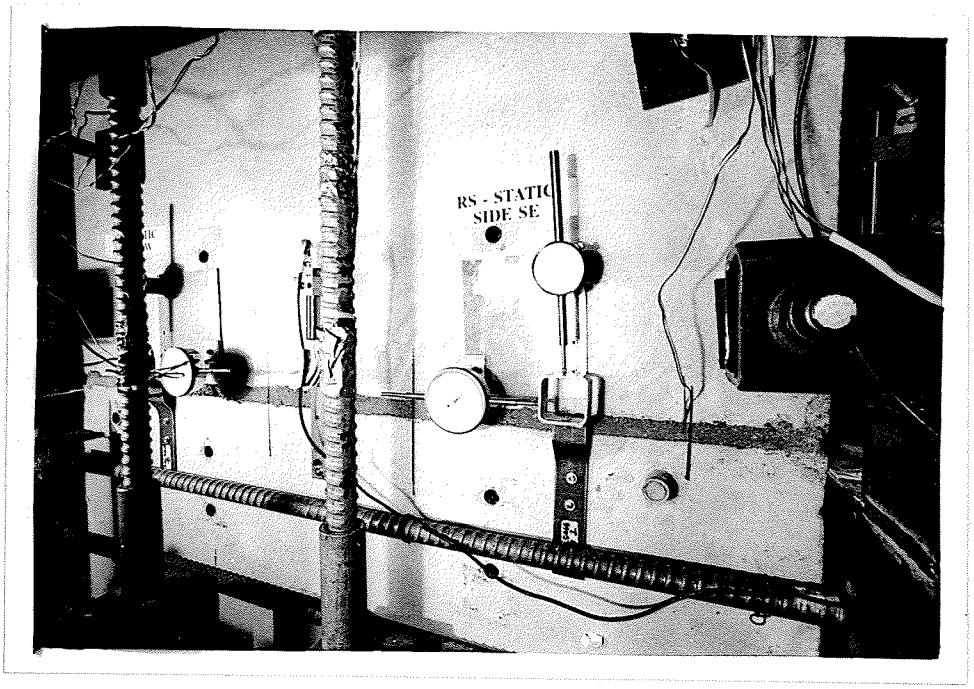

Figure 5.7(a) Condition of connection for specimen RS-S: at start

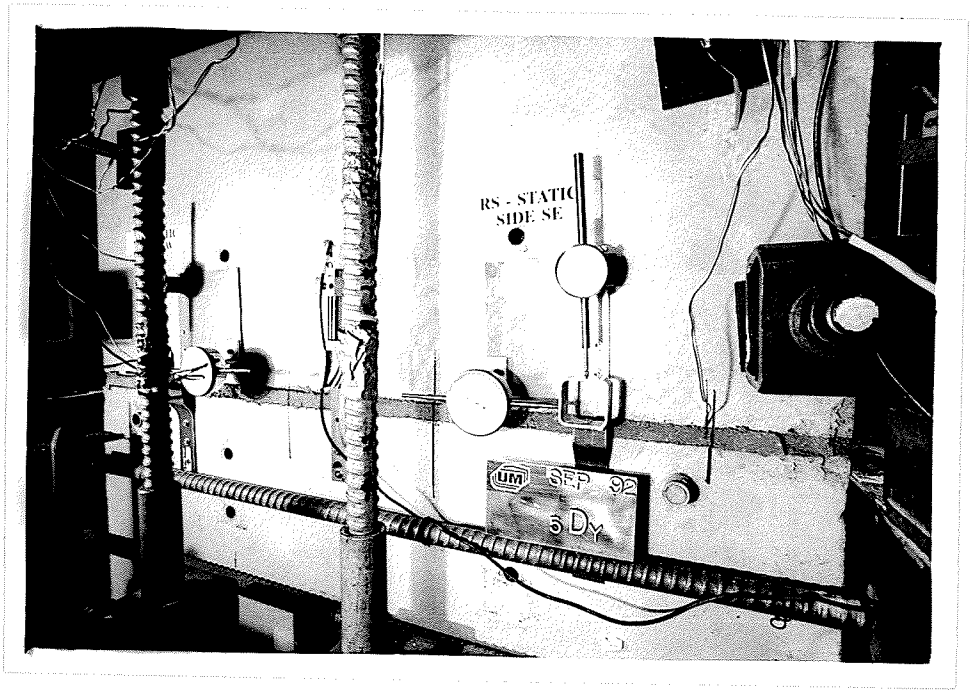

Figure 5.7(b) Condition of connection for specimen RS-S: at 5Dy

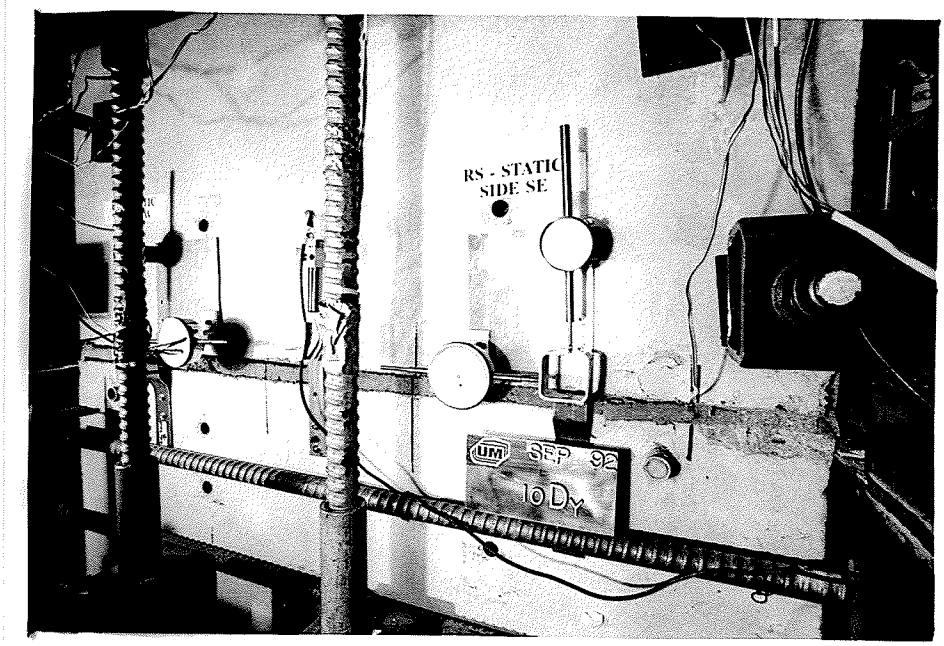

Figure 5.7(c) Condition of connection for specimen RS-S: at 10Dy (failure)

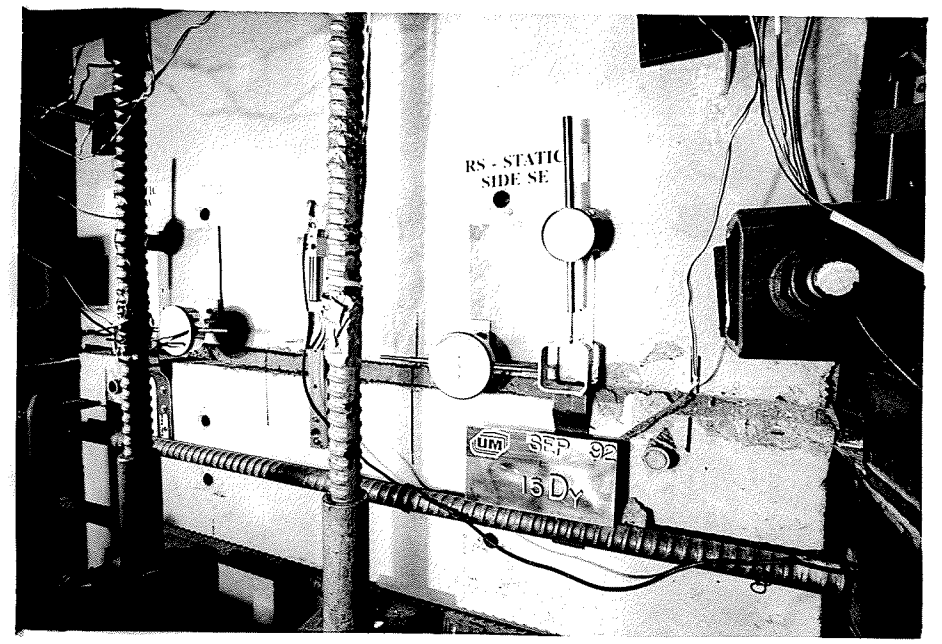

Figure 5.7(d) Condition of connection for specimen RS-S: at 15Dy (post-failure)

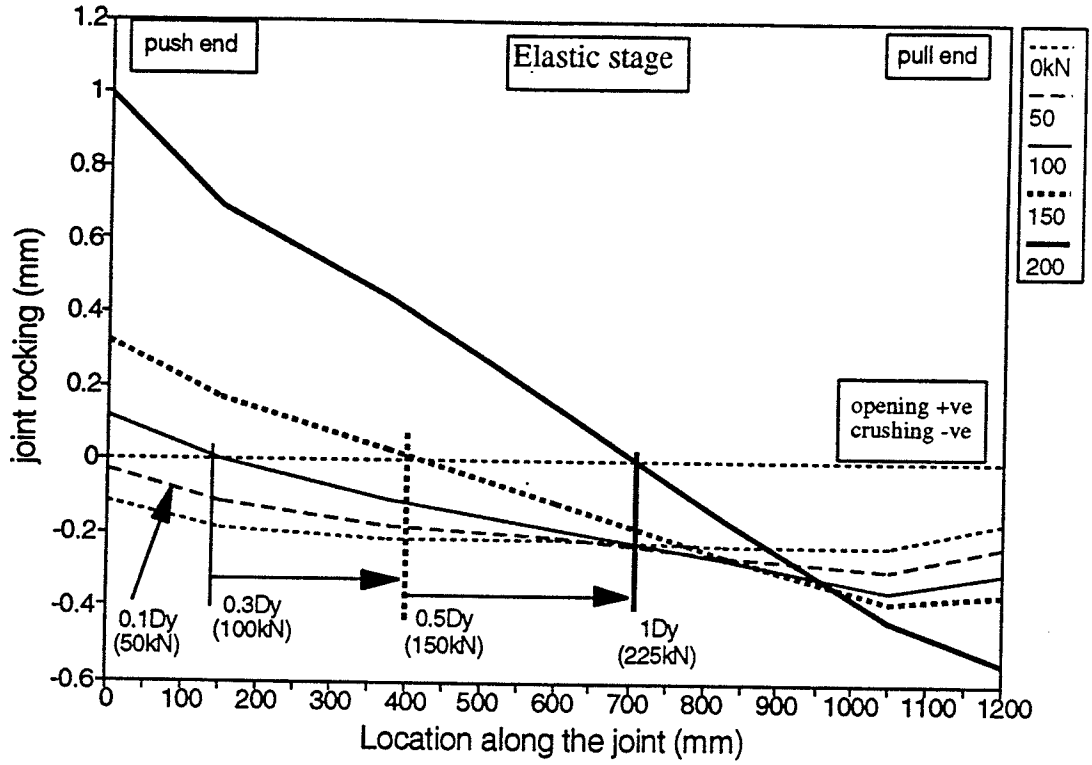

Figure 5.8(a) Rocking behaviour for specimen RS-S: elastic stage

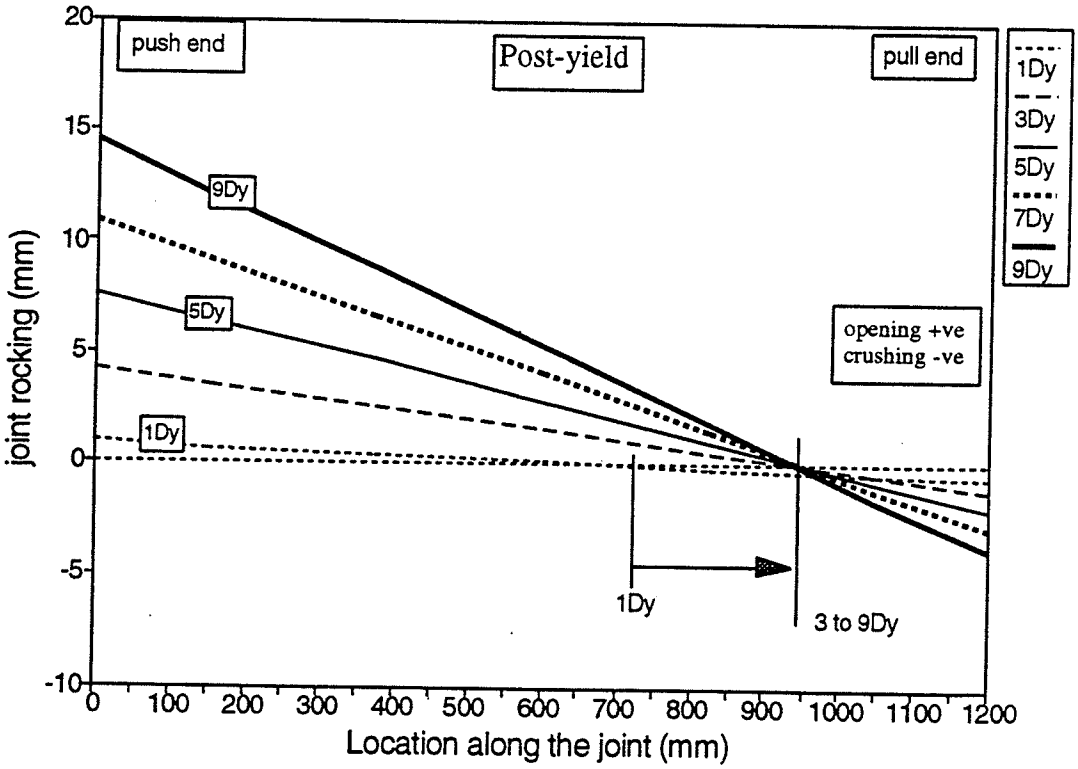

Figure 5.8(b) Rocking behaviour for specimen RS-S: post-yield stage

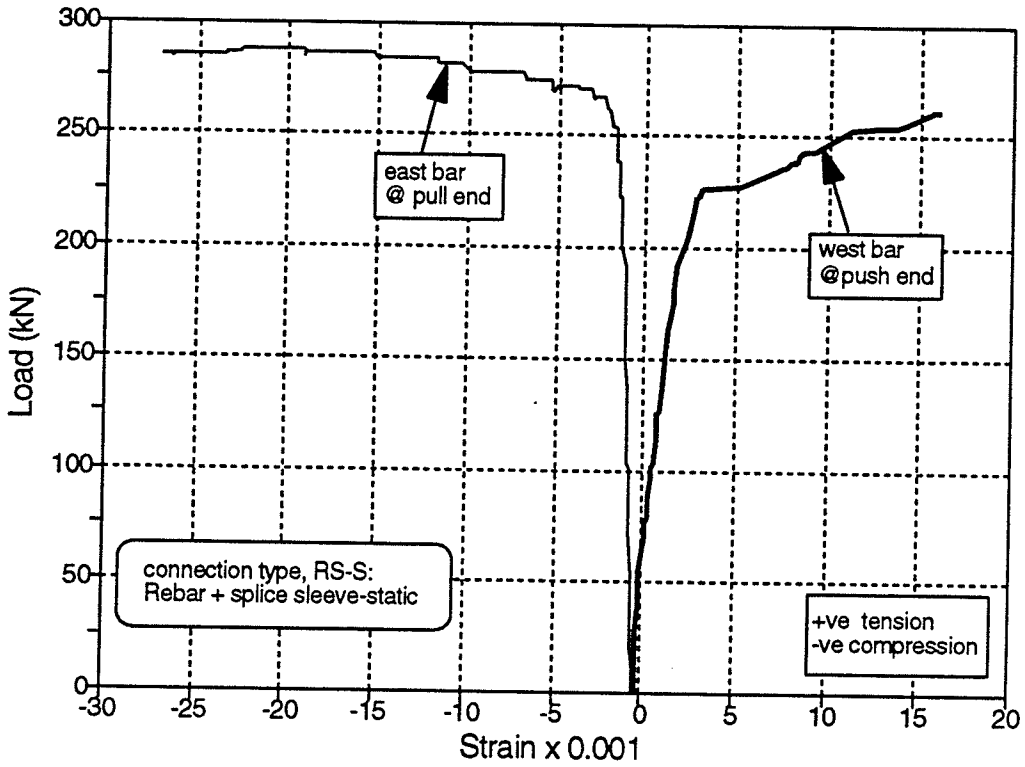

Figure 5.9 Load versus strain relationship for specimen RS-S: west and east bar

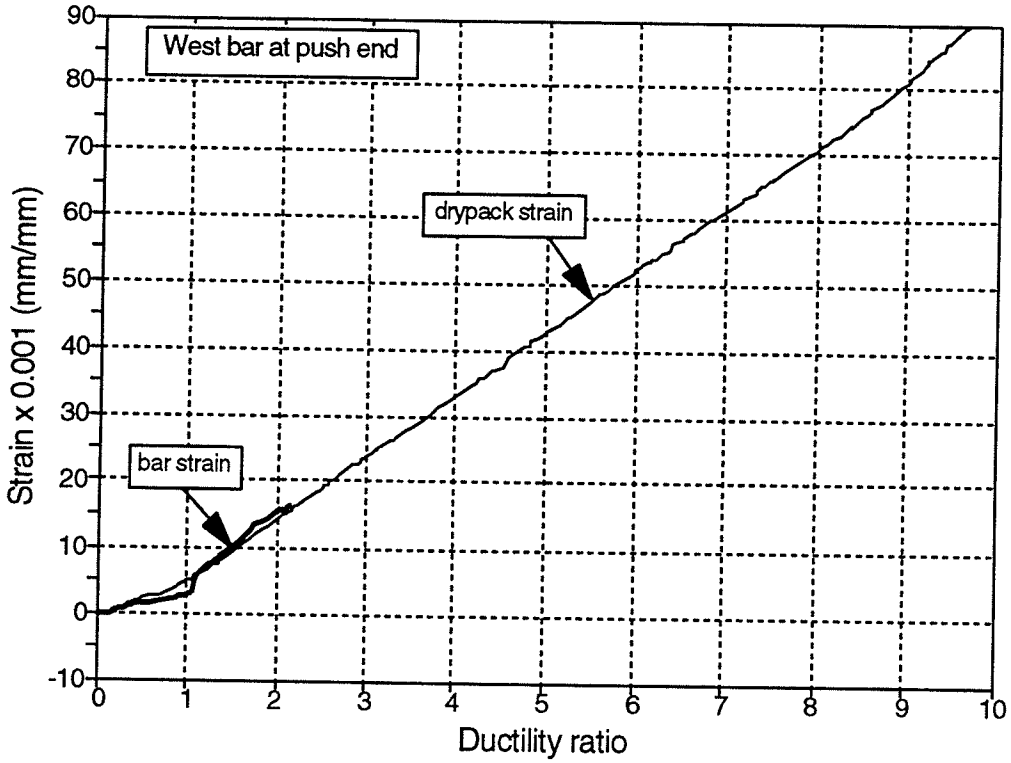

Figure 5.10(a) Comparison of bar and drypack strain at push end for specimen RS-S

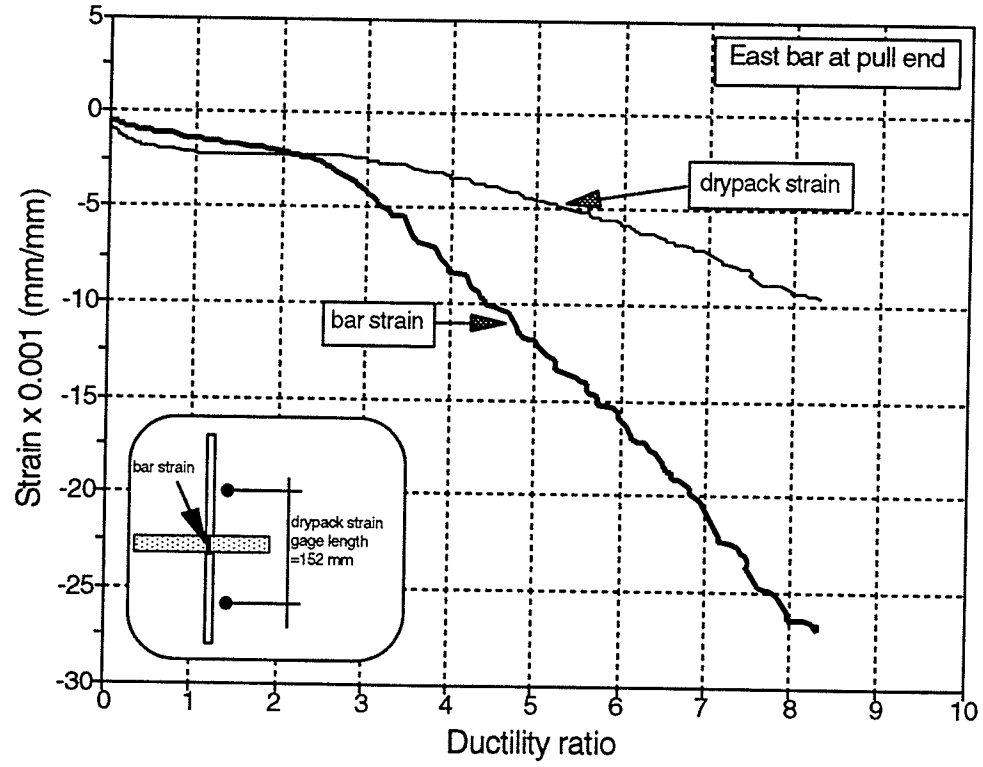

Figure 5.10(b) Comparison of bar and drypack strain at pull end for specimen RS-S

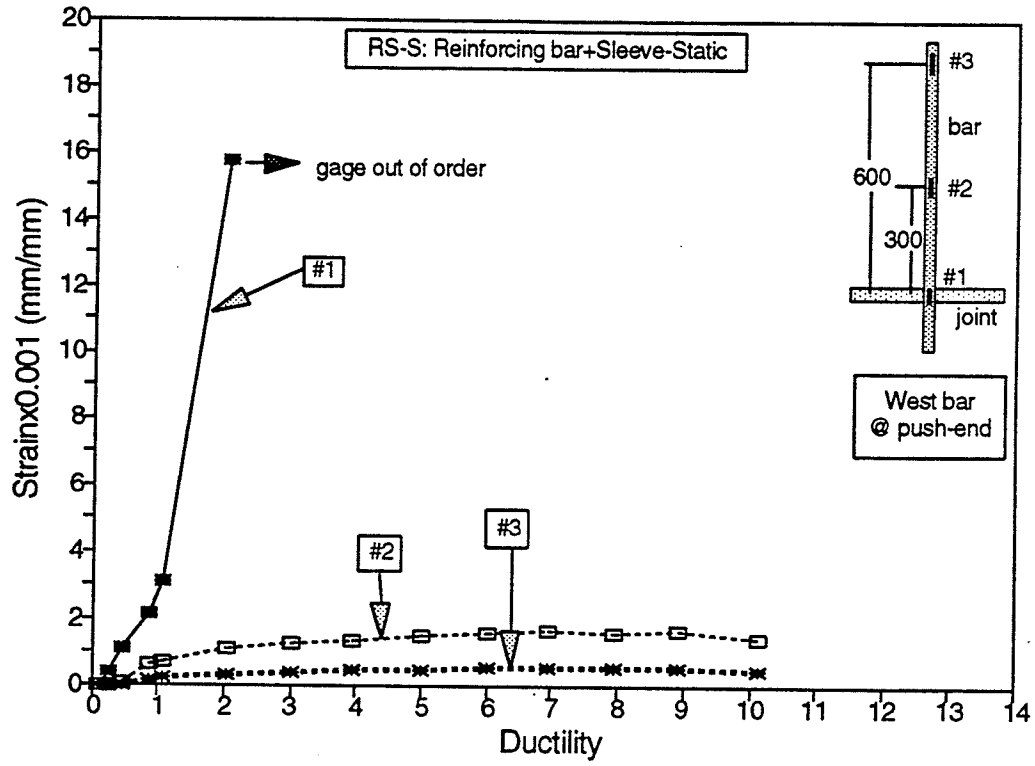

Figure 5.11(a) Tension bar strain at gages #1, #2 and #3 for specimen RS-S

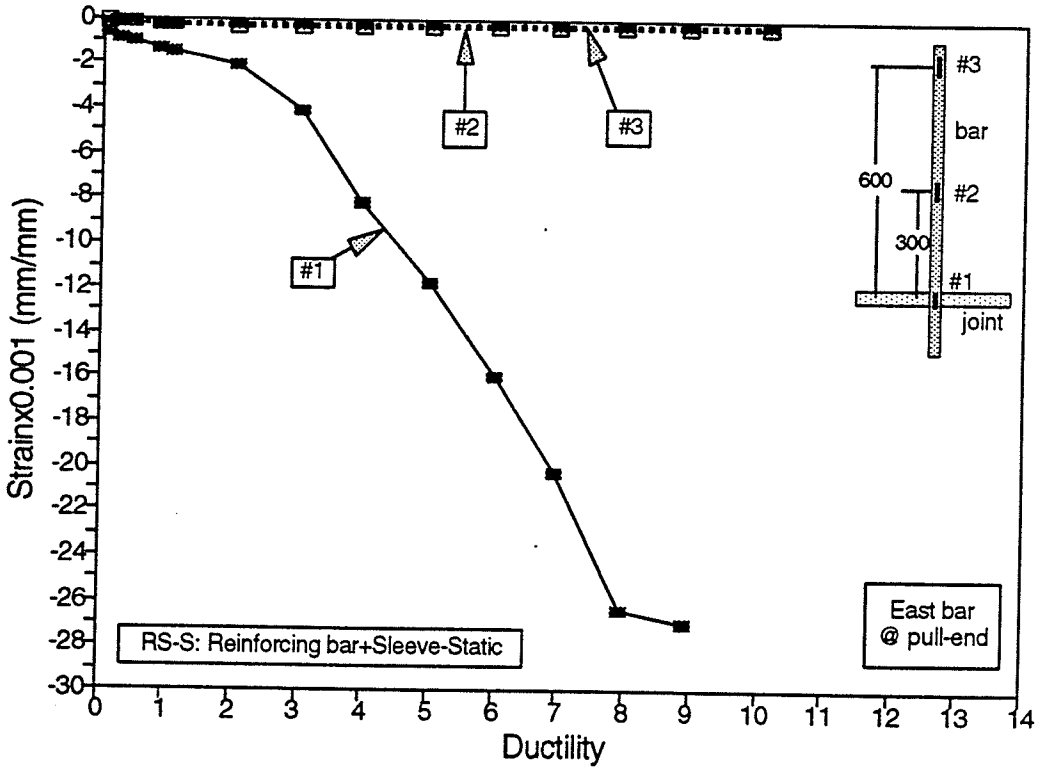

Figure 5.11(b) Compression bar strain at gages #1, #2 and #3 for specimen RS-S

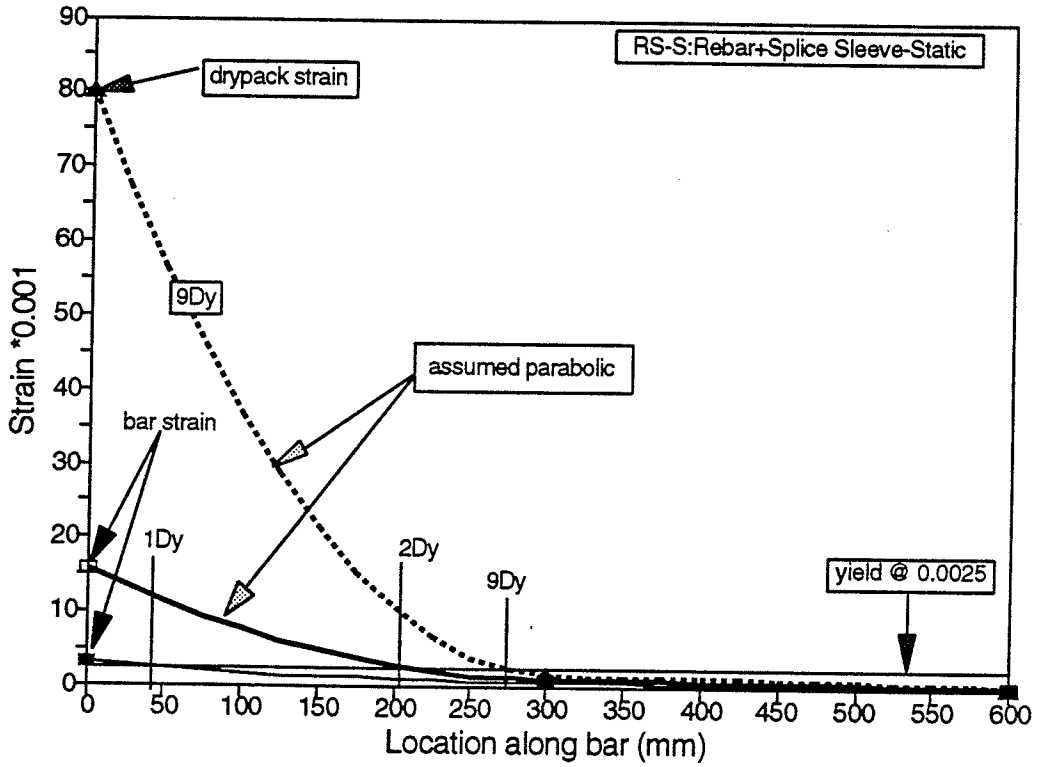

Figure 5.12 Extent of tension bar yielding at different ductility levels for specimen RS-S

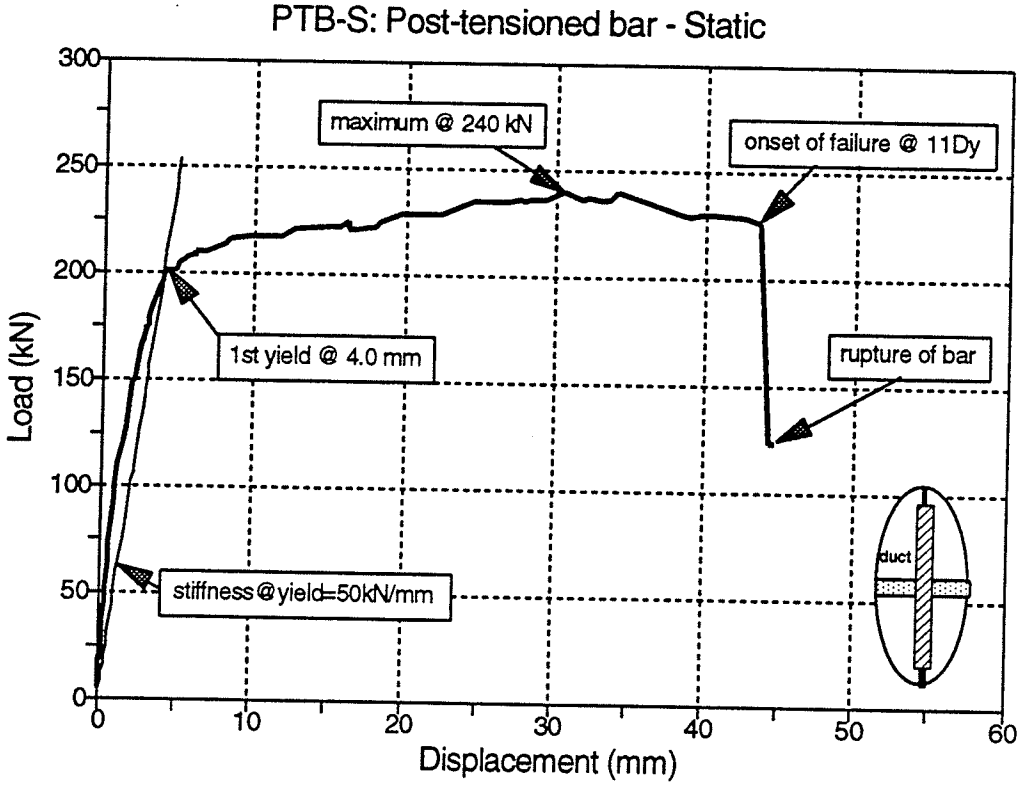

Figure 5.13 Load versus displacement relationship for specimen PTB-S

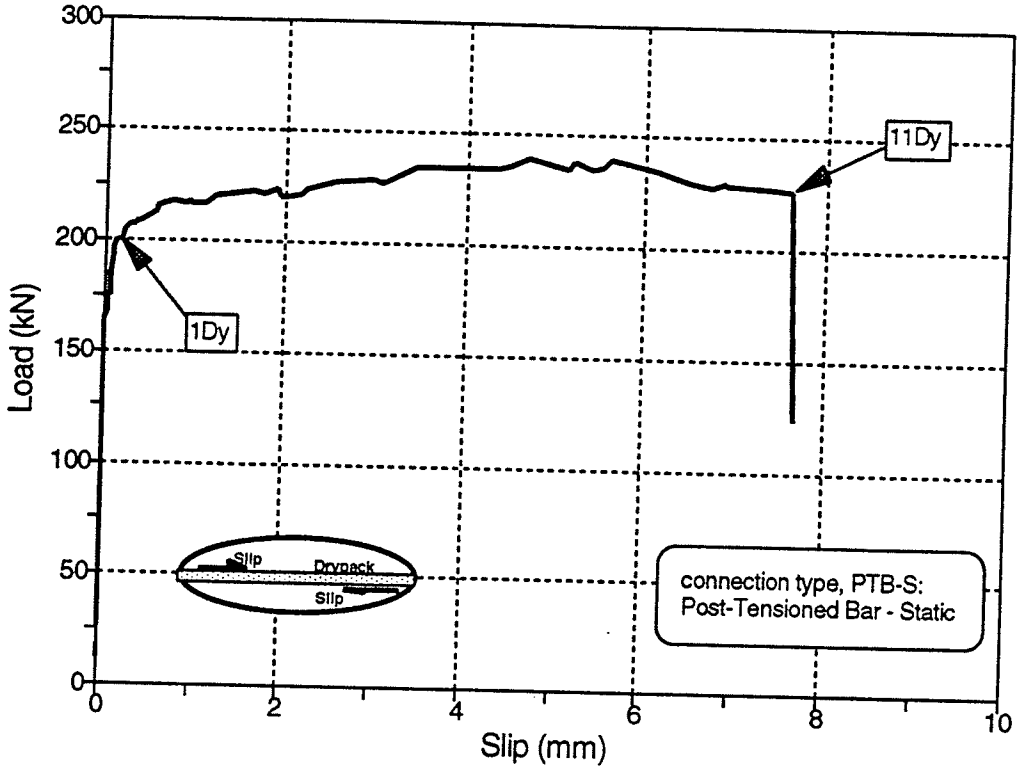

Figure 5.14 Load versus horizontal slip behaviour for specimen PTB-S

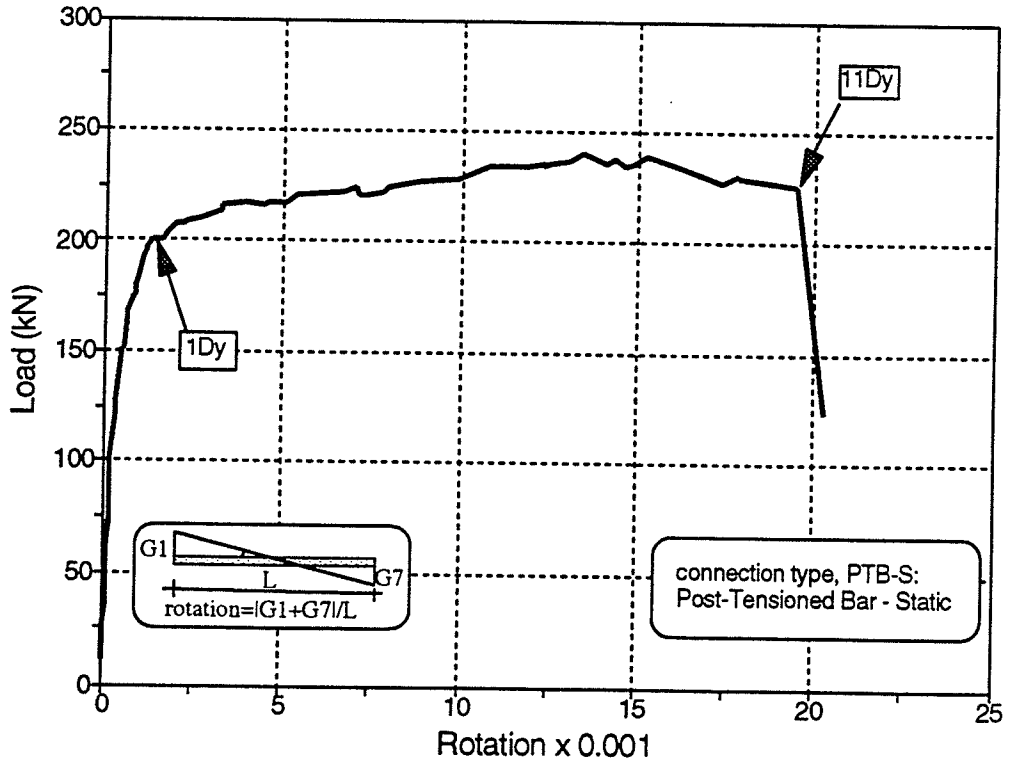

Figure 5.15 Load versus rotation relationship for specimen PTB-S

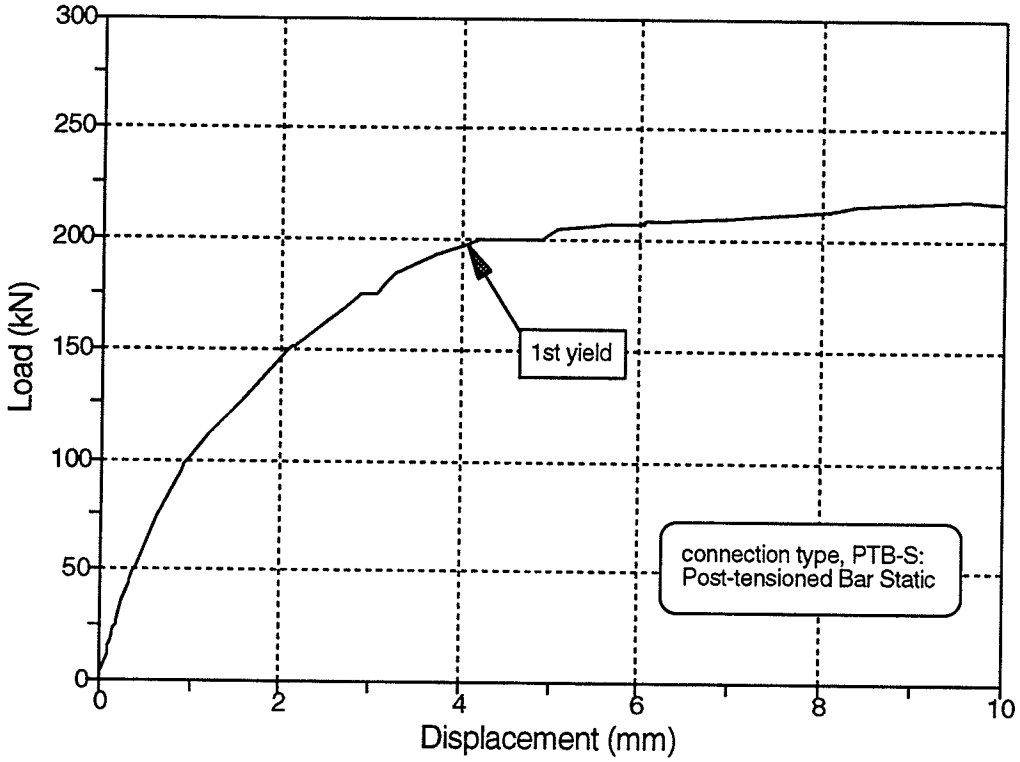

Figure 5.16 First yield response per load-displacement relationship for specimen PTB-S

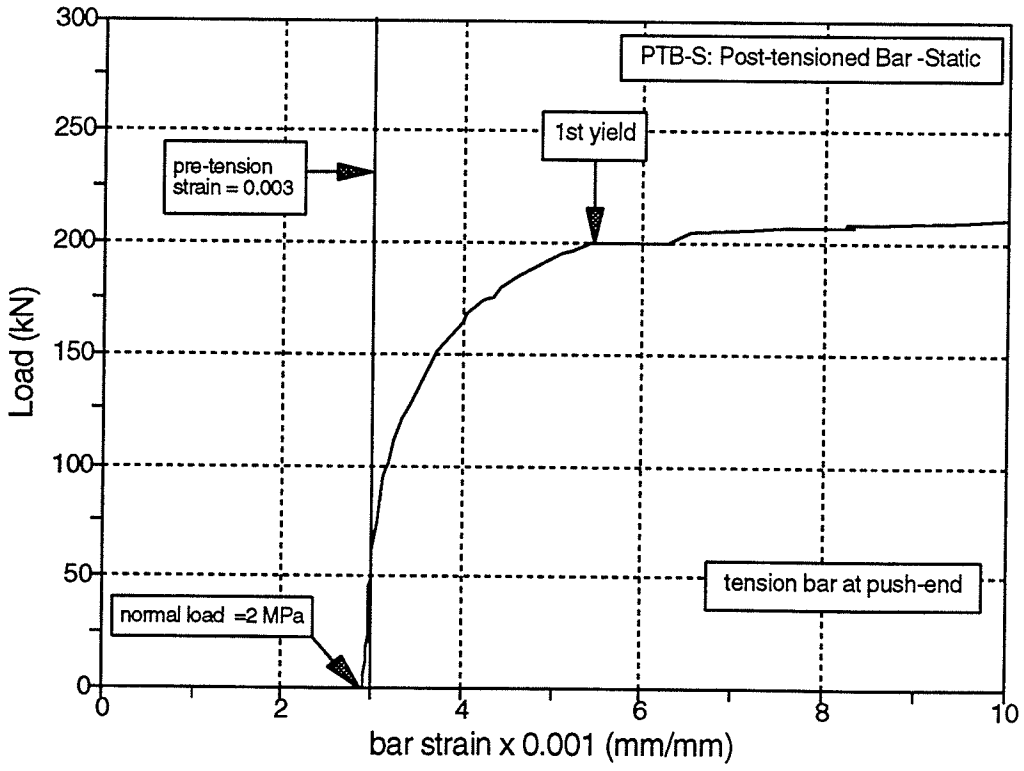

Figure 5.17 First yield response per load vs. tension bar strain for specimen PTB-S

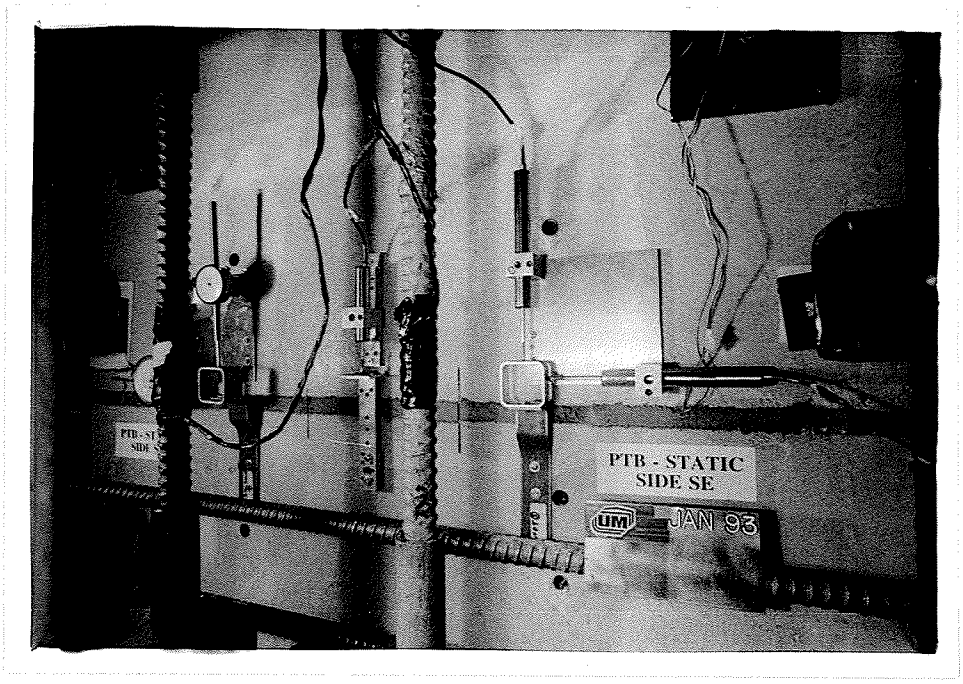

Figure 5.18(a) Condition of connection for specimen PTB-S: at start

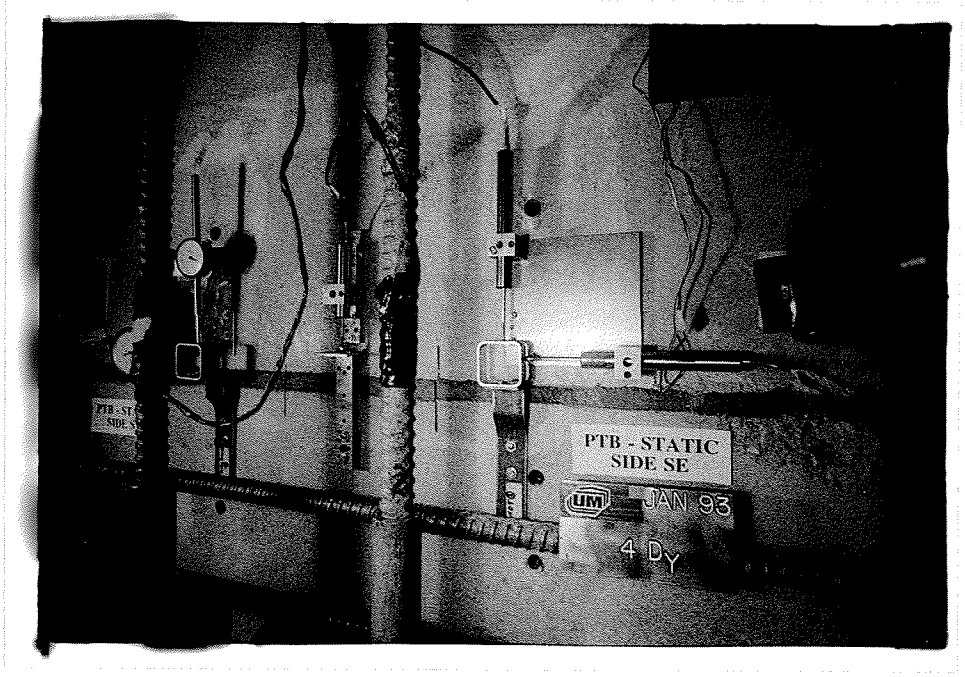

Figure 5.18(b) Condition of connection for specimen PTB-S: at 4Dy

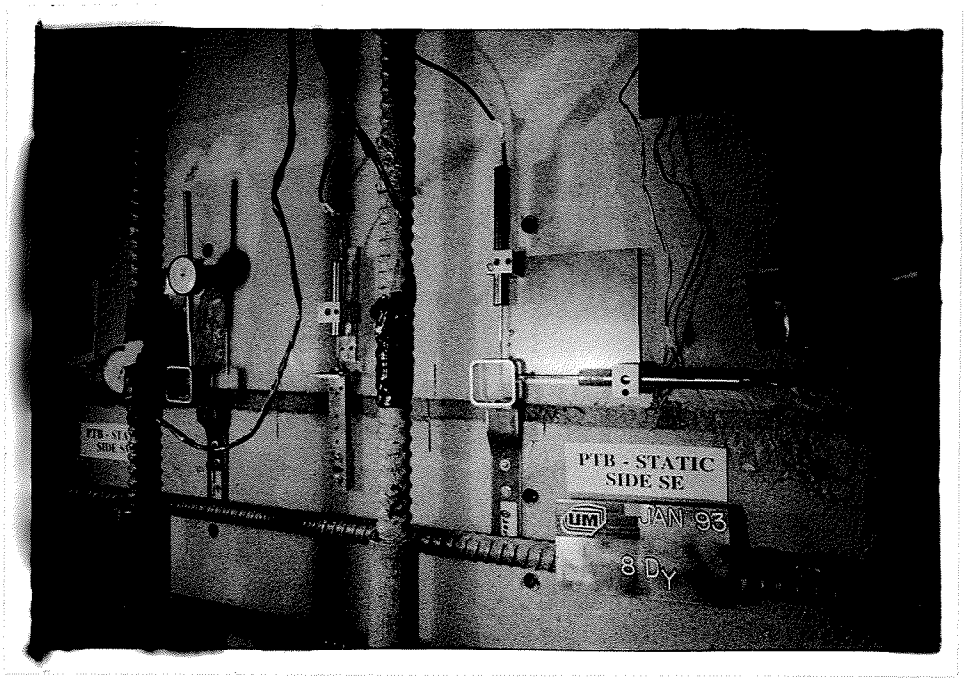

Figure 5.18(c) Condition of connection for specimen PTB-S: at 8Dy

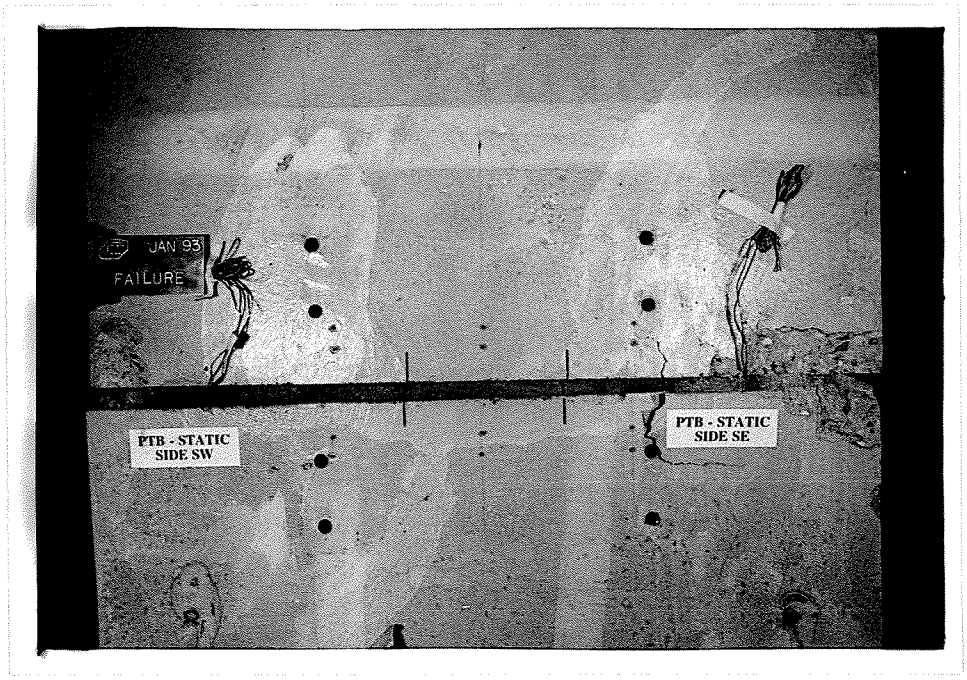

Figure 5.18(d) Condition of connection for specimen PTB-S: at 11Dy (failure)

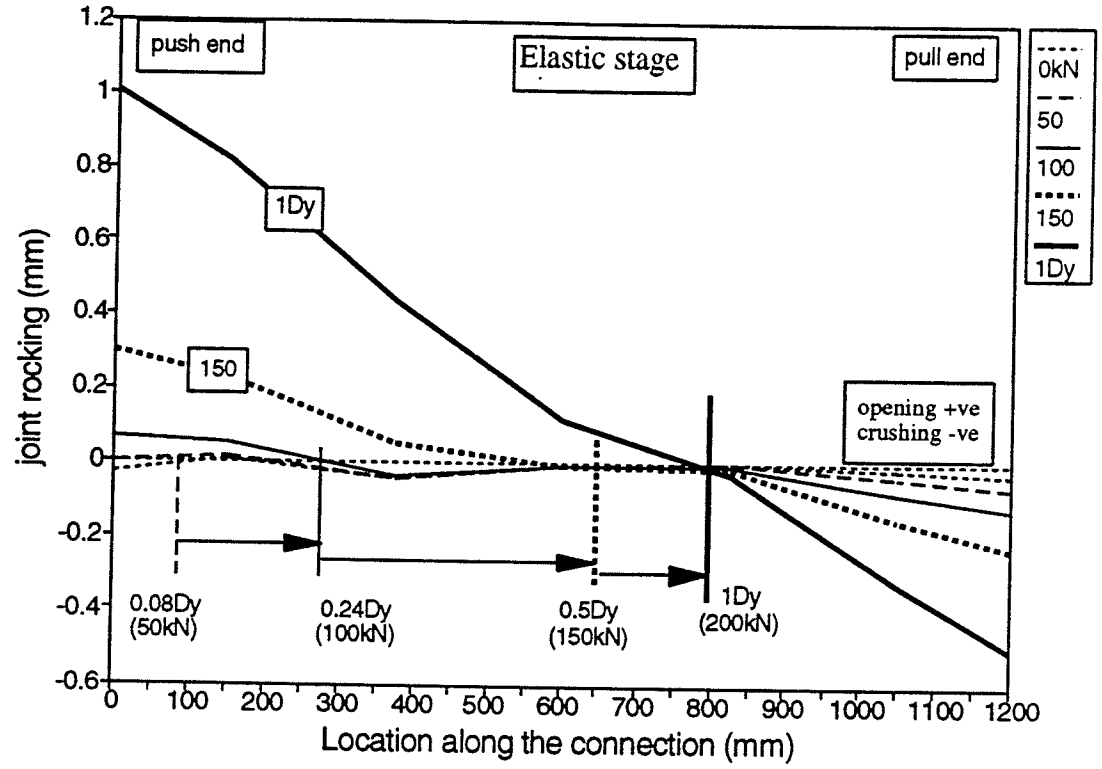

Figure 5.19(a) Rocking behaviour for specimen PTB-S: elastic stage

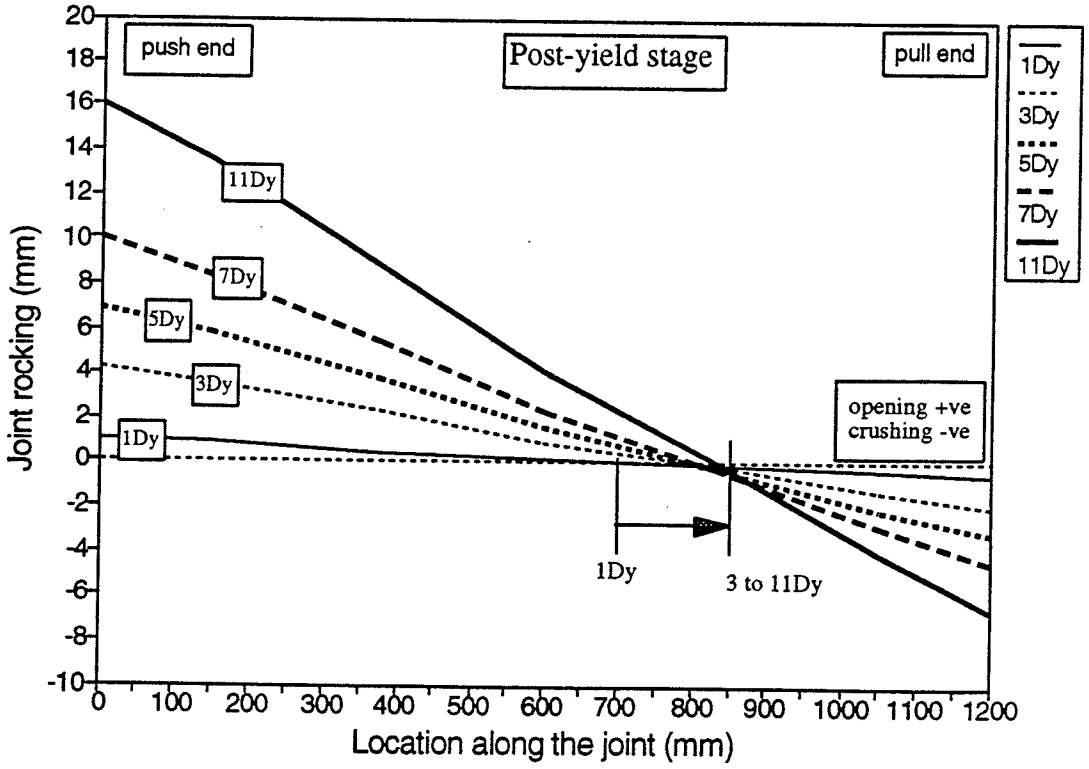

Figure 5.19(b) Rocking behaviour for specimen PTB-S: post-yield stage

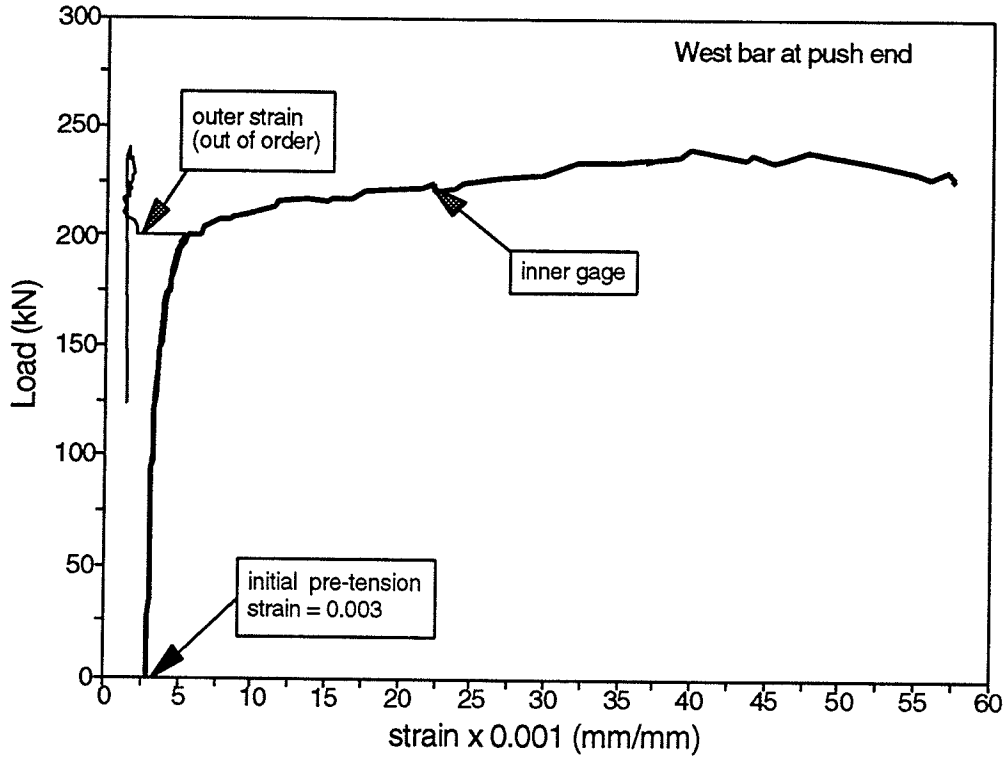

Figure 5.20(a) Load vs. strain of west bar at the push end for specimen PTB-S

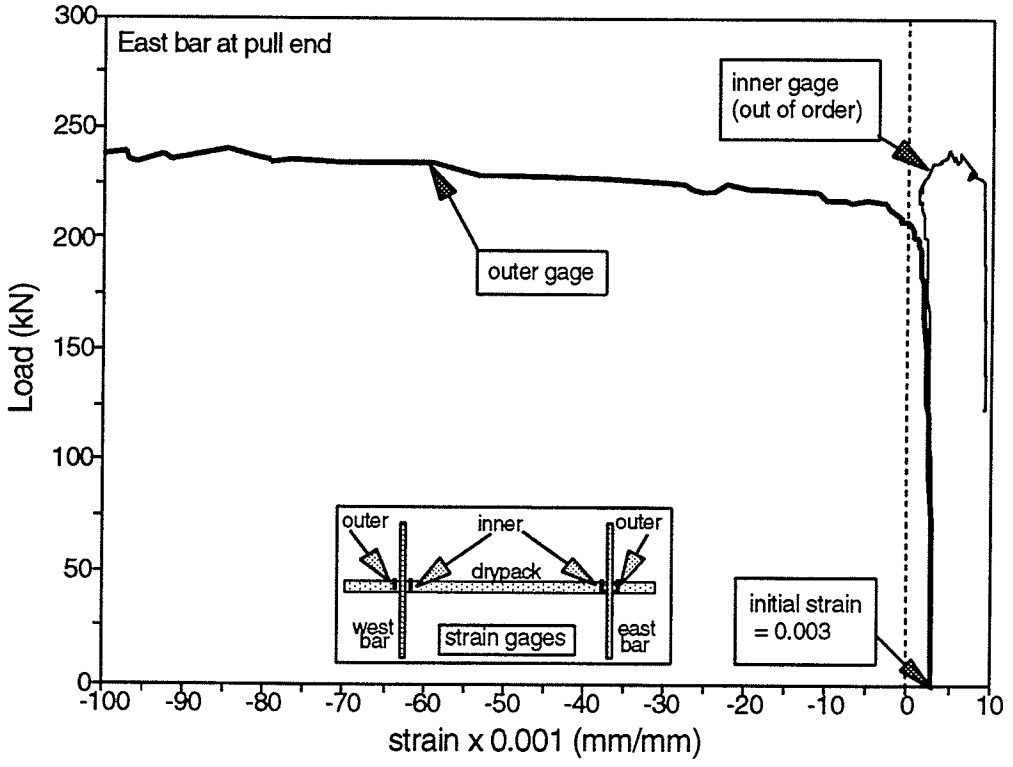

Figure 5.20(b) Load vs. strain of east bar at the pull end for specimen PTB-S

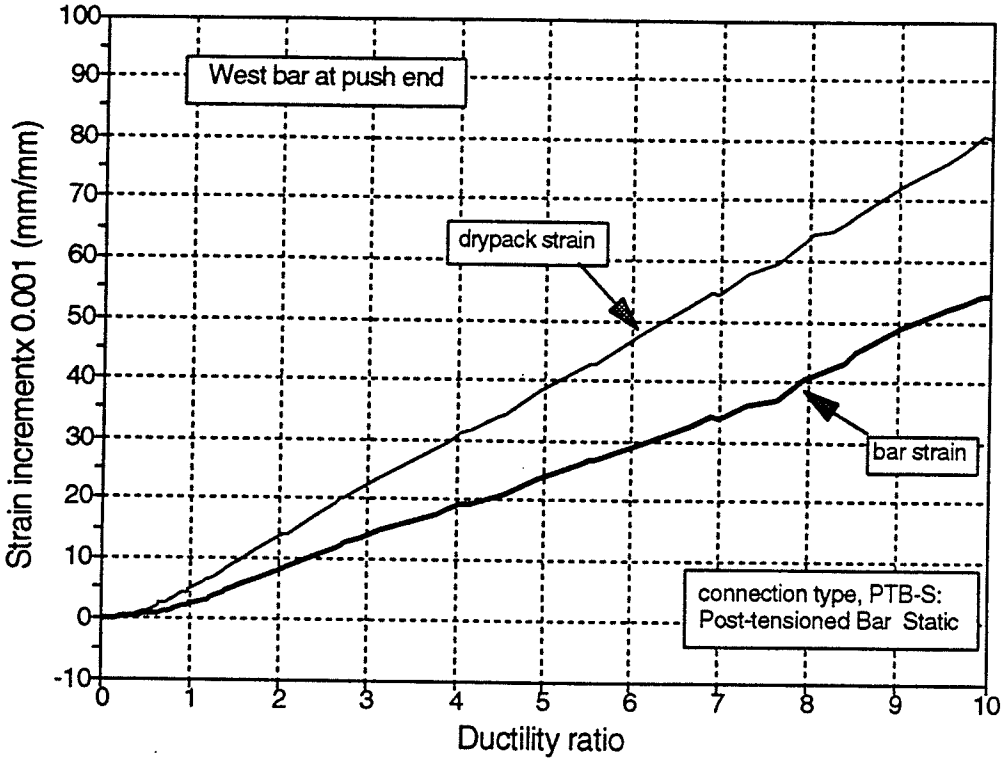

Figure 5.21(a) Comparison of bar and drypack strain at the push-end for specimen PTB-S

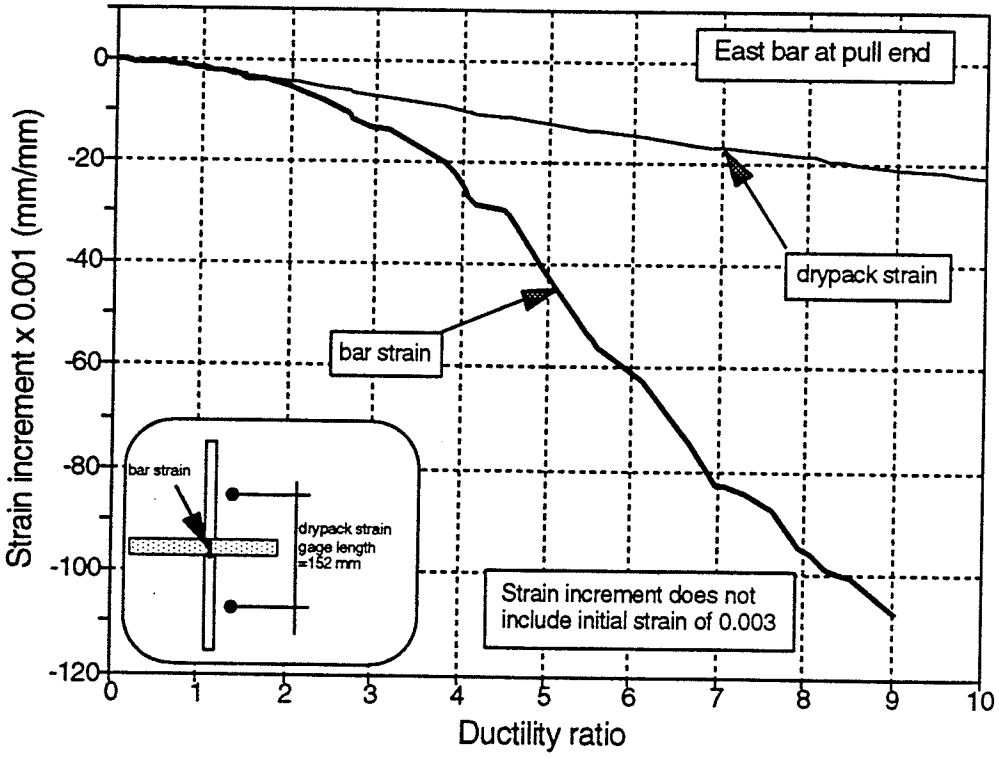

Figure 5.21(b) Comparison of bar and drypack strain at the pull end for specimen PTB-S

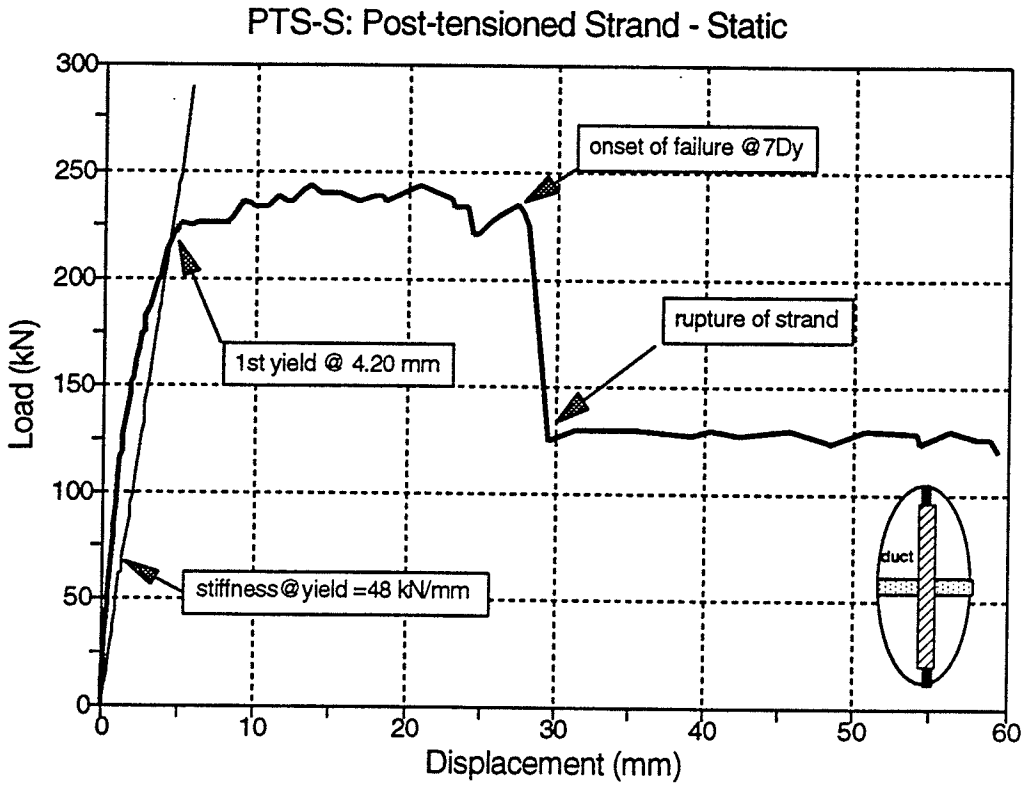

Figure 5.22 Load versus displacement relationship for specimen PTS-S

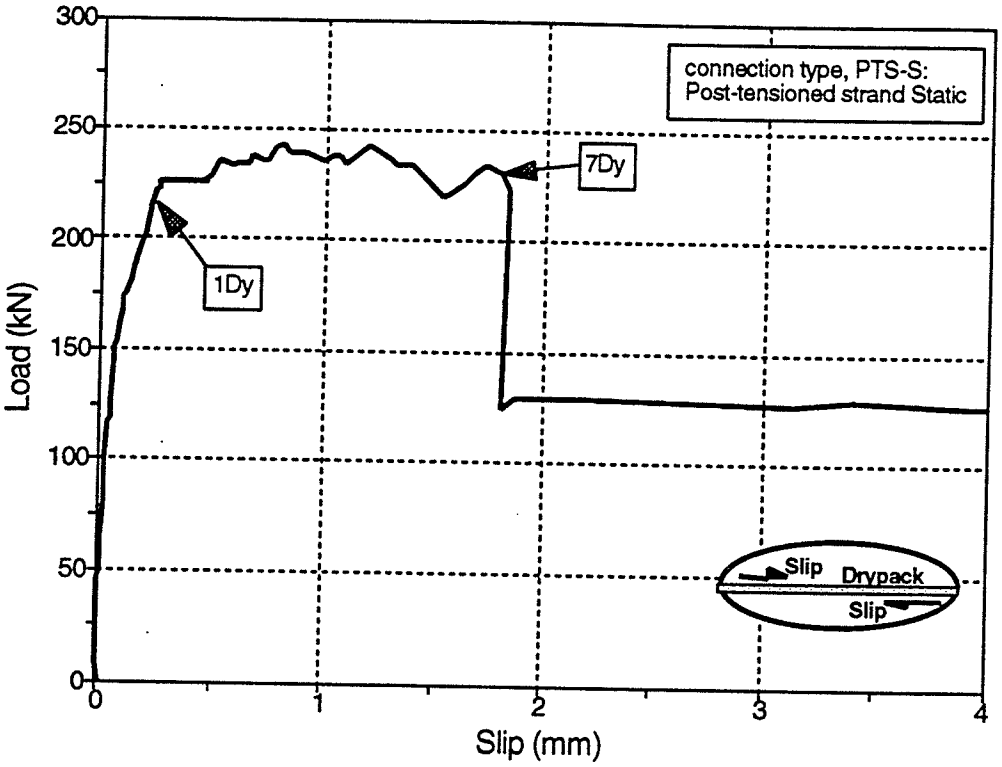

Figure 5.23 Load versus horizontal slip behaviour for specimen PTS-S

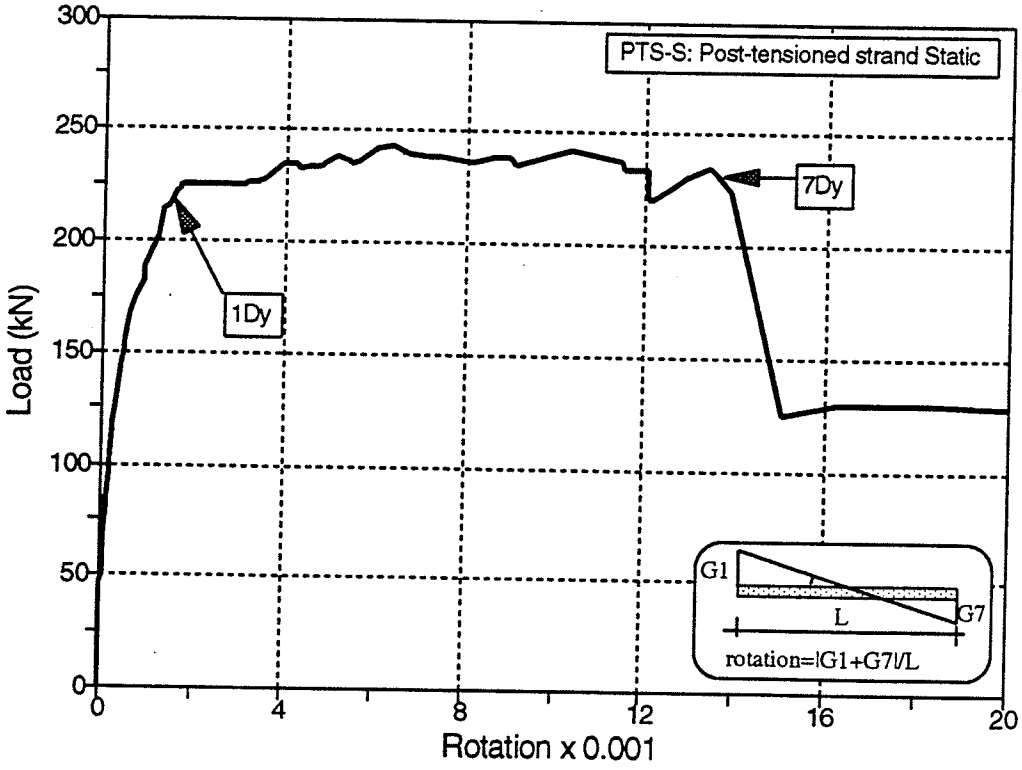

Figure 5.24 Load versus rotation relationship for specimen PTS-S

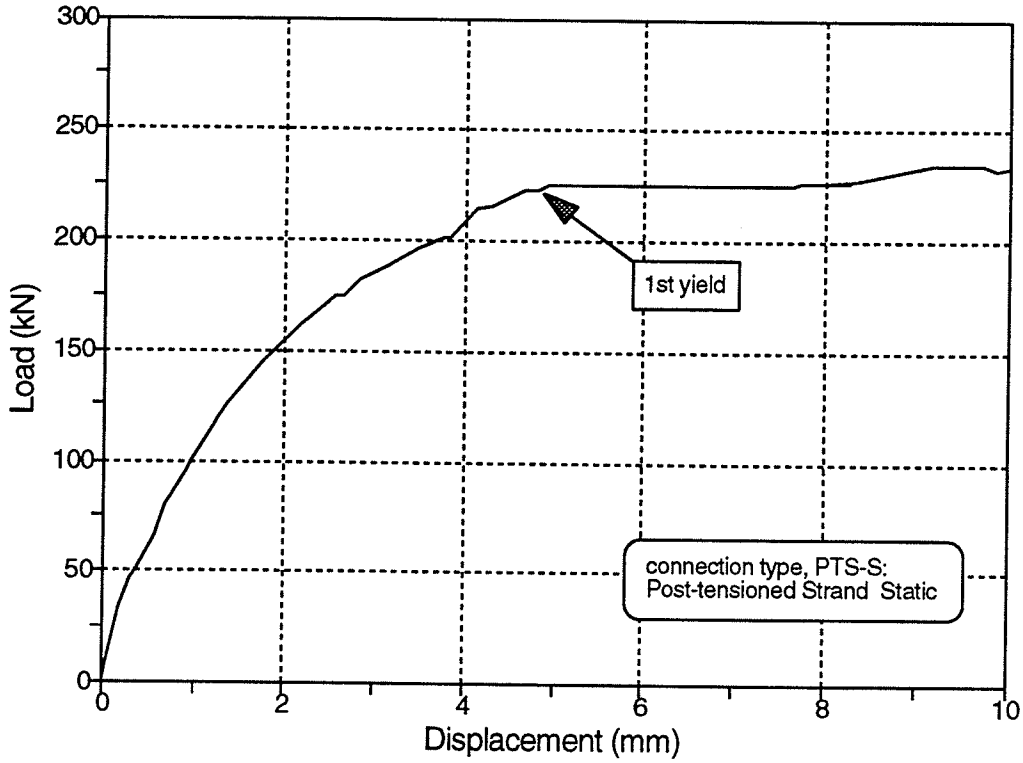

Figure 5.25 First yield response per load-displacement relationship for specimen PTS-S

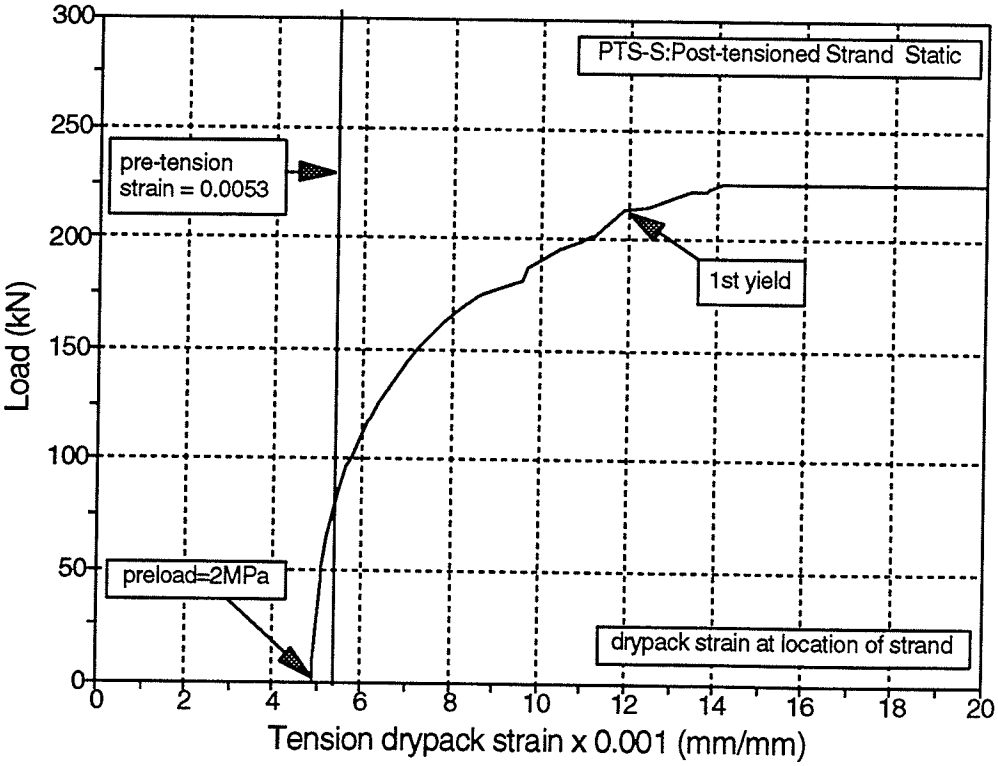

Figure 5.26 First yield response per load vs. tension drypack strain for specimen PTS-S

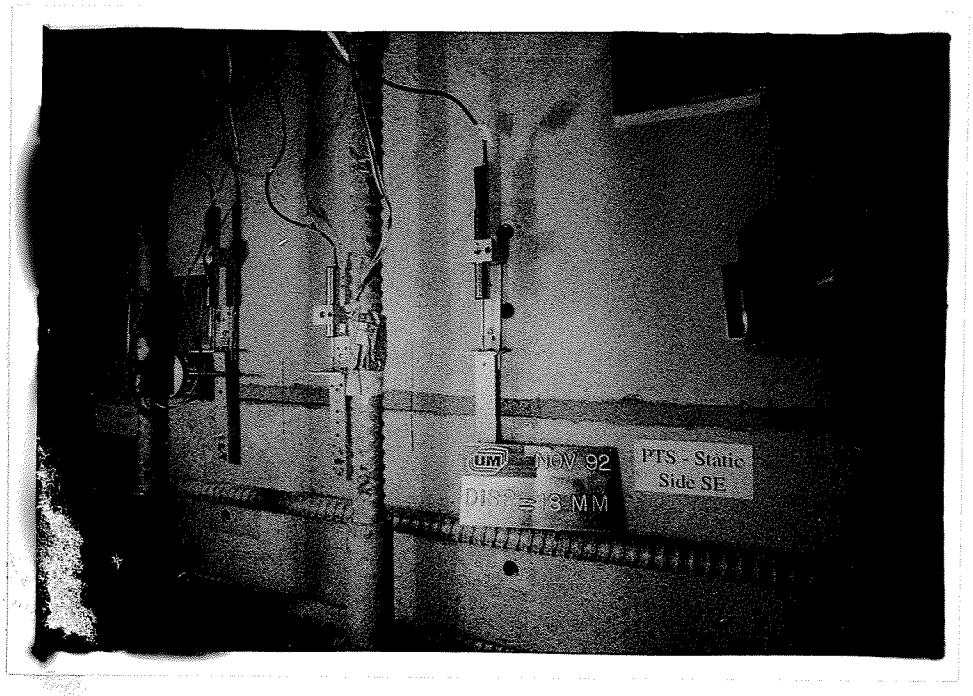

Figure 5.27(a) Condition of connection - specimen PTS-S: at 4Dy (18 mm,no damage)

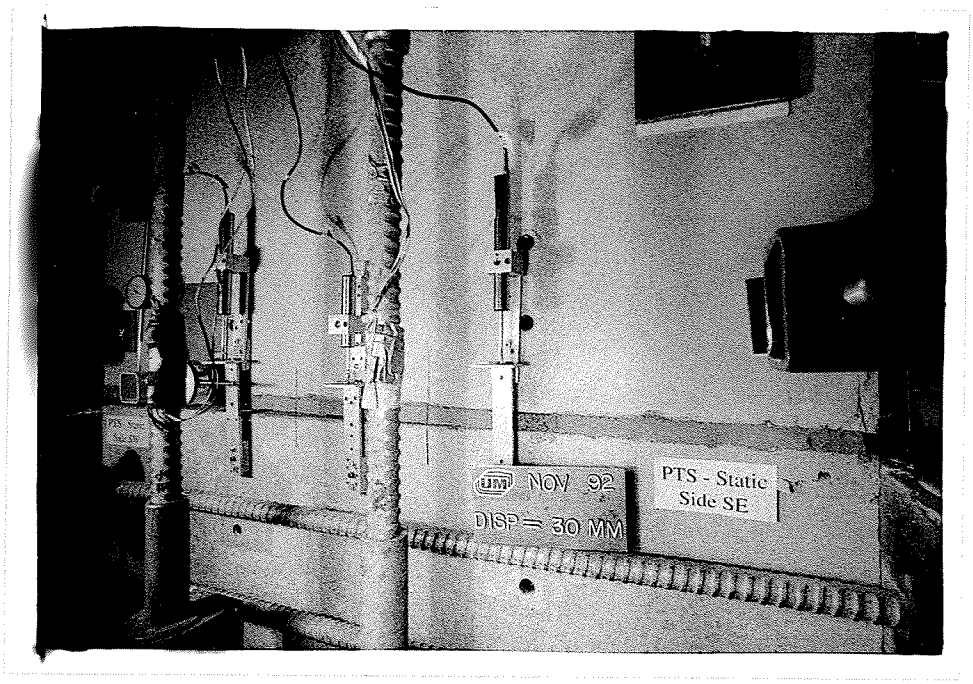

Figure 5.27(b) Condition of connection for specimen PTS-S: at 7.5Dy (30 mm, failure)

Figure 5.27(c) Condition of connection for specimen PTS-S: post-failure

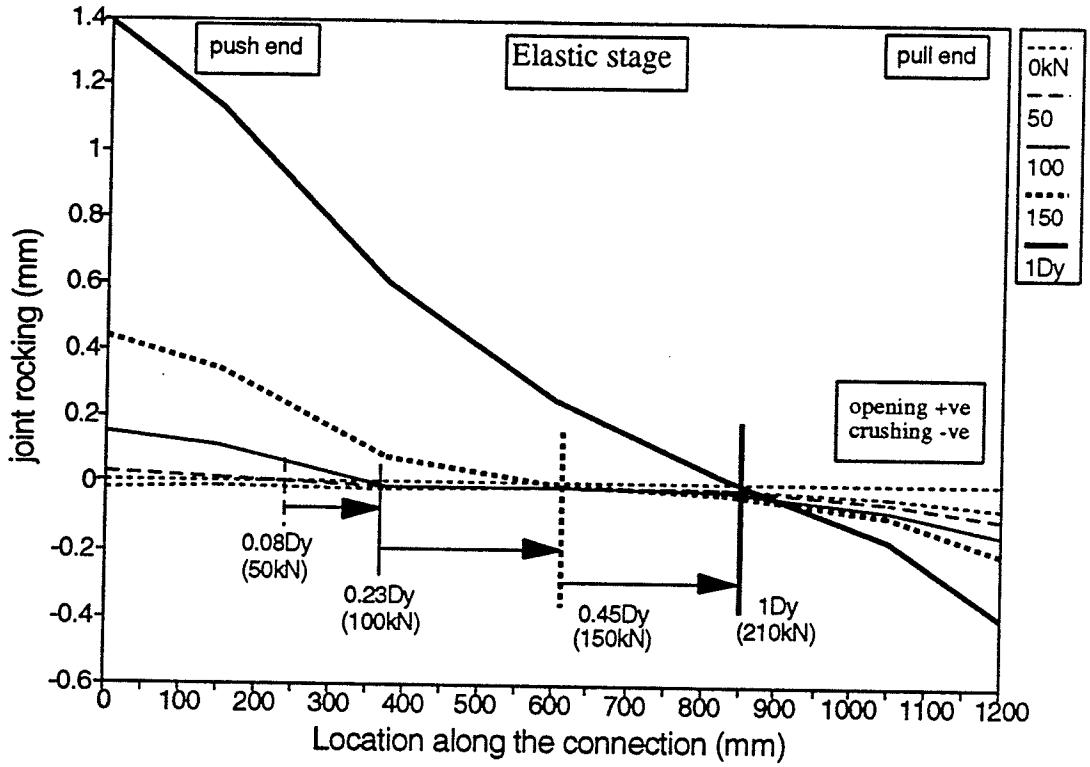

Figure 5.28(a) Rocking behaviour for specimen PTS-S: elastic stage

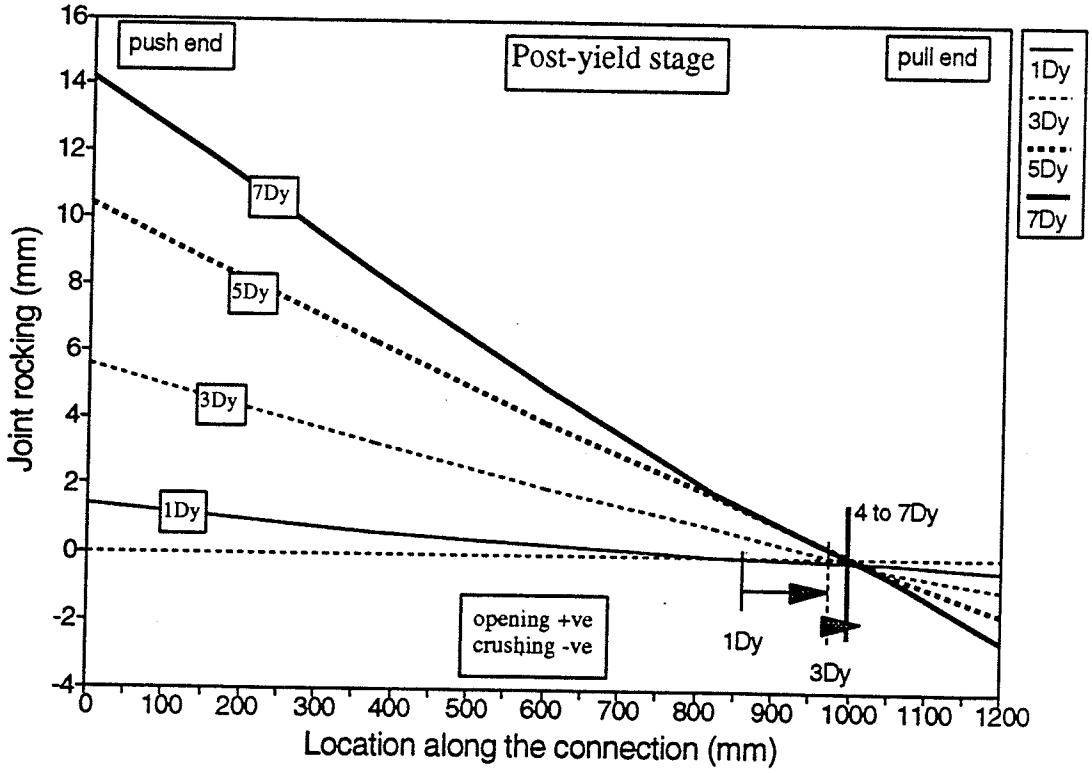

Figure 5.28(b) Rocking behaviour for specimen PTS-S: post-yield stage

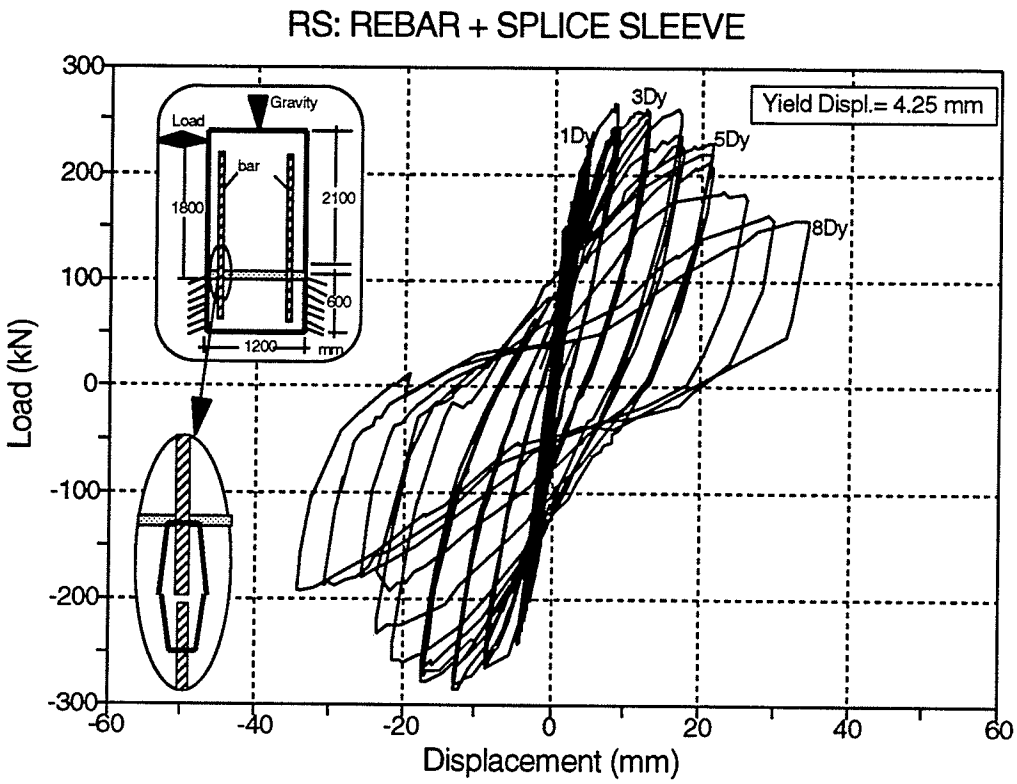

Figure 5.29(a) Hysteresis loops of load versus displacement behaviour for specimen RS

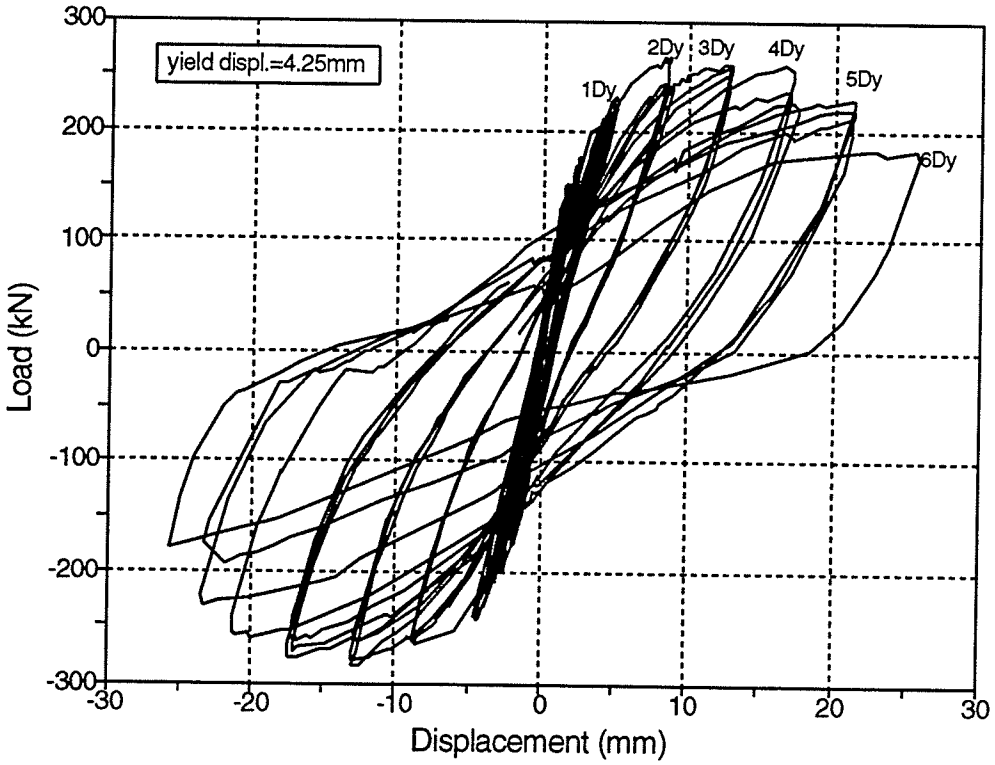

Figure 5.29(b) Magnified hysteresis loops of load vs. displacement for specimen RS

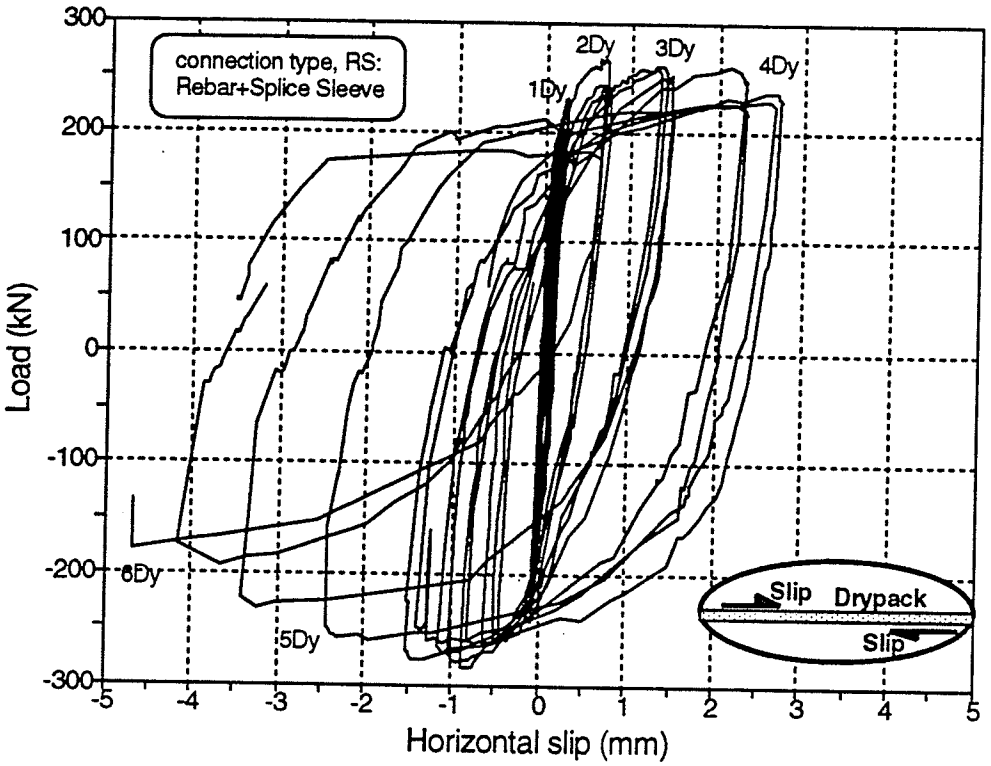

Figure 5.30 Hysteresis loops of load versus horizontal slip for specimen RS

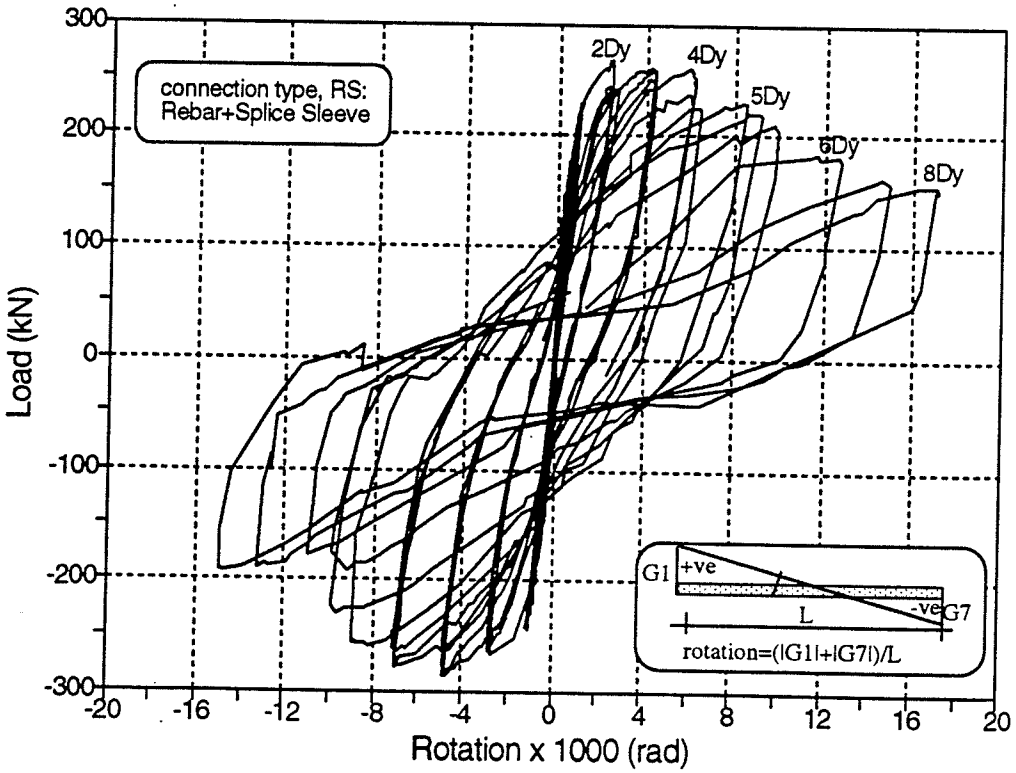

Figure 5.31 Hysteresis loops of load versus rotation for specimen RS

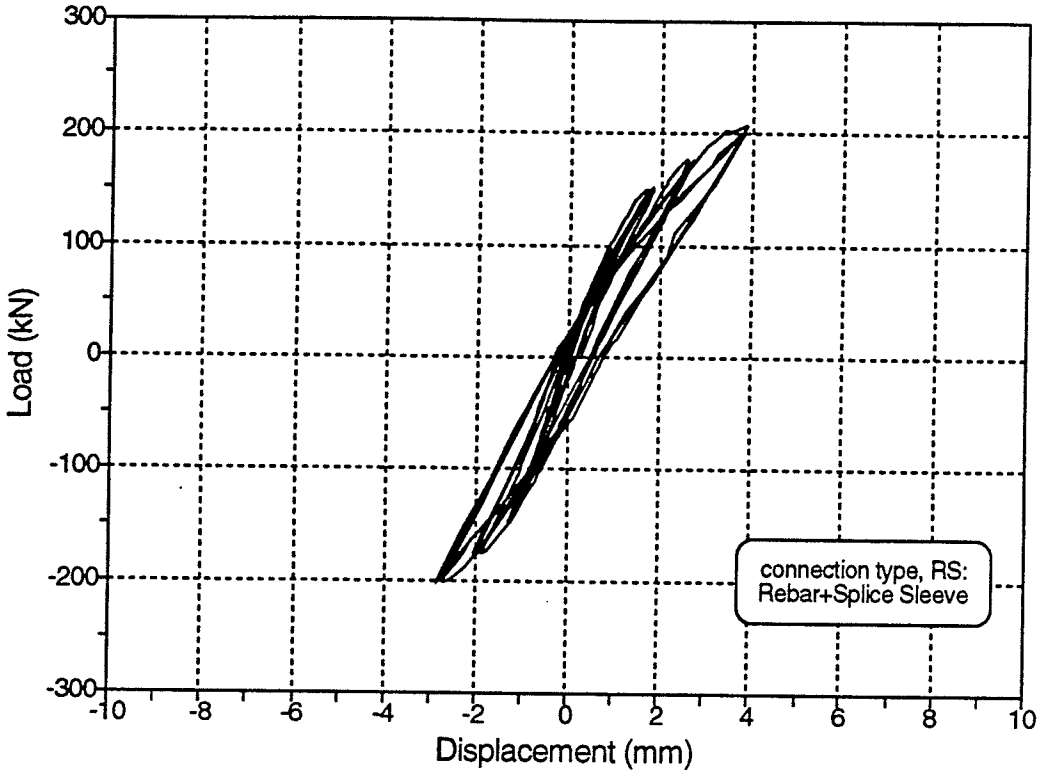

Figure 5.32 Elastic load-displacement behaviour for specimen RS

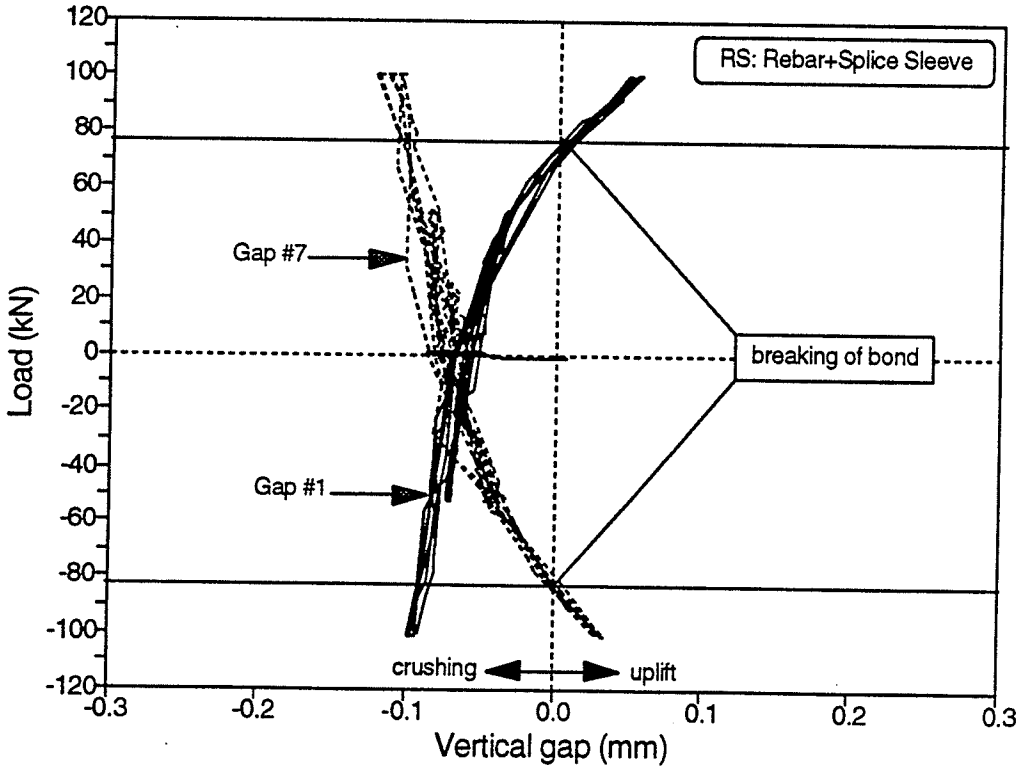

Figure 5.33 Onset of breaking of bond in load-gap relationship for specimen RS

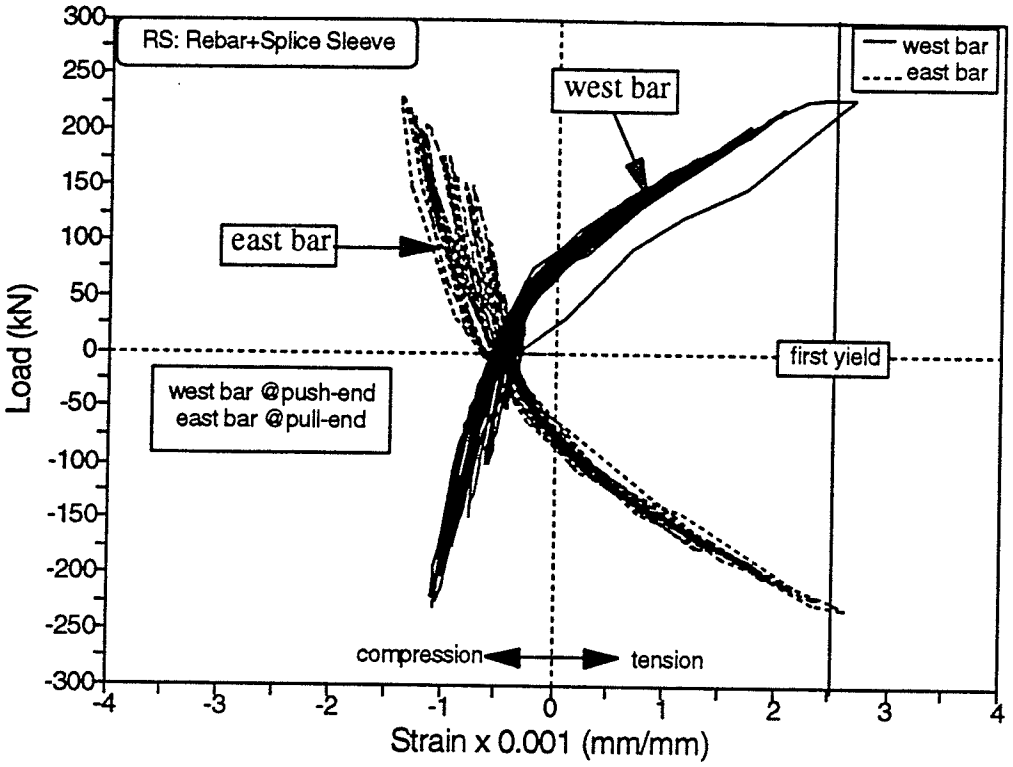

Figure 5.34 Onset of yield in load-bar strain relationship for specimen RS

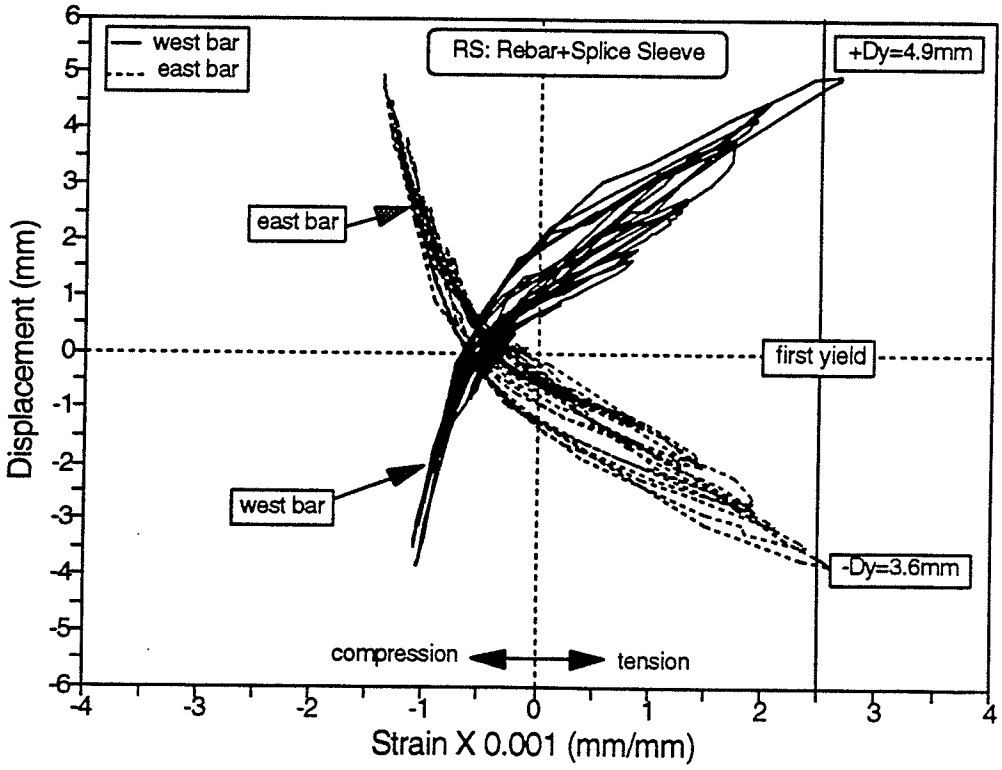

Figure 5.35 Onset of yield in bar strain-displacement relationship for specimen RS

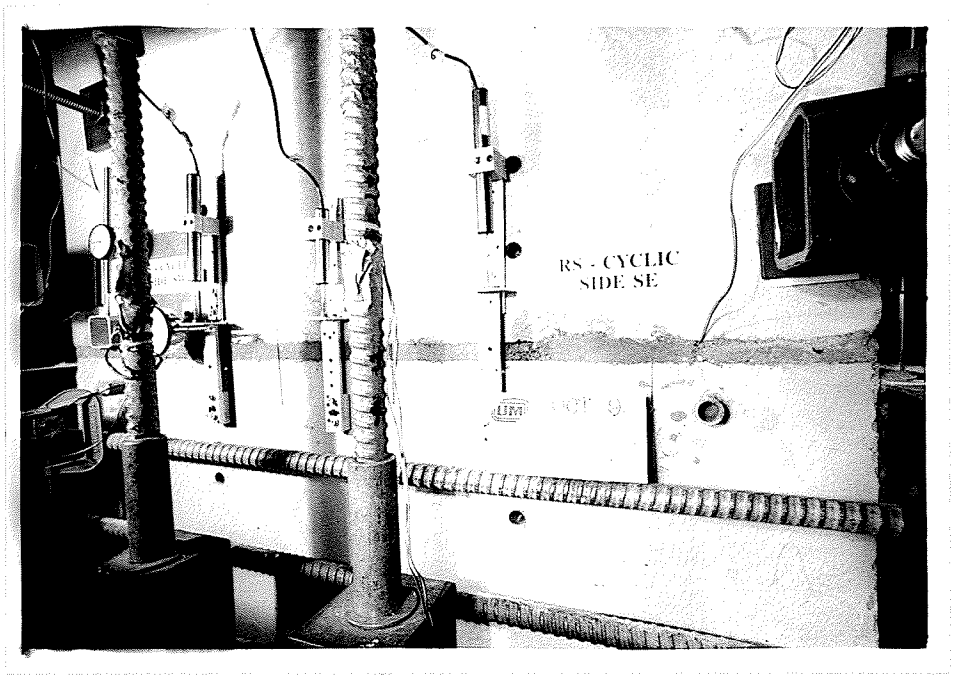

Figure 5.36(a) Condition of connection for specimen RS: at start

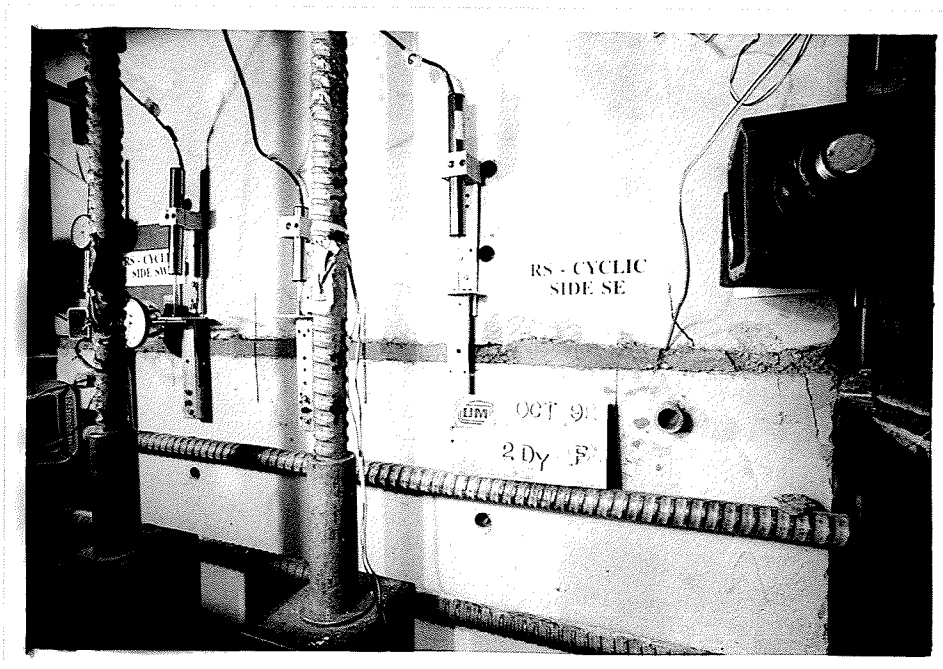

Figure 5.36(b) Condition of connection for specimen RS: at 2Dy

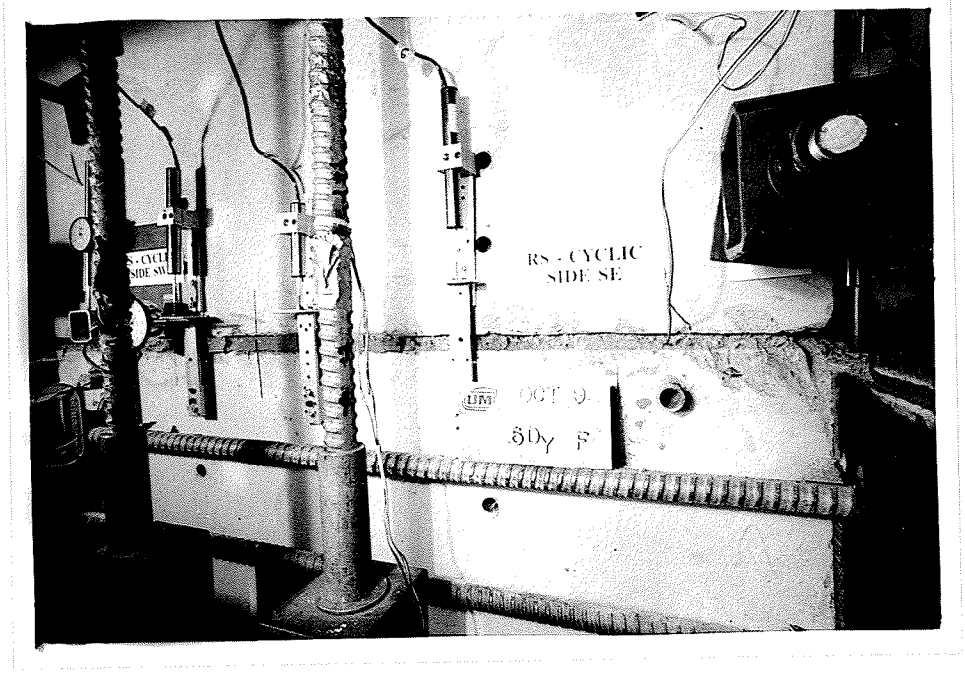

Figure 5.36(c) Condition of connection for specimen RS: at 5Dy (failure)

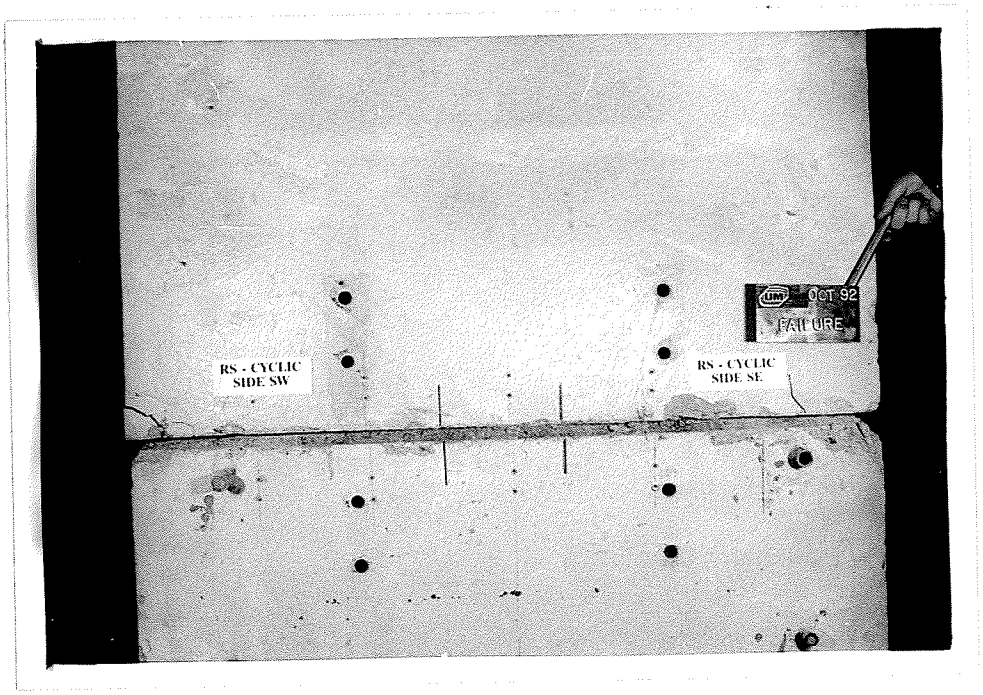

Figure 5.36(d) Condition of connection for specimen RS: post-failure outside frame

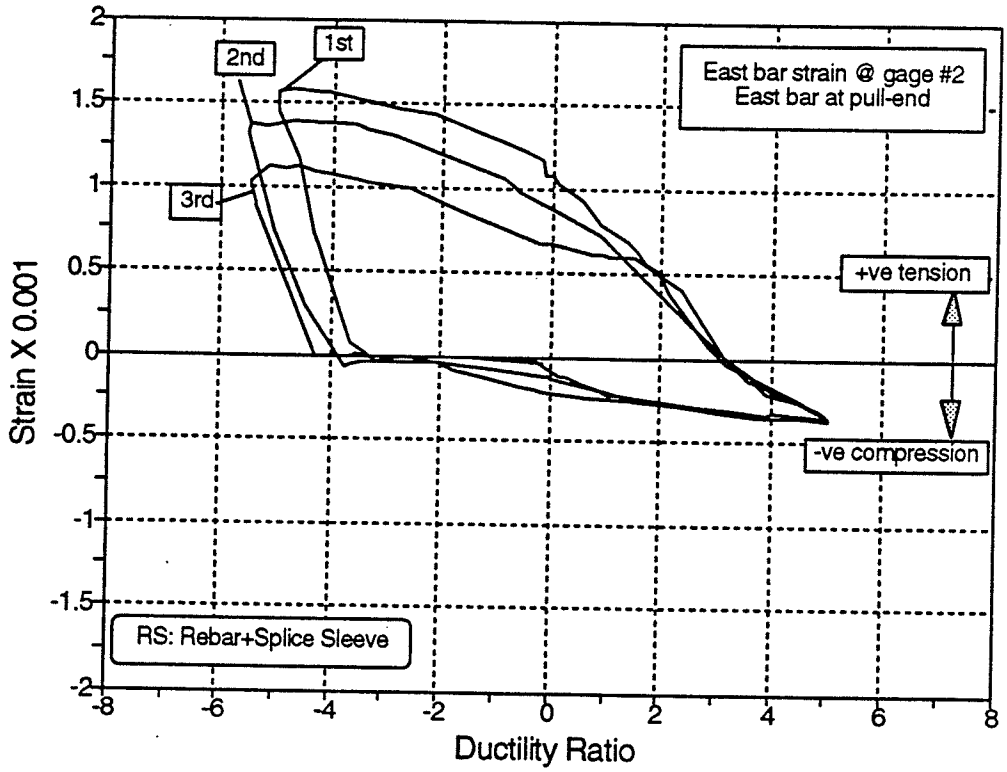

Figure 5.37 Onset of east bar pull-out per strain gage #2 at 5Dy for specimen RS

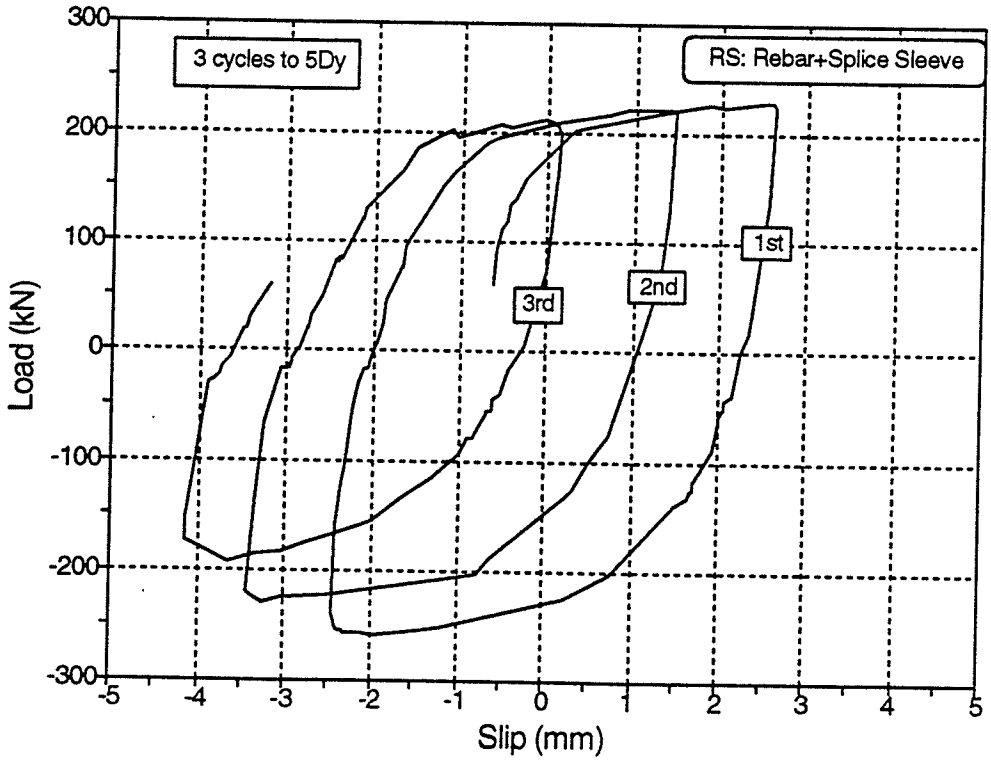

Figure 5.38 Shift in slip @ cycles to 5Dy for specimen RS

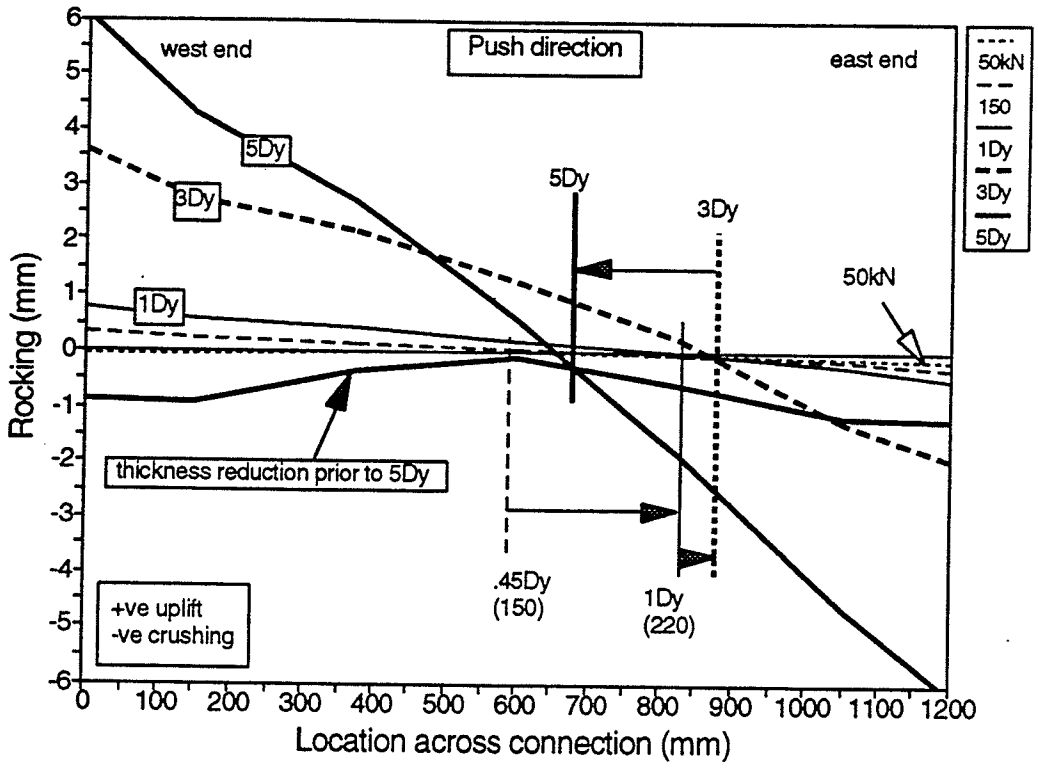

Figure 5.39(a) Rocking behaviour in the push direction for specimen RS

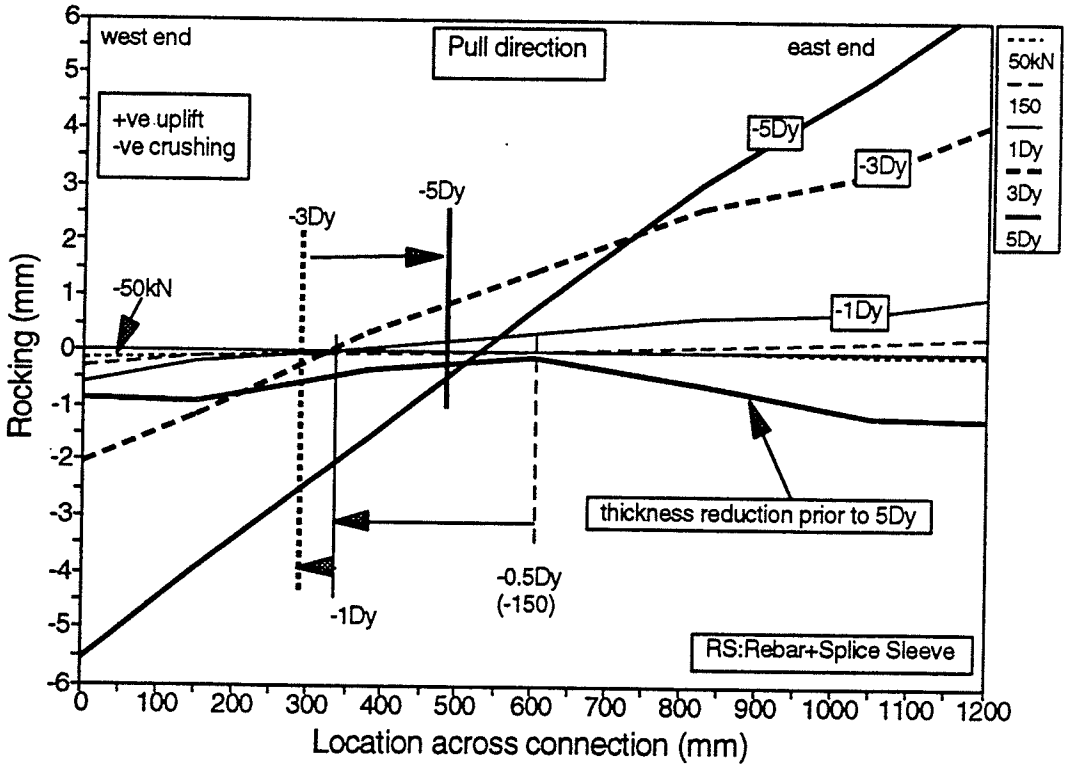

Figure 5.39(b) Rocking behaviour in the pull-direction for specimen RS

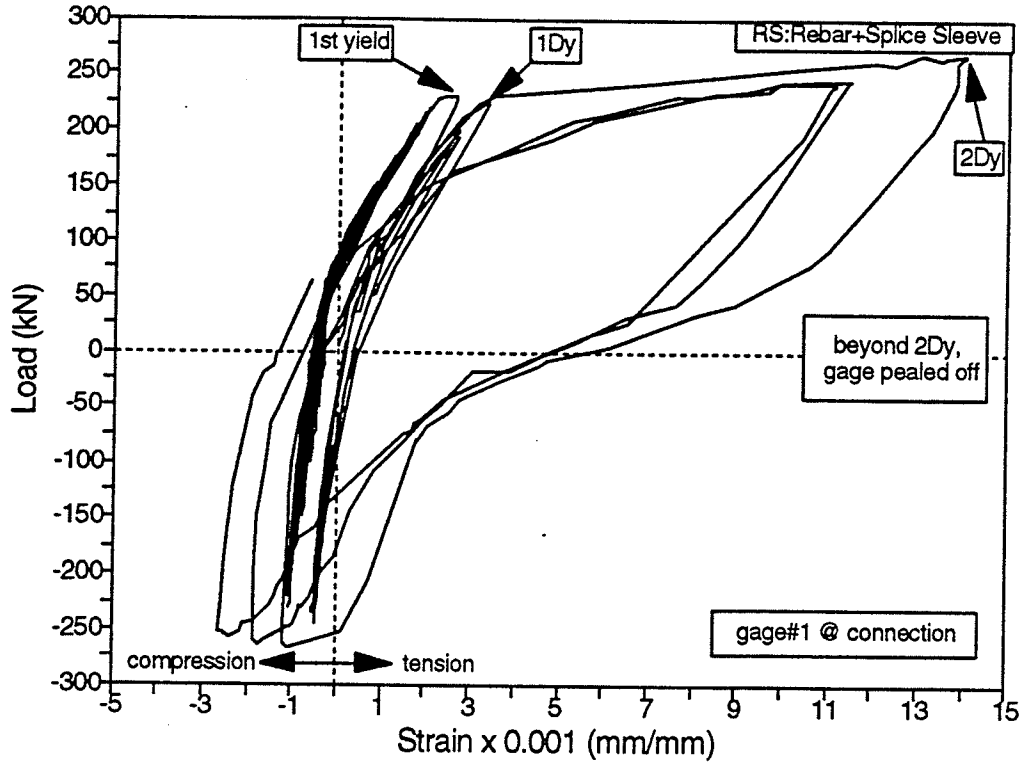

Figure 5.40(a) West bar strain gage #1 at connection push-end for specimen RS

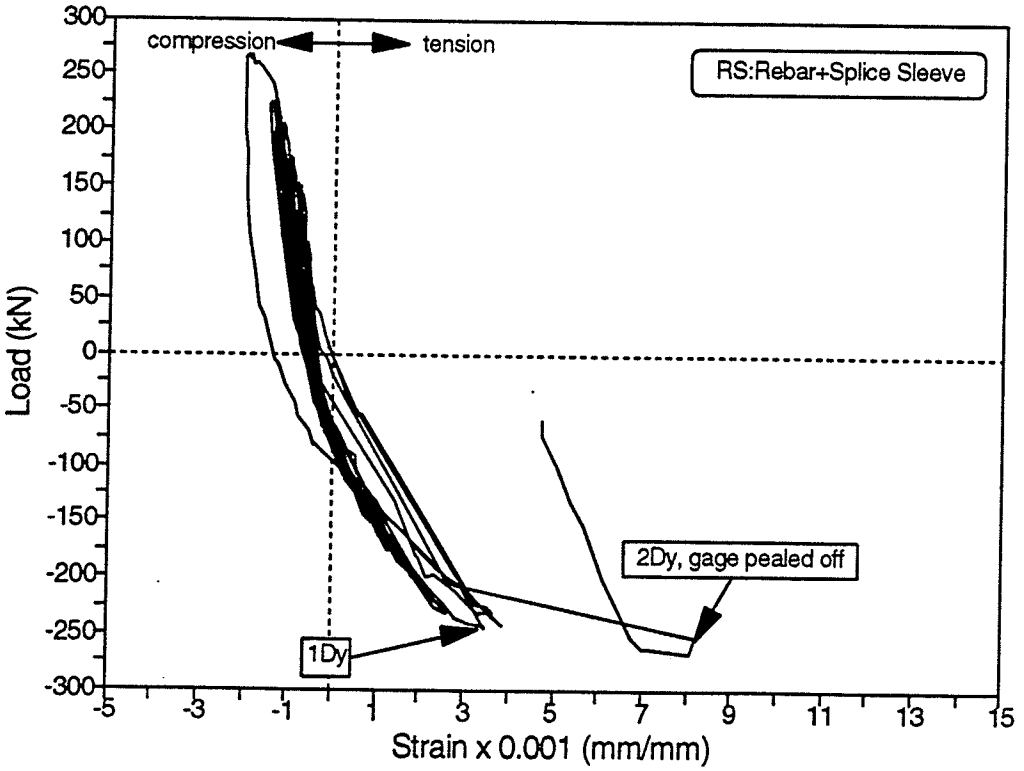

Figure 5.40(b) East bar strain gage #1 at connection pull-end for specimen RS

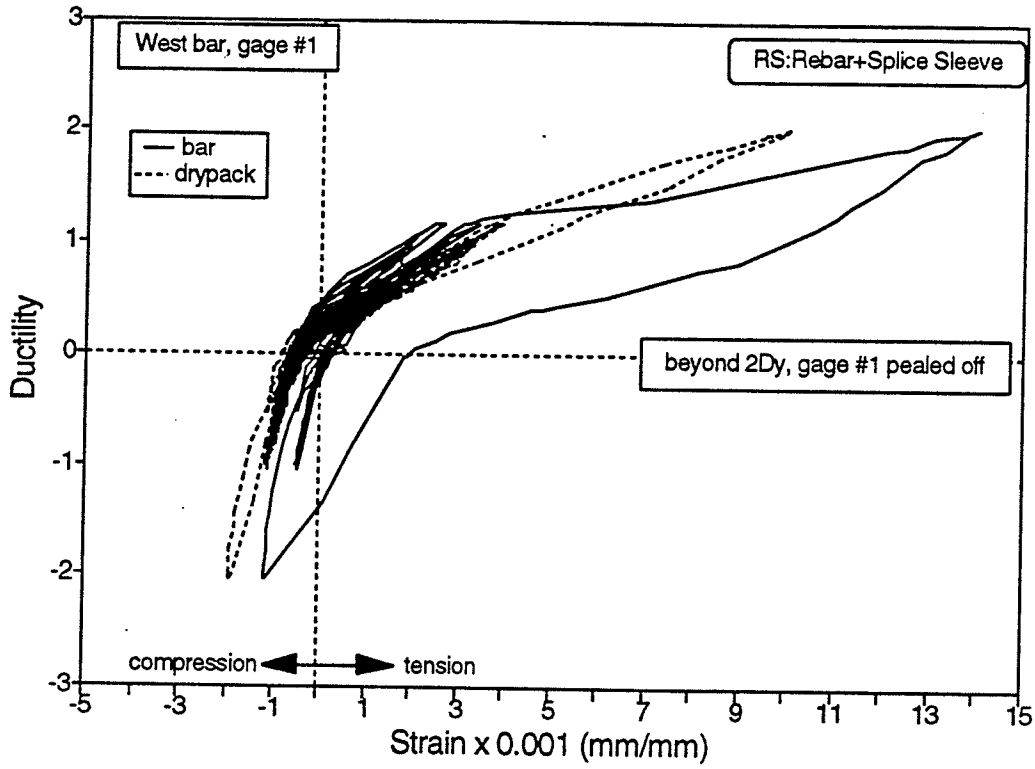

Figure 5.41(a) Comparison of west bar strain and drypack strain at joint for specimen RS

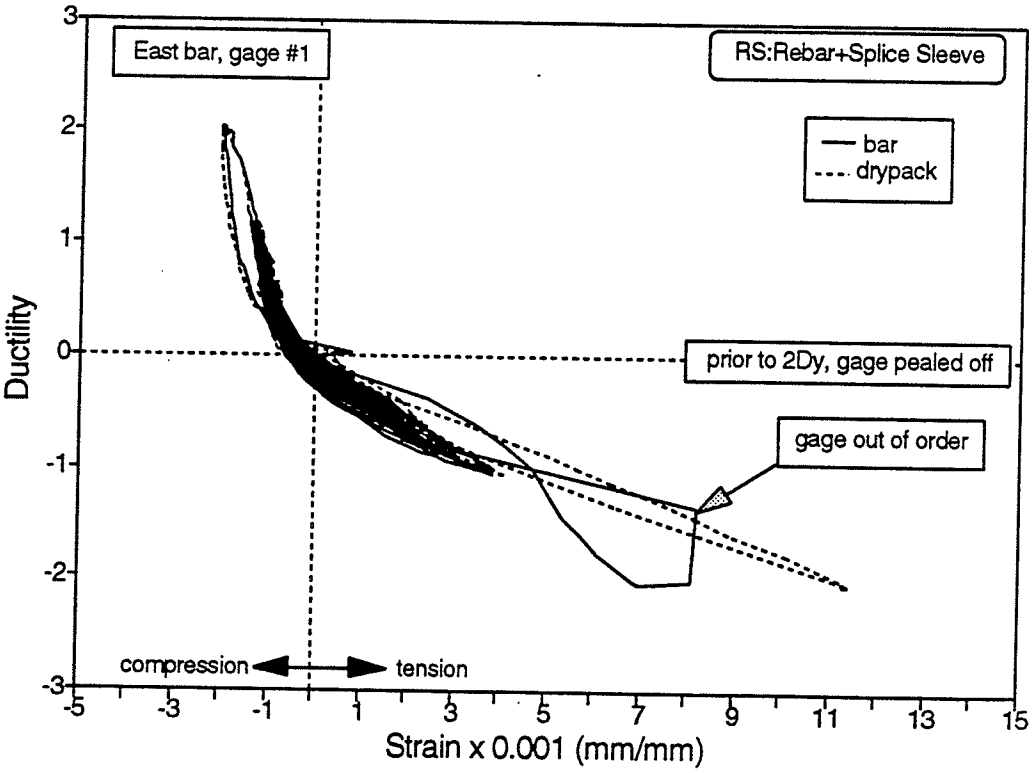

Figure 5.41(b) Comparison of east bar strain and drypack strain at joint for specimen RS

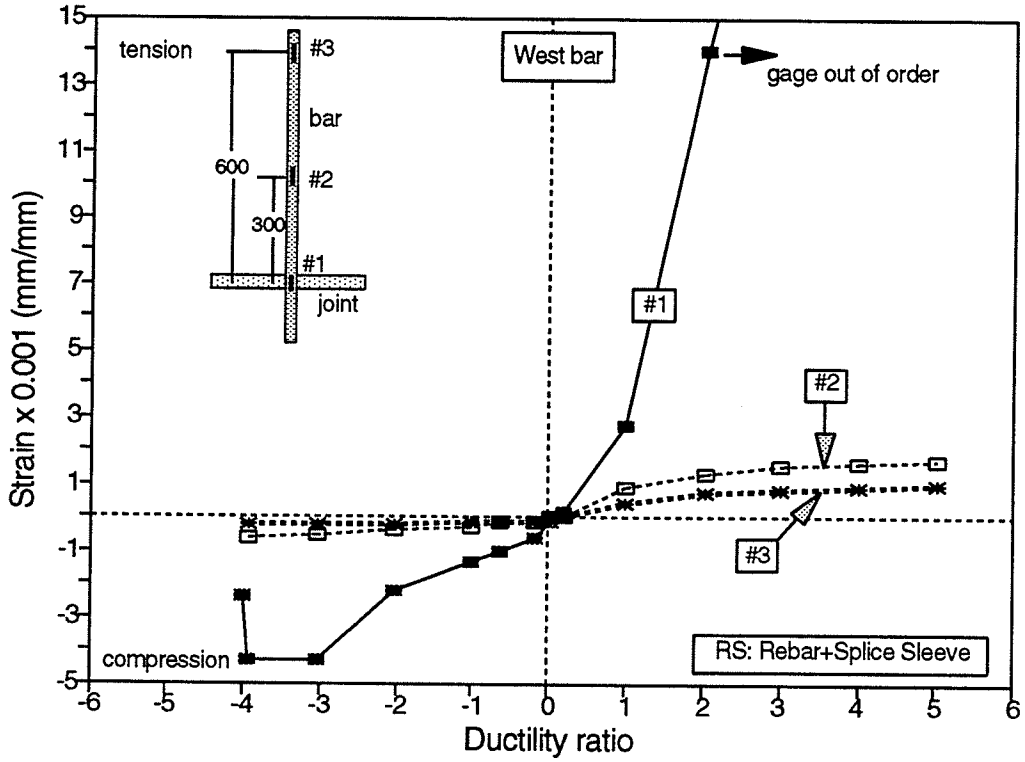

Figure 5.42(a) West bar strain at gages #1, #2 and #3 for specimen RS

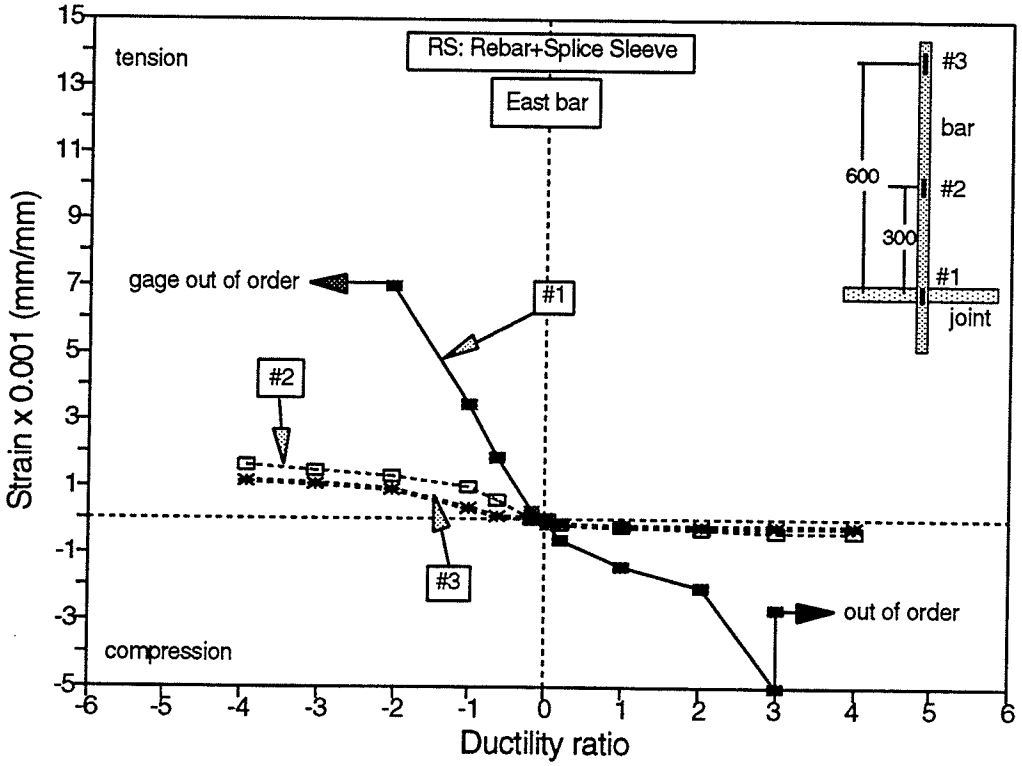

Figure 5.42(b) East bar strain at gages #1, #2 and #3 for specimen RS

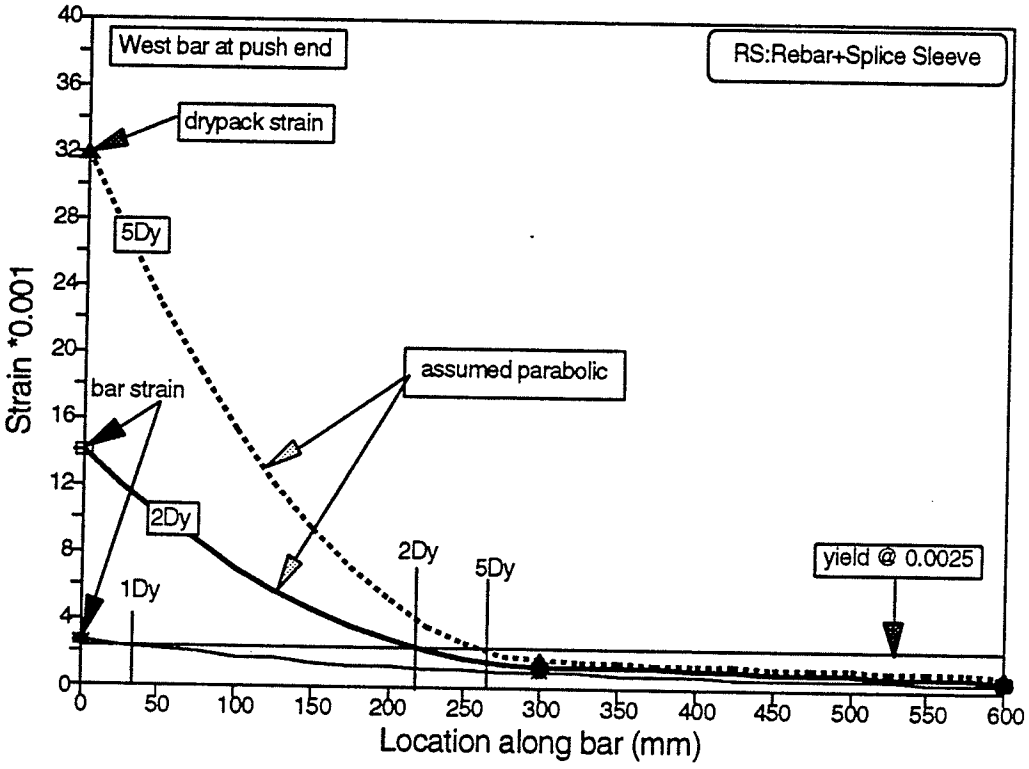

Figure 5.43 Extent of yielding for west bar at different ductility levels for specimen RS

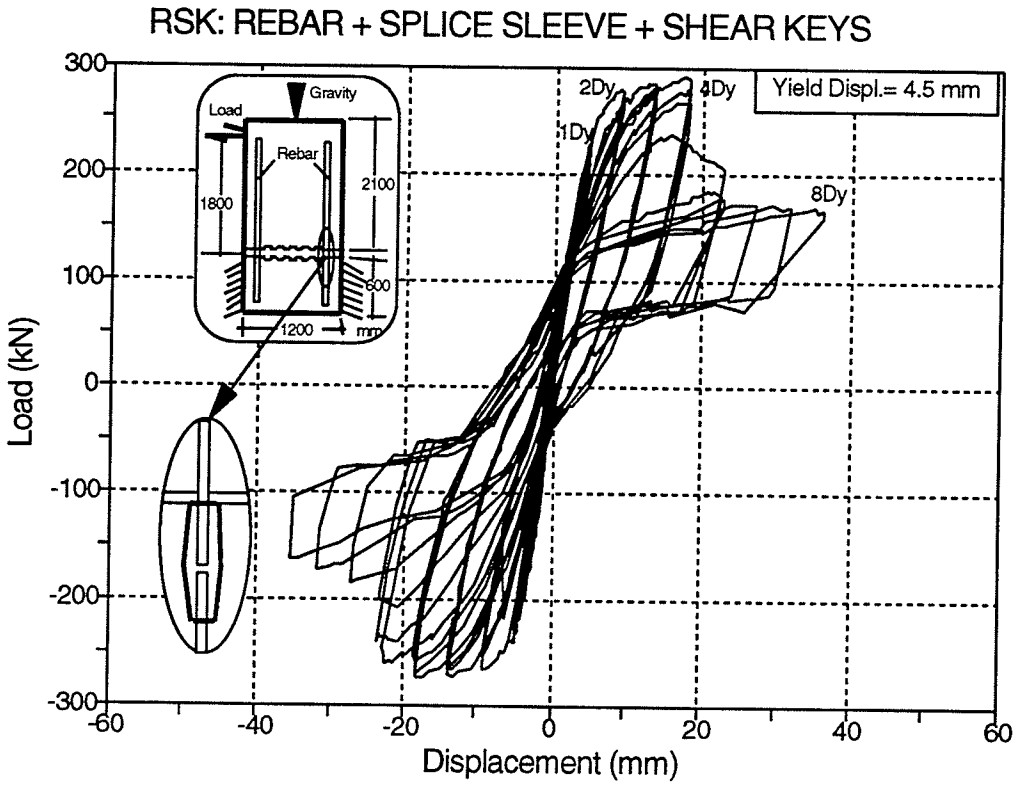

Figure 5.44(a) Hysteresis loops of load versus displacement for specimen RSK

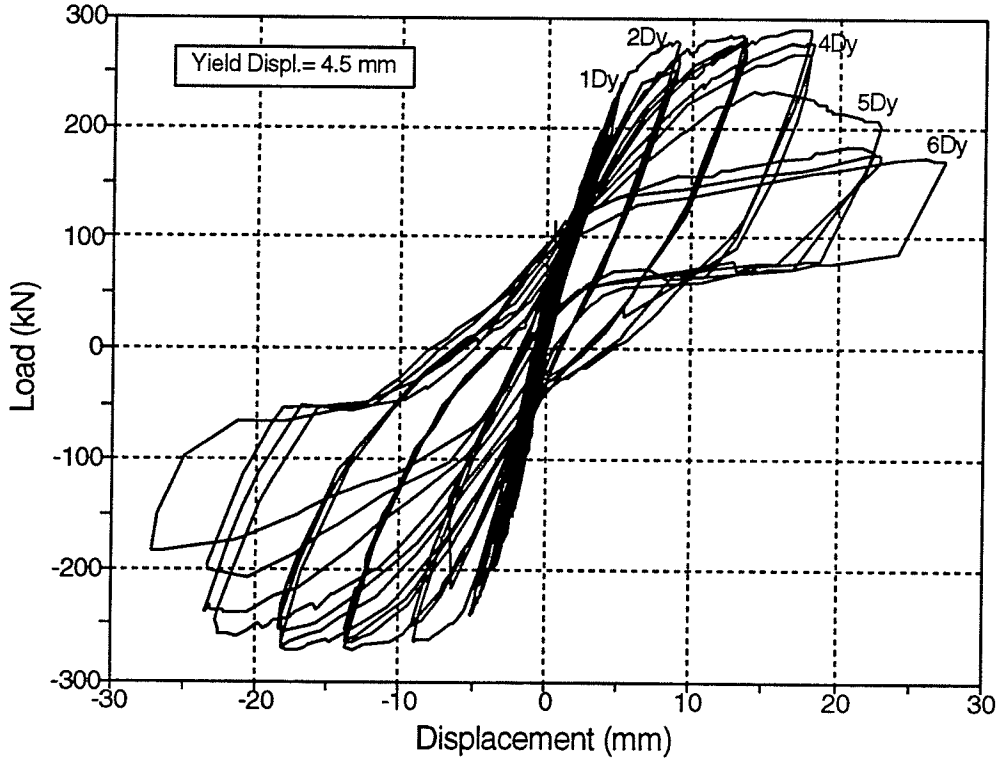

Figure 5.44(b) Magnified hysteresis loops of load vs. displacement for specimen RSK

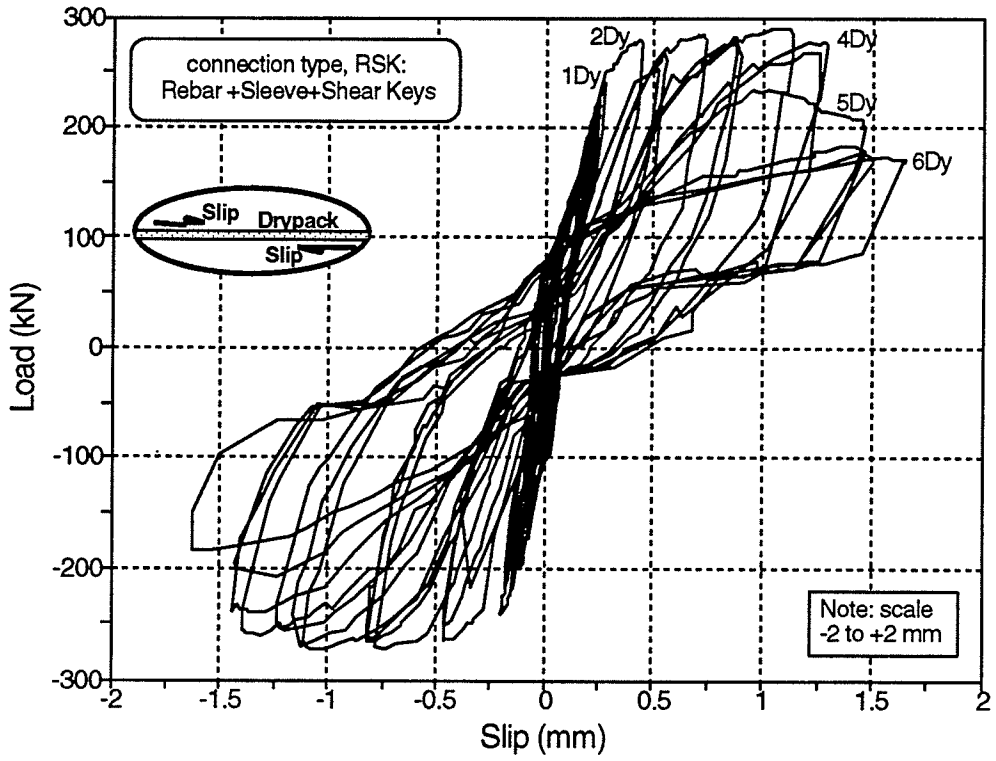

Figure 5.45 Hysteresis loops of load versus horizontal slip behaviour for specimen RSK

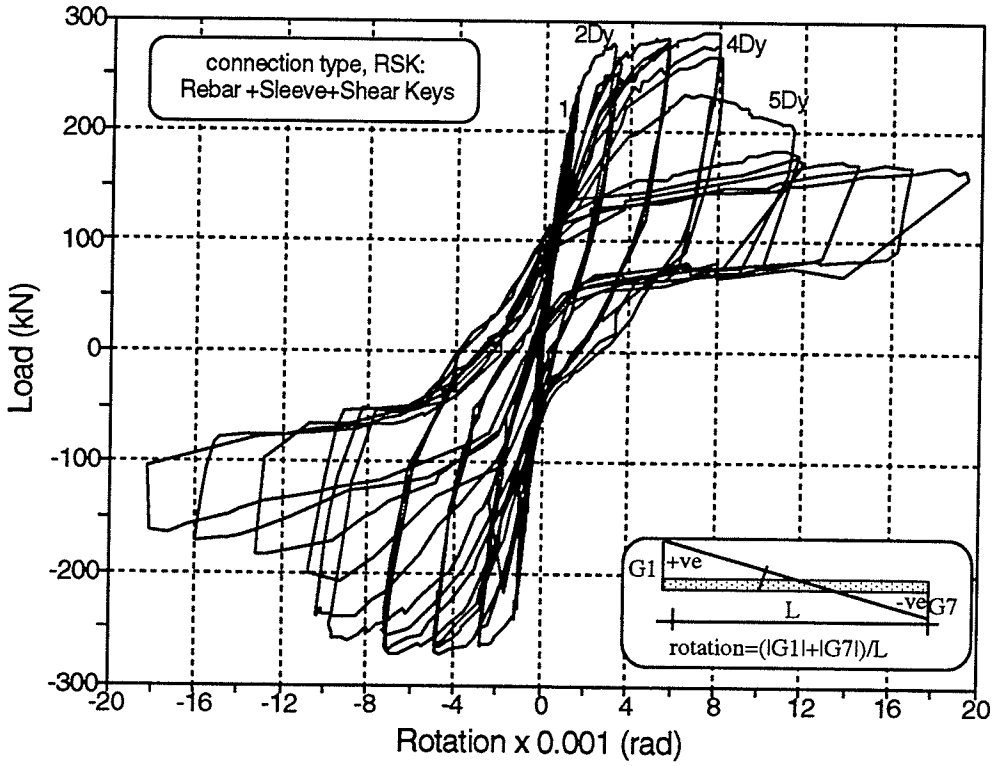

Figure 5.46 Hysteresis loops of load versus joint rotation for specimen RSK

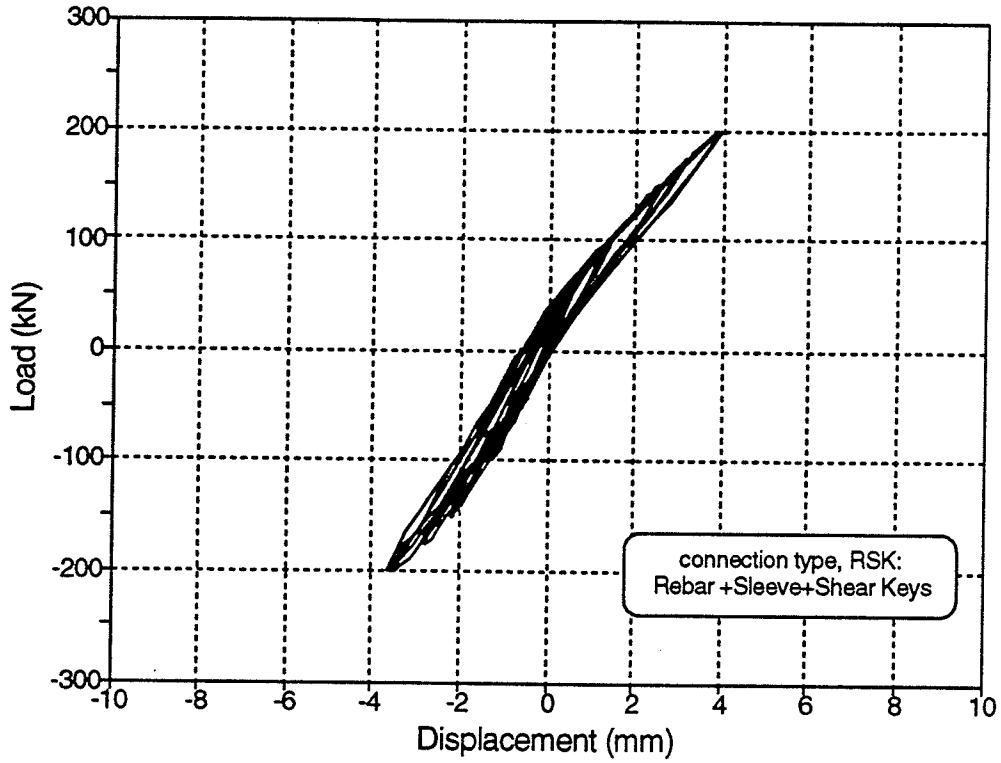

Figure 5.47 Elastic load versus displacement behavior for specimen RSK

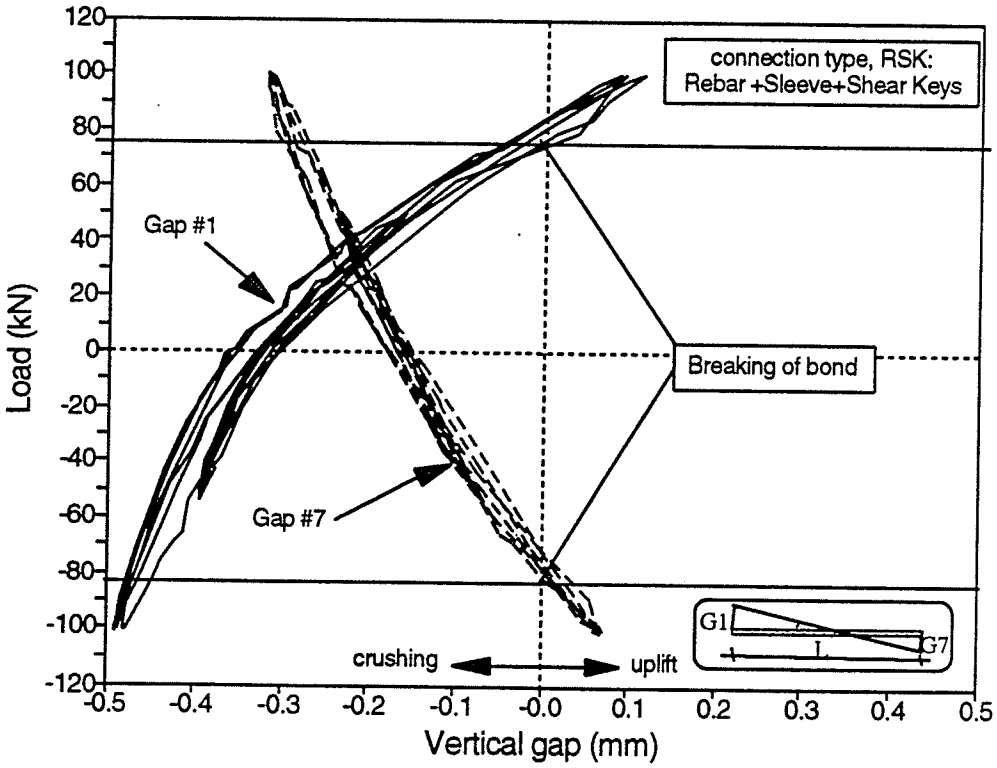

Figure 5.48 Onset of breaking of bond in load versus gap hysteresis for specimen RSK

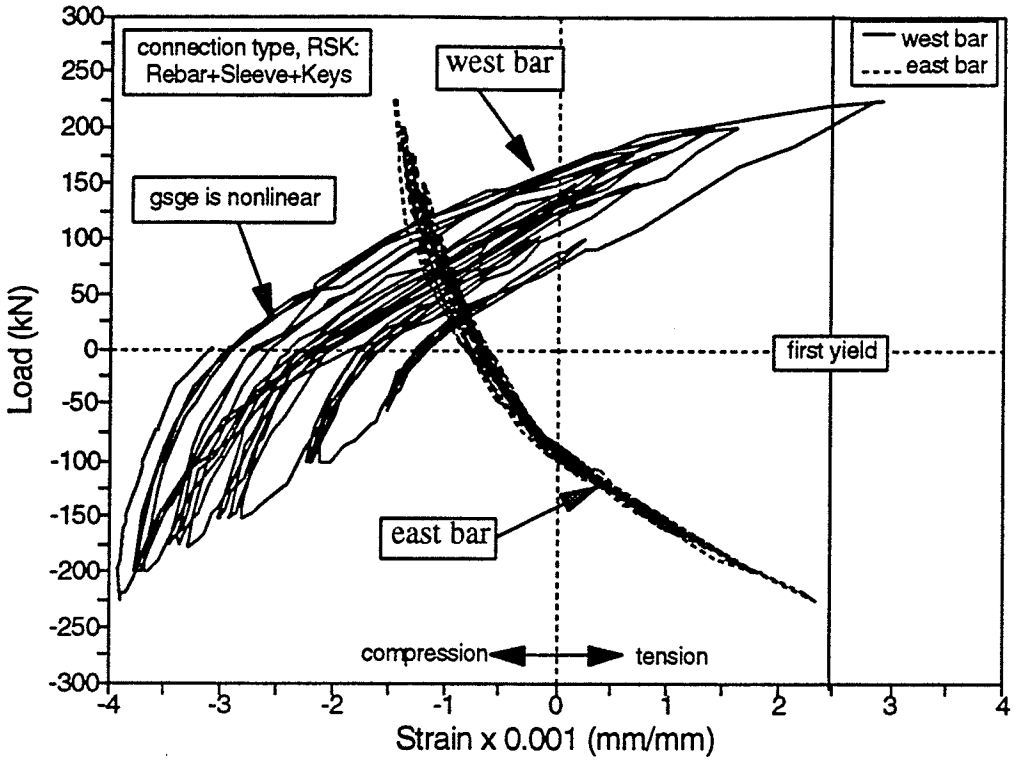

Figure 5.49 Onset of yield in load-bar strain relationship for specimen RSK

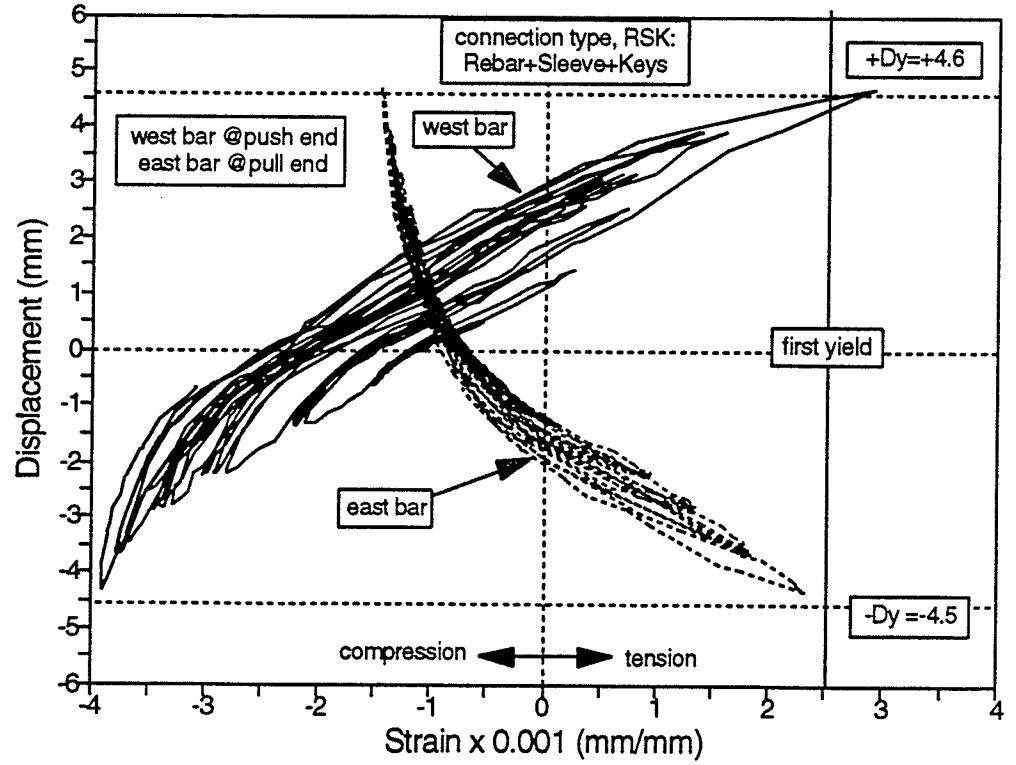

Figure 5.50 Onset of yield in bar strain-displacement relationship for specimen RSK

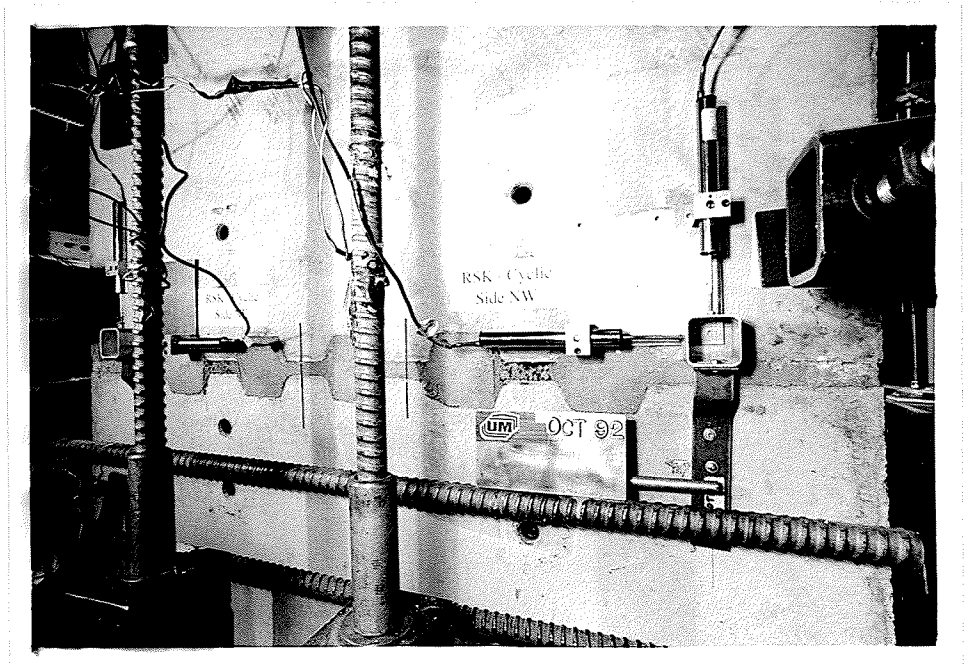

Figure 5.51(a) Condition of connection for specimen RSK: at start

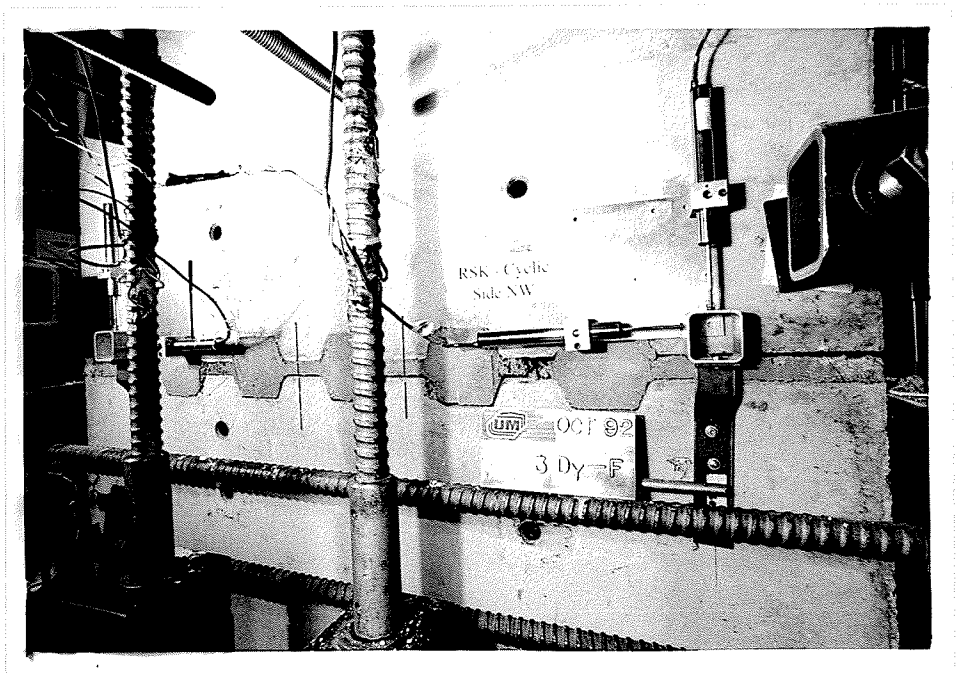

Figure 5.51(b) Condition of connection for specimen RSK: at 3Dy

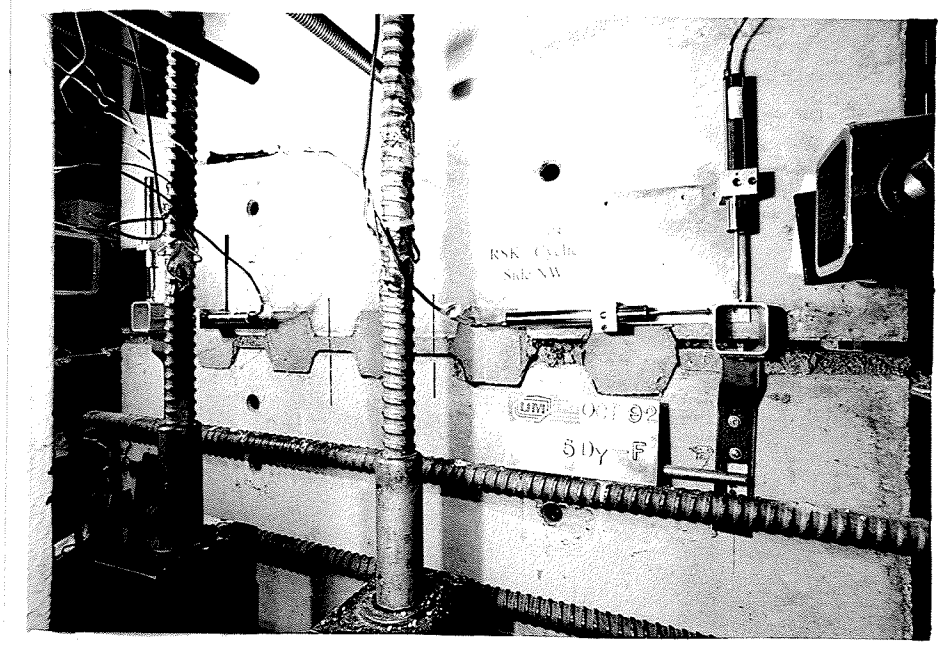

Figure 5.51(c) Condition of connection for specimen RSK: at 5Dy (failure)

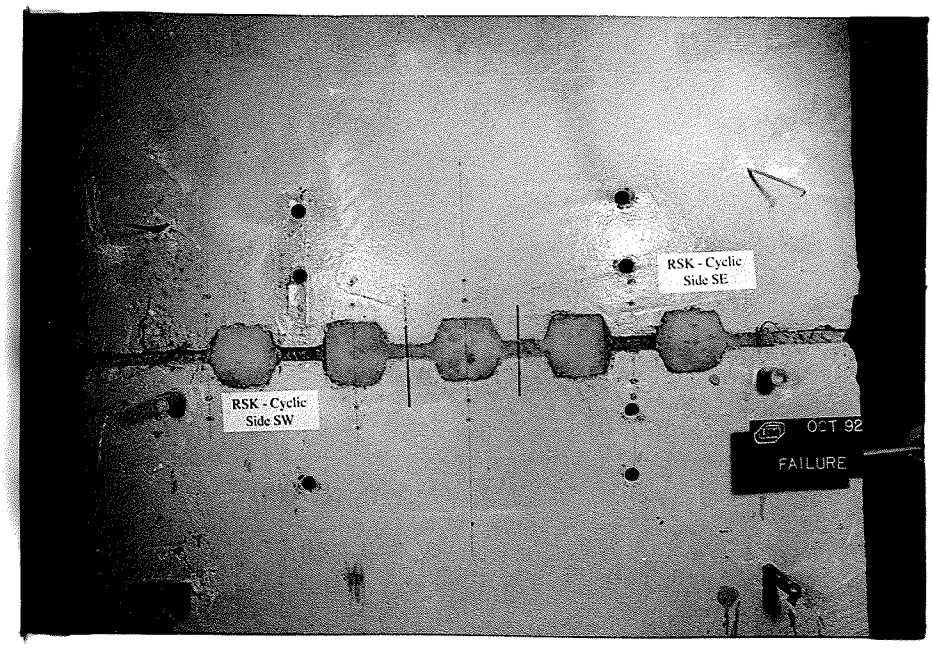

Figure 5.51(d) Condition of connection for specimen RSK: post-failure outside frame

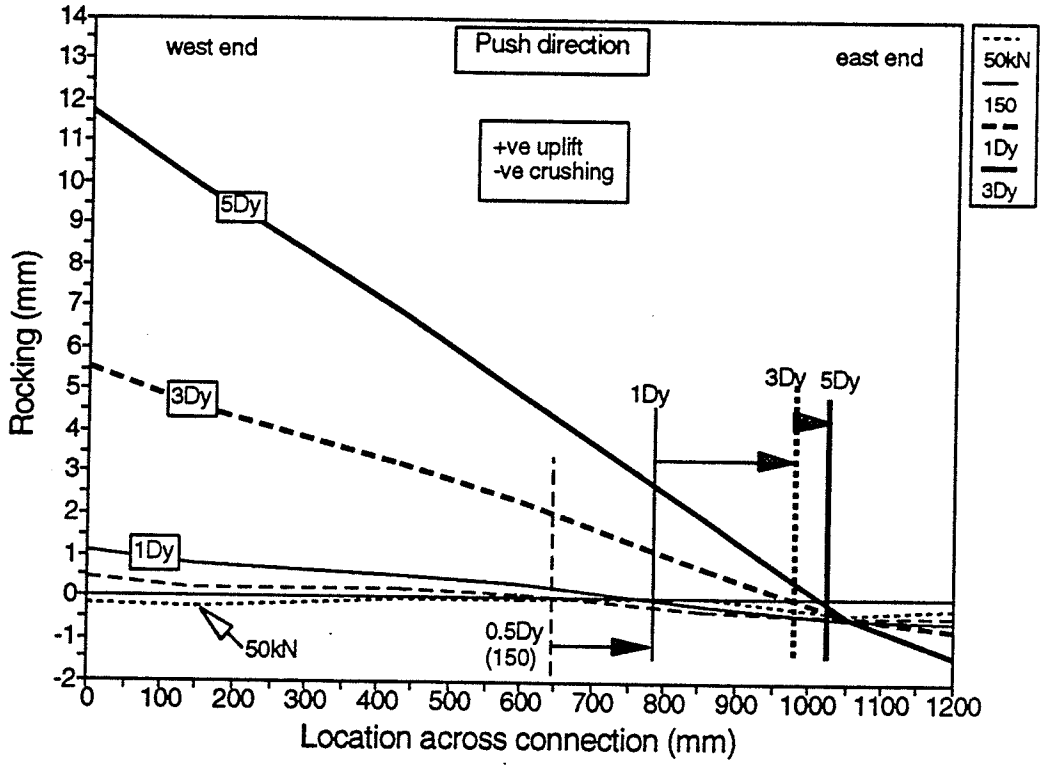

Figure 5.52(a) Rocking behaviour in the push direction for specimen RSK

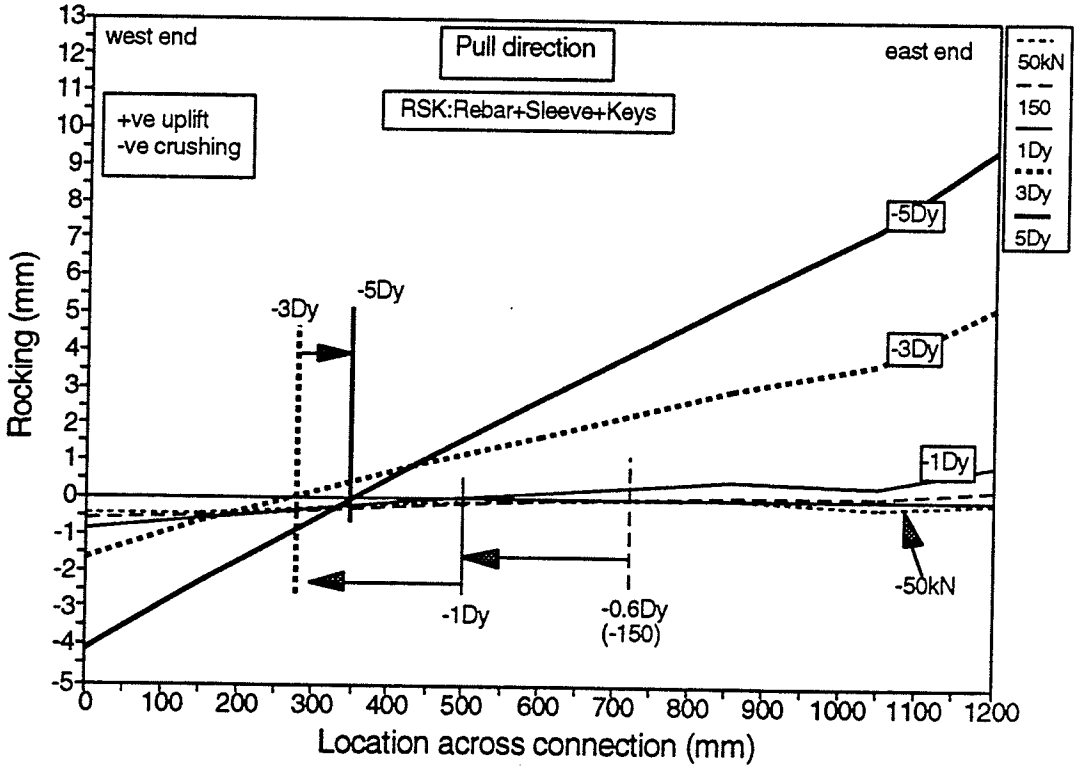

Figure 5.52(b) Rocking behaviour in the pull-direction for specimen RSK

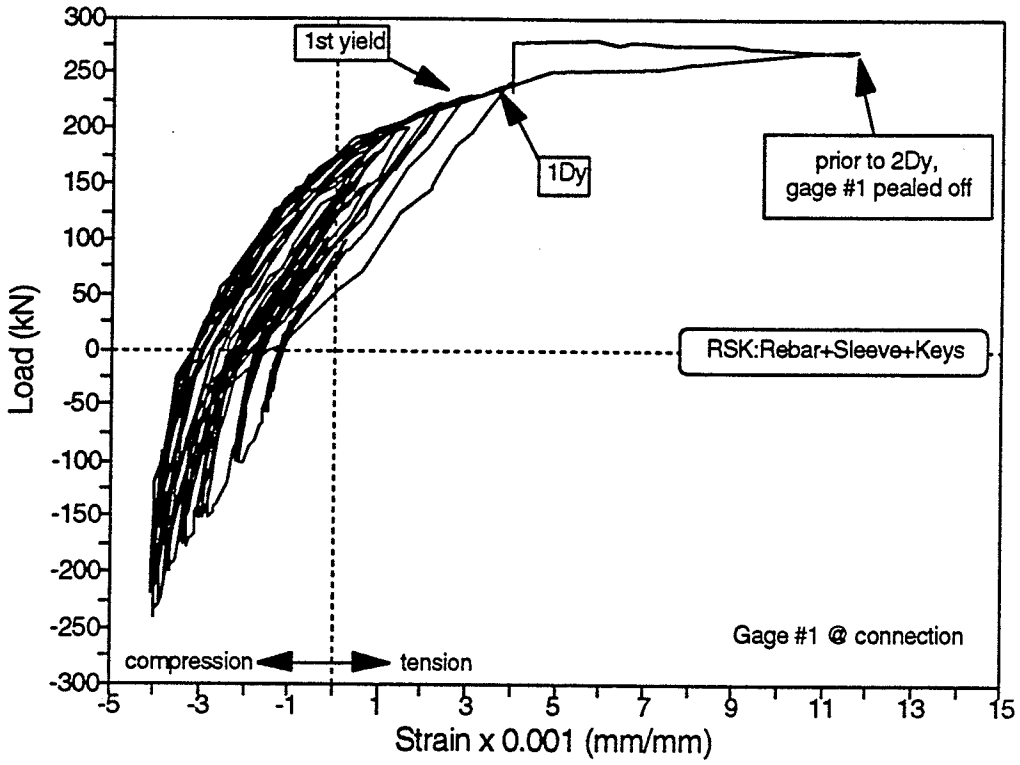

Figure 5.53(a) West bar strain gage #1 at connection push-end for specimen RSK

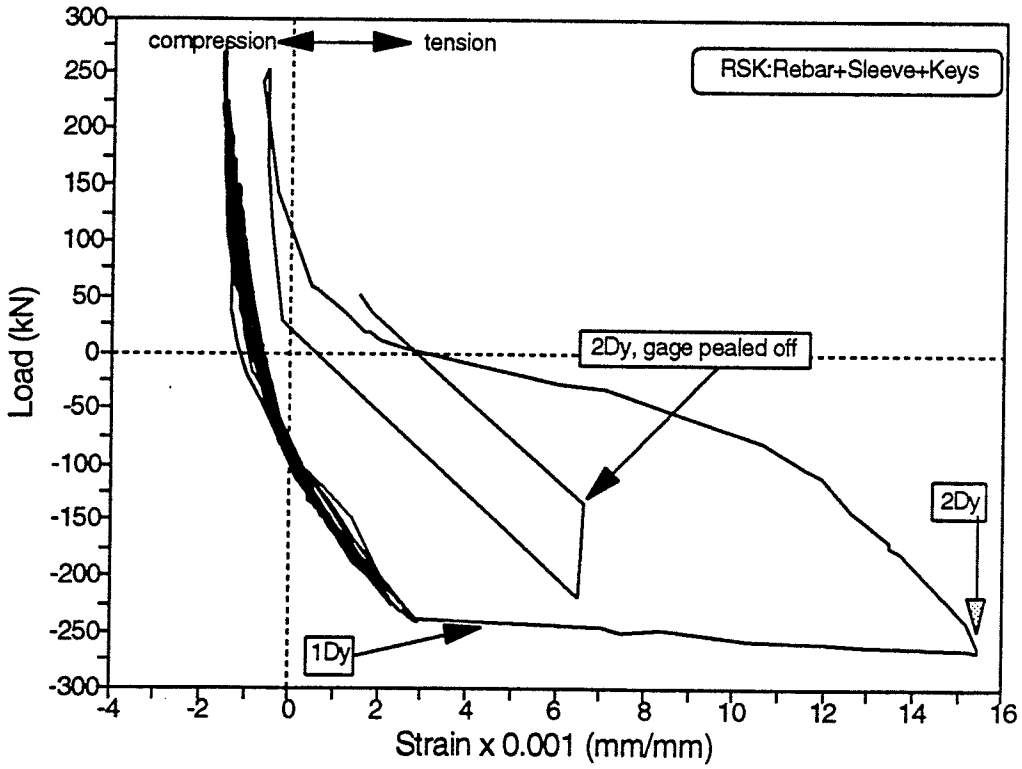

Figure 5.53(b) East bar strain gage #1 at connection pull-end for specimen RSK

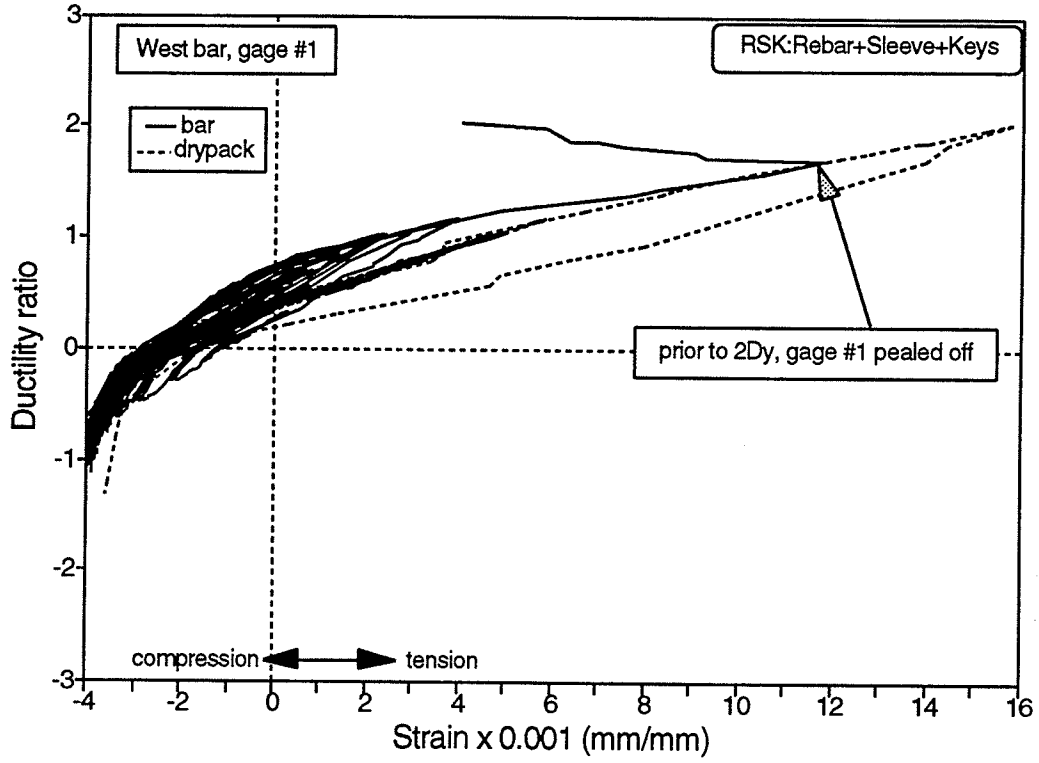

Figure 5.54(a) Comparison of west bar and drypack strain at joint for specimen RSK

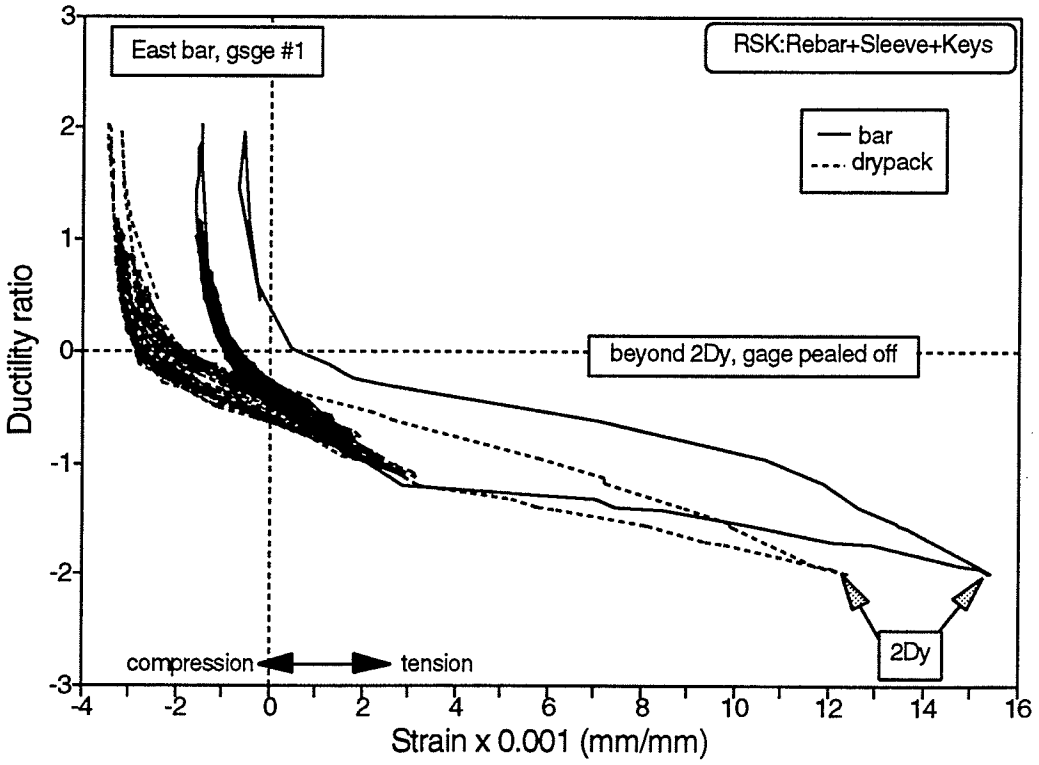

Figure 5.54(b) Comparison of east bar and drypack strain at joint for specimen RSK

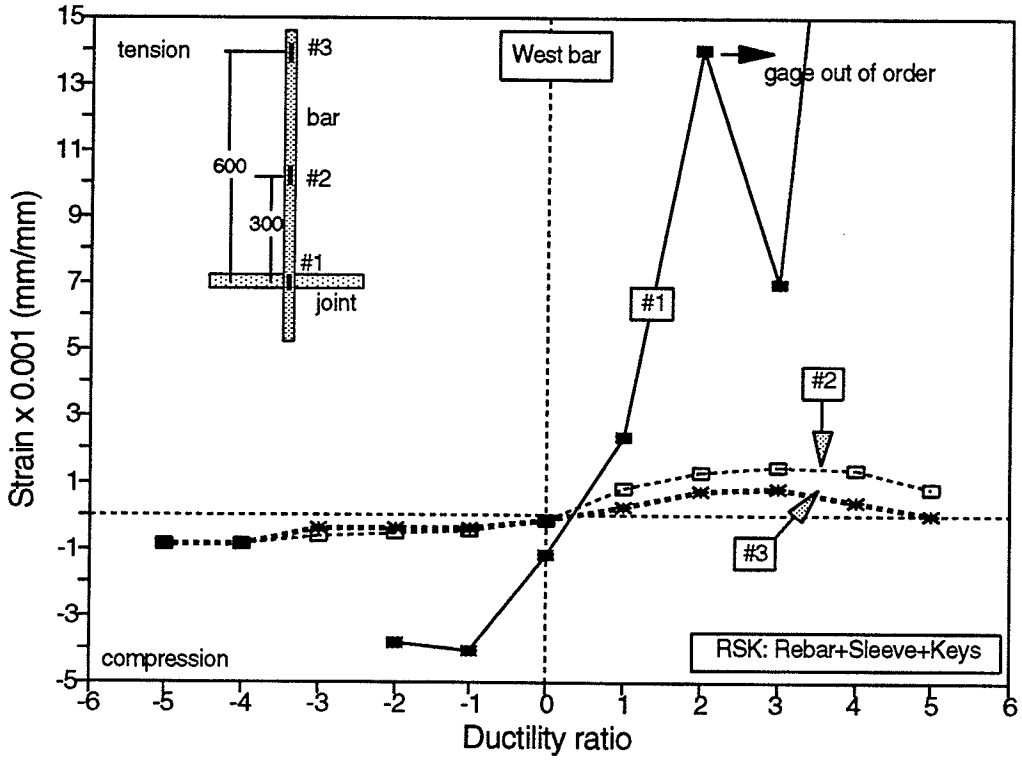

Figure 5.55(a) West bar strain at gages #1, #2 and #3 for specimen RSK

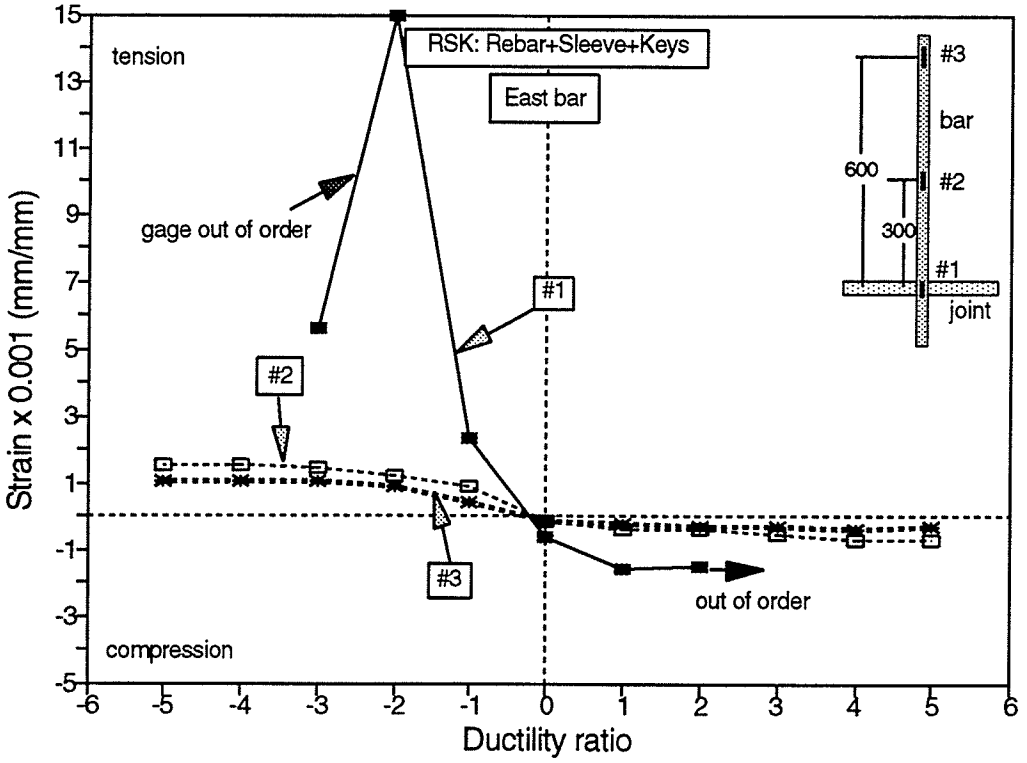

Figure 5.55(b) East bar strain at gages #1, #2 and #3 for specimen RSK

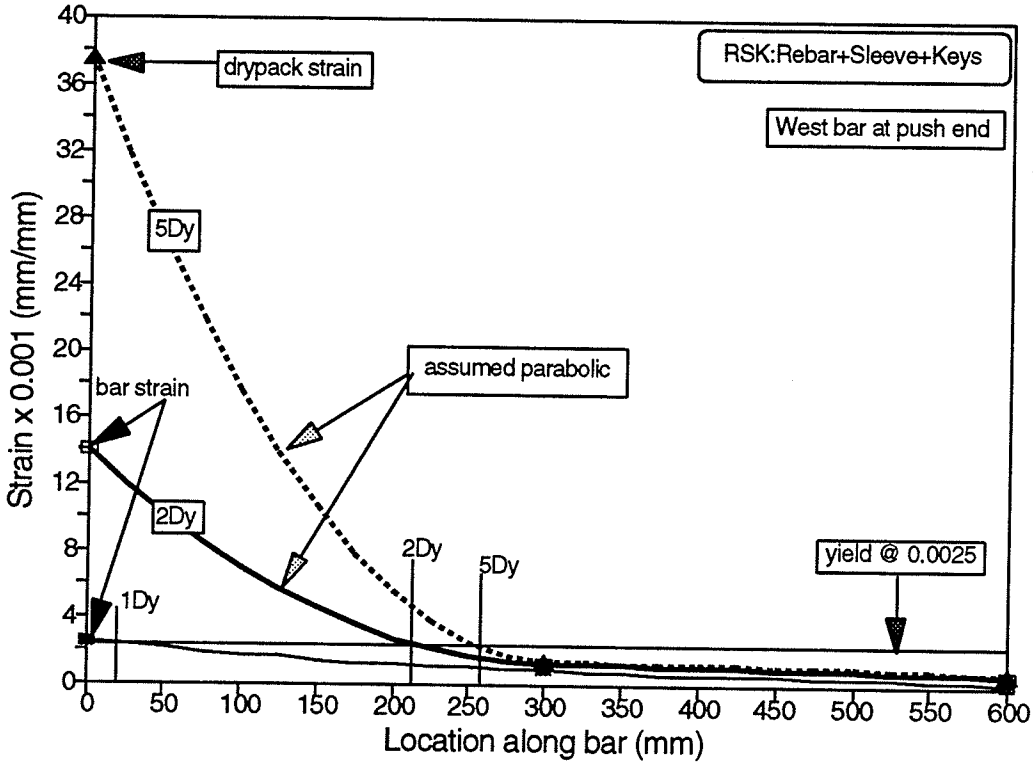

Figure 5.56 Extent of yielding for west bar at different ductility levels for specimen RSK

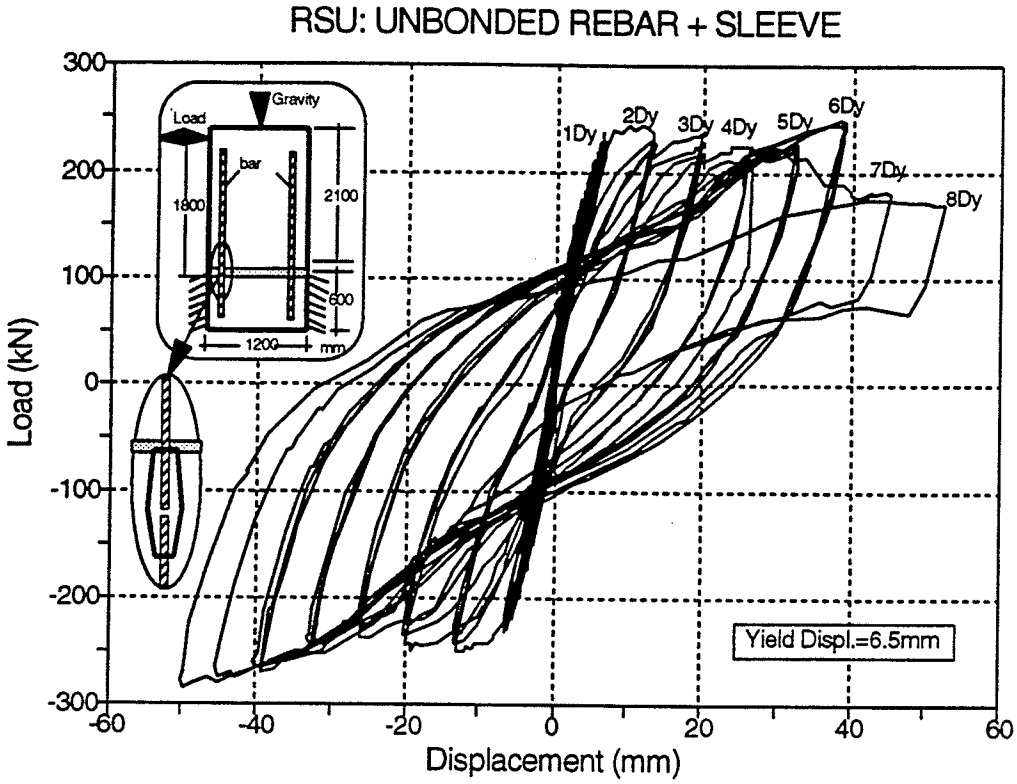

Figure 5.57(a) Hysteresis loops of load versus displacement behaviour for specimen RSU

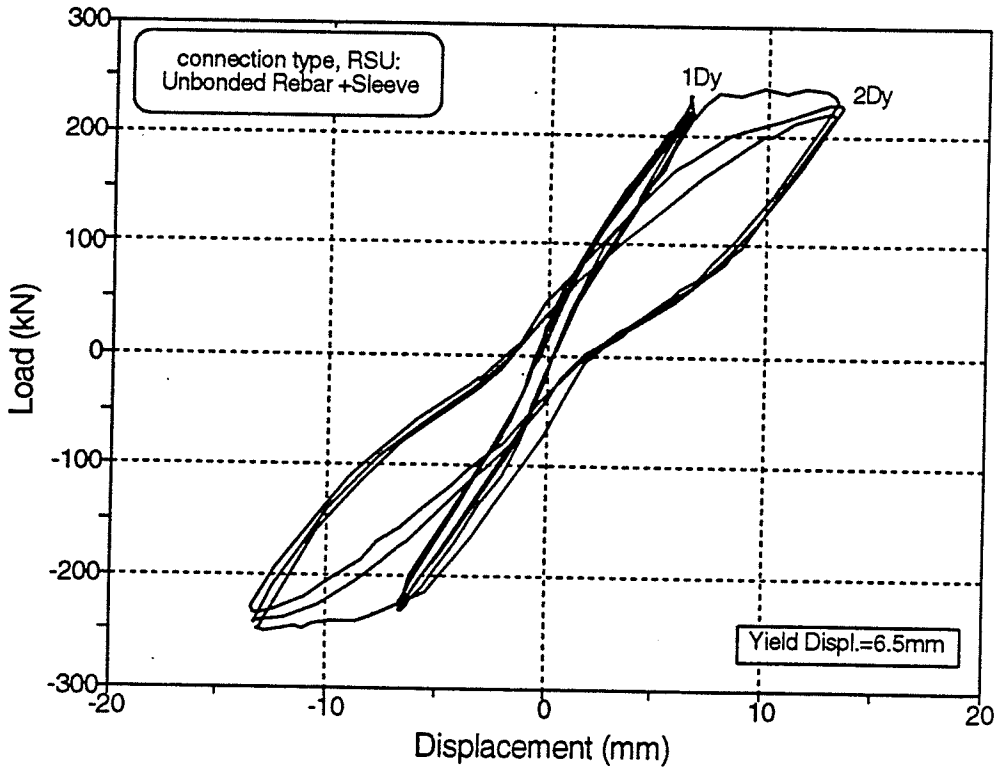

Figure 5.57(b) Hysteresis load-displacement loops at 1&2Dy cycles for specimen RSU

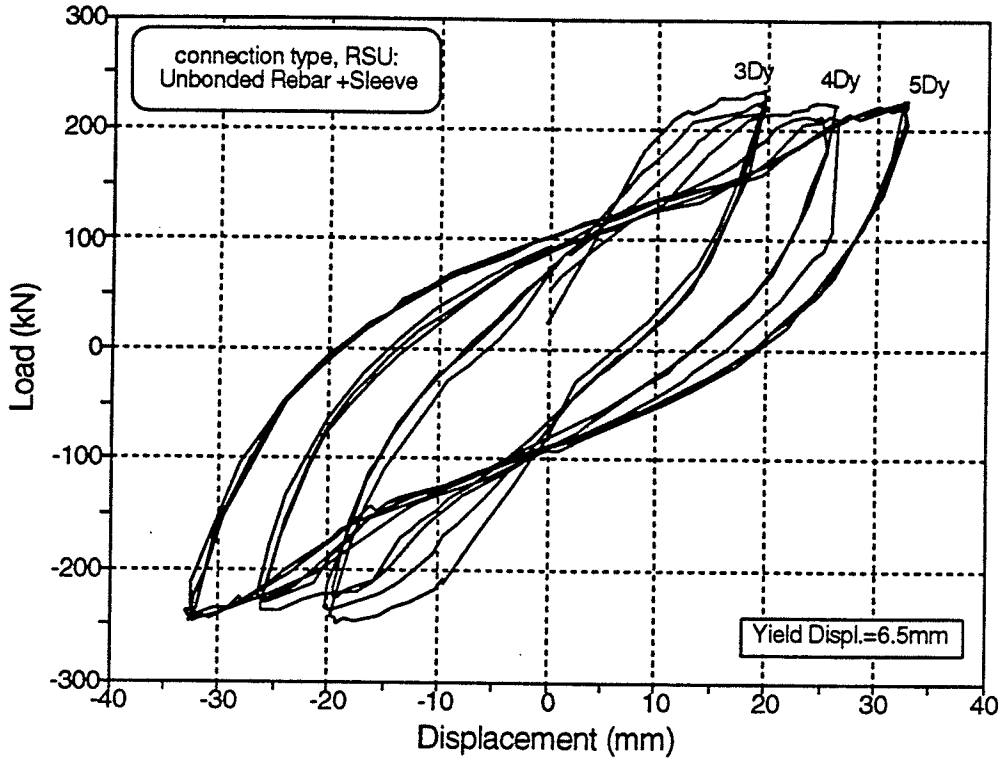

Figure 5.57(c) Hysteresis load-displacement loops at 3, 4&5Dy cycles for specimen RSU

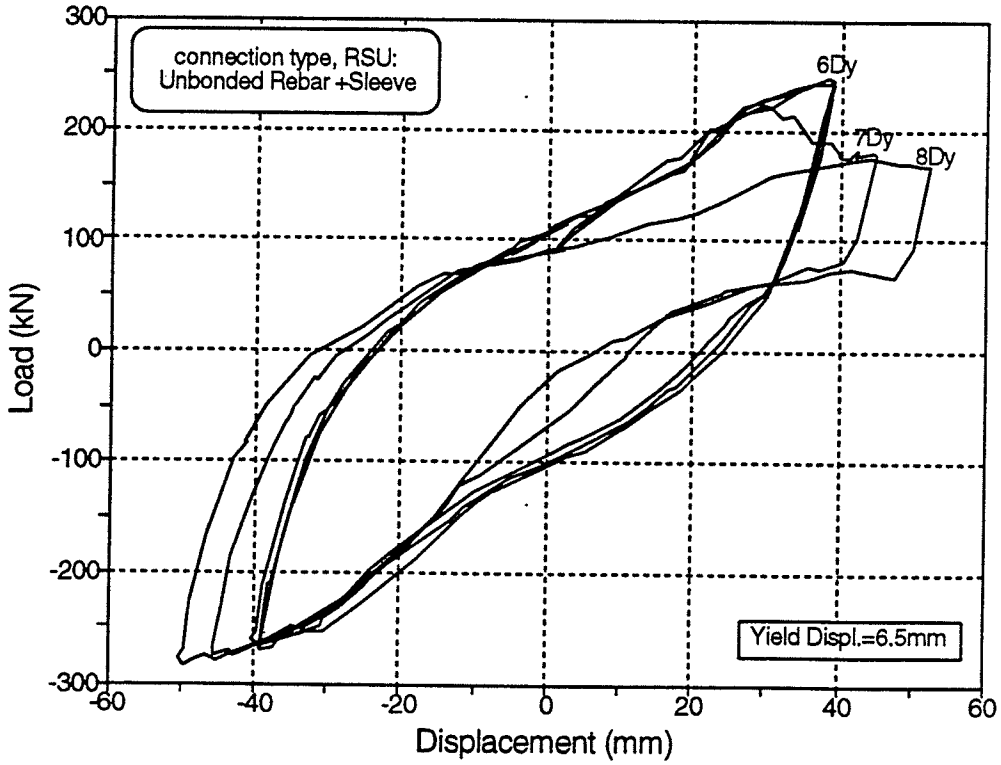

Figure 5.57(d) Hysteresis load-displacement loops at 6, 7&8Dy cycles for specimen RSU

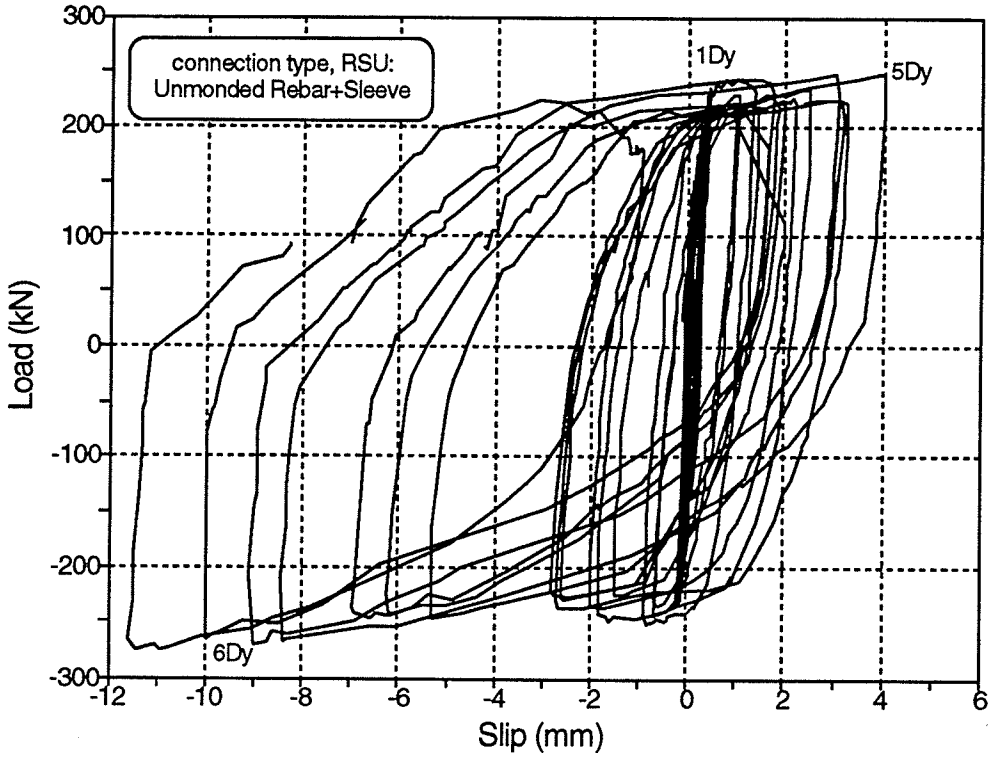

Figure 5.58(a) Hysteresis loops of load vs. horizontal slip behaviour for specimen RSU

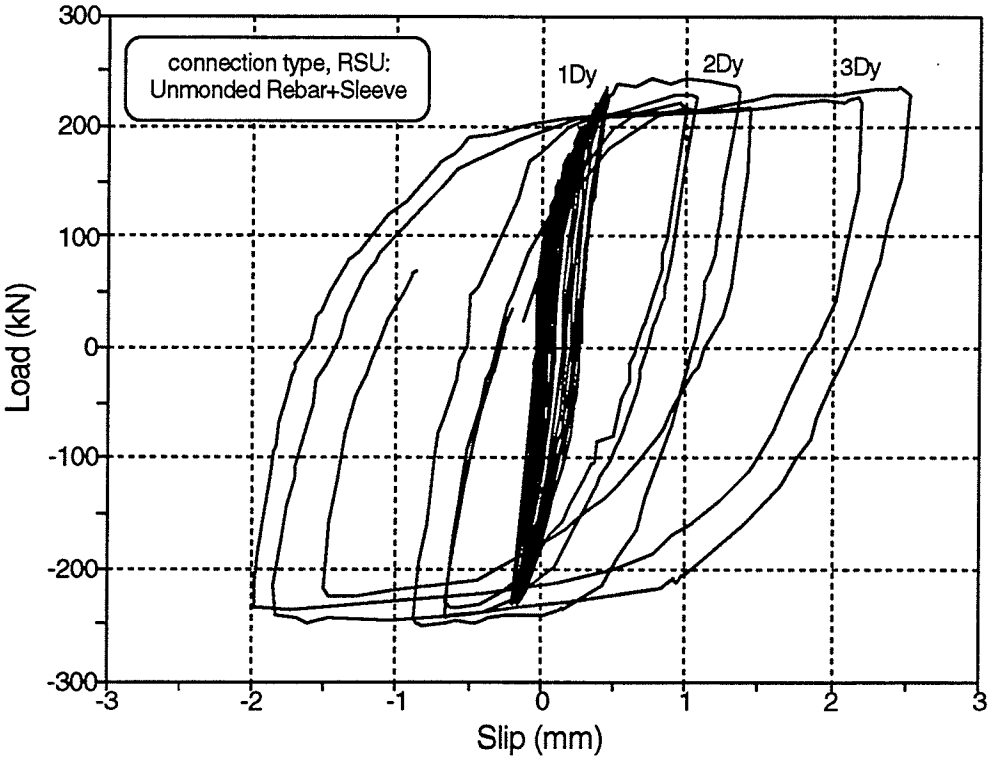

Figure 5.58(b) Slip behaviour at cycles to 1, 2 and 3Dy for specimen RSU

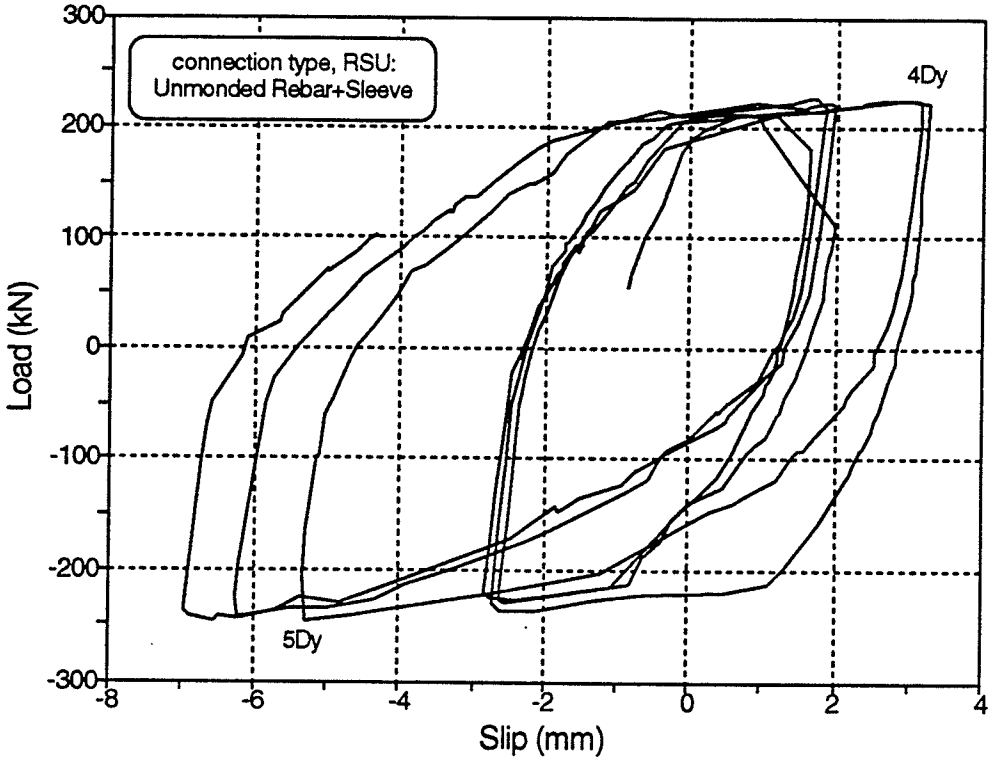

Figure 5.58(c) Slip behaviour at cycles to 4 and 5 Dy for specimen RSU

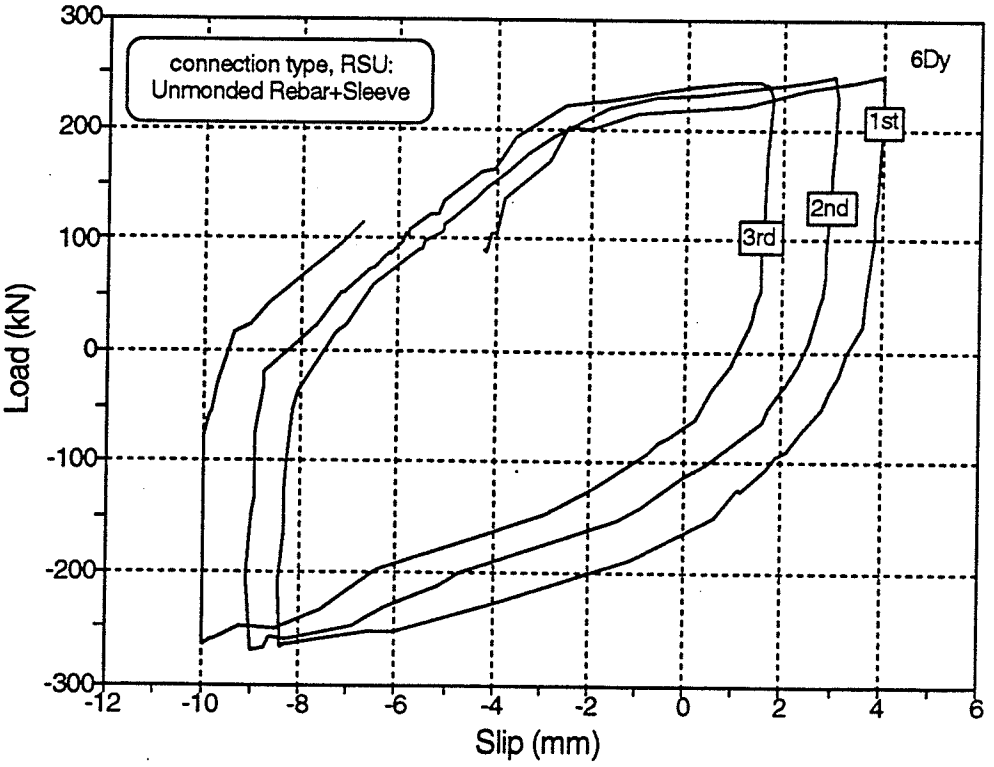

Figure 5.58(d) Slip behaviour at cycles to 6Dy for specimen RSU

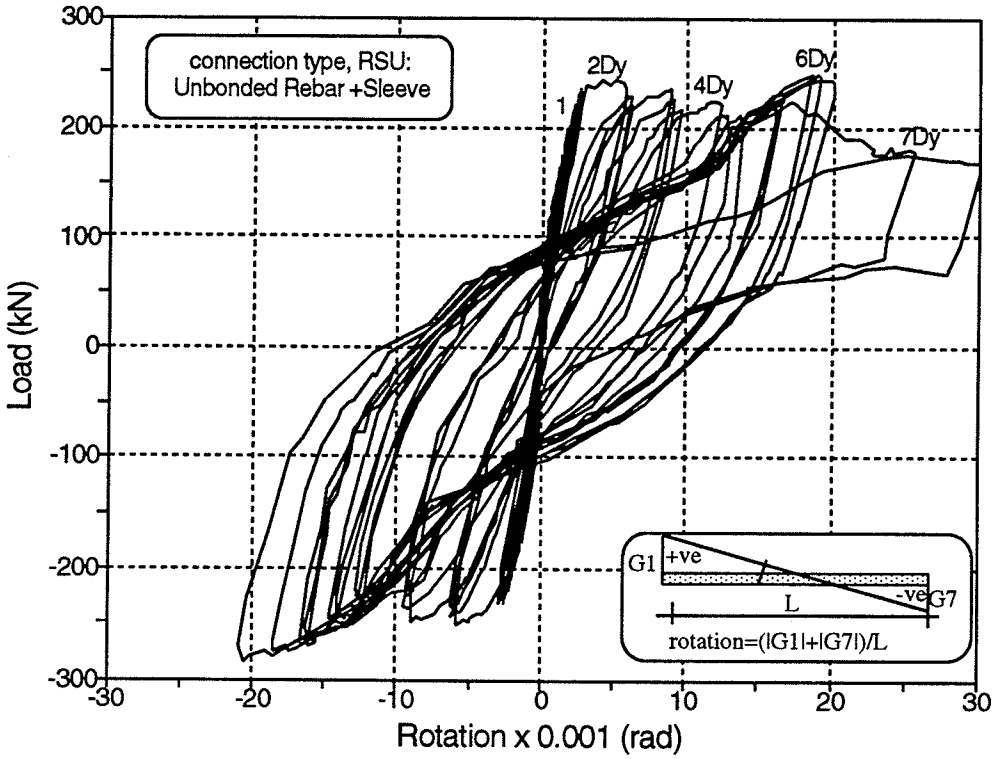

Figure 5.59 Hysteresis loops of load versus joint rotation for specimen RSU

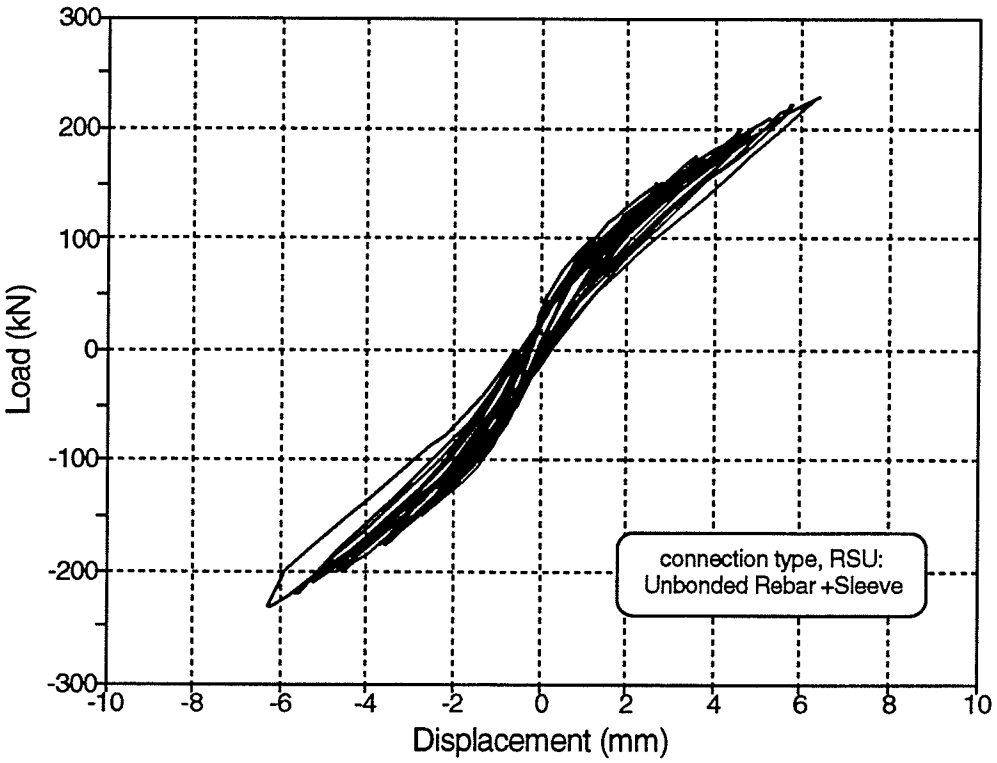

Figure 5.60 Elastic load vrs. displacement behavior for specimen RSU

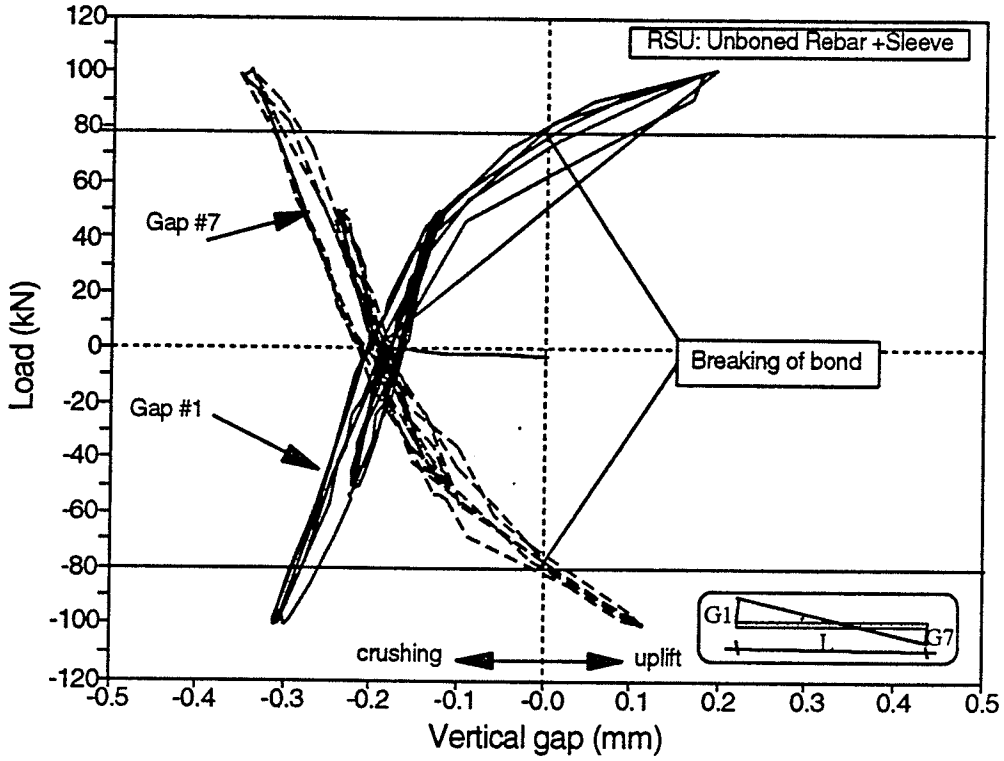

Figure 5.61 Onset of breaking of bond in load versus gap hysteresis for specimen RSU

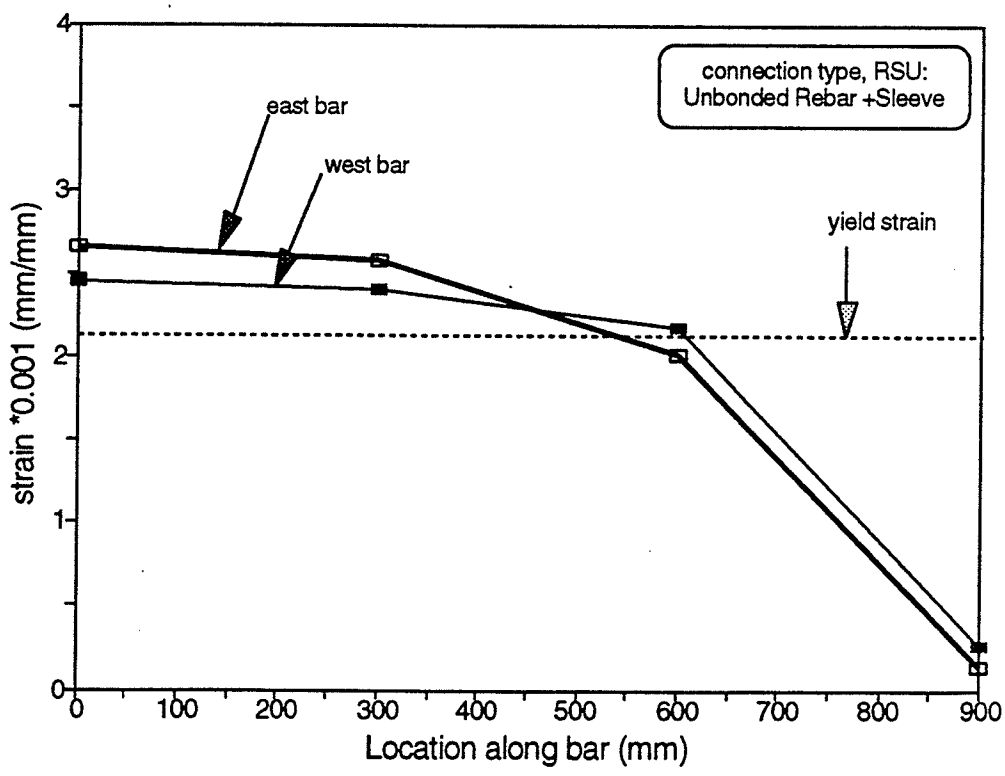

Figure 5.62 Extent of bar yield for specimen RSU

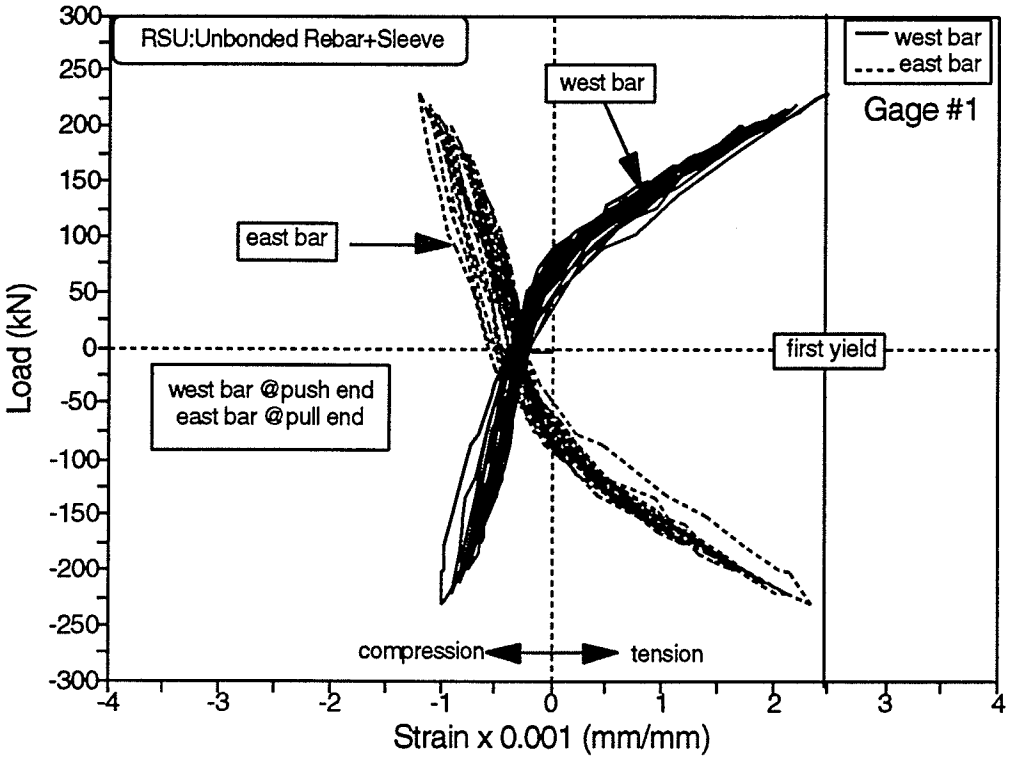

Figure 5.63 Onset of yield in load vs. bar strain at gage #1 for specimen RSU

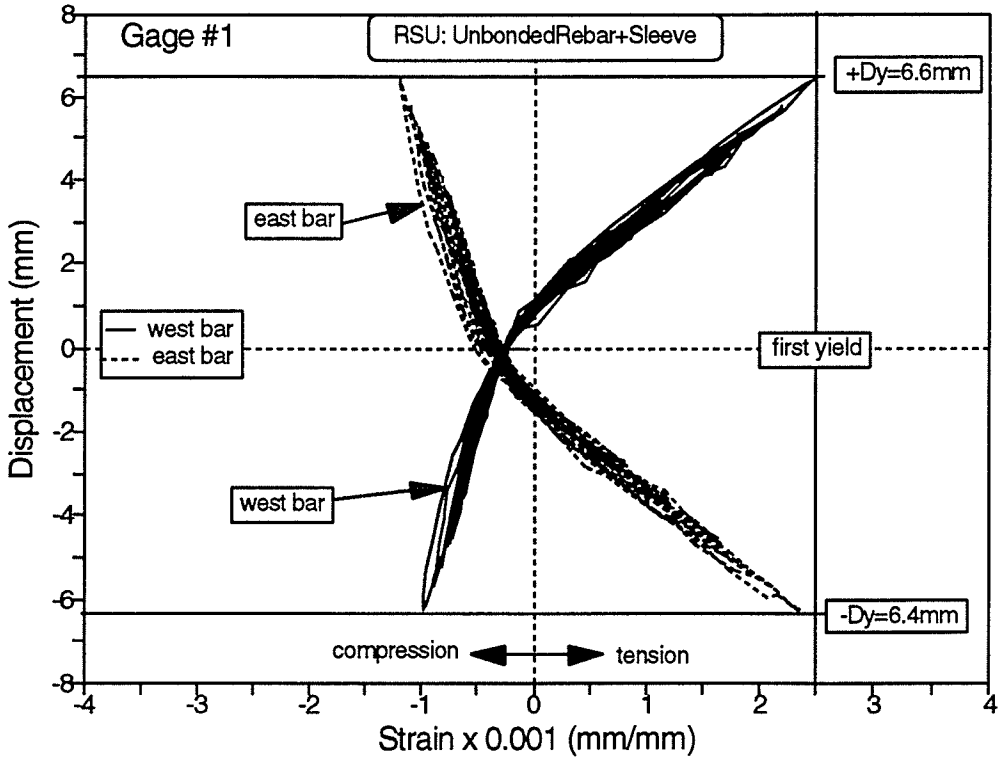

Figure 5.64 Onset of yield in displacement vs. bar strain at gage #1 for specimen RSU

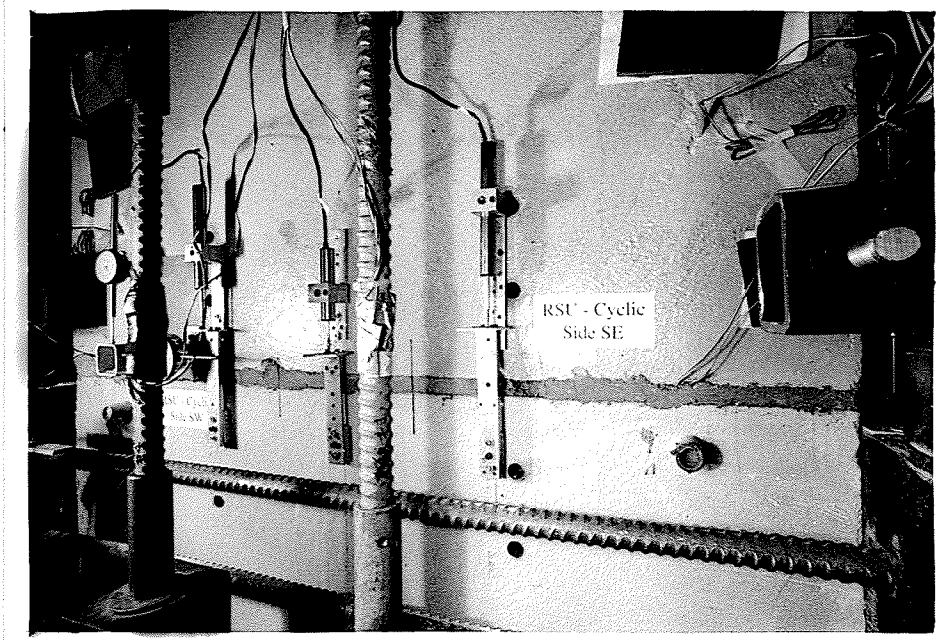

Figure 5.65(a) Condition of connection for specimen RSU: at start

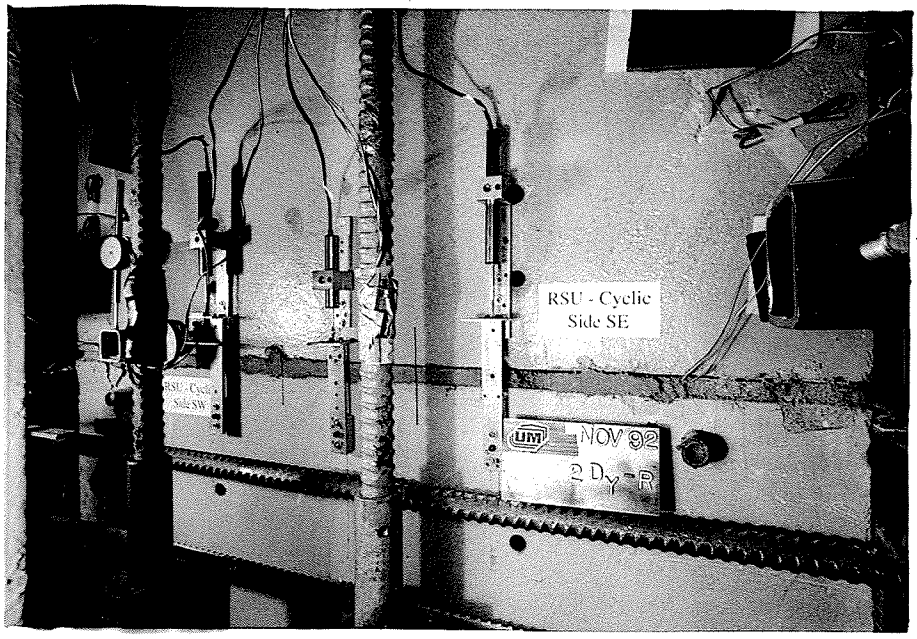

Figure 5.65(b) Condition of connection for specimen RSU: at 2Dy

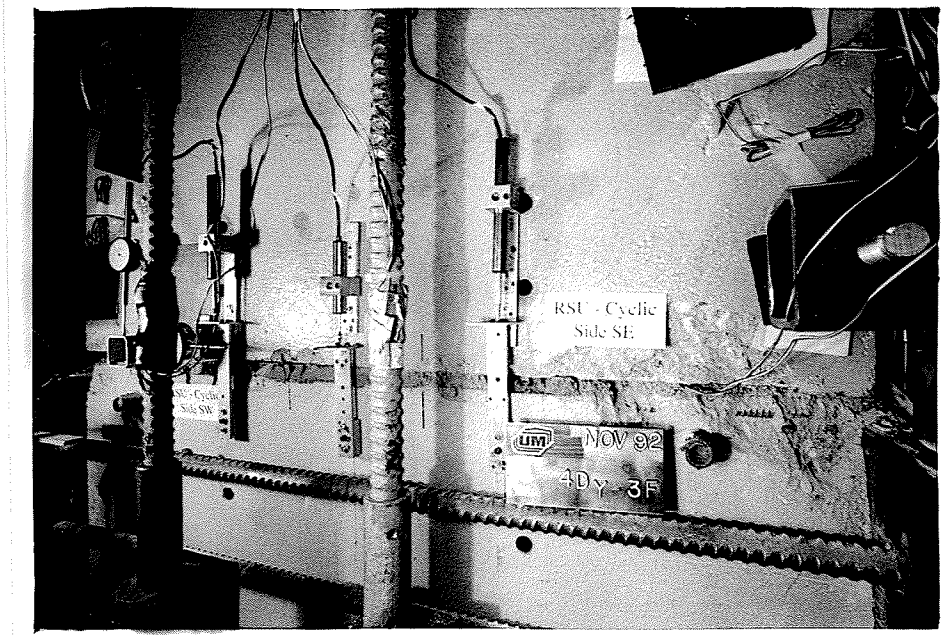

Figure 5.65(c) Condition of connection for specimen RSU: at 4Dy

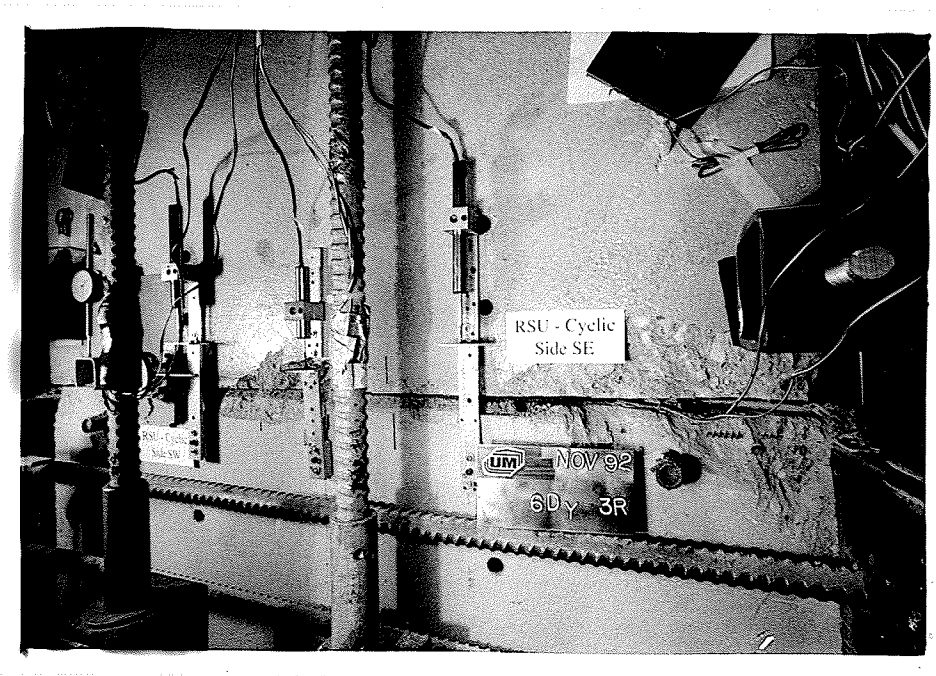

Figure 5.65(d) Condition of connection for specimen RSU: at 6Dy (failure)

Figure 5.65(e) Condition of connection for specimen RSU: post-failure outside frame

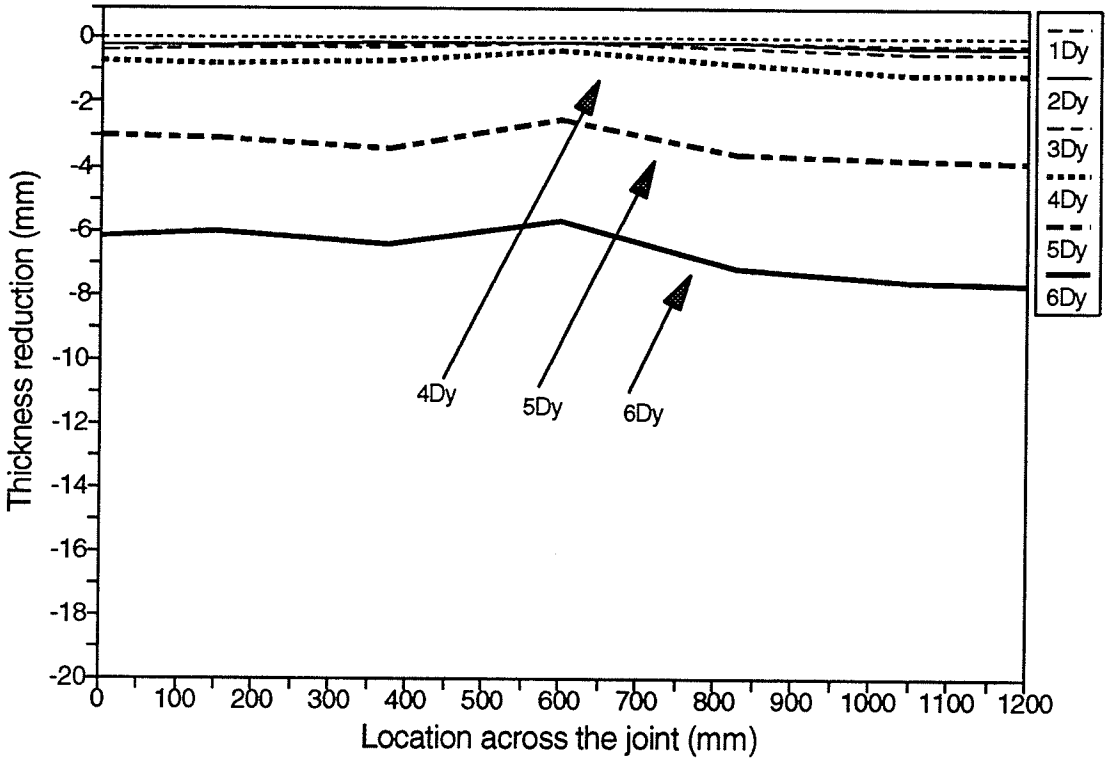

Figure 5.66(a) Rocking mechanism for specimen RSU: drypack thickness reduction

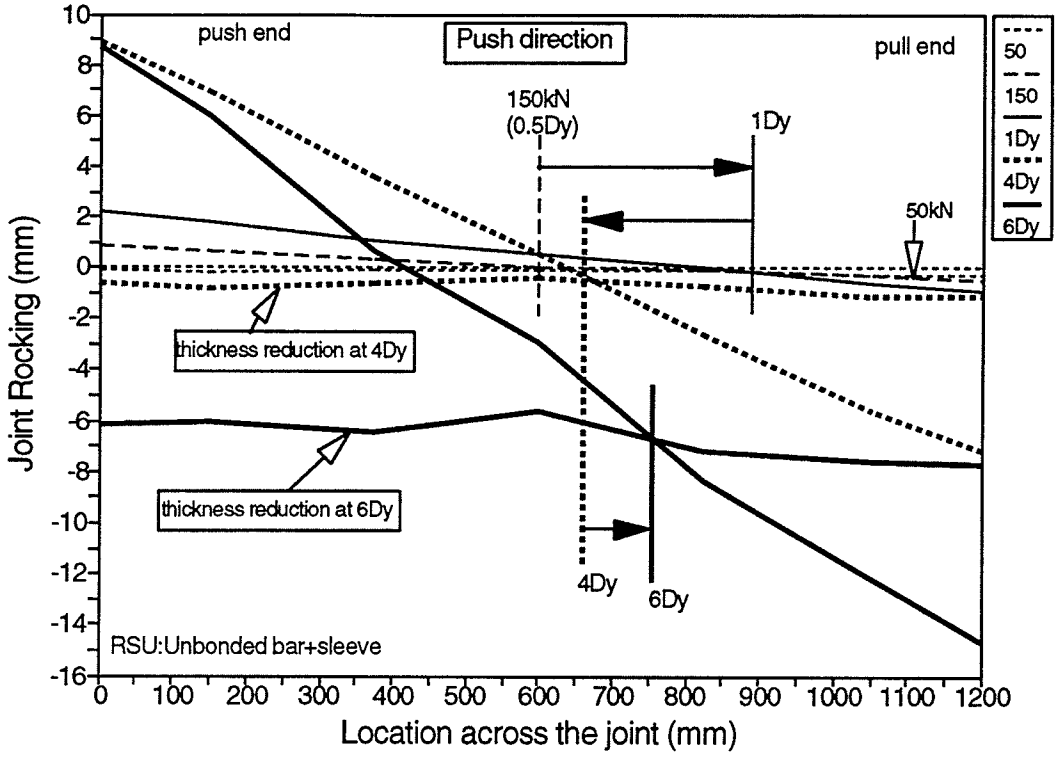

Figure 5.66(b) Rocking behaviour for specimen RSU: push direction

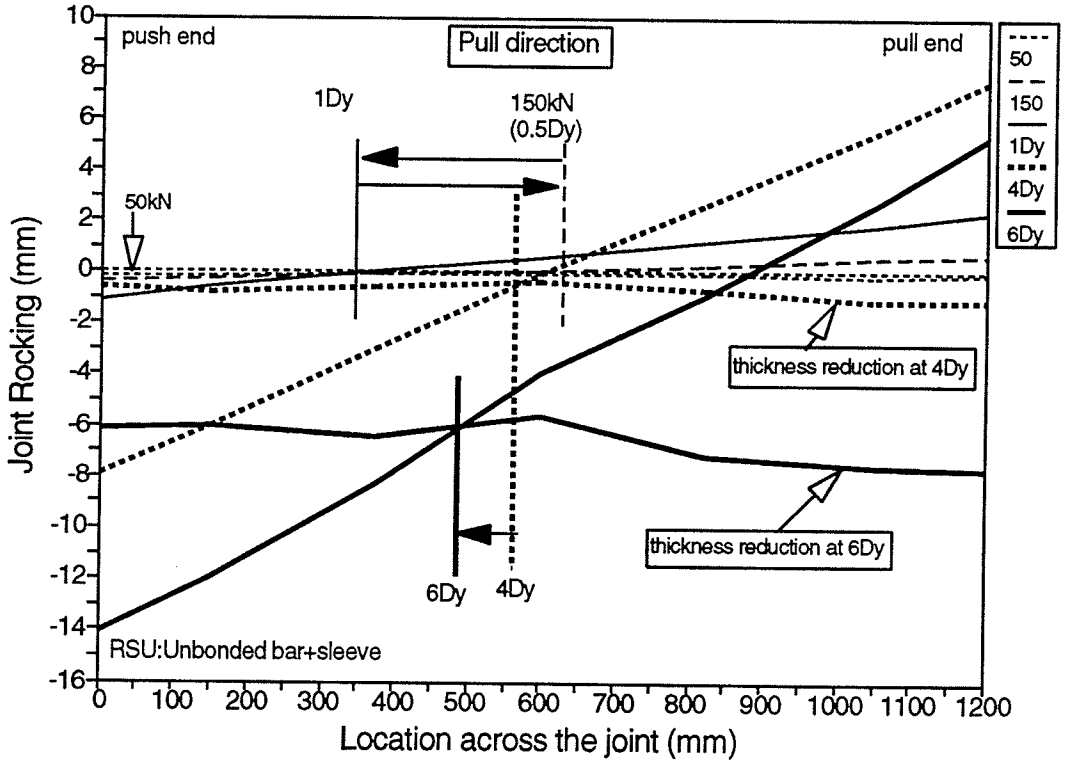

Figure 5.66(c) Rocking behaviour for specimen RSU: pull direction

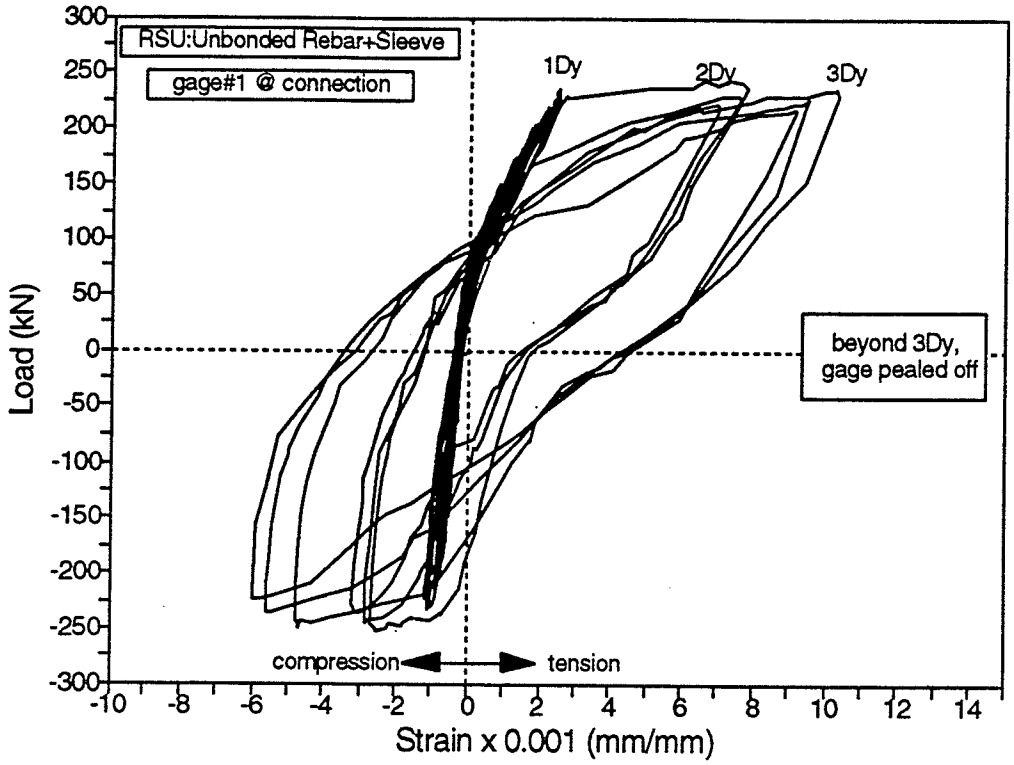

Figure 5.67(a) West bar strain gage #1 at connection push-end for specimen RSU

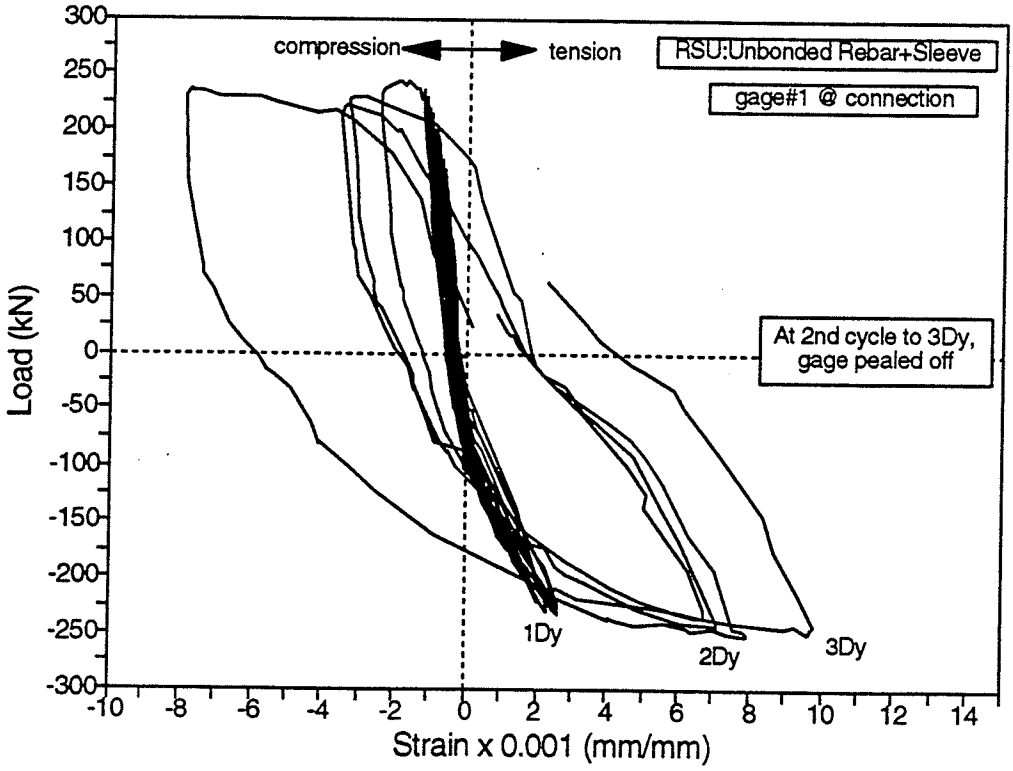

Figure 5.67(b) East bar strain gage #1 at connection pull-end for specimen RSU

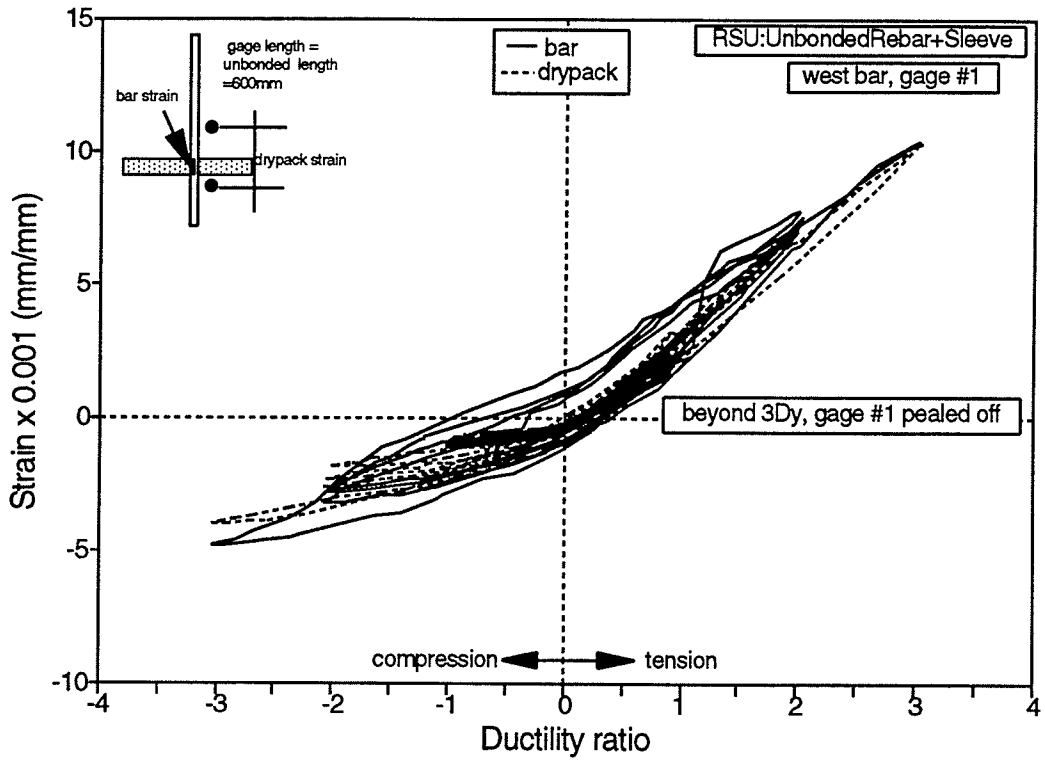

Figure 5.68(a) Comparison of west bar and drypack strain at joint for specimen RSU

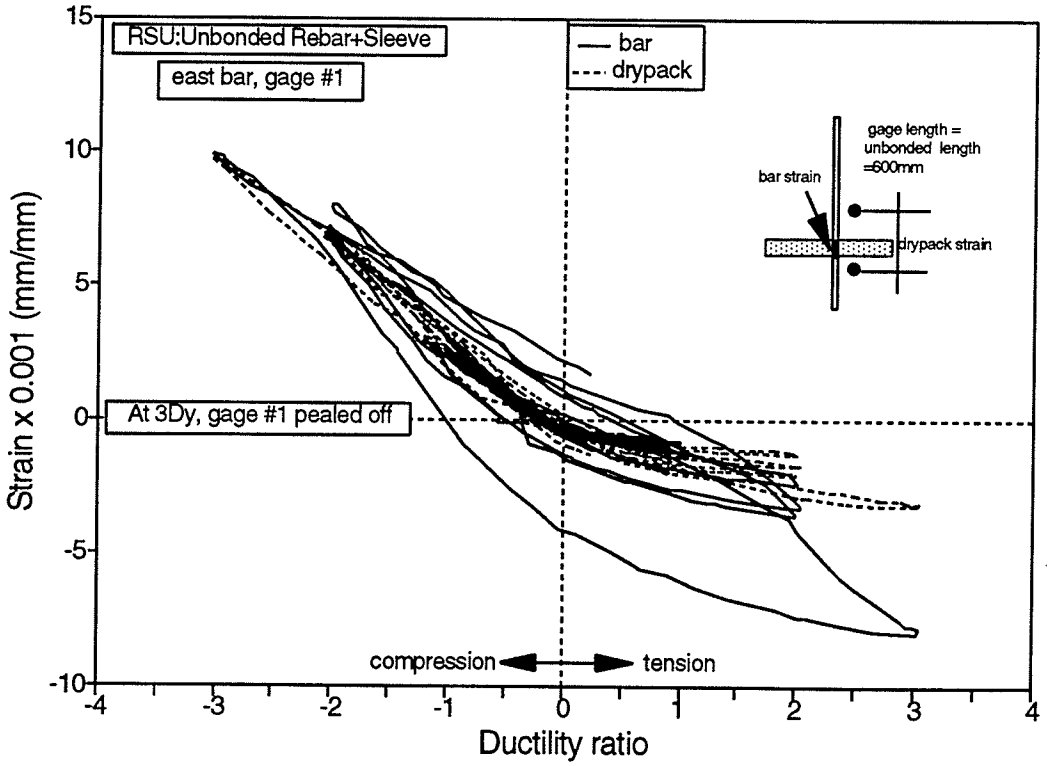

Figure 5.68(b) Comparison of east bar and drypack strain at joint for specimen RSU

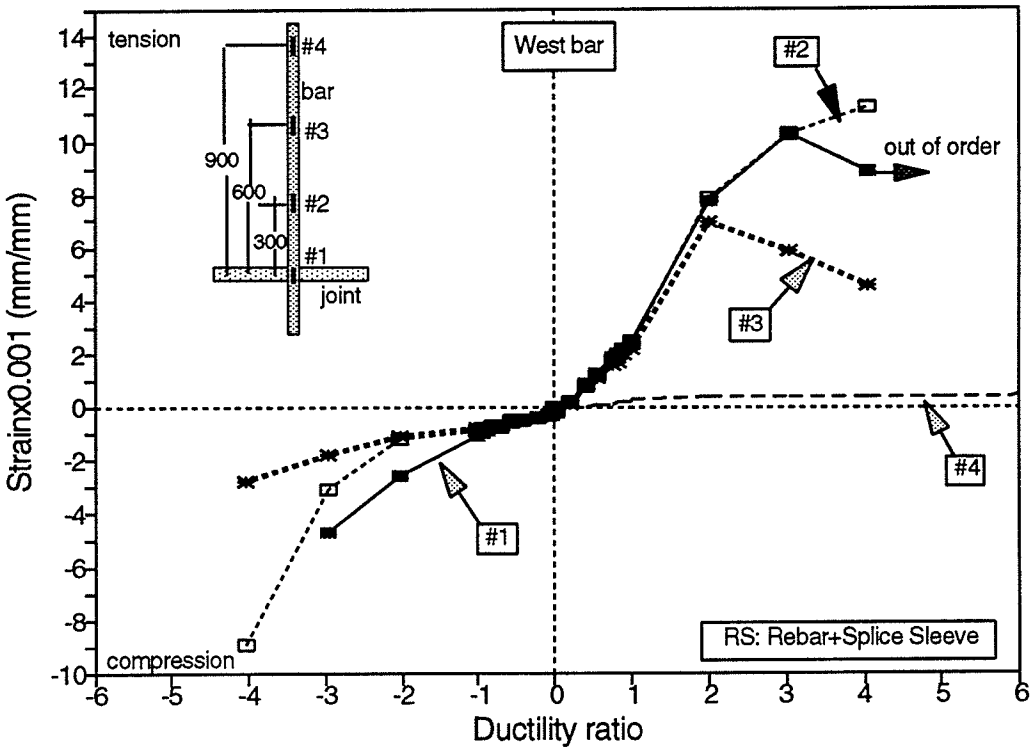

Figure 5.69(a) West bar strain at gages #1through #4 for specimen RSU

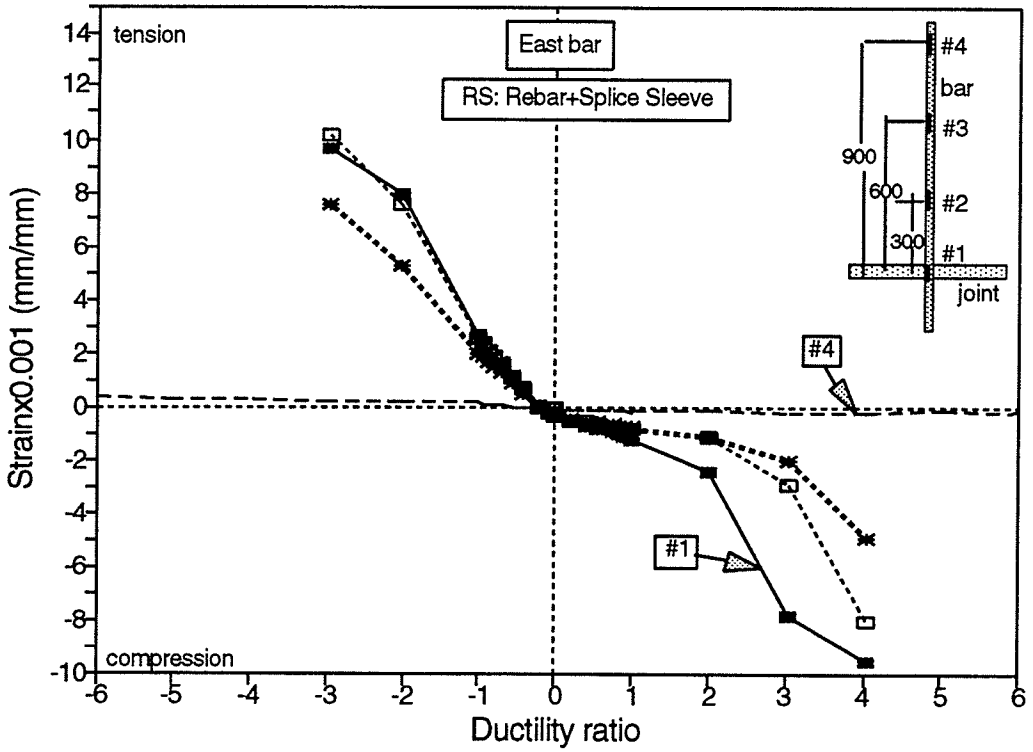

Figure 5.69(b) East bar strain at gages #1through #4 for specimen RSU

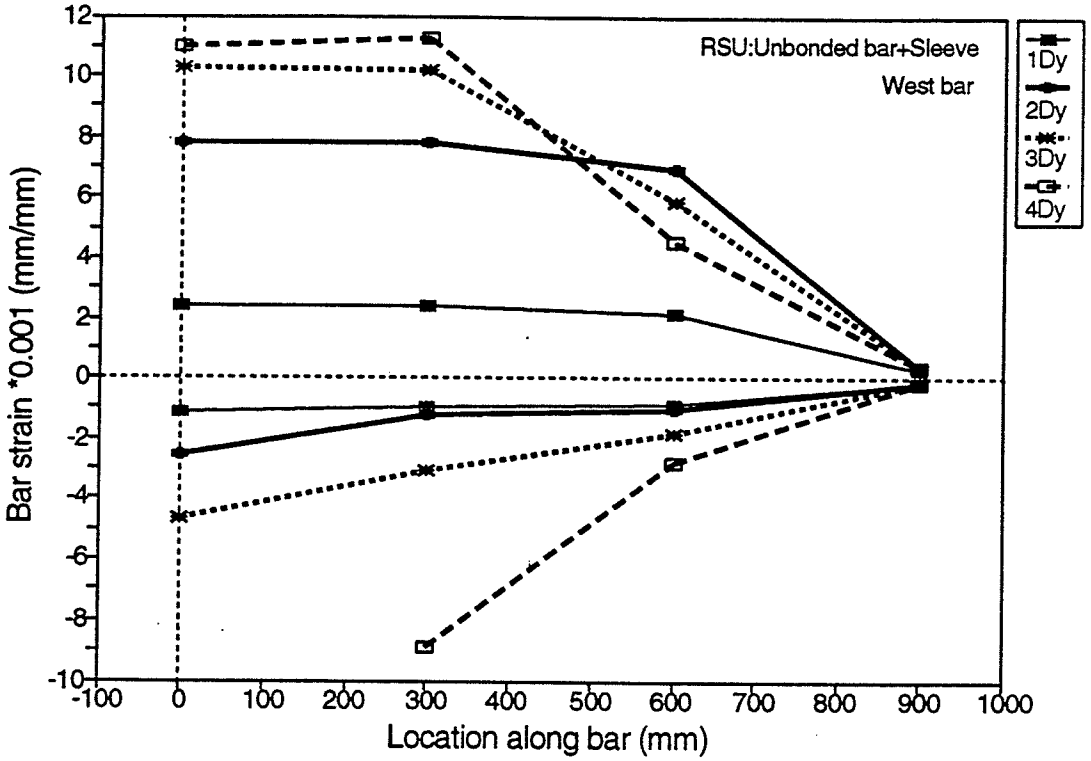

Figure 5.70(a) Extent of yield for specimen RSU at 1, 2, 3 and 4Dy: west bar

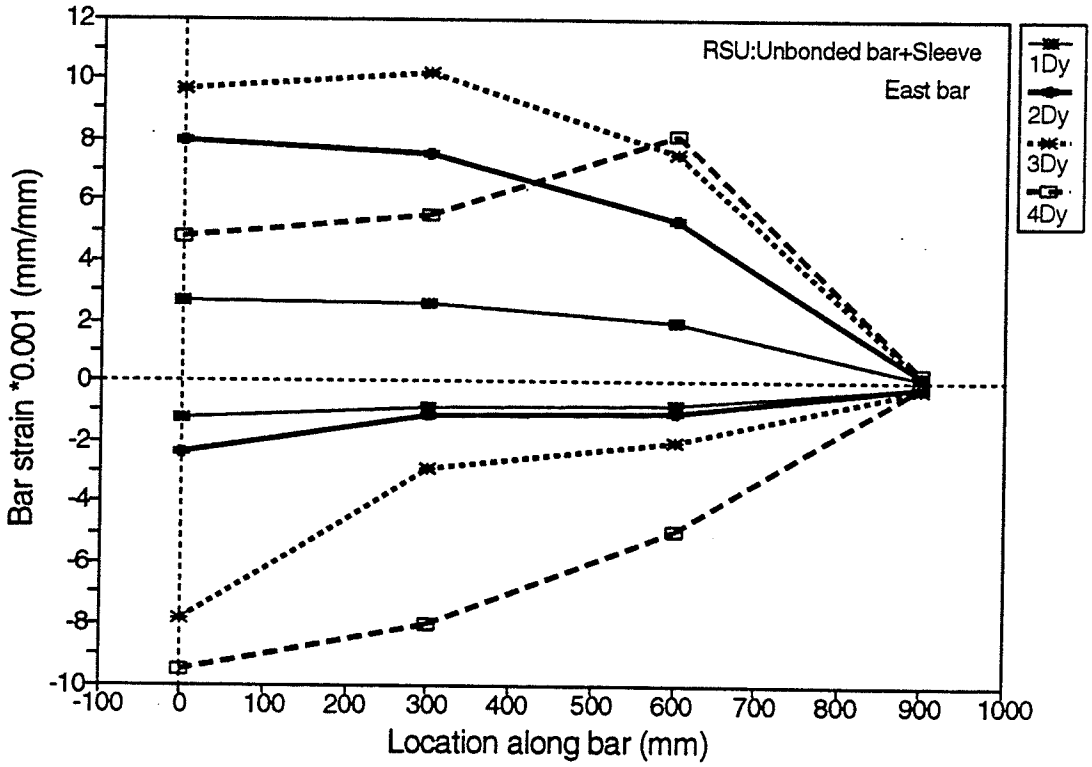

Figure 5.70(b) Extent of yield for specimen RSU at 1, 2, 3 and 4Dy: east bar

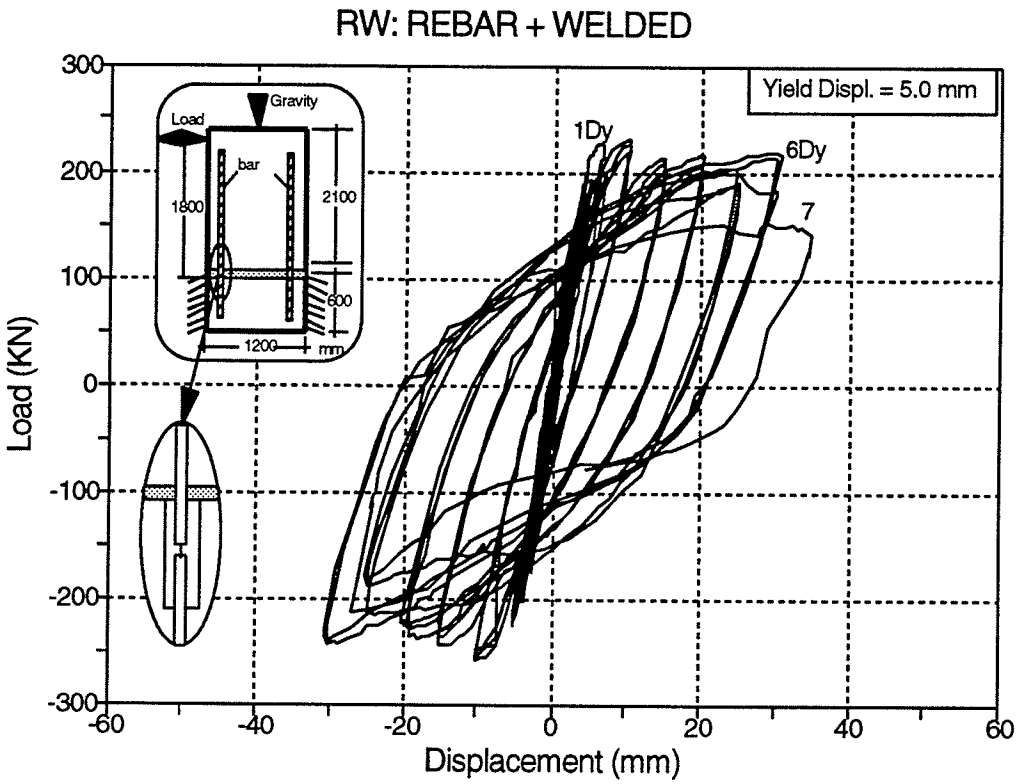

Figure 5.71(a) Hysteresis loops of load versus displacement behaviour for specimen RW

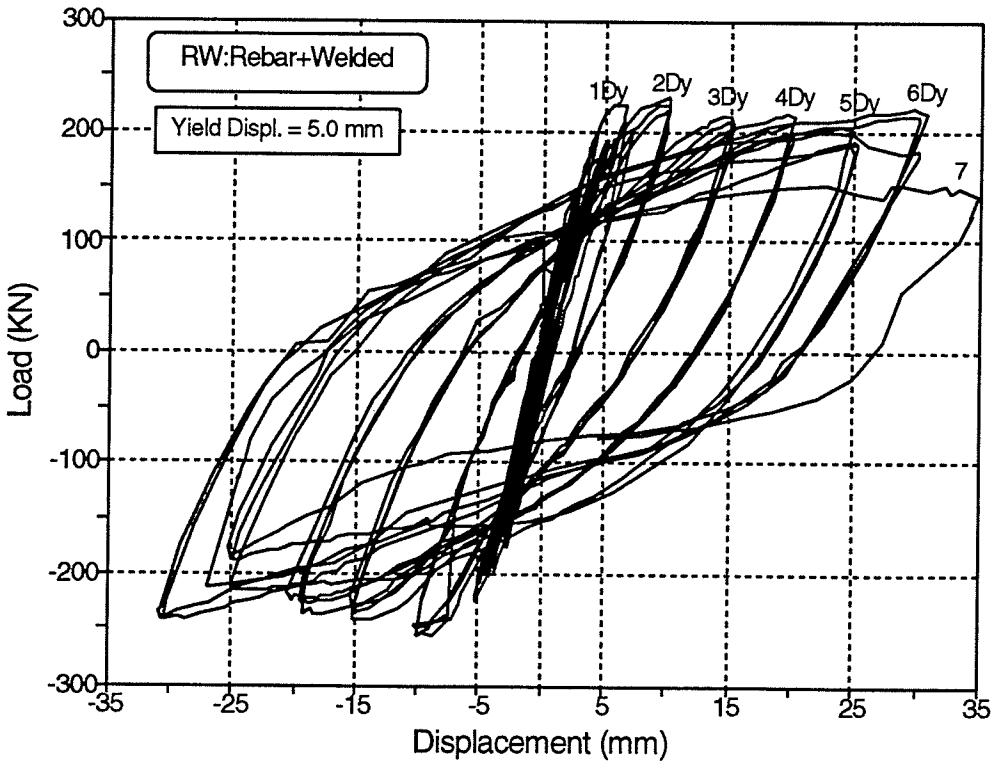

Figure 5.71(b) Magnified hysteresis loops of load vs. displacement for specimen RW

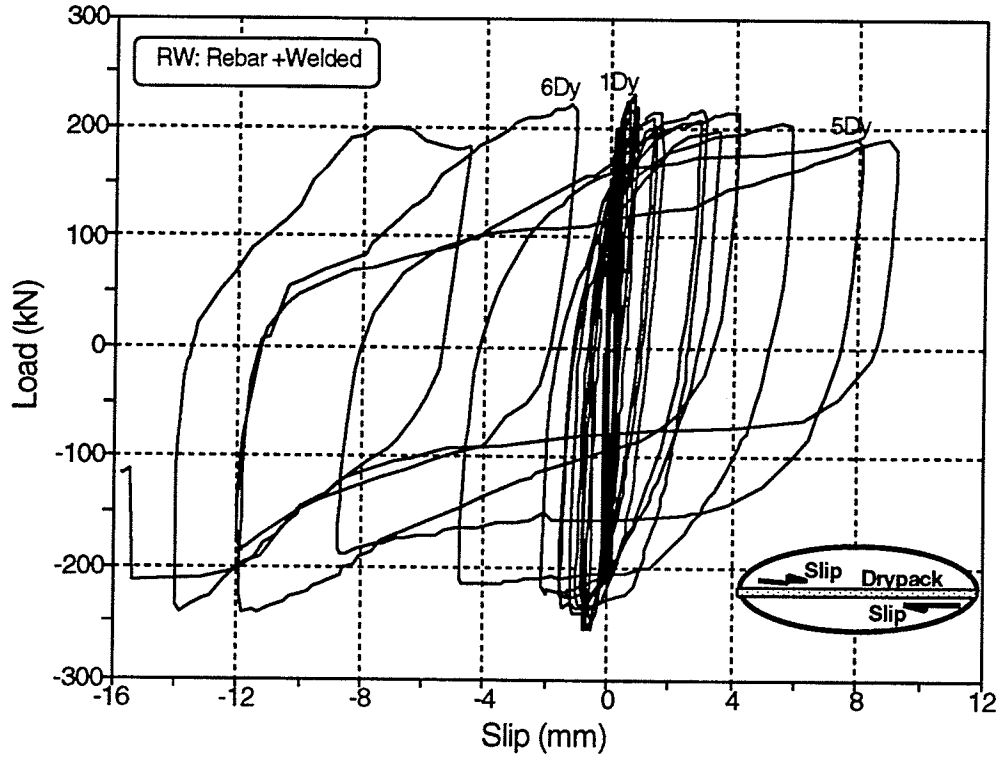

Figure 5.72(a) Hysteresis loops of load vs. horizontal slip behaviour for specimen RW

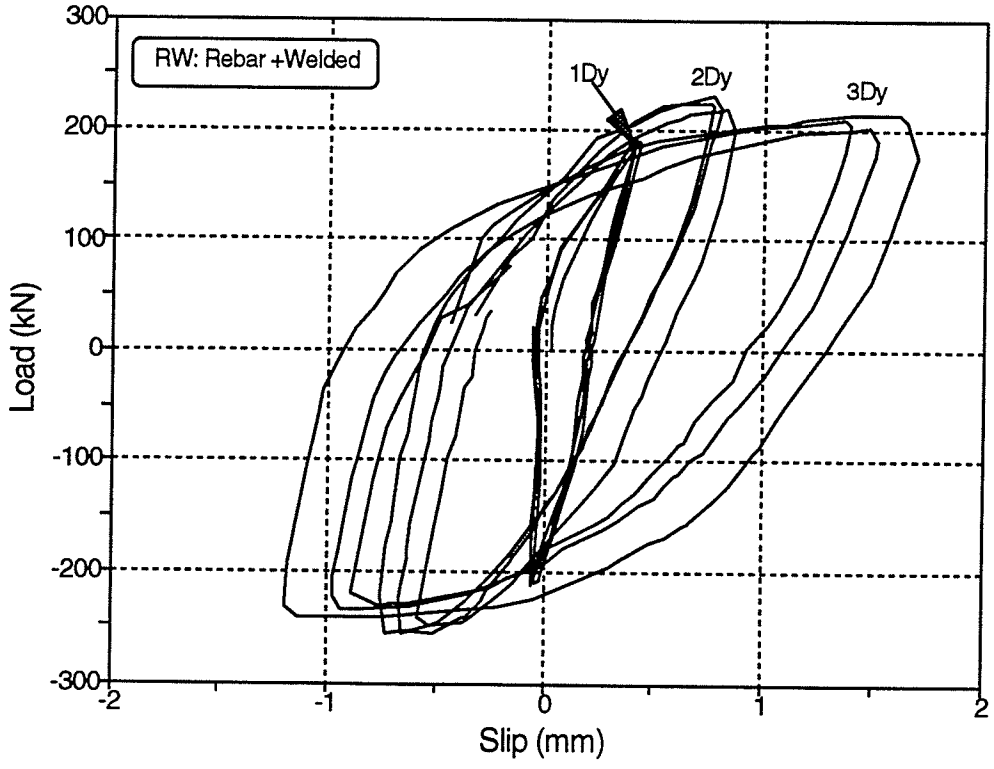

Figure 5.72(b) Slip behaviour at cycles to 1, 2 and 3Dy for specimen RW

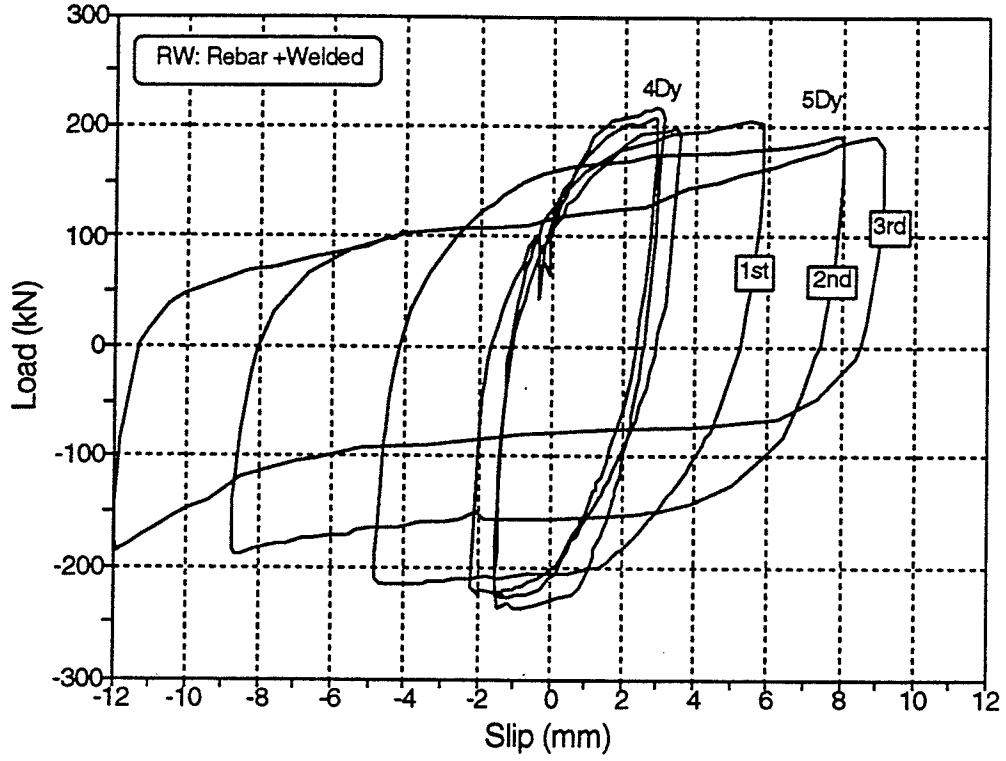

Figure 5.72(c) Slip behaviour at cycles to 4 and 5Dy for specimen RW

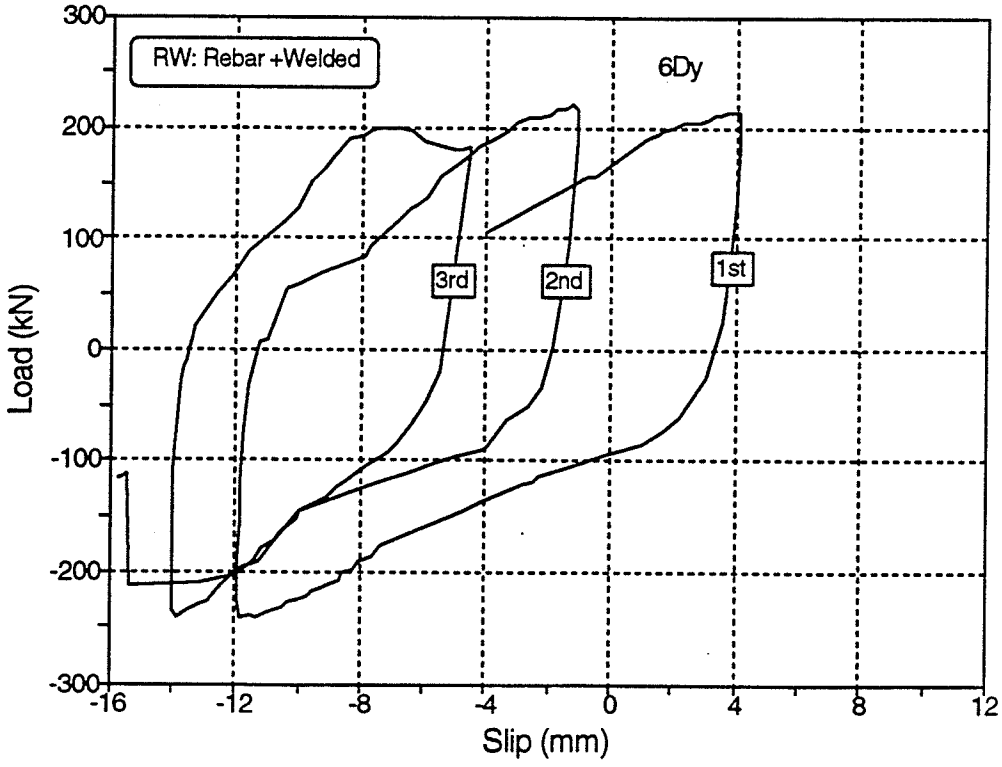

Figure 5.72(d) Slip behaviour at cycles to 6Dy for specimen RW

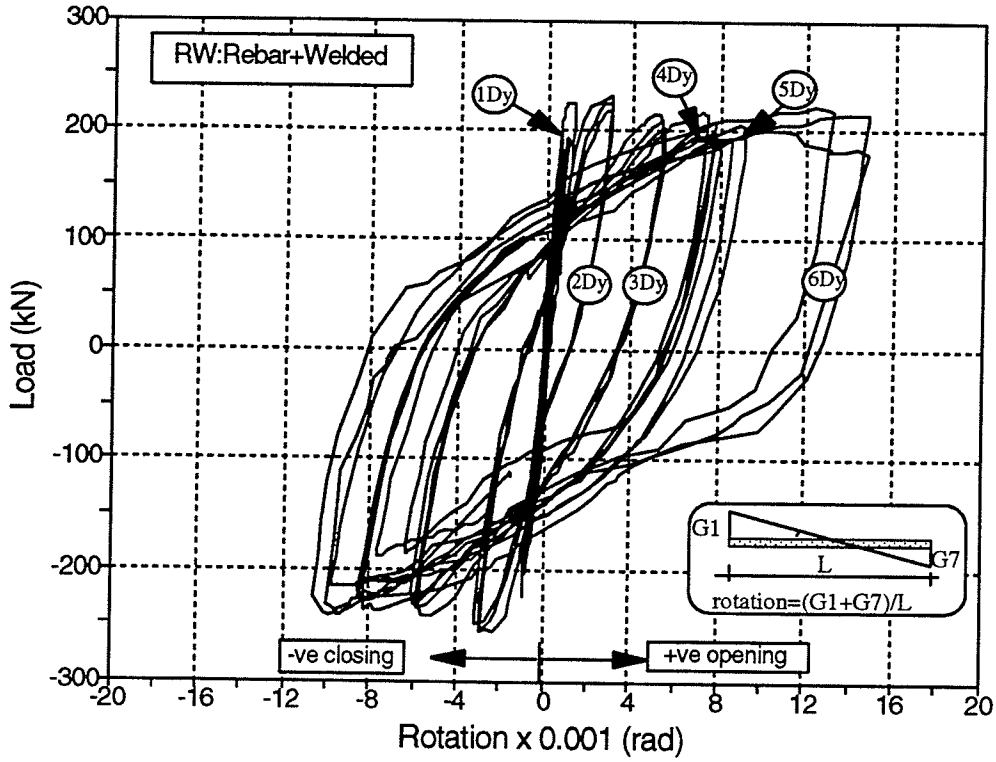

Figure 5.73 Hysteresis loops of load versus rotation for specimen RW

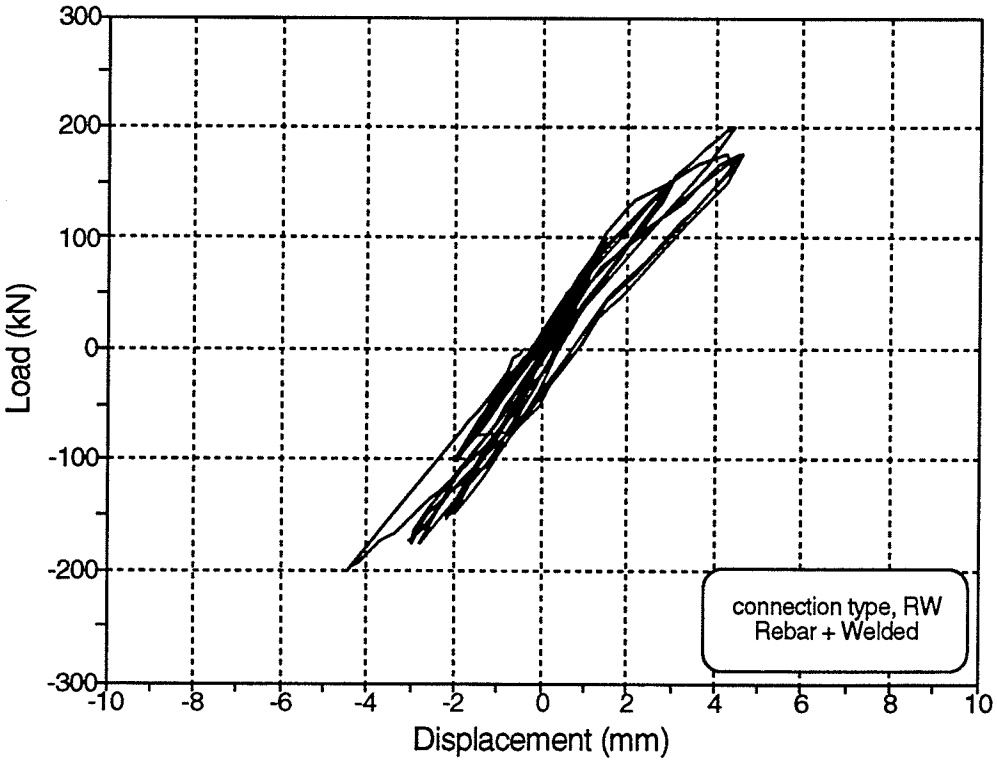

Figure 5.74 Elastic load-displacement behaviour for specimen RW

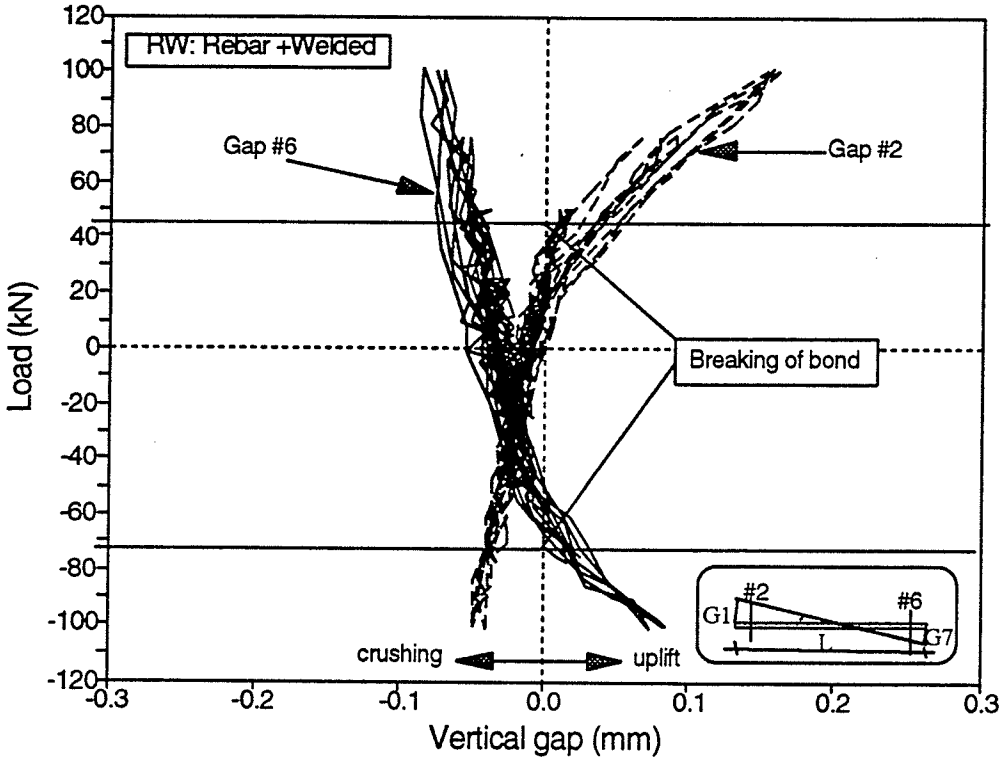

Figure 5.75 Onset of breaking of bond in load versus gap hysteresis for specimen RW

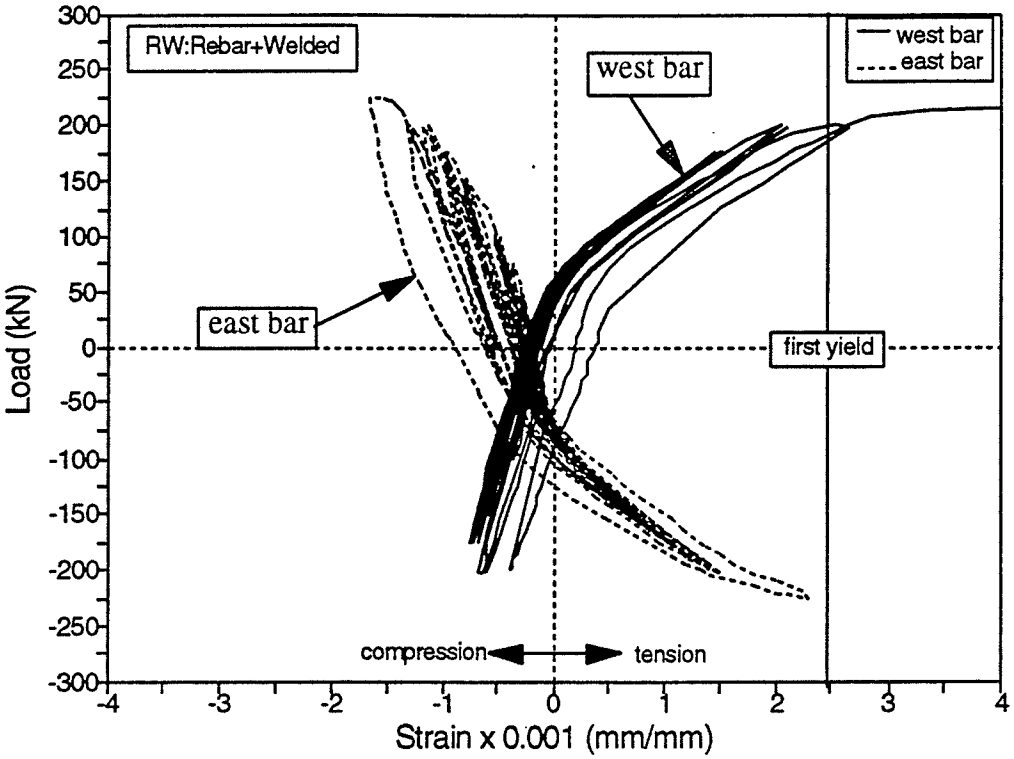

Figure 5.76 Onset of yield in load-bar strain relationship for specimen RW

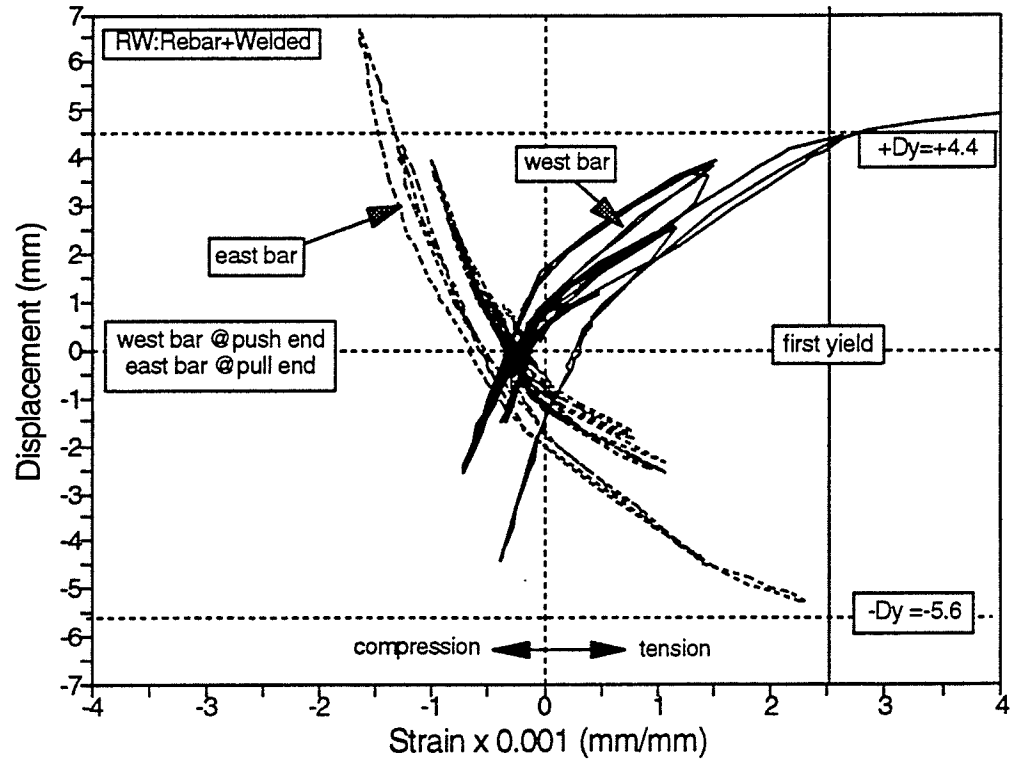

Figure 5.77 Onset of yield in bar strain-displacement relationship for specimen RW

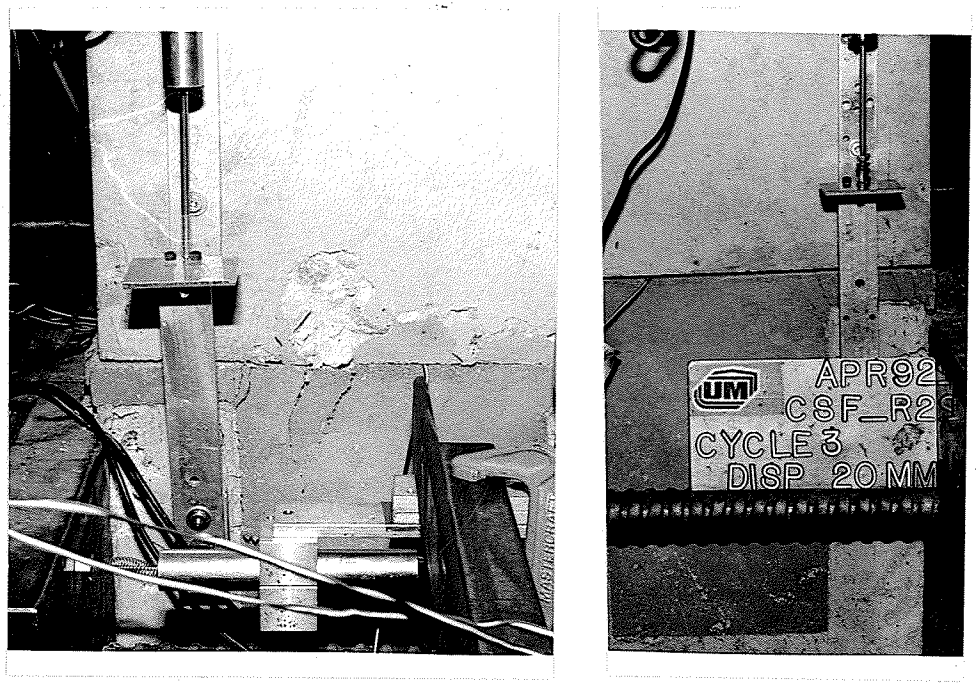

Figure 5.78(a) Condition of connection for specimen RW: at 2Dy

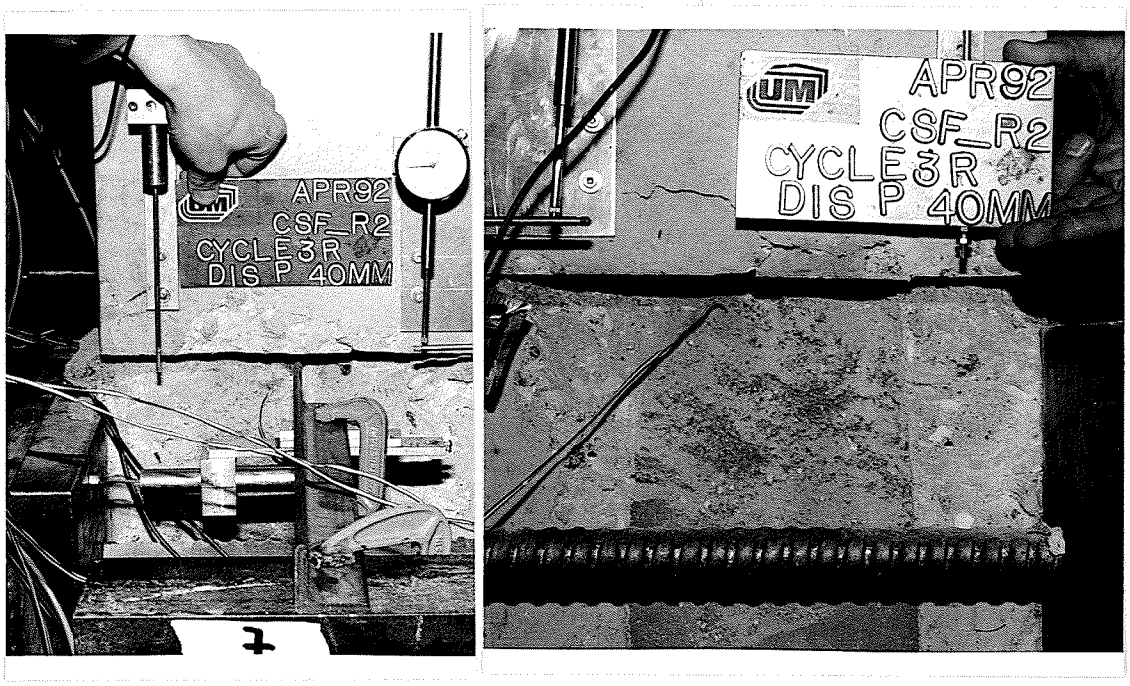

Figure 5.78(b) Condition of connection for specimen RW: at 4Dy

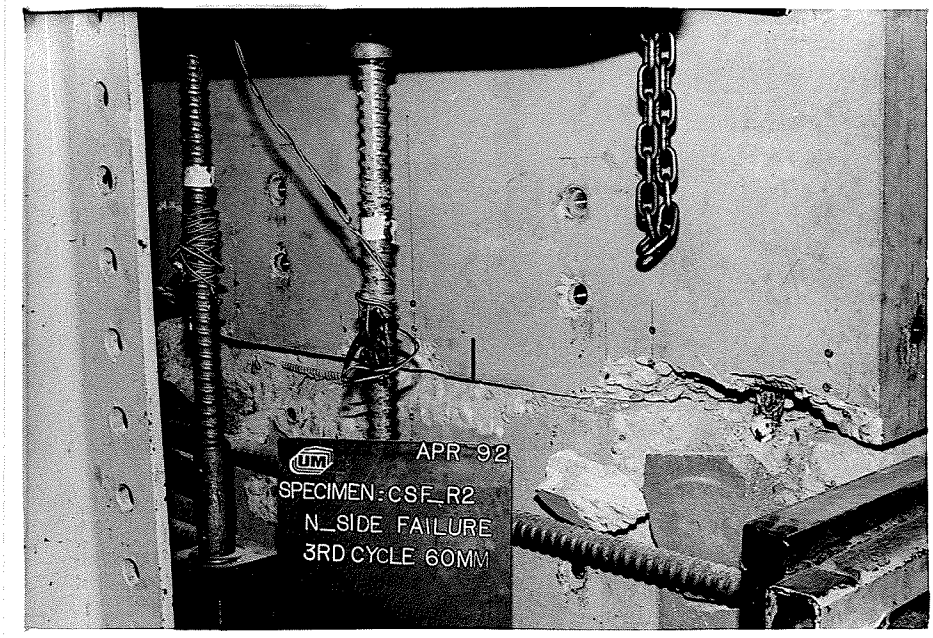

Figure 5.78(c) Condition of connection for specimen RW: at 6Dy (failure)

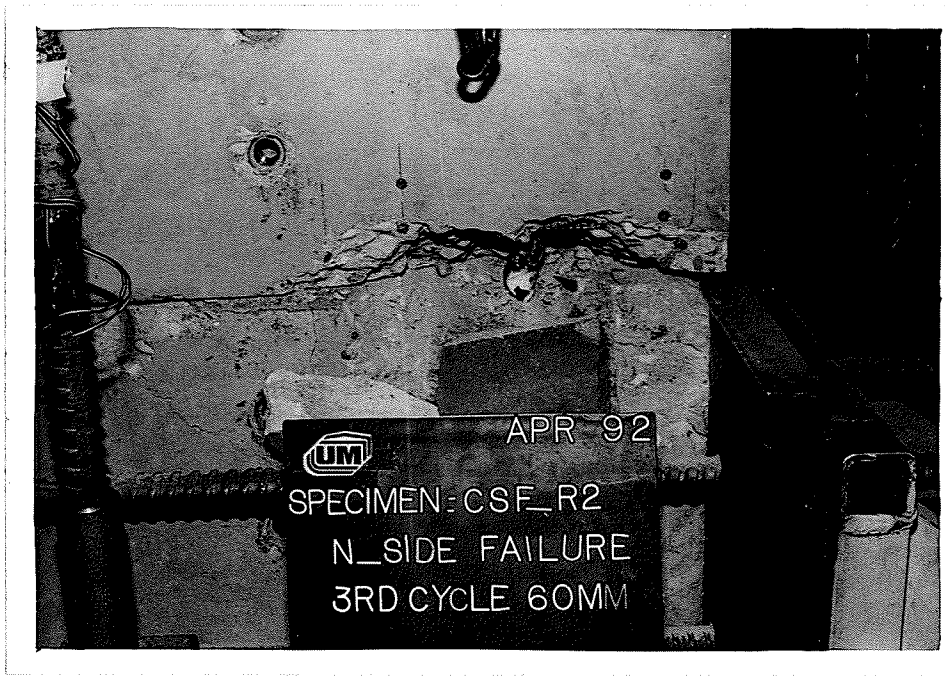

Figure 5.78(d) Condition of connection for specimen RW: buckling of bar (closeup)

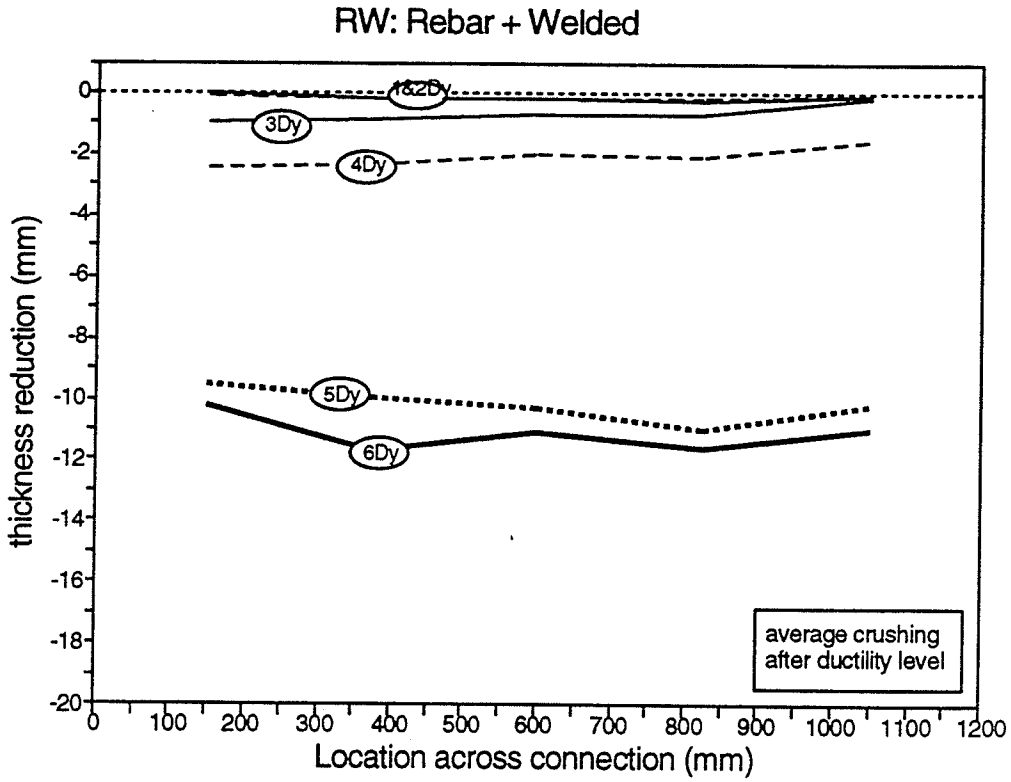

Figure 5.79(a) Rocking mechanism for specimen RW: drypack thickness reduction

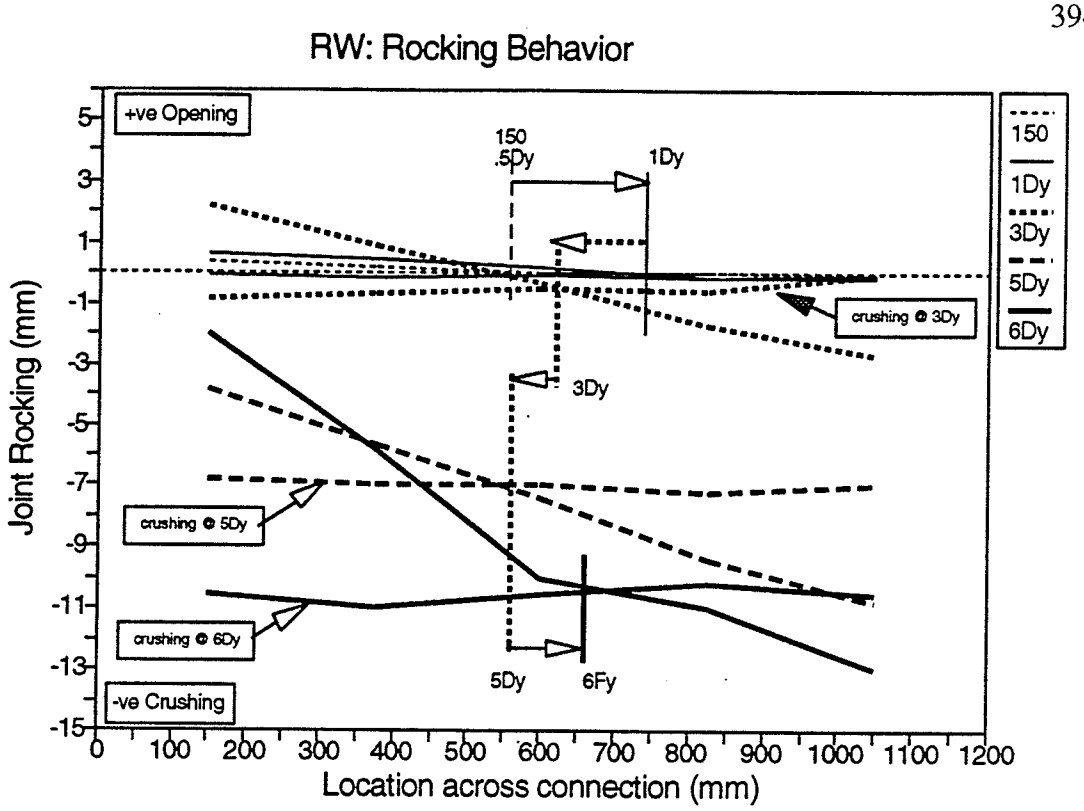

Figure 5.79(b) Rocking behaviour for specimen RW: push direction

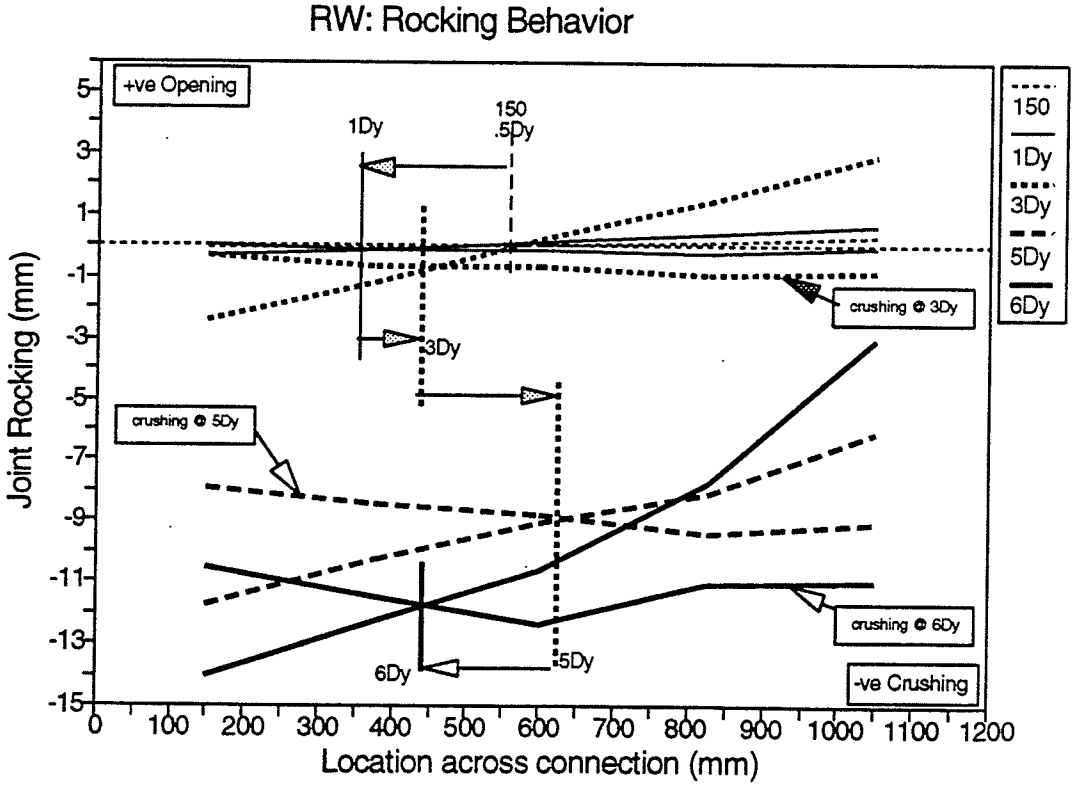

Figure 5.79(c) Rocking behaviour for specimen RW: pull direction

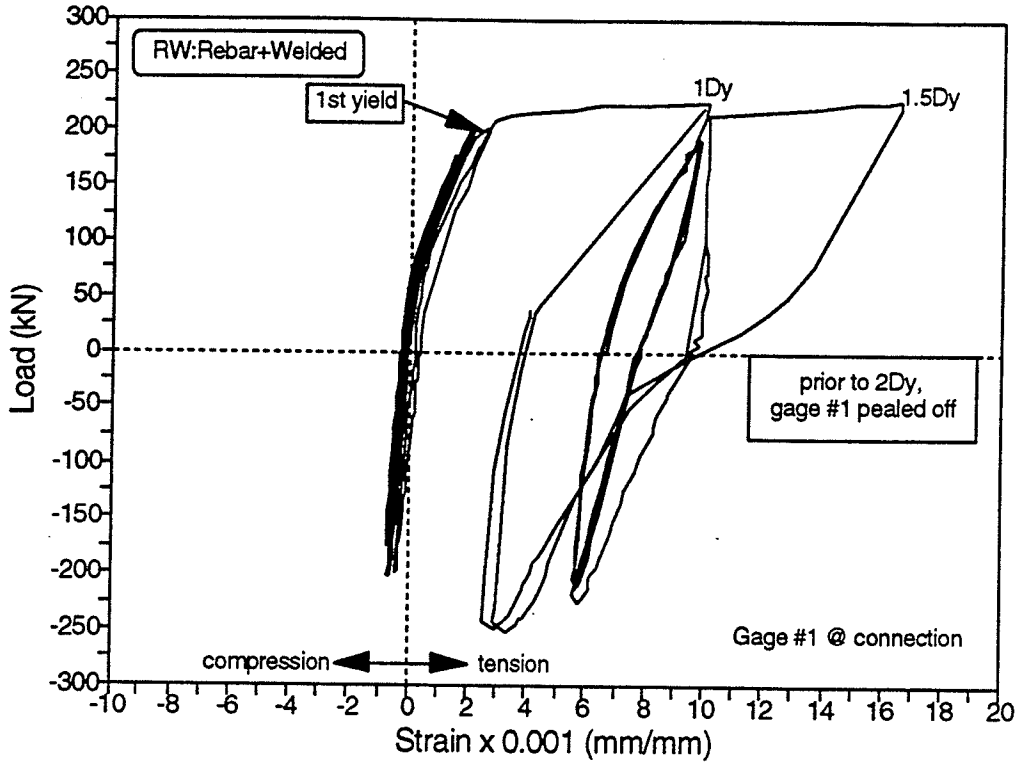

Figure 5.80(a) West bar strain gage #1 at connection push-end for specimen RW

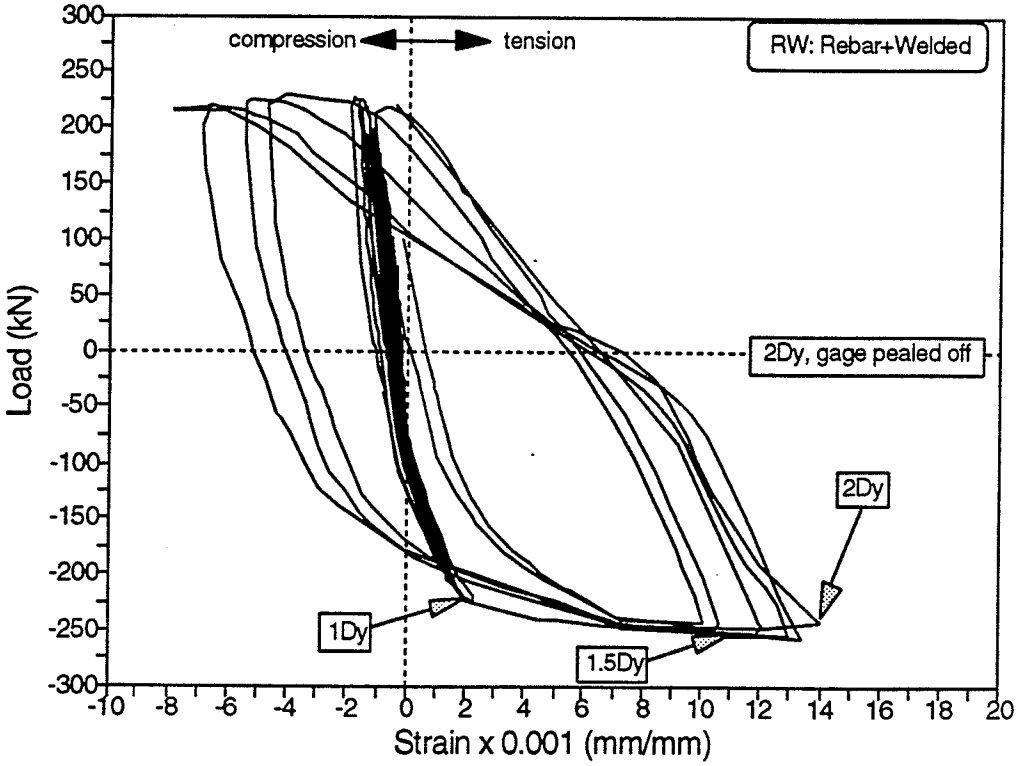

Figure 5.80(b) East bar strain gage #1 at connection pull-end for specimen RW

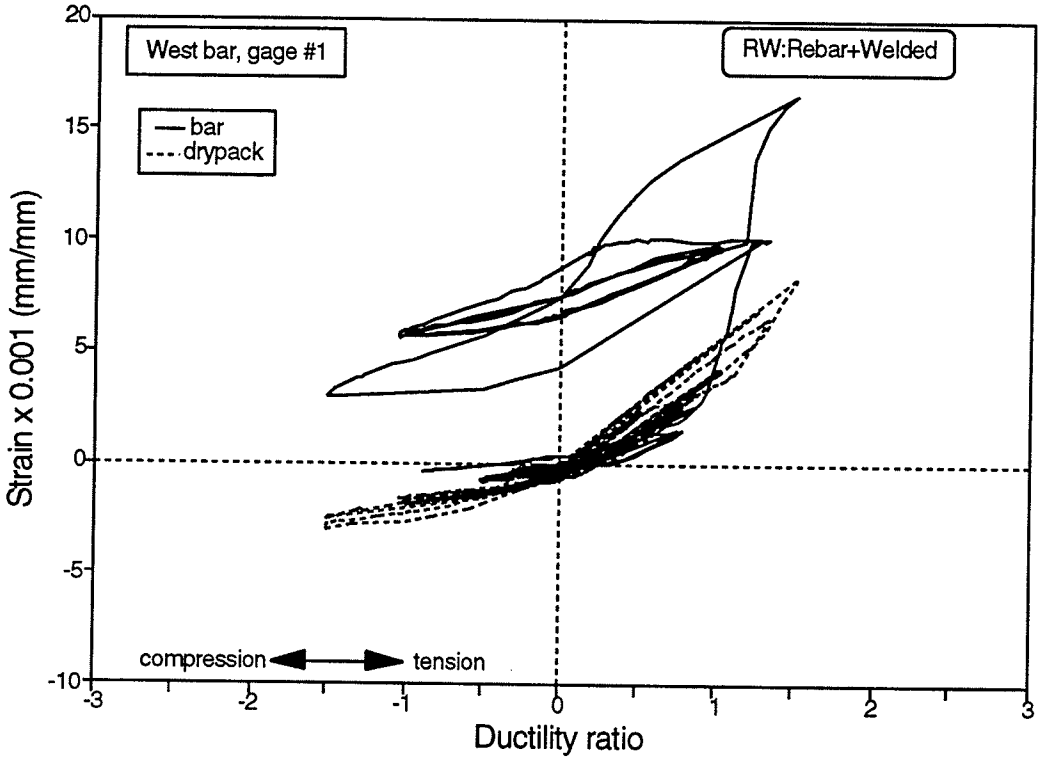

Figure 5.81(a) Comparison of west bar and drypack strain at joint for specimen RW

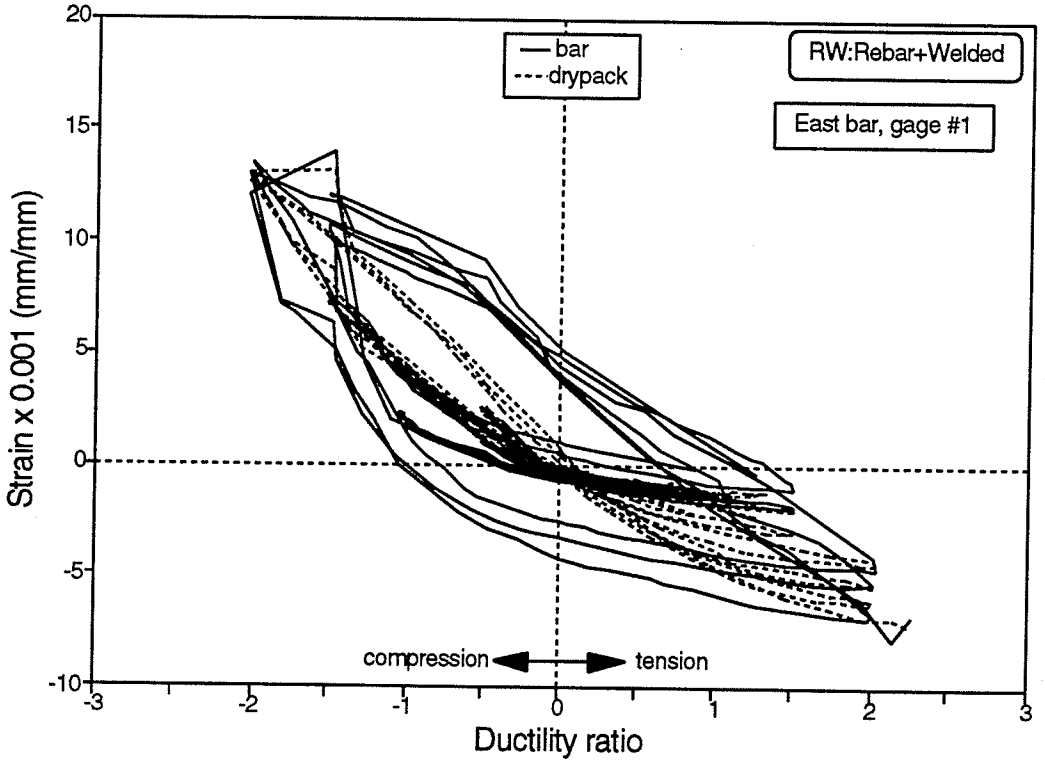

Figure 5.81(b) Comparison of east bar and drypack strain at joint for specimen RW

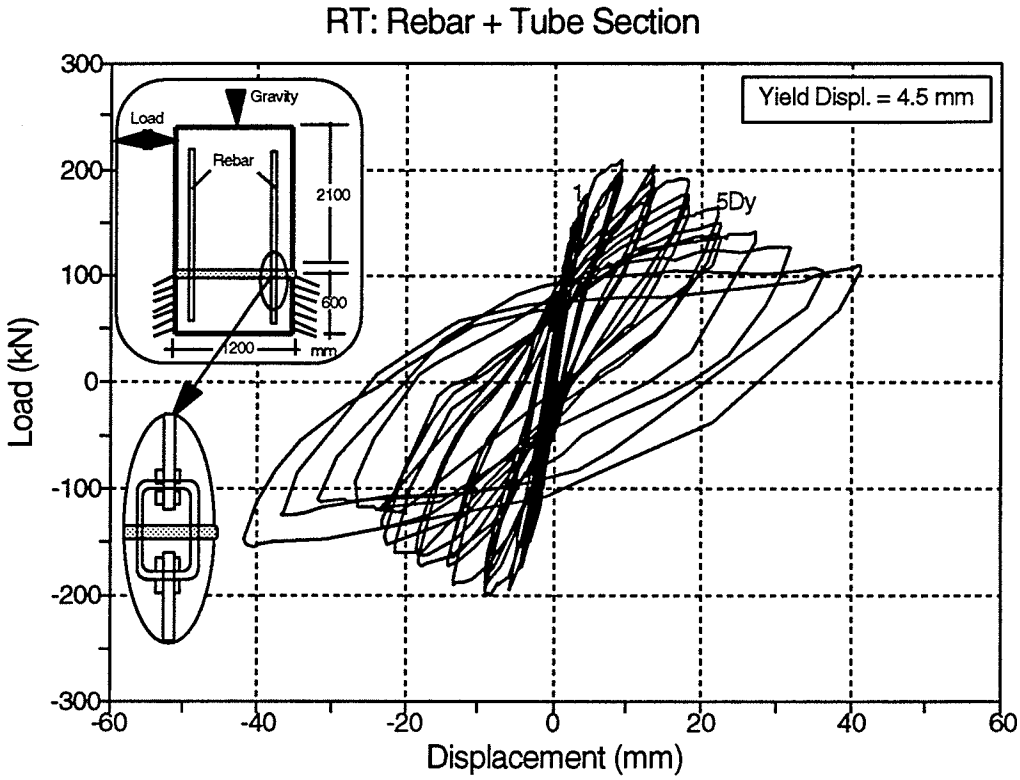

Figure 5.82(a) Hysteresis loops of load vs. displacement relationship for specimen RT

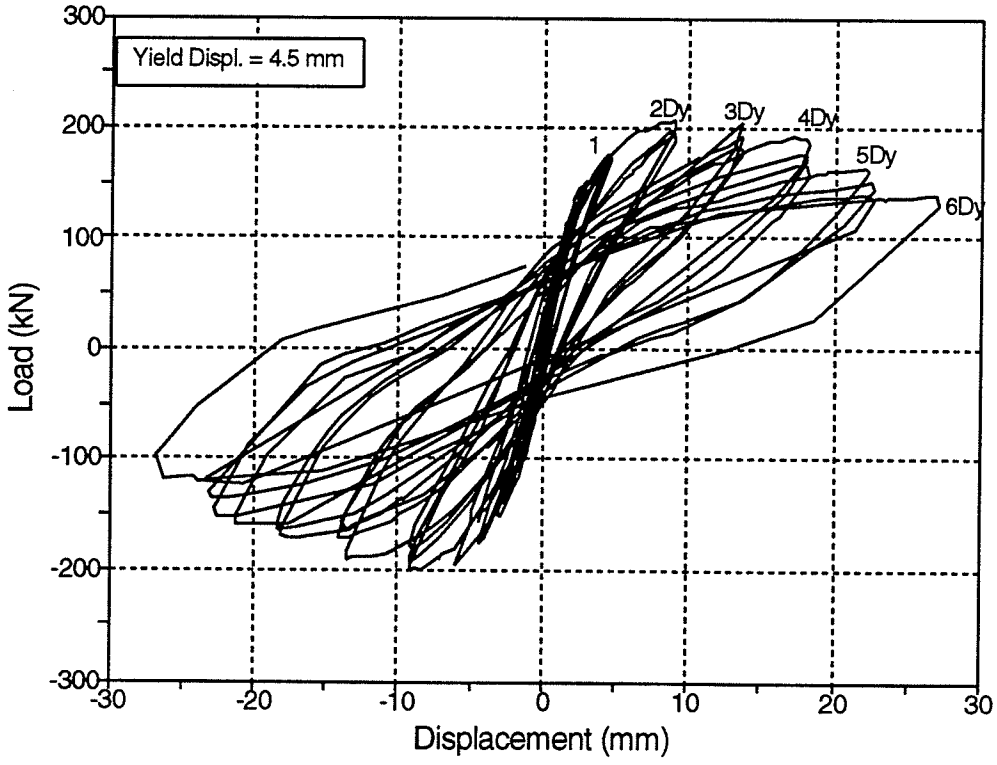

Figure 5.82(b) Magnified hysteresis loops of load vs. displacement for specimen RT

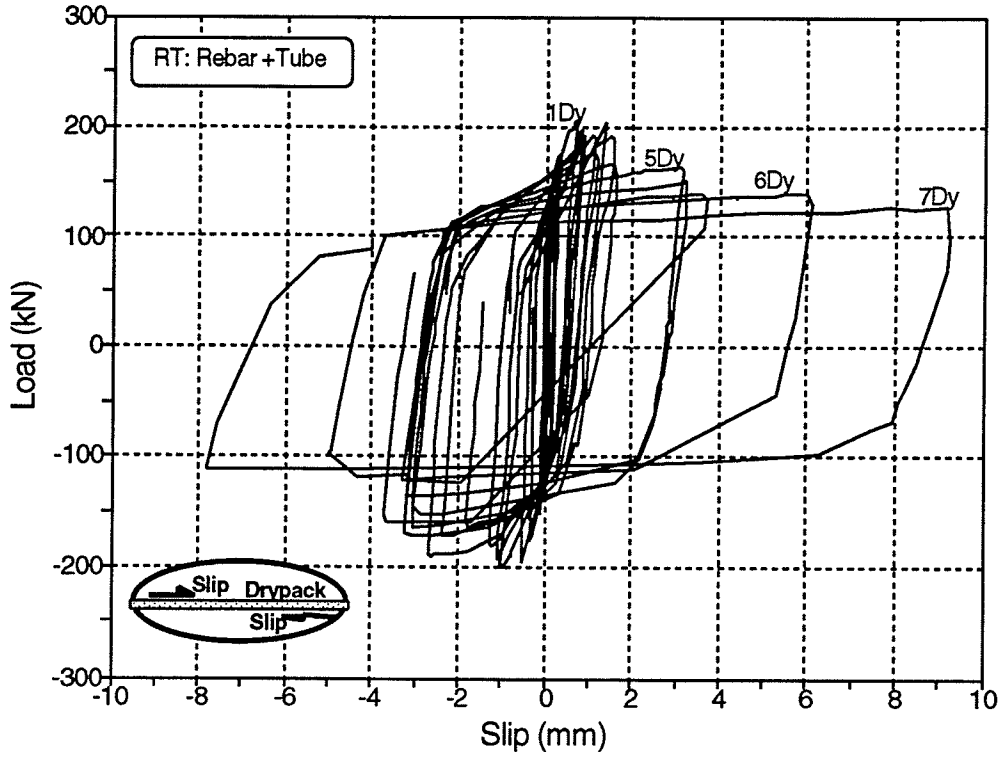

Figure 5.83(a) Hysteresis loops of load vs. horizontal slip behaviour for specimen RT

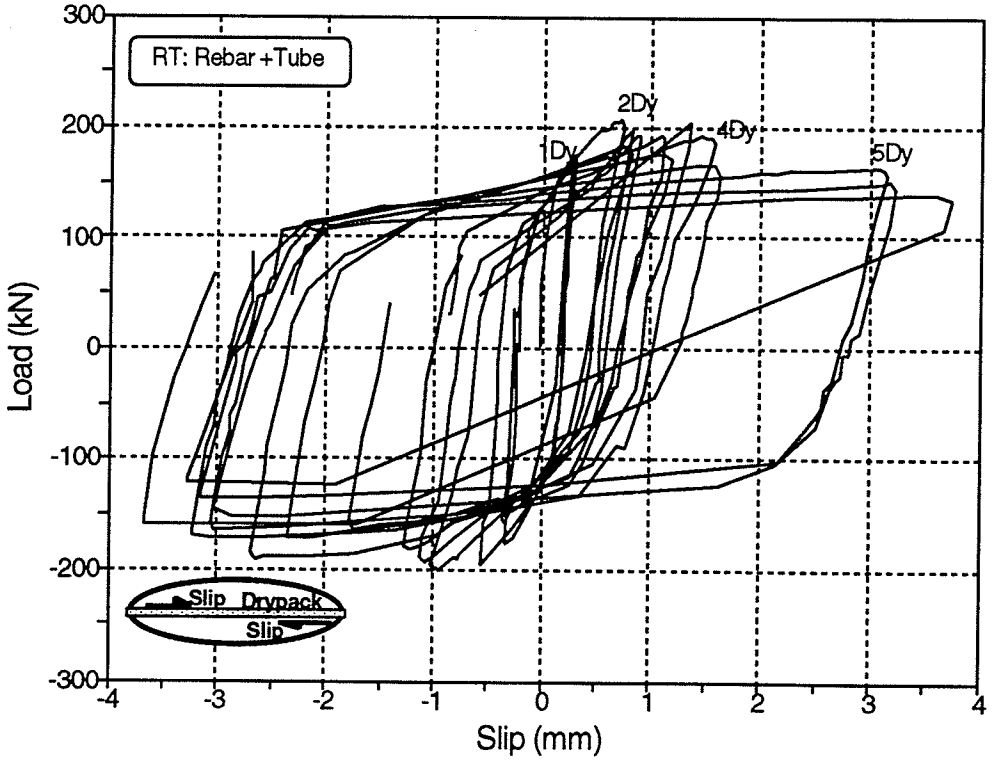

Figure 5.83(b) Magnified hysteresis loops of load vs. horizontal slip for specimen RT

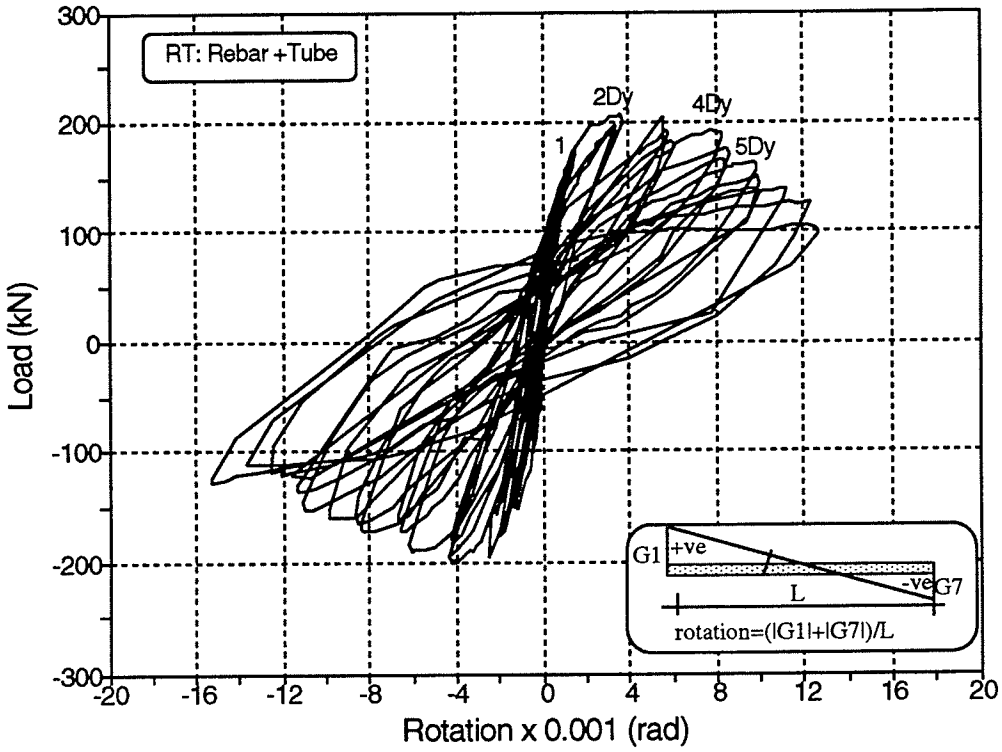

Figure 5.84 Hysteresis loops of load versus joint rotation for specimen RT

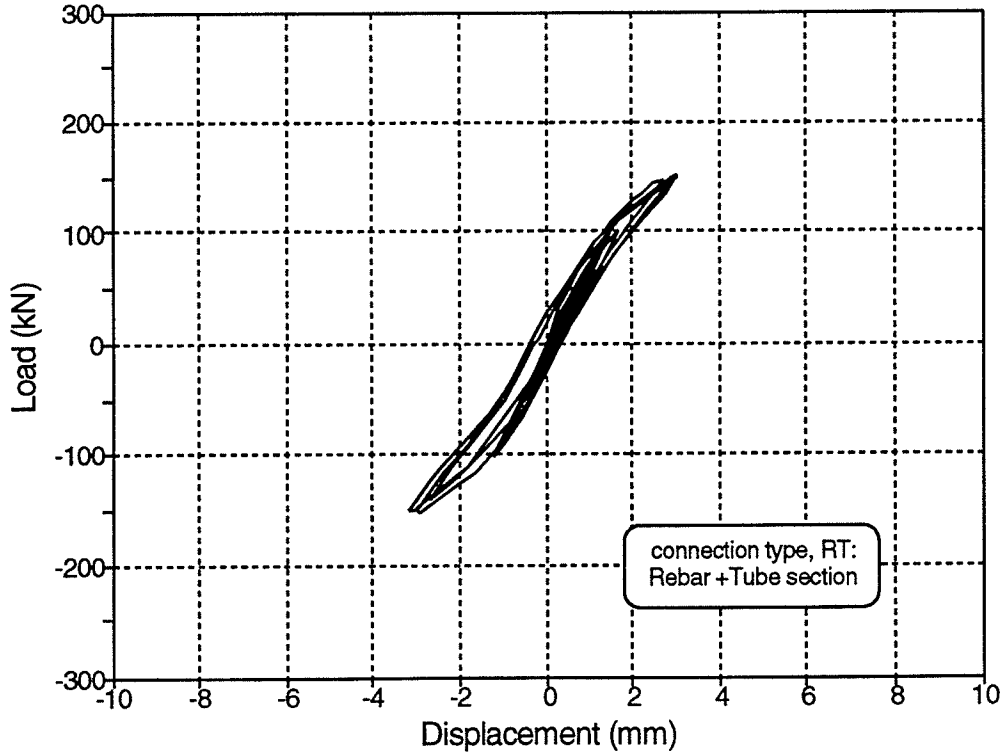

Figure 5.85 Elastic load-displacement behavior for specimen RT

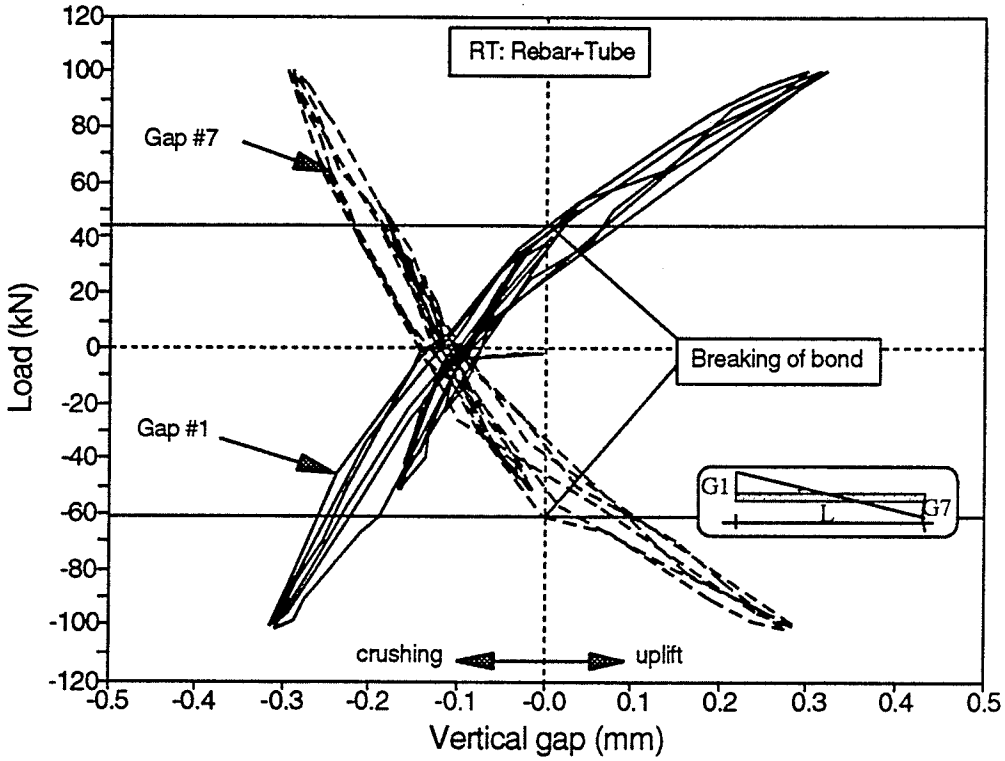

Figure 5.86 Onset of breaking of bond in load versus gap hysteresis for specimen RT

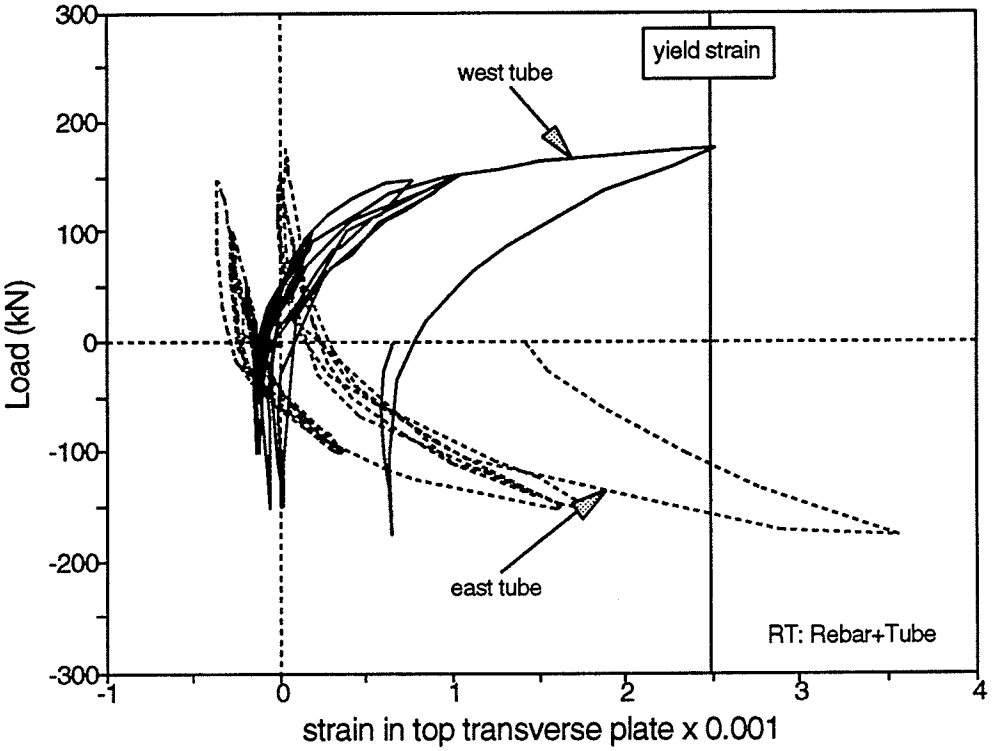

Figure 5.87 Onset of yield in load vs. top transverse plate strain for specimen RT

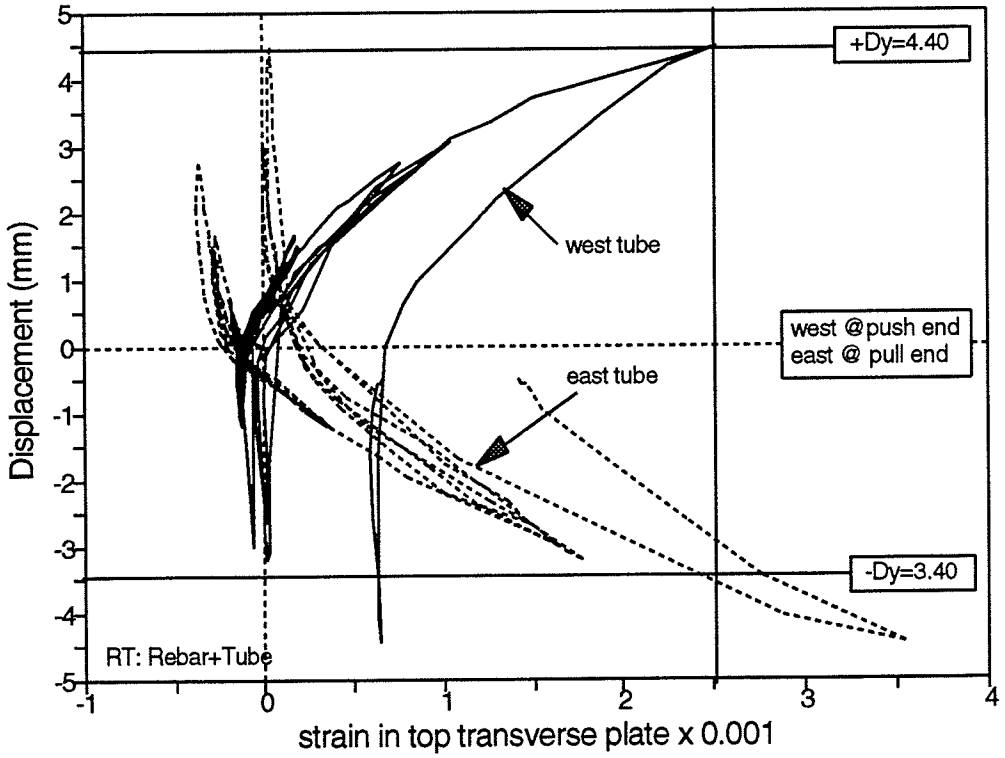

Figure 5.88 Onset of yield in transverse plate strain vs. displacement for specimen RT

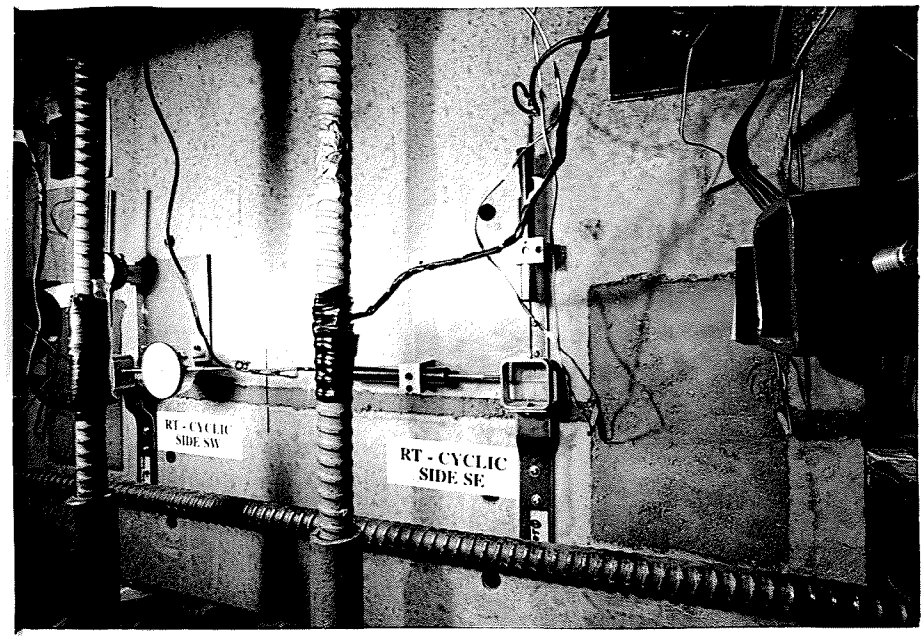

Figure 5.89(a) Condition of connection for specimen RT: at start

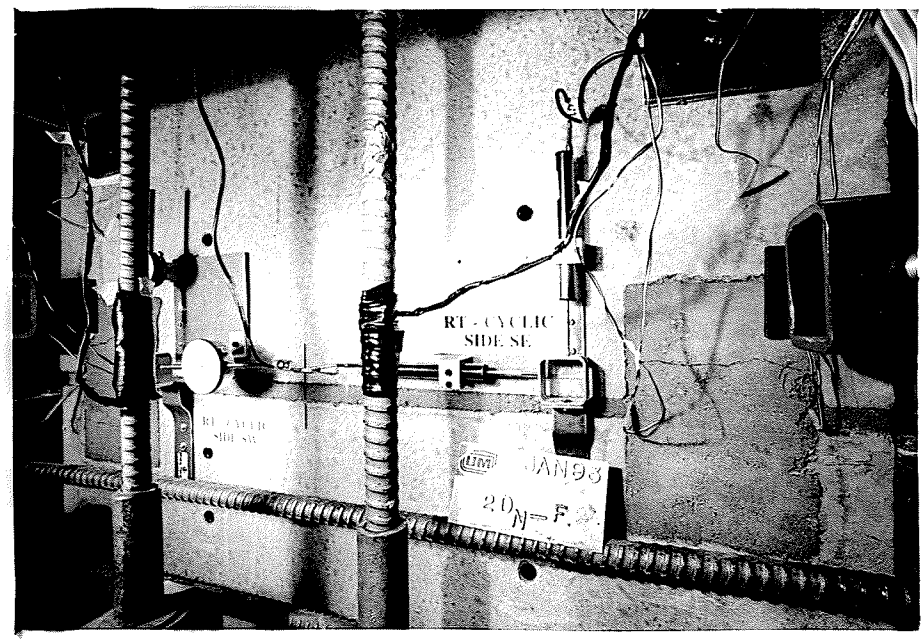

Figure 5.89(b) Condition of connection for specimen RT: at 2Dy

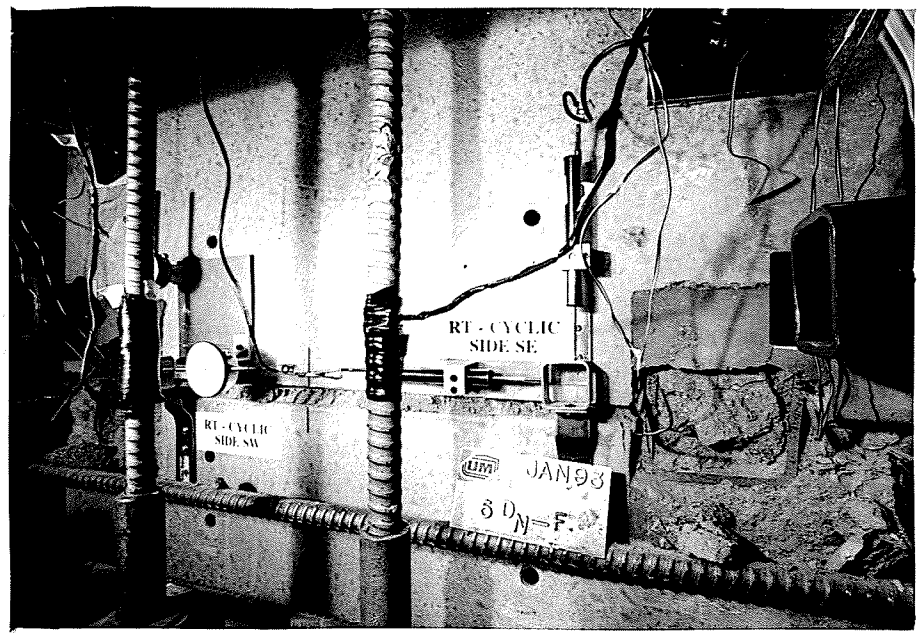

Figure 5.89(c) Condition of connection for specimen RT: at 5Dy

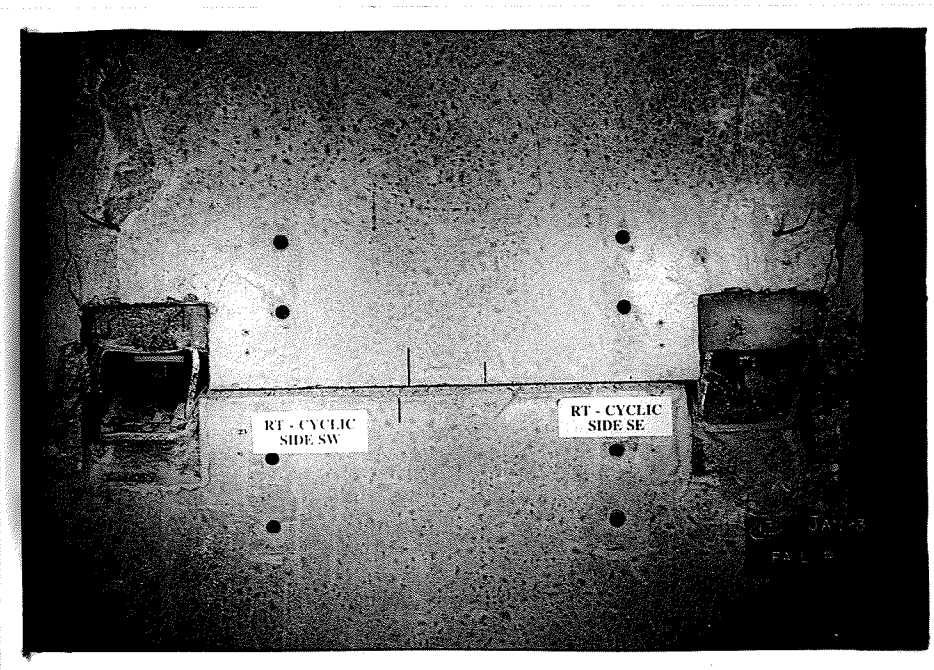

Figure 5.89(d) Condition of connection - specimen RT:post-failure outside frame(8Dy)

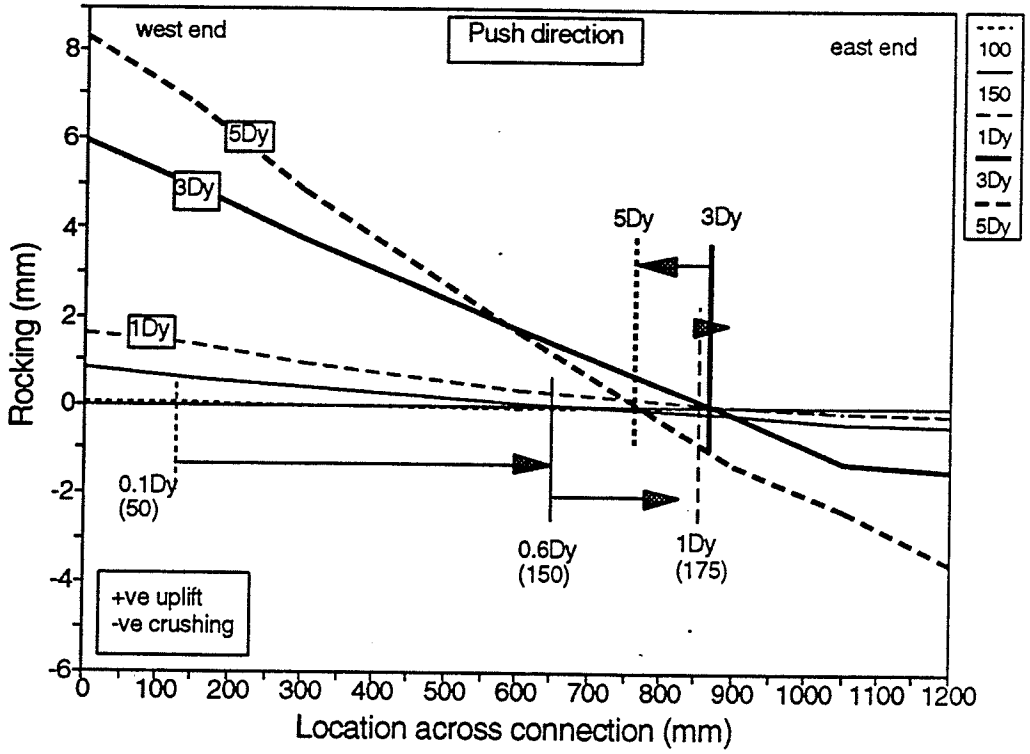

Figure 5.90(a) Rocking behaviour in the push direction for specimen RT

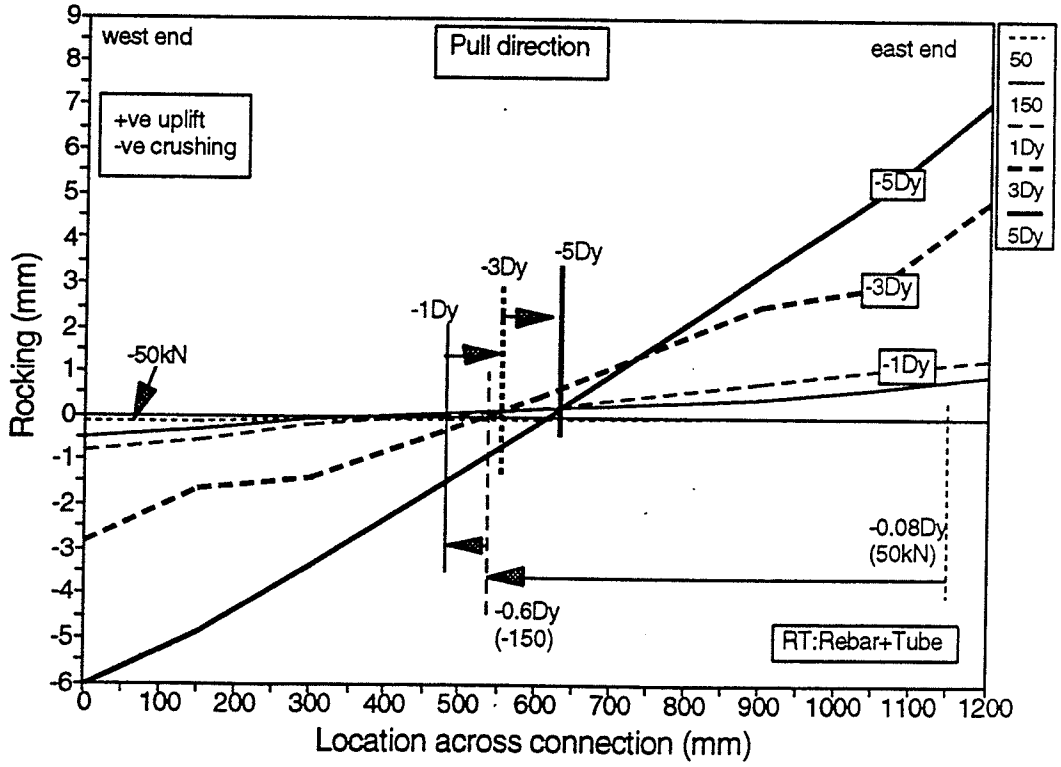

Figure 5.90(b) Rocking behaviour in the pull-direction for specimen RT

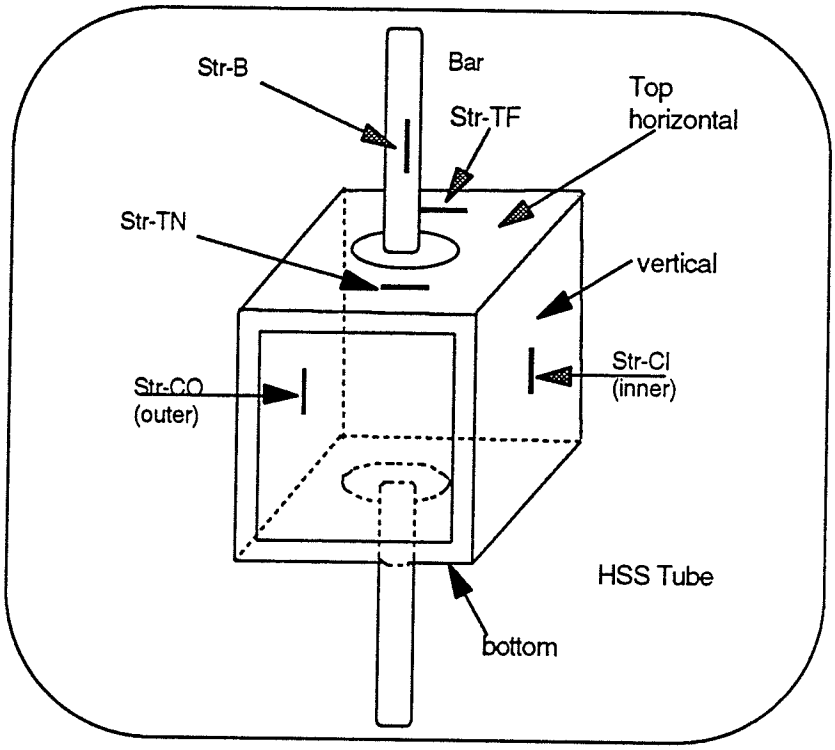

Figure 5.91 Schematic of strain gage layout on HSS tube section

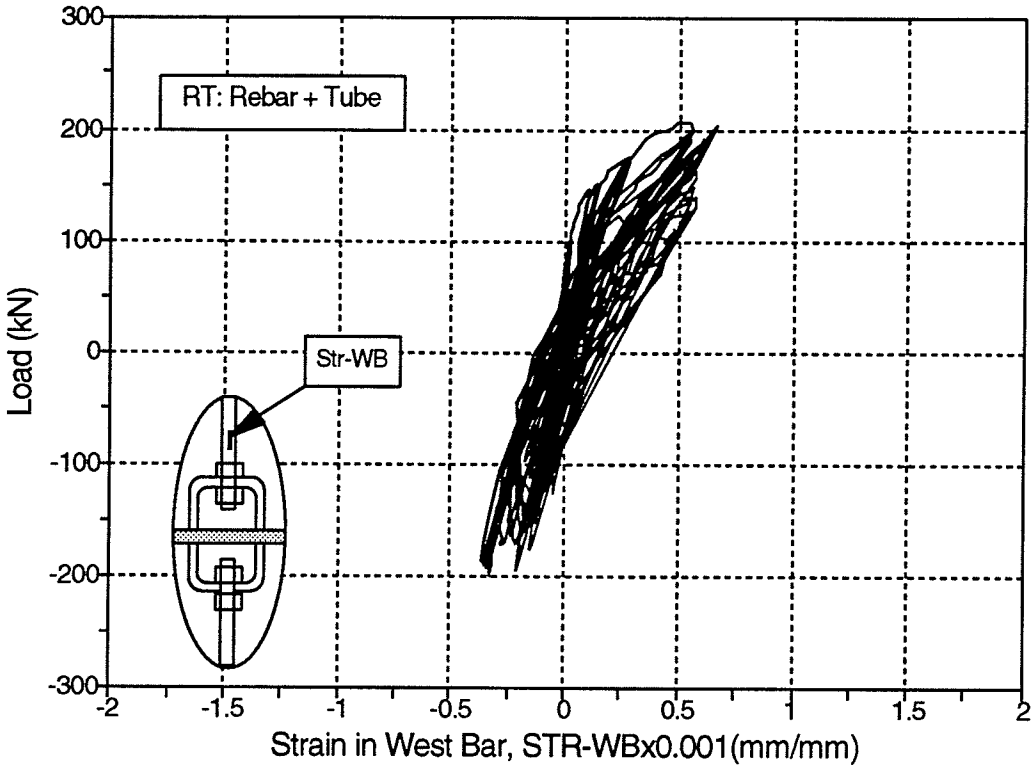

Figure 5.92(a) West bar load vs. strain behaviour for specimen RT

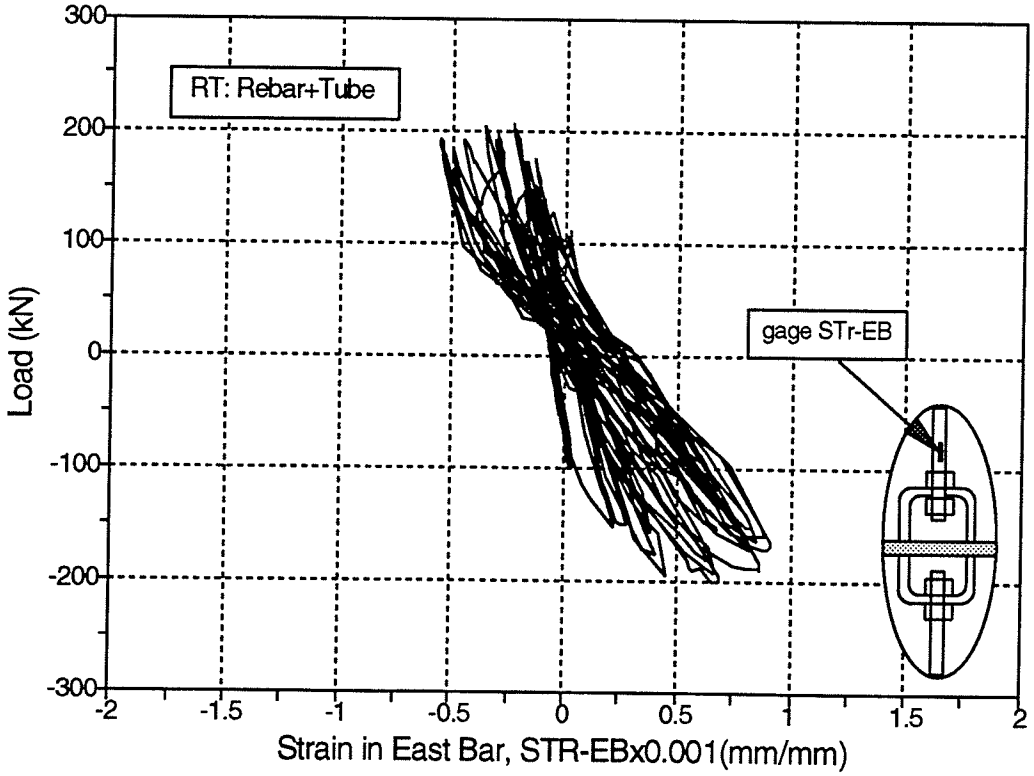

Figure 5.92(b) East bar load vs. strain behaviour for specimen RT

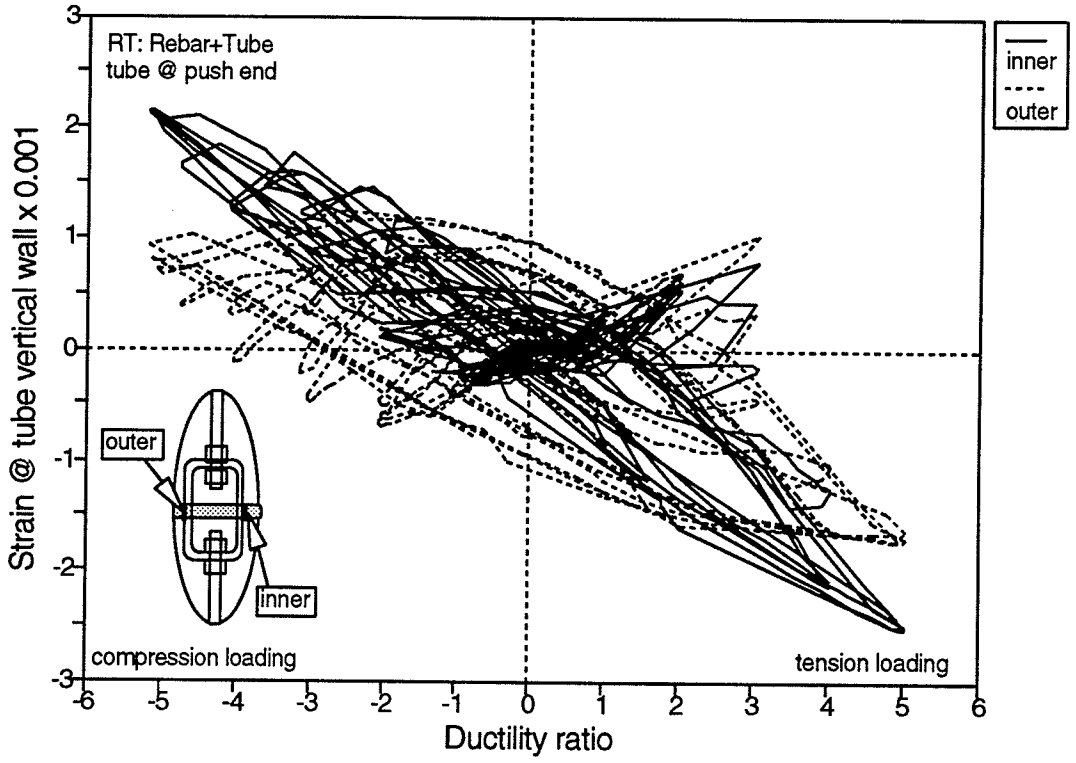

Figure 5.93(a) Strain behaviour of vertical walls of push-end tube for specimen RT

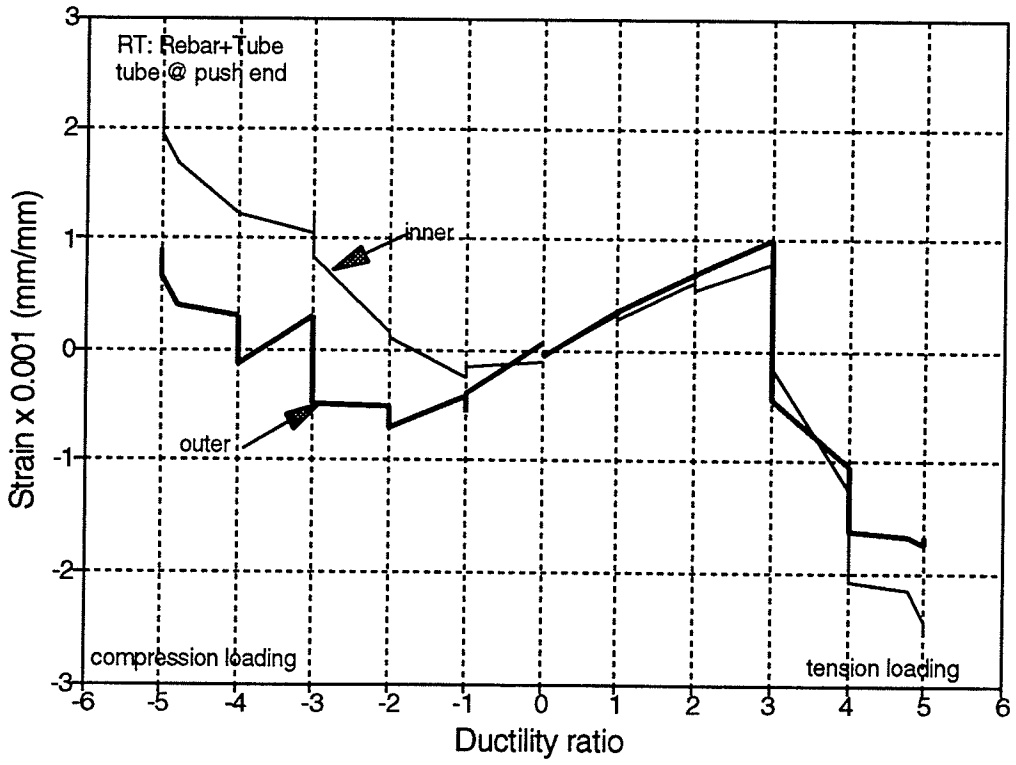

Figure 5.93(b) Envelope of strain of vertical walls in push-end tube for specimen RT

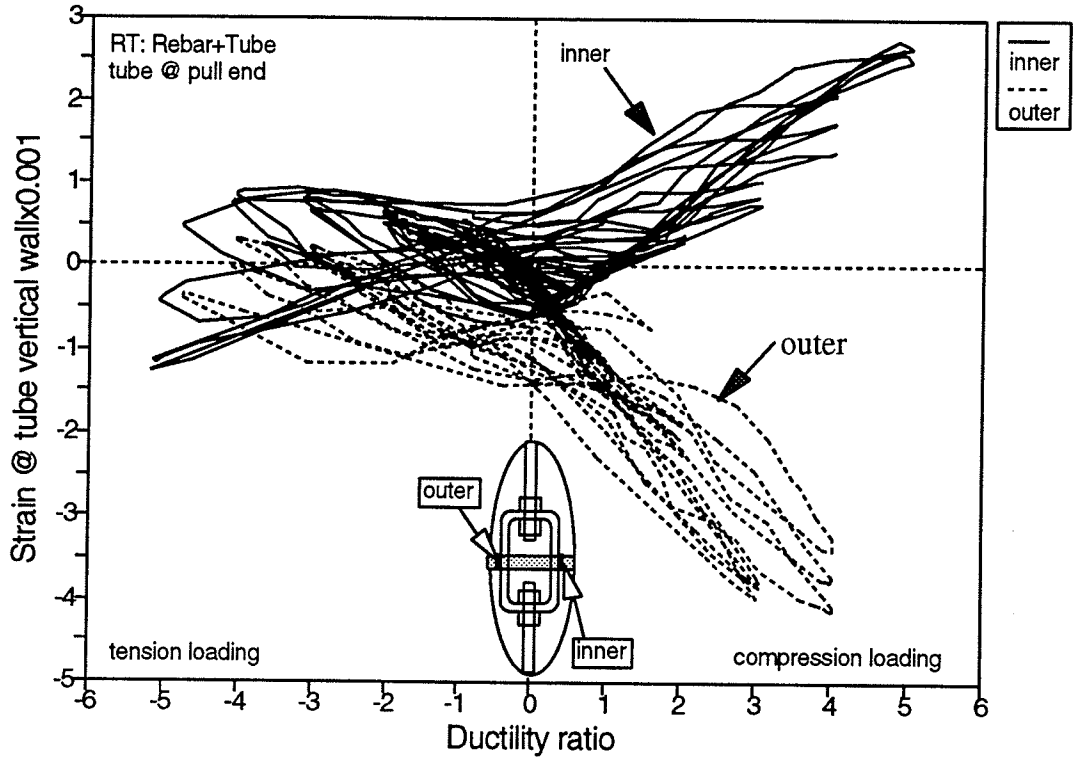

Figure 5.94(a) Strain behaviour of vertical walls of pull-end tube for specimen RT

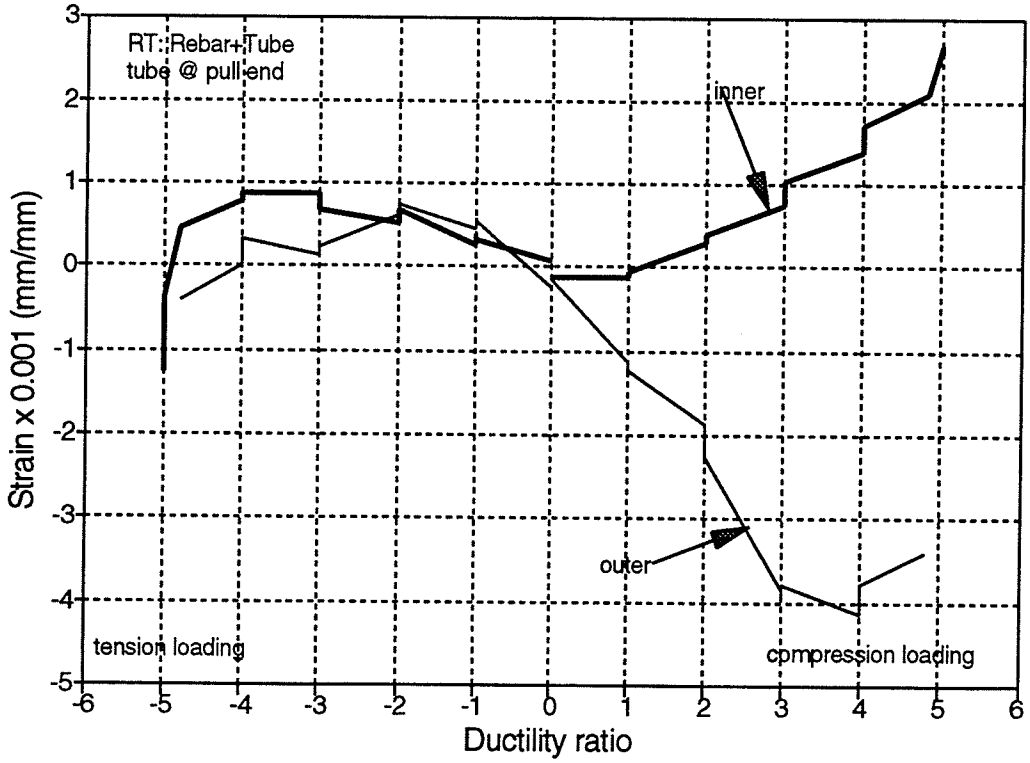

Figure 5.94(b) Envelope of strain of vertical walls in pull-end tube for specimen RT

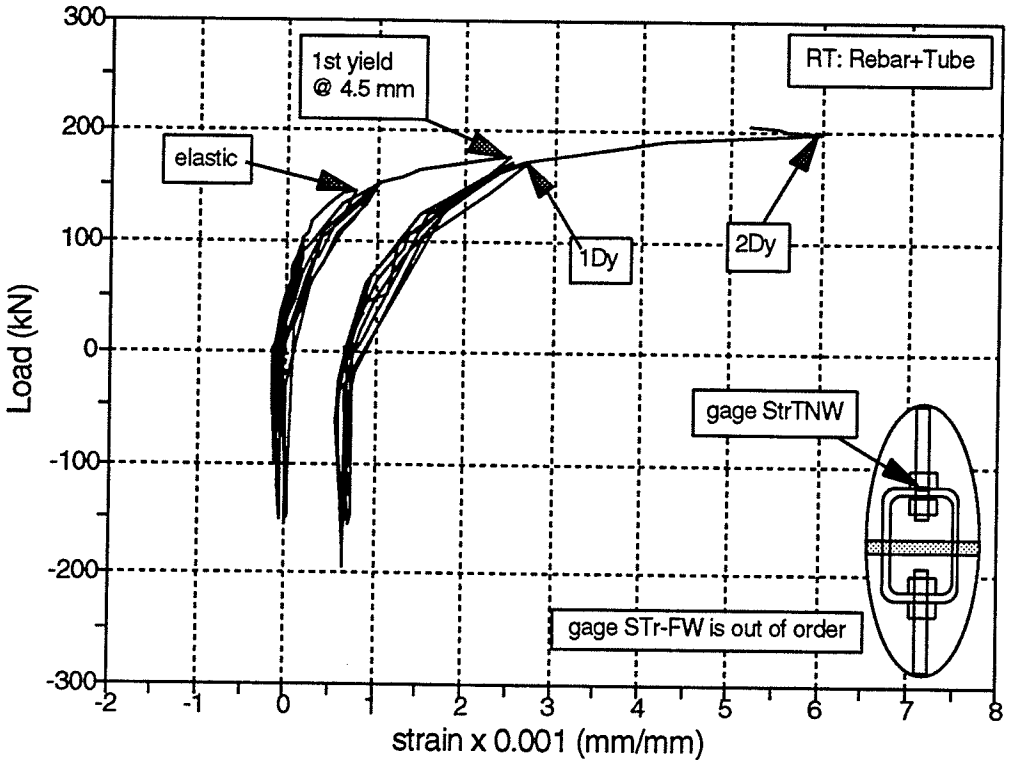

Figure 5.95(a) Strain behaviour of horizontal plate in push-end tube for specimen RT

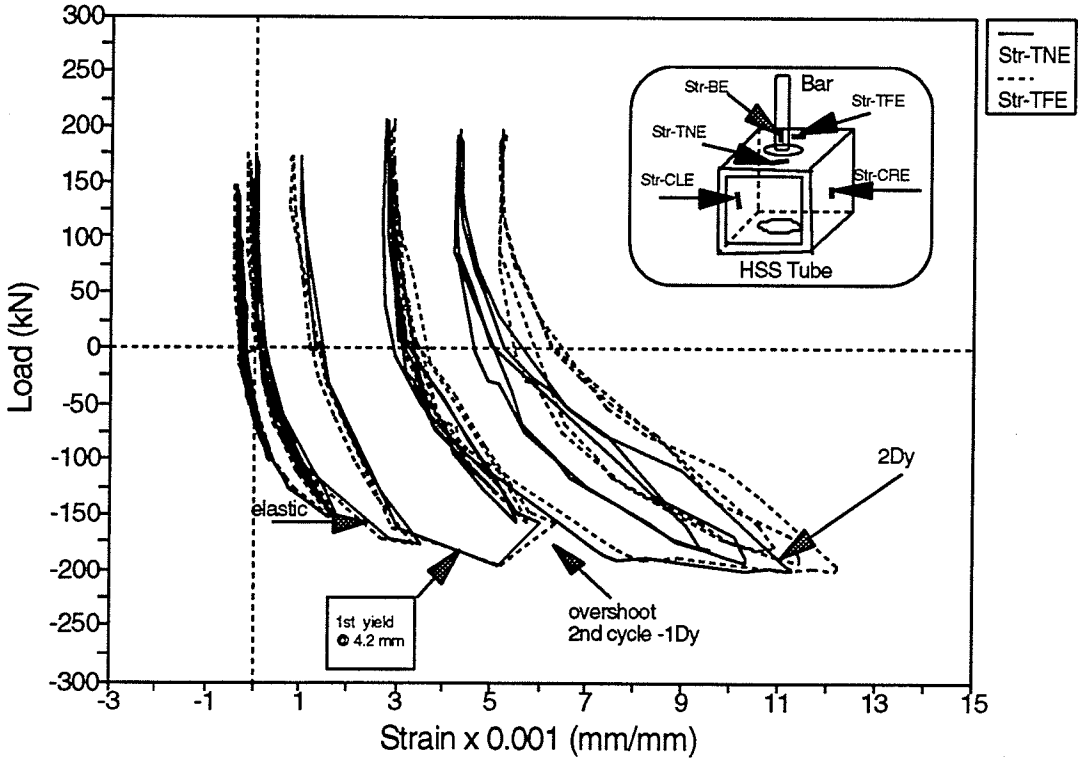

Figure 5.95(b) Strain behaviour of horizontal plate in pull-end tube for specimen RT

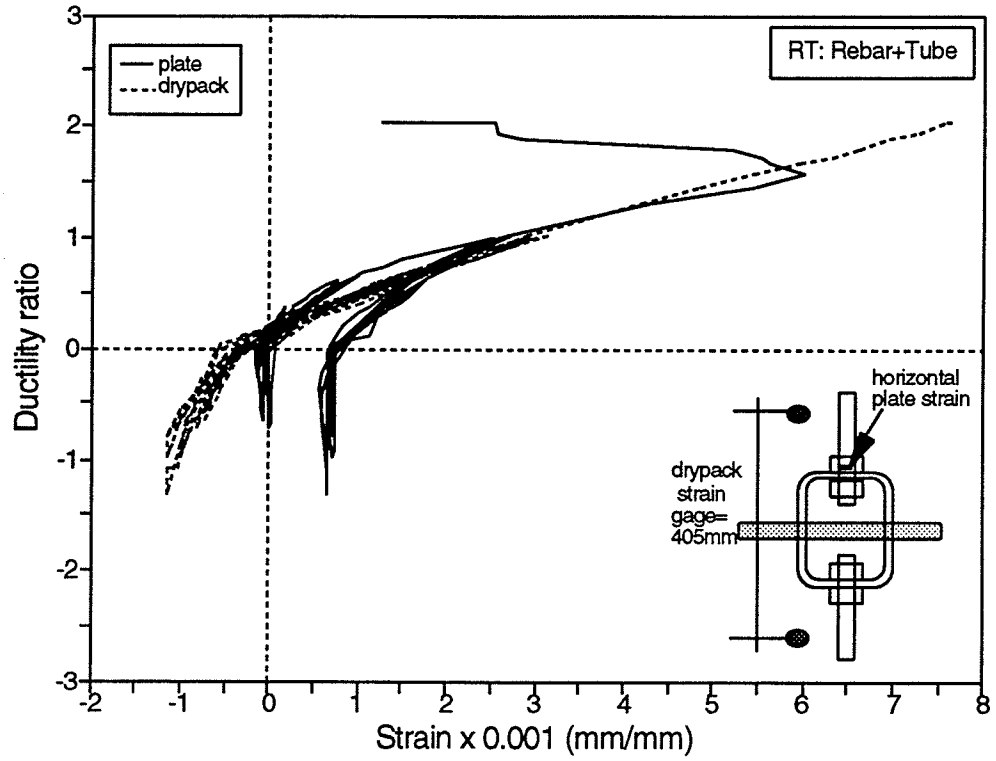

Figure 5.96(a) Comparison of west tube horizontal plate & drypack strain: specimen RT

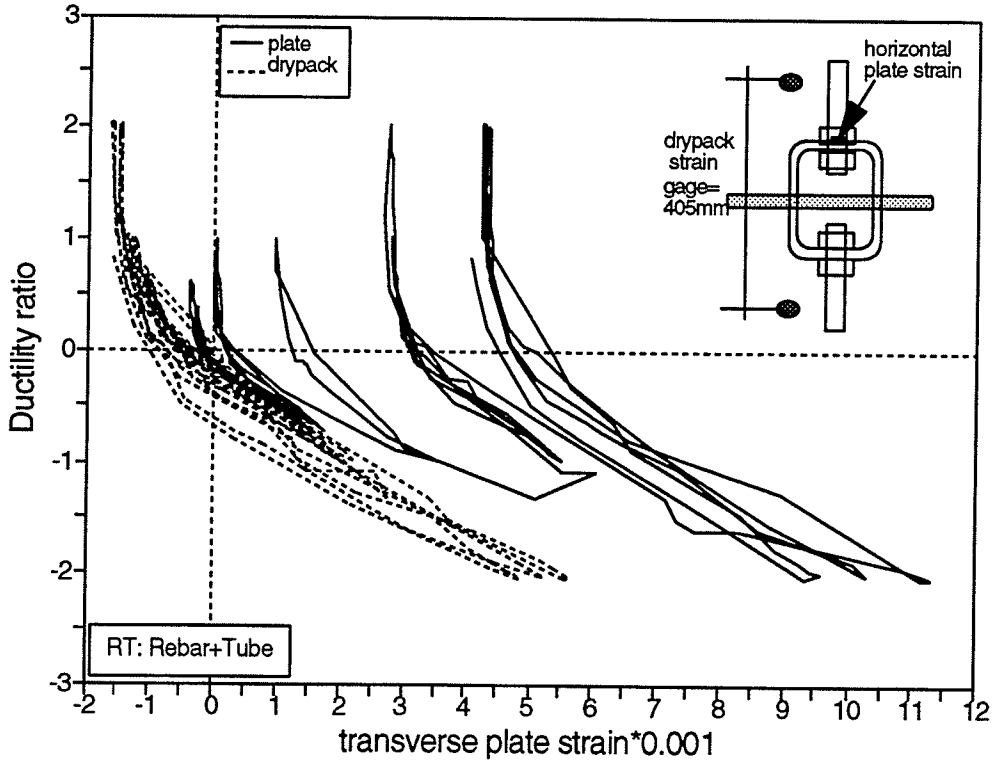

Figure 5.96(b) Comparison of east tube horizontal plate & drypack strain: specimen RT

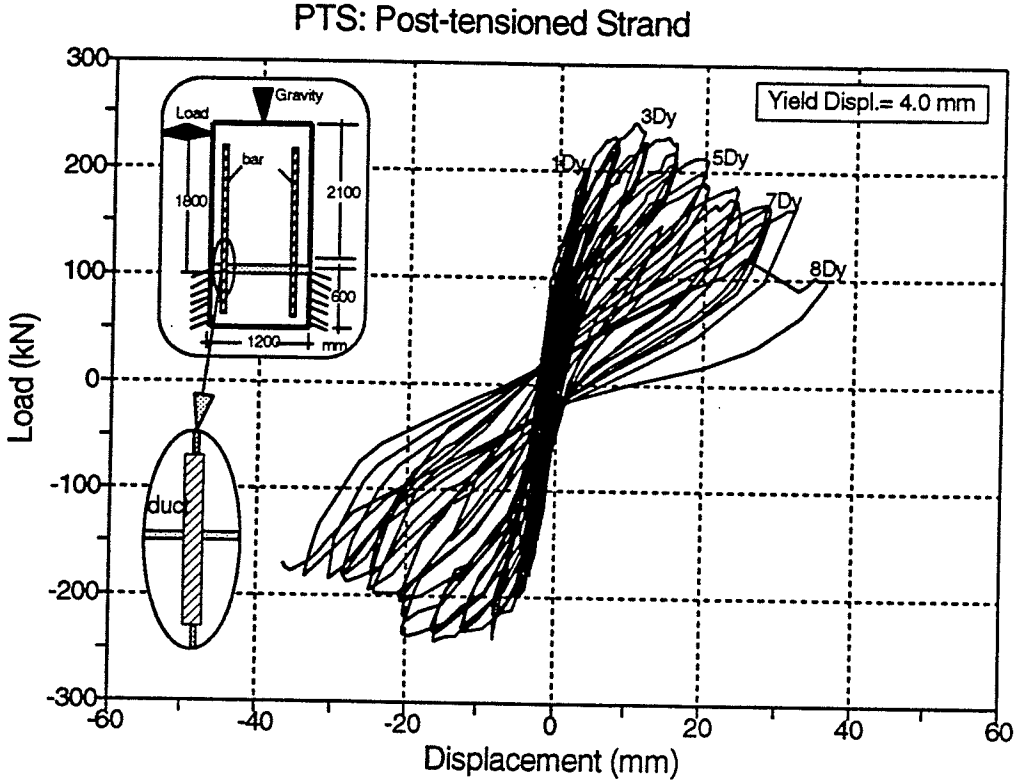

Figure 5.97(a) Hysteresis loops of load versus displacement behaviour for specimen PTS

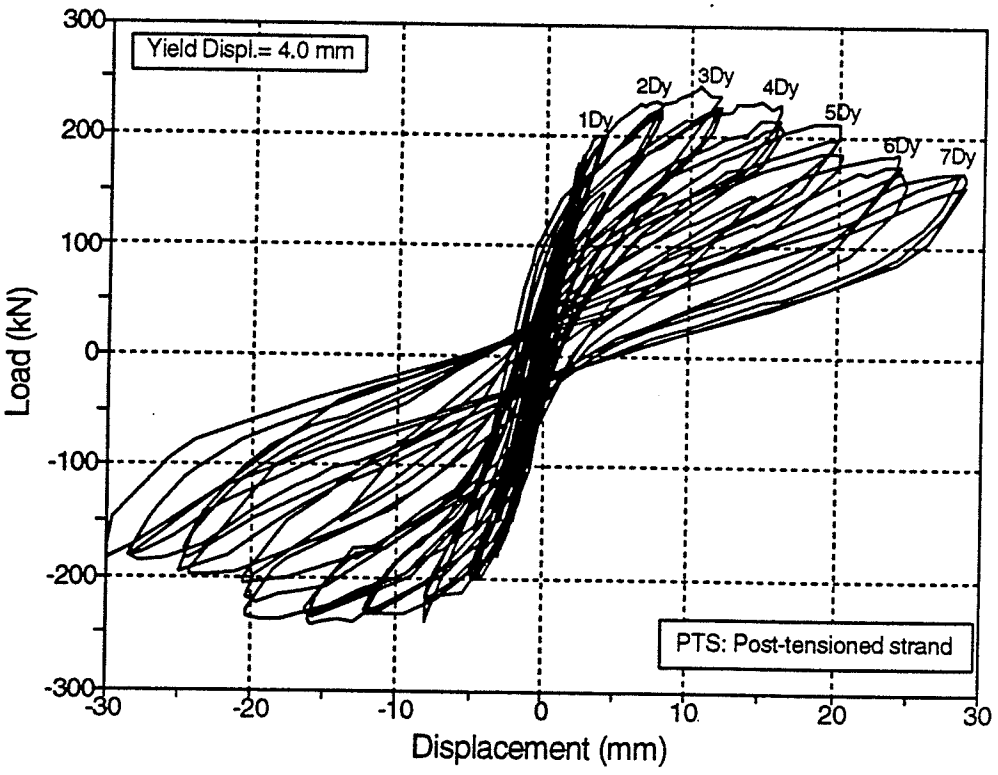

Figure 5.97(b) Magnified hysteresis loops of load versus displacement for specimen PTS

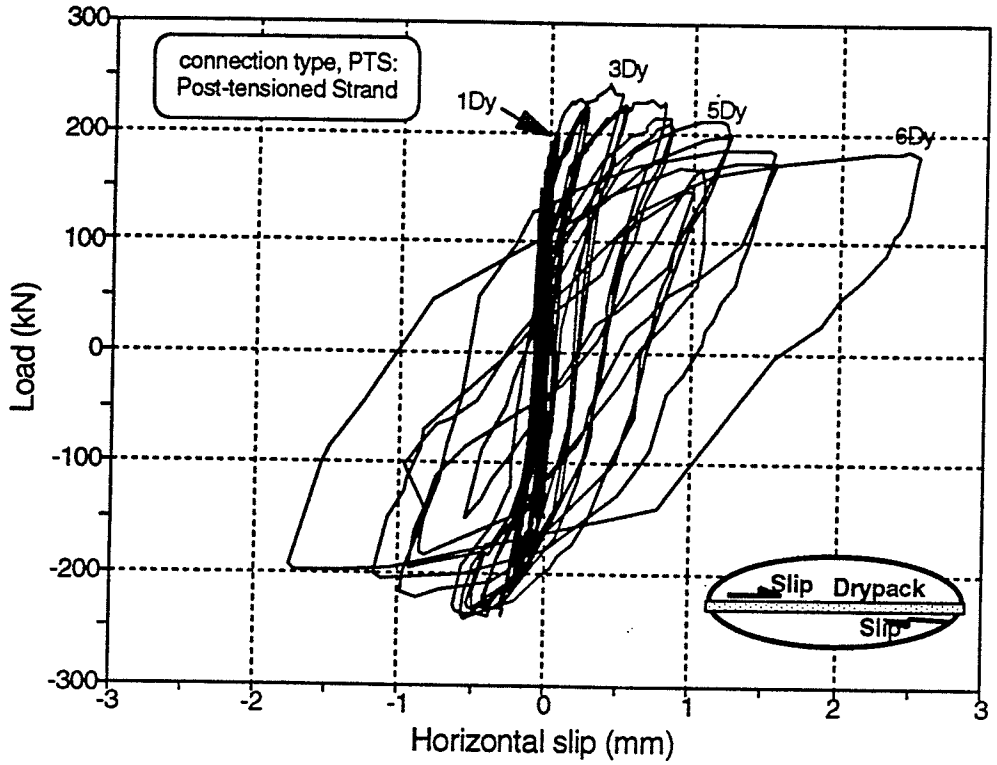

Figure 5.98 Hysteresis loops of load versus horizontal slip for specimen PTS

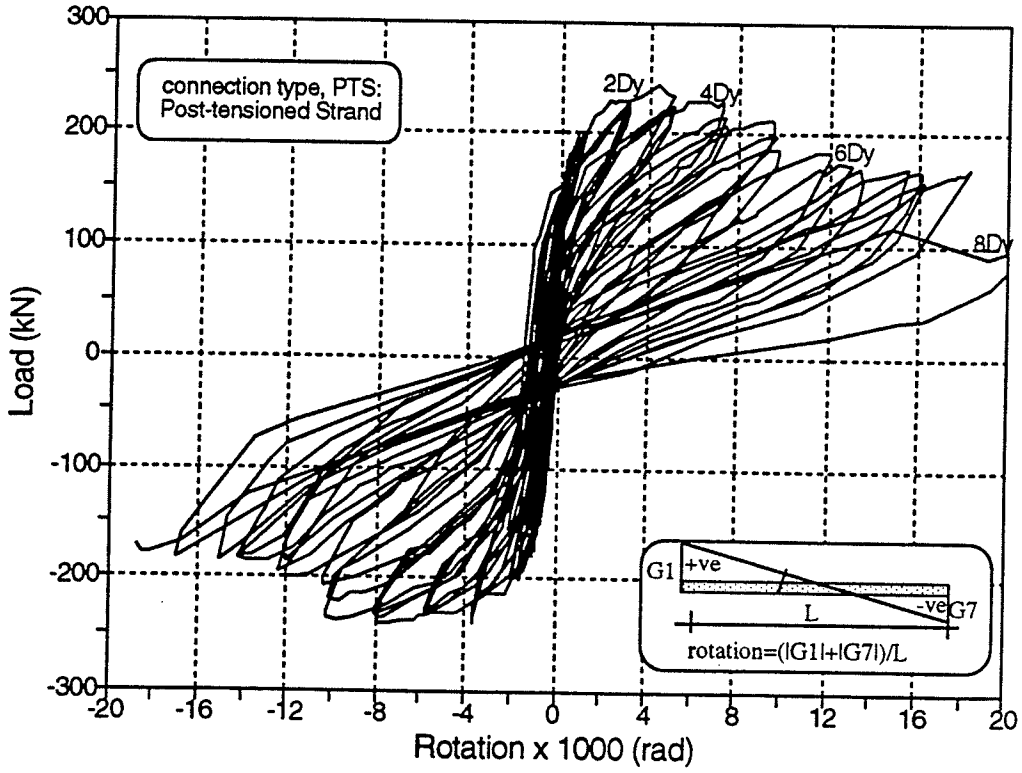

Figure 5.99 Hysteresis loops of load versus rotation for specimen PTS

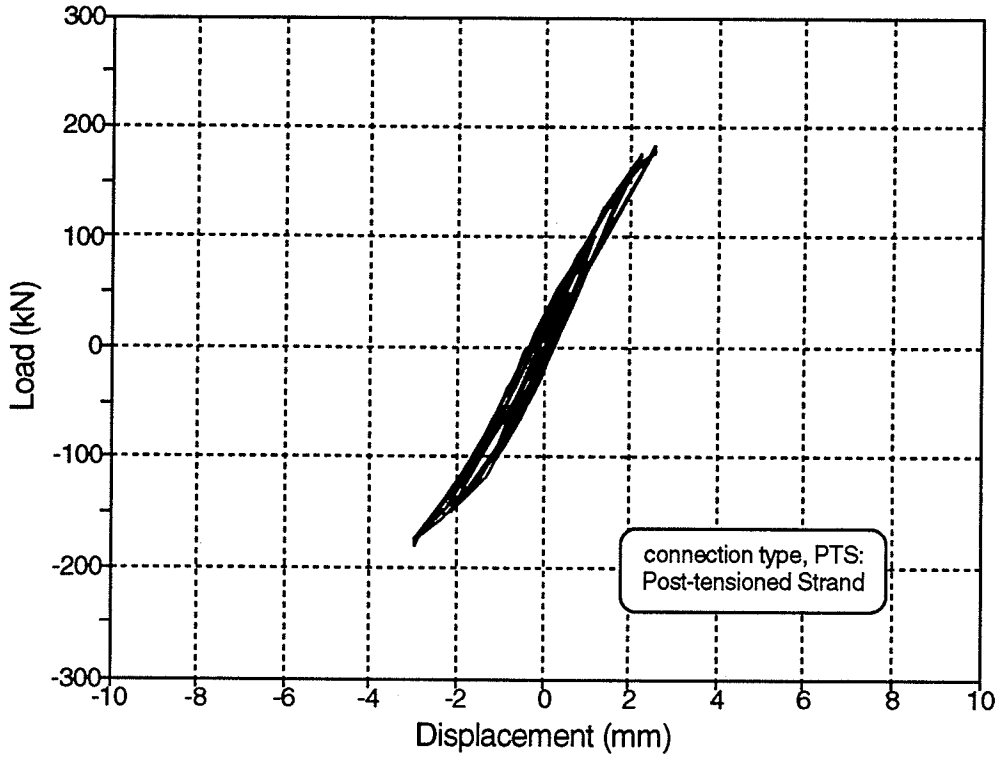

Figure 5.100 Elastic load vs. displacement behavior for specimen PTS

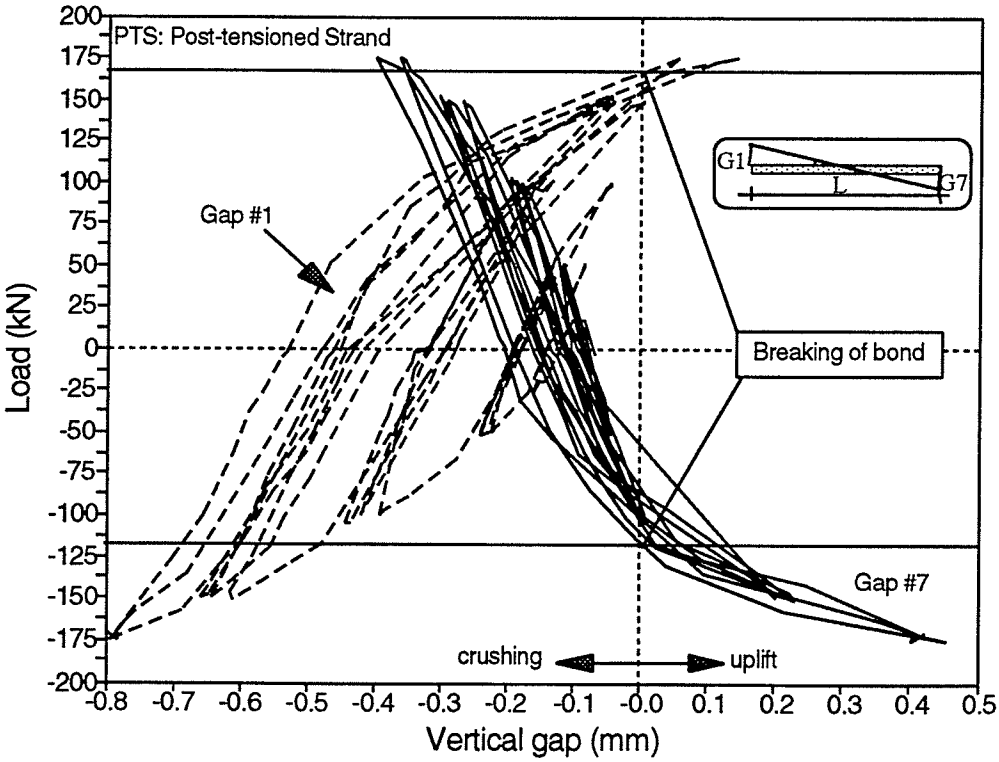

Figure 5.101 Onset of breaking of bond in load vs. gap hysteresis for specimen PTS

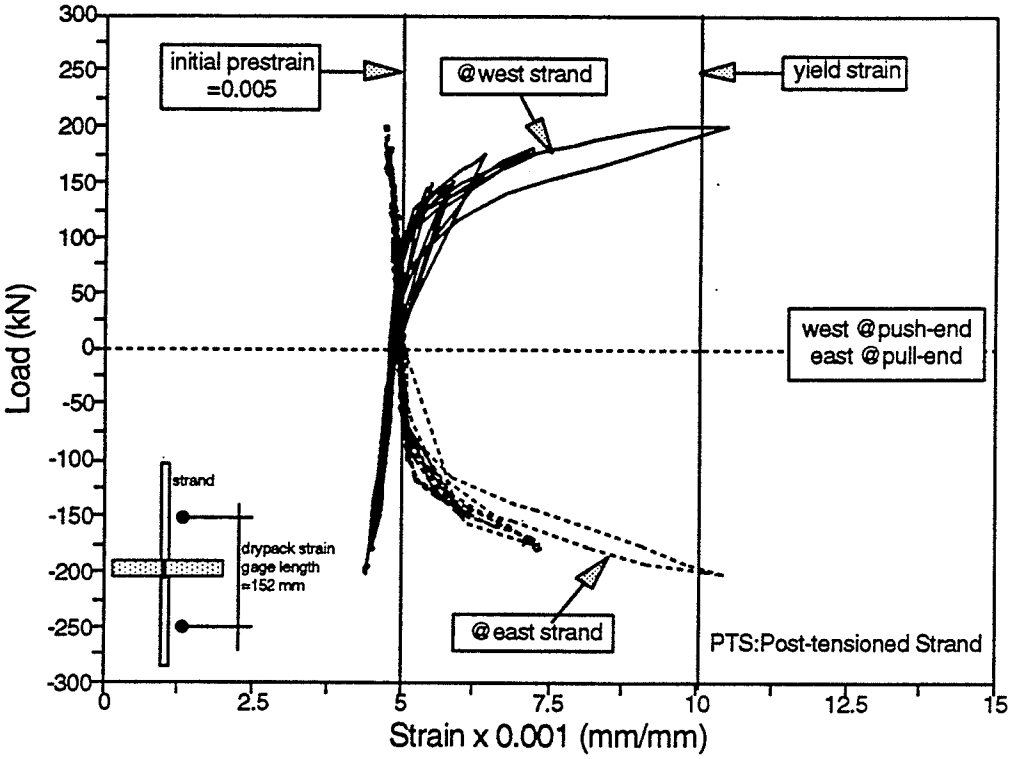

Figure 5.102 Onset of yield in load-drypack strain relationship for specimen PTS

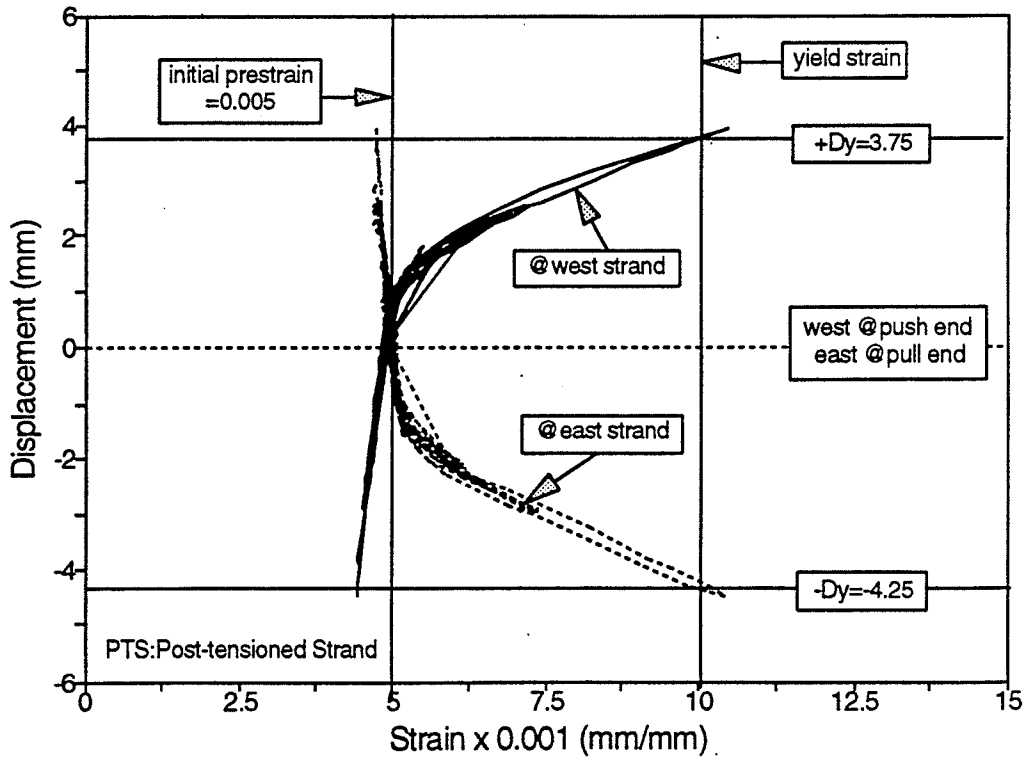

Figure 5.103 Onset of yield in drypack strain versus displacement for specimen PTS

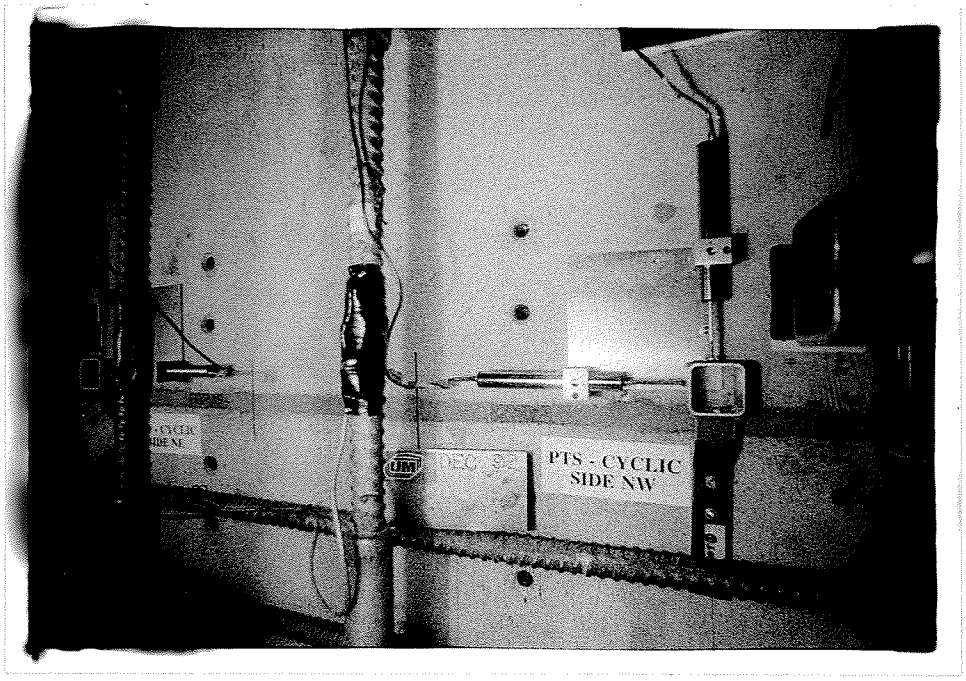

Figure 5.104(a) Condition of connection for specimen PTS: at start

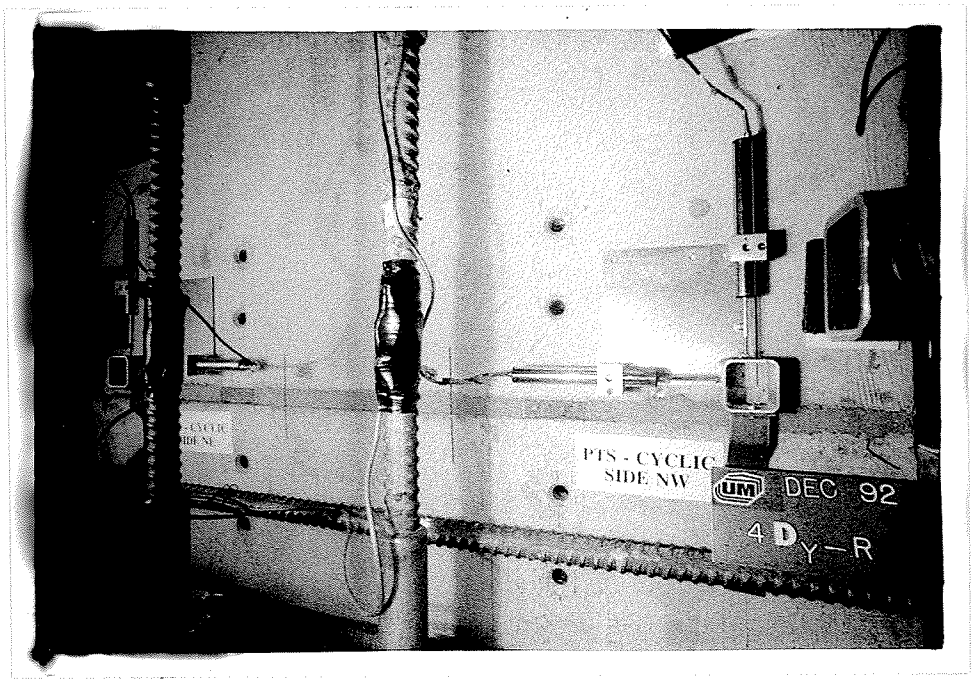

Figure 5.104(b) Condition of connection for specimen PTS: at 4Dy

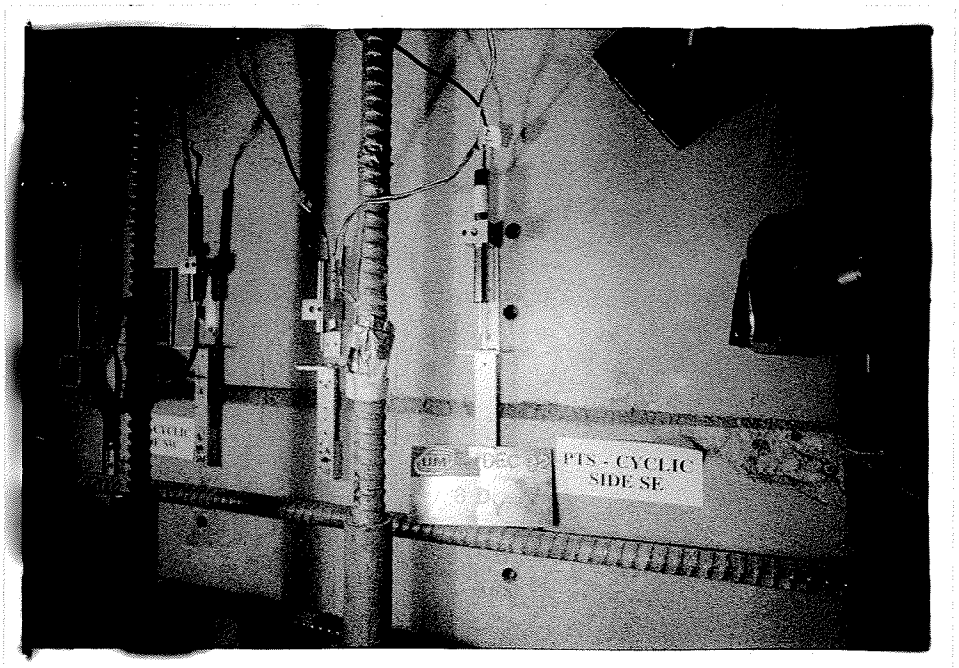

Figure 5.104(c) Condition of connection for specimen PTS: at 6Dy

Figure 5.104(d) Condition of connection for specimen PTS: at 8Dy (rupture of strand)

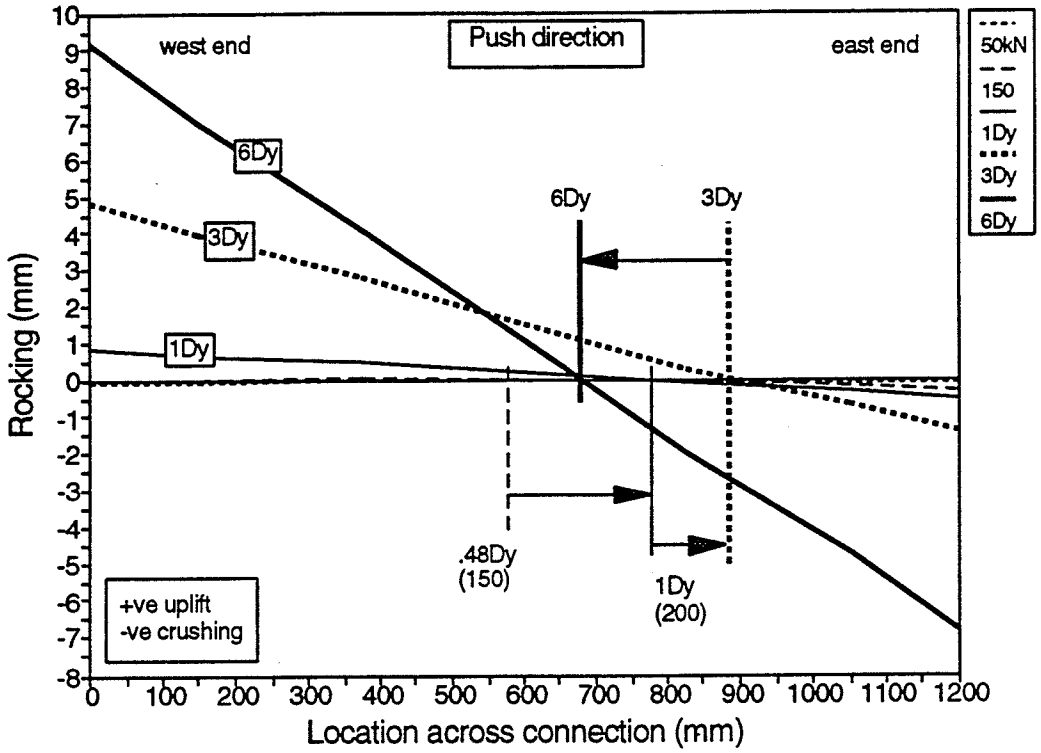

Figure 5.105(a) Rocking behaviour in the push direction for specimen PTS

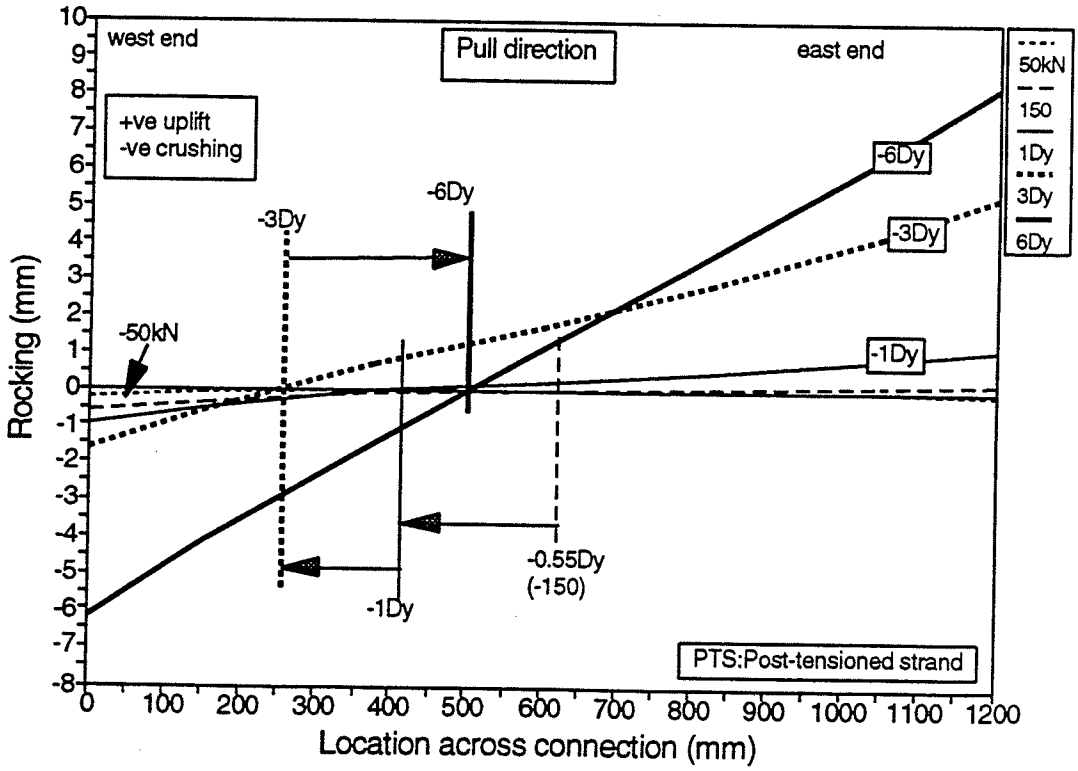

Figure 5.105(b) Rocking behaviour in the pull-direction for specimen PTS

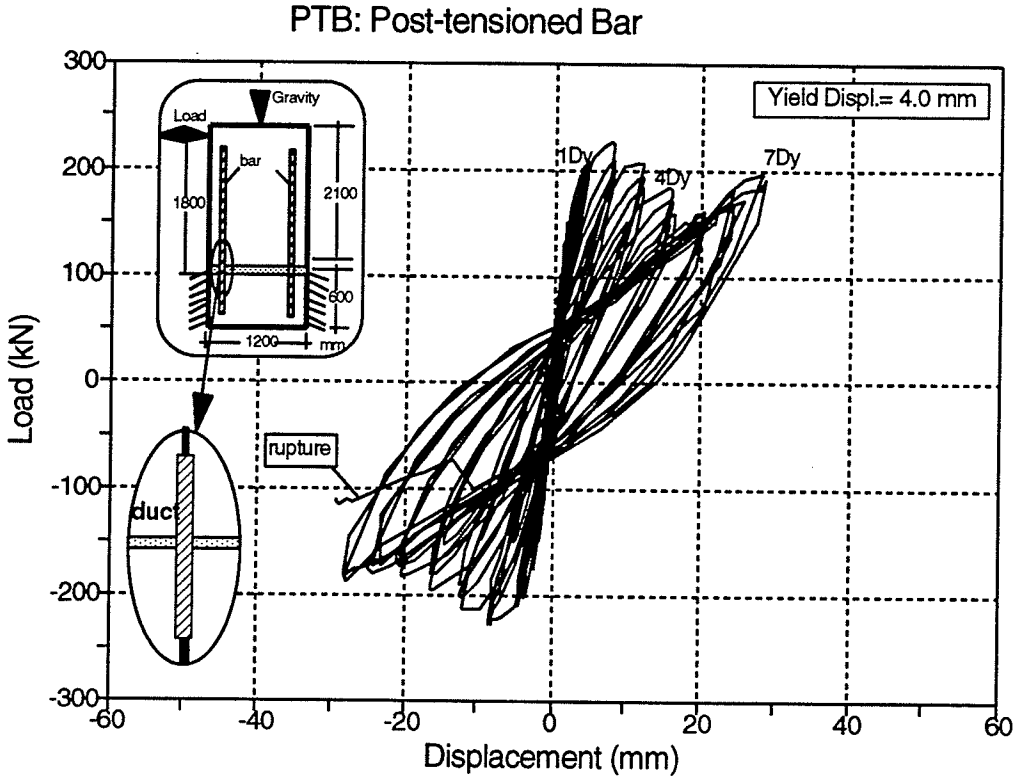

Figure 5.106(a) Hysteresis loops of load vs. displacement behaviour for specimen PTB

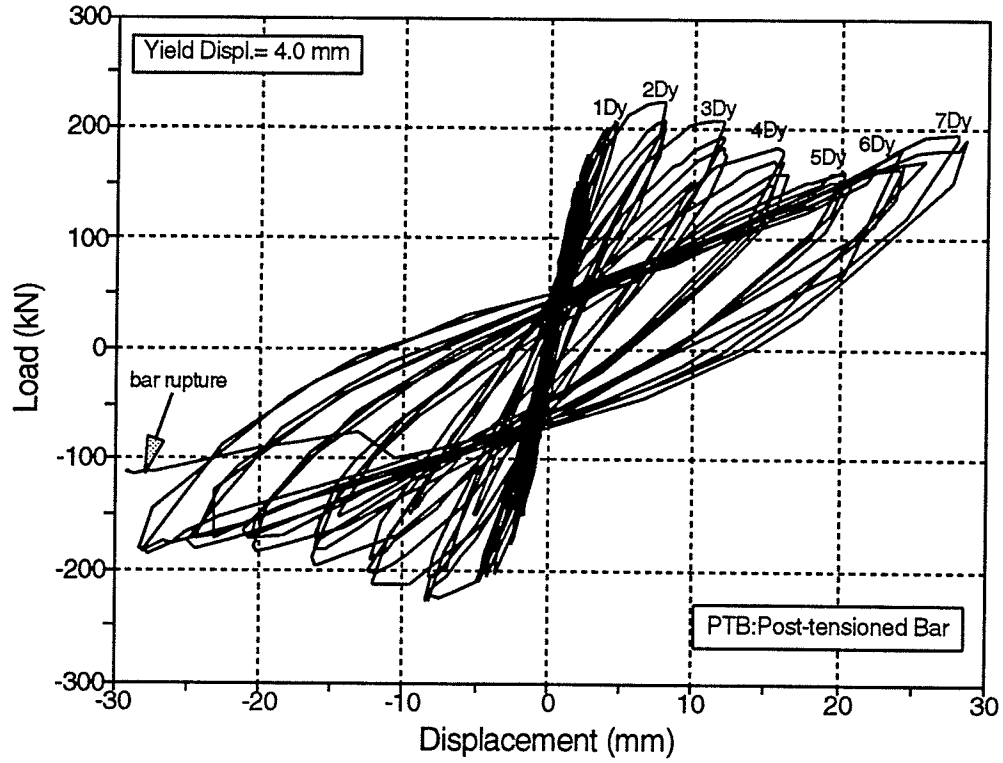

Figure 5.106(b) Magnified hysteresis loops of load vs. displacement for specimen PTB

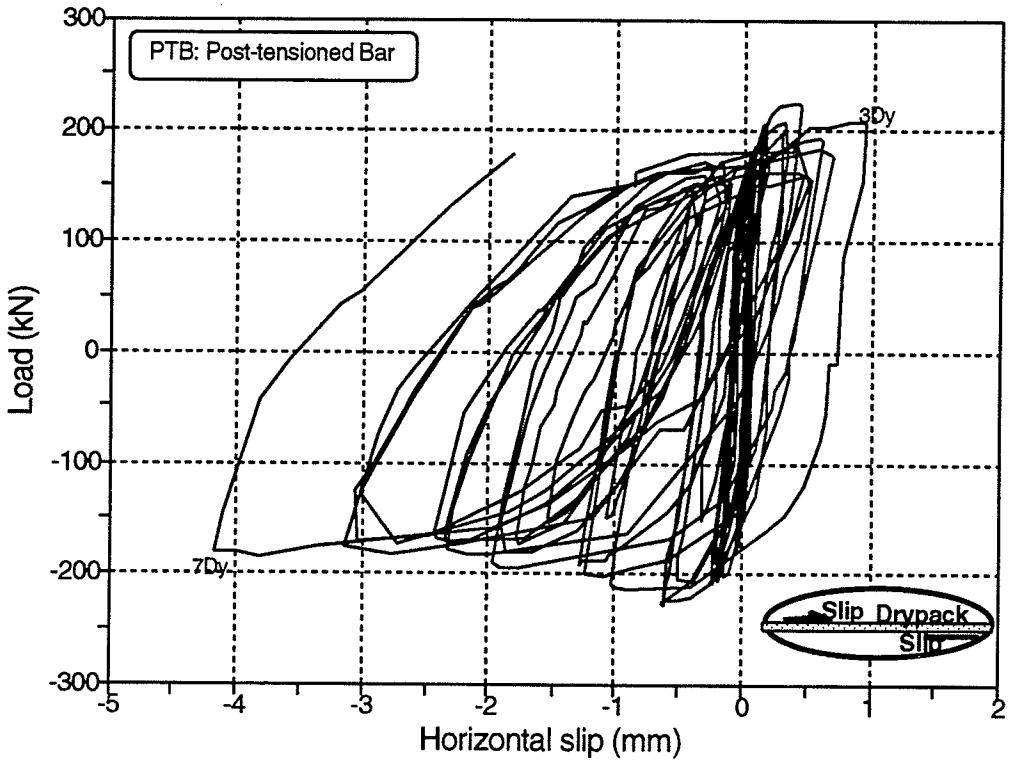

Figure 5.107(a) Hysteresis loops of load vs. horizontal slip for specimen PTB

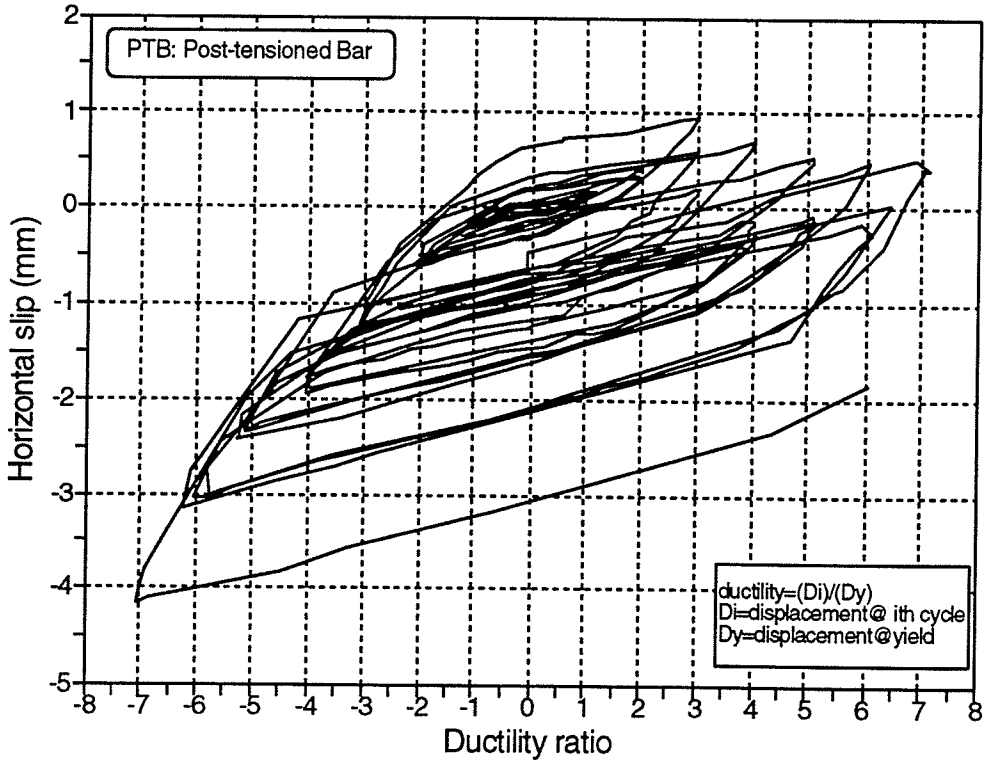

Figure 5.107(b) Hysteresis loops of horizontal slip vs. ductility for specimen PTB

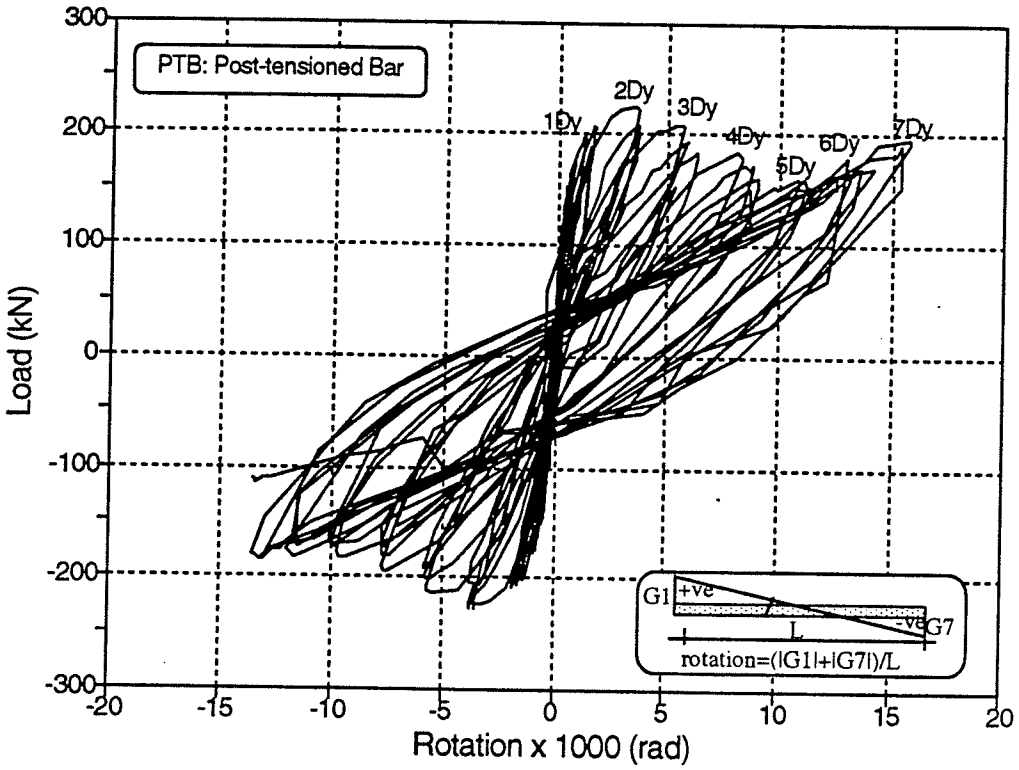

Figure 5.108 Hysteresis loops of load versus rotation for specimen PTB

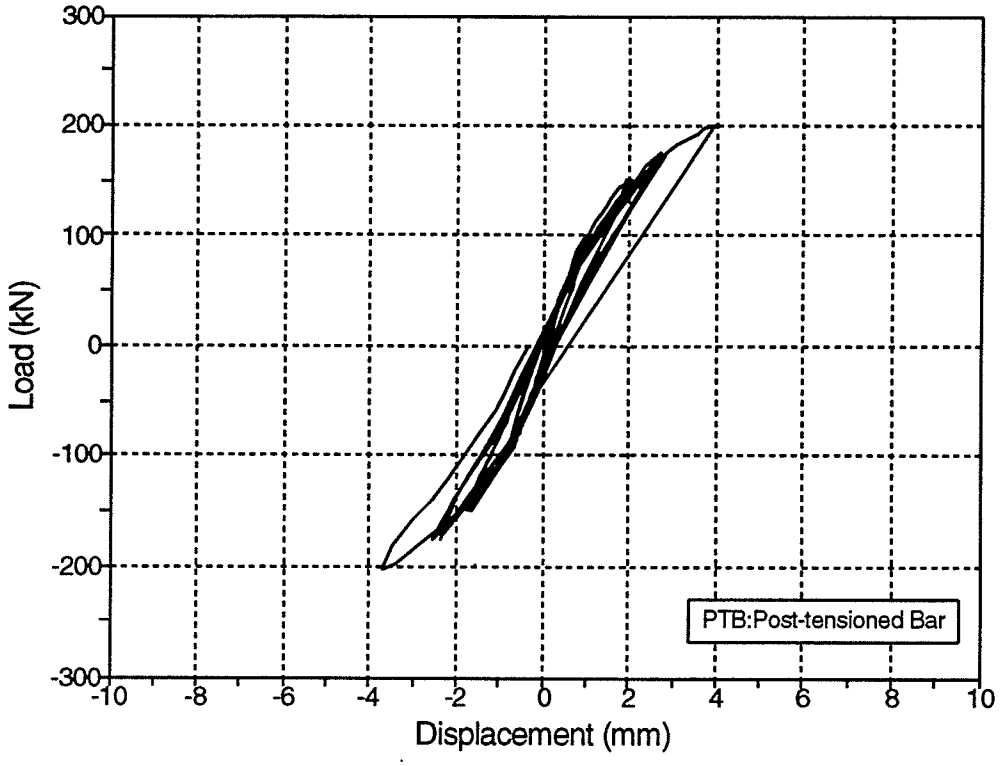

Figure 5.109 Elastic hysteresis loops of load vs. displacement for specimen PTB

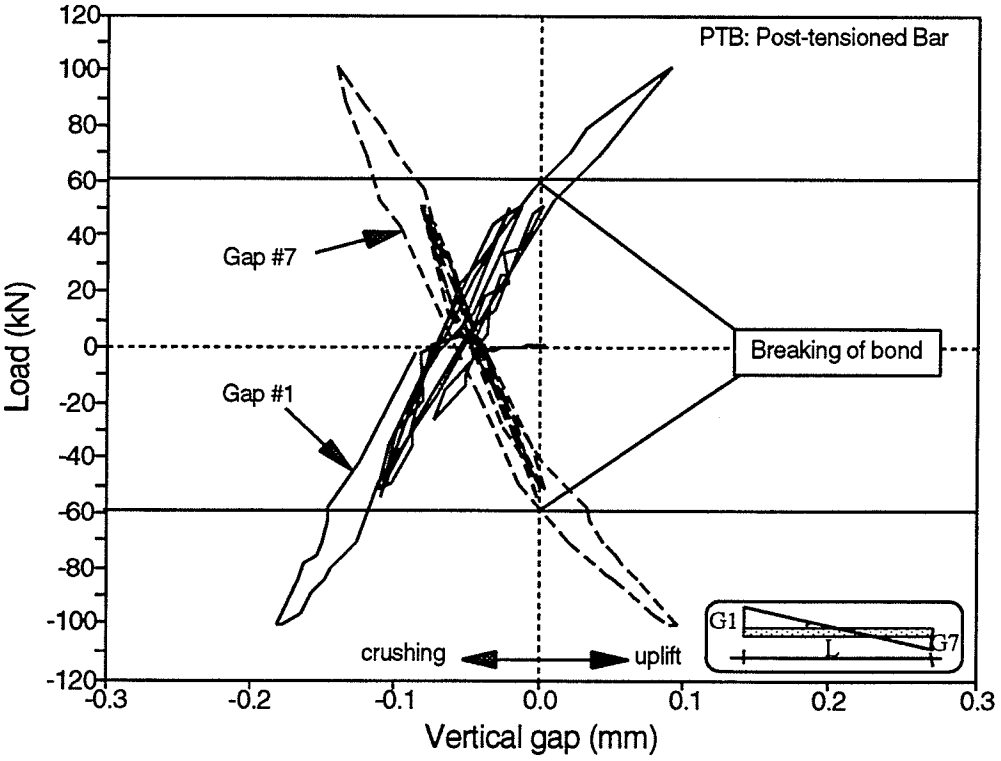

Figure 5.110 Onset of breaking of bond in load vs. gap hysteresis for specimen PTB

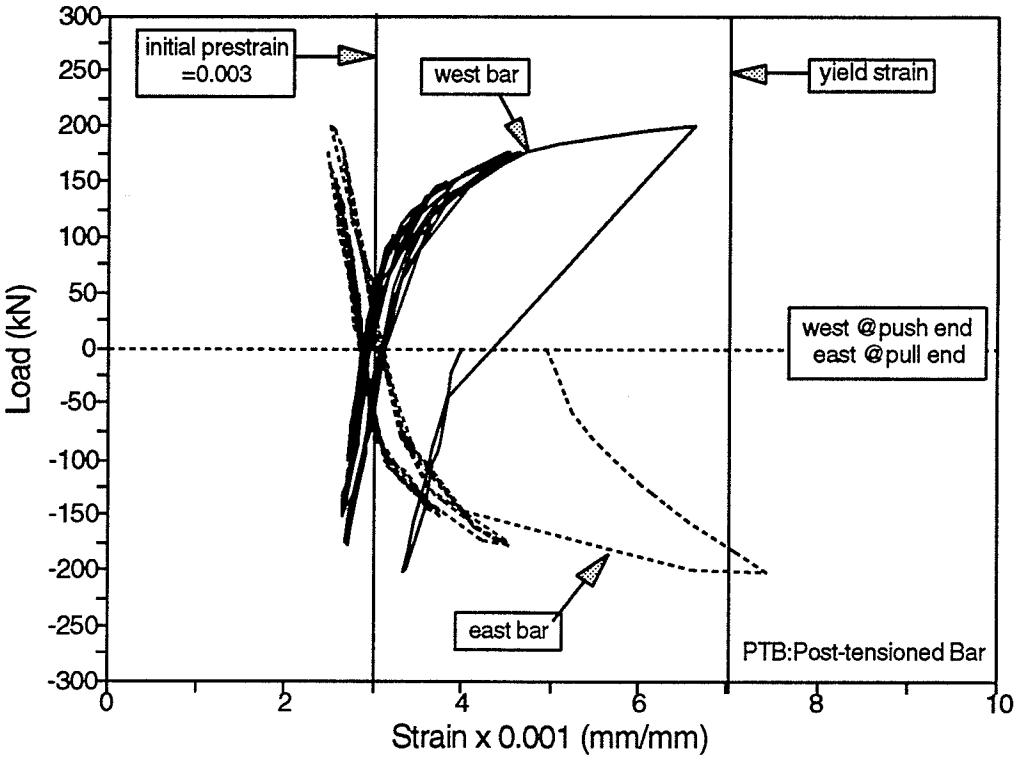

Figure 5.111 Onset of yield in load vs. bar strain relationship for specimen PTB

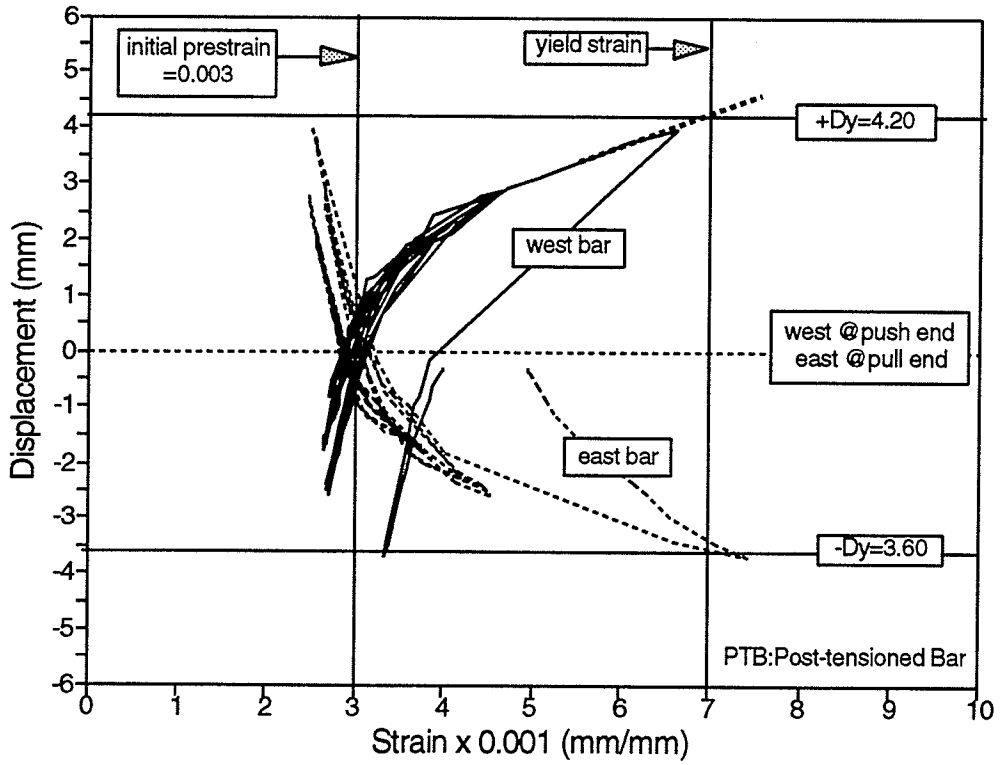

Figure 5.112 Onset of yield in bar strain vs. displacement relationship for specimen PTB

Figure 5.113(a) Condition of connection for specimen PTB: at start

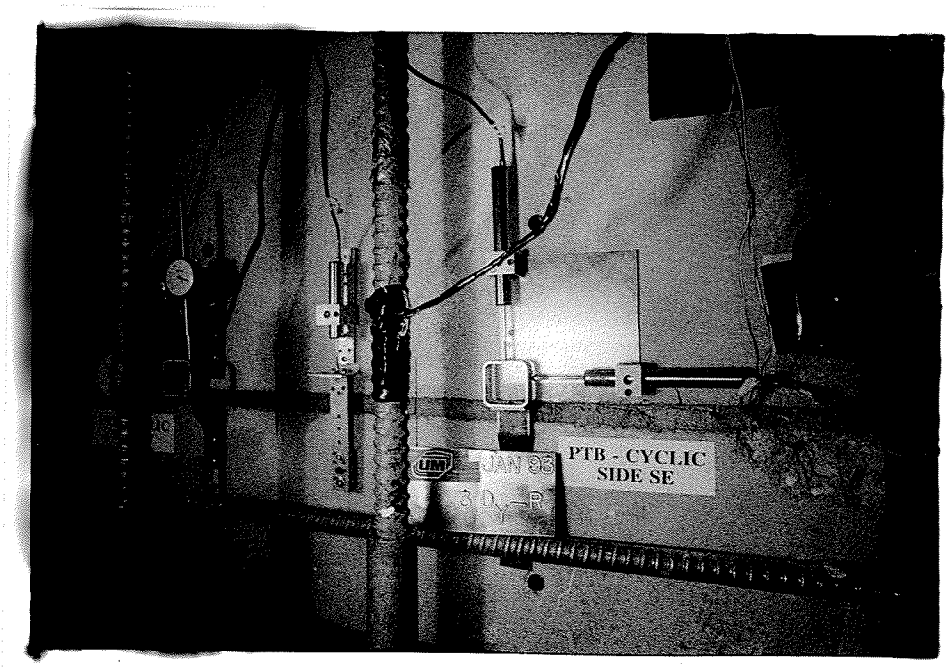

Figure 5.113(b) Condition of connection for specimen PTB: at 3Dy

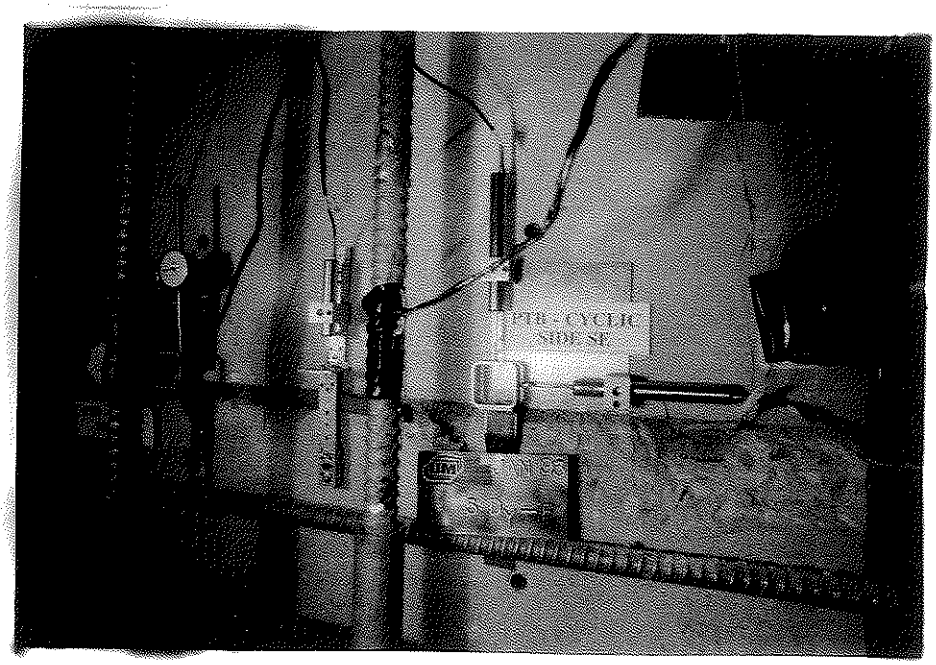

Figure 5.113(c) Condition of connection for specimen PTB: at 5Dy

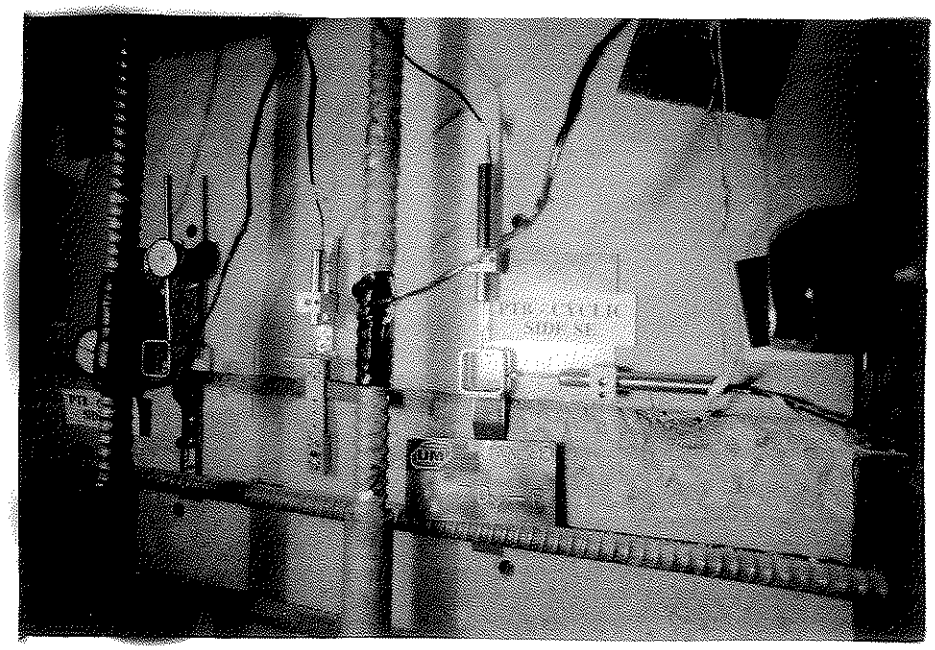

Figure 5.113(d) Condition of connection for specimen PTB: at 7Dy (failure)

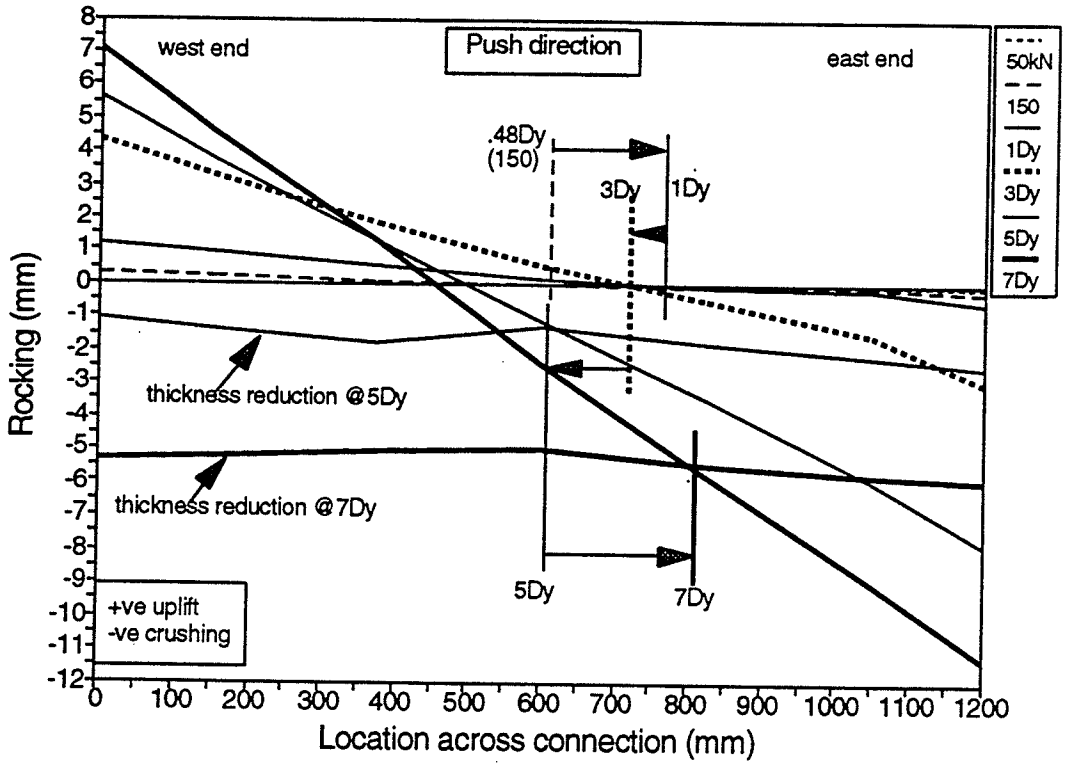

Figure 5.114(a) Rocking behaviour in the push direction for specimen PTB

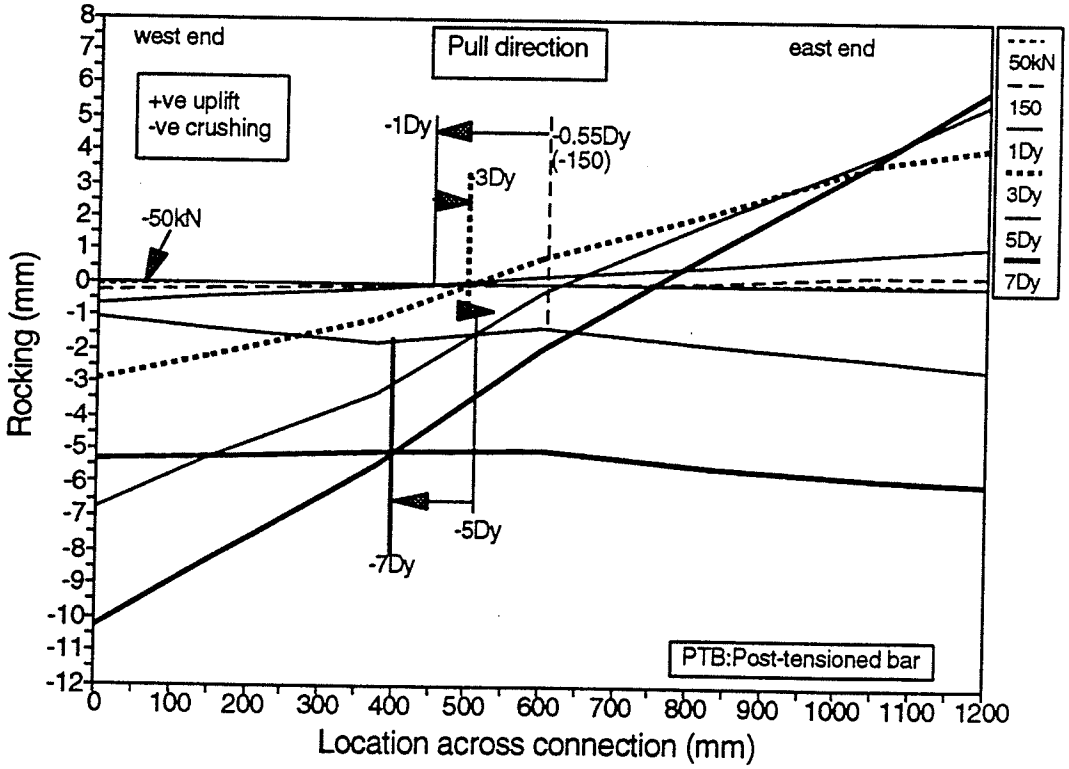

Figure 5.114(b) Rocking behaviour in the pull-direction for specimen PTB

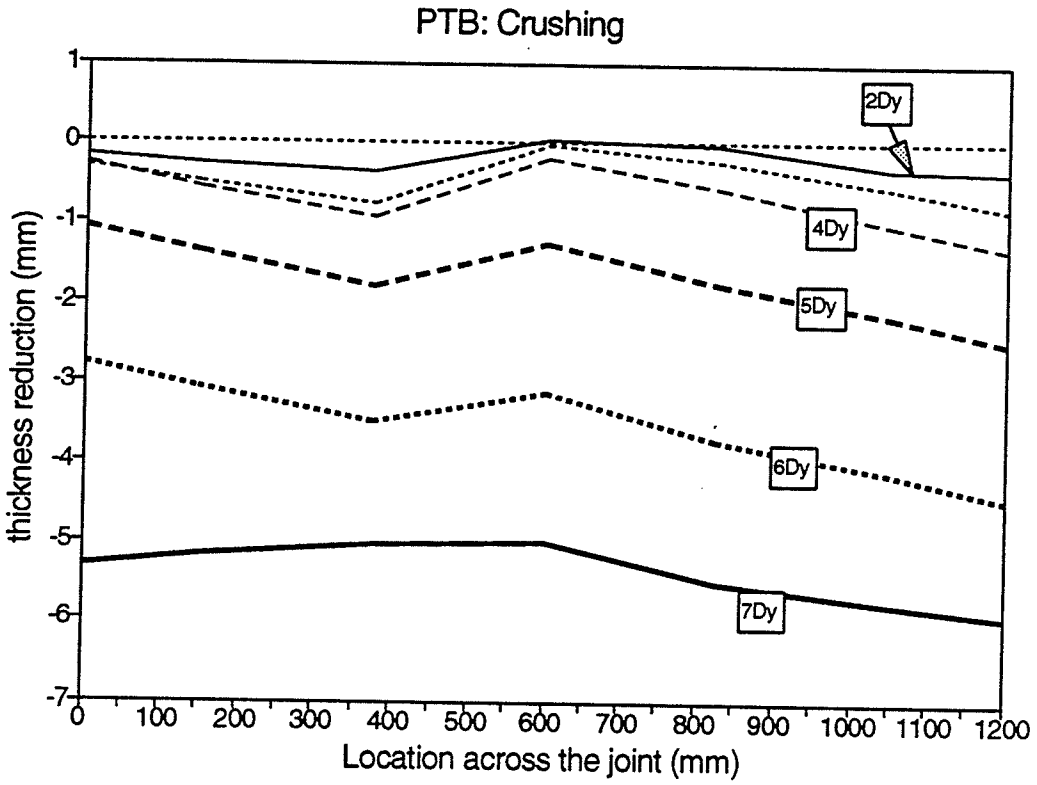

Figure 5.114(c) Rocking behavior for specimen PTB: thickness reduction

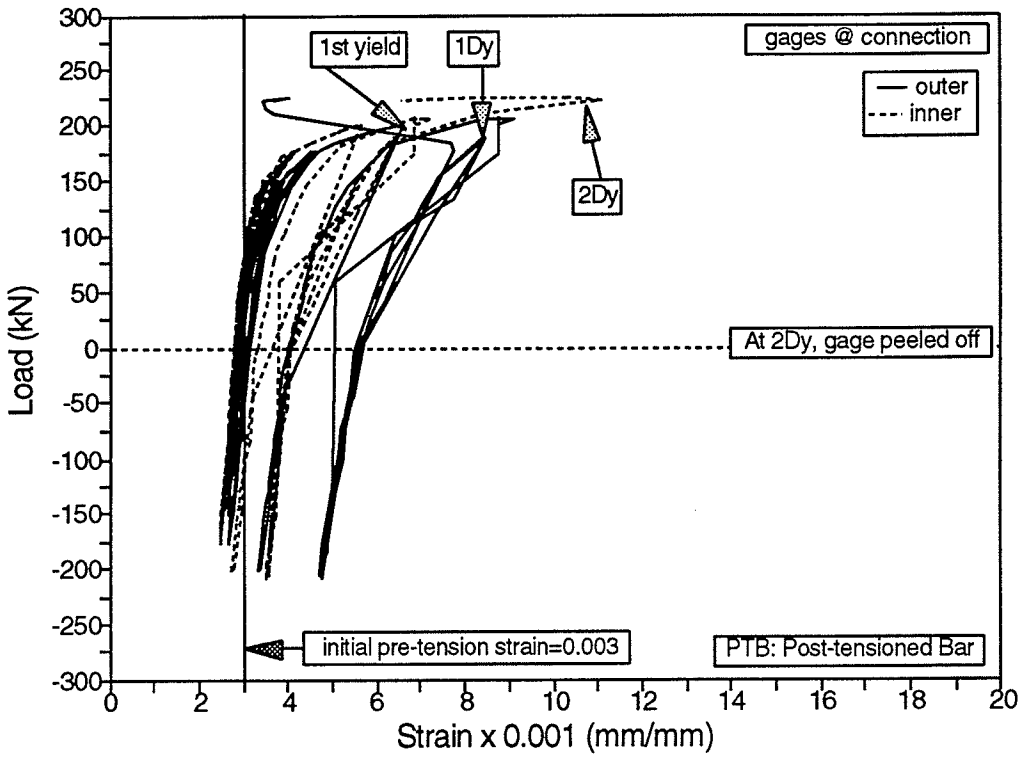

Figure 5.115(a) West bar inner & outer strain at connection push end for specimen PTB

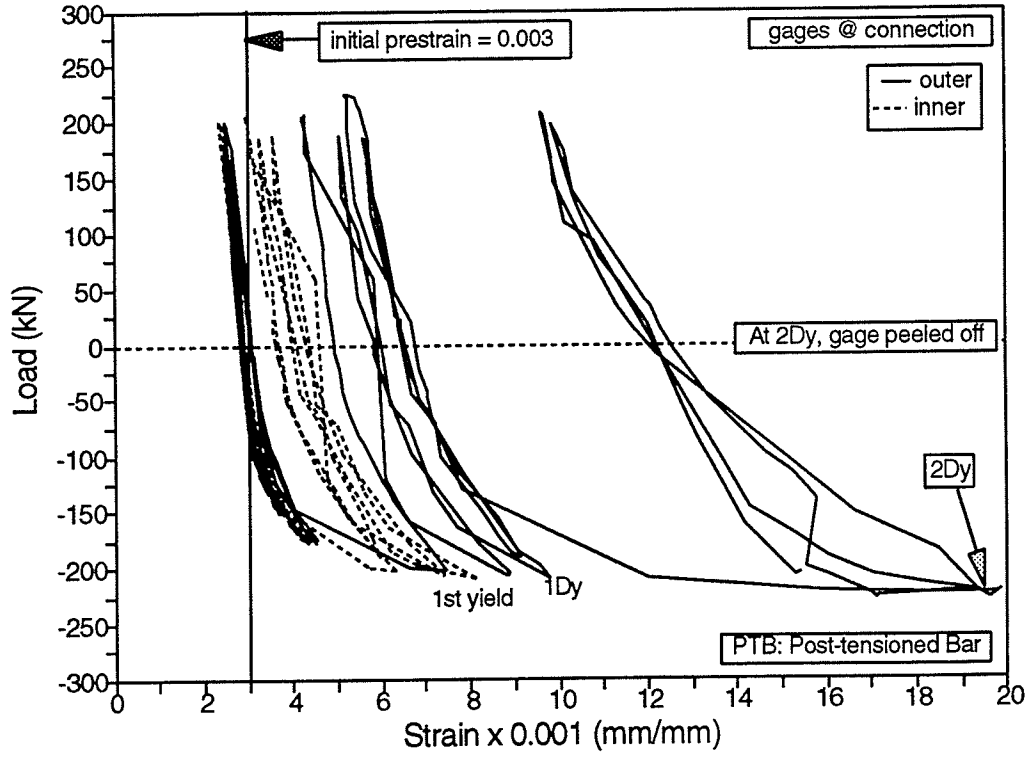

Figure 5.115(b) East bar inner & outer strain at connection push end for specimen PTB

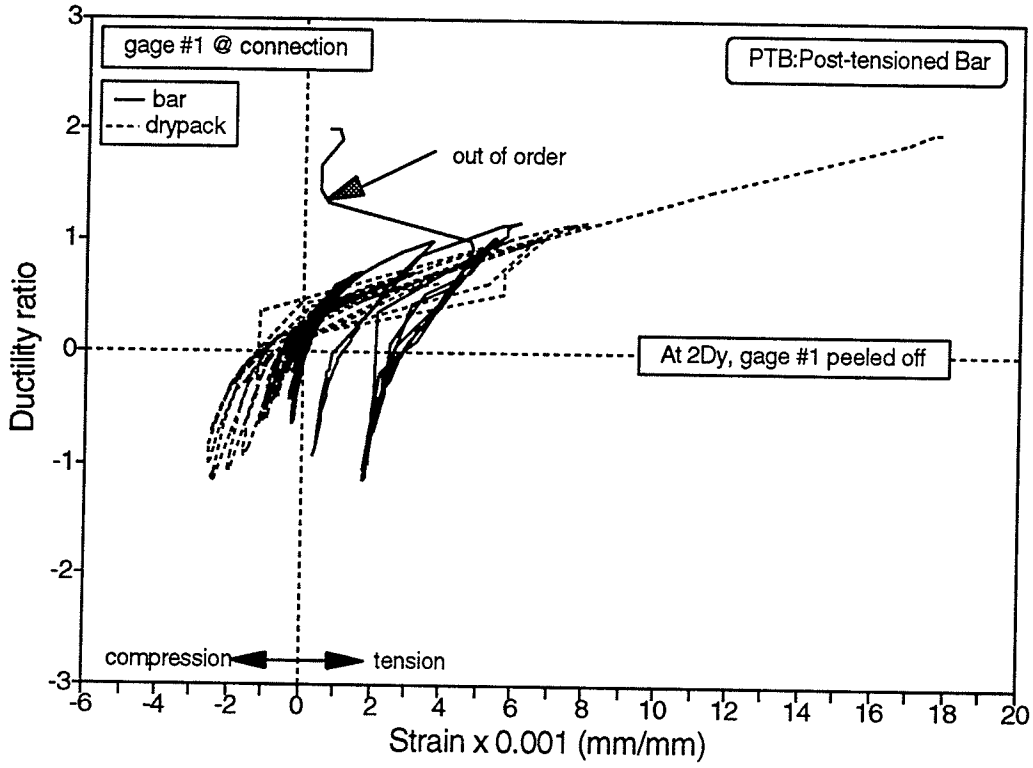

Figure 5.116(a) Comparison of bar and drypack strain at joint push end for specimen PTB

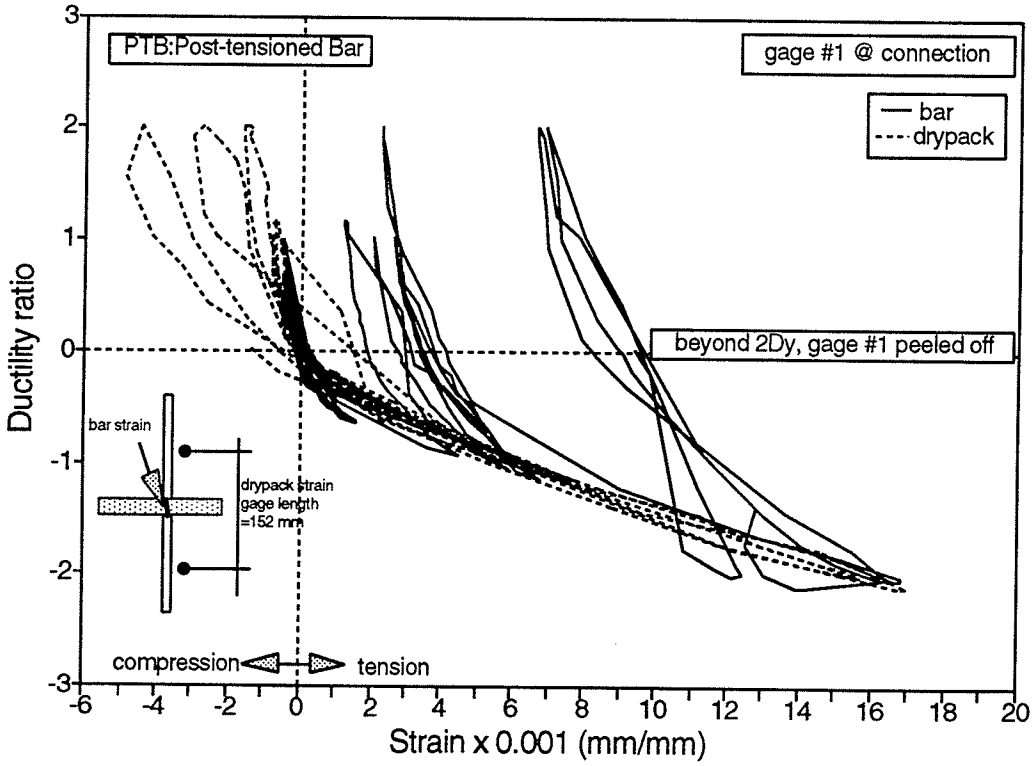

Figure 5.116(b) Comparison of bar and drypack strain at joint pull end for specimen PTB

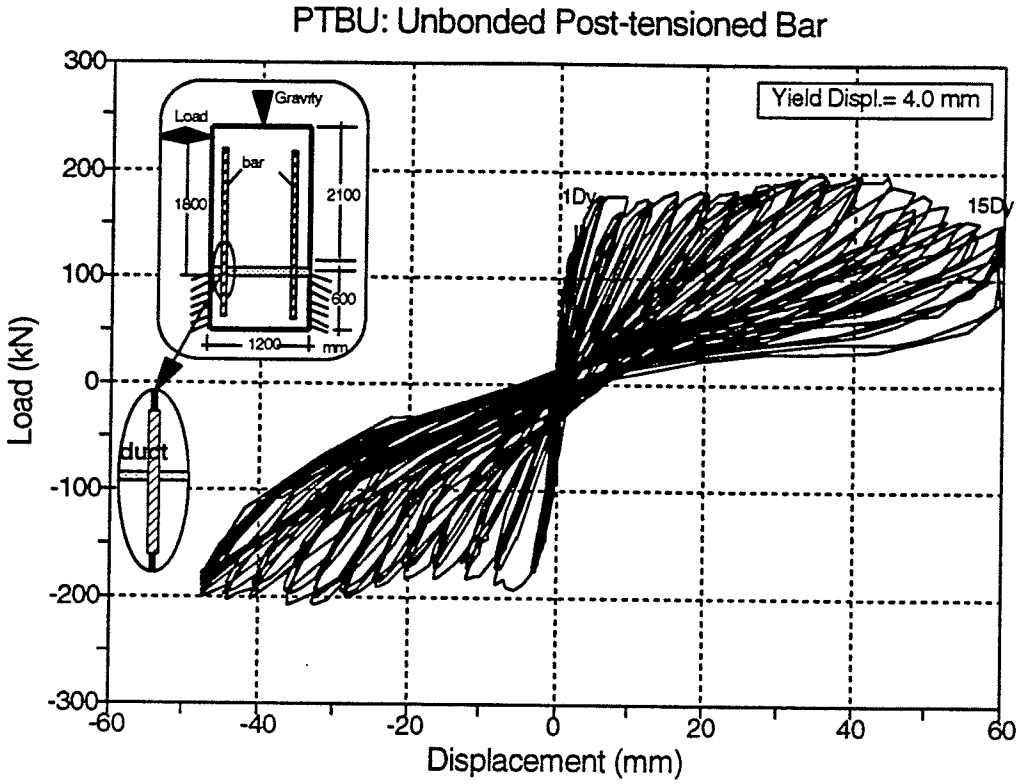

Figure 5.117(a) Hysteresis loops of load vs. displacement behaviour for specimen PTBU

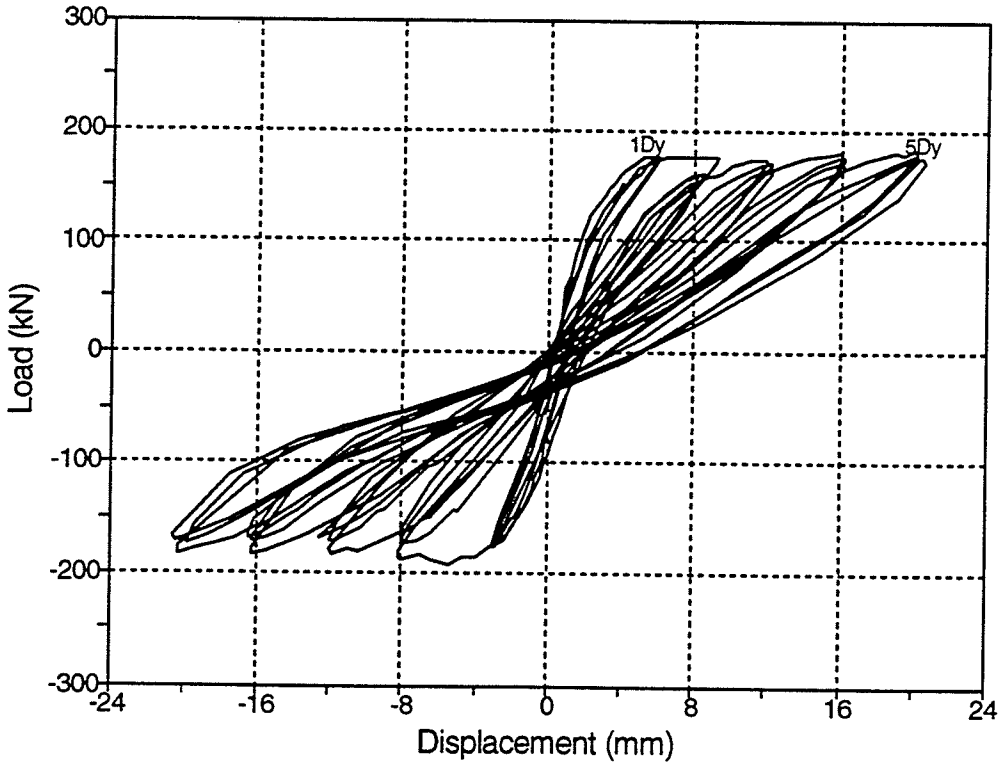

Figure 5.117(b) Hysteresis load-displacement at 1Dy to 5Dy cycles for specimen PTBU

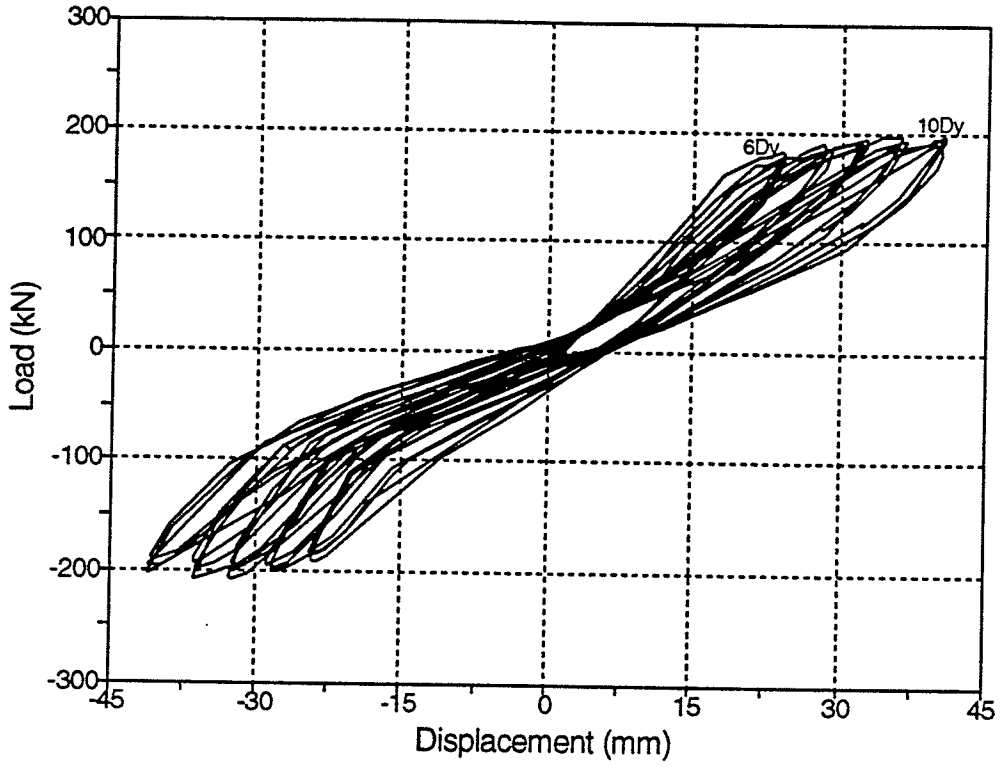

Figure 5.117(c) Hysteresis load-displacement cycles at 6Dy to 9Dy for specimen PTBU

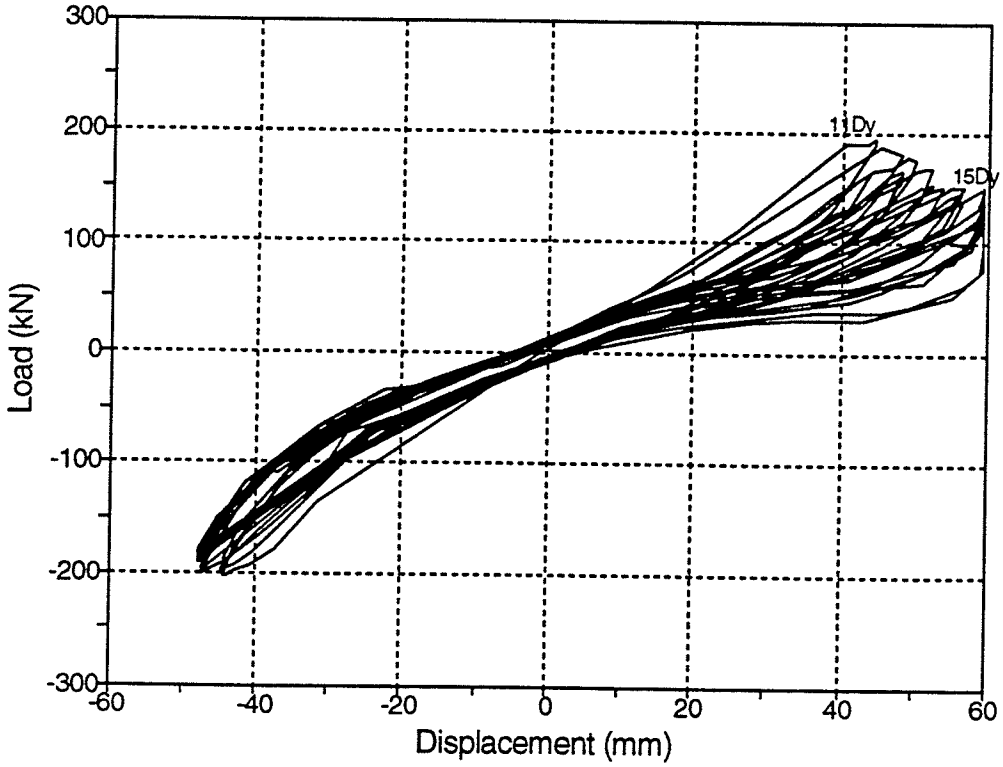

Figure 5.117(d)Hysteresis load-displacement cycles at 11Dy to 15Dy for specimen PTBU

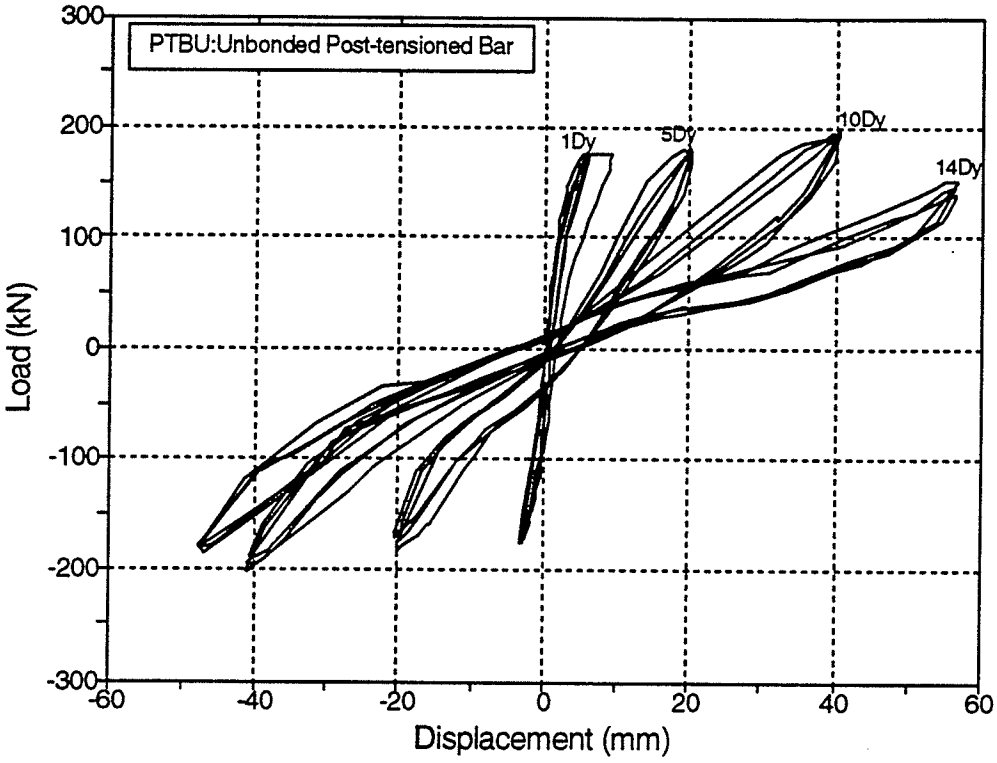

Figure 5.117(e) Hysteresis load-displacement cycles at 1, 5, 10, 14Dy of specimen PTBU

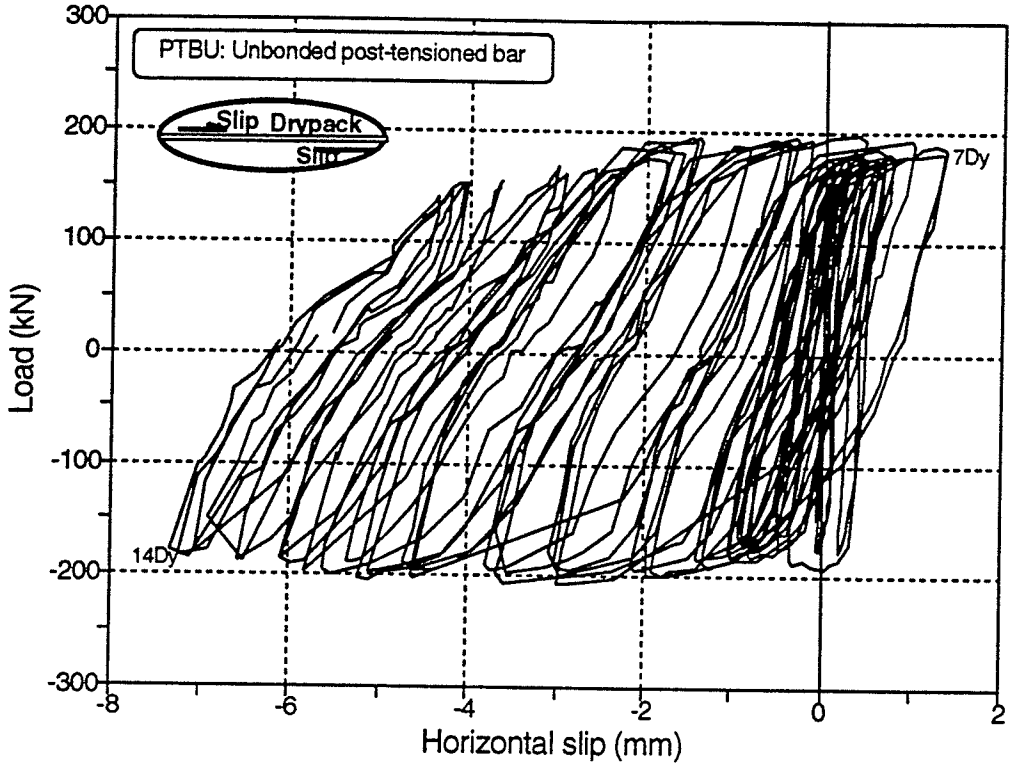

Figure 5.118(a) Hysteresis loops of load versus horizontal slip for specimen PTBU

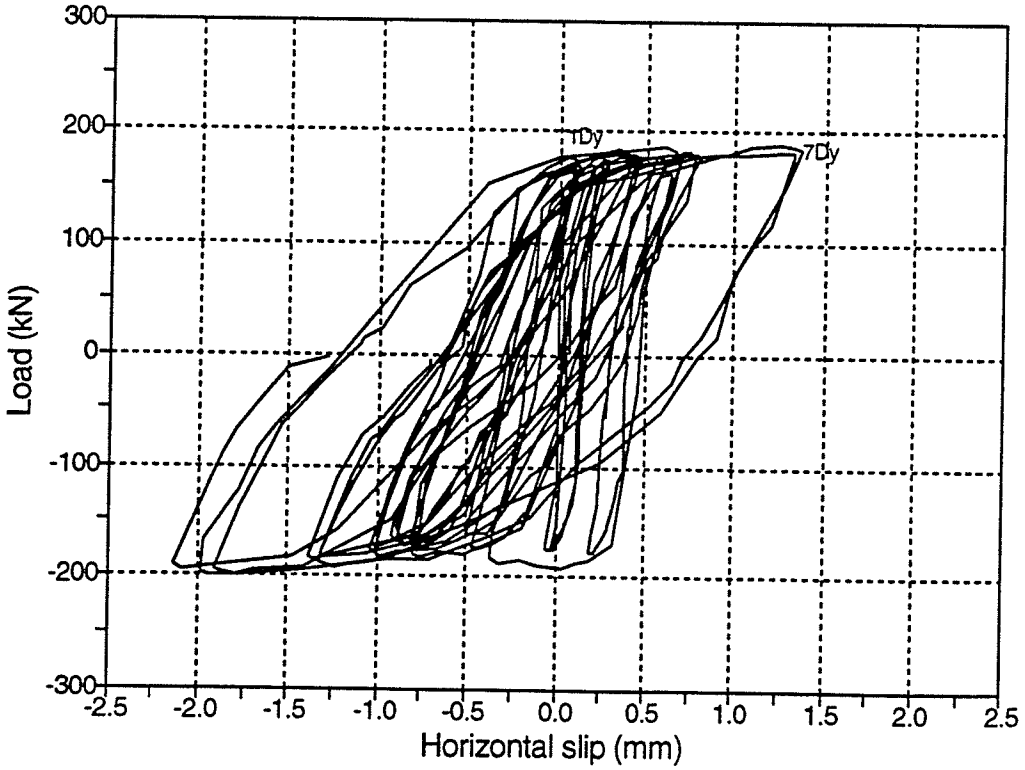

Figure 5.118(b) Slip hysteresis loops for specimen PTBU: 1 to 7Dy cycles

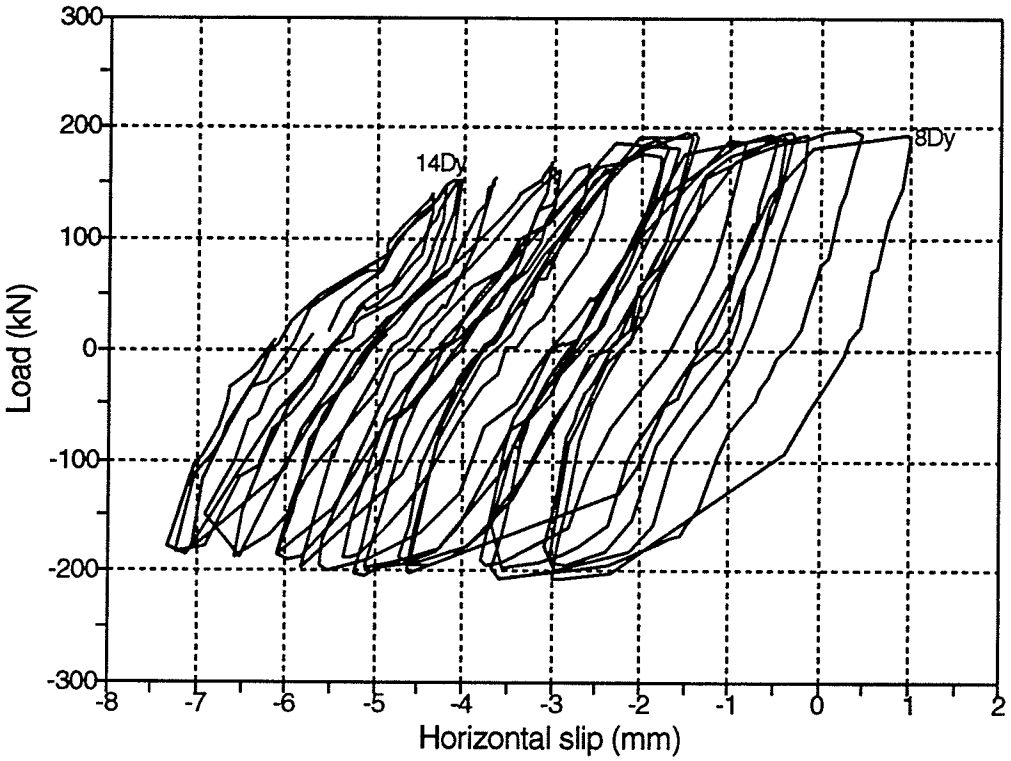

Figure 5.118(c) Slip hysteresis loops for specimen PTBU: 8 to 14 Dy cycles

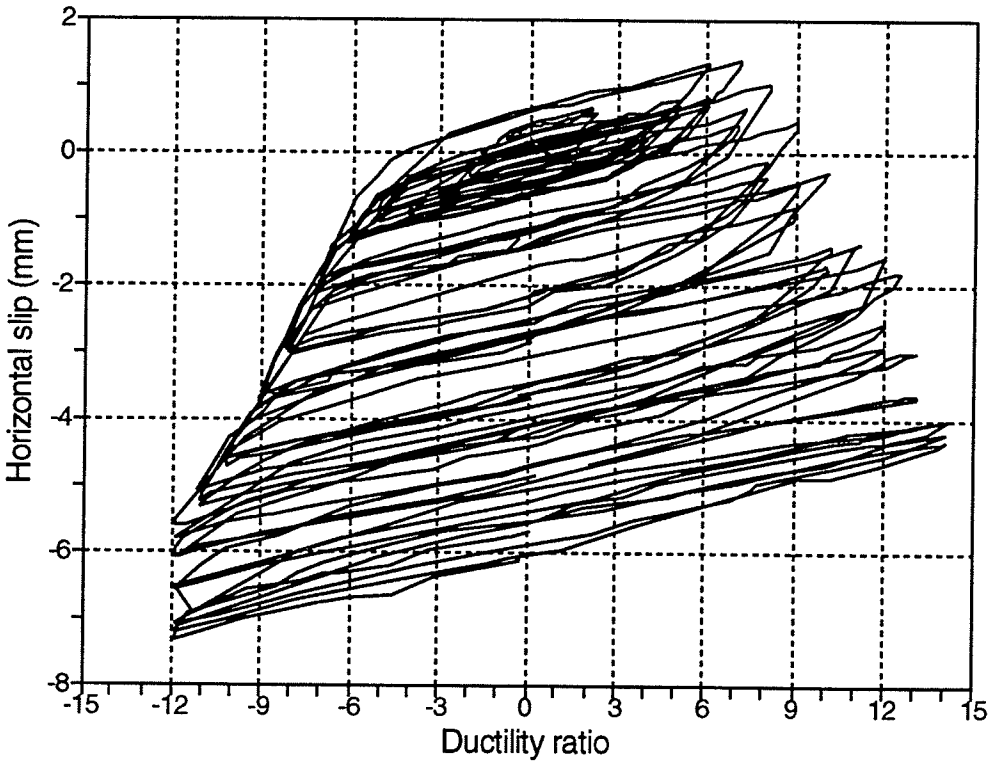

Figure 5.118(d) Hysteresis loops of horizontal slip vs. ductility for specimen PTBU

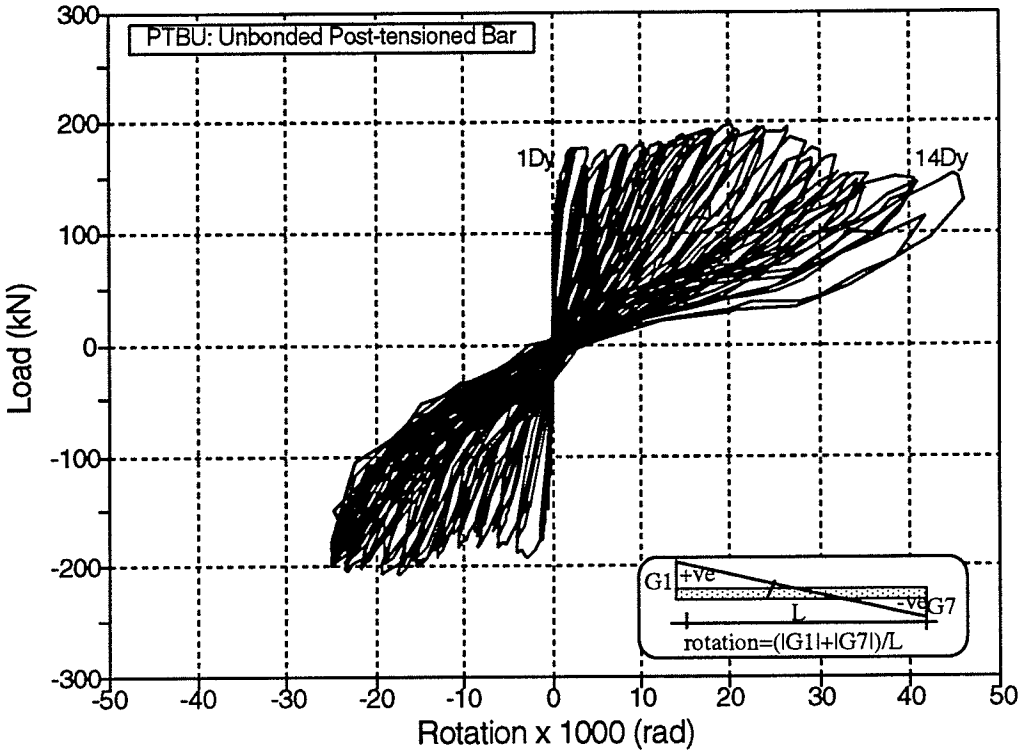

Figure 5.119 Hysteresis loops of load vs. rotation for specimen PTBU

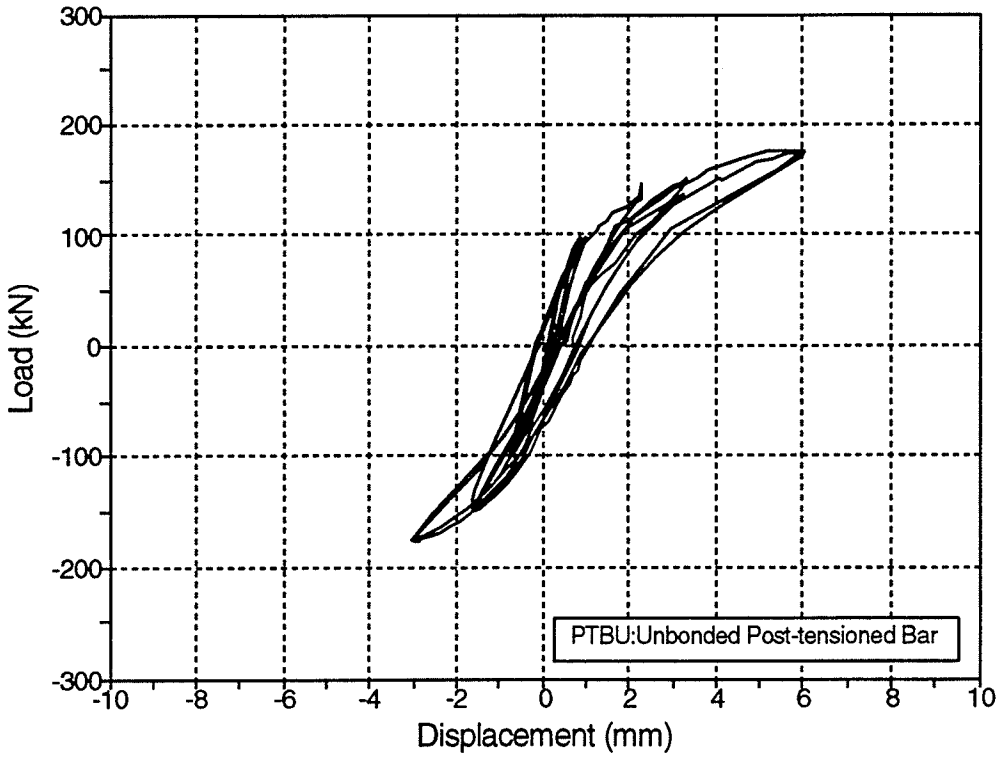

Figure 5.120 Elastic hysteresis loops of load vs. displacement for specimen PTBU

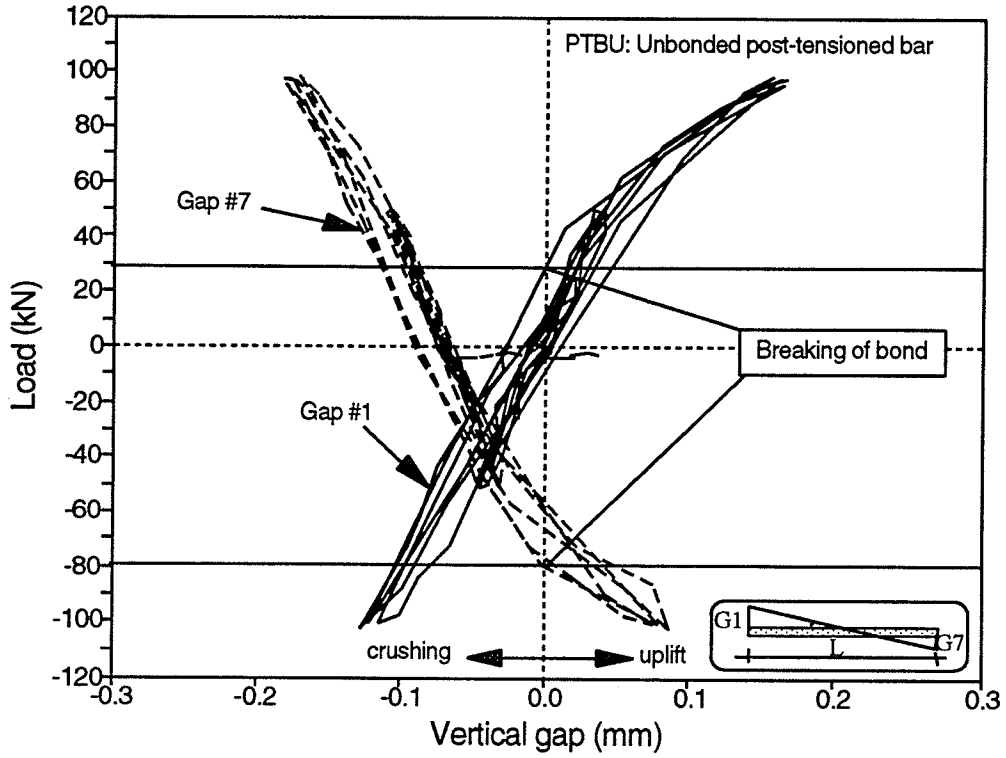

Figure 5.121 Onset of breaking of bond in load vs. gap hysteresis for specimen PTBU

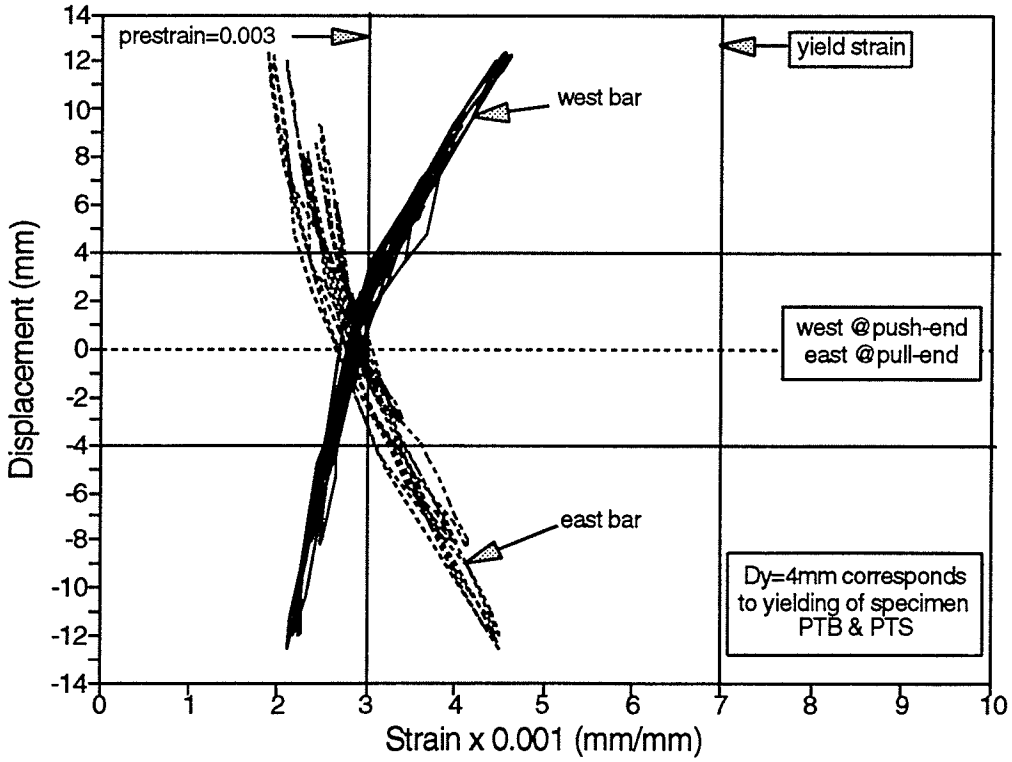

Figure 5.122 Bar strain vs. displacement relationship for specimen PTBU: initial stage

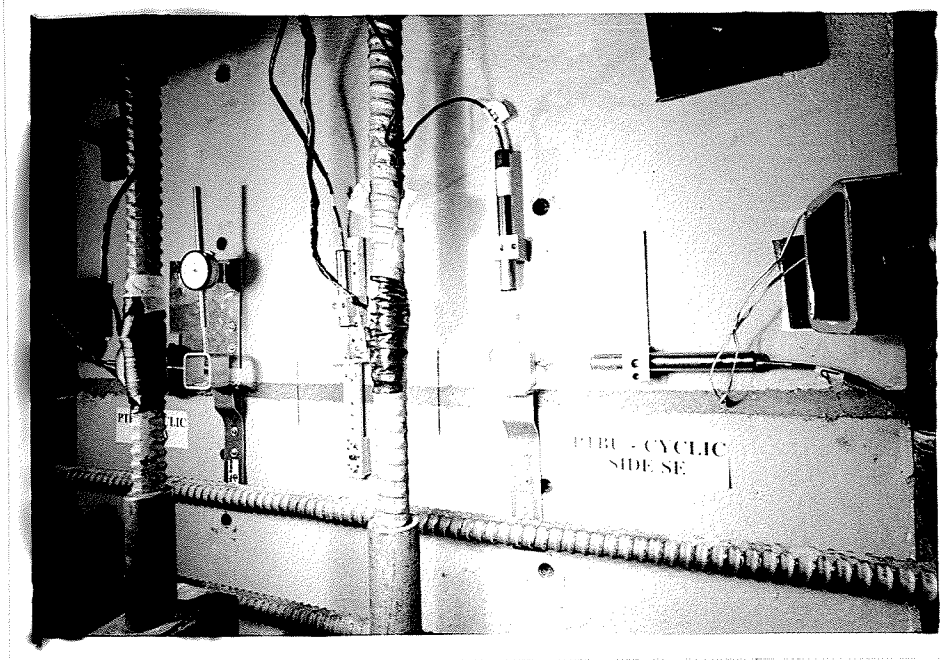

Figure 5.123(a) Condition of connection for specimen PTBU: at start

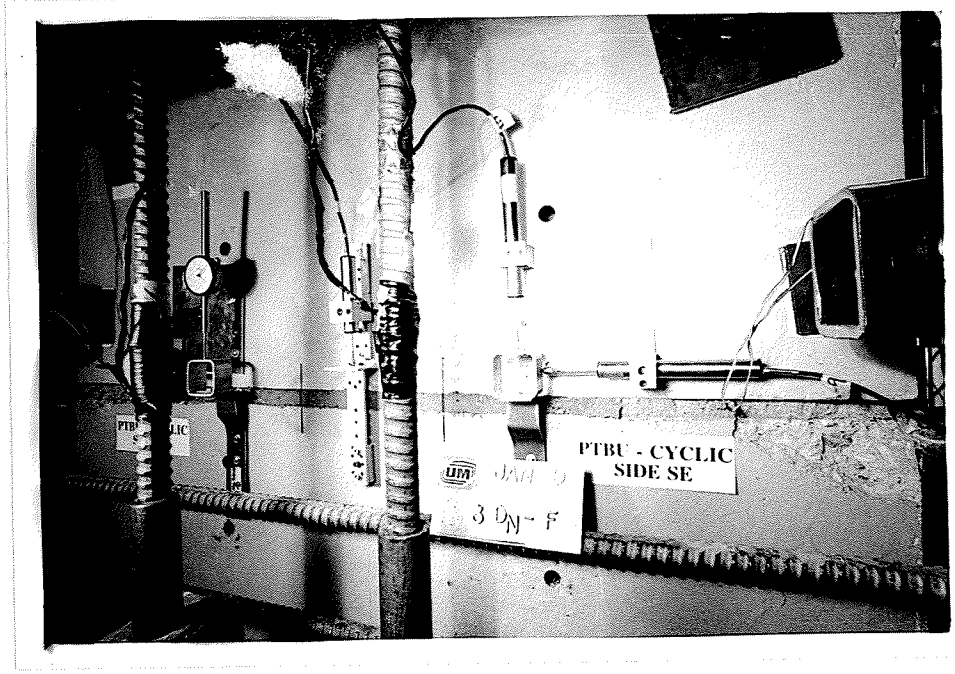

Figure 5.123(b) Condition of connection for specimen PTBU: at 3Dy

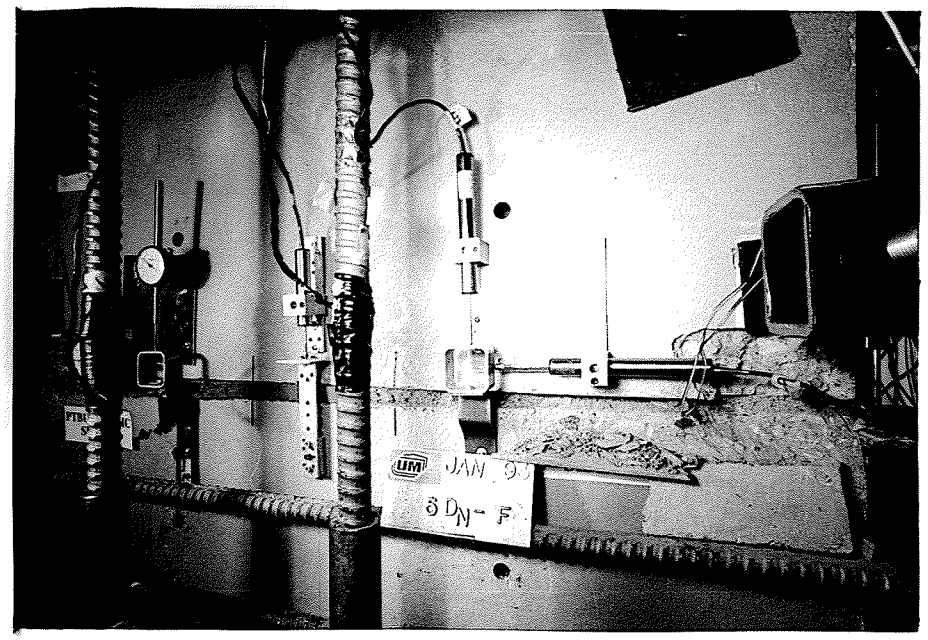

Figure 5.123(c) Condition of connection for specimen PTBU: at 5Dy

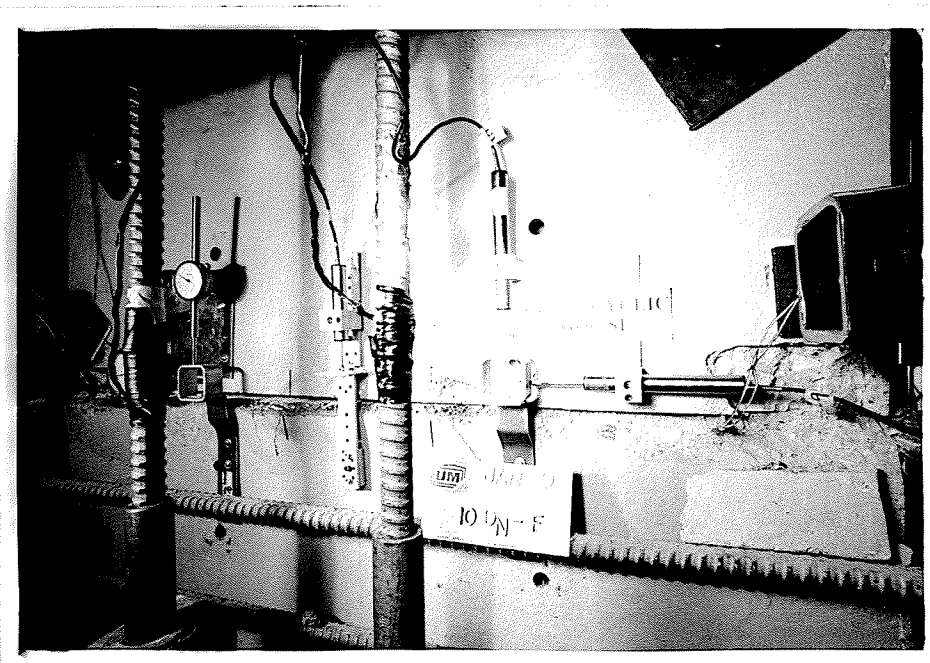

Figure 5.123(d) Condition of connection for specimen PTBU: at 10Dy

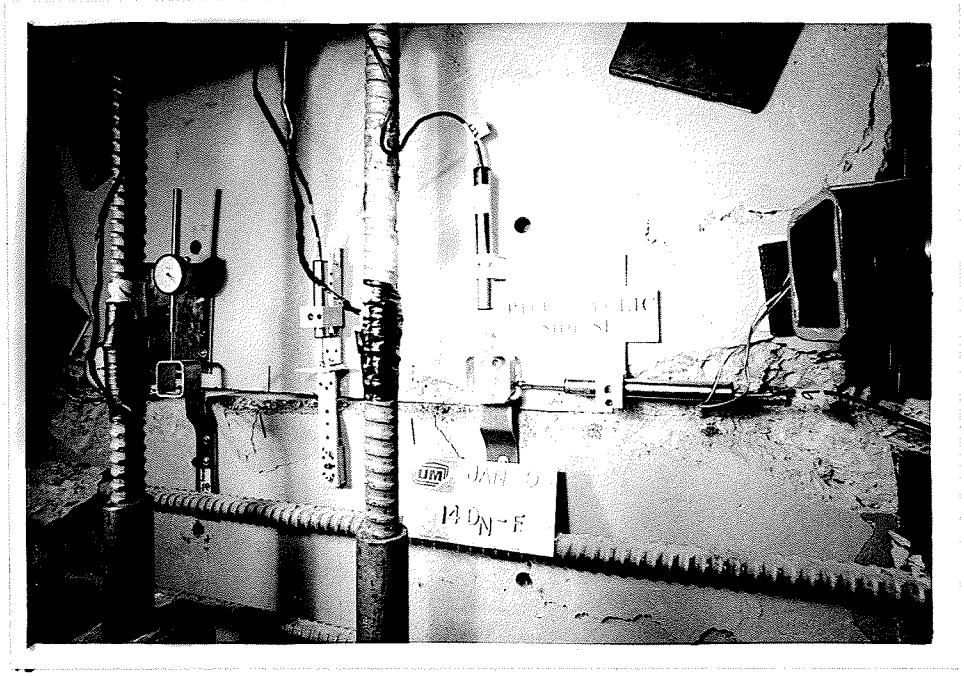

Figure 5.123(e) Condition of connection for specimen PTBU: at 14Dy

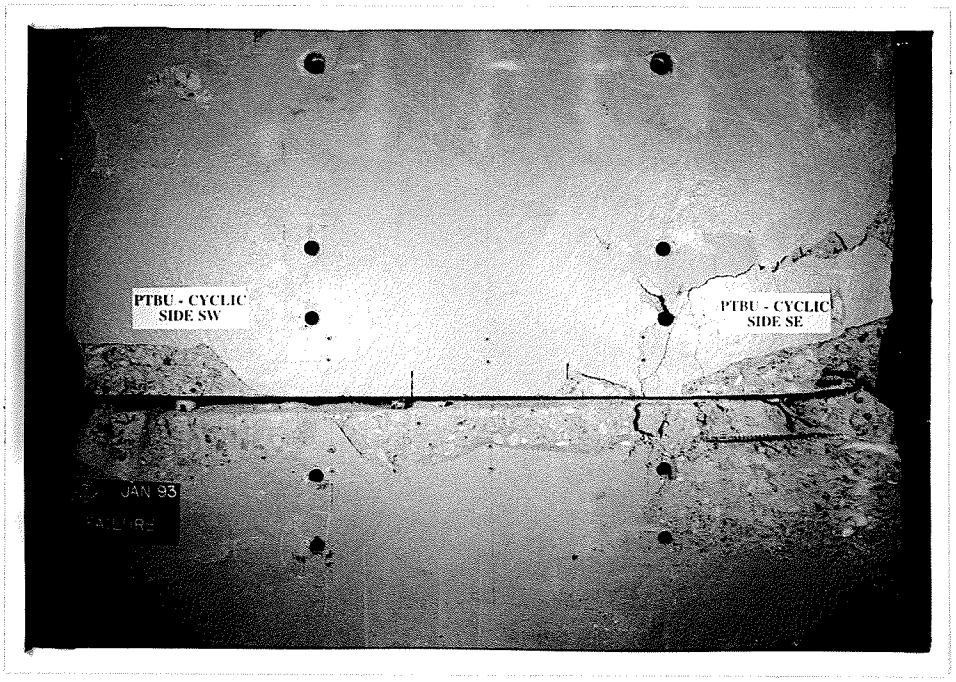

Figure 5.123(f) Condition of connection specimen PTBU: post-failure outside frame

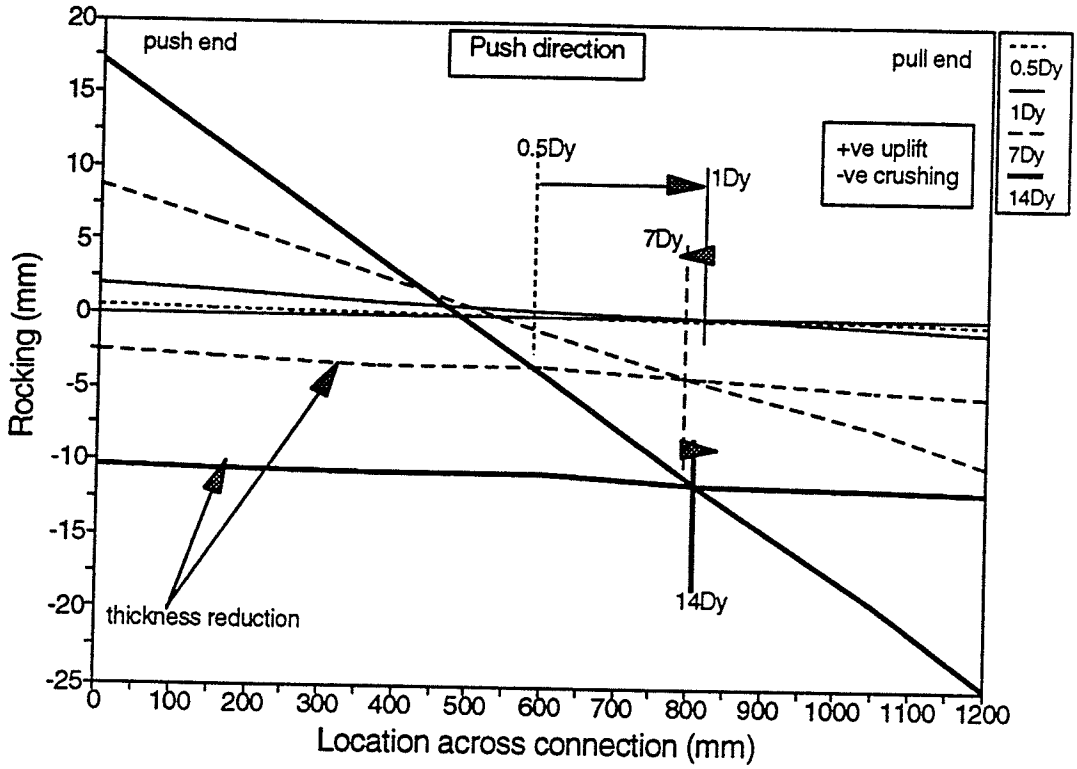

Figure 5.124(a) Rocking behaviour in the push direction for specimen PTBU

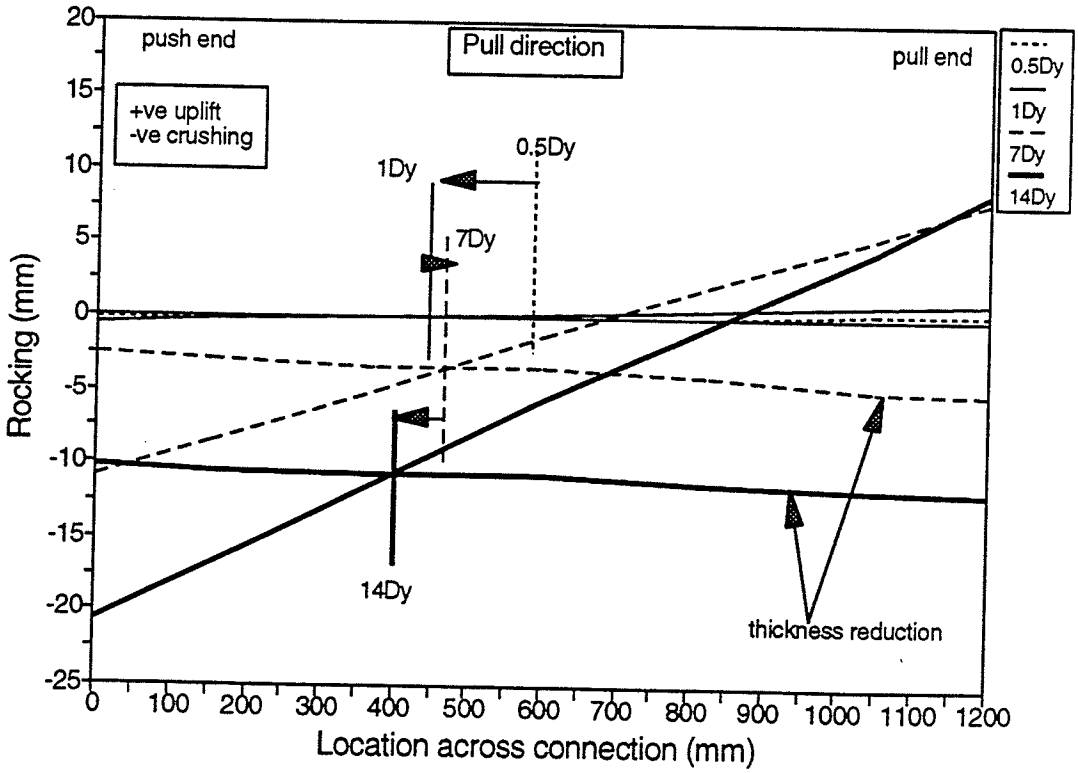

Figure 5.124(b) Rocking behaviour in the pull direction for specimen PTBU

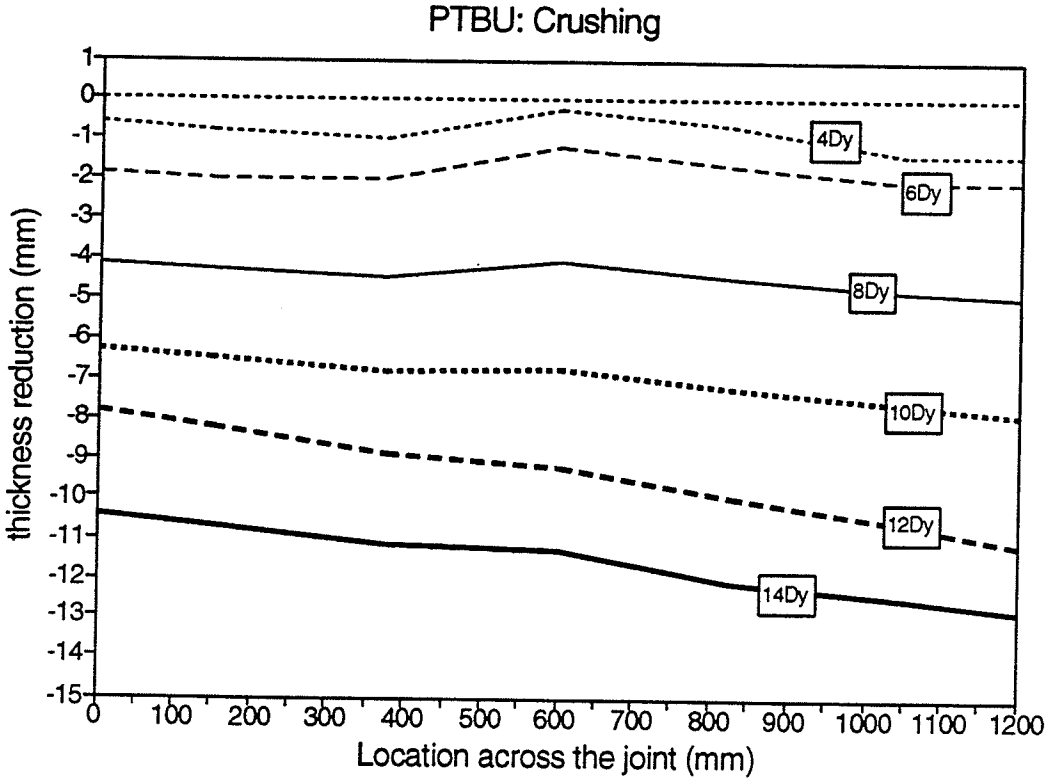

Figure 5.124(c) Rocking behavior for specimen PTBU: thickness reduction

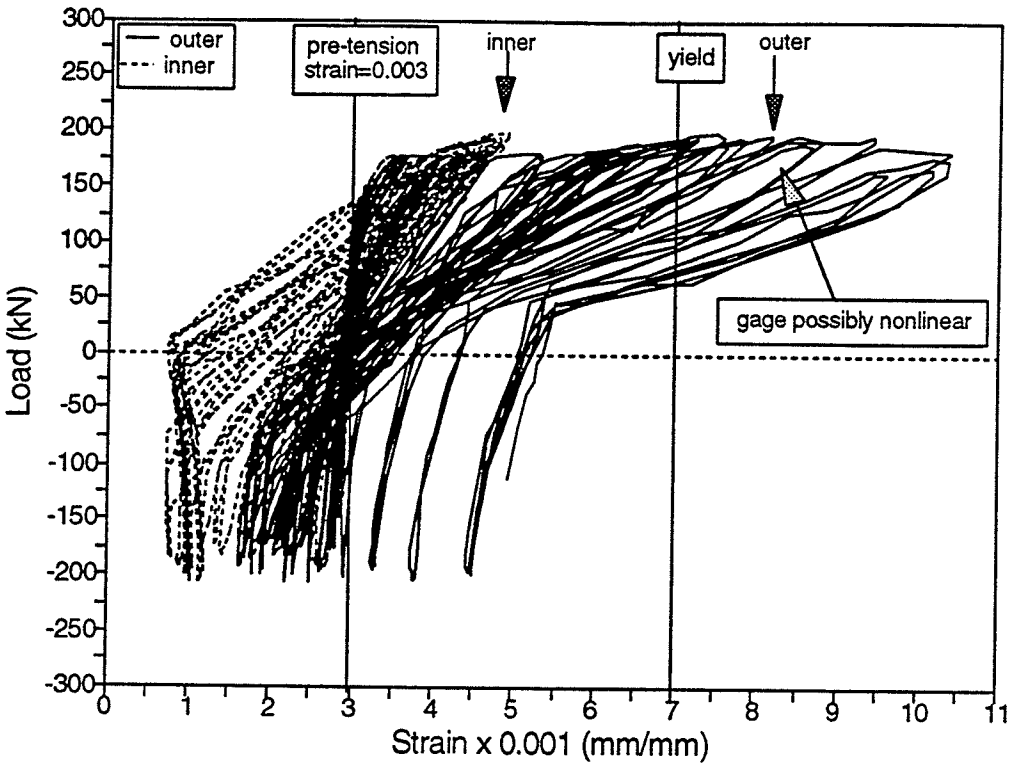

Figure 5.125(a) Strain at inner & outer gage on push end bar for specimen PTBU

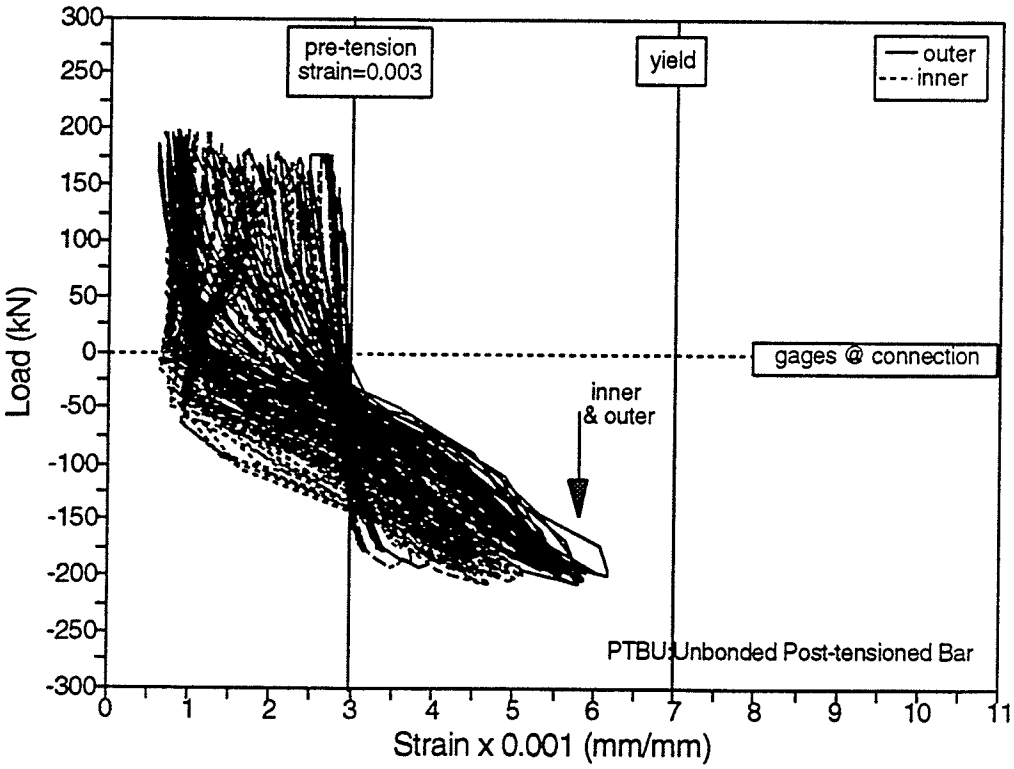

Figure 5.125(b) Strain at inner & outer gage on pull end bar for specimen PTBU

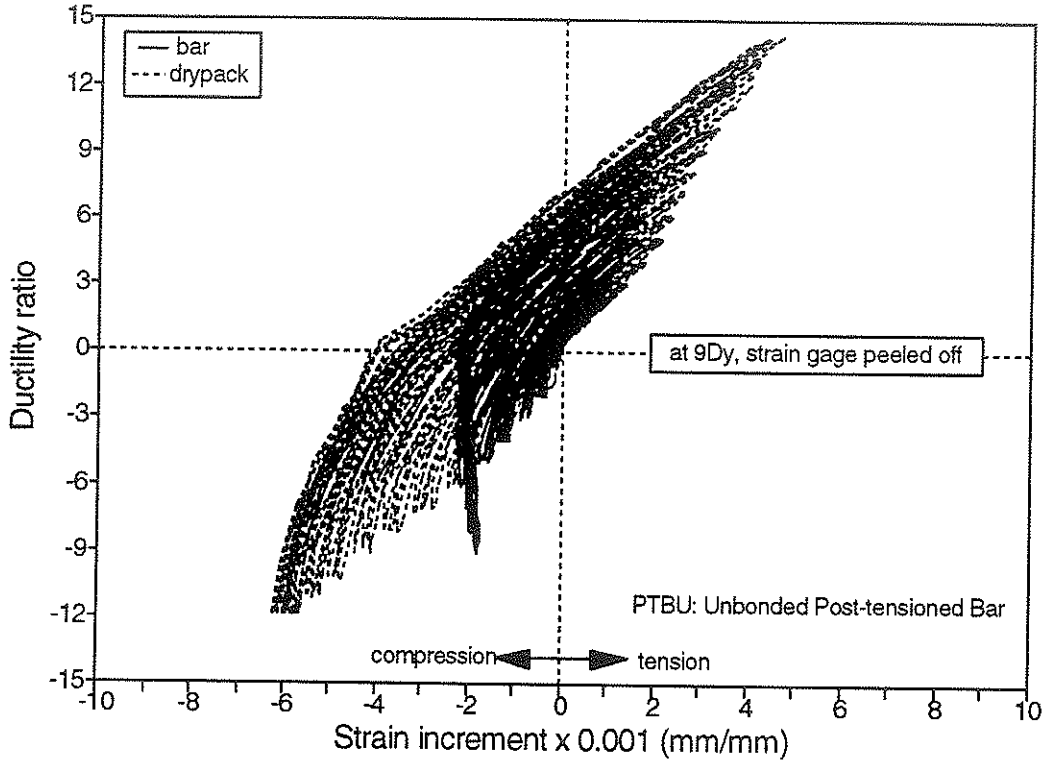

Figure 5.126(a) Comparison of bar and drypack strain at push end for specimen PTBU

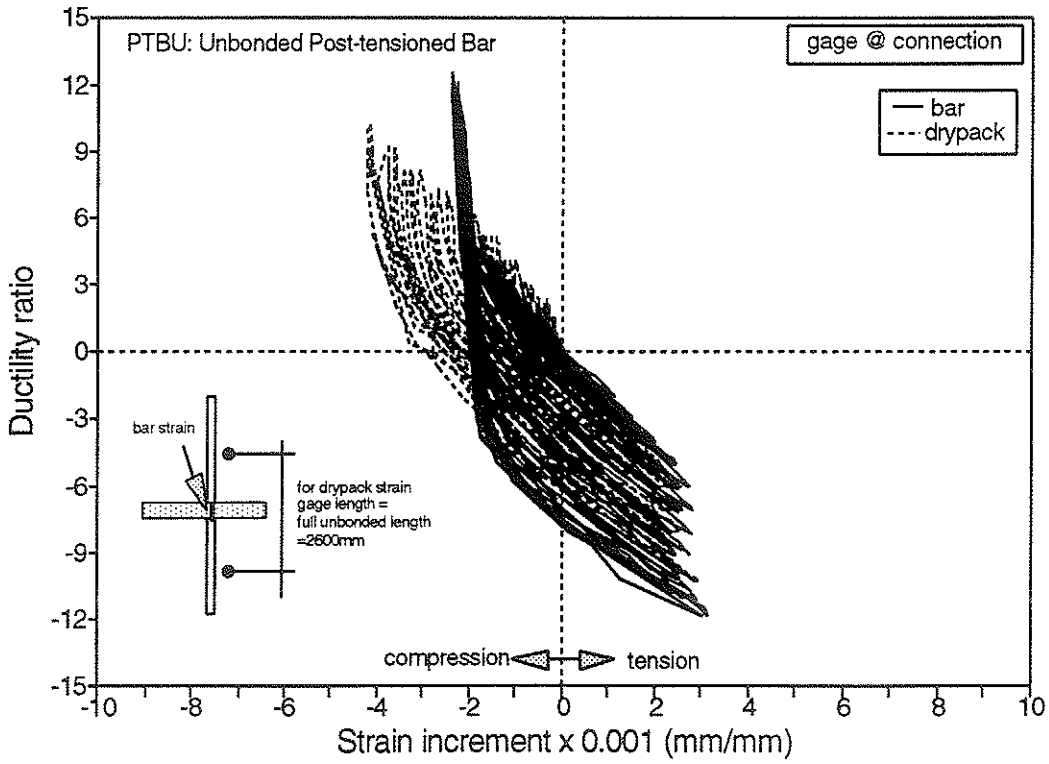

Figure 5.126(b) Comparison of bar and drypack strain at pull end for specimen PTBU

CHAPTER 6

DISCUSSION OF FLEXURE/SHEAR TEST RESULTS

6.1 INTRODUCTION

This chapter discusses in detail the results of the combined flexure/shear experiments. The specimens under monotonic loading condition are treated first in section 6.2. The specimens with mild steel reinforcement subjected to cyclic load are discussed in section 6.3 and the cyclic specimens with prestressing reinforcement are discussed in section 6.4. Each section begins with a brief overview of the general performance and the observed damage at failure for the particular test group. This is followed by a more detailed discussion of critical response characteristics including, where applicable, overall load-displacement strength envelopes and various limits states; local joint rocking and joint slip; stiffness degradation; strength; ductility; and energy dissipation capacity. (The energy dissipation and stiffness loss were not observed in the monotonic specimens and are characteristics of the cyclic specimens only). Comparisons of the performance among the specimens in each test group are made based on the different response characteristics. This made it possible to identify the contribution of the different configurations and experimental variables in each test group to the behaviour of precast wall connections. The rationalization of the resistance mechanisms for such connections is presented later in Chapter 7.

6.2 SPECIMENS SUBJECTED TO MONOTONIC LOADING

6.2.1 General

The results of specimens tested under monotonic loading conditions are discussed in this section. These specimens will be referred to henceforth as the monotonic specimens. Three specimens (RS-S, PTB-S, and PTS-S) were tested to study the monotonic behaviour of three different types of continuity reinforcement across the joint, namely: mild steel reinforcement, prestressing bars and prestressing strands. Each monotonic specimen had a companion cyclic specimen with identical configuration and material properties.

Each specimen was monotonically loaded in one direction. The specimen was subjected to elastic load-control increments until yielding of the reinforcement continuity, followed by displacement-control increments of the yield displacement. Throughout the test the 2 MPa vertical axial load was kept constant.

6.2.2 Performance and Damage Observations

The observed performance of the three static specimens was very similar. In general, the response was characterized by progressive crushing at one end of the connection in the compression zone and opening at the other end in the tension zone. At failure of the mild steel specimen, the bar pulled out from the NMB splice sleeve after undergoing strain similar to the rupture strain for a bar in tension. For the prestressed specimens, rupture of the prestressing bar or strand occurred at failure. The drypack within the compression zone remained almost intact with minor crushing and some spalling noted at the outer edges. Local shear deformation of the continuity reinforcement, mild-steel and prestressing, occurred in the compression zone of the

connection as well. Very minor compression-flexural cracking was noted in the top and bottom panels. Thus failure of the monotonic specimens was characterized by minor to moderate damage. The degree and extent of damage experienced by these specimens was not nearly as severe as in the case of the companion cyclic specimens. Since no load reversal was applied, the severe drypack deterioration along the connection length observed in the cyclic specimens did not occur and drypack crushing concentrated only at the connection end region within the compression zone. Also, progressive drypack deterioration due to the grinding action observed in the cyclic specimens did not occur.

6.2.3 Overall Specimen Response

In general, the monotonic specimens had similar overall response characteristics. The overall response is compared in terms of load-displacement relationships as shown in Figure 6.1. The load-displacement relationships were bilinear elasto-plastic and the behaviour was characterized by three distinct phases:

Phase I: Elastic behaviour - prior to yielding of continuity reinforcement: the behaviour is elastic almost linear without any visible damage.

Phase II: Plastic behaviour - following the yielding of continuity reinforcement without significant joint deterioration: the behaviour was plastic with hinging and minor damage without extensive crushing. The connection strength was very stable and remained almost constant during this phase.

Phase III: Residual behaviour - after failure with significant reduction in the load carrying capacity under increased deformation. This stage was characterized by hinging at one end of the joint with

moderate crushing and rupture of the prestressing steel or pull-out from sleeve of the mild steel reinforcement at the other end.

The three phases of the behaviour are illustrated in the load-displacement curves in Figures 6.1. The effect of the different continuity reinforcement on the overall response is also shown in these figures. It is obvious from Figure 6.1 that the reinforcement type had little or no influence on the connection stiffness as all three specimens had almost identical initial stiffness. The three specimens exhibited pronounced nonlinear behaviour at around the same displacement level and the measured yield displacement was identical for the three specimens. The specimen with mild steel reinforcement (RS-S), as designed, had higher connection strength than the post-tensioned specimens (PTB-S & PTS-S). Also, the strength of the connection post-tensioned with strands was slightly higher than that of the connection post-tensioned with prestressing bars. The failure modes of the different connections are also indicated in Figure 6.1. Failure of specimens post-tensioned with strands or bars was abrupt as shown by the sudden drop in the load at ultimate due to rupture of the prestressing bar/strand. Failure of the specimen with mild steel reinforcement was gradual, as seen in the load-displacement plot, due to the gradual pull-out of bar from the sleeve. With regard to the ultimate displacement capacity of the different connections, the specimen with prestressing strand had the lowest ultimate ductility while the specimen with post-tensioned bars had the highest ductility capacity. Thus the latter specimen showed the best performance as it had the largest ductility.

The relative performance of the specimens was compared in terms of normalized load versus ductility relationship shown in Figure 6.2. The normalized load is the ratio of the load to the maximum measured load and the ductility is the

ratio of measured displacement to yield displacement of the given connection. It is clear from Figure 6.2 that the three specimens had very similar overall response characteristics.

6.2.4 Connection Local Response

Due to the inherent low reinforcement content typically used for this type of connection and the relatively low elastic modulus of the drypack in comparison to the concrete walls, all inelastic deformations and damage were expected to be concentrated in the connection region. The basic response mechanisms of deformation in the connection could be characterized as a combination of: (i) Rocking associated with vertical opening of the drypack gap region at one extreme end while pivoting about the opposite end of the joint region; and (ii) Horizontal slip at the interface of the panel to the drypack. All the static specimens showed similar response characteristics in terms of rocking and slip. The behaviour of the two specimens with bars, mild steel (RS-S) and prestressed (PTB-S), was characterized by rocking with initially limited slip in the joint region at the early stages (up to 3Dy) followed by major slip with large displacement at onset of failure. The specimen with prestressing strands (PTS-S) had a limited slip mechanism throughout the duration of the test. The following paragraphs discuss and compare the rocking and slip behaviour of the three monotonic specimens.

6.2.4.1 Rocking Behaviour

The rocking behaviour was monitored by seven LVDT gap stations mounted vertically along the length of the connection. The layout of the instrumentation was explained

in section 3.9. Severe drypack deterioration along the connection length did not occur and crushing concentrated over the compression zone of the connection. The three specimens showed very similar rocking characteristics. Typical rocking behaviour is given in Figures 6.3, which shows the distribution of measured vertical gap deformations across the length of the connection at various loading increments for specimen PTB-S. Two stages of the response could be identified: (1) initial elastic and (2) post-yield behaviour. The rocking at the joint region was slightly nonlinear for the initial elastic load increments as shown in Figure 6.3(a). The post-yield rocking behaviour was almost linear as shown in Figure 6.3(b). Figures 6.3 demonstrates how the neutral axis migrated within the connection length as the moment was increased. The behaviour went from pure compression to rocking about the centre line of the connection to hinging towards the connection ends. During hinging, the compression zone length remained constant as the displacement ductility was increased while the compression area was slightly reduced due to crushing of the drypack. The hinging phenomenon is evident in Figure 6.3(b).

A similar rocking characteristic was observed for specimens RS-S and PTS-S with elastic and post-yield rocking stages. The only difference was in the extent of horizontal hinge length at the connection end: specimen PTB-S hinged at about L/3, specimen RS-S hinged at about L/5 and specimen PTS-S hinged at about L/6, where L is the connection length. The variation of measured compression zone depth versus displacement ductility ratio is shown in Figure 6.4 for the three specimens. The different hinging ranges of the specimens are evident in Figure 6.4. The rocking behaviour was further compared in terms of rotation versus ductility relationship as shown in Figure 6.5. The rotation was defined in Figure 5.1(a) as the ratio of the

absolute summation of the gap stations at the opposite ends of the connection to the connection length. Figure 6.5 indicates again that the three specimens had very similar rocking characteristics. Looking closely at Figure 6.5, it could be seen that in the initial elastic stage below yield, the rotational capacity of the three specimens was almost identical. During the post-yield phase, the rotational capacity of the two specimens with bars, mild steel (RS-S) and prestressed (PTB-S), was close while that of the specimen with prestressing strands (PTS-S) was higher. The rotation of specimen PTS-S was about 20% higher than specimen RS-S while the rotation of specimen PTB-S was only 5% higher than that of RS-S for a given ductility ratio. This suggested that PTS-S was more flexible than PTB-S and RS-S in the nonlinear range. This can be attributed to the lower stiffness of the strand relative to that of the bars. This behaviour occurred after loss of prestress due to deterioration of grout. However, it should be noted that the variation was rather small.

6.2.4.2 Slip Behaviour

The horizontal slip behaviour was measured by two LVDT slip stations, one at each end of the connection. The slip characteristic of the specimen with strands was different from that of the specimens with bars as shown in Figure 6.6, which compares the slip versus ductility relationship for the three specimens. The two specimens with bars, mild steel (RS-S) and prestressed (PTB-S), had initially limited slip at early stages with the slip accounting for less than 5% of the total deformation. The connection response was governed mainly by rocking at this initial stage. This stage was then followed by a nonlinear increase in the slip up to a maximum of about 17% and 14% of the total deformation at onset of failure for specimens PTB-S and RS-S, respectively. The increase in slip occurred as a result of drypack crushing in the

compression zone. On the other hand, the specimen with prestressing strands (PTS-S) had a limited slip mechanism throughout the duration of the test with the slip maintaining around 5% of the total deformation. The percentage of slip to displacement ratio at different ductility levels is presented in Figure 6.7. The different stages of the slip response for the specimens with bars are clearly indicated in Figure 6.7. It is clear from the figure that specimen PTS-S had consistently the lowest slip contribution to the total deformation at all ductility levels.

The shear-force-slip mechanism was mainly resisted by a Coulomb-type friction at the panel-to-drypack interface in the compression zone region since the drypack grout remained intact at all stages of loading. The contribution of the steel reinforcement to the slip mechanism appeared to be negligible. The magnitude of the measured slip was too small, about 50% lower than in the pure shear tests, to activate any clamping action of the compression reinforcement. Also, the gap opening (uplift) of the connection at the location of the tension reinforcement and the inherent flexibility of the reinforcement would increase the link length over which the horizontal shear was transferred to the reinforcement and would make the contribution of the tension reinforcement almost nil. However, to include the contribution of the reinforcement in shear resistance, the apparent coefficient of friction, μ, was calculated as the ratio of the applied shear (measured horizontal load) to the drypack compressive force as follows:

$$\mu = \frac{V}{C_d} \tag{6.1}$$

where

V = connection shear resistance, measured horizontal load

C_d = drypack compressive force in the compression zone

μ = coefficient of friction

The drypack compressive force, C_d, was calculated from equilibrium of forces in the connection region using measured material properties. From the measured results, apparent coefficients of friction about 0.65, 0.55 and 0.40 were determined for specimens RS-S, PTB-S and PTS-S, respectively, under combined flexure and shear loading. It is worth noting that the average coefficient of friction of a similar specimen tested under cyclic pure shear loading condition was in the order of 0.80 (West, 1993). Also, as was evident in the pure shear tests (West, 1993), it was virtually impossible to quantify the magnitude of the slip deformation. The pure shear test results indicated that the shear–force—shear–slip relationship was an unconfined elasto-plastic mechanism. Thus the slip contribution to the overall response would be represented as a percentage of the total deformation.

The distinct similarity between the load versus rotation and load versus slip relationships indicates that flexural and slip deformations might be coupled. In general, sliding at one end was in phase with uplift at the other end of the connection and the peak slip displacement was in proportion to the uplift. Thus coupling of the flexural and shear displacements could be quantified experimentally by means of slip versus rotation relationship shown in Figure 6.8. Figure 6.8 shows an almost linear relationship between slip and rotation. The slope of the slip-rotation relationship was determined by linear regression to be 32%, 38%, and 11% for specimens RS-S, PTB-S and PTS-S, respectively. Thus the slip to rotation was about 35% for connections with bars and 11% for connections with strands.

6.2.5 Connection Stiffness

The stiffness of the connection in the test specimen was expressed as the slope of the graph of the horizontal load versus the displacement at the top of the upper panel. Due to the nonlinear characteristic of the drypack material, the load-displacement relationship exhibited nonlinearity during the elastic loading stage. Thus the initial elastic stiffness cannot be evaluated definitively. However, the initial tangent stiffness, K_t, and the stiffness at yield, K_y, could be easily determined. The tangent stiffness was defined as the slope of the tangent at the origin of the load-displacement curve. The measured tangent stiffnesses for specimens RS-S, PTB-S and PTS-S were 120, 140 and 150 KN/mm, respectively. The tangent stiffness values had a 20% variability among the specimens. This could be attributed to the initial nonlinearity of the material or to the lack of accuracy of the instrumentation in the initial stages. The yield stiffness, a secant stiffness, was given as the ratio of the yield load to the yield displacement. The measured yield stiffnesses for the specimens were very close at about 55, 48, and 50 kN/mm for specimens RS-S, PTB-S and PTS-S, respectively. The variability in the measured yield stiffness values was only 12%. The stiffness evaluation for the monotonic specimens is presented in Figures 6.9 to 6.11. The tangent stiffness and the yield stiffness are evident in these Figures. The specimen elastic stiffness is somewhere between the tangent stiffness and the yield stiffness. As a guide, the PRESSS program (Priestley, *et al.,* 1992) defined the elastic stiffness, K_e, as the secant stiffness corresponding to a load of 75% of the maximum nominal load. This elastic stiffness is also shown in Figures 6.9 to 6.11. For specimen RS-S, the load corresponding to 75% of the maximum is the same as the yield load and thus the elastic stiffness coincides with the stiffness at yield.

6.2.6 Connection Strength

The maximum connection strengths for the static connections tested are given in terms of the maximum measured load in Table 6.1. The measured maximum load was achieved at or close to the ultimate displacement of the connection. In general, the measured strength of the connection with mild steel reinforcement (RS-S) was 20% higher than the connection with prestressed bars (PTB-S) or strands (PTS-S). This was mainly due to the differences in size and material characteristic of the reinforcement type. The strengths of the two prestressed connections (PTB-S and PTS-S) were within 1% difference.

6.2.7 Connection Ductility

The large connection deformability associated with rocking and slip allowed the precast shear wall subassemblage to withstand large magnitude of deformation up to onset of failure. Failure resulted from the inability of the connection to sustain additional load. The deformational capacity of the system is expressed in terms of the ultimate displacement ductility or the drift. The ultimate displacement ductility is defined as the ratio of the displacement at failure to the displacement at yield as follows:

$$\mu_{\Delta} = \frac{\Delta_u}{\Delta_y} \tag{6.2}$$

Table 6.1 gives the ultimate displacement ductilities, and maximum drift for the three static specimens. Also given in Table 6.1 are values for the connection stiffness at yield and the percent slip to displacement ratio. The ultimate drift is defined as the

ratio of the ultimate displacement at the top wall panel to the effective height of the top panel above connection region.

While the yield displacement of the three specimens was the same, the ultimate ductility was different. The ultimate displacement ductility for the specimen with mild steel reinforcement (RS-S) was 9 and the drift was 2%. The post-tensioned connection with prestressing bars, specimen PTB-S, had a ductility of 11 and a drift of 2.44%. Specimen PTS-S, post-tensioned with prestressing strands, had the lowest displacement ductility of 7 and drift of 1.56%. The lower ultimate ductility achieved by specimen PTS-S could be attributed to the material stress-strain characteristic of the prestressing strand.

In summary, specimen PTB post-tensioned with bars showed the best deformational capacity with the highest ultimate ductility. The ductility of the specimen PTB-S was 20% higher than specimen RS-S. The ductility of PTB-S, with prestressed bars, was about 60% higher than that of PTS-S, with prestressing strands. This increase in ductility can be attributed to the differences in prestressing reinforcement. The ductility of specimen RS-S, with mild steel reinforcement, was about 30% higher than that of specimen PTS-S, with prestressing strands.

6.3 MILD STEEL SPECIMEN SUBJECTED TO REVERSED CYCLIC LOAD

6.3.1 General

Five specimens with mild steel reinforcement continuity across the joint were tested under cyclic loading: specimen RS, RSK, RSU, RW, and RT. These specimens will be referred to in the discussion as the mild steel specimens. (The specimen nomenclature was explained earlier in section 3.2). All the mild steel specimens, with the exception of specimen RSK, had a plain surface joint. The experimental variables include:

1. Condition of joint surface:

a) plain surface (RS) versus b) shear keys (RSK)

2. Type of bar coupling:

a) splice sleeve (RS); b) welded to angle (RW); and c) bolted to tube (RT)

3. bar to panel concrete condition:

a) bonded reinforcement (RS) versus b) partially unbonded reinforcement(RSU)

Specimen RS, plain surface joint with bar mechanically spliced with a splice sleeve, will be used as the "control" or "reference" specimen. The behaviour of the remaining four specimens will be discussed in comparison to specimen RS. The behaviour of the companion monotonic specimen RS-S is also compared to that of specimen RS.

Each specimen was subjected to a two-phase cyclic loading history: load-control cycles and displacement-control cycles. The load-control cycles consisted of 3 cycles at increasing increments of the theoretical load up to the connection yield. The displacement-control cycles were multiples of the yield displacement. Three

cycles were applied at each displacement ductility level, followed by a lower service level cycle. The top displacement is the relative top panel to bottom panel displacement measured at the location of the applied horizontal load as explained in section 5.1. The applied displacement ductility ratio was increased as the test progressed. Throughout test, the normal stress applied to the top of the wall was kept constant at 2 MPa. A more detailed description of the cyclic loading history could be found in section 3.8.

6.3.2 Performance and Damage Observations

In general, the cyclic response of the mild steel specimens was similar and could be identified by the following stages:

1. Rocking: continuous opening and closing of the joint region.
2. Crushing of drypack and panel concrete in the compression zone at joint ends.
3. Yielding of continuity reinforcement at connection level.
4. Subsequent buckling of vertical reinforcement through the joint.
5. Spalling of concrete and drypack adjacent to the buckled bars.
6. Limited formation of flexural-shear cracks in the panel.
7. Hinge formation and deterioration of drypack in the joint region.
7. Progressive drypack crushing and spalling along the length of the connection.
8. Rupture of reinforcing bar at the weld toes in the RW (welded detail) and pull-out of the bar from the splice sleeve in the RS (splice sleeve detail) and severe wall deformations of the tube in specimen RT (tube detail).

The degree and extent of damage observed at failure varied among the specimens. Specimen RSU, RW and RT had major drypack deterioration at failure. Specimen RS had moderate damage across the connection length while specimen RSK

had moderate damage at the connection ends and no damage or minor damage to the shear keys which remained intact at failure. The behaviour of the mild steel specimens was detailed in section 5.3. The following is a brief recapulation of the behaviour of each specimen at failure:

Specimen RS failed by pull-out of the east bar from the sleeve in the 3rd cycle of loading increment to - 5Dy in the pull direction. Bar pull-out occurred after reaching strain levels corresponding to rupture of the bar. Drypack crushing concentrated at the connection end region, around 1/3 the connection length, and was ground to a very thin layer. However, the spread of crushing along the full length of the connection was limited. Average drypack crushing along the connection length was rather moderate at about 5% of the initial thickness. Few cracks were observed at the concrete panels around the connection region and no cracks were observed elsewhere. The crack pattern was limited to compression-type cracks. The slip at onset of failure was permanently shifted in one direction and tended to be slightly more towards the pull than the push-direction of loading. (The push/pull-directions of the load were explained in Figure 5.1). Slip consisted of 13 percent of the total deformation at failure.

Failure of specimen RSK occurred by pull-out of the west bar from the sleeve in the first cycle to + 5Dy in the push direction. No damage was observed in the shear keys which remained intact. Very minor cracking was noted in the concrete wall panel in the form of vertical compression crack. Moderate drypack crushing and spalling occurred at the connection end region and was concentrated over 1/6 the connection length from either end. Average drypack crushing did not occur as in the case of the RS connection. The shear-slip followed the loading direction and was limited to approximately 7 percent of the total deformation; thus the response was

predominantly flexural.

Severe drypack deterioration over the entire connection length occurred at failure of specimen RSU. The drypack was literally ground to dust in the connection region and the compression force was transferred to the wall panel concrete. Failure was by pull-out of the bar from the sleeve at the 1st cycle at + 7Dy. Average drypack crushing was over the entire connection length and was about 40% of the initial thickness of the joint. Cracking in the wall panels occurred by spalling off the concrete cover at the panel end region at the connection region. Buckling of the continuity reinforcement occurred. The slip was permanently shifted towards the pull than the push-direction of loading. The slip constituted about 15% of the displacement at failure.

The behaviour of specimen RW at failure was similar to that of specimen RSU with extensive drypack crushing and spalling. Overall crushing along the entire connection length was in the order of 60% of the initial thickness. Buckling of the compression reinforcement caused permanent shift in the force-slip behaviour. The slip was more towards the pull than the push-direction of loading and was about 35% of the total deformation. Onset of severe crushing and major slip was the 3rd cycle to 5Dy. The response stabilized during the cycles of 6Dy and failure occurred by rupture of the east bar during the 3rd cycle of -6Dy in pull direction.

Specimen RT failed at the 1st cycle of + 5Dy. Failure was characterized by severe drypack crushing and spalling at the connection extreme end, severe crushing and partial spalling of the drypack within the tube section and local buckling of the tube section due to shear deformations. Vertical compression cracks were noted in the wall panels. Average drypack crushing along the connection length was less than 1%. Slip was symmetric and consisted of about 14% of the total deformation.

6.3.3 Overall Specimen Response

The overall cyclic response of each specimen was monitored by hysteresis loops of the load versus the displacement relationship. The load was the applied horizontal load at the top of the upper panel and the top displacement was defined as difference between the top panel displacement at location of the applied load and the displacement of the bottom panel close to the joint region. A typical cyclic response strength-envelope is shown in Figure 6.12. The measured cyclic responses of all the mild steel specimens are shown in Figures 6.13 to 6.17. These figures also include the strength envelopes of the cyclic response for each specimen tested. The strength envelope is the envelope of the measured absolute maximum/minimum loads at different displacement increments. The strength envelopes will be compared later in this section to discuss the relative performance of the different mild steel specimens.

As seen in Figures 6.13 to 6.17 all the mild steel specimens had very similar cyclic response characteristics. All specimens showed very good ability to maintain peak resistance with continued cycling beyond first yield. The mild steel specimens exhibited stable hysteretic behaviour until onset of failure, followed by degraded slightly pinched loops during post-failure cycles. Failure of the different connections is also indicated in Figures 6.13 to 6.17: specimens where the reinforcing bar was coupled with a splice sleeve (RS, RSK, RSU) or with the tube section (RT) had a gradual failure. The specimen where the reinforcing bar was welded (RW) had an abrupt failure by rupture of the bar. In general, the overall behaviour of the connection can be characterized by three distinct phases depending on the degree of joint deterioration:

Phase I: Initial linear elastic behaviour prior to connection yield without

any visible damage.

Phase II: Post-yield behaviour without significant joint deterioration - behaviour was consistent with nearly stable hysteresis loops and minor damage without extensive crushing.

Phase III: Post-yield behaviour with significant joint deterioration - with significant reduction in load carrying capacity under increased deformation. This stage was characterized by bar rupture at the weld or pull-out of bar from sleeve, and by crushing and spalling of drypack and concrete at the connection level.

The three phases of the connection behaviour are illustrated in the strength envelope plots in Figures 6.13 to 6.17. The response characteristics of the five mild steel specimens are compared by means of the strength envelopes as shown in Figure 6.18. It is clear from Figures 6.18 that the five specimens had similar overall response characteristics. Looking closely at Figure 6.18, for a given connection, the response in the push (+ve) and pull (-ve) directions was not perfectly symmetrical. However, the difference in strength between push and pull was less than 10%. This difference could be attributed to the progressive deterioration of the drypack at the extreme ends of the connection as loading alternates from the push and pull direction. The difference in strength among the mild steel specimens, with the exception of specimen RT, was less than 15%. In this regards, with the exception of specimen RT, specimen RSK had the highest strengths about 275 kN and specimen RW had the lowest strength about 240 kN. The strength of specimen RT was 205 kN. Also, it seems that the different configurations tested had minor influence on the connection initial stiffness. Different specimens exhibited nonlinear behaviour at different displacement

levels and the measured yield displacement varied for the five configurations tested. specimen RS, with the bonded bar had the lowest yield displacement of 4.25 mm and specimen RSU with the unbonded bar had the highest yield displacement of 6.5 mm, as would be expected due to the effect of debonding. With respect to ultimate displacement capacity, the specimen with the tube section (RT) had the lowest displacement capacity of about 20 mm and the specimen with the unbonded bar (RSU) had the highest displacement capacity of 40 mm.

The normalized performances of the specimens are compared in terms of the normalized load versus ductility relationship shown in Figure 6.19. The normalized load is the ratio of the load to the maximum measured load and the ductility is the ratio of measured displacement to yield displacement. Figure 6.19 indicates that the connections had very similar response and were able to maintain their individual peak loads up to large ductility levels well beyond yield point. Nondimensionalizing the deformability capacity relative to a specimen's own yield provided a conservative estimate of the ductility characteristic as will be discussed in section 6.2.6.

To better compare the effect of the different connection configurations to the response, Figure 6.18 was split into four comparison plots each including strength envelopes for two specimens only: the control specimen RS compared separately to each of the other four specimens. The comparison plots are presented in Figures 6.20(a) through 6.20(d). The effect of welded versus mechanically spliced connection detail is shown in Figure 6.20(a). Both these connection details had similar overall response characteristics. However, the mechanically spliced detail showed slightly higher initial stiffness and maximum load compared to the welded one, even though

the welded detail had higher deformation capacity mainly due to the flexibility of the welded connector in comparison to the rigid splice sleeve. The effect of bolting the bar to a tube section versus mechanically spliced detail is shown in Figure 6.20(b). The connection with tube section had slightly lower initial stiffness, significantly lower strength and lower ultimate displacement capacity in comparison to the mechanically spliced detail. Figure 6.20(c) compares the two mechanically spliced reinforcing bar connections with and without shear keys at the joint interface. Again the comparison was very good; both these connections showed similar response characteristics in terms of stiffness, maximum load and deformability of the joint. The shear key connection configuration had consistently limited slip response compared to the plain surface joint as will be discussed later in section 6.3.4.3. The effect of debonding of continuity reinforcing bar on the behaviour is illustrated in Figure 6.20(d) that compares two mechanically spliced reinforcing bar connections: the one with the reinforcing bar fully bonded to the concrete and the other with the reinforcing bar partially unbonded inside the top panel of the test specimen. Looking at Figure 6.20(d) it is evident that the connection with the debonded reinforcing bar gives much more favourable connection performance in terms of deformation capacity while maintaining strength and stiffness. The effect of reversed cyclic loading on the behaviour of the connection with mild steel reinforcement is given in Figure 6.20(e). The figure compares two identical specimens tested under monotonic and cyclic loading conditions. The cyclic loading seems to have little effect on the maximum measured strength. However, the ultimate deformation capacity was reduced significantly due to the severe damage induced by cyclic loading.

Table 6.2(a) summarizes the response characteristics for the five mild steel

connections in terms of strength, stiffness, ductility and percent slip-to-displacement ratio. Table 6.2(b) compares the strength degradation, stiffness degradation, slip-to-displacement ratio, and energy dissipation quantities for the mild steel connections at 4Dy. This ductility level was chosen since all the connections were capable of withstanding 4Dy. It is worth noting that at 4Dy, no significant reduction in the strength was measured, as indicated in Table 6.2(b). The comparisons in Table 6.2(b) reveal the similarities and differences in the response among the different configurations as will be discussed in the following sections.

6.3.4 Connection Local Response

Similar to the behaviour of the specimens tested monotonically, all the inelastic deformation and damage in the specimens with mild steel reinforcement tested under cyclic loading were concentrated at the connection region. The basic response mechanisms at the connection were characterized by: (i) Rocking associated with vertical gap opening (uplift) at one extreme end and gap closing (crushing) at the other end of the connection; (ii) Permanent reduction in the thickness of the drypack due to the progressive deterioration (crushing and spalling) caused by the grinding action of the cyclic loading; and, (iii) Horizontal shear slip at the panel to drypack interface.

All the mild steel specimens with a plain surface connection region (RS, RSU, RW, RT) showed very similar rocking and slip behaviour. The behaviour of the specimen was characterized by rocking with initially limited slip in the joint region at early stages followed by major slip at the onset of failure. Specimen RSK, with multiple shear keys along the connection had a limited slip mechanism throughout the entire test duration. As such the rocking behaviour of specimen RSK was slightly

different from that of the rest of the mild steel specimens.

Reduction in the thickness of the connection due to the deterioration of the drypack grout by the cyclic loading varied among the specimens. While specimens RSU and RW sustained major reduction in the connection thickness, moderate reduction was measured for specimen RS, minor reduction for specimen RT and no reduction was noted for specimen RSK at the onset of failure.

6.3.4.1 Rocking Behaviour

All mild steel specimens displayed similar rocking behaviour. A typical rocking behaviour is given in Figure 6.21, which shows the distribution of the measured gap deformations across the length of the connection at various loading increments for specimen RS. Figure 6.21(a) gives the response for loading cycles in the push (forward) direction and Figure 6.21(b) shows the response in the pull (reverse) direction. It is evident from Figure 6.21(a) and (b), that the rocking response was almost linear and symmetrical between the push and pull directions. Figures 6.21 demonstrate how the neutral axis moved within the connection length as the applied moment was increased. The behaviour ranged from pure compression followed by rocking about the center line of the connection to hinging around the end zone of the connection. At large lateral deformation (5Dy), due to significant drypack crushing and appreciable reduction in the thickness of the drypack, the neutral axis shifted back towards the center line as shown in Figure 6.21. In all the specimens with mild steel reinforcement, hinging occurred at ductility levels between 1Dy and 3Dy. During hinging, the depth of the compression zone remained the same and thus the neutral axis position remained approximately constant. As the applied displacement was

increased, the compression area slightly reduced due to crushing of the drypack. The hinge length depended on the type of the connection. For specimens RS and RSU, the hinge length was about L/4, specimen RT and RW had a hinge length of about L/3, and specimen RSK had hinge length of about L/5, where L is the connection length. As soon as significant drypack crushing occurred in the connection region, the neutral axis shifted toward the centre line of the connection. The motion of the neutral axis was to compensate the loss of drypack resistance due to crushing at the outer edges of the connection and to maintain equilibrium between the compression and tension forces. This phenomenon was observed for specimens RSU, RW and RT, but not for specimen RSK, due to the presence of the shear keys which remained intact at onset of failure and therefore prevented the reverse movement of the neutral axis. The variation of measured compression zone length versus applied displacement ductility ratio is shown in Figures 6.22 to 6.26 for the five mild steel specimens subjected to cyclic loading. The measured compression zone lengths for the push and pull directions of loading are shown in these figures. It is clear from these figures that the length of the compression zone in the push direction was not always identical to that in the pull direction. However, the difference was at most 15% and could be attributed partly to the variability in the characteristic of the drypack material from one end of the connection to the other and partly due to the lack of accuracy of the instrumentation. The average compression zone lengths of the different mild steel specimens are compared in Figure 6.27(a). The average length of the compression zone is the average of the two depths measured in the push and pull directions for each specimen. The normalized compression zone length relative to the connection length is compared in Figure 6.27(b). The similarity in the hinging behaviour among the mild steel connections was very obvious in these figures.

The rocking behaviour in terms of rotation versus displacement relationship of all specimens with mild steel reinforcement subjected to cyclic loading is shown in Figure 6.28. Figure 6.28 reveals that the all five specimens had nearly identical rocking characteristics, mainly due to the fact that all specimens were subjected to the same moment-to-shear ratio (M/VL), for the same connection length, L. The linear relationship of the rotation-displacement relationship shown in Figure 6.28 confirmed the rigid-body-type motion of the top panel relative to the bottom panel at the connection region. The rocking behaviour of the specimens is compared versus the ductility ratio in Figure 6.29. The ductility ratio in the figure is the ratio of the applied displacement to the yield displacement for the given connection. The magnitude of the yield displacement varied among the specimens: specimen RS had the lowest yield displacement of 4.25 mm while specimen RSU had the highest yield displacement of 6.5 mm. Figure 6.29 shows that all the specimens had a similar rocking characteristic. All specimens with bonded reinforcing bars had nearly identical rotation-ductility relationships. Specimen RSU, with partially unbonded reinforcing bar, had much higher rotational capacity in comparison to the rest of the specimens mainly because the unbonded reinforcing bar in that specimen. Thus, comparing the rocking response in terms of the ductility ratio, a nondimensional quantity, did not give the relative behaviour of the different connections. However, the rotation versus displacement gave a better comparison.

6.3.4.2 Reduction of Connection Thickness

A reduction in the thickness of the connection in the form of permanent deterioration due to crushing and spalling of the drypack along the connection length was observed for all the cyclic specimens with plain surface connection connected by reinforcing

bars. No reduction in the thickness was observed for the shear key specimen (RSK) as the shear keys remained intact during cyclic loading and the drypack crushing concentrated at the connection ends only. The shear keys in the connection region remained intact possibly due to a strut-tie mechanism within the keys which enhanced the shear resistance. No measurable overall thickness reduction was observed for the specimen tested under monotonic loading since crushing of the drypack concentrated in the compression zone only. Thus it seems that overall thickness reduction could be an additional limit-state only due to cyclic loading.

The degree of deterioration in the cyclic specimens with plain surface region varied from severe for specimens RSU and RW to moderate for specimen RS to minor for specimen RT. The variation of the percent reduction in the thickness versus ductility for the specimens with plain surface connection subjected to cyclic loading is given in Figures 6.30 to 6.33. The reduction in the thickness in these figures was measured at the zero displacement position and at the completion of the three cycles of the applied ductility level. Figure 6.30 gives the thickness reduction for specimen RS. It is clear from the figure that overall drypack deterioration along the length of the connection was moderate. The measured percent reduction at failure, 3rd cycle to 5Dy, was less than 5%. The reduction in thickness for specimen RSU is presented in Figure 6.31. It is evident that up to 4Dy, the reduction was minor. During cycles of 5Dy, major overall crushing occurred and the connection thickness reduced significantly. Progressive thickness reduction continued during cycles of 6Dy. After the drypack was severely crushed the compression resistance mechanism was transferred to the concrete panels. The percent reduction at failure, 1st cycle to 7Dy, was 35% for specimen RSU. The thickness reduction for specimen RW was similar

to that of specimen RSU and is shown in Figure 6.32. Again prior to 4Dy, the reduction was minor. At 4Dy cycles, the reduction was moderate at 10%. During the 5Dy cycles, extensive drypack crushing and spalling occurred and significant continued reduction in thickness was measured. The thickness reduction stabilized at 6Dy. The percent reduction at failure, 3rd cycle to 6Dy, was 55%. Very minor overall thickness reduction was measured for specimen RT and the percent reduction at failure, 1st cycle to 5Dy, was less than 1% as can be seen in Figure 6.33. The severe drypack crushing concentrated mainly at the tube location and at the connection ends.

6.3.4.3 Slip Behaviour

All mild steel specimens exhibited some amount of horizontal slip between the top and bottom panels at the connection region. The slip behaviour of the five mild steel specimens subjected to cyclic loading is given by hysteresis loops of slip versus displacement relationship as shown in Figures 6.34 to 6.38. The slip in these figures is the average of the slip measured by two LVDT slip stations mounted at both ends of the connection. The displacement is the applied displacement at the top of the upper panel. Figures 6.34 to 6.38 also include the envelopes of cyclic slip response for each specimen. The slip envelopes represent points of absolute maximum and minimum slip at different displacement increments.

The specimens with a plain surface connection (specimens RS, RSU, RW, RT) had very similar slip response. In general, all four specimens with plain surface connections had minor slip at the initial stages of loading. The slip was almost symmetrical and fully recoverable when the applied displacement returned to zero.

At this initial stage, the response was mainly governed by the rocking mechanism.

At large displacement increments, the slip magnitude was moderate to major. The magnitude of slip was in proportion to the amount of drypack deterioration from the cyclic loading. The slip hysteresis loops were fat and formed an irrecoverable mechanism with a permanent residual slip at the zero displacement level. The slip was symmetrical in push and pull for specimen RT with the tube section as seen in Figure 6.38 but was permanently shifted towards the push direction for specimens RS, RSU and RW with bars as seen in Figures 6.34, 6.36 and 6.37, respectively. The permanently shifted slip of these specimens was possibly due to permanent local shear deformation of the bar at the connection region and/or pull-out of the bar from the sleeve. At failure, specimen RS and RT had moderate slip and specimens RSU and RW had major slip. On the other hand, the specimen with multiple shear keys across the connection (specimen RSK) exhibited consistently minor slip at all ductility levels as clear in Figure 6.36. Presence of shear keys at connection interface prevented the extensive slip that occurred in plain surface connections. The slip was symmetrical in push and pull and fully recoverable when applied displacement returns to zero.

A comparison of the slip envelopes for the mild steel specimens is presented in Figure 6.39. It is clear that all specimens, with the exception of specimen RSK, had similar slip characteristics. The slip-displacement relationship prior to significant drypack deterioration was almost linear, indicating a constant rate of slippage. Extensive crushing and spalling observed in specimens RSU and RW altered the slip resistance mechanism causing a sudden change in the slip rate. The increase in the measured slip, as seen in Figure 6.39, could have resulted from a reduction in the

coefficient of friction due to significant drypack crushing. Specimen RSK with shear keys had consistently the lowest slip contribution at all displacement levels.

The slip to displacement ratio in percentage is plotted in Figures 6.40 to 6.44 for all the specimens connected by reinforcing bars. The percentage of slip per cycle is given for the push and pull cycles at the different ductility levels. These Figures revealed the similarity in the slip characteristic for all four specimens with plain surface connections and the distinct slip behaviour of the specimen with shear keys. For all specimens, up to 1Dy, the slip was limited to 5% of the total deformation. The slip for specimen RSK with shear keys continued to be limited and symmetrical in push and pull at all ductility levels as seen in Figure 6.41. The slip for all other specimens varied from moderate to major at failure. Specimen RS had moderate slip with the average push/pull slip at 14% of the total deformation as seen in Figure 6.40. The slip for specimens RSU and RW was major at failure with the average slip at 17% and 32% of the total deformation as seen in Figures 6.42 and 6.43. At failure, the slip in these specimens RS, RSU, and RW was permanently shifted and tended to be more towards the pull direction. The onset of permanent shift in slip behaviour was at the 3rd cycle of 5Dy for specimen RS, at the 2nd cycle to 5Dy for specimen RW and at the 1st cycle to 6Dy for specimen RSU. The onset of permanent shift in the slip behaviour corresponded to severe drypack deterioration and dowel action due to local shear deformation of the bar. The slip response for specimen RT with the tube section was symmetrical and moderate at 13% as seen in Figure 6.44.

Figure 6.45 compares the maximum slip/displacement percentage versus ductility for the five mild steel specimens. The different stages of the slip response

are clear in this comparison plot. Specimen RW had the highest percentage of slip-to-displacement at 35% and specimen RSK had the lowest percent slip at 6% of the displacement at failure.

As in the specimen subjected to monotonic load, the shear-slip resistance mechanism was mainly through a Coulomb-type friction in the compression zone of the connection. The contribution of the compression reinforcement to the resistance was negligible since the clamping action of the reinforcement did not occur because the measured slip at ultimate in the flexural specimens was less than 50% of the slip at which clamping action occurred in the pure shear tests. The tension steel reinforcement provided no clamping action and its inherent flexibility made its contribution almost nil.

To include any contribution of the reinforcement in the shear resistance, an apparent coefficient of friction, μ, was calculated as the ratio of the connection shear resistance, V, (applied horizontal load) to the compressive force of the drypack, C_d, in the compression zone using equation 6.1. From the test results, apparent coefficients of friction of about 0.55, 0.45 and 0.50 were determined respectively for specimens RS and RSU and RW under combined flexure and shear loading. The coefficient of friction of connection type RW with mild steel reinforcement tested under cyclic pure shear loading condition was 0.80 (West, *et al*, 1993). It is worth noting that the cyclic shear test results indicate that the shear force-shear slip relationship is an unconfined elasto-plastic mechanism. It was virtually impossible to quantify the magnitude of the slip deformation versus load. Therefore, the slip contribution to the overall response could possibly be represented as a percentage of the total deformation.

6.3.5 Connection Stiffness and Stiffness Degradation

The stiffness loss or stiffness degradation for the specimens connected by reinforcing bar and subjected to cyclic load, is discussed in this section. Stiffness loss is examined at different ductility levels and at the service cycle after completion of each ductility level. The service cycle was taken at a 150 kN load level which represents about 60% of the maximum load. The stiffnesses at yield of the five mild steel specimens are compared in Table 6.2(a). These stiffnesses were of the same order of magnitude with a maximum variability of 35%. This variation could be due to the variability in the material characteristics or the connection configuration.

Figures 6.46 to 6.50 give the load-displacement cycles for the intermediate equivalent service cycles after each displacement increment. It is clear from these figures that the mild steel specimens had similar service cyclic response. The service load-displacement loops for specimen RS were narrow up to 5Dy, beyond which the service loops widened and became severely degraded, as shown in Figure 6.46. This was due mainly to the crushing and spalling of the drypack and pull-out of the reinforcing bar from the sleeve. The service cycles for specimen RSU were narrow up to 3Dy. Beyond 3Dy, the service behaviour was nonlinear elastic and the hysteresis loops were wide as shown in Figure 6.48. For the other specimens, the service load-displacement cycles remained in the elastic range and the hysteresis loops were consistently narrow. This behaviour is shown clearly in Figure 6.47, 6.49 and 6.50 for specimens RSK, RW and RT, respectively.

Figures 6.51 to 6.55 give the measured stiffness degradation in term of the ductility level. The stiffness per cycle was determined as the slope of the peak-to-peak load-displacement hysteresis relationship at the service cycle after completion of the cycles of each ductility increment. The load was the horizontal load applied at the top of the upper panel and the displacement was the measured displacement at the location of the applied load. The initial elastic stiffness of the connection, was obtained by regression analysis as the slope of the best-fit line of the load-displacement elastic cycles in the initial excursions prior to yield. The stiffness at yield was the peak-to-peak slope in the push and pull direction of the load-displacement cycle at connection yield. In general, the initial stiffness was about twice the stiffness at yield. Figures 6.51 to 6.55 reveals that all specimens tested had very similar response in terms of stiffness degradation. One thing was obvious in these figures: the stiffness at the service cycle after the completion of each ductility level was slightly higher than the stiffness at a load corresponding to the same ductility level.

Comparison of the stiffness degradation for the mild steel specimens is shown in Figures 6.56(a) and (b). Figure 6.56(a) gives the stiffness degradation to each ductility level while Figure 6.56(b) gives the stiffness degradation at the service cycle after the completion of each ductility level. Figure 6.56 reveals that all the specimens had very similar stiffness degradation. The highest and lowest stiffnesses at yield were 50 kN/mm and 35 kN/mm for specimens RS and RSU, respectively. The difference between these stiffnesses is about 35%. This difference could be attributed mainly due to the use of bonded reinforcement in specimen RS versus unbonded reinforcement in specimen RSU. The measured stiffness was compared to the stiffness

at yield in Figure 6.57(a) at each ductility level while Figure 6.57(b) represents the same quantity at the service cycle after the completion of each ductility level. Again Figure 6.57 reflects similar stiffness degradation characteristic for the tested specimens connected with reinforcing bars. Figure 6.57(a) reveals that, at a given ductility level, the percent stiffness degradation of the specimens was similar. In particular at 4Dy, the average stiffness degradation for the different connection types, as given in Table 6.2(b), was about 27%. The stiffness at failure was about 20% of the initial stiffness at yield. On the other hand, the percent service stiffness to yield stiffness-ductility relationship in Figure 6.57(b) has a wider scatter among the specimens suggesting that the degradation of the stiffness at the service cycles for specimen RW and RSK was considerably less than the other specimens.

The most important feature revealed in Figures 6.56 and 6.57 was the sharp decrease in stiffness versus increase in ductility. Such decrease in stiffness with increasing ductility seems to be a characteristic of degrading systems and has been observed by other researchers testing concrete structures (ATC8, 1981). This loss of stiffness was due mainly to the progressive deterioration of the drypack material by continued crushing, loss of compression zone area by spalling of the drypack, cracking and spalling of the concrete at the connection edges, and the nonlinear behaviour of the material.

6.3.6 Connection Strength

The measured connection strengths for the five mild steel specimens are given in Table 6.2(a). The connection strength is expressed in terms of the maximum measured horizontal load which was achieved close to the ultimate displacement of the connection. In general, the percent variability in the connection strength among the mild steel specimens, with the exception of specimen RT with tube section, was less than 14%. The connection strength in specimen RT with the tube was about 25% lower than the average strength value of the other specimens. This lower strength was due mainly to the lower resistance of the tube section relative to the sleeve or welded connector. The strength reduction for the different connections is compared at 4Dy in Table 6.2(b). At this stage, specimen RSU, RW and RT had only 10% strength reduction while specimens RSK and RS had less than 3% reduction. Above 4Dy, comparison of strength degradation among connections was not possible since different connections reached different ductilities.

6.3.7 Connection Ductility

All mild steel specimens were capable of maintaining peak resistance with cycling at large displacements well beyond first yield. No sudden loss of load carrying capacity was noted with appreciable deformation, and failure was rather gradual. The overall performance of the specimen is given by its deformational capacity. The deformational capacity is expressed in terms of either the ultimate displacement ductility or the ultimate drift. The ultimate displacement ductility, μ_D, is defined as the ratio of the displacement at failure, D_u, to the displacement at yield, D_y, as given in equation 6.2. The ultimate drift, θ, is the ratio of the displacement at failure, D_u, to the effective height, H, of the upper panel above the connection region. The

effective height was the same for all specimens at 1800 mm. Values for the ultimate ductility and ultimate drift for the mild steel specimens are given in Table 6.2(a).

In terms of the overall deformational capacity, specimen RSK with shear keys and specimen RT with the tube section had the lowest ductility ratio of 4. Specimen RS, a plain surface connection with a mechanically spliced reinforcing bar, had a displacement ductility ratio of 5 and an ultimate drift of 1.2%. Specimen RW, the welded-reinforcing-bar configuration, had an ultimate ductility ratio of 5 and a drift of 1.38%. The lower ductility achieved by specimen RS compared to that of specimen RW could be attributed to material characteristics or to the early pull-out of the bar from the sleeve prior to overall drypack crushing in the connection or to the flexibility of the welded connector relative to the rigid splice sleeve. Specimen RSU with unbonded reinforcement had the highest displacement ductility ratio of more than 6. The ultimate drift for specimen RSU was 2.16%. Therefore, comparing the deformational capacities of the five specimens it can be seen that the capacity of specimen RS was 20% higher than that of specimens RT and RSK. The capacity of specimen RW was 20% higher than specimen RS. The capacity of specimen RSU, with unbonded reinforcement, was 80% higher than specimen RS, with bonded reinforcement.

6.3.8 Energy Dissipation

The energy dissipated by each specimen during a test was defined as the area enclosed by the load versus displacement hysteresis relationship. The area was calculated by numerical integration. For each specimen the energy dissipation per cycle (e) and the cumulative energy dissipation (E) were computed up to failure. The energy dissipation per cycle (e) was defined as the energy dissipated at a given cycle for a given ductility level. The cumulative energy dissipation was the summation of the energy per cycle at any given point in the test ($E=\Sigma e_i$). Also, for each specimen an estimate was made of how much of this energy was dissipated by rocking and how much was dissipated by slip. The contribution of the slip to the energy dissipation (E_s or e_s) was calculated by deducting the flexural energy dissipation (E_r or e_r) determined by the load versus flexural deformation plot from the total energy dissipation (E_t or e_t) determined by the load-displacement plot. The flexural deformation was given as the total displacement minus the horizontal slip deformation. The energy dissipation response exhibited by specimens RS, RSK, RSU, RW and RT is given in Figures 6.58 through 6.62, respectively. Each figure shows: (a) the energy dissipation per cycle and (b) the cumulative energy dissipation. Also shown in each plot is the contribution of slip and rocking to the energy dissipation (a) per cycle and (b) at the cumulative level. As can be seen from Figures 6.58(a) through 6.62(a), the energy dissipation per cycle was consistent at each ductility level. The percent energy due to slip versus the total energy was, in general, less than 30%. The cumulative energy dissipation for all specimens was characterized by nonlinear as shown in Figures 6.58(b) to 6.62(b). The contribution of slip to the energy was small and also nonlinear.

Comparison of the average percentage energy dissipated per cycle due to slip to the total energy is shown in Figure 6.63. Specimen RSK had the lowest percent energy due to slip and specimen RT had the highest. Specimens RS, RSU and RW exhibited very similar contribution of slip to energy dissipation.

Comparison of the average energy dissipation per cycle plots at a given ductility level is shown in Figure 6.64. The cumulative energy dissipation for all specimens are compared in Figure 6.65. Looking closely at Figures 6.64 and 6.65, the following was noted: the energy dissipation per cycle capability of specimens RSK and RS, mechanically spliced reinforcing bar connections with and without shear keys, was nearly identical. The cumulative energy dissipation for the RS specimen was higher as it failed at a higher ductility level. The welded connection detail, specimen RW, had a slightly higher energy dissipation per cycle than specimen RS. Specimen RW also had a higher cumulative energy dissipation as failure occurred at a higher ductility than RS specimen. Specimen RT has the lowest energy dissipation per cycle and the lowest cumulative energy dissipation; this is due to the fact that specimen RT had a significantly lower strength than the other specimens (the strength of specimen RT was about 70% of that of the rest of the specimens). Specimen RSU, with unbonded bar, had by far the best cumulative energy dissipation characteristics in comparison to all other specimens.

In order to give a nondimensionalized representation of the energy dissipation for each specimen, an attempt was made to normalize the energy dissipated relative to the elastic energy absorbed by the specimen at yield. The energy dissipation index was defined as the ratio of the energy at a given ductility level to the energy at yield. The elastic energy at yield was determined as:

$$E_y=\frac{1}{2}(P_y^+\Delta_y^+ + P_y^-\Delta_y^-) \tag{6.3}$$

The yield load and yield displacement in this equation were defined in Figure 6.1 and corresponded to the push (+ve) and pull (-ve) cycles of the response. The energy dissipation index per cycle is presented in Figure 6.66. The cumulative energy dissipation index is shown in Figure 6.67. The wide range observed in the energy dissipation per cycle was somewhat reduced as energy dissipation index values were closer to each other. Yet Some specimens still had a higher dissipation index than others. The cumulative energy dissipation index in Figure 6.67 revealed similar trend of behaviour as well.

6.4 PRESTRESSED SPECIMEN SUBJECTED TO REVERSED CYCLIC LOAD

6.4.1 General

This section discusses the results of the prestressed specimens subjected to reversed cyclic loading. Three prestressed specimens were tested: specimen PTB, PTS, and PTBU. The specimen nomenclature was explained earlier in section 3.2. All prestressed specimens were post-tensioned to an equivalent prestress of 1.2 MPa on the connection. The specimens had a plain surface joint region. The experimental variables included:

1. Type of prestressing reinforcement:

a) prestressing bars (PTB) versus b) prestressing strands (PTS)

2. Bar to panel concrete condition:

a) bonded reinforcement (PTB) versus b) fully unbonded reinforcement(PTBU)

Specimen PTB with bonded prestressing bars will be used as the reference specimen. The behaviour of the other two prestressed specimens will be compared to specimen PTB. The behaviour of prestressed specimens tested under cyclic loading conditions was compared to specimens tested under monotonic loading conditions.

As in the mild steel specimens, the prestressed specimens were subjected to the cyclic loading history as explained in section 3.8.

6.4.2 Performance and Damage Observations

The observed response of the prestressed specimens was similar to that of the mild steel specimens and can be given by the following stages:

1. Rocking in terms of continuous opening and closing of the joint region.
2. Crushing of drypack and panel concrete in the compression zone at the joint ends.
3. Yielding of prestressing reinforcement (specimen PTB and PTS).
4. Subsequent buckling of the prestressed bars (specimen PTB and PTBU).
5. Spalling of concrete and drypack adjacent to the buckled bars.
6. Panel cracking in the form of compression cracks at the connection extreme ends.
7. Progressive drypack crushing and spalling along the length of the connection.
8. Rupture of the prestressing bar or strand at the connection region (specimens PTB and PTS) at failure.

The extent of observed damage at failure varied. Specimens PTB and PTS had moderate damage across the connection length while specimen PTBU had major drypack deterioration at failure. The observed behaviour of the prestressed specimens was detailed in section 5.4. A brief recapulation of the behaviour of each specimen at failure is as follows:

Specimen PTS failed by rupture of the prestressing strand at the 2nd cycle to 8Dy in the push direction. Severe crushing and spalling of the drypack grout accompanied the rupture of the strand. The drypack was ground to a thin layer over about L/6 from the connection ends. Drypack crushing progressed towards the connection centre line where very minor crushing occurred. The average thickness reduction along the connection length was minor at about 5% of the initial thickness.

Concrete cracking and spalling concentrated at the connection extreme ends in the form of surface cracks mainly in the lower panel. A big concrete cover piece in the lower panel at the push end spalled off. The slip was symmetrical and consisted of 12% of displacement at failure. The ductility of the connection was 6.

Specimen PTB failed by rupture of the prestressing bar at the 3rd cycle of 7Dy in the pull direction. The drypack at the connection ends was reduced to a very thin layer. Drypack crushing progressed along the full connection length. The average drypack crushing along the connection at failure was moderate with a 25% reduction from the initial thickness. Concrete cracking and spalling was mainly in the lower panel at the connection edges. The cracking was in the form of compression surface cracks. The slip was permanently shifted and tended to be more towards the pull end possibly because of local shear deformation of the bar in dowel action. The slip at failure was 12% of the displacement. The ultimate ductility was 6.

Failure of specimen PTBU was characterized by severe drypack deterioration over the entire connection length and significant crushing in the extreme ends of the concrete panels. The drypack was literally ground to dust in the connection region and the compression force was transferred to the wall panel concrete. Rupture of the bar did not occur at failure. The average drypack crushing over the entire connection length was 60% of the initial thickness. Cracking in the wall panels occurred by spalling off concrete cover at the panel end region near the connection region. Buckling of the continuity reinforcement occurred. The slip was permanently shifted towards the pull than the push-direction of loading. The slip constituted about 14% of the displacement at failure. The ultimate ductility was 14.

6.4.3 Overall Specimen Response

The overall cyclic response of the prestressed specimens was monitored by the load versus displacement hysteresis relationship. The response was similar to that of the specimens with mild steel reinforcement; however, the hysteresis loops were narrower and the plastic deformation was smaller, possibly due to the prestressing effect. Figures 6.68 to 6.70 give the measured load-displacement hysteresis loops and include the strength envelope of the cyclic response. In these figures, the load was applied at the top of the upper panel and the displacement was measured at the location of the applied load relative to the bottom panel. The strength envelope connects absolute maximum measured loads of cycles at different displacement increments. The strength envelopes will be later compared to evaluate the relative performance of the prestressed specimens.

The cyclic behaviour of the three prestressed specimens was very similar as is evident in Figures 6.68 to 6.70. The hysteresis loops for specimen PTBU, with unbonded bars, were narrower and more pinched in comparison to loops for specimens PTB and PTS, with bonded reinforcement. This behaviour was a consequence of unbonding the prestressing reinforcement. All specimens showed stable hysteretic behaviour and were able to maintain peak resistance after cycling well beyond first yield. Failure of the connection is evident in Figures 6.68 to 6.70: the two specimens with bonded prestressing reinforcement failed abruptly by rupture of the bar or strand while the specimen with unbonded bar had a gradual failure. The envelope of the connection behaviour can be characterized by three phases as illustrated in Figures 6.68 to 6.70 depending on the degree of joint deterioration:

I: Initial linear elastic prior to yield without any visible damage.

II: Ductile phase characterized by stable hysteresis loops and minor to

moderate damage without extensive crushing.

III: Ultimate stage (failure) with significant reduction in the load carrying capacity under increased deformation and severe damage. This stage was characterized by extensive crushing and spalling of drypack and panel concrete at both sides of the joint. Rupture of the prestressed reinforcement, in the bonded specimens, occurred at this stage.

The response characteristics of the prestressed specimens are compared using the strength envelopes in Figure 6.71. The three specimens had similar overall characteristics. The response, however, was not perfectly symmetrical between the push and pull directions. The strength difference between push and pull was less than 10%. This difference could be attributed to the progressive deterioration due to cyclic between the push and pull directions. The maximum strength of specimens with bonded prestressed bars or strands was within 1%. The strength of the specimen with unbonded bars was 15% lower than the one with bonded bars and was a direct consequence of the unbonding of the bars. Specimen PTS had the highest strength of 240 kN, specimen PTB had a slightly lower strength of 225 kN, and specimen PTBU had the lowest strength of 205 kN. The connection configuration had no influence on the initial stiffness of the connection which was almost identical for the three specimens as is clear in Figure 6.71. The prestressed specimens exhibited nonlinear behaviour at different displacement levels but the yield displacement was the same for the three configurations tested. The yield displacement for all specimens was 4.0 mm. This displacement corresponds to the yielding of the bars and strands in specimens PTB and PTS, respectively. The unbonded bars in specimen PTBU did not yield and therefore the equivalent-to-yield displacement was chosen as the yield displacement

of specimen PTB. The ultimate displacement capacity at onset of failure varied among the specimens: the two specimens with bonded prestressed bars and strands (PTB and PTS) had the same displacement capacity of 24 mm and the specimen with unbonded bar (PTBU) had the highest displacement capacity of 56 mm.

Figure 6.72 provides a nondimensionalized response of the three prestressed specimens. The normalized performances are given in terms of the normalized load versus ductility ratio. The normalized load is the ratio of the load to the maximum measured load. Since the same yield displacement was used for the three specimens, nondimensionalizing the deformability capacity did not give a different comparison alternative.

Figure 6.71 is split into two comparison plots, Figure 6.73(a) and 6.73(b), each including strength envelopes for only two specimens to highlight the effect of the different configurations to the response. The effect of bonded bars versus bonded strands is shown in Figure 6.73(a). Both these connection details had very similar overall response characteristics in terms of stiffness, yield and ultimate displacement. The specimen with strands had a slightly higher maximum load compared to the specimen with bars. The strength was maintained over a longer displacement range in the specimen with strands. The effect of debonding of the prestressing bars on the behaviour is illustrated in Figure 6.73(b) which compares two prestressed connections: fully bonded bars and fully unbonded bars. Relative to the specimen with bonded bars, the specimen with unbonded bars had significantly enhanced connection deformability capacity. The strength of the unbonded specimen was slightly lower than that of the bonded specimen while the stiffness was almost the same. Therefore,

unbonded bars give much more favourable connection performance than bonded bars in terms of deformation capacity.

The effect of the reversed cyclic loading on the behaviour of prestressed specimens is given in Figures 6.73(c) and (d) for specimens with bars and strands, respectively. Each figure compares the response of two identical specimens tested under monotonic and cyclic loading conditions. Figure 6.73(c) compares specimens PTB and PTB-S, prestressed with bars, and Figure 6.73(d) compares specimens PTS and PTS-S, prestressed with strands. The cyclic loading did not affect the maximum measured strength. However, the ultimate displacement capacity was significantly reduced due to the severe damage induced by cyclic loading.

Table 6.3(a) summarizes the response characteristics of the prestressed connections in terms of strength, stiffness, ductility and percent slip to deformation ratio. Table 6.3(b) compares the strength degradation, stiffness degradation, slip to deformation ratio and energy dissipation quantities for the prestressed connections at 6Dy. This ductility level was chosen since all the connections were capable of withstanding 6Dy. The similarities and differences of response among the different configurations will be discussed in the following sections.

6.4.4 Connection Local Response

As for the mild steel specimens, the mechanisms at the connection of the prestressed specimens were: (i) rocking associated with vertical gap opening and closing; (ii) permanent reduction in drypacked connection thickness through severe drypack deterioration and, (iii) horizontal shear slip at the panel to drypack interface.

All the prestressed specimens (PTS, PTB and PTBU) showed similar rocking and slip response. Initially, the behaviour was characterized by rocking with limited slip at early stages followed by major slip at the onset of failure. Specimens PTB and PTBU had permanent shift in slip at failure. Thickness reduction due to deterioration of the drypack grout varied among the specimens. Specimen PTBU showed a major reduction in the connection thickness, moderate reduction was measured for specimen PTB and minor reduction for specimen PTS, at the onset of failure.

6.4.4.1 Rocking Behaviour

The rocking behaviour for all prestressed specimens was similar. Typical rocking behaviour of the prestressed specimens is given in Figures 6.74(a) and (b) for rocking in the push and pull loading directions, respectively. The rocking response was almost linear and symmetrical between the push and pull directions. Figures 6.74 illustrates the movement of the neutral axis within the connection length as loading was increased. The behaviour started initially by pure compression followed by rocking about the centre line of the connection to hinging around the end zone of the connection. At large ductility levels, due to significant drypack crushing and some reduction in the thickness of the drypack, the neutral axis shifted back toward the centre line as shown in Figure 6.74. The neutral axis moved back to compensate for the loss of drypack resistance due to crushing and to maintain equilibrium between compression and tension forces.

In the prestressed specimens with bonded reinforcement, hinging occurred at ductility levels between 1Dy and 3Dy, while hinging of the unbonded specimen occurred between 1Dy and 14Dy. During hinging, the depth of the compression zone

remained the same and thus the position of the neutral axis remained approximately constant. The hinge length depended on the type of the connection. Specimen PTS hinge length was about L/4 while specimen PTB and PTBU had a hinge length about L/3, where L is the connection length. As soon as significant drypack crushing occurred in the connection region, the neutral axis shifted back closer towards the centre line of the connection and the compression depth increases. This phenomena was observed for specimens PTB and PTS but not for specimen PTBU. The variation of measured compression zone length versus applied displacement ductility ratio is shown in Figures 6.75 to 6.77 for the three prestressed specimens subjected to cyclic loading. The measured compression zone lengths for the push and pull directions of loading are shown in these figures. The length of the compression zone in the push direction was not always identical to that in the pull direction. The difference was at most 15% and could be attributed to the variability in the characteristic of the drypack material or to the accuracy of the instrumentation. The average compression zone lengths of the three prestressed specimens are compared in Figure 6.78(a). The average compression zone length was the average of the two lengths measured in the push and pull directions for each specimen. The normalized compression zone lengths relative to the connection length is compared in Figure 6.78(b). The similarity in the rocking behaviour is very obvious in these figures.

The rotation versus displacement relationship of the prestressed specimens subjected to cyclic loading is shown in Figure 6.79(a). Figure 6.79(a) reveals that the all specimens had very similar rocking characteristics, mainly due to the fact that all specimens were subjected to the same moment-to-shear ratio (M/VL), for the same connection length, L. The linearity in the relationship of the rotation-displacement shown in Figure 6.79(a) confirmed the rigid-body-type motion of the top panel relative

to the bottom panel at the connection region. The two specimens with bonded reinforcement had nearly identical rotation-ductility relationships. Specimen PTBU with unbonded bar, had a higher rotational capacity in comparison to the bonded specimens mainly because the unbonded bar in that specimen. The rocking behaviour of the specimens was compared versus the ductility ratio in Figure 6.79(b) to nondimensionalize the results. Similar behaviour is evident in Figure 6.79(b) among the three specimens.

6.4.4.2 Reduction of Connection Thickness

Permanent reduction in the thickness of the connection caused by crushing and spalling of the drypack along the connection length was observed for all prestressed specimens subjected to cyclic loading, while no measurable thickness reduction was noted for companion specimens (PTB-S and PTS-S) tested under monotonic loading. Thus thickness reduction could be an additional limit-state due to cyclic loading only.

The degree of deterioration in the prestressed specimens varied from severe for specimens PTBU to moderate for specimen PTB to minor for specimen PTS. The percent reduction in the thickness versus ductility for the prestressed specimens subjected to cyclic loading is given in Figures 6.80 to 6.82. The reduction in the thickness in these figures was measured at the zero displacement position after the completion of three cycles of the applied ductility level. Figure 6.80 gives the thickness reduction for specimen PTS. The drypack deterioration along the length of this connection was minor. The measured percent reduction at onset of failure, 6Dy, was about 3%. The thickness reduction for specimen PTB is presented in Figure 6.81. Up to 4Dy, minor reduction was noted with 4% reduction at 4Dy. Between 4Dy and

6Dy, major crushing occurred and the connection thickness reduced. The percent reduction at failure, 6Dy, was 20%. The thickness reduction for specimen PTBU is shown in Figure 6.82. Again prior to 4Dy, the reduction was minor. At 6Dy cycles reduction was moderate at 10%. During cycles of 6Dy to 14Dy, extensive crushing and spalling of the drypack and concrete occurred. Continued reduction in the thickness was measured. The thickness reduction stabilized at during cycles to 14Dy. The percent reduction at onset of failure, 3rd cycle to 14Dy, was 55%.

6.4.4.3 Slip Behaviour

The slip behaviour of the three prestressed specimens subjected to cyclic loading (specimens PTS, PTB and PTBU) is given by hysteresis loops of slip versus displacement as shown in Figures 6.83 to 6.85. In these figures, the average slip measured by two LVDT slip stations, mounted at both ends of the connection, was reported. Also included in these figures was the envelope of cyclic slip response for each specimen. In general, all three specimens with prestressed reinforcement had similar response. All specimens had minor slip at the initial loading stages. The slip was almost symmetrical and fully recoverable at the zero displacement level. At large displacement increments, the slip formed an irrecoverable mechanism with permanent residual slip at zero displacement. The slip hysteresis loops were somewhat fat for specimens PTB and PTS with bonded steel but rather narrow for specimen PTBU with unbonded bars. The slip was symmetrical in push and pull for specimen PTS up to the 1st cycle to 24 mm (6Dy), as seen in Figure 6.83, beyond which the slip stations were lost and the slip response could not be determined. The slip was permanently shifted towards the pull direction for specimens PTB and PTBU with bars as seen in Figures 6.84 and 6.85, respectively. The shift in slip response was more pronounced

in specimen PTBU with the unbonded bar than in specimen PTB with bonded bars. This was possibly due to local shear deformation of the bar at the connection region or loss of prestressing force or instrumentation error. At failure, the magnitude of slip was in proportion to the extent of drypack deterioration. Specimens PTS and PTB had moderate slip and specimens PTBU had major slip.

The slip envelopes for the prestressed specimens are compared in Figure 6.86. The similarity in the slip response among the three specimens is obvious. The slip behaviour prior to significant drypack deterioration was almost linear with constant rate of slippage. Extensive crushing and spalling resulted in sudden change in the slip rate as seen in Figure 6.86. The sudden increase in the measured slip could have resulted from a reduction in the coefficient of friction at the connection interface due to severe crushing. Specimen PTS consistently had the lowest slip contribution at all displacement levels while specimen PTBU had the highest slip at ultimate.

Figures 6.87 to 6.89 give percentage of slip to displacement ratio in the push and pull cycles at different ductility levels for the three prestressed specimens. Again, the similarity in the slip characteristic for all three prestressed specimens is evident. For all specimens, up to 1Dy, the slip was limited to 5% of the total deformation. The slip for specimen PTS increased slightly to 6% of the displacement at the 1st cycle of 5Dy and then jumped to 10% of the displacement at the 1st cycle of 6Dy. In specimen PTB, the rate of slip increase was higher. The slip increased to 10% of the displacement at 3Dy and maintained a maximum of 12% of the displacement between 4Dy and 6Dy. It is evident from Figure 6.88 that the slip was permanently shifted and tended to be more towards the pull than the push direction. The onset of shift in slip

response is at the 3rd cycle of 3Dy. At the 2nd cycle of 4Dy in the push direction, some negative slip contribution was recorded. The negative slip to displacement ratio means that the measured slip is opposite to the direction of the applied displacement. This negative slip contribution was repeated for two push cycles of 5Dy and one push cycle of 6Dy. During these push cycles, the local motion in the connection was dominated by the rigid body rotation of the top panel at the connection region. When the top panel rotates at the pull end, the lower edge of the panel moves towards the pull end at the connection region, thus producing a negative slip contribution. In specimen PTBU, the slip maintained below 6% of the displacement up to 7Dy. Beyond 7Dy, the slip increased at a constant rate up to 14% of the displacement at 14Dy. Between 7Dy to 14Dy, the slip response was permanently shifted towards the pull direction as evident in measured negative slip during these ductility levels.

The maximum slip to displacement ratio in percentage versus ductility for the three prestressed specimens is compared in Figure 6.90. At 6Dy, the percent slip to displacement ratio was lowest for specimen PTBU at 6% while specimens PTS and PTB had similar percent slip to displacement ratio of 11% and 12%, respectively. This behaviour is possibly because specimens PTB and PTS experienced severe degradation and may had more prestress loss at 6Dy than specimen PTBU with unbonded bars. The comparison is given in Table 6.3(b). At ultimate of specimen PTBU, 14Dy, the percent slip to displacement ratio is 14%.

Again, the shear force-slip resistance mechanism was characterized as Coulomb-friction in the compression zone of the connection. The contribution of the prestressed reinforcement to the resistance was through the effective prestress force

only and not by dowel action. The effect of the prestressing on the shear resistance was included by calculating an apparent coefficient of friction, μ. The measured apparent coefficients of friction varied from 0.35 to 0.5 for specimens PTBU, PTB and PTS under combined flexure and shear loading. Coefficient of friction of similar prestressed specimens tested under cyclic pure shear loading was 0.90 (West, Soudki and Rizkalla 1993).

6.4.5 Connection Stiffness Degradation

The stiffness degradation for the prestressed specimens subjected to cyclic load was examined at the ductility level and at the service cycle after completion of the ductility level. The service cycle was considered as equivalent to 60% of the connection strength: at 150 kN for specimens PTB and PTS, and at 100 kN for specimen PTBU. Minor variation was recorded among the stiffness of the different specimens, mainly due to the variability in the material characteristics or the connection configuration.

Figures 6.91 to 6.93 give the response at service of the prestressed specimens in terms of the load-displacement after each ductility level. It is clear from these figures that the service cyclic response of specimens with bonded steel (PTS and PTB) was different from the specimen with unbonded steel (PTBU). The service load-displacement loops for specimens PTB and PTS were narrow up to 2Dy, beyond which the loops became fat and degraded as shown in Figure 6.91 and 6.92. The service cycles for specimen PTBU were consistently narrow at all ductility levels up to failure as shown in Figure 6.93. The loops were narrow mainly due to the unbonding of the bars. The service cycles of specimen PTBU were severely degraded after 5Dy. The degraded response is mainly due to the severe deterioration of the

connection region from cyclic load.

The measured stiffness degradation versus ductility is given in Figures 6.94 to 6.96. At any given cycle, the stiffness is determined as the slope of the peak-to-peak load-displacement hysteresis relationship. The initial elastic stiffness is obtained by regression analysis as the slope of the best-fit line of the load-displacement elastic cycles in the initial excursions prior to yield. The stiffness at yield is the peak to peak slope in the push and pull direction of the load-displacement cycle at yield. In general, as evident in Figures 6.94 to 6.96, the initial stiffness was about twice the stiffness at yield. Figures 6.94 to 6.96 reveal that all prestressed specimens had very similar response in terms of stiffness degradation. The degradation was nonlinear with a very sharp decrease in the stiffness. Also evident in Figures 6.94 to 6.96 is that the stiffness at service cycle after the completion of each ductility level was higher than the stiffness at a load corresponding to the same ductility level.

Comparison of stiffness degradation for the prestressed specimens is shown in Figures 6.97(a) and (b). Figure 6.97(a) gives the stiffness degradation at the ductility level while Figure 6.97(b) gives the stiffness degradation at the service cycle after the completion of the ductility level. These figures reveal the similarity in the stiffness degradation among the specimens. At yield, the highest and lowest stiffness were 47 kN/m for specimen PTB and 40 kN/m for specimen PTBU. The variability among these stiffness was only 15%. This difference could be attributed mainly due to the use of bonded reinforcement in specimen PTB versus unbonded reinforcement in specimen PTBU. The measured stiffness was further compared to the stiffness at yield in Figure 6.98(a) at the ductility level and in Figure 6.98(b) at the service cycle after

completion of the ductility level. Again, Figures 6.98 reflect the similarity in the stiffness degradation characteristic. The percent stiffness degradation of the specimens was rather identical. At 6Dy, the stiffness degradation was about 16% for the three specimens as shown in Figure 6.98(a) and given in Table 6.3(b). At ultimate of PTBU, 14Dy, the residual stiffness was about 10% of the yield stiffness for specimen PTBU, as shown in Figure 6.98(a). On the other hand, the percent service stiffness to yield stiffness - ductility relationship in Figure 6.98(b) had a wider scatter among the specimens suggesting that the stiffness degradation at the service cycles for specimen PTS with strands was considerably less than the other two specimens bars. This could be due to the higher loss of prestress in the bars versus strands and/or the severe connection deterioration observed in the specimens with bars versus specimen with strands.

As in the mild steel specimens, the most important feature revealed in Figures 6.97 and 6.98 was the severe stiffness degradation of the prestressed specimens in terms of the sharp decrease in stiffness versus increase in ductility. It was mainly due to the progressive deterioration of the drypack material by continued crushing and spalling.

6.4.6 Connection Strength

Table 6.3 gives the connection strength for the three prestressed specimens tested under cyclic loading. The maximum measured load-carrying capacity was almost the same for specimens PTB and PTS. The capacity of specimen PTBU was about 87% of specimen PTB. This could be due to the lack of grout in the ducts for the unbonded bar used for specimen PTBU. The strength reduction is compared for the

three specimens at 6Dy in Table 6.3(b). At 6Dy, specimens PTB and PTS has reached ultimate with strength 77% and 83% of the maximum measured while specimen PTBU still maintained 94% of the maximum load.

6.4.7 Connection Ductility

All prestressed specimens were capable of maintaining peak resistance with cycling at large displacement increments well beyond first yield. The overall performance of the specimen is given by its ultimate displacement ductility, μ_D, or the ultimate drift. Definitions of the ductility terms are found in section 6.3.7. Table 6.3 gives the ultimate displacement ductility and the ultimate drift for the three prestressed specimens tested under cyclic loading.

In terms of overall response, the deformational capacity of specimen PTBU with unbonded bars was more than twice that of specimens with bonded steel (PTB and PTS). Specimens PTB and PTS had the same ductility capacity. These specimens had an ultimate ductility of 6 and an ultimate drift of 1.33%. Specimen PTBU, with unbonded bars, had the highest ductility of 14 and ultimate drift of 3.11%.

6.4.8 Energy Dissipation

The energy dissipation per cycle (e) and the cumulative energy dissipation (E) were computed up to failure, for all the three prestressed specimens. The energy dissipation per cycle (e) was the energy dissipated at a given cycle for a given ductility level. The energy dissipated was defined as the area enclosed by the load versus displacement hysteresis relationship. The cumulative energy dissipation was the summation of the energy per cycle at any given point in the test ($E=\Sigma e_i$). Also for each specimen, the contribution of slip and rocking to the energy dissipation was identified. The slip contribution to the total energy dissipation (E_s or e_s) was calculated by deducting the total energy dissipation (E_t or e_t) from the flexural energy dissipation (E_r or e_r). The flexural energy was determined from the load versus flexural (rocking) deformation hysteresis plot. The flexural deformation was the total displacement minus the horizontal slip.

The energy dissipation response for the three prestressed specimens is given in Figures 6.99 to 6.101 for specimens PTS, PTB, and PTBU, respectively. Each figure is split into: (a) the energy dissipation per cycle and (b) the cumulative energy dissipation. The contribution of slip and rocking to the energy dissipation at (a) the per cycle and (b) the cumulative level, is also shown in each plot. As can be seen from Figures 6.99(a) through 6.101(a), energy dissipation per cycle was consistent at each ductility level and was characterized by nonlinear behaviour. The contribution of slip to the energy was small and also nonlinear. The percent energy due to slip versus total energy was in general less than 20%. Since the cumulative energy is a linear summation of the energy per cycle, the variation of the cumulative energy dissipation for all specimens was nonlinear as shown in Figures 6.99(b) to 6.101(b).

Figure 6.102 compares the average energy per cycle due to slip to the total energy in percentage for the different specimens. Specimen PTS had the lowest percent energy due to slip and specimen PTB had the highest. Specimens PTB and PTBU exhibited very similar slip contribution to energy dissipation.

The average energy dissipation per cycle versus ductility is compared in Figure 6.103 for the three specimens. The average energy was the algebraic average of the energy of three cycles. The cumulative energy dissipation for all specimens are compared in Figure 6.104. Looking closely at Figures 6.103 and 6.104, the following was noted: Specimen PTB prestressed with bonded bars had the highest energy dissipation per cycle and specimen PTBU with unbonded bars had the lowest energy dissipation per cycle. specimen PTS with strands had the lowest cumulative energy dissipation while specimen PTBU (unbonded bars) had the highest cumulative energy dissipation as it failed at a much higher ductility level.

In order to give a nondimensionalized representation of the energy dissipation for each specimen, the energy dissipated was normalized relative to the elastic energy absorbed by the specimen at yield. The energy dissipation index is then given as the ratio of the energy at a given ductility level to the energy at yield. The elastic energy at yield was determined using equation 6.3. The energy dissipation index was presented per cycle in Figure 6.105 and on a cumulative energy in Figure 6.106. The wide range observed in the energy per cycle comparison plot was not reduced in the energy dissipation index plots. The comparisons using the energy index revealed similar behaviour as Figures 6.103 and 6.104.

Table 6.1 Comparison of test results for static (monotonic) specimens

specimen	Maximum Strength (kN)	Yield displ. (mm)	Ductility	Drift (%)	Stiffness, K (kN/mm)		slip/disp
		Dy	μ_D	Du/H (%)	Ky	Ku/Ky (%)	Su/Du (%)
RS-S	275	4.0	9	2	65	-	13.6
PTB-S	235	4.0	11	2.44	66	-	15.6
PTS-S	230	4.0	7	1.56	65	-	5.8

Dy displacement corresponding to yielding of continuity reinforcement
Du displacement corresponding to ultimate strain in continuity reinforcement
Su slip at ultimate level
μ_Δ displacement ductility = Du/Dy
Ky initial stiffness at yield
Ku stiffness at ultimate after degradation due to cyclic loading

Table 6.2(a) Comparison of test results for mild steel specimens subjected to cyclic load

specimen	Maximum Strength (kN)	yield displ. Dy (mm)	Ductility μ_D	Drift (%) Du/H (%)	Stiffness, K (kN/mm) K_y	K_u/K_y (%)	slip/disp Su/Du (%)
RS	270	4.25	5	1.18	50	20	17.8
RSK	278	4.5	4	1	47.5	30	7.0
RSU	258	6.5	6	2.16	34	22	25
RW	243	5.0	5	1.39	39	20	35
RT	205	4.5	4	1	35	25	17.8

Table 6.2(b) Comparison of response quantities for mild steel specimen at 4Dy

specimen	Strength degradation P_{4Dy}/P_m (%)	stiffness degradation K_{4Dy}/K_y (%)	slip/disp S/4Dy (%)	Energy dissipation per cycle e (kN-mm)
RS	97	30	15.9	5578
RSK	100	30	7	4720
RSU	93	25.2	12.3	7735
RW	92	26.6	17.5	6835
RT	88	26	18	3190

Dy displacement corresponding to yielding of continuity reinforcement
Du displacement corresponding to ultimate strain of continuity reinforcement
Su slip at ultimate level
μ_D displacement ductility = Du/Dy
K_y initial stiffness at yield
K_u stiffness at ultimate after degradation due to cyclic loading

Table 6.3(a) Comparison of test results for prestressed specimens subjected to cyclic load

specimen	Maximum Strength (kN)	yield displ. Dy (mm)	Ductility μ_D	Drift (%) Du/H (%)	Stiffness, K (kN/mm) K_y	K_u/K_y (%)	slip/disp Su/Du (%)
PTS	240	4.0	6	1.33	44	16	10.8
PTB	223	4.0	6	1.33	47.5	15	12.5
PTBU	201	4.0	14	3.11	39	7	15.2

Table 6.3(b) Comparison of response quantities for prestressed specimen at 6Dy

specimen	Strength degradation P_{6Dy}/P_m (%)	stiffness degradation K_{6Dy}/K_y (%)	slip/disp S/6Dy (%)	Energy dissipation per cycle e (kN-mm)
PTS	83	16	10.8	2825
PTB	77	15	12.5	4170
PTBU	94	16	5.8	1466

Dy displacement corresponding to yielding of continuity reinforcement
Du displacement corresponding to ultimate strain of continuity reinforcement
Su slip at ultimate level
μ_D displacement ductility = Du/Dy
K_y initial stiffness at yield
K_u stiffness at ultimate after degradation due to cyclic loading

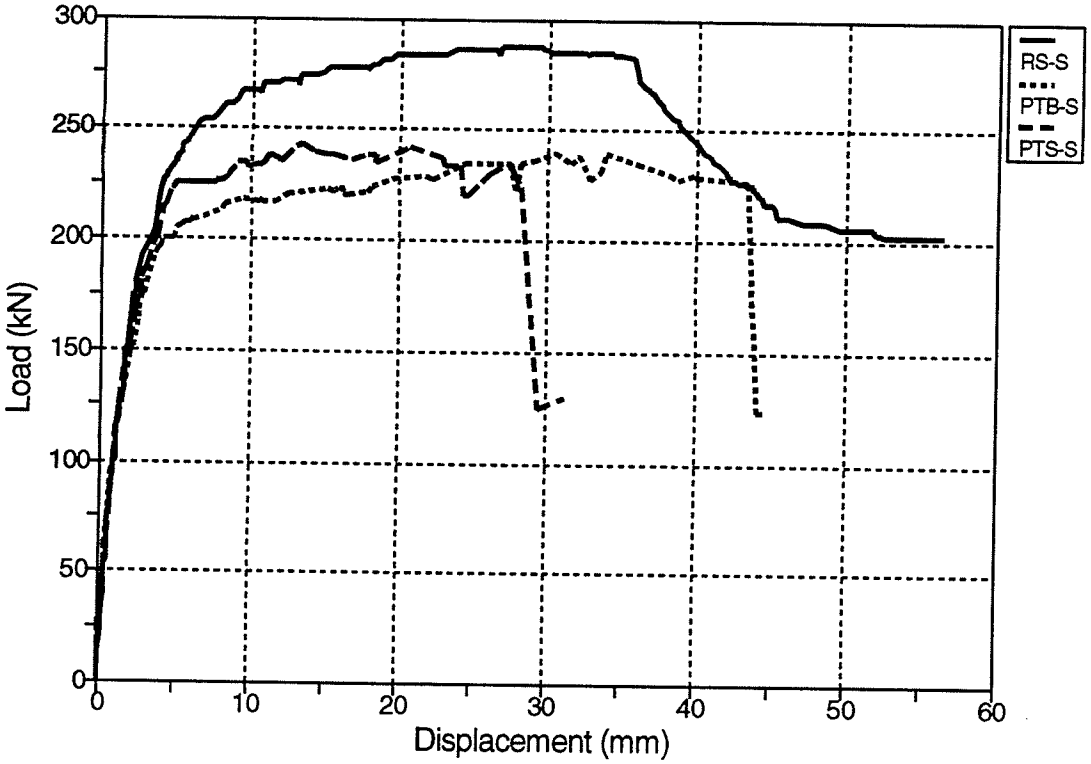

Figure 6.1 Comparison of load vs. displacement relationship for static specimens

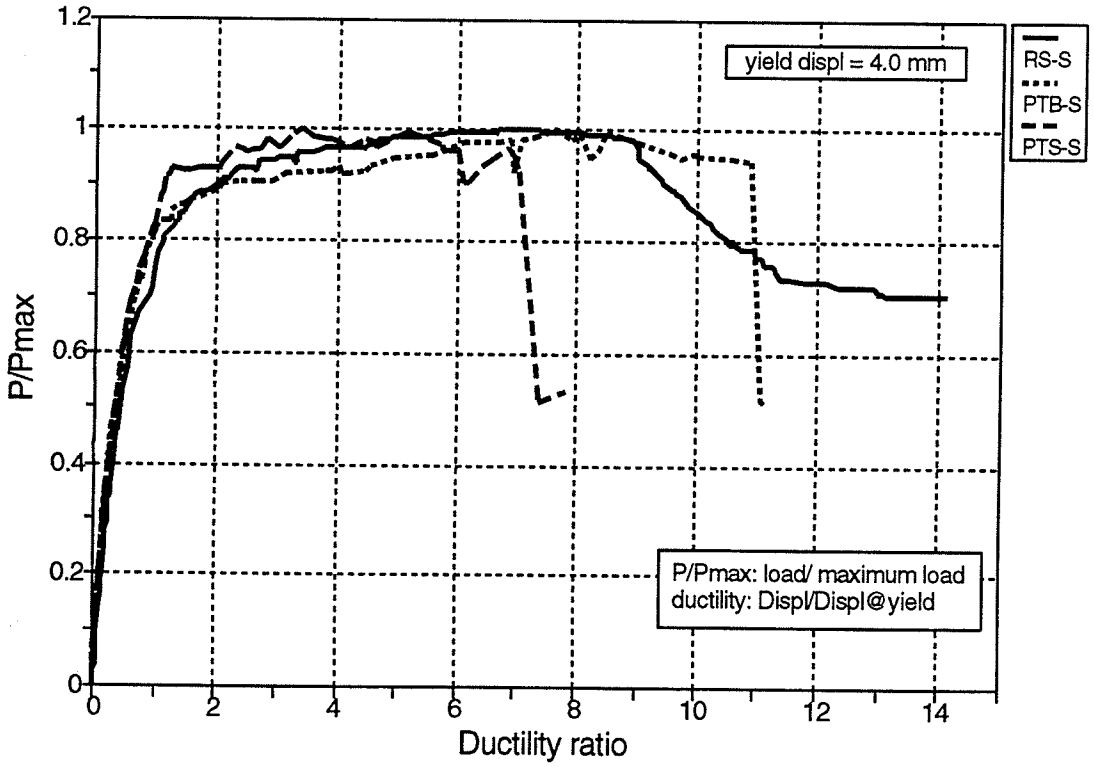

Figure 6.2 Comparison of normalized load vs. ductility for static specimens

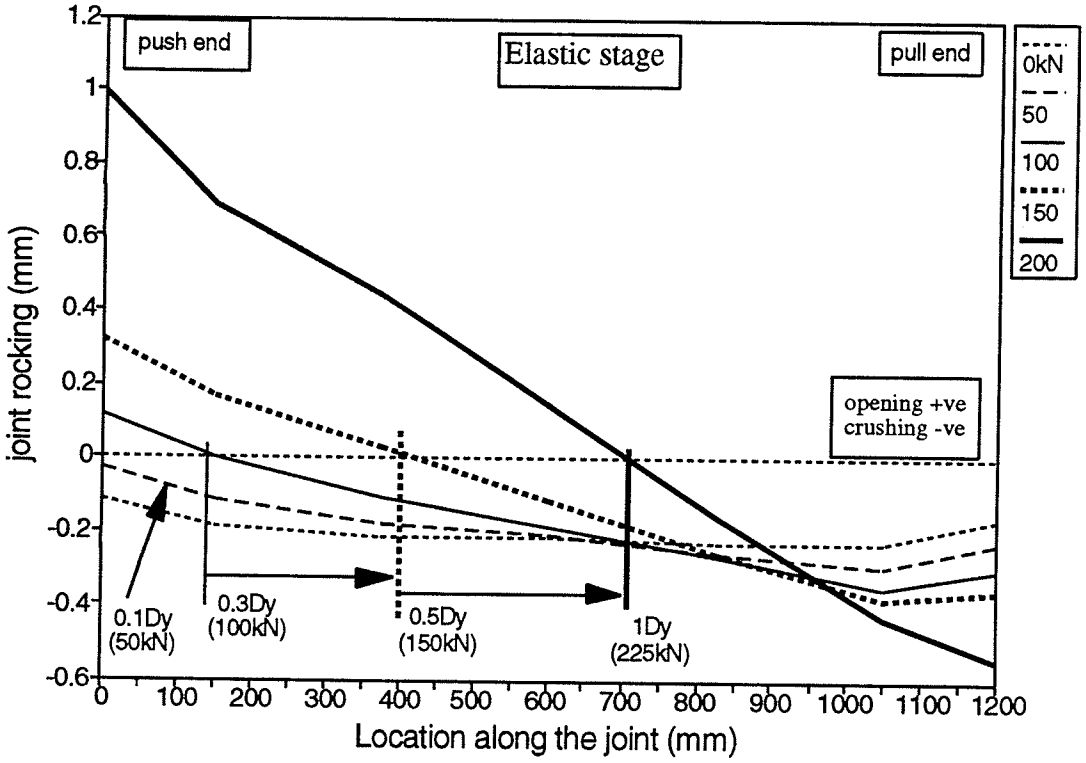

Figure 6.3(a) Typical rocking behaviour in elastic stage (specimen RS-S)

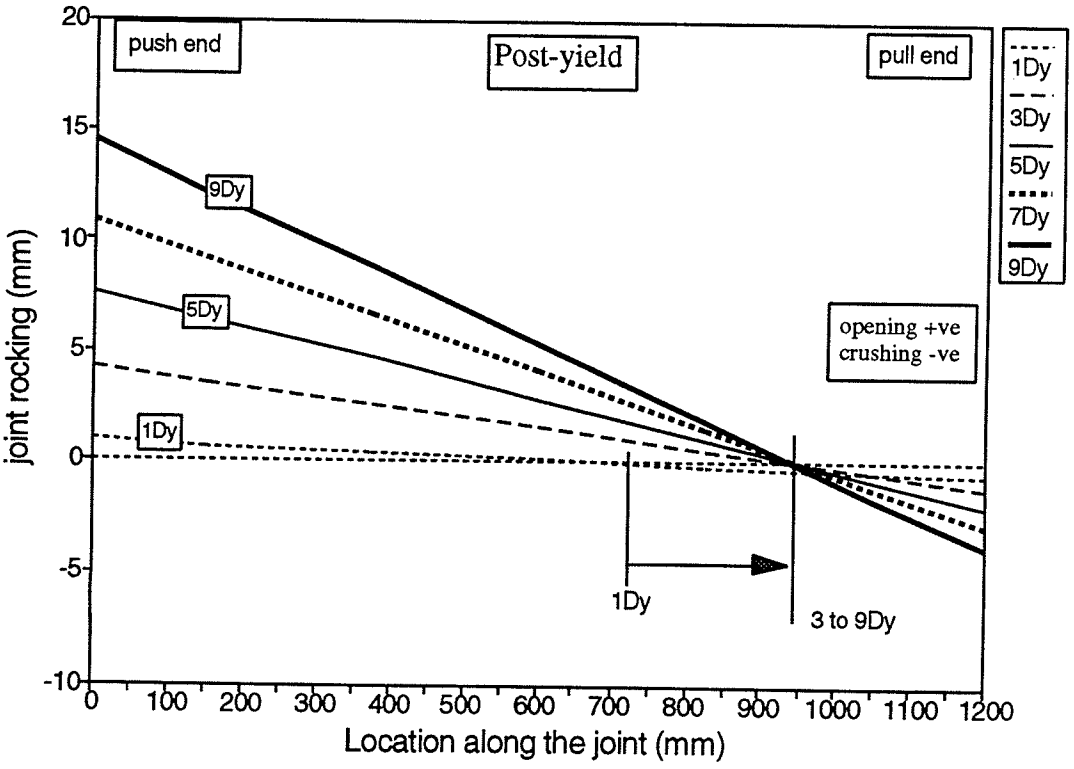

Figure 6.3(b) Typical rocking behaviour in post-yield stage (specimen RS-S)

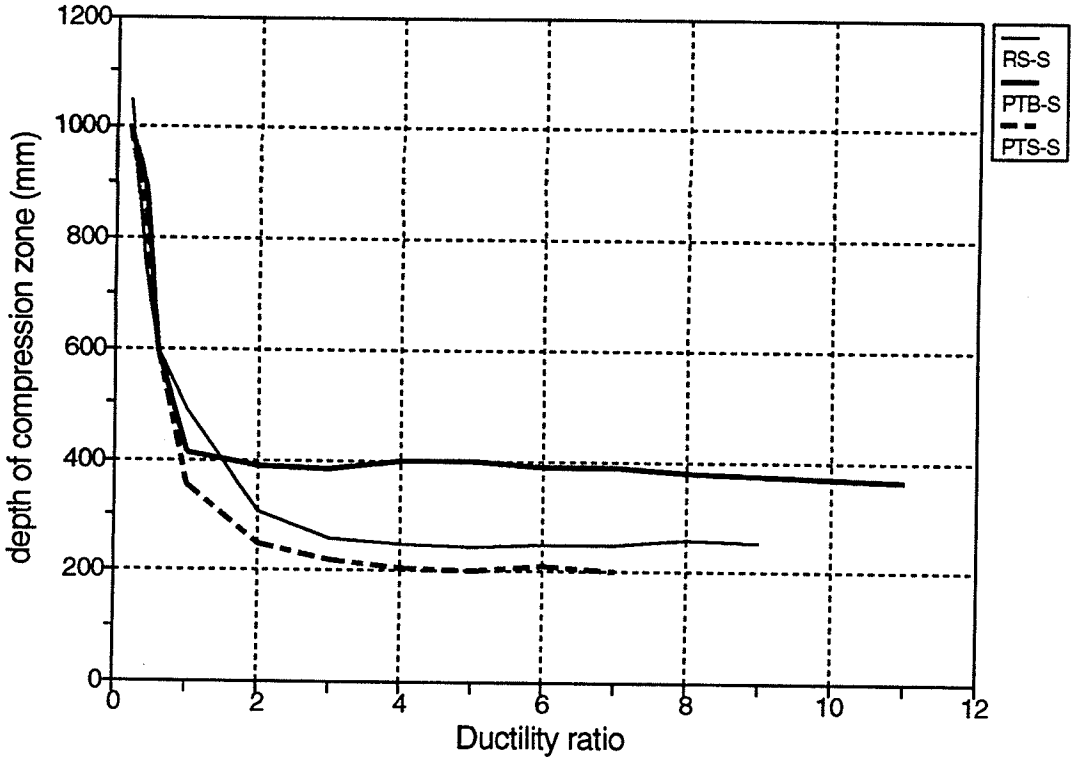

Figure 6.4 Comparison of compression zone depths vs. ductility for the static specimens

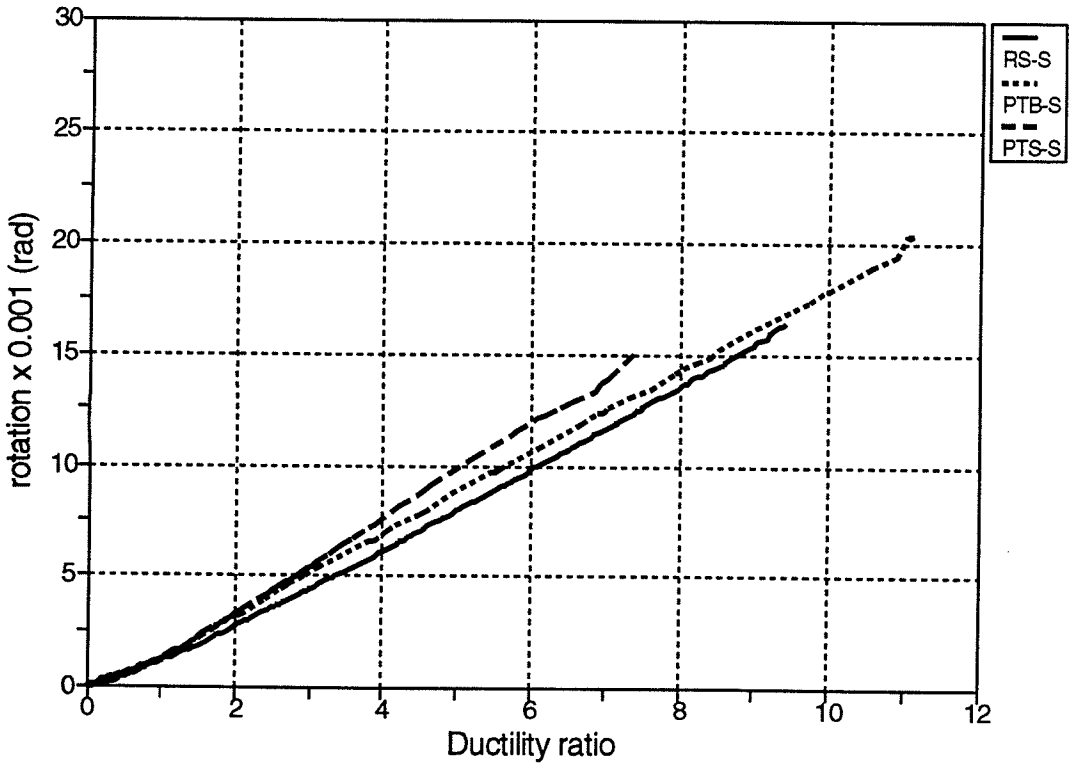

Figure 6.5 Comparison of rotation vs. ductility relationship for the static specimens

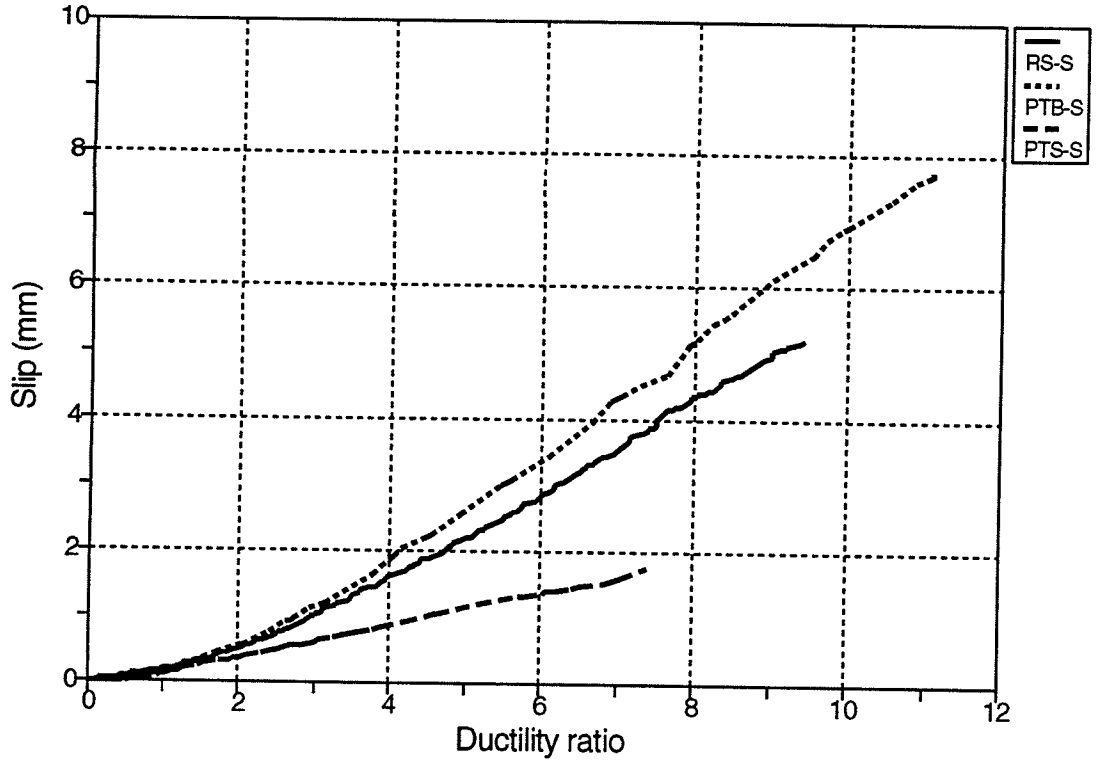

Figure 6.6 Comparison of slip vs. ductility relationship for the static specimens

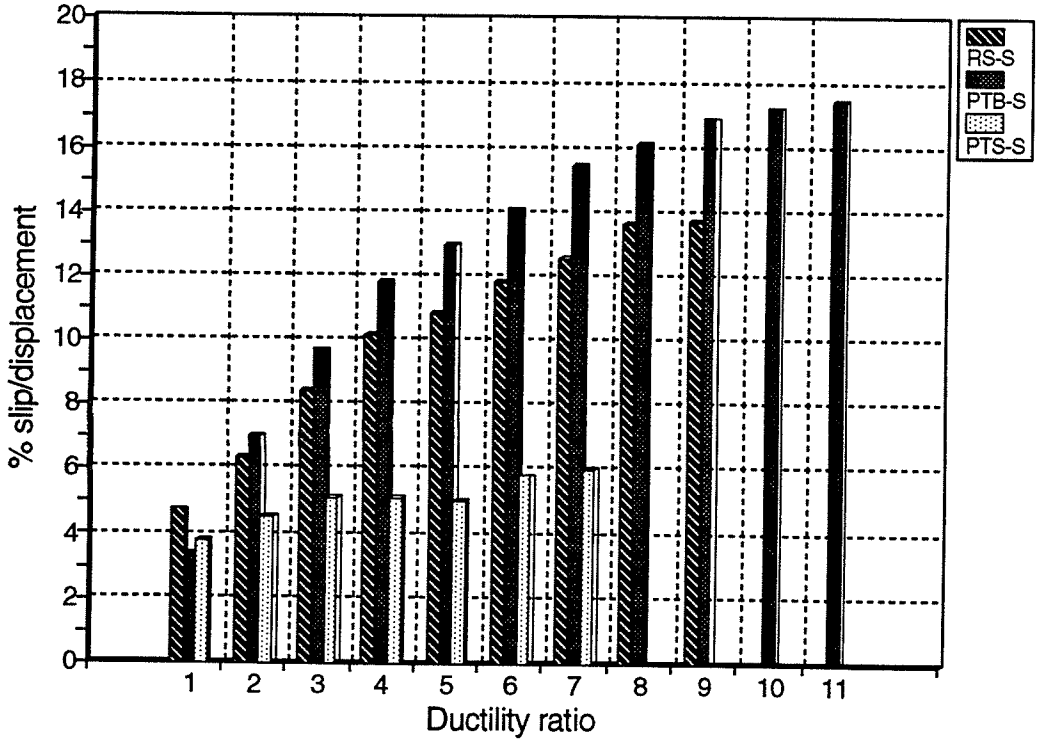

Figure 6.7 Comparison of % slip/displacement vs. ductility for the static specimens

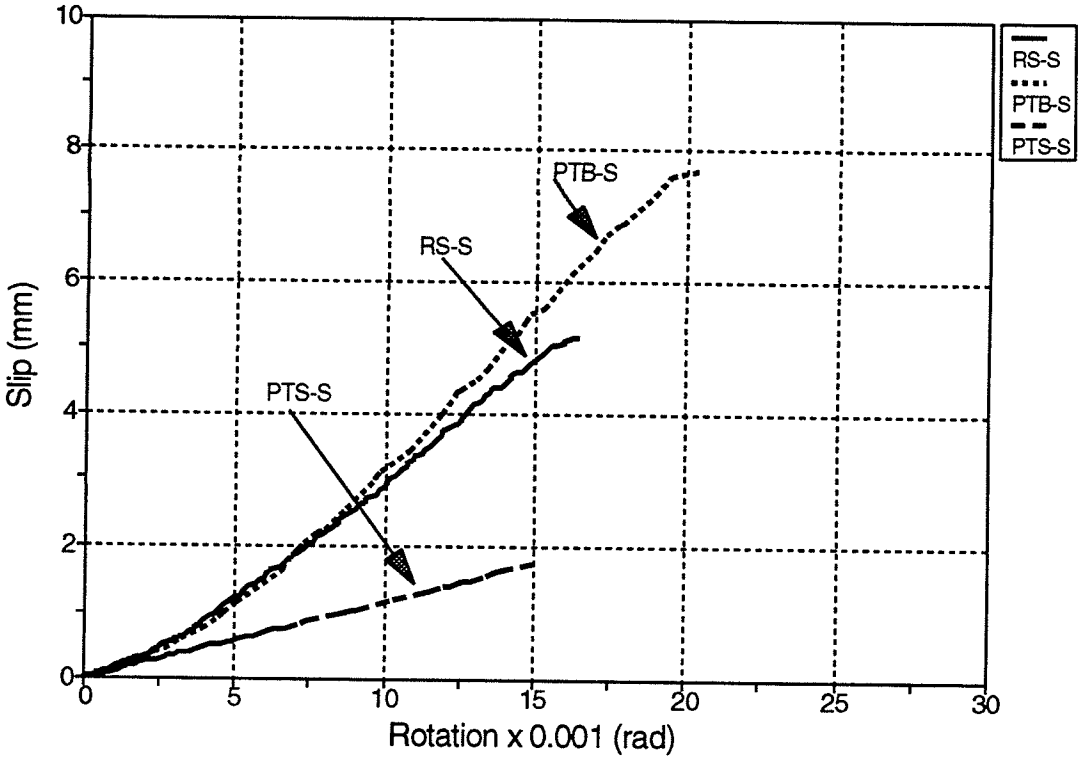

Figure 6.8 Comparison of slip vs. rotation relationship for the static specimens

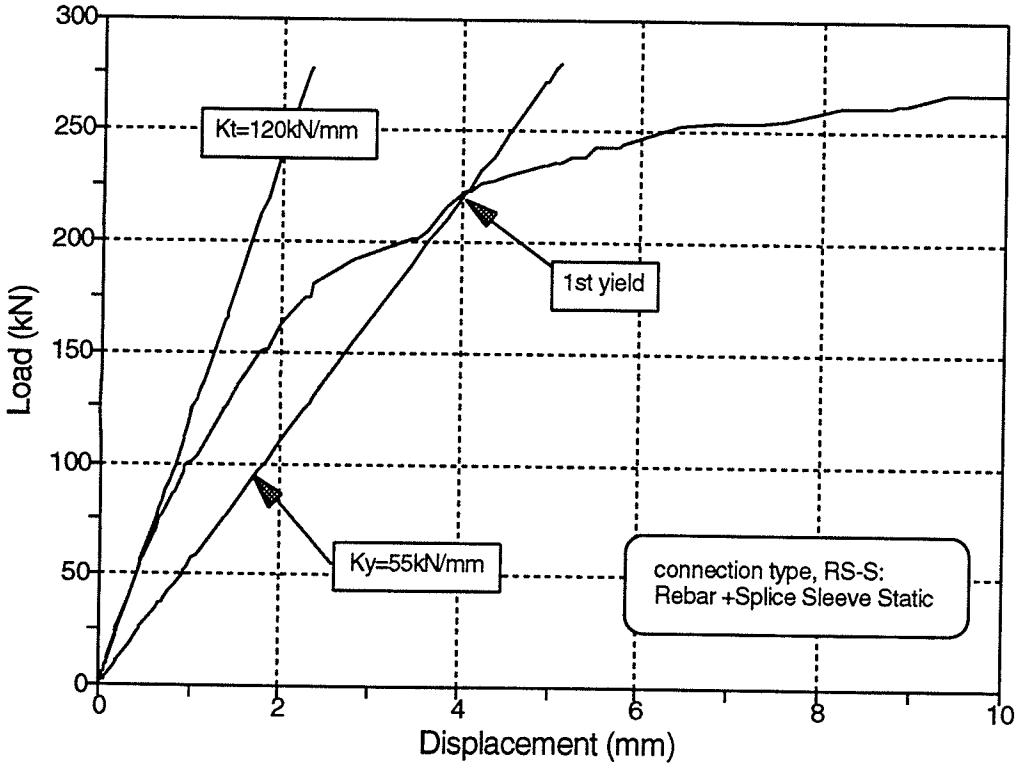

Figure 6.9 Stiffness evaluation in terms of load vs. displacement for specimen RS-S

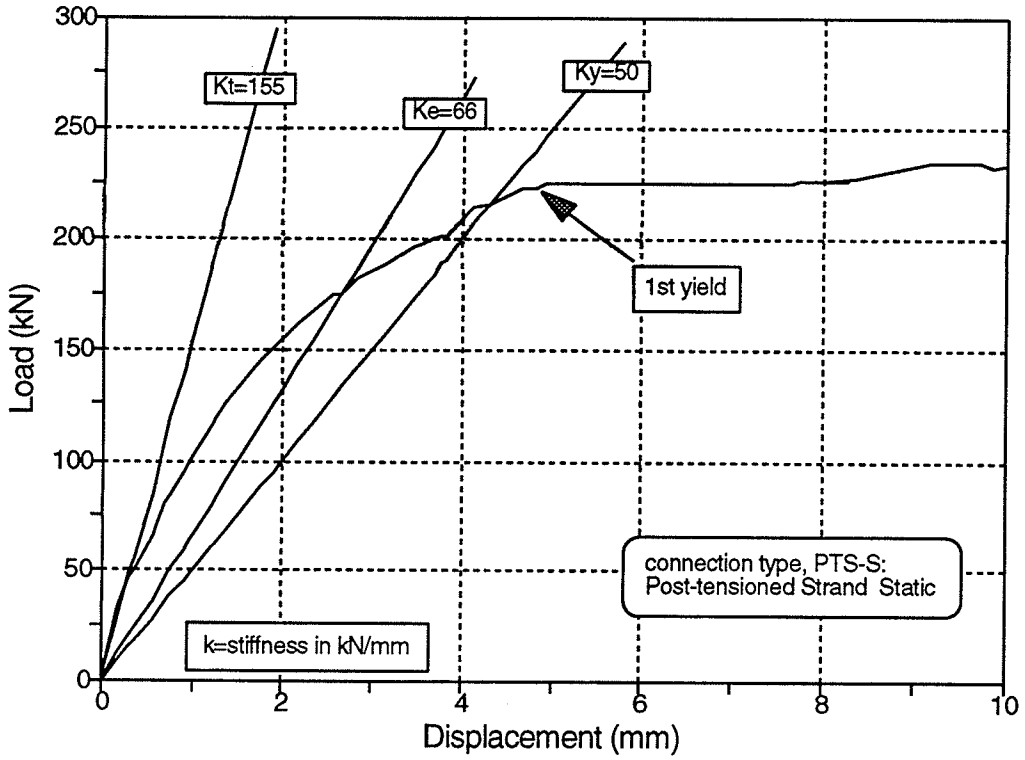

Figure 6.10 Stiffness evaluation in terms of load vs. displacement for specimen PTS-S

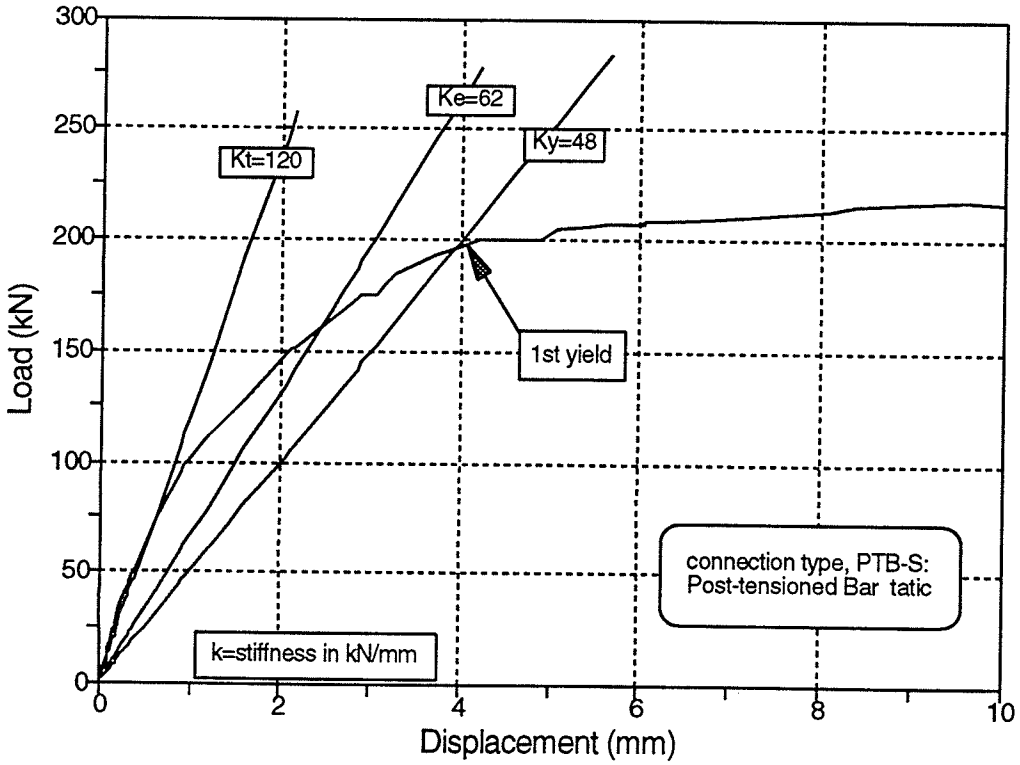

Figure 6.11 Stiffness evaluation in terms of load vs. displacement for specimen PTB-S

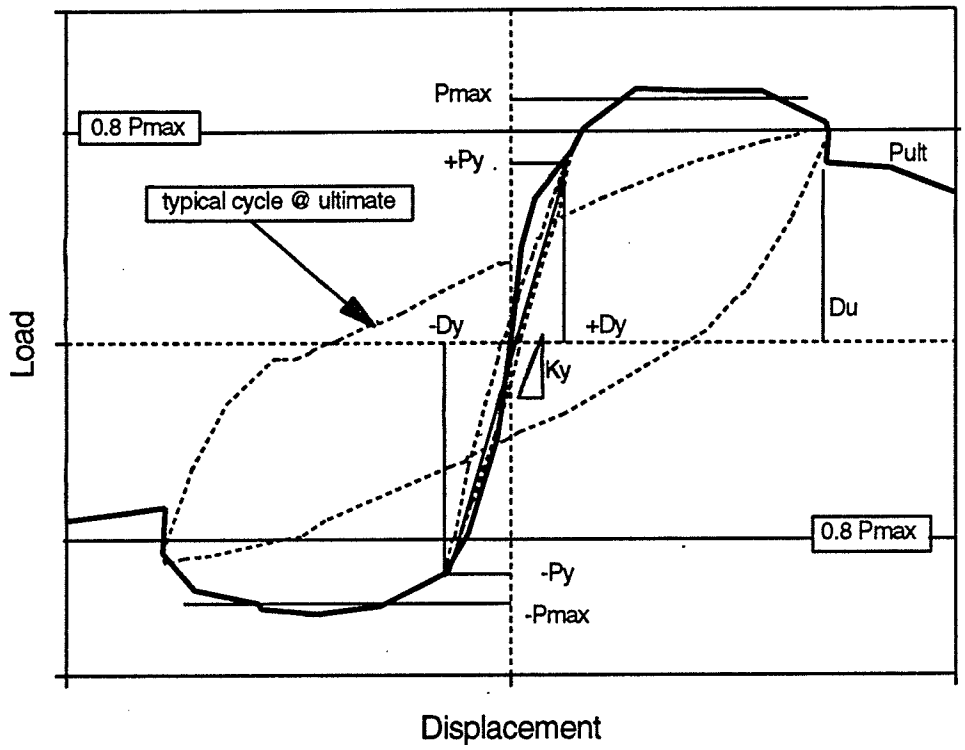

Figure 6.12 Typical strength envelope of load-displacement response

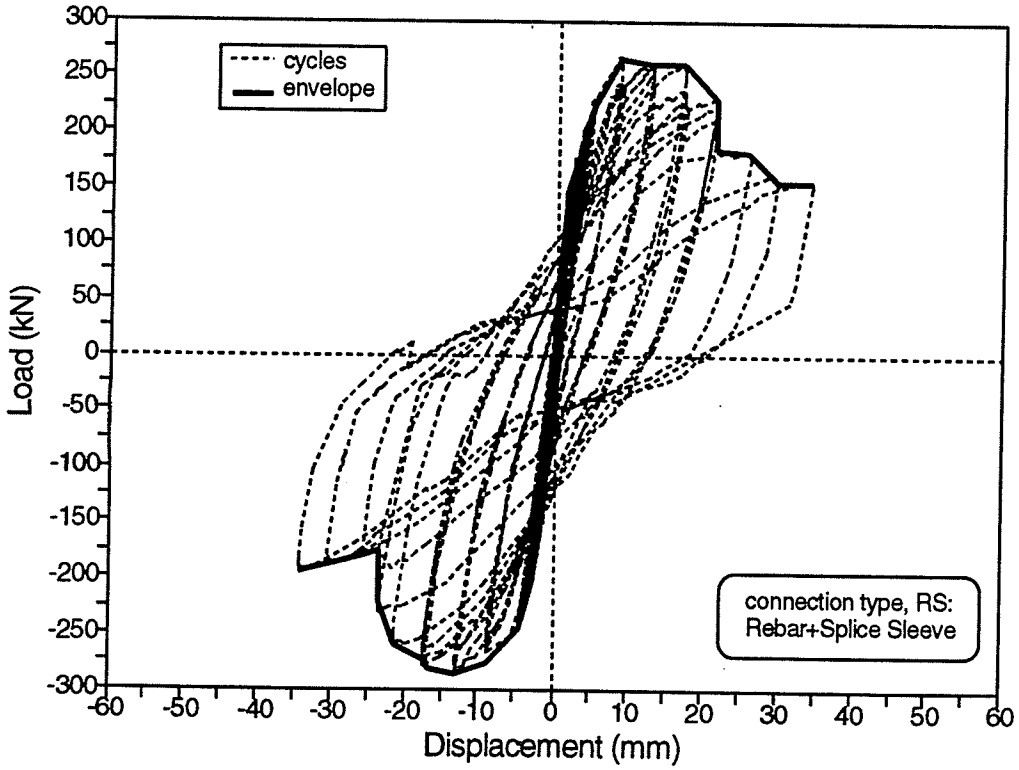

Figure 6.13 Strength envelope of response for specimen RS

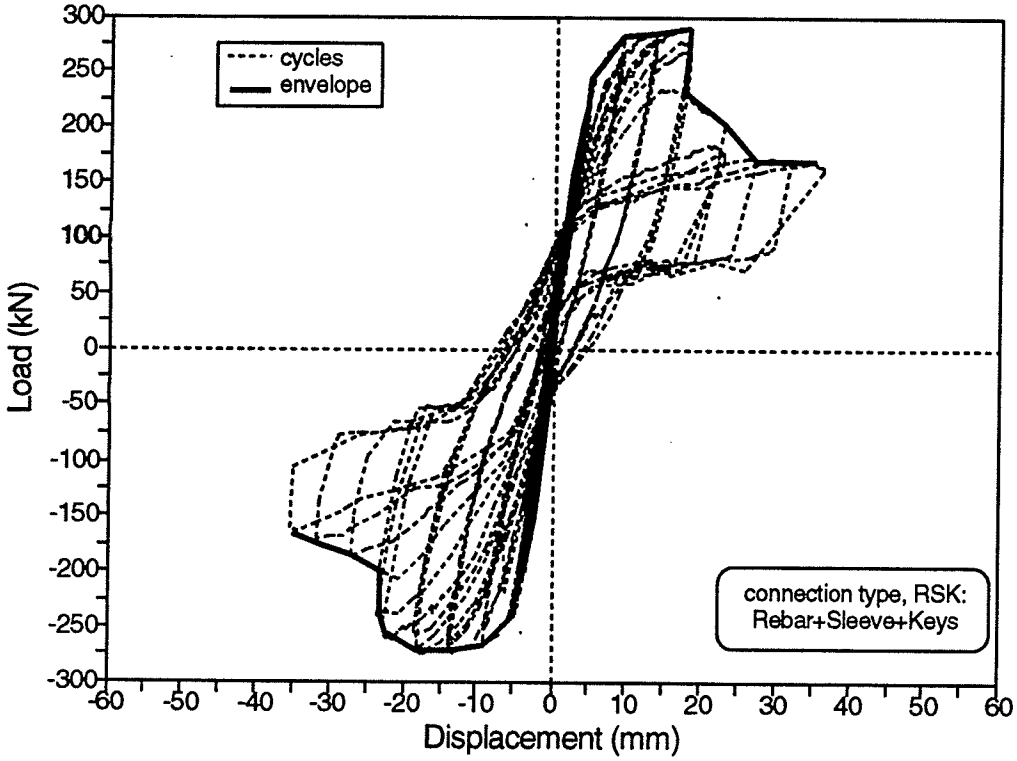

Figure 6.14 Strength envelope of response for specimen RSK

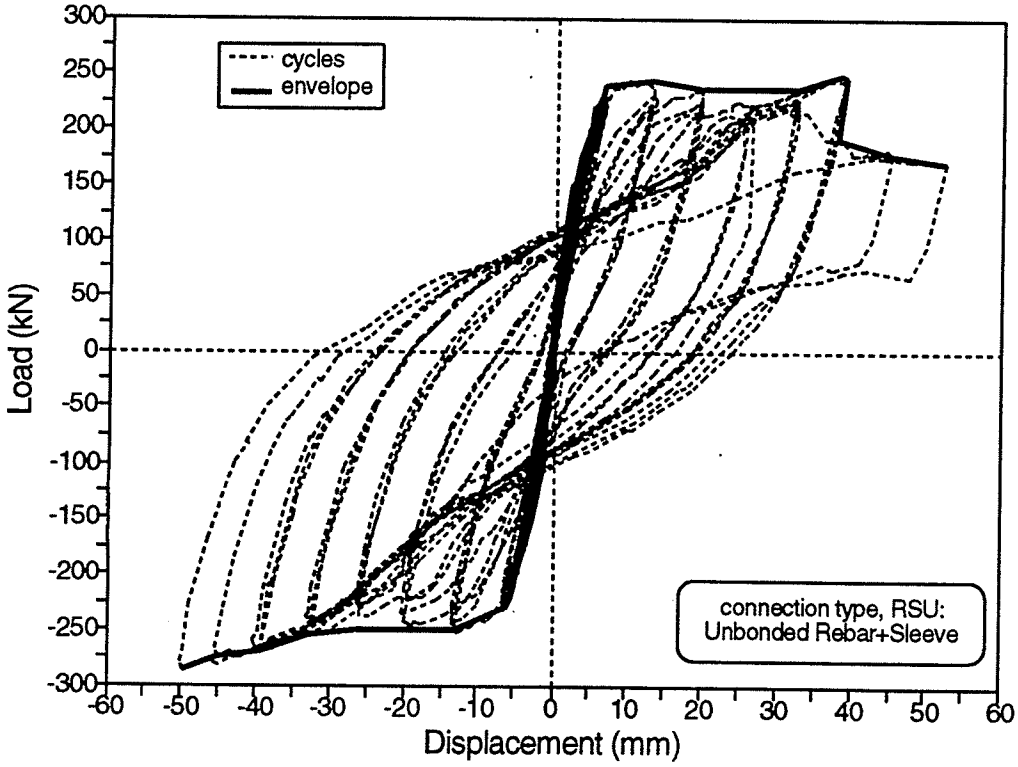

Figure 6.15 Strength envelope of response for specimen RSU

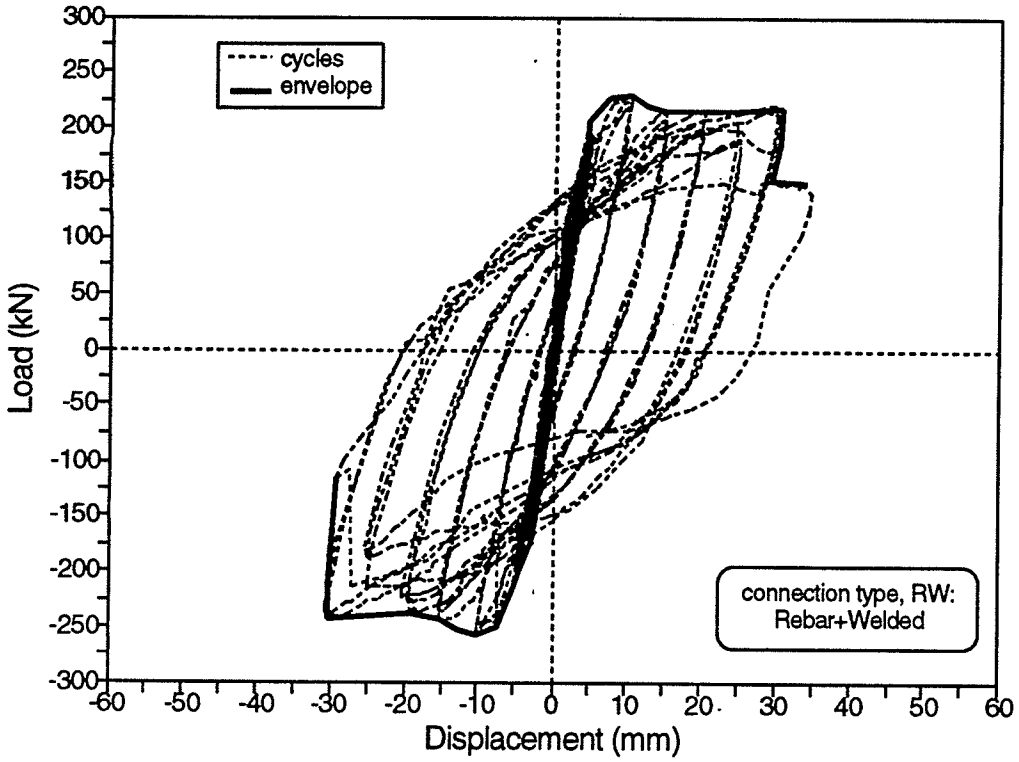

Figure 6.16 Strength envelope of response for specimen RW

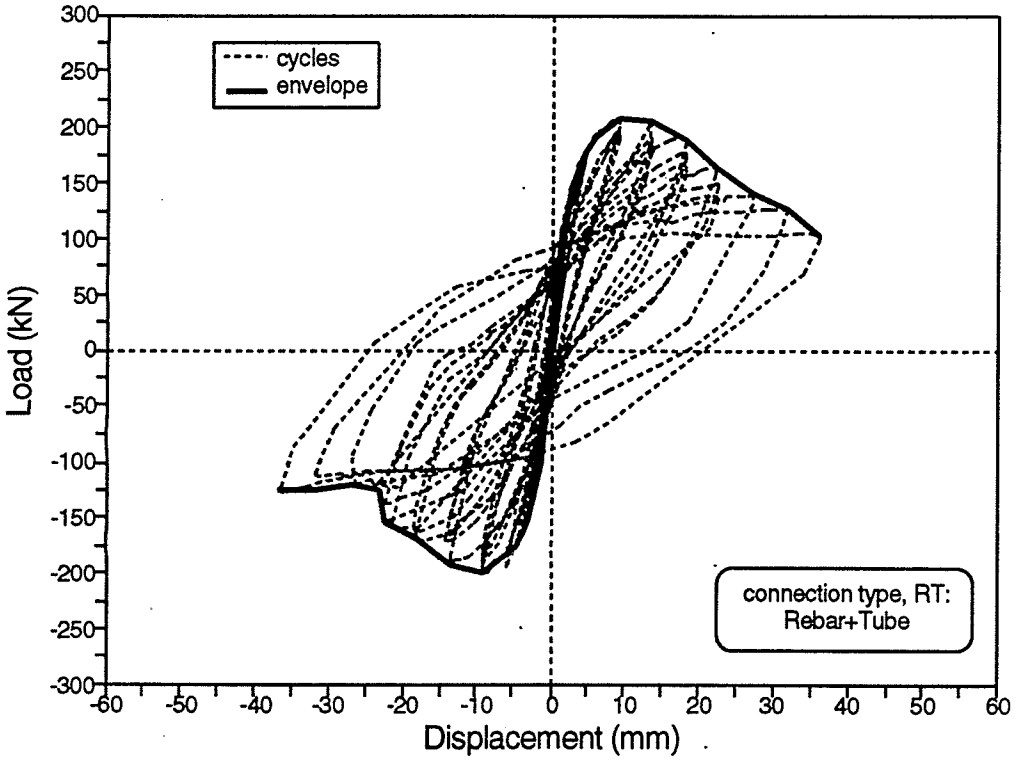

Figure 6.17 Strength envelope of response for specimen RT

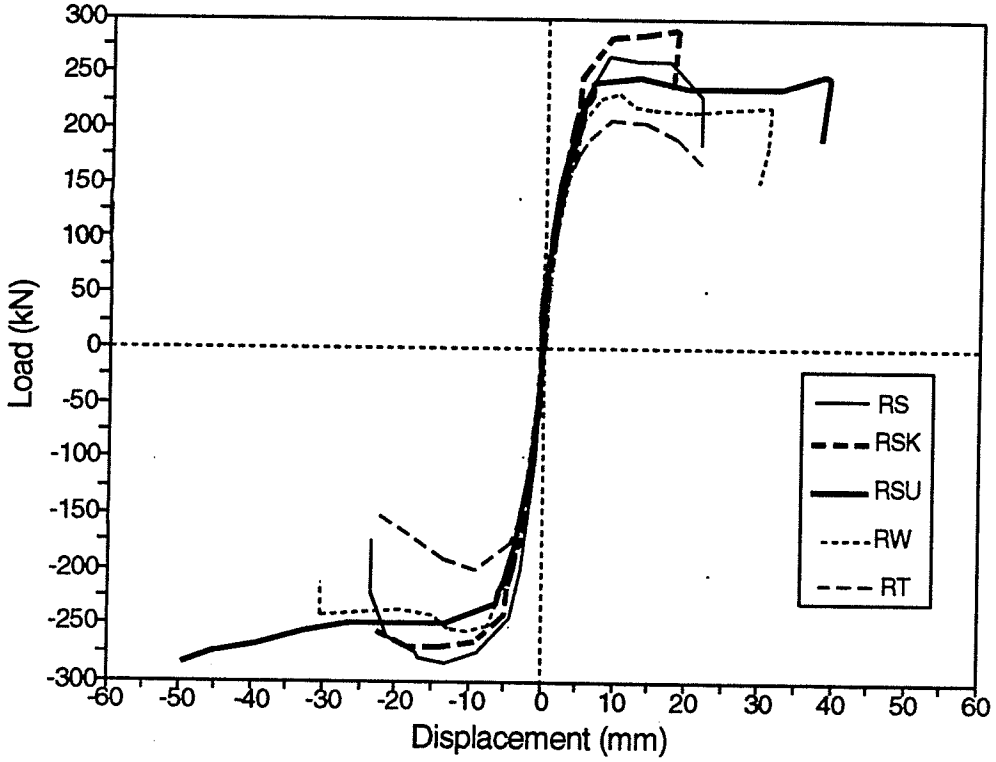

Figure 6.18 Comparison of strength envelopes for specimens with mild steel bars

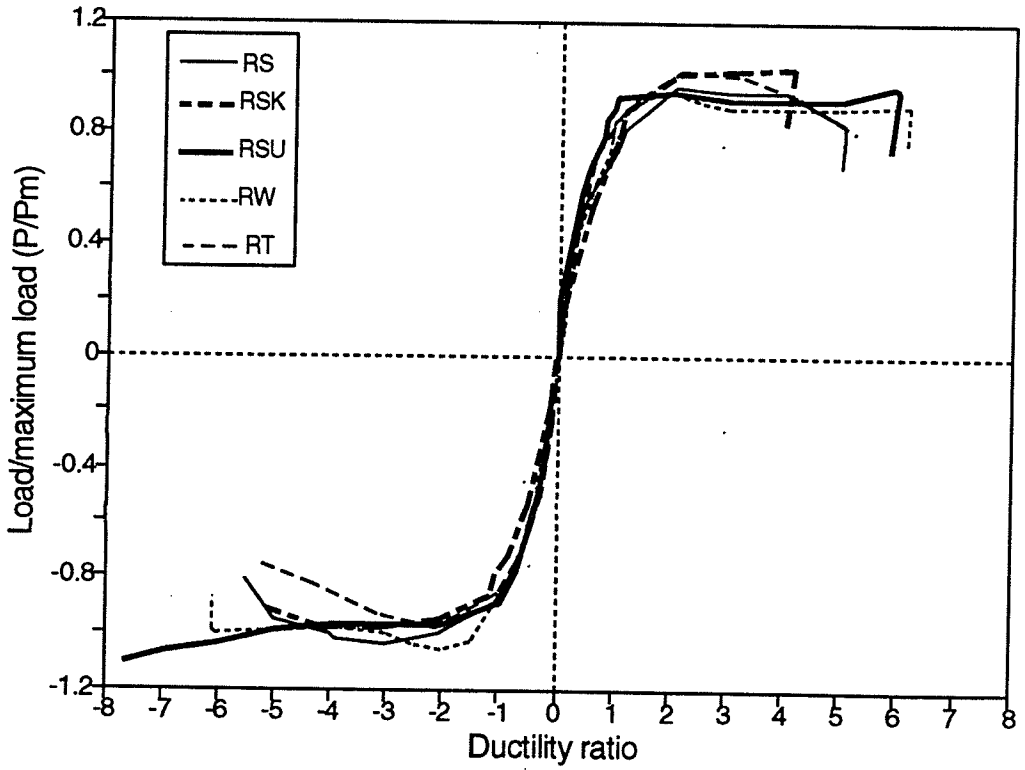

Figure 6.19 Comparison of normalized envelopes for specimens with mild steel bars

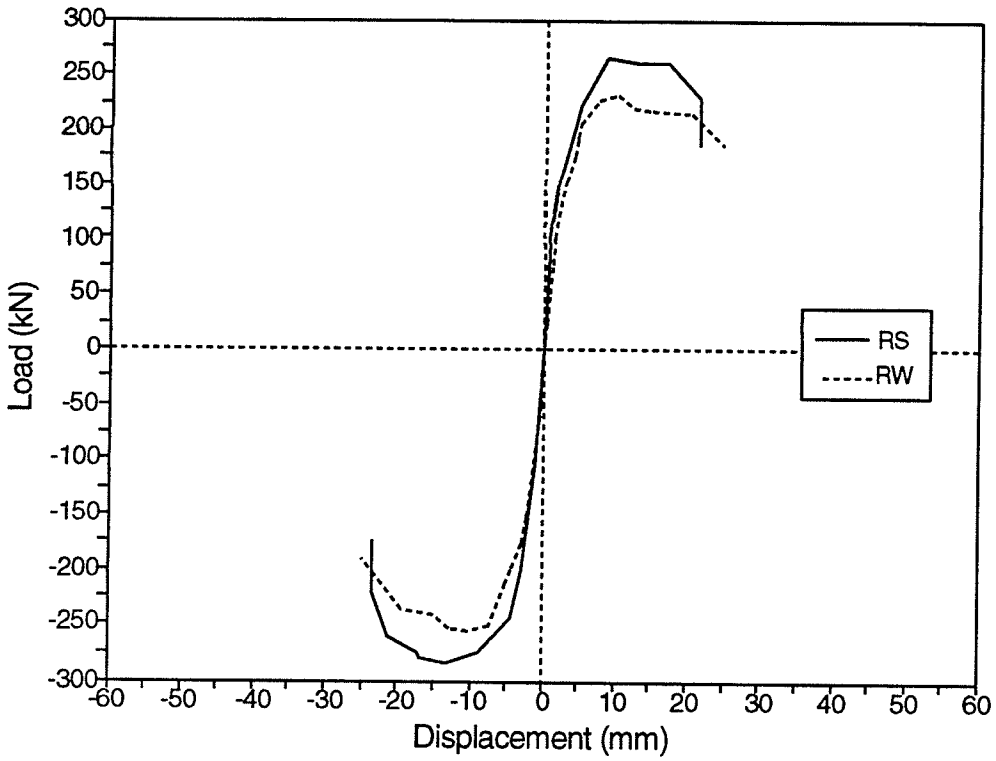

Figure 6.20(a) Comparison of strength envelopes: specimen RW vs. RS

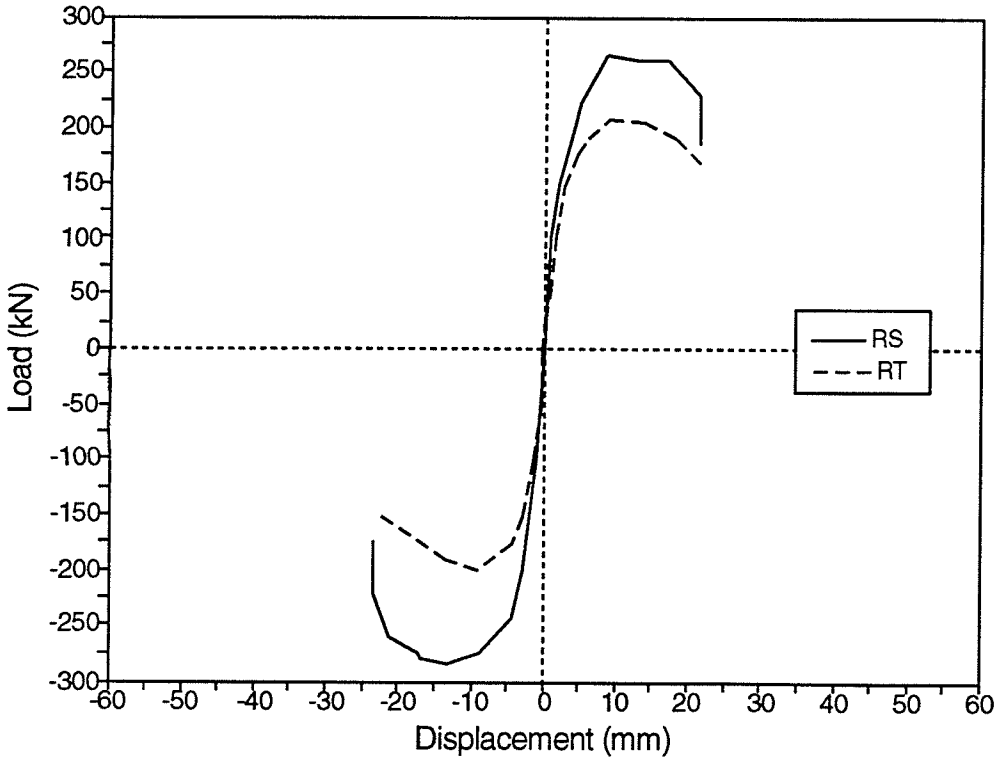

Figure 6.20(b) Comparison of strength envelopes : specimen RT vs. RS

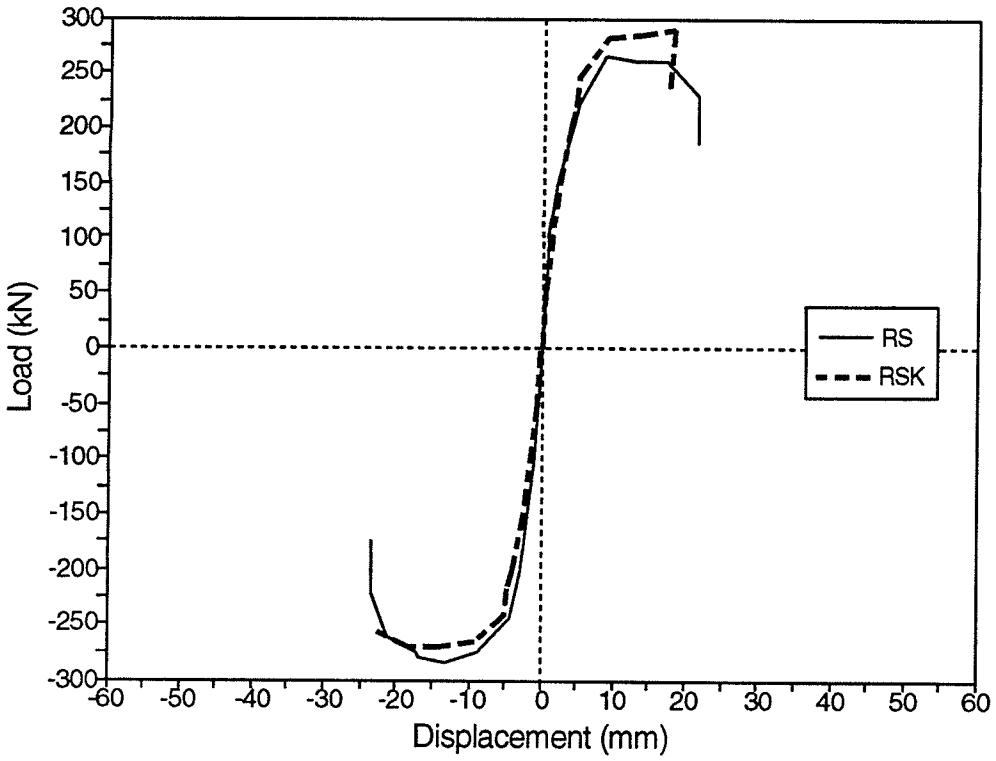

Figure 6.20(c) Comparison of strength envelopes : specimen RSK vs. RS

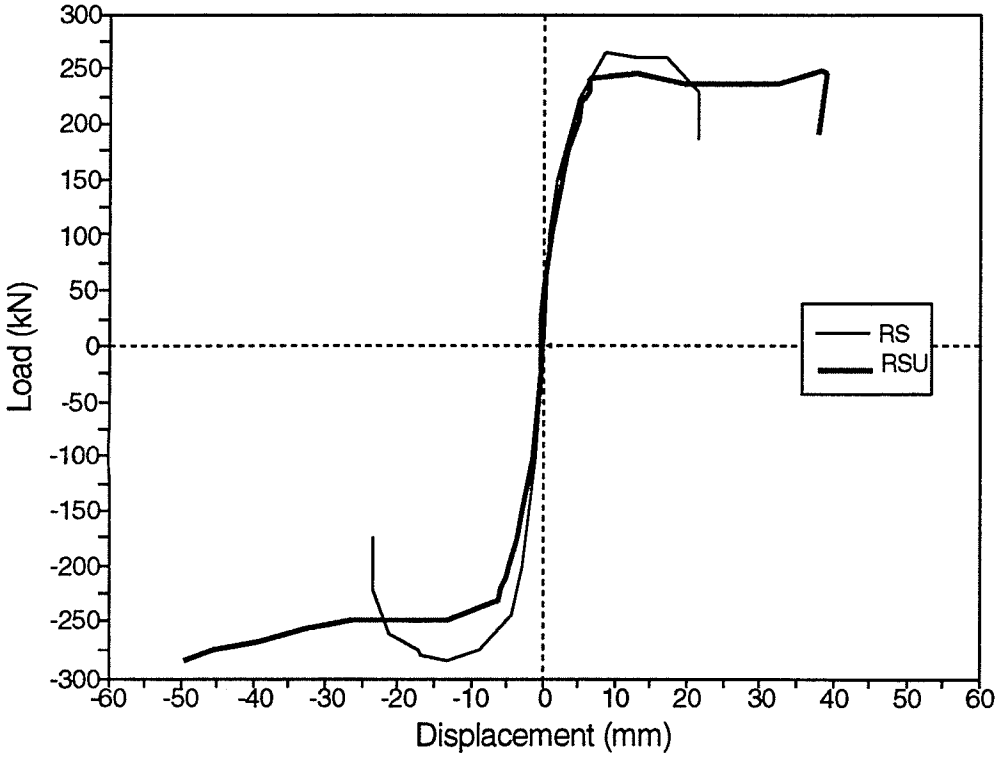

Figure 6.20(d) Comparison of strength envelopes: specimen RSU vs. RS

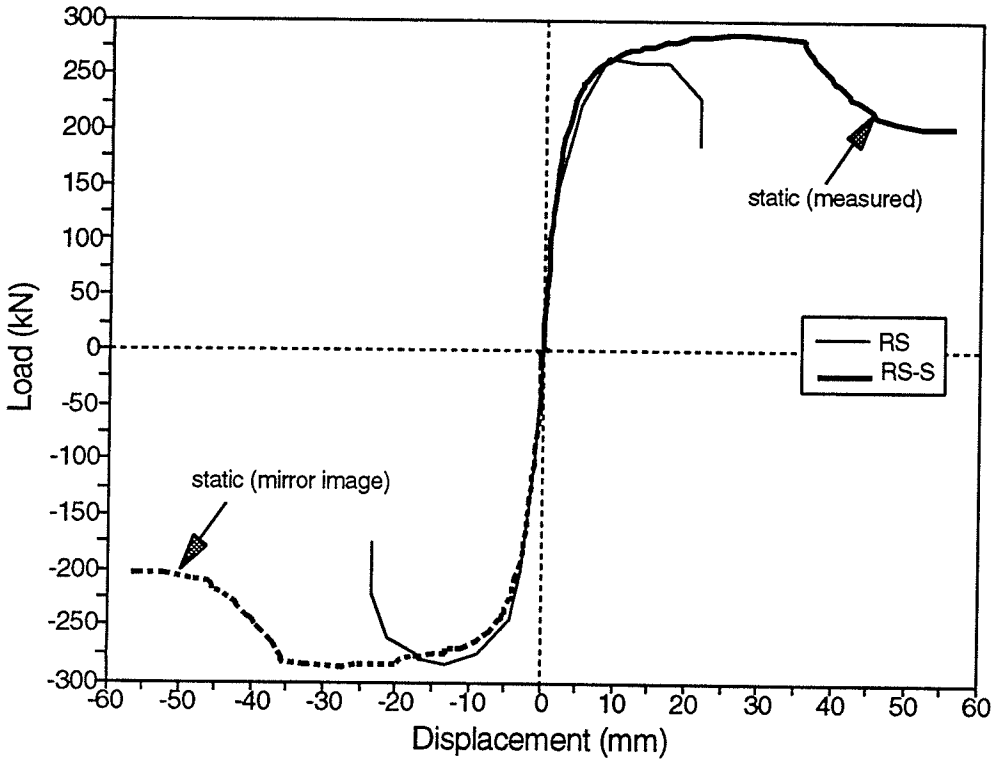

Figure 6.20(e) Comparison of strength envelopes: specimen RS vs. RS-S

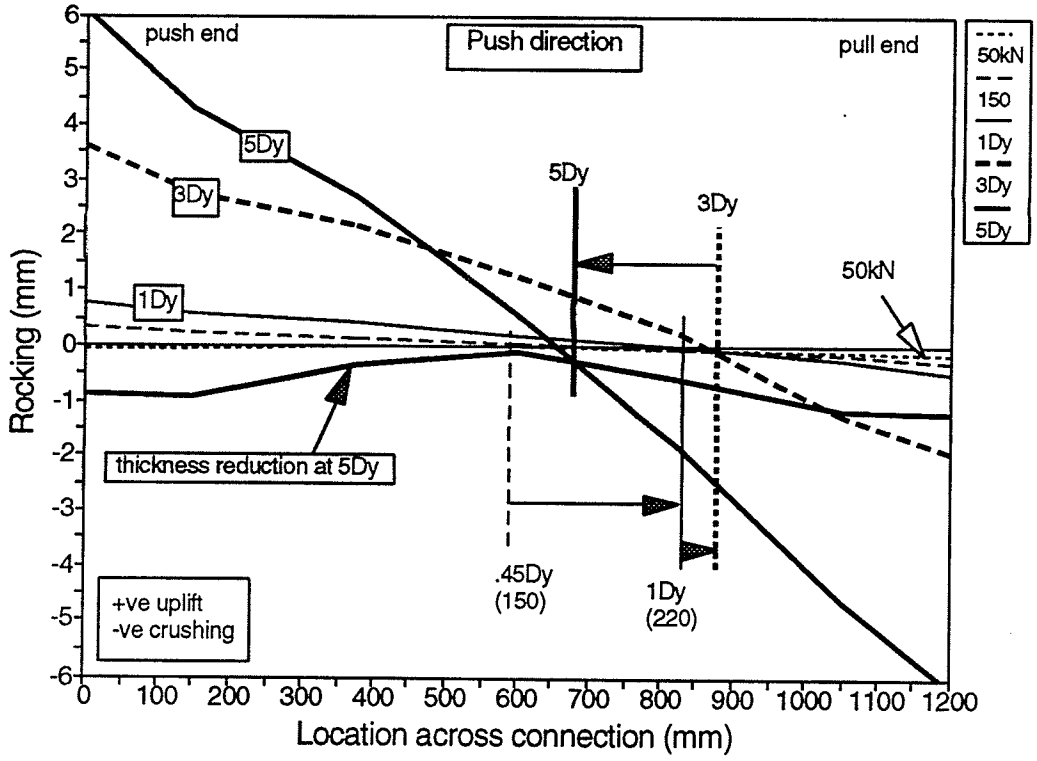

Figure 6.21(a) Typical rocking behaviour in the push direction (specimen RS)

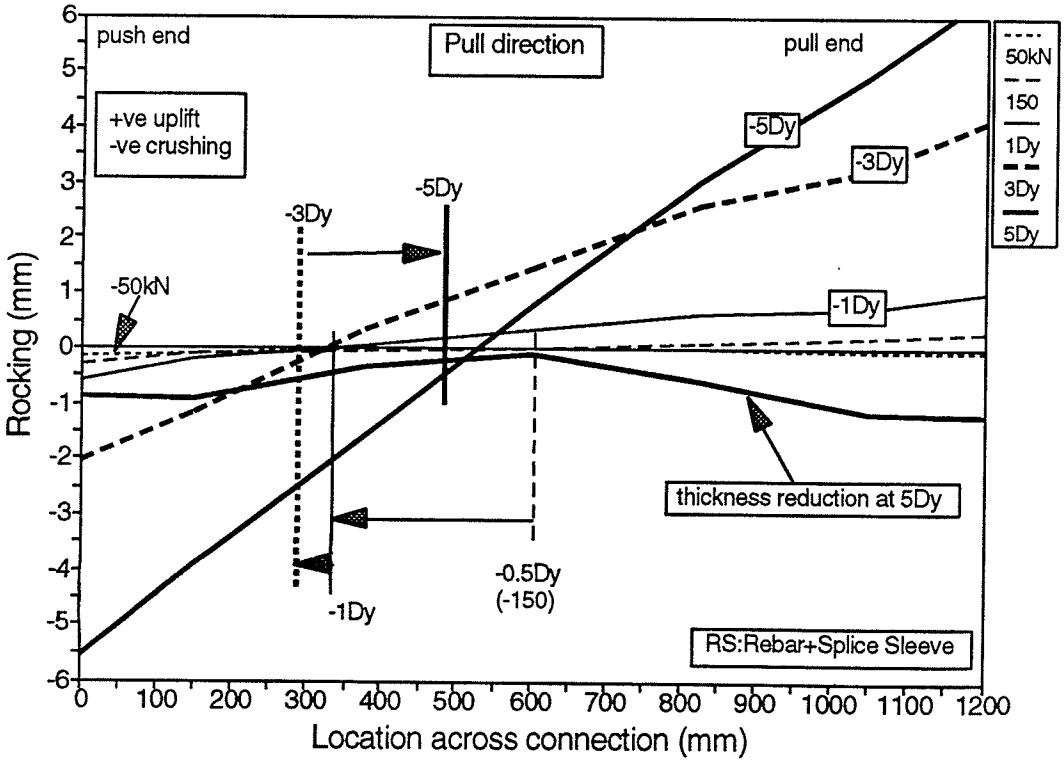

Figure 6.21(b) Typical rocking behaviour in the pull direction (specimen RS)

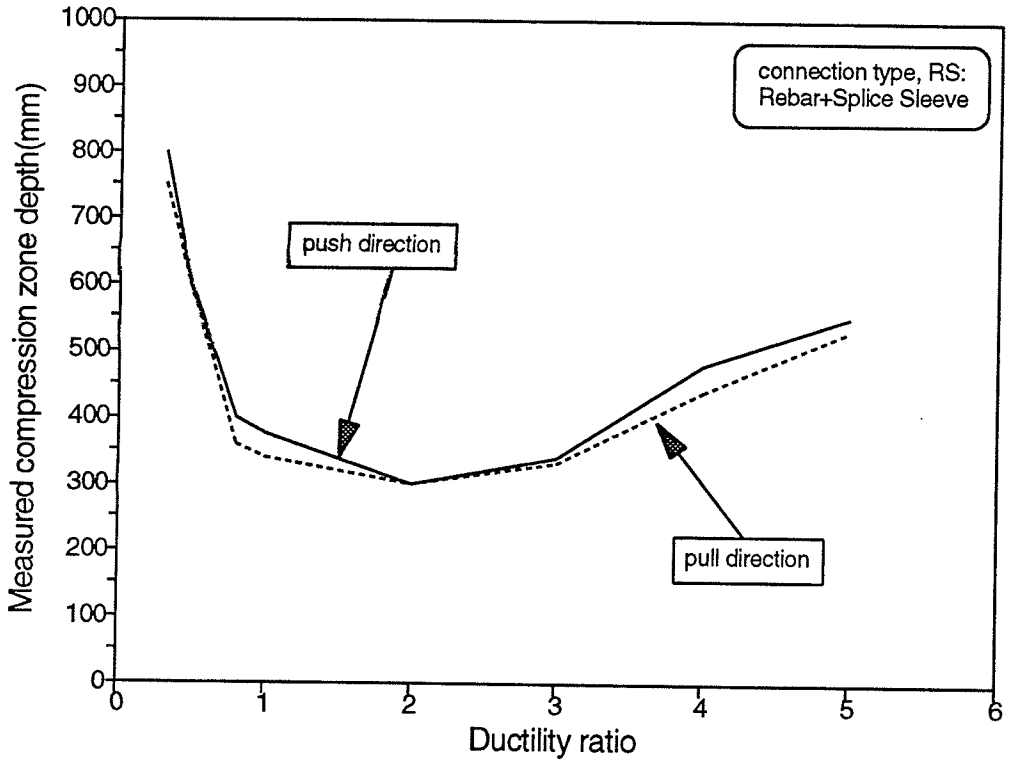

Figure 6.22 Variation of compression zone depth for specimen RS

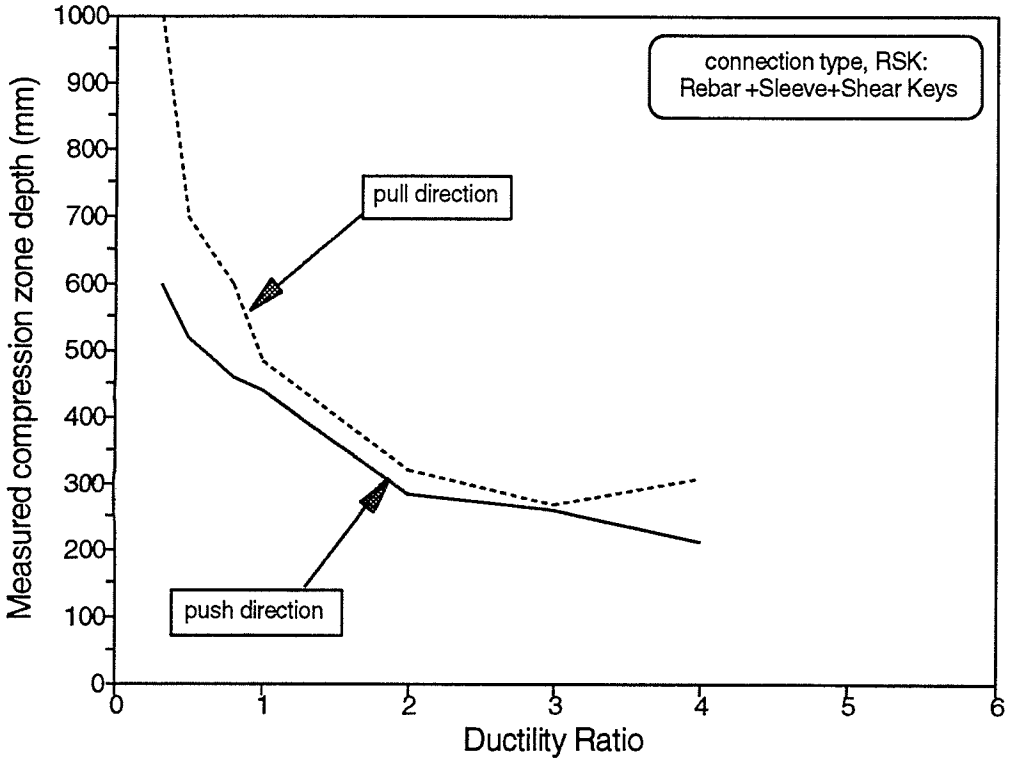

Figure 6.23 Variation of compression zone depth for specimen RSK

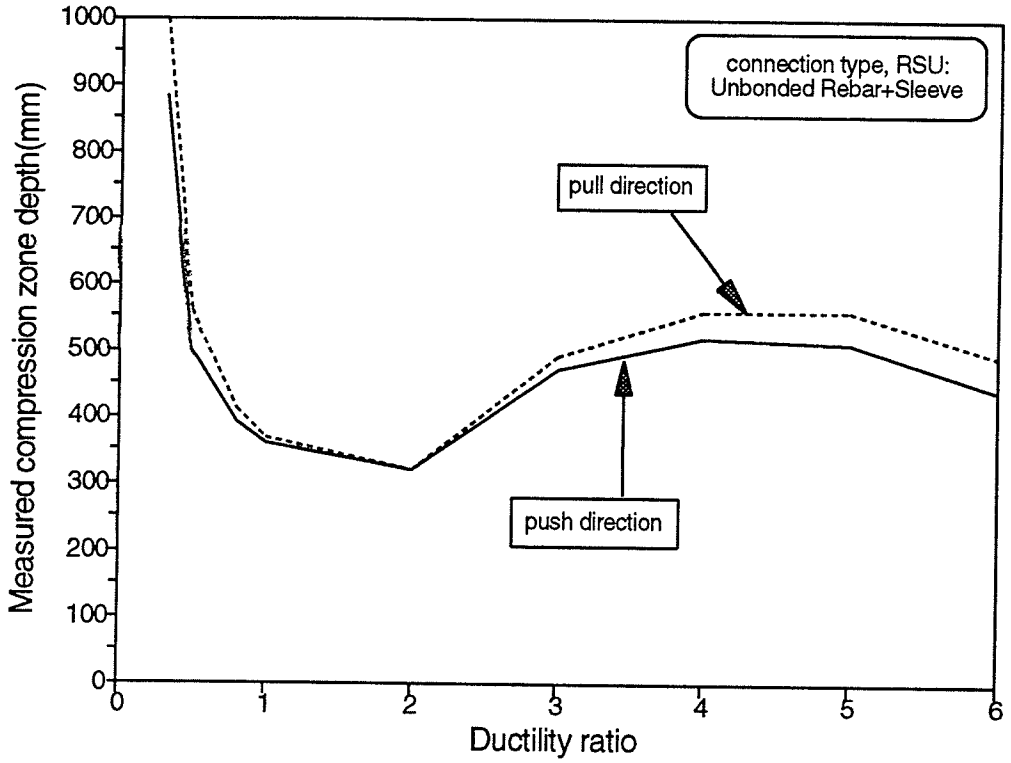

Figure 6.24 Variation of compression zone depth for specimen RSU

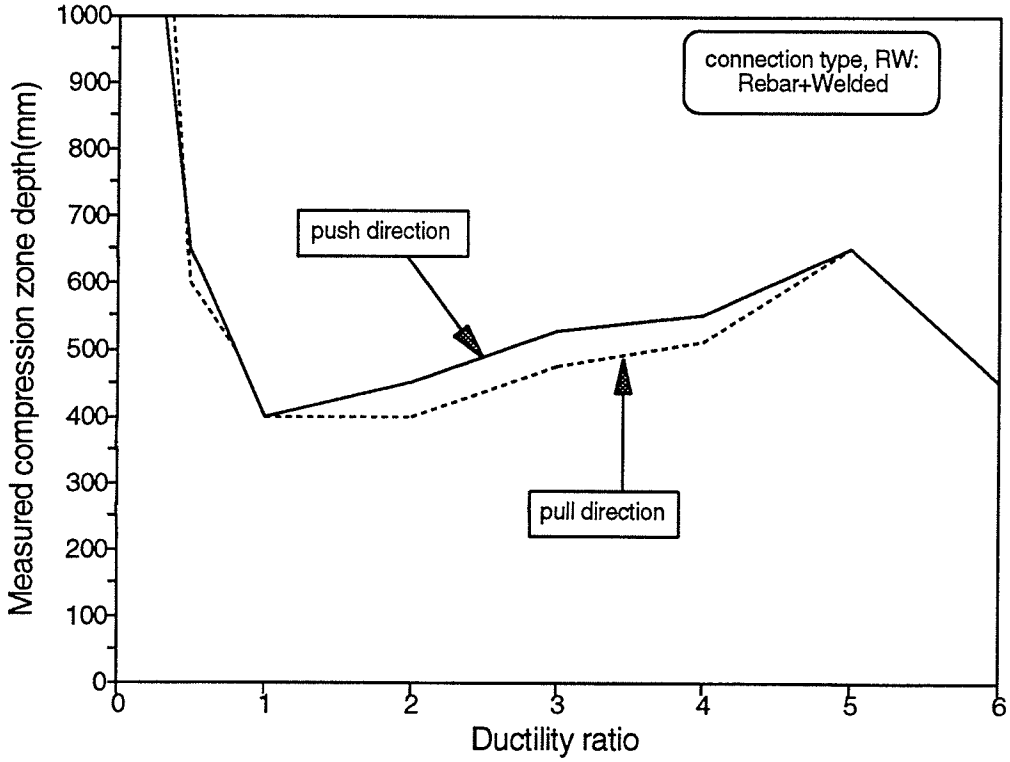

Figure 6. 25 Variation of compression zone depth for specimen RW

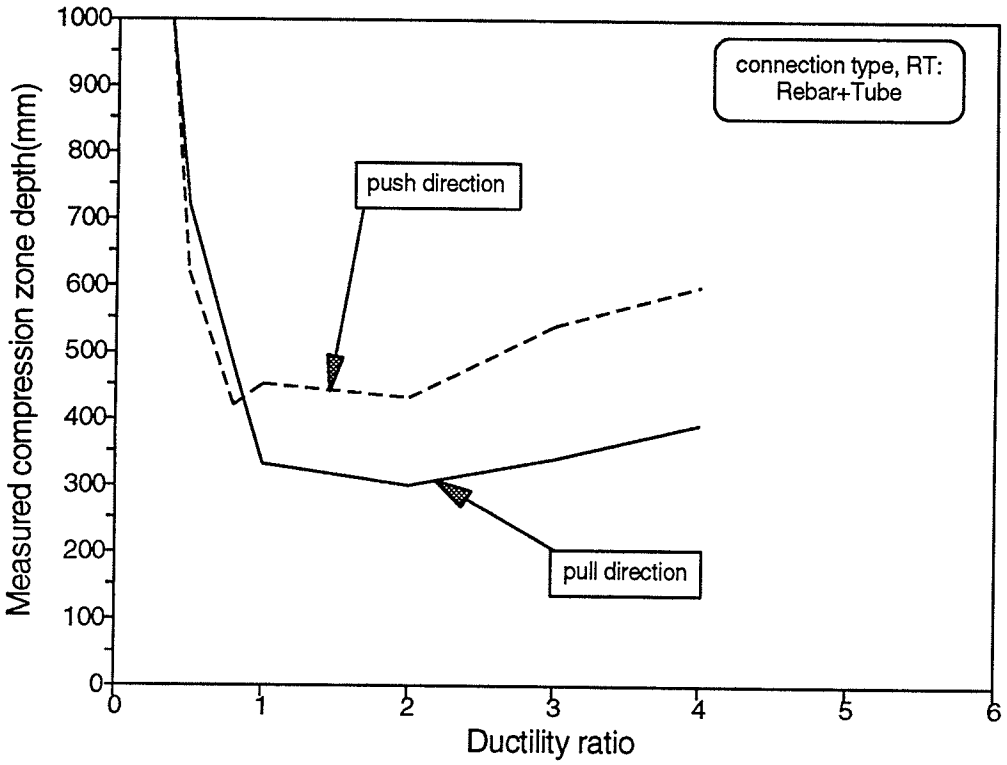

Figure 6.26 Variation of compression zone depth for specimen RT

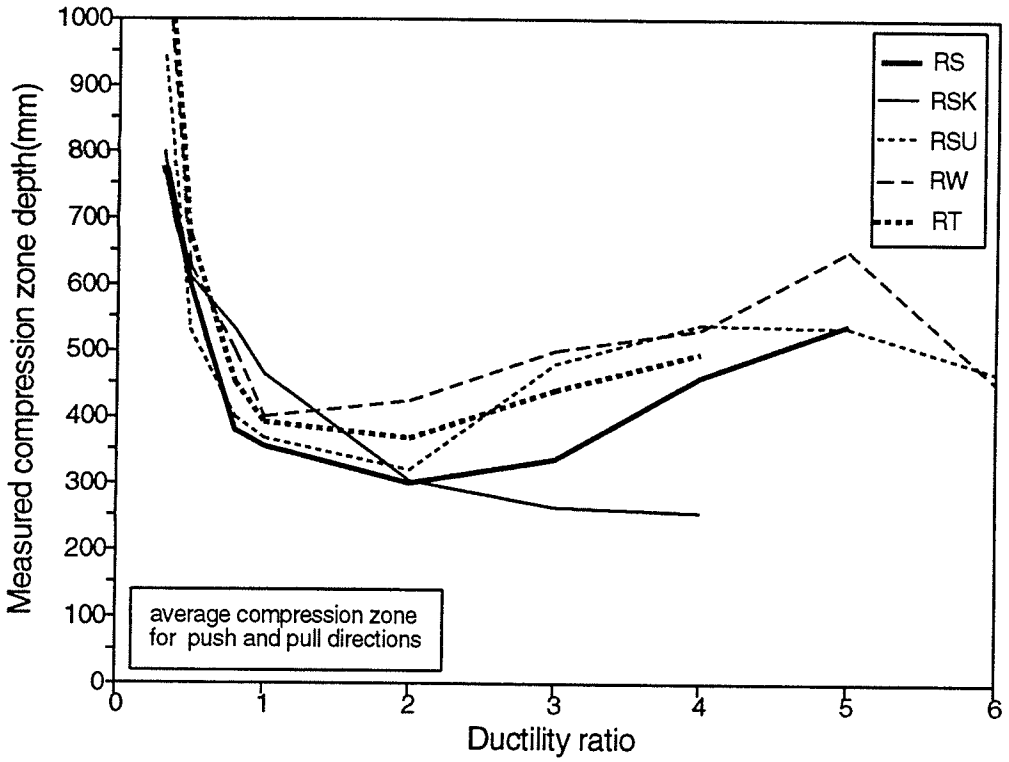

Figure 6.27(a) Comparison of variation of compression zone depth for rebar specimens

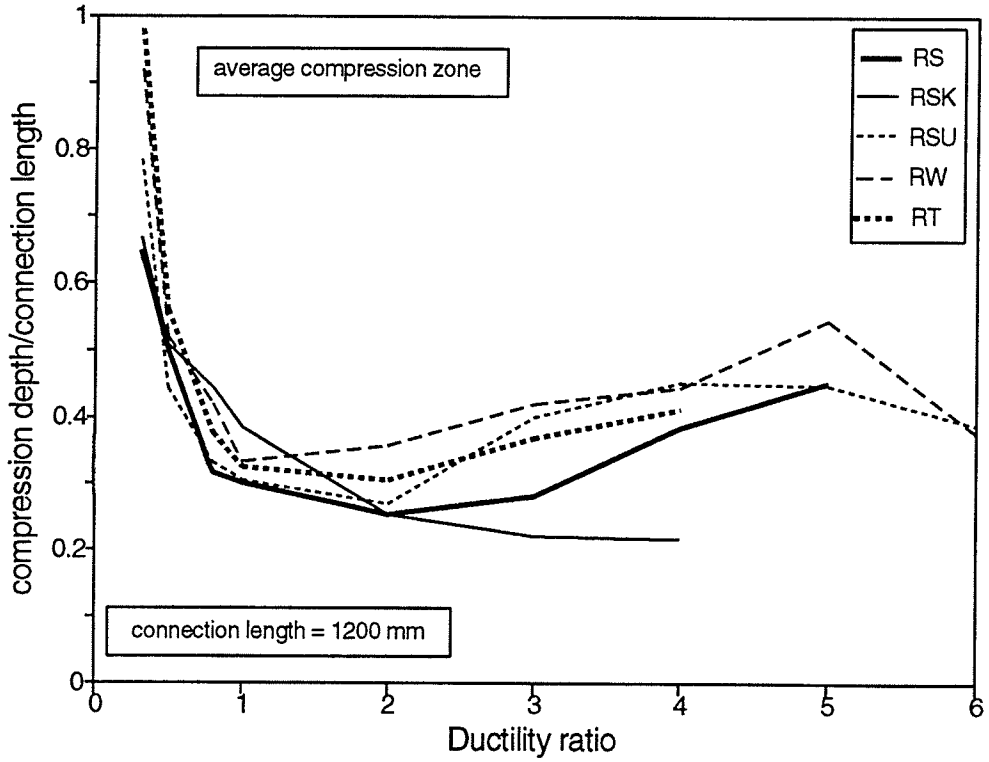

Figure 6.27(b) Comparison of normalized compression zone depth for rebar specimens

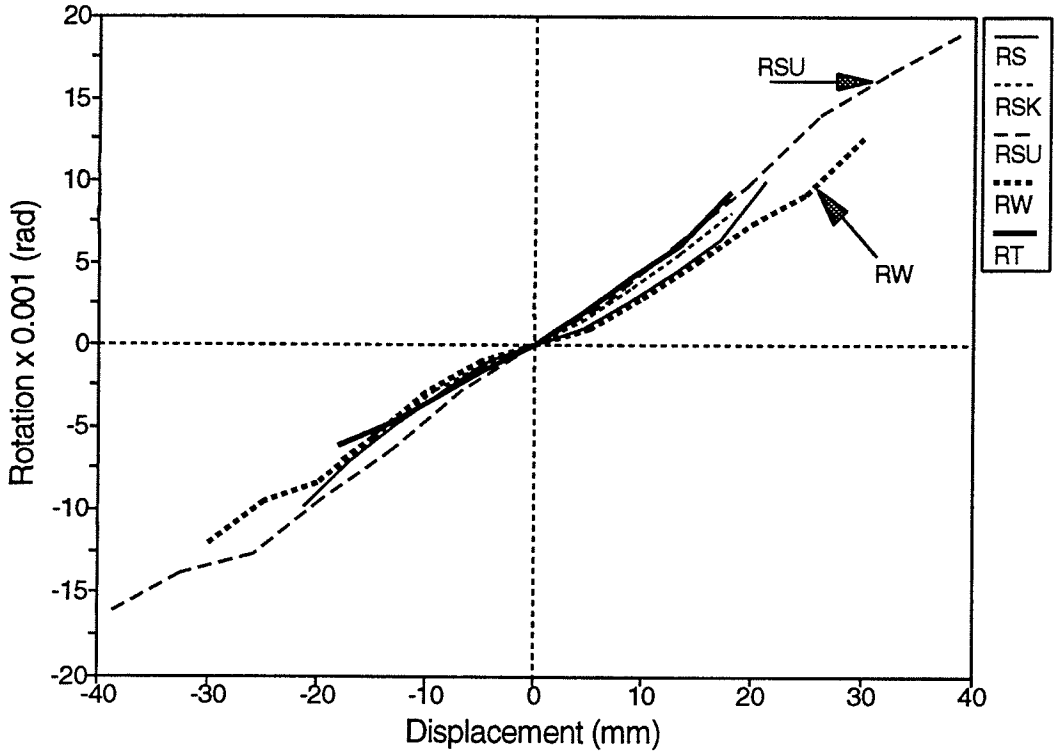

Figure 6.28 Rotation vs. displacement relationship for mild steel specimens

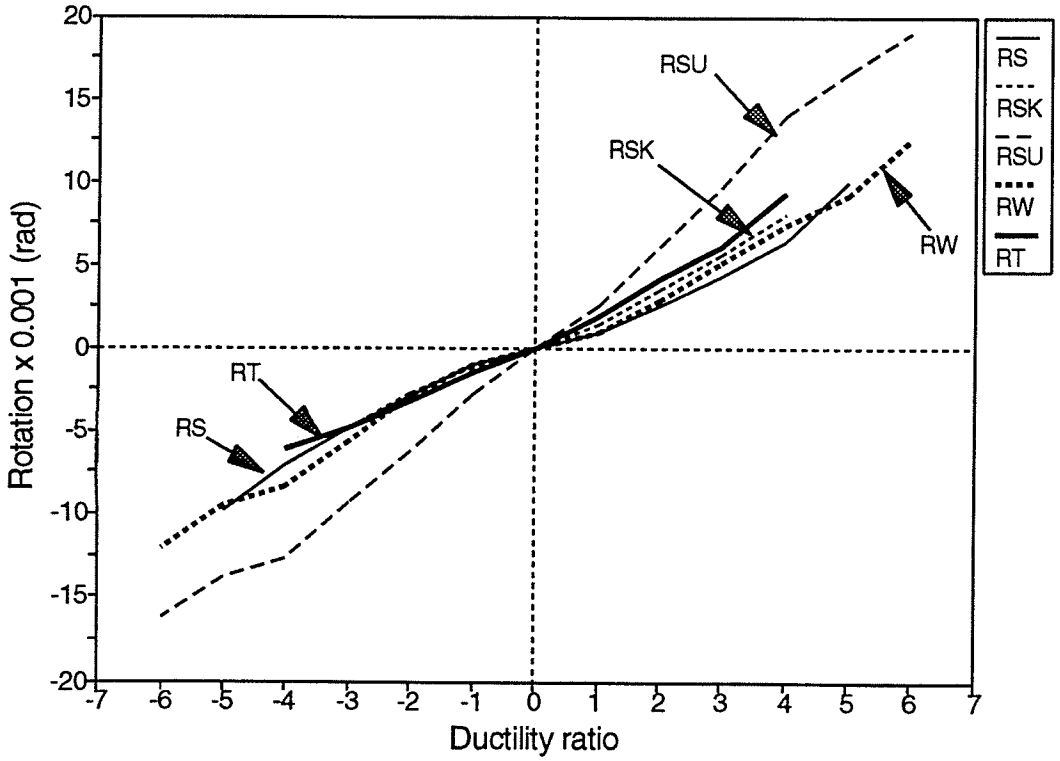

Figure 6.29 Rotation vs. ductility relationships for mild steel specimens

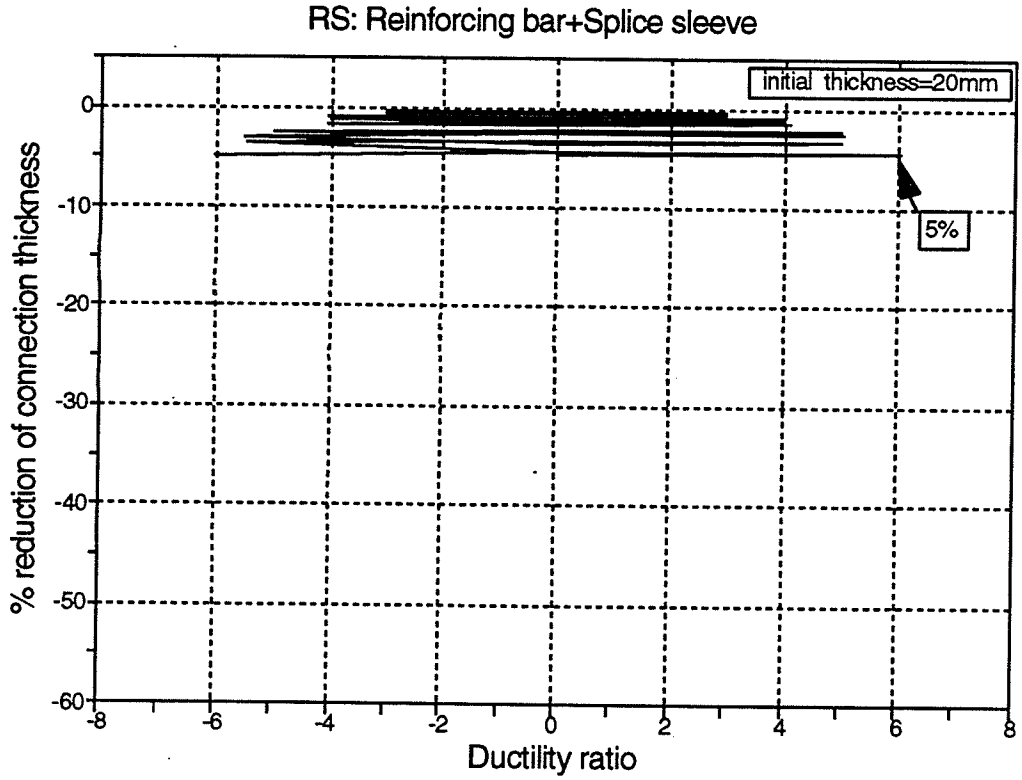

Figure 6.30 Percent reduction in connection thickness for specimen RS

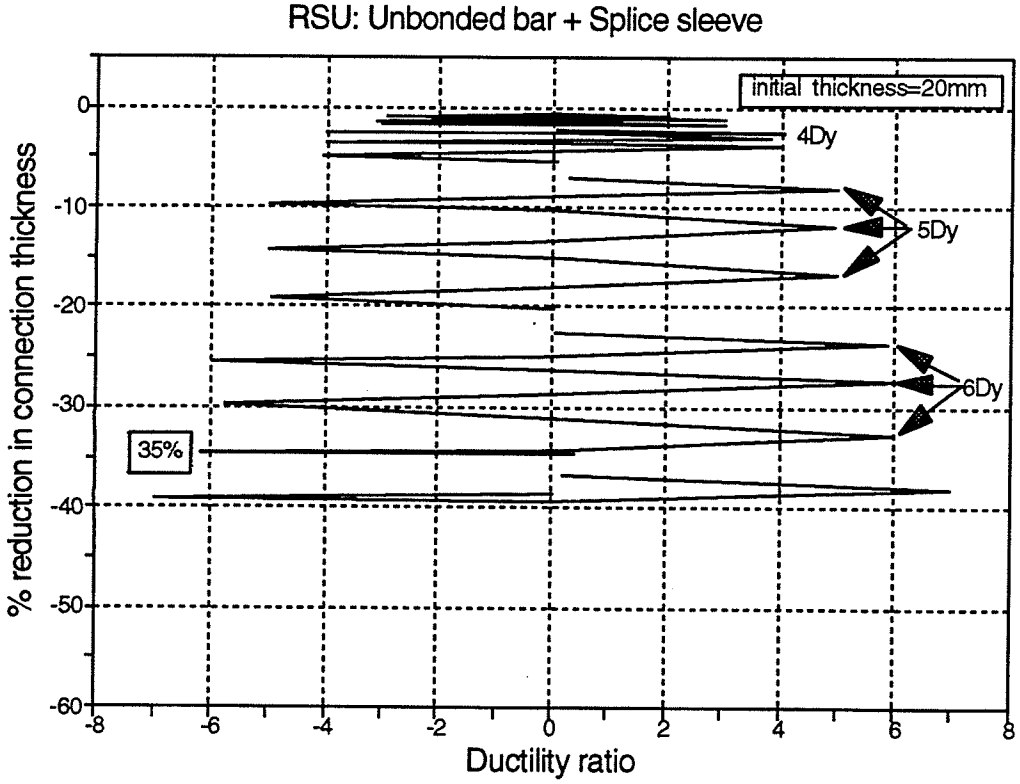

Figure 6.31 Percent reduction in connection thickness for specimen RSU

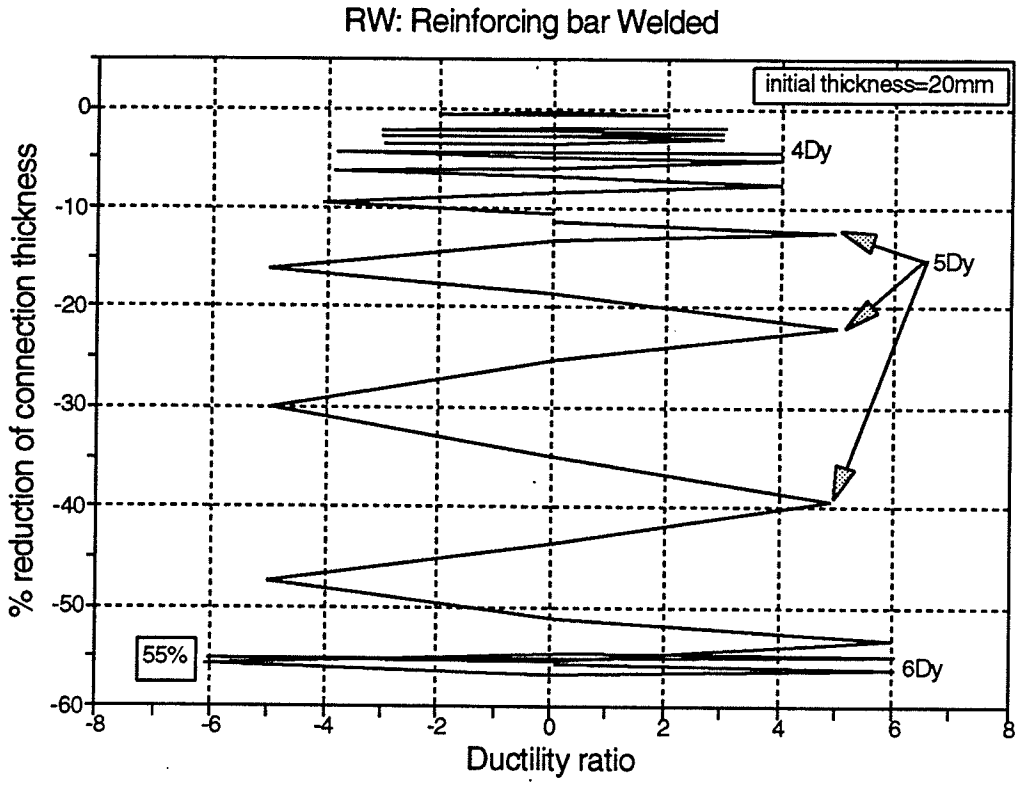

Figure 6.32 Percent reduction in connection thickness for specimen RW

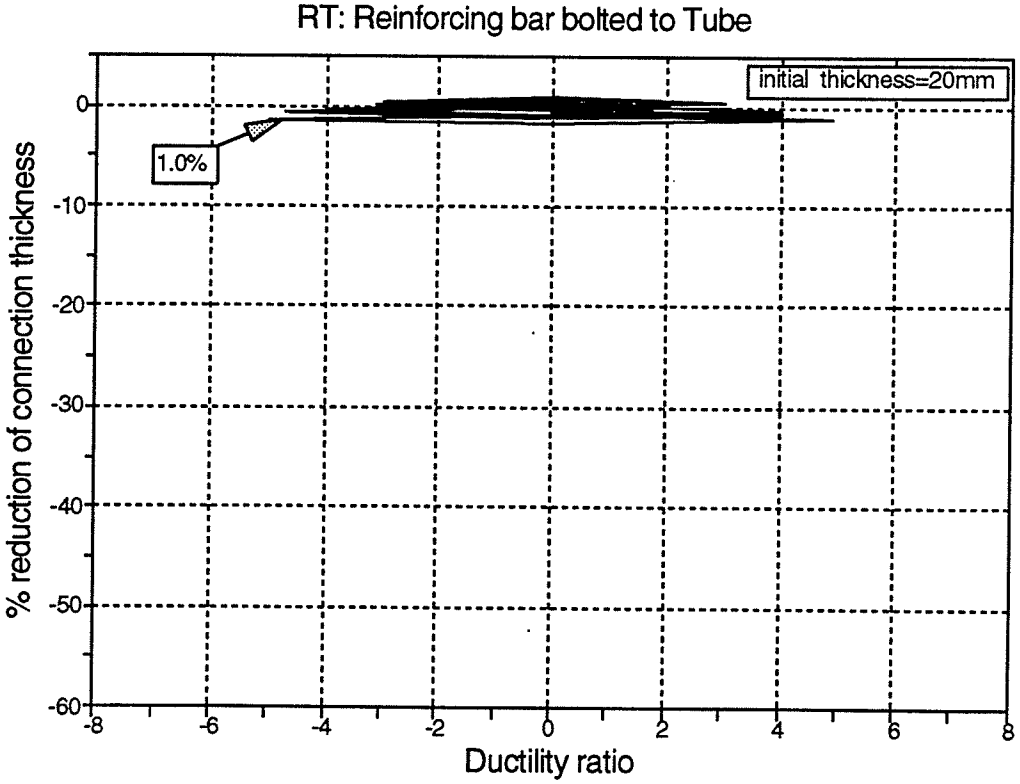

Figure 6.33 Percent reduction in connection thickness for specimen RT

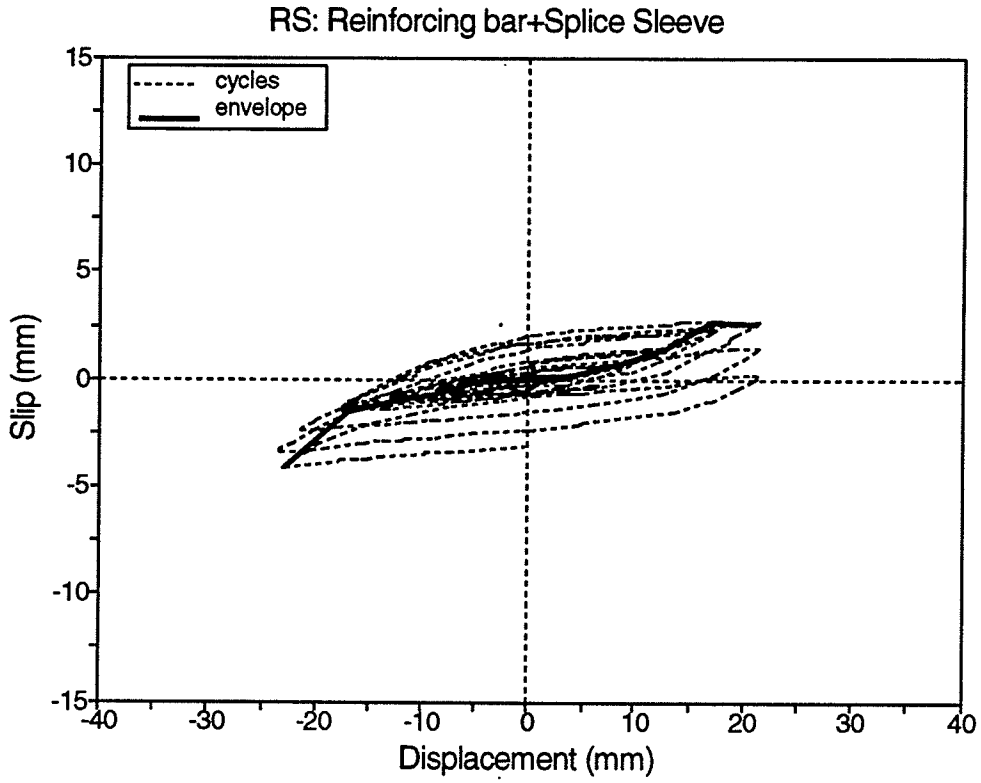

Figure 6.34 Slip-envelope for specimen RS

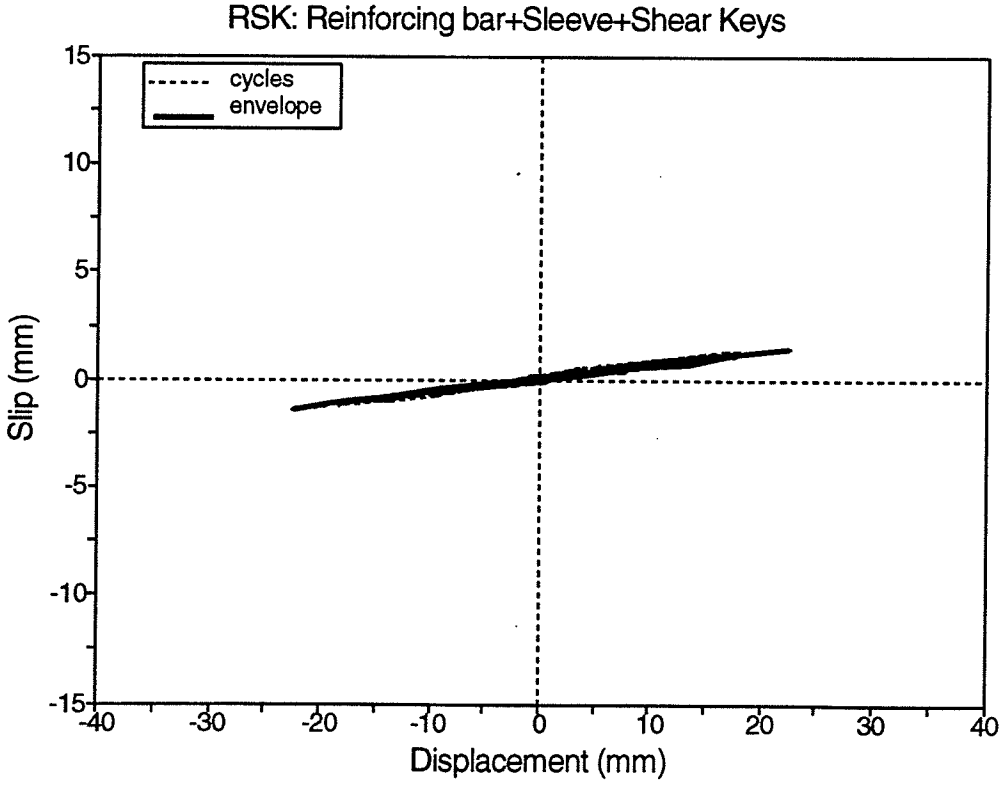

Figure 6.35 Slip-envelope for specimen RSK

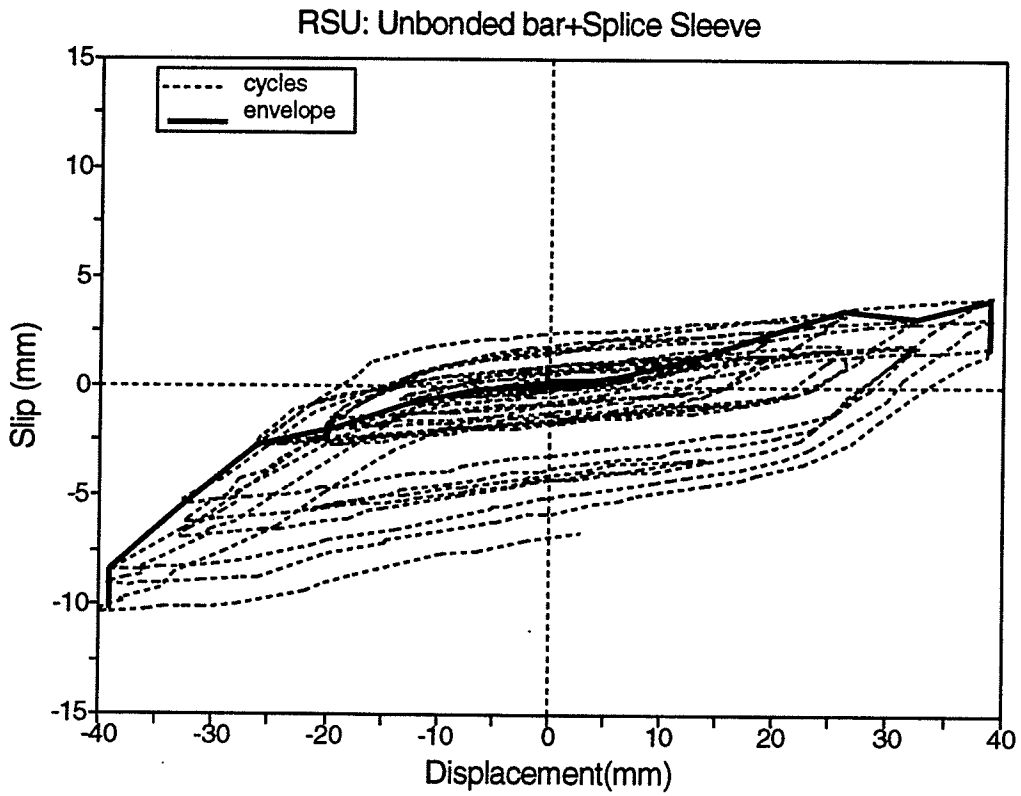

Figure 6.36 Slip-envelope for specimen RSU

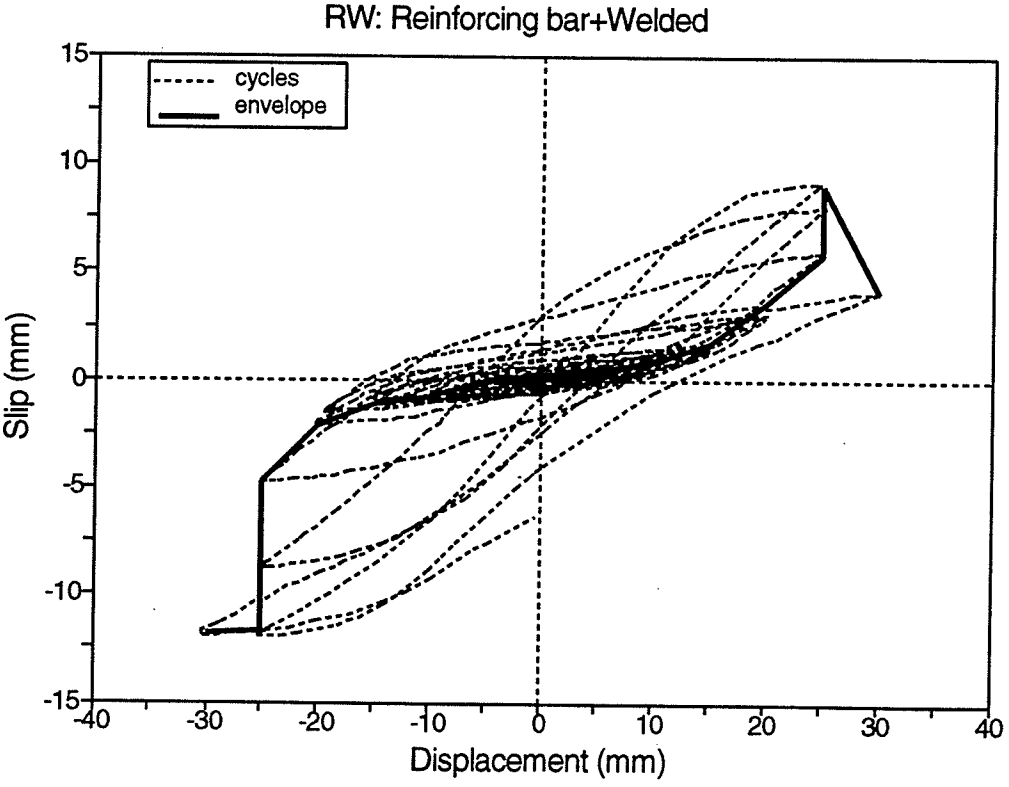

Figure 6.37 Slip-envelope for specimen RW

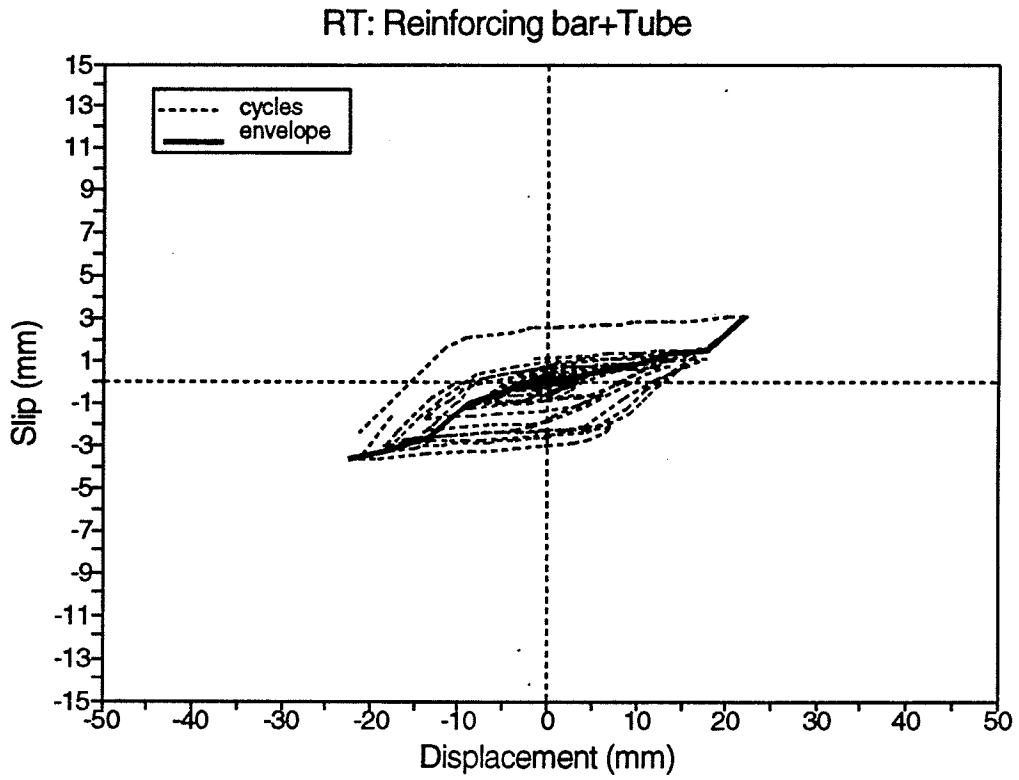

Figure 6.38 Slip-envelope for specimen RT

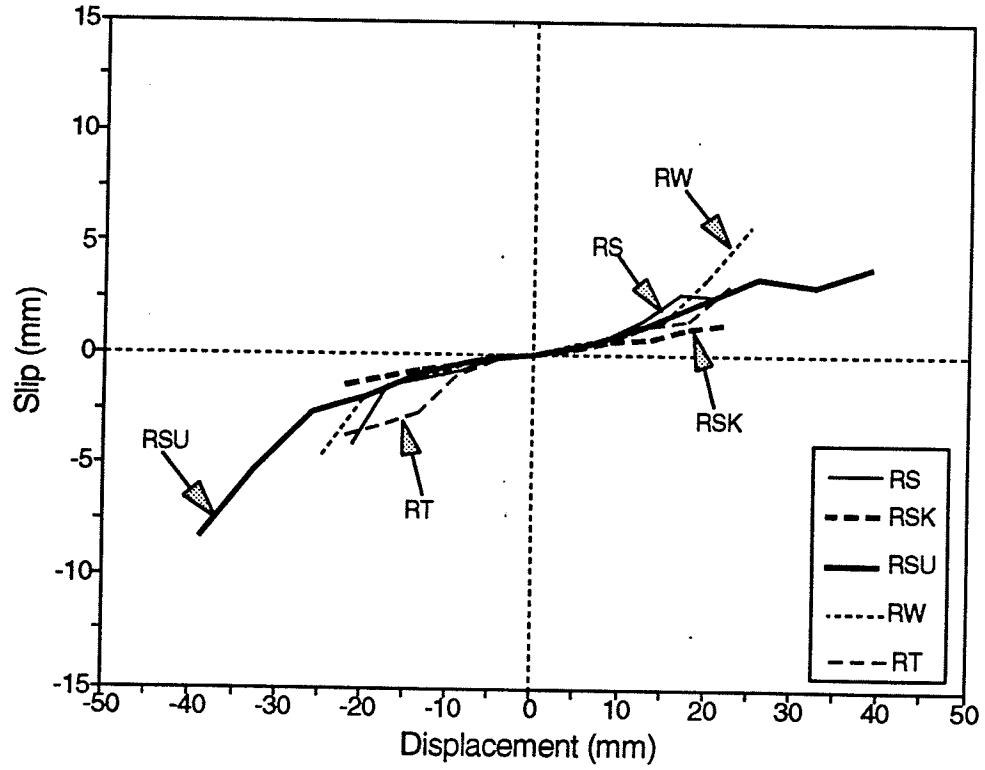

Figure 6.39 Comparison of slip envelopes for the cyclic reinforcing bar specimens

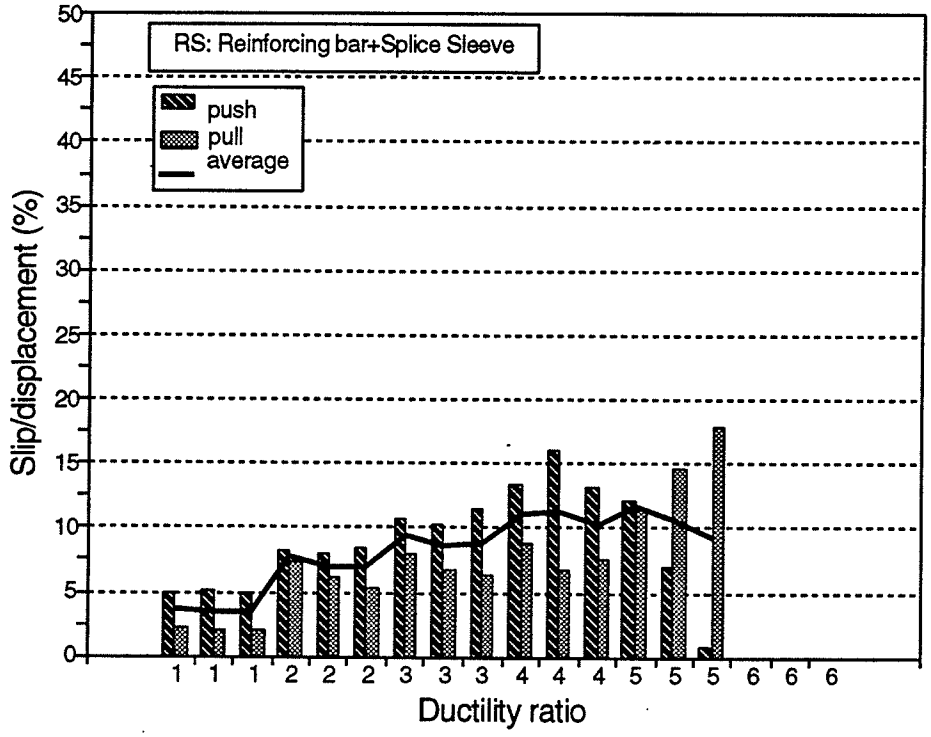

Figure 6.40 Percent slip/displacement per cycle versus ductility for specimen RS

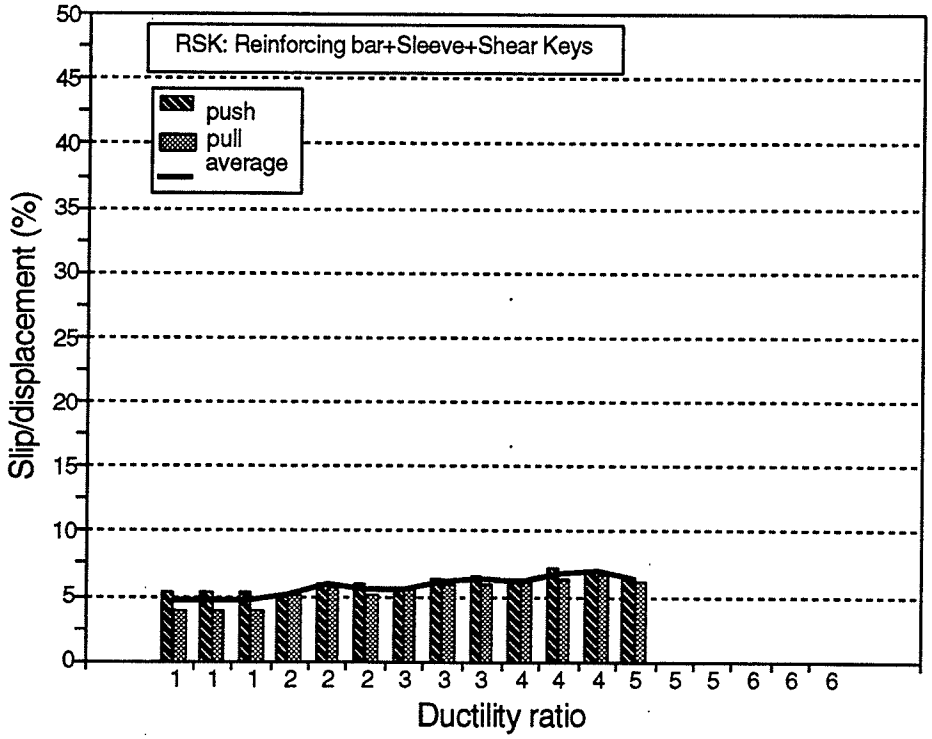

Figure 6.41 Percent slip/displacement per cycle versus ductility for specimen RSK

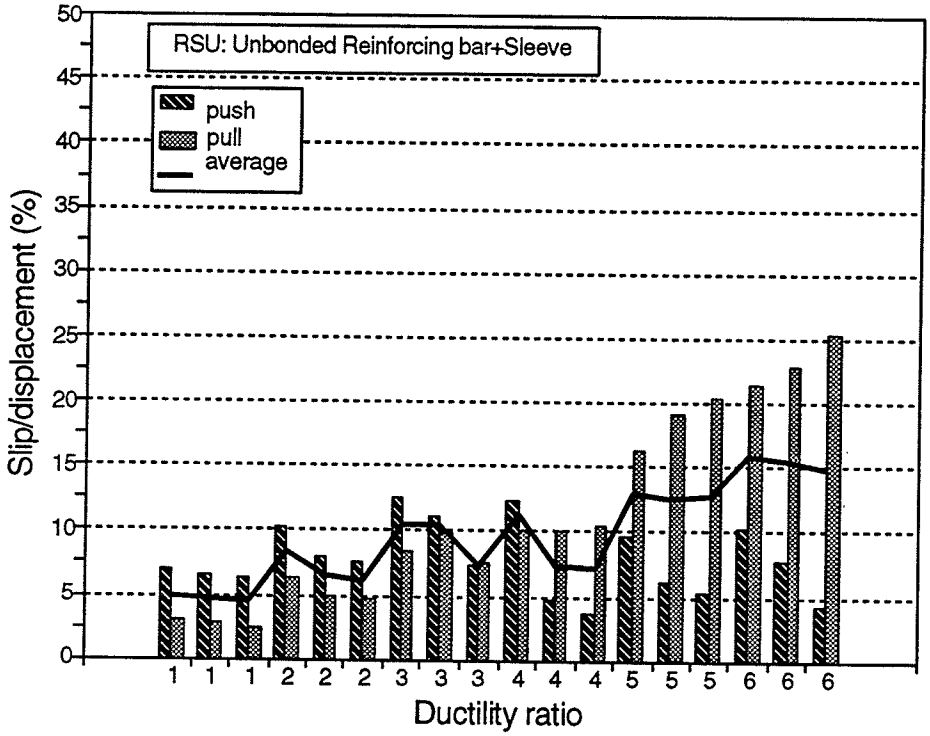

Figure 6.42 Percent slip/displacement per cycle versus ductility for specimen RSU

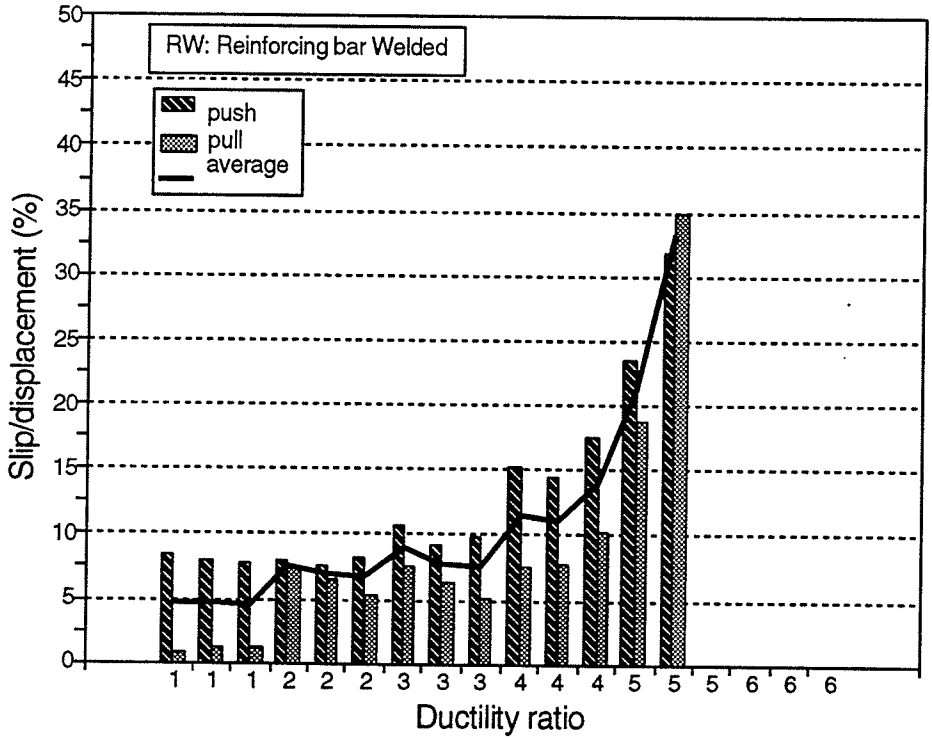

Figure 6.43 Percent slip/displacement per cycle versus ductility for specimen RW

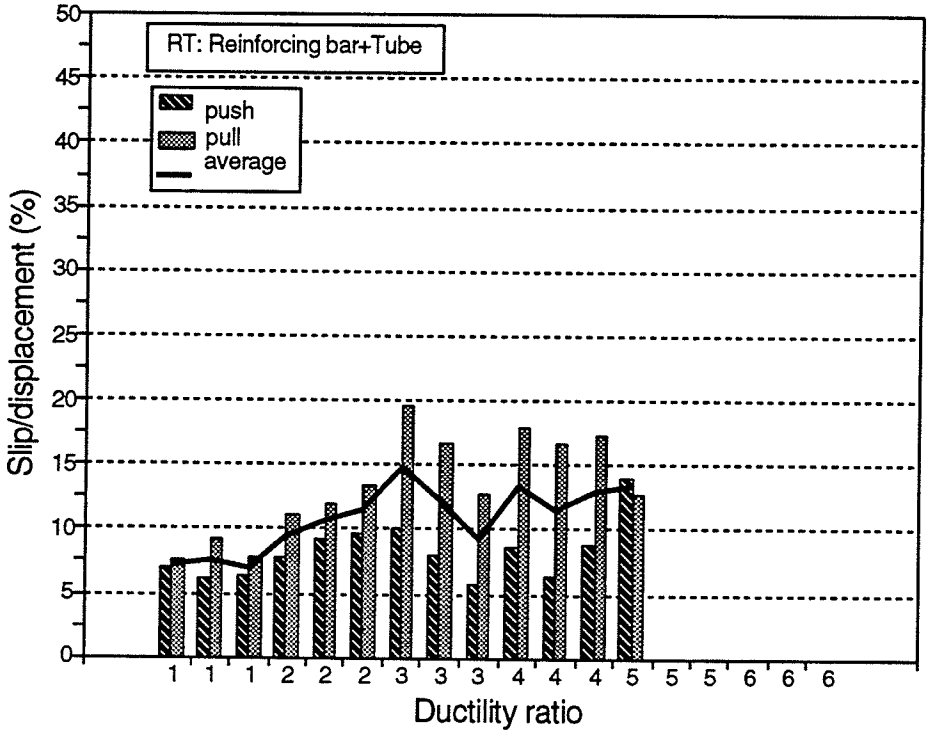

Figure 6.44 Percent slip/displacement per cycle versus ductility for specimen RT

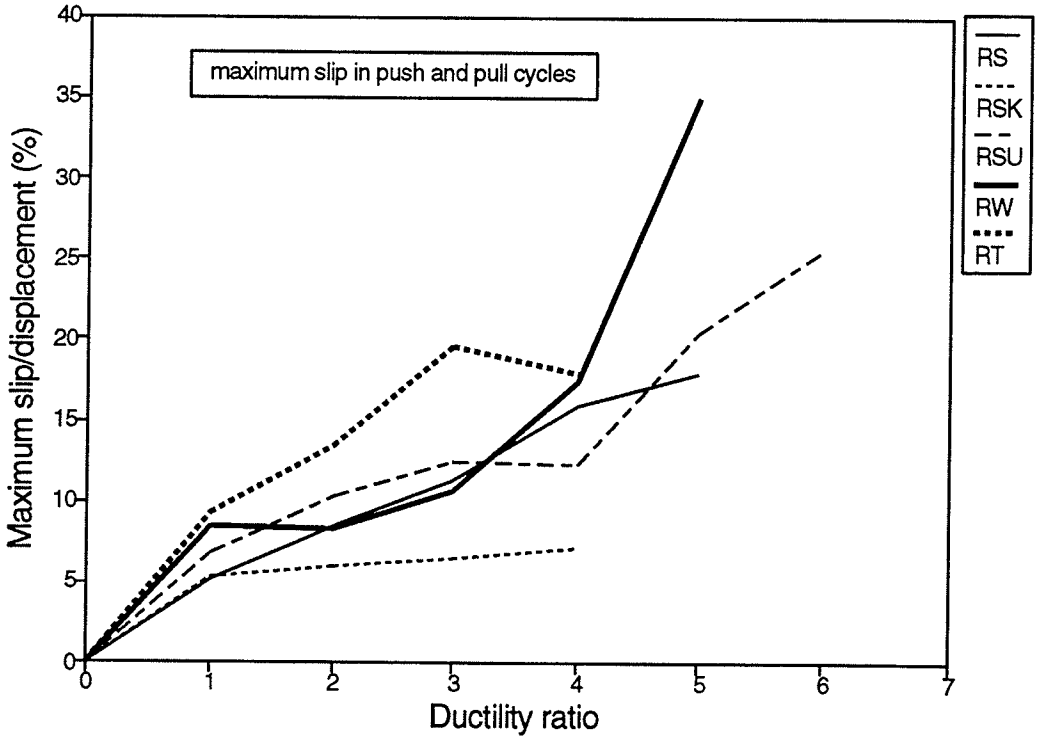

Figure 6.45 Comparison of percent slip/displacement for reinforcing bar specimens

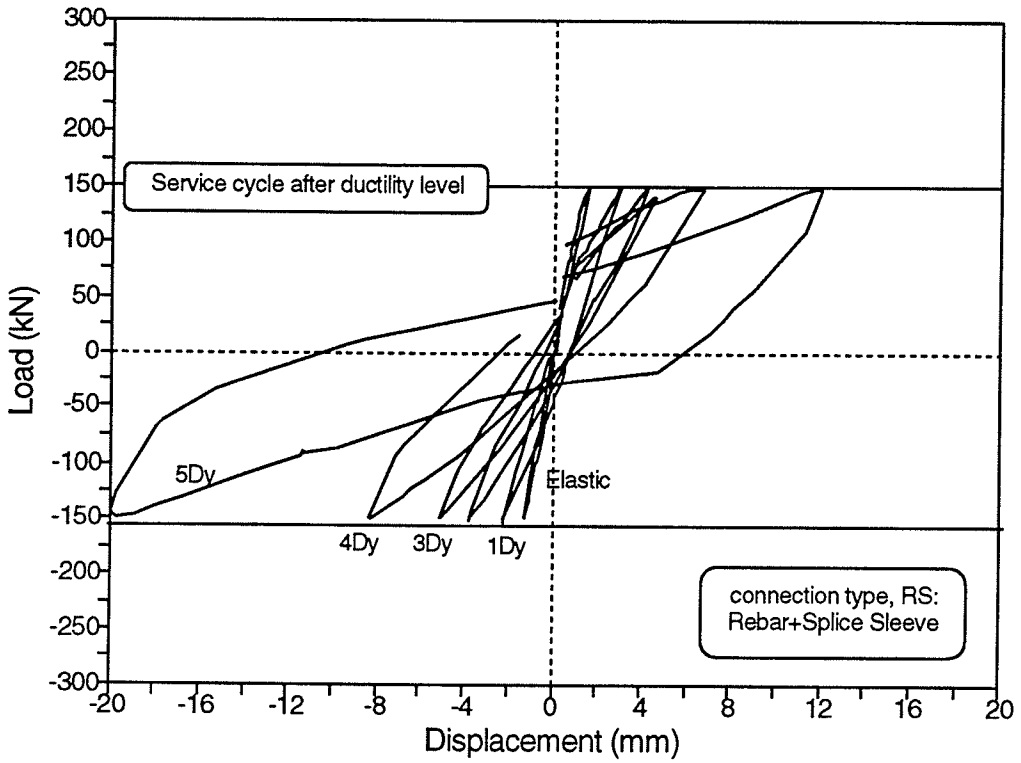

Figure 6.46 Service load-displacement cycles for specimen RS

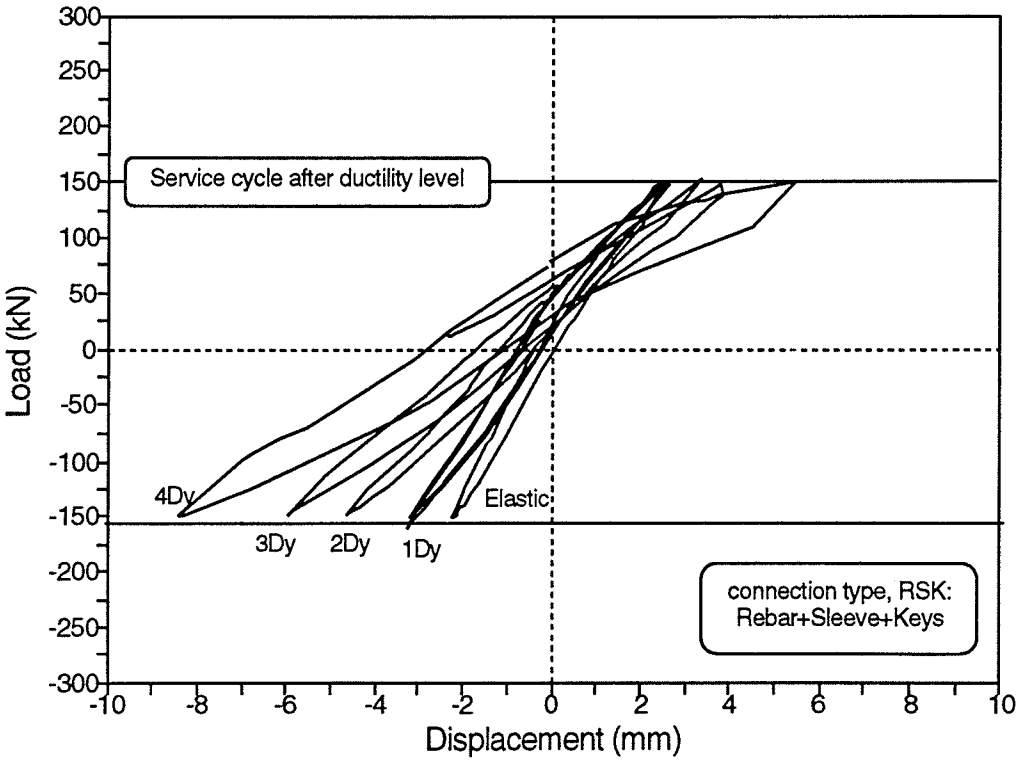

Figure 6.47 Service load-displacement cycles for specimen RSK

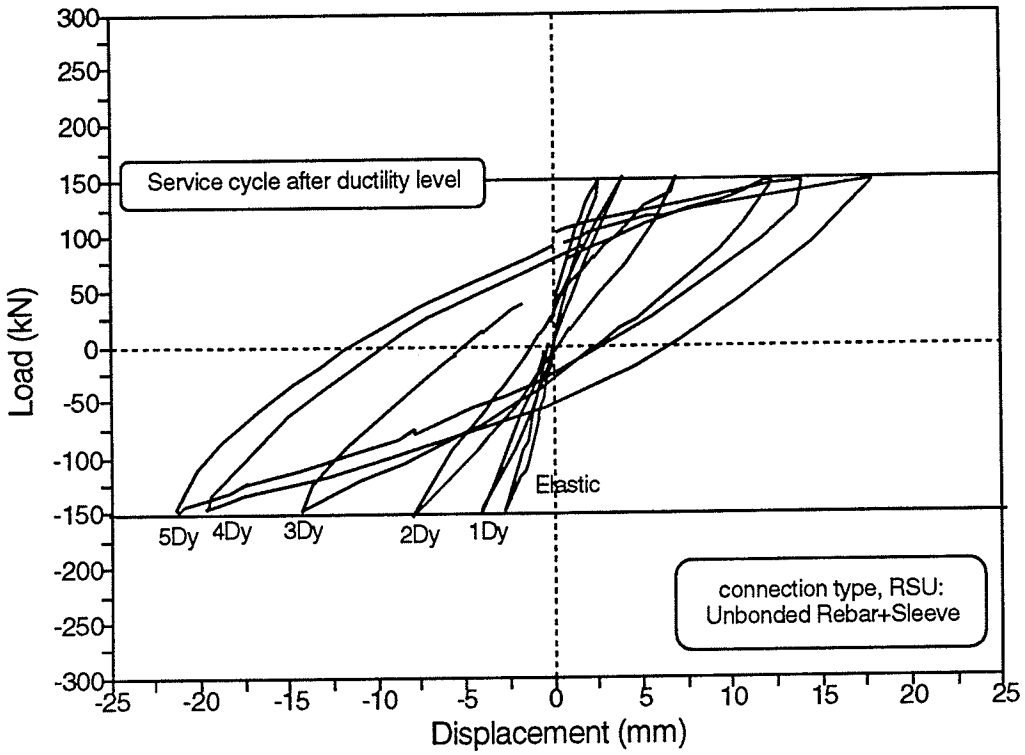

Figure 6.48 Service load-displacement cycles for specimen RSU

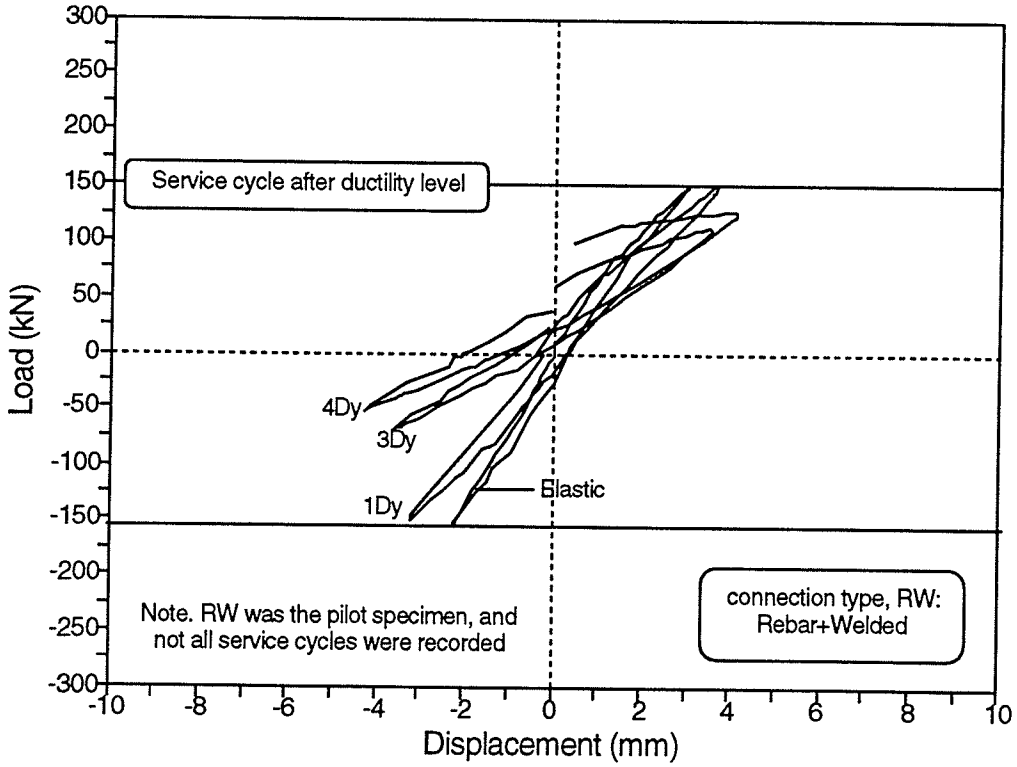

Figure 6.49 Service load-displacement cycles for specimen RW

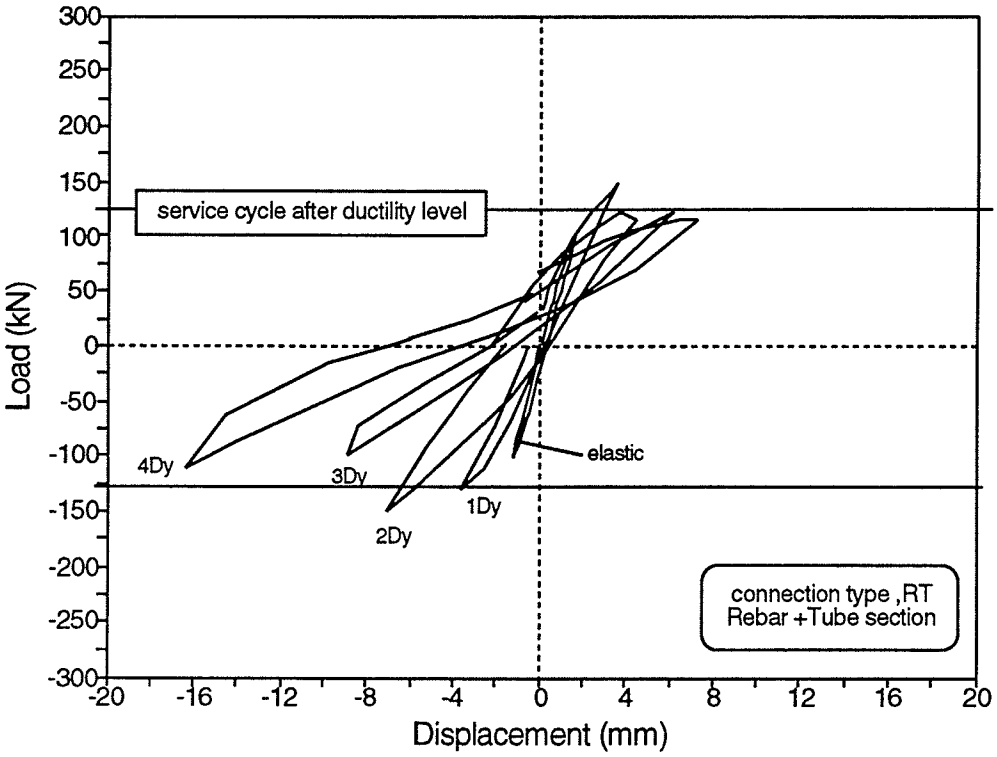

Figure 6.50 Service load-displacement cycles for specimen RT

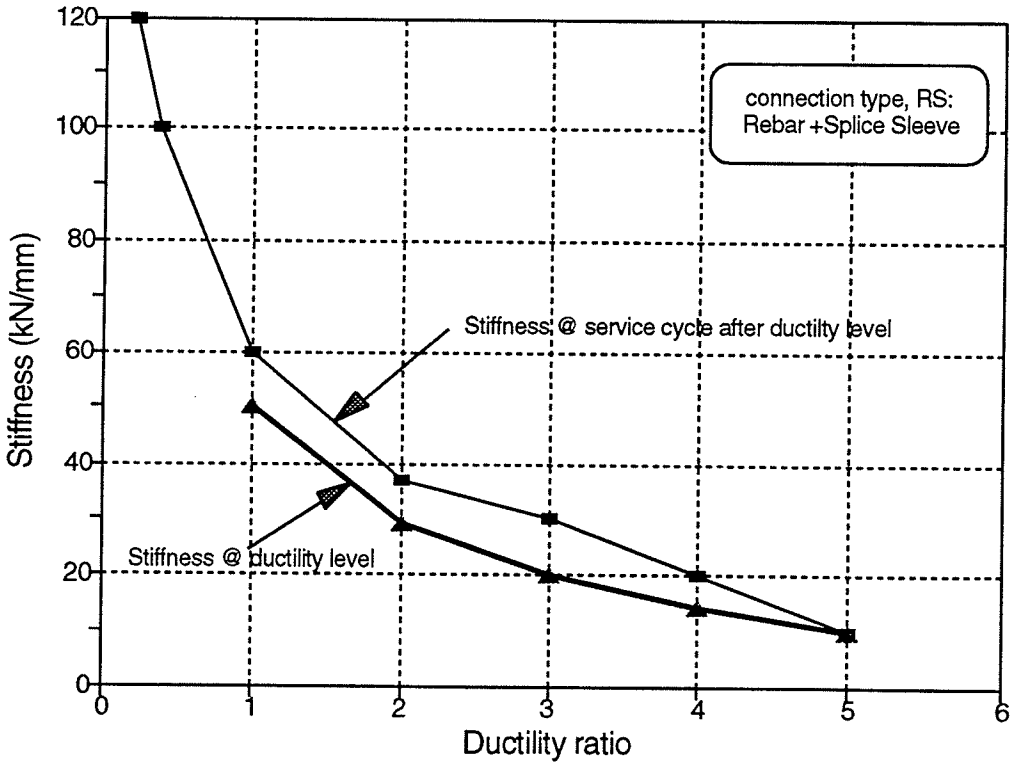

Figure 6.51 Stiffness degradation versus ductility for specimen RS

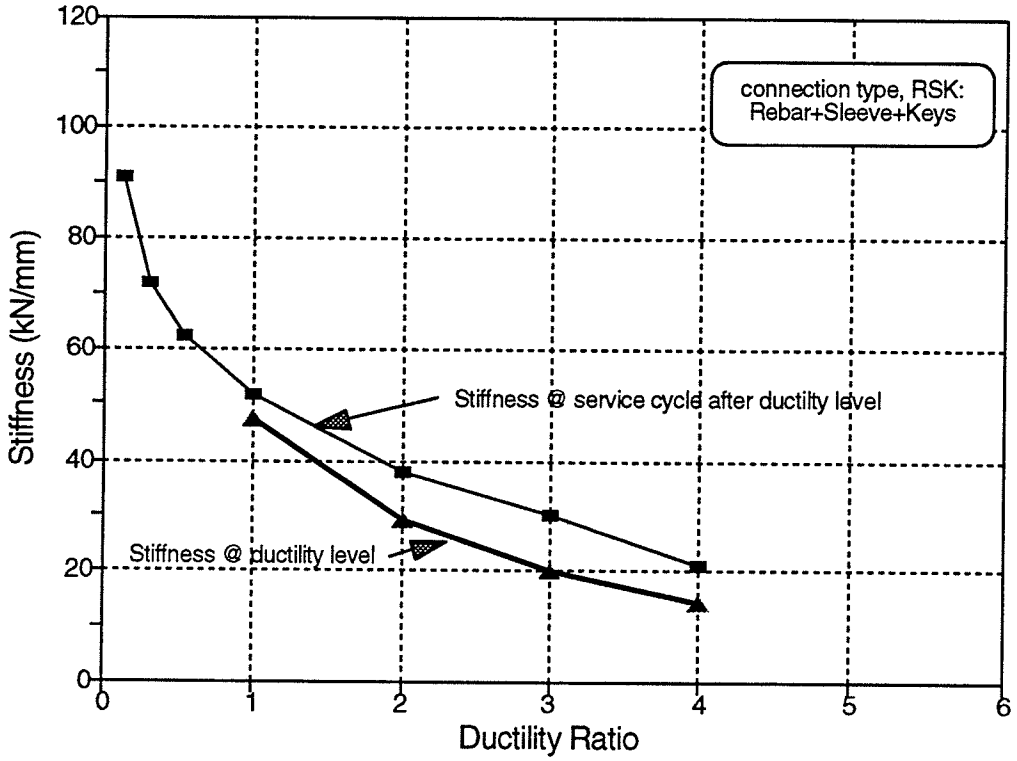

Figure 6.52 Stiffness degradation versus ductility for specimen RSK

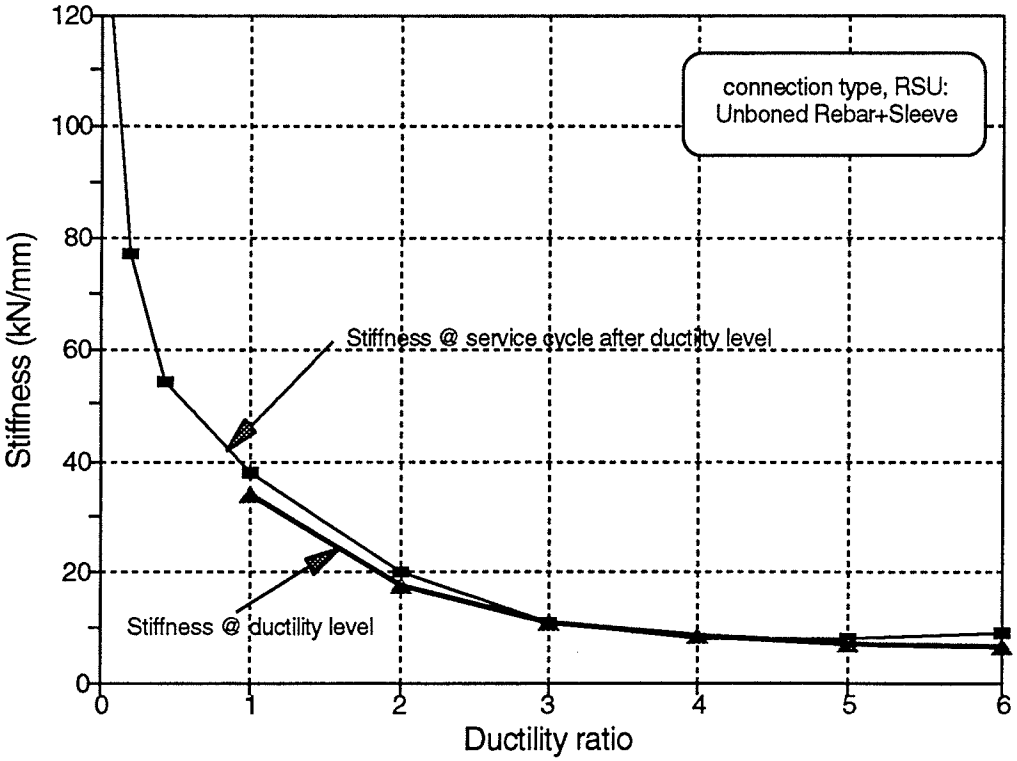

Figure 6.53 Stiffness degradation versus ductility for specimen RSU

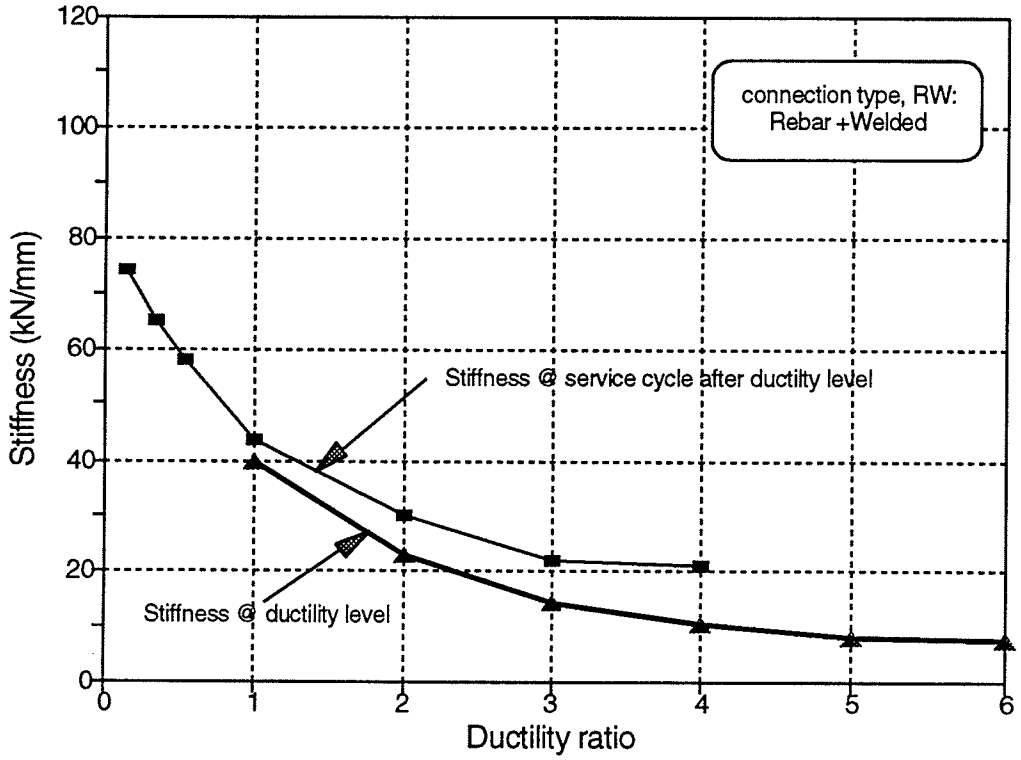

Figure 6.54 Stiffness degradation versus ductility for specimen RW

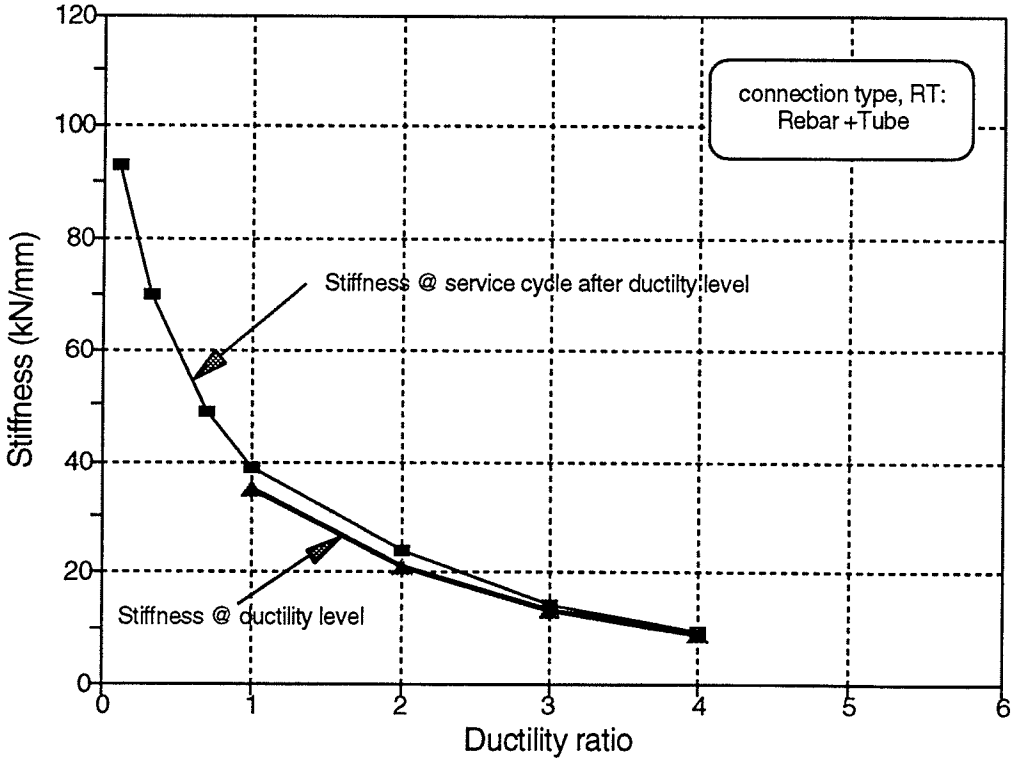

Figure 6.55 Stiffness degradation versus ductility for specimen RT

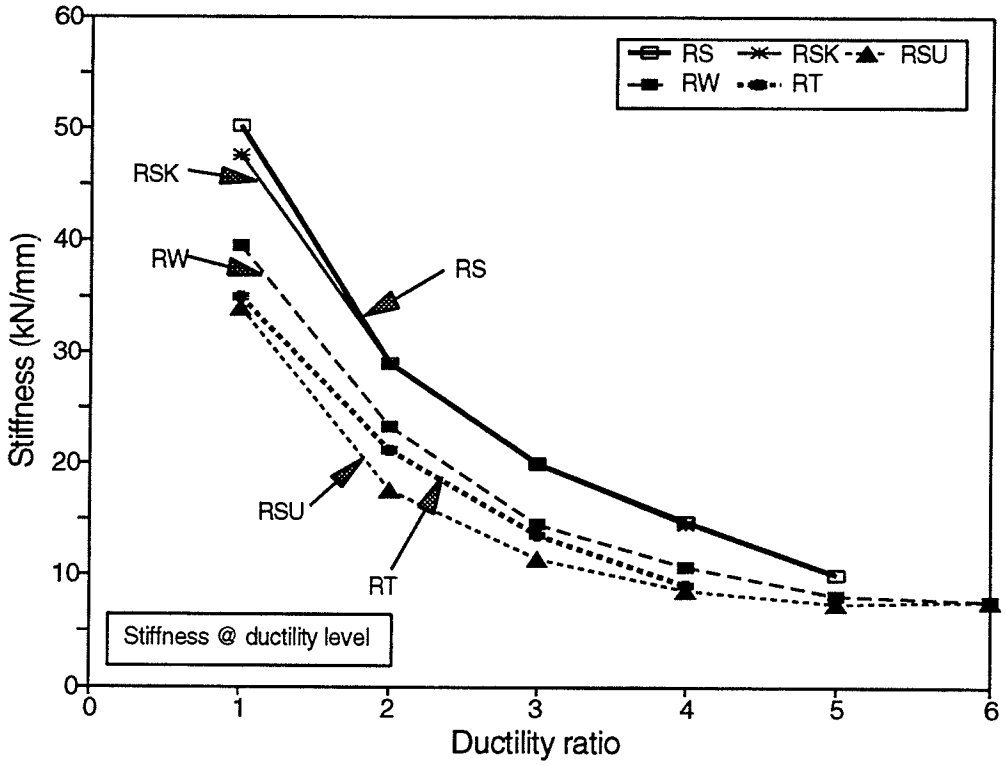

Figure 6.56(a) Comparison of stiffness degradation for specimen with mild steel bars

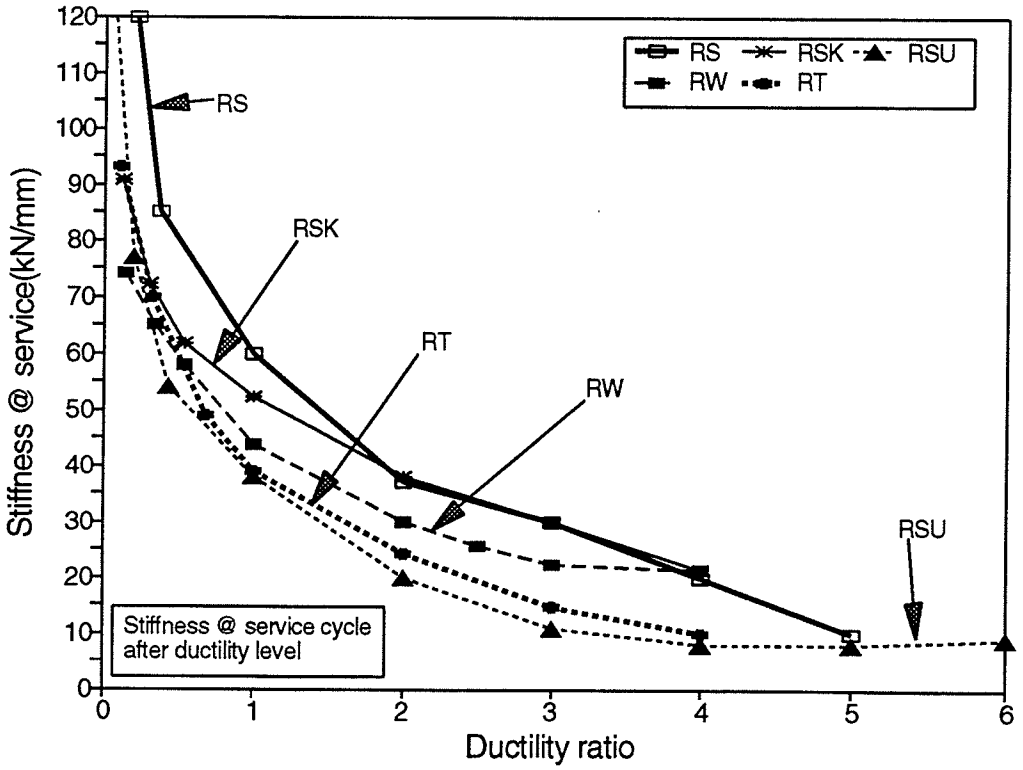

Figure 6.56(b) Comparison of service stiffness degradation: specimen with mild steel bars

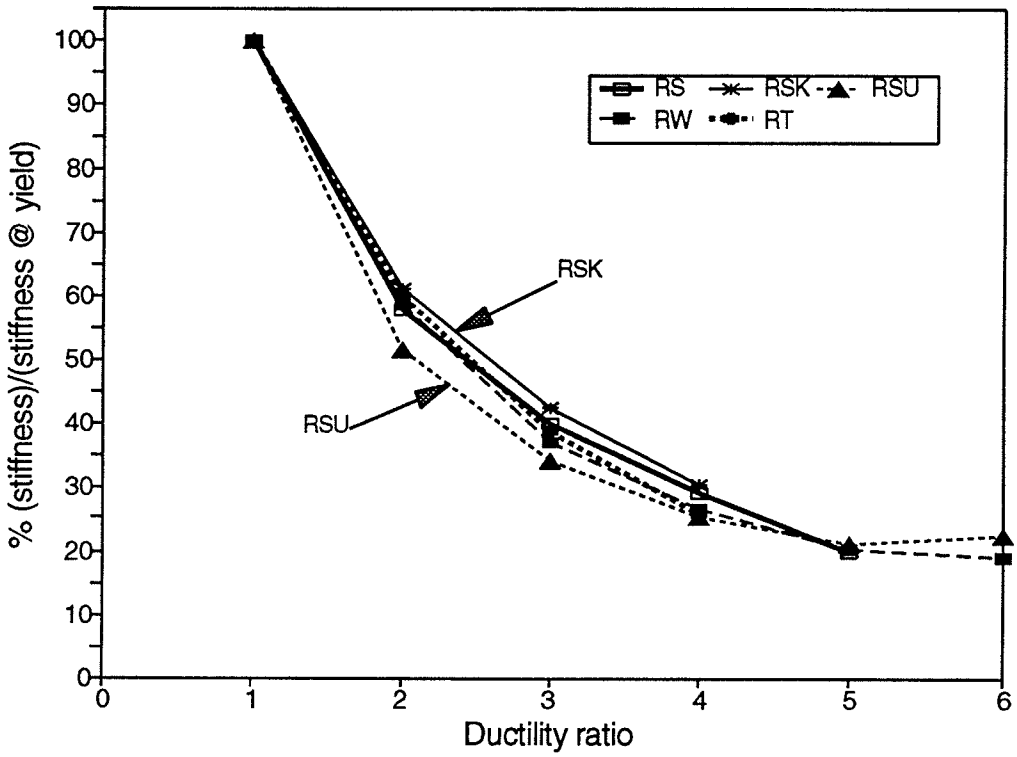

Figure 6.57(a) Comparison of % stiffness degradation for specimen with mild steel bars

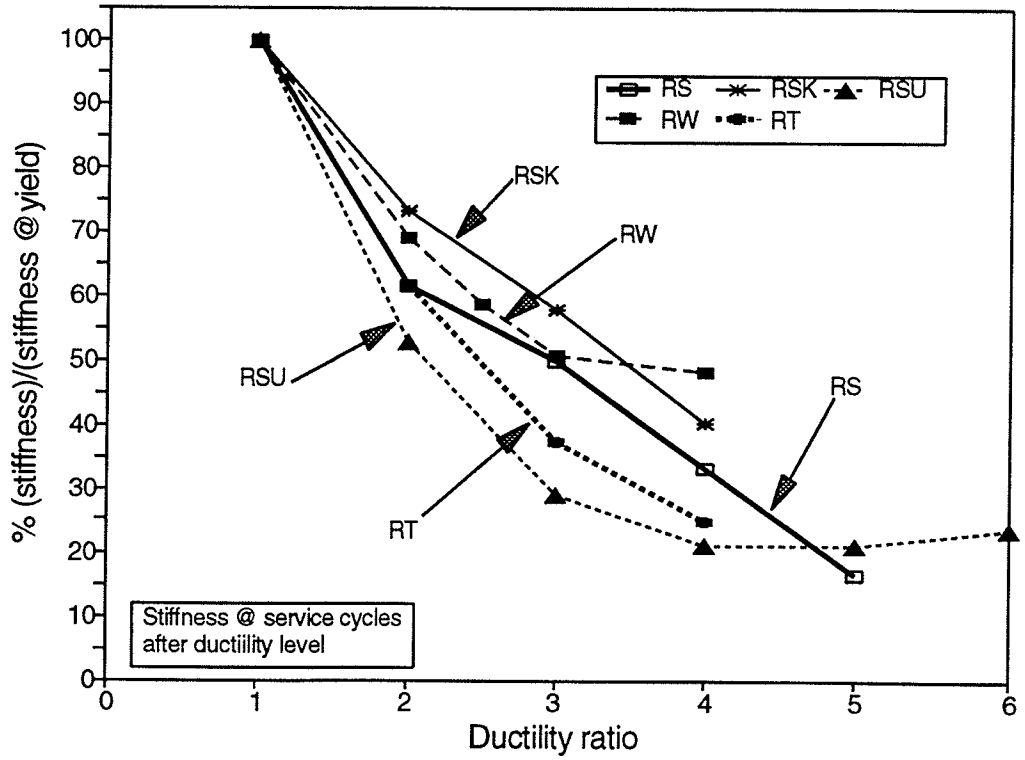

Figure 6.57(b) Comparison of % service stiffness degradation: mild steel specimen

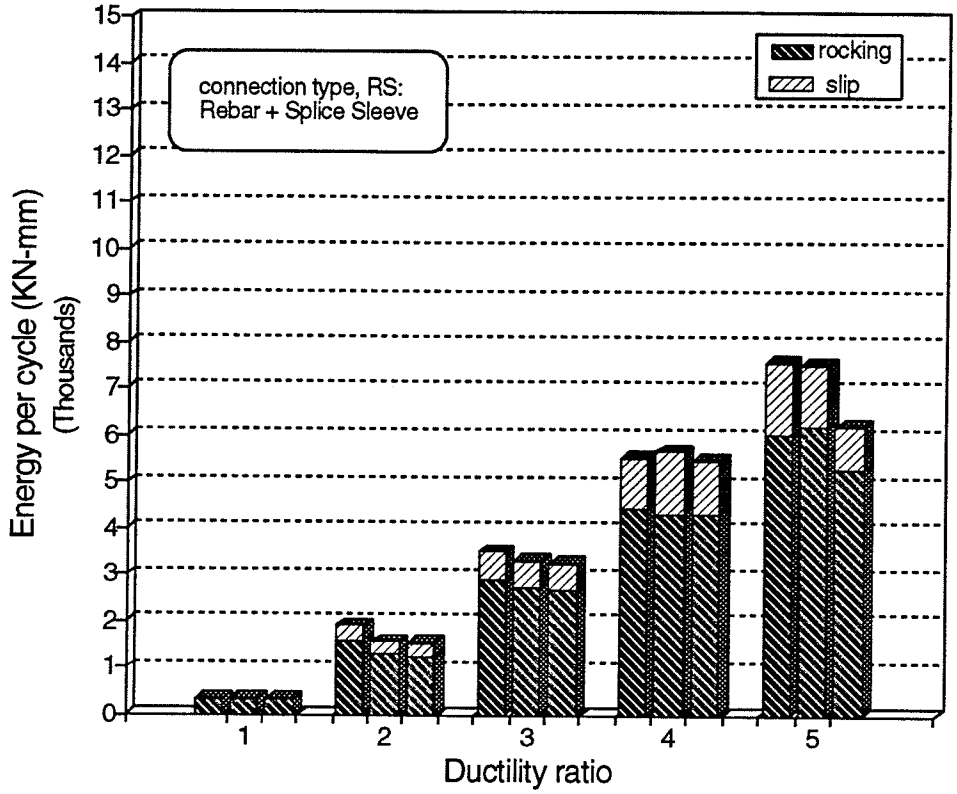

Figure 6.58(a) Per cycle energy dissipated by specimen RS

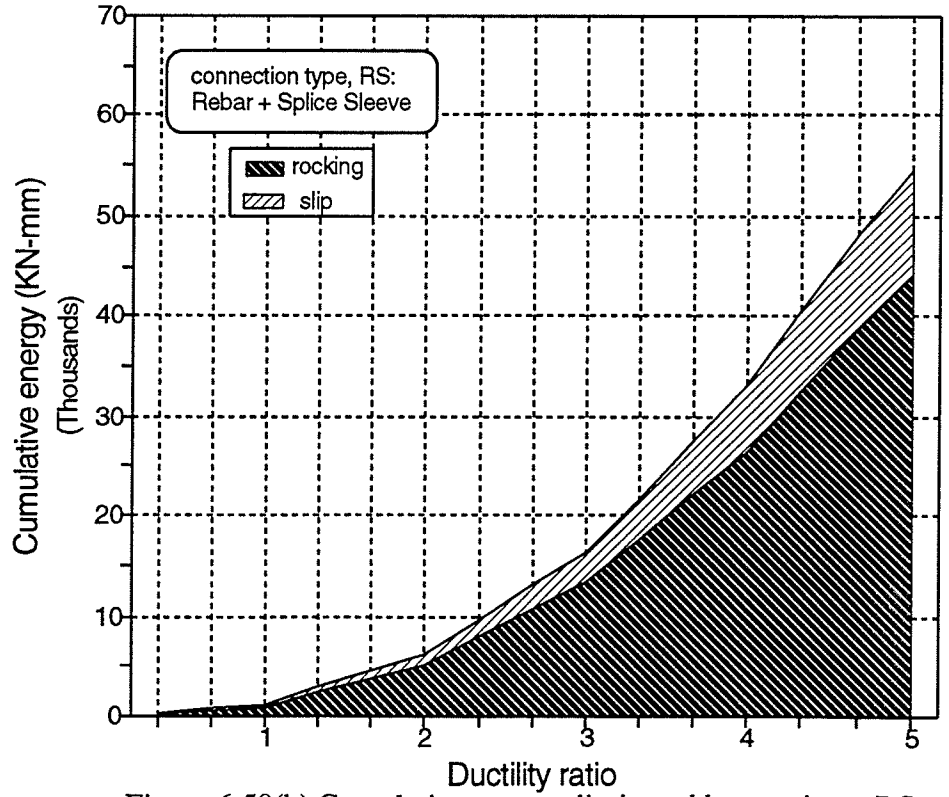

Figure 6.58(b) Cumulative energy dissipated by specimen RS

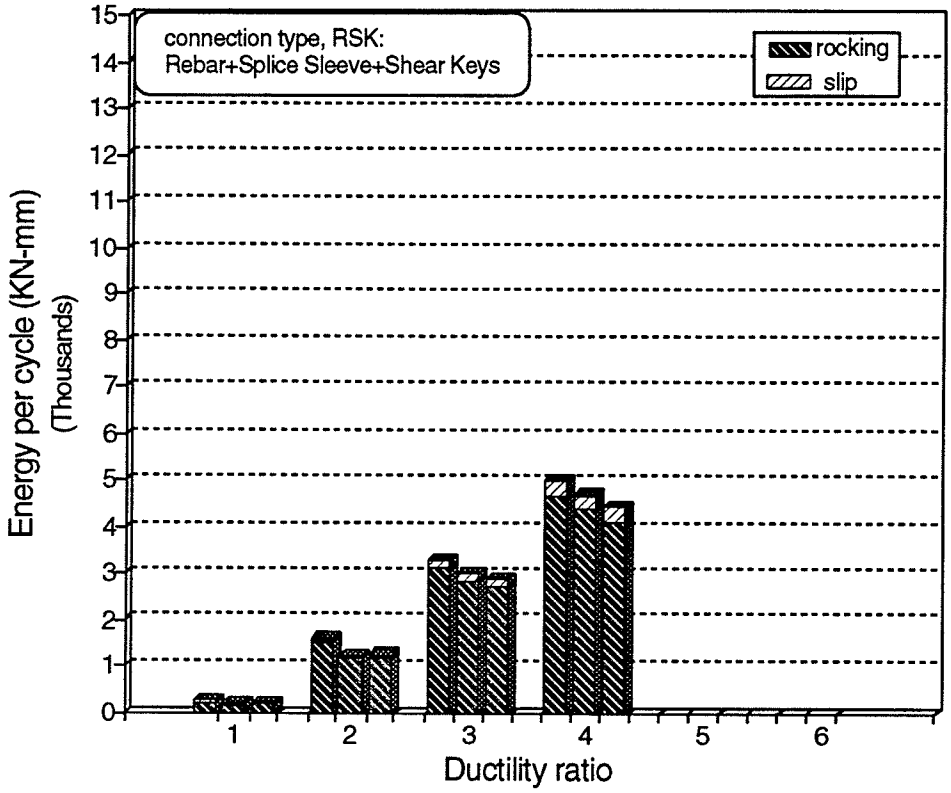

Figure 6.59(a) Per cycle energy dissipated by specimen RSK

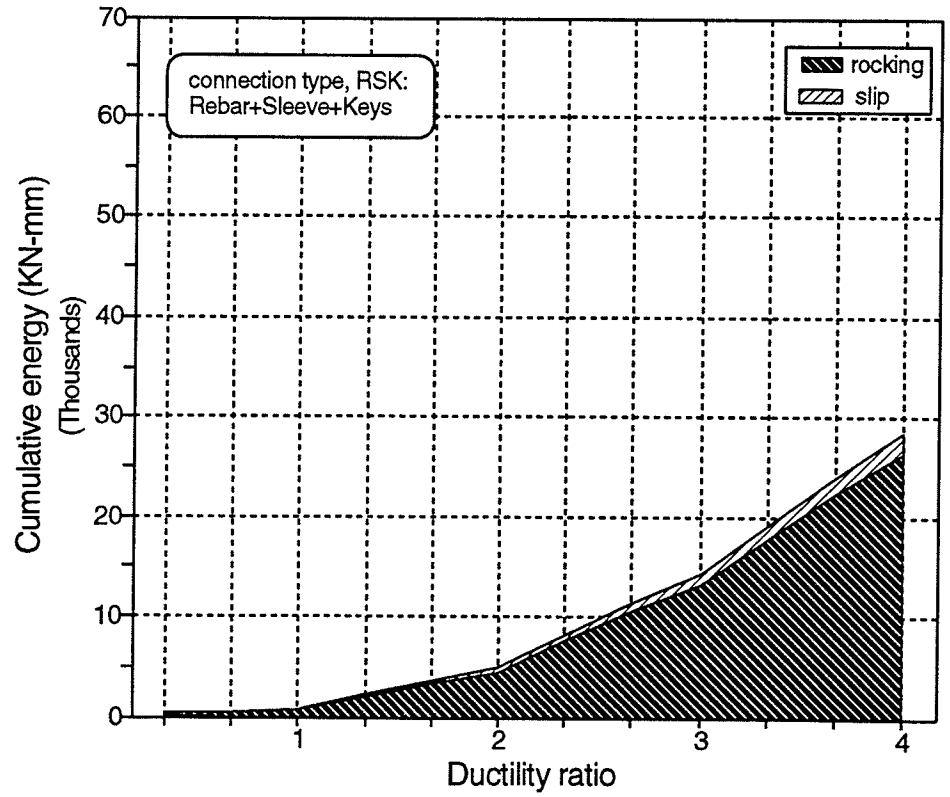

Figure 6.59(b) Cumulative energy dissipated by specimen RSK

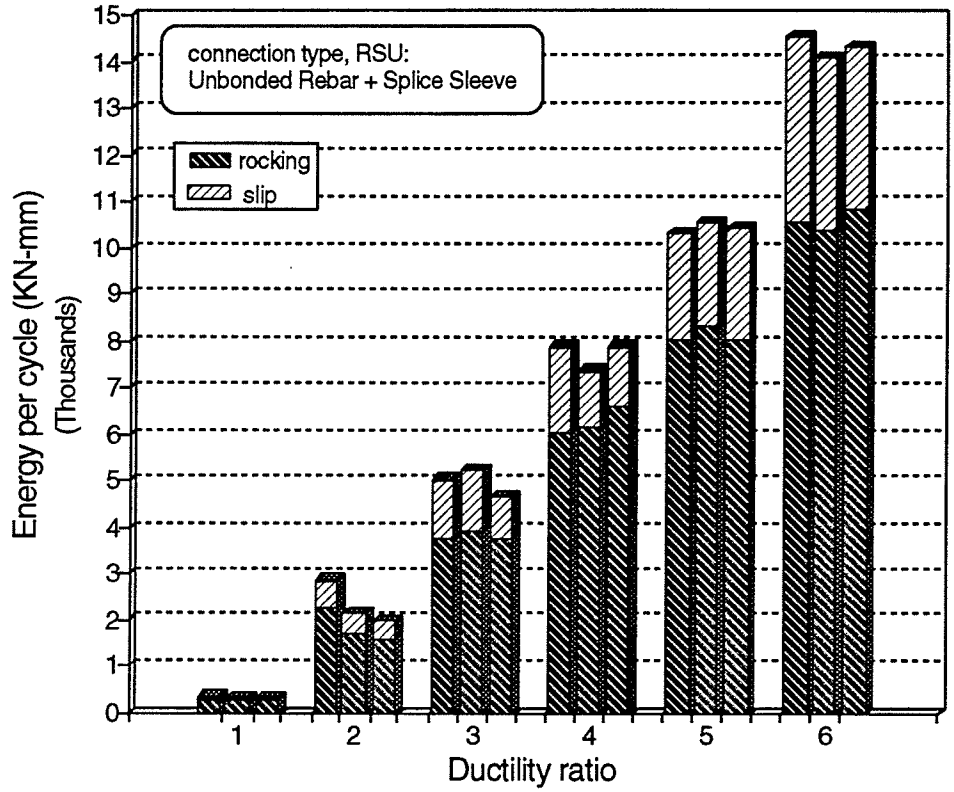

Figure 6.60(a) Per cycle energy dissipated by specimen RSU

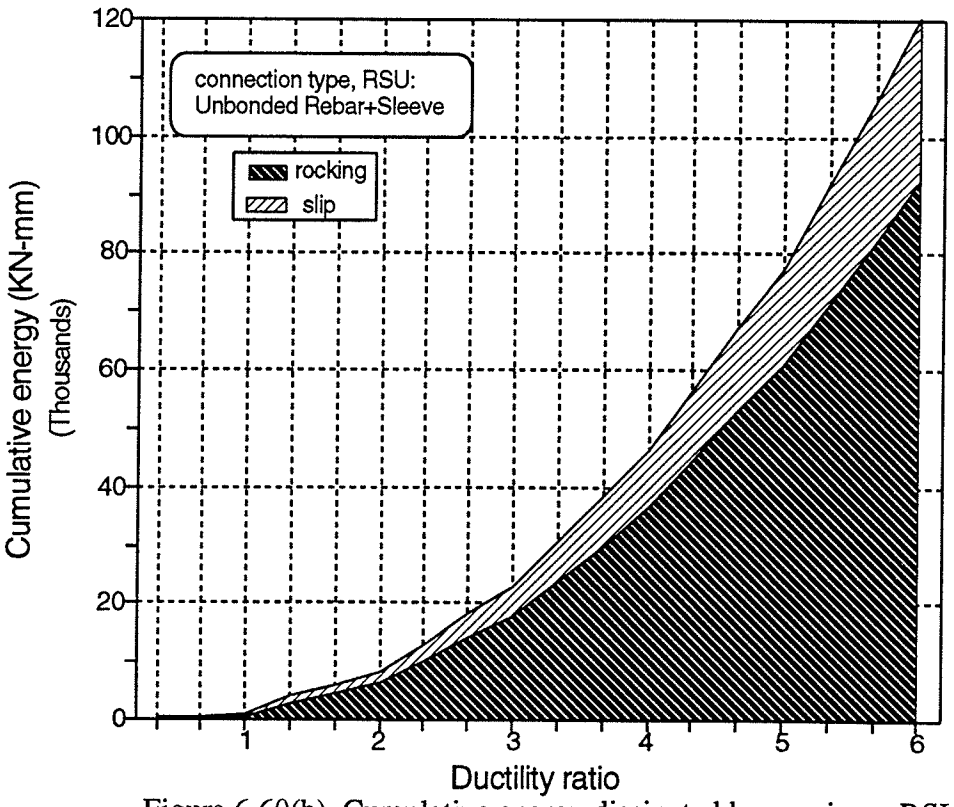

Figure 6.60(b) Cumulative energy dissipated by specimen RSU

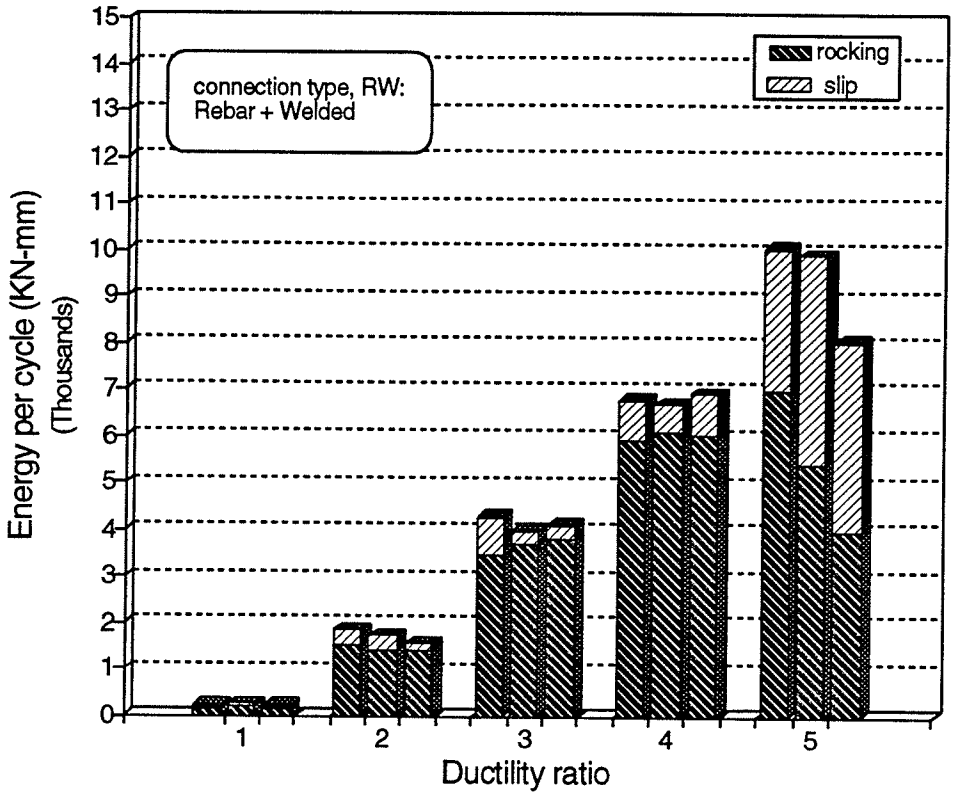

Figure 6.61(a) Per cycle energy dissipated by specimen RW

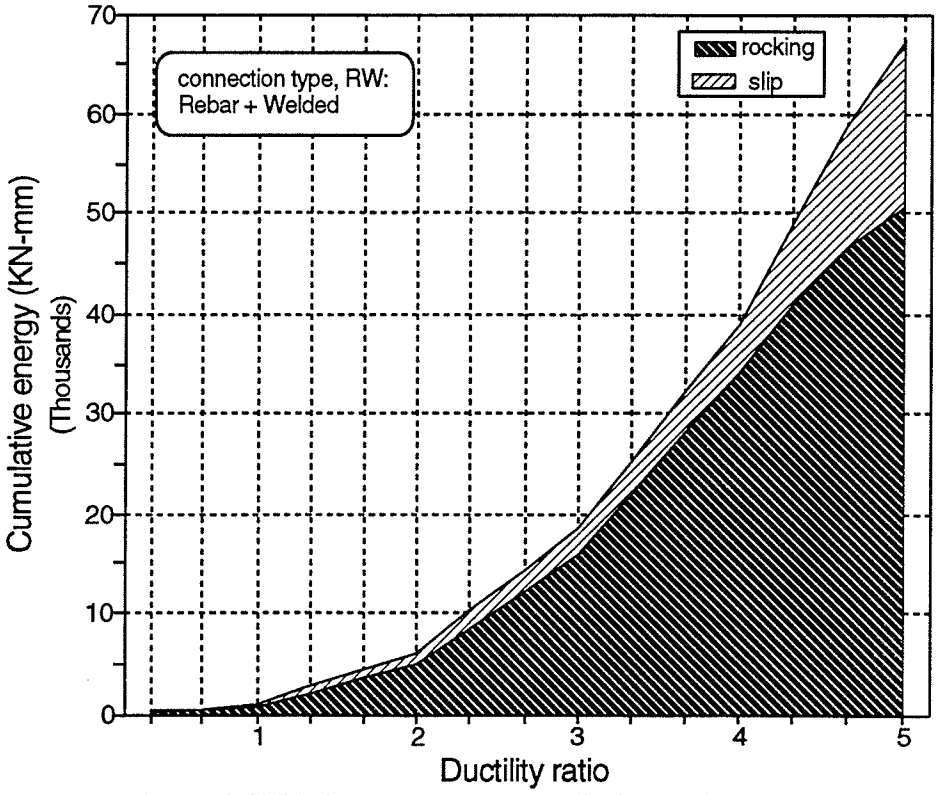

Figure 6.61(b) Cumulative energy dissipated by specimen RW

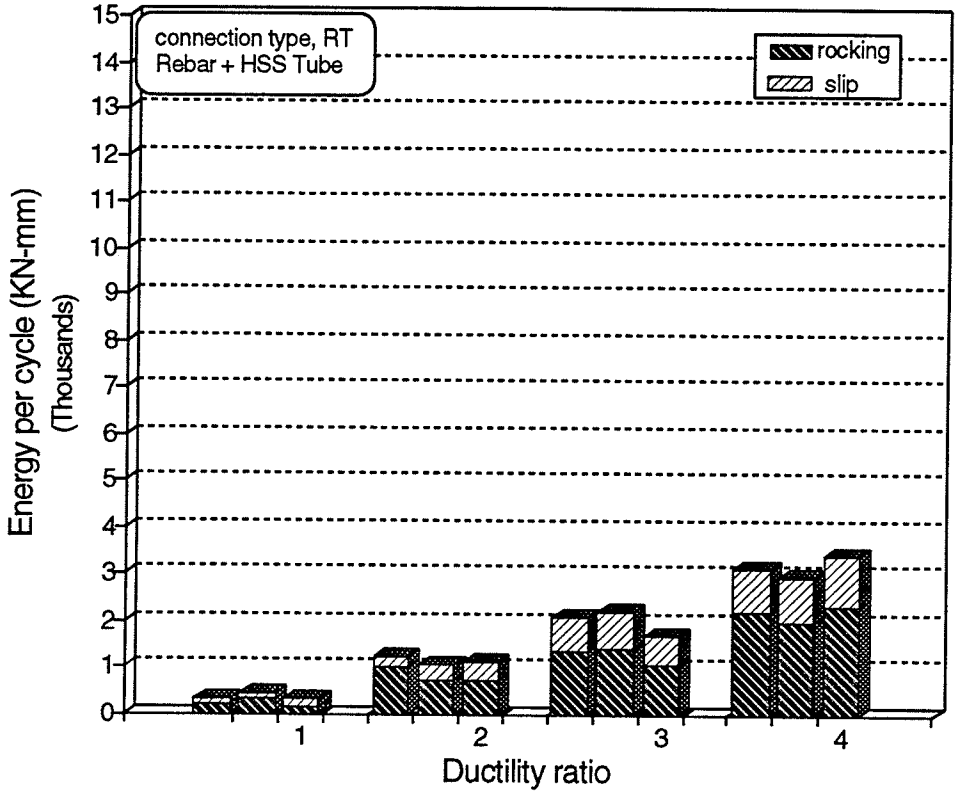

Figure 6.62(a) Per cycle energy dissipated by specimen RT

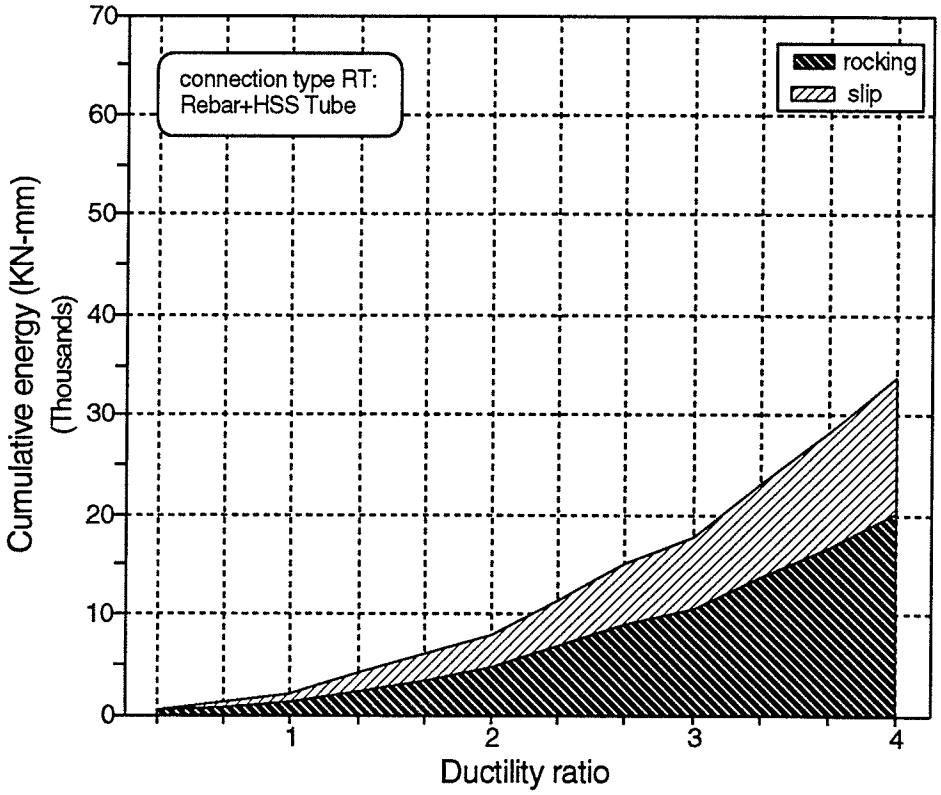

Figure 6.62(b) Cumulative energy dissipated by specimen RT

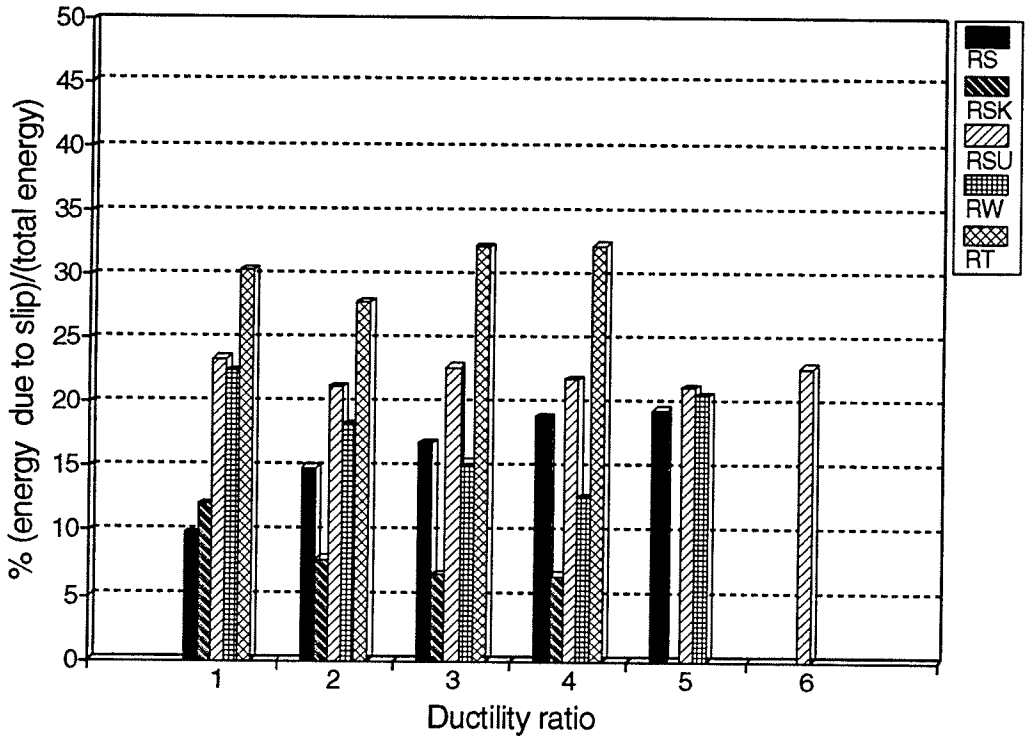

Figure 6.63 Percentage of energy due to slip to total energy for mild steel specimens

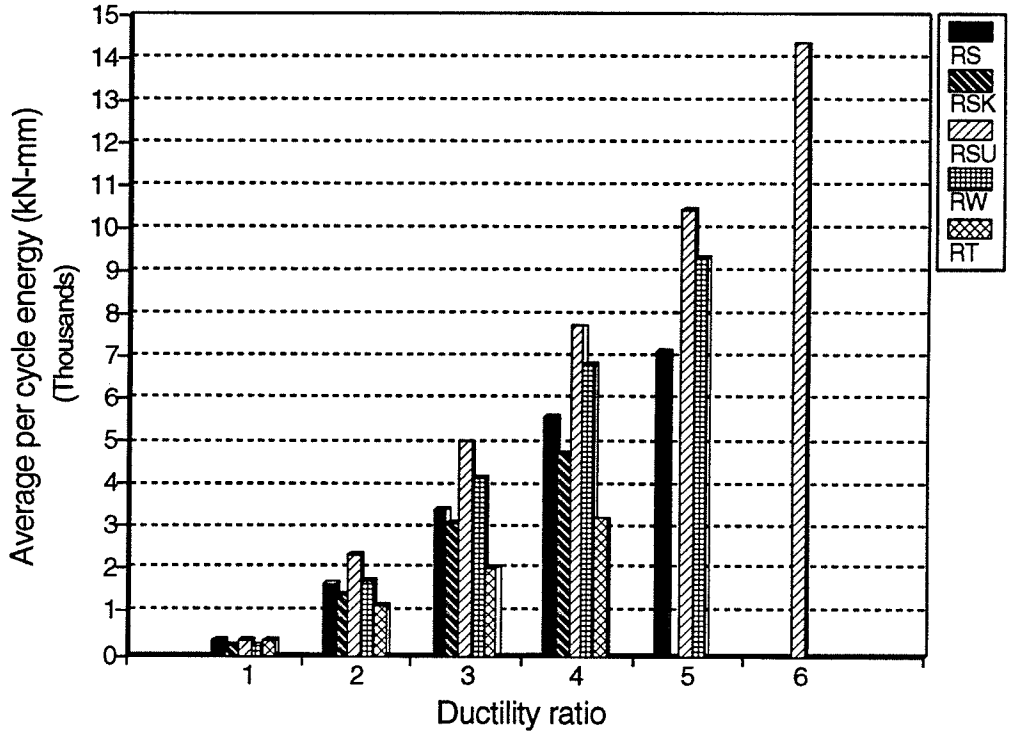

Figure 6.64 Average per cycle energy for specimen with mild steel reinforcement

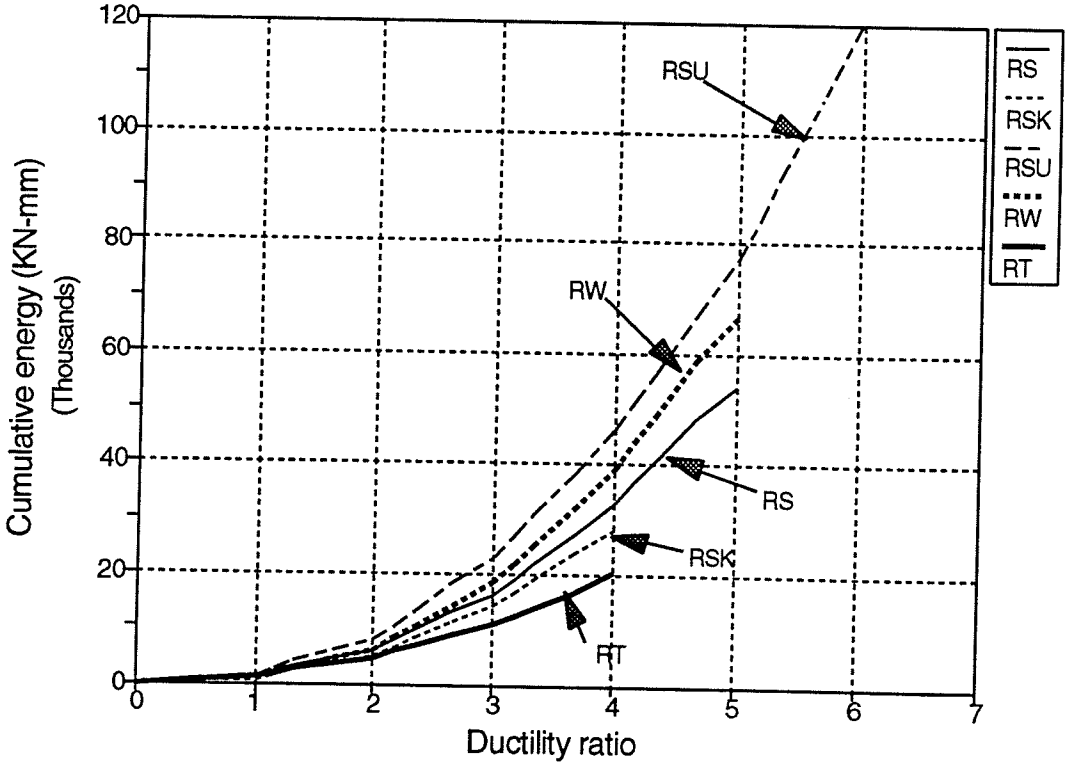

Figure 6.65 Comparison of cumulative energy dissipation for mild steel specimens

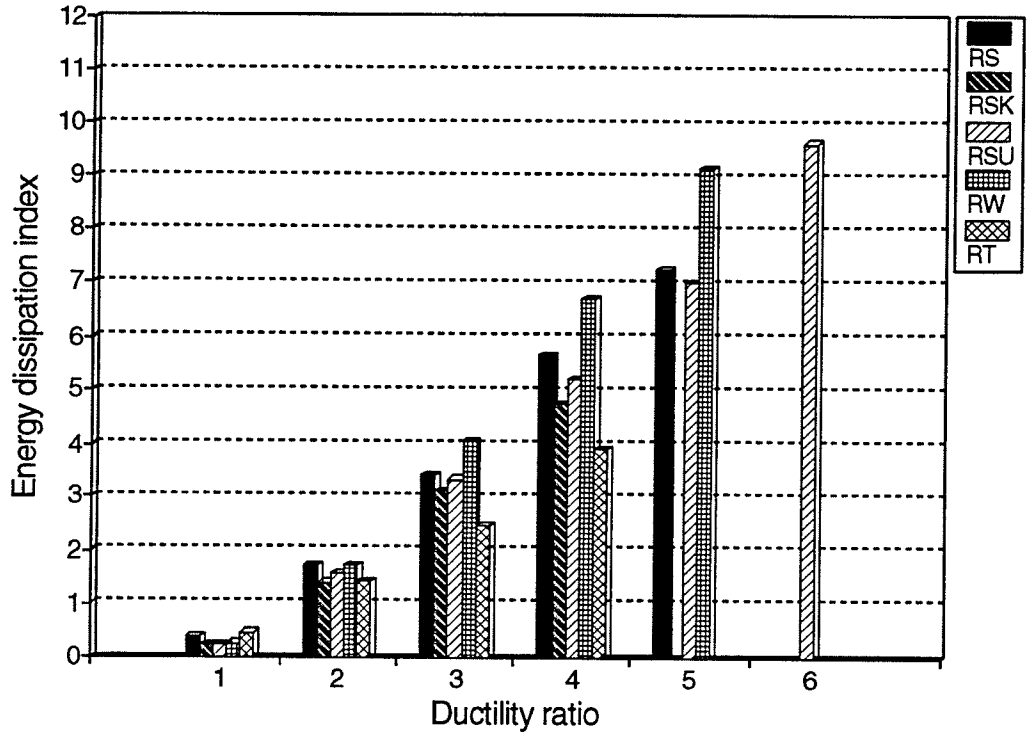

Figure 6.66 Per cycle energy dissipation index for mild steel specimen

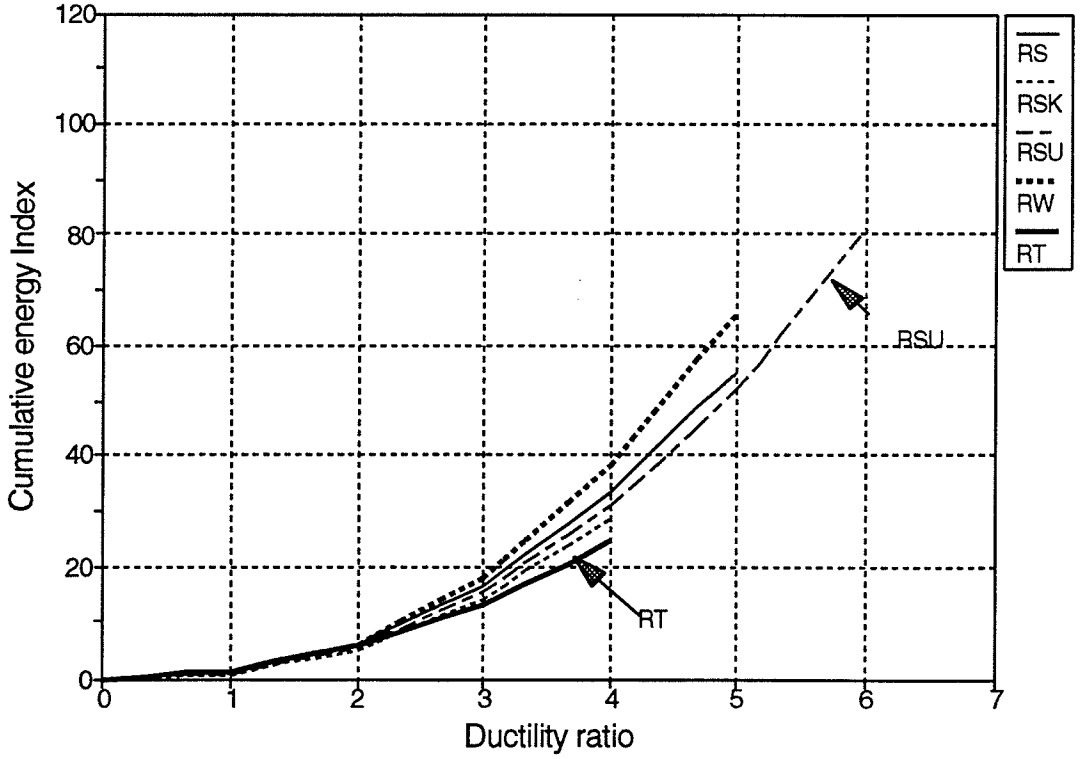

Figure 6.67 Cumulative energy dissipation index for mild steel specimen

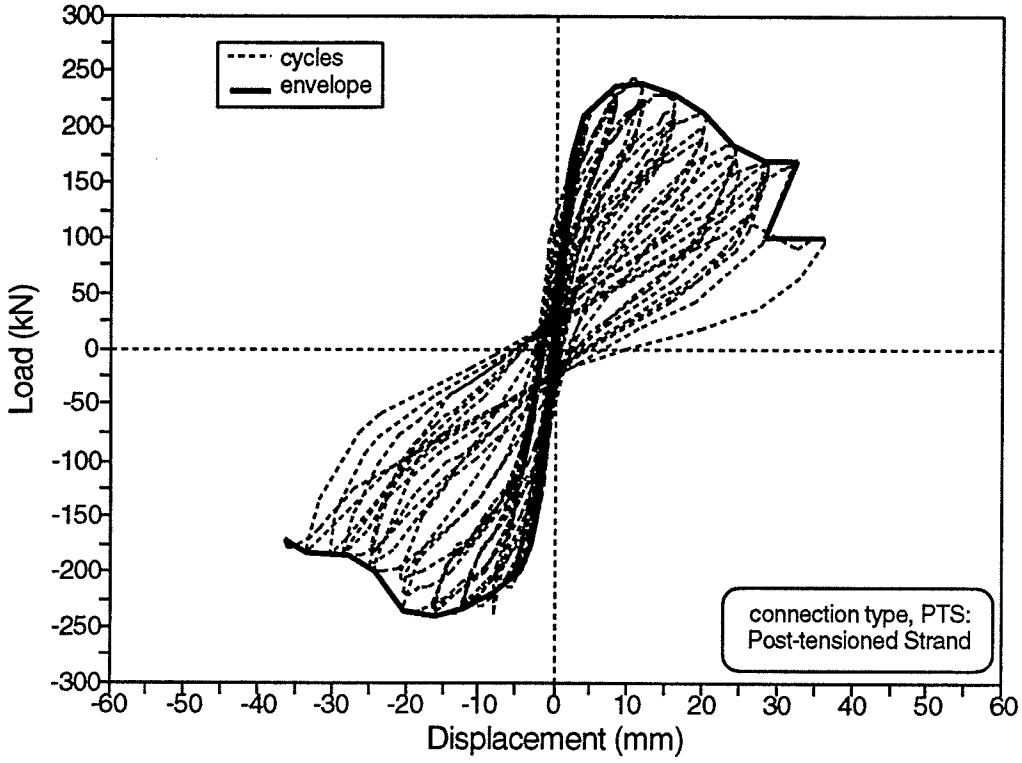

Figure 6.68 Strength envelope of response for specimen PTS

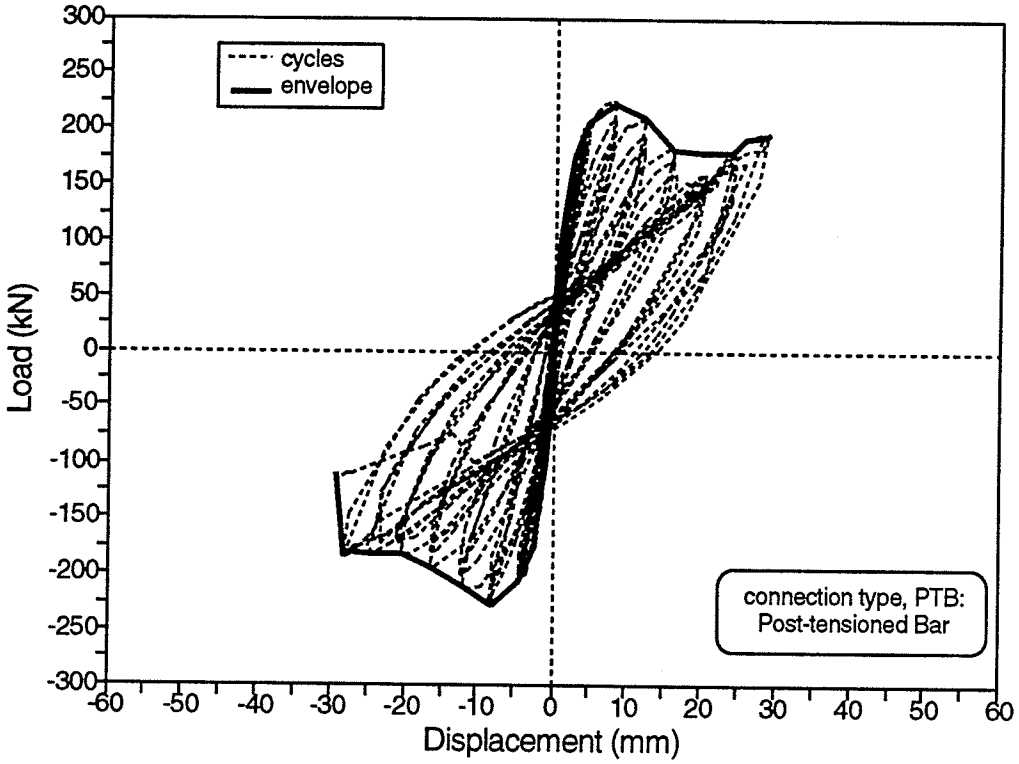

Figure 6.69 Strength envelope of response for specimen PTB

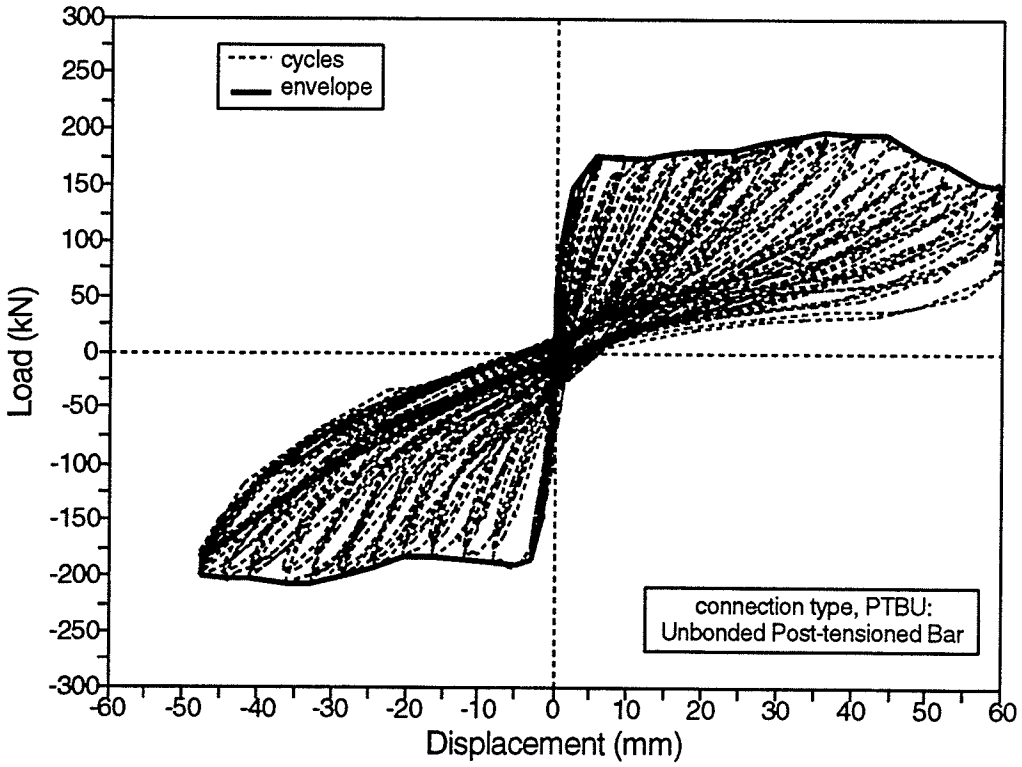

Figure 6.70 Strength envelope of response for specimen PTBU

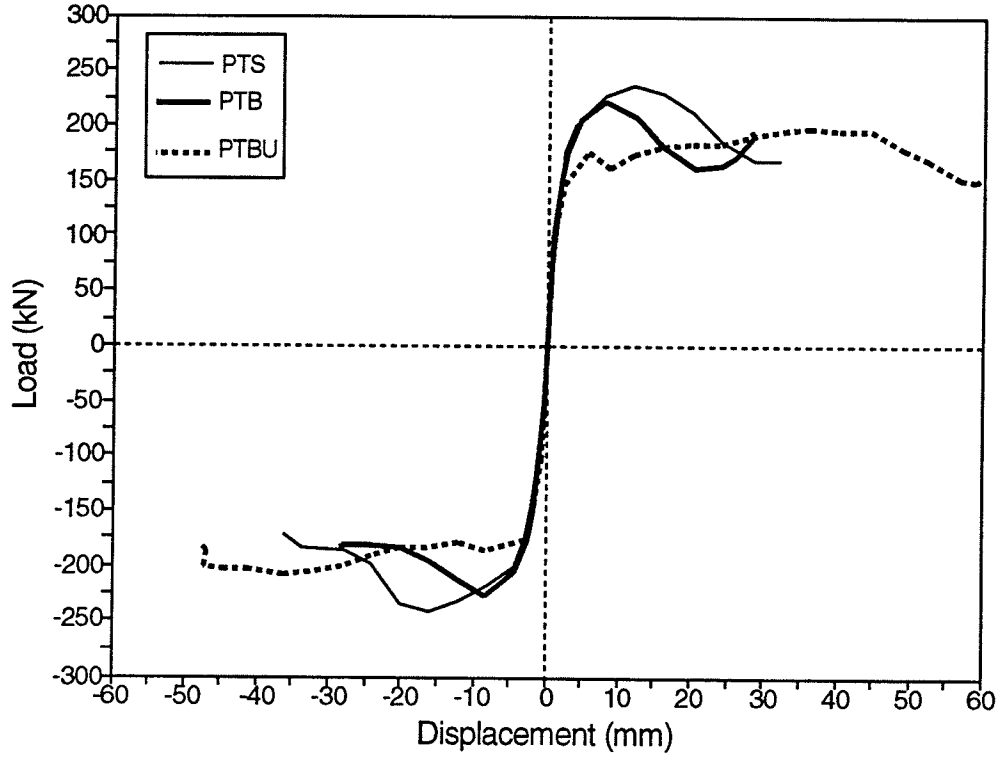

Figure 6.71 Comparison of strength envelopes for prestressed specimens

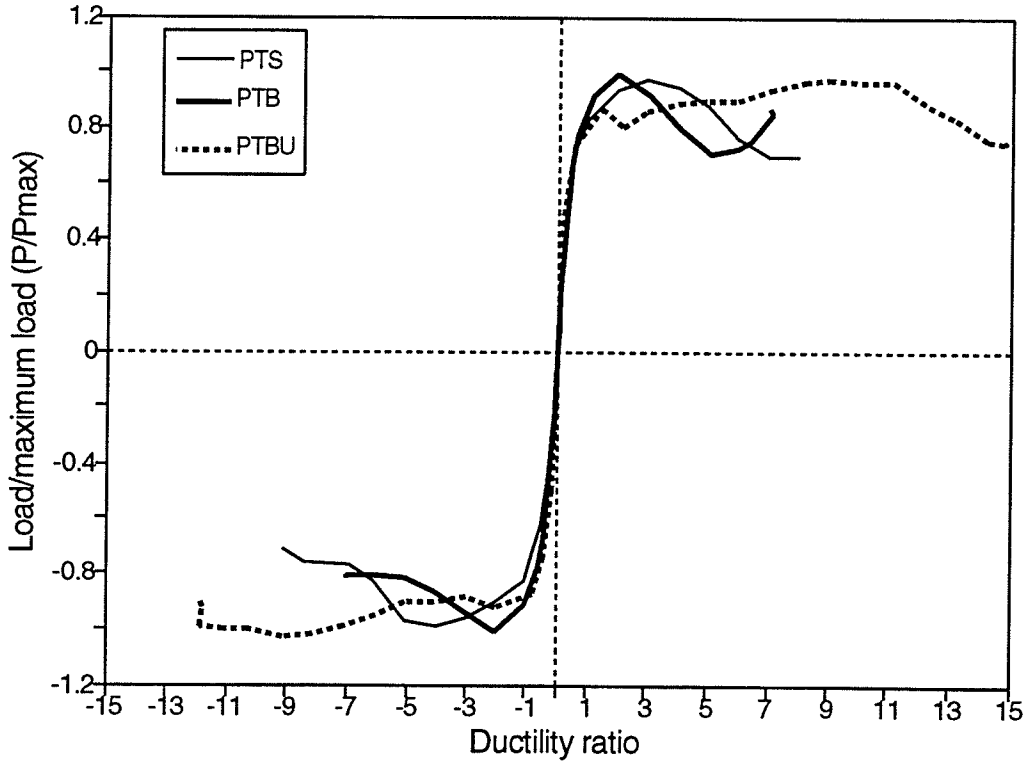

Figure 6.72 Comparison of normalized envelopes for prestressed specimens

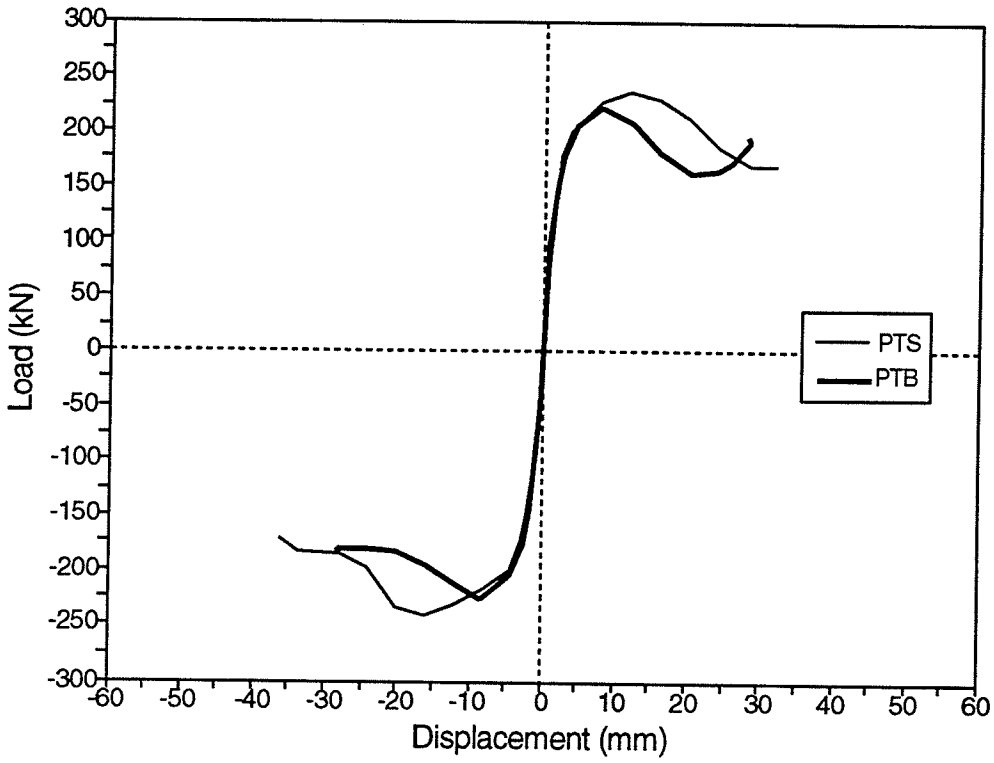

Figure 6.73(a) Comparison of strength envelopes: specimen PTS vrs PTB

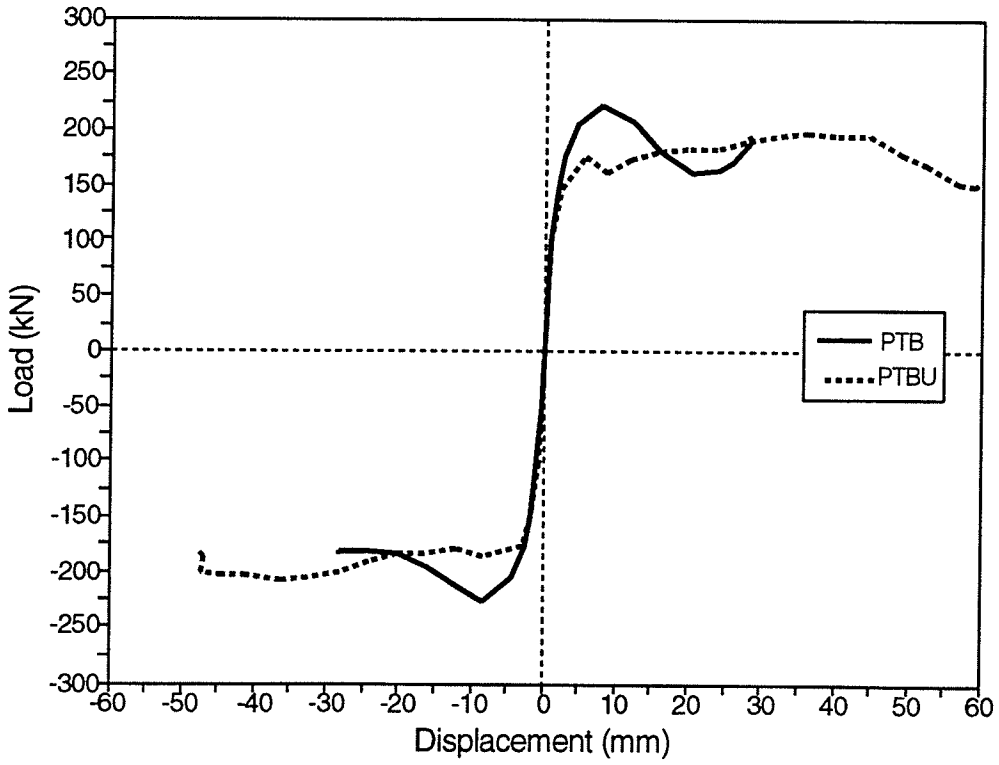

Figure 6.73(b) Comparison of strength envelopes: specimen PTBU vrs PTB

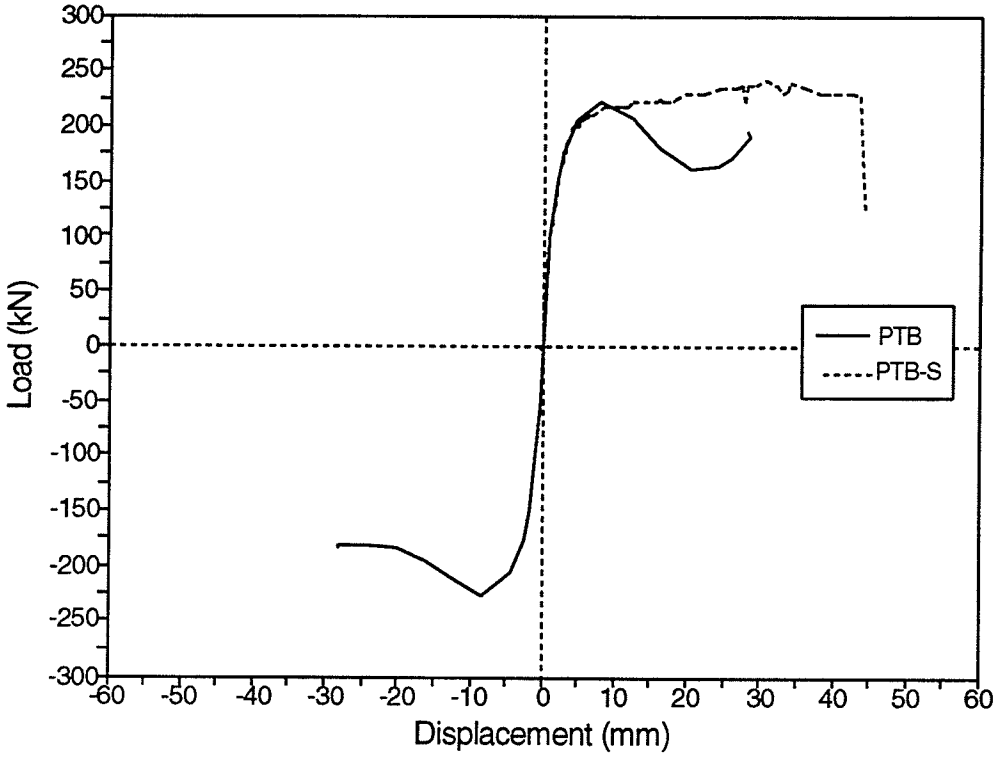

Figure 6.73(c) Comparison of strength envelopes: specimen PTB-S vrs PTB

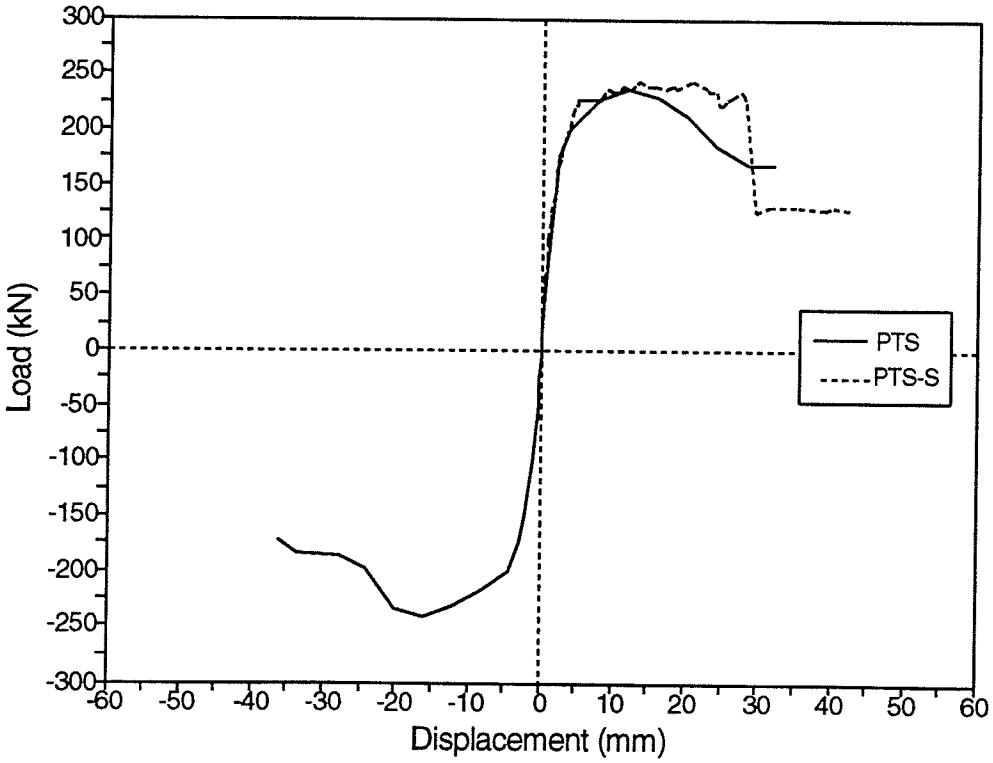

Figure 6.73(d) Comparison of strength envelopes: specimen PTS-S vrs PTS

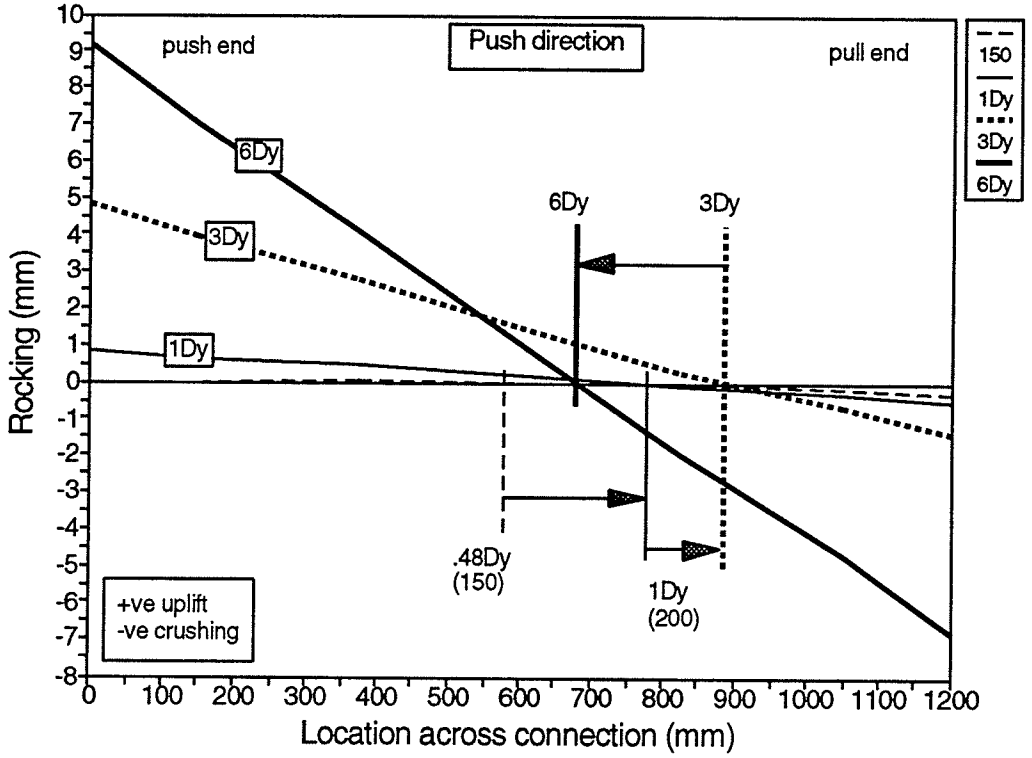

Figure 6.74(a) Typical rocking in the push direction for prestressed specimen (PTS)

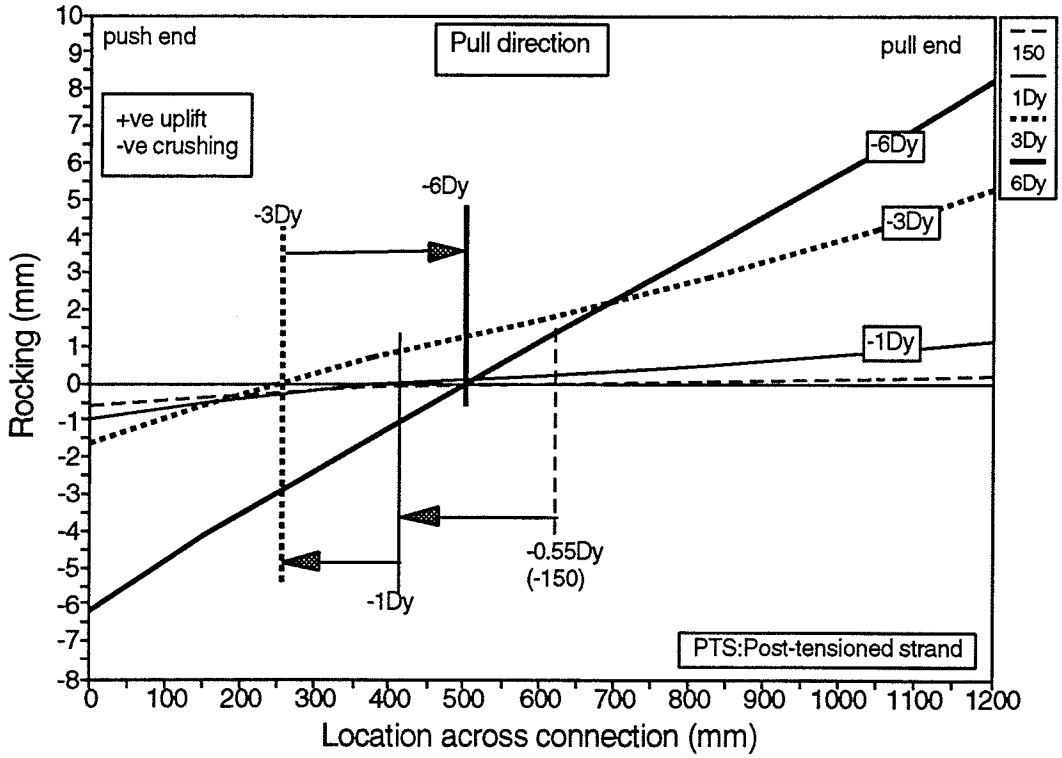

Figure 6.74(b) Typical rocking in pull direction for prestressed specimen (PTS)

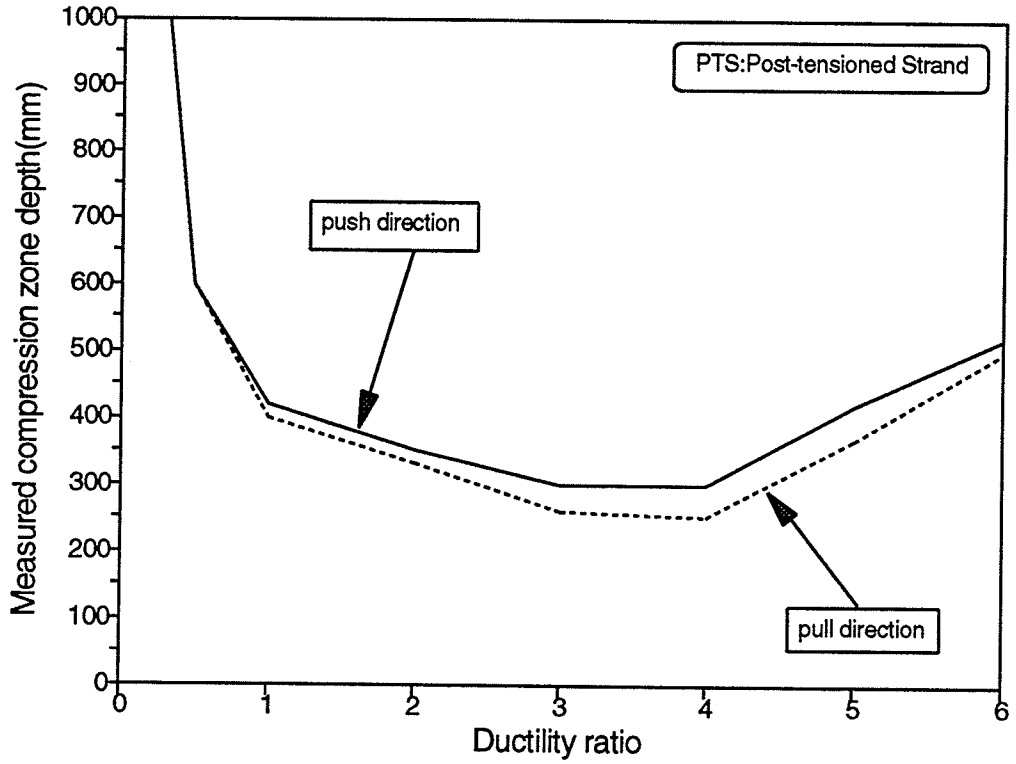

Figure 6.75 Variation of compression zone depth for specimen PTS

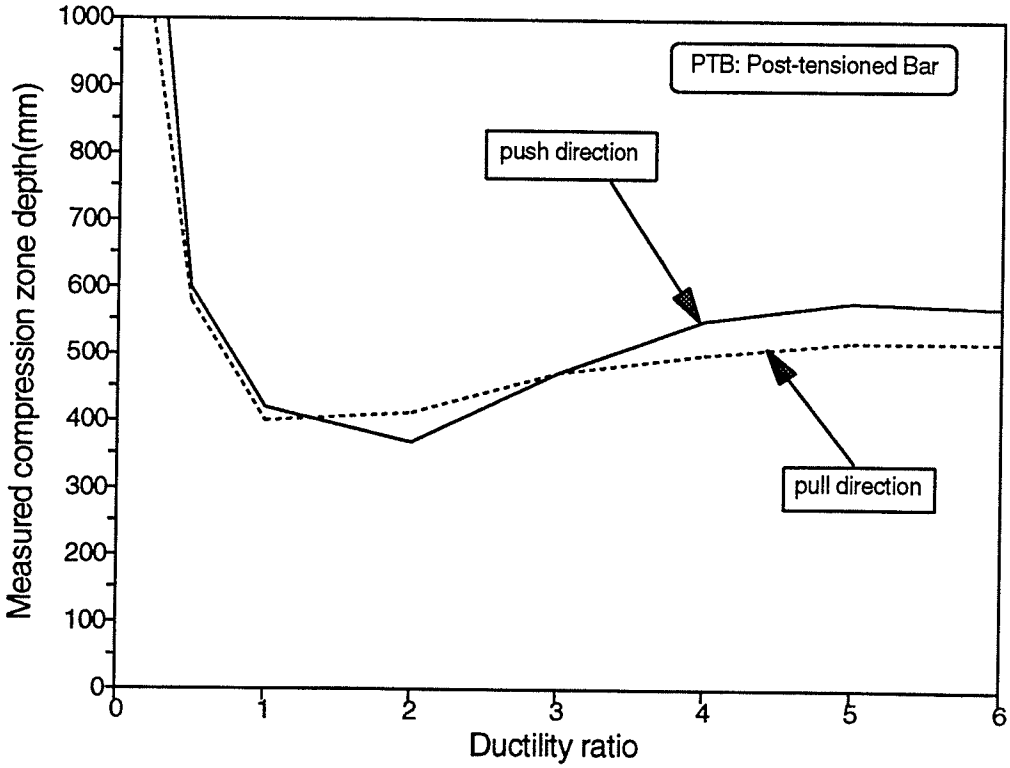

Figure 6.76 Variation of compression zone depth for specimen PTB

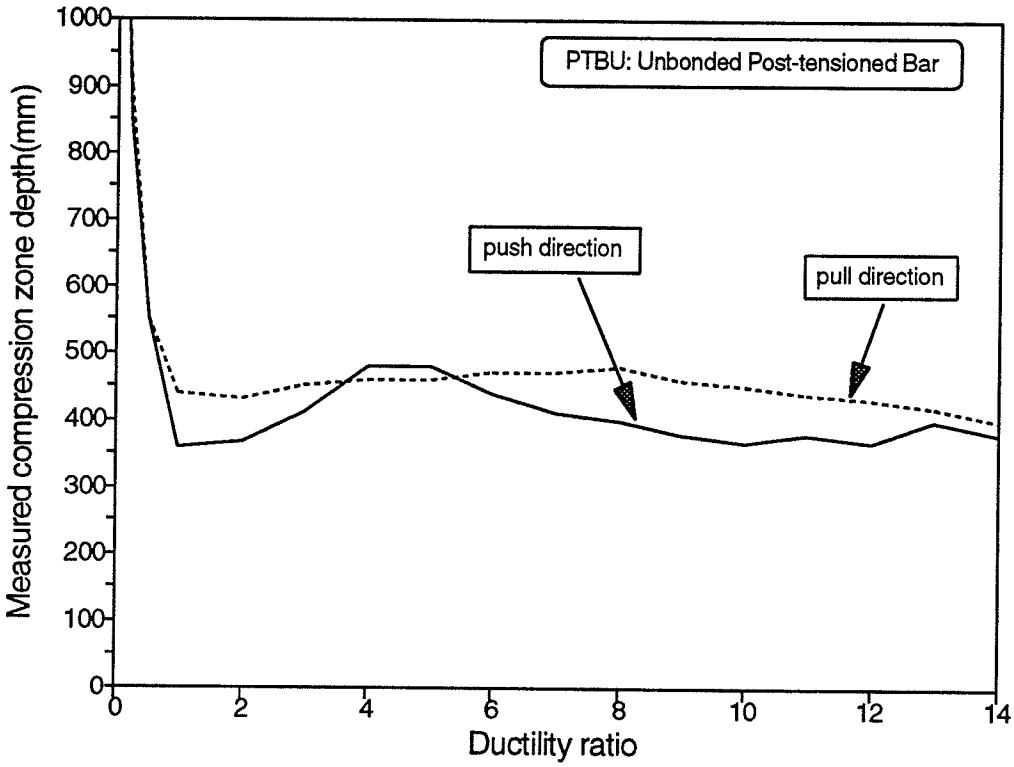

Figure 6.77 Variation of compression zone depth for specimen PTBU

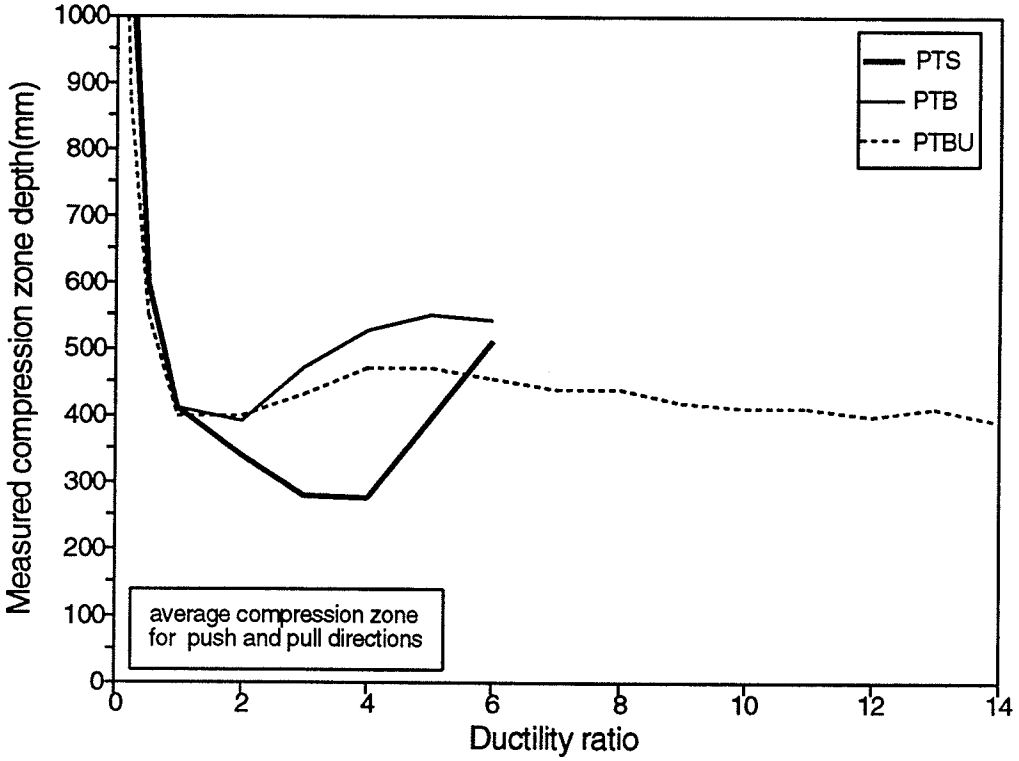

Figure 6.78(a) Comparison of compression zone depths for prestressed specimens

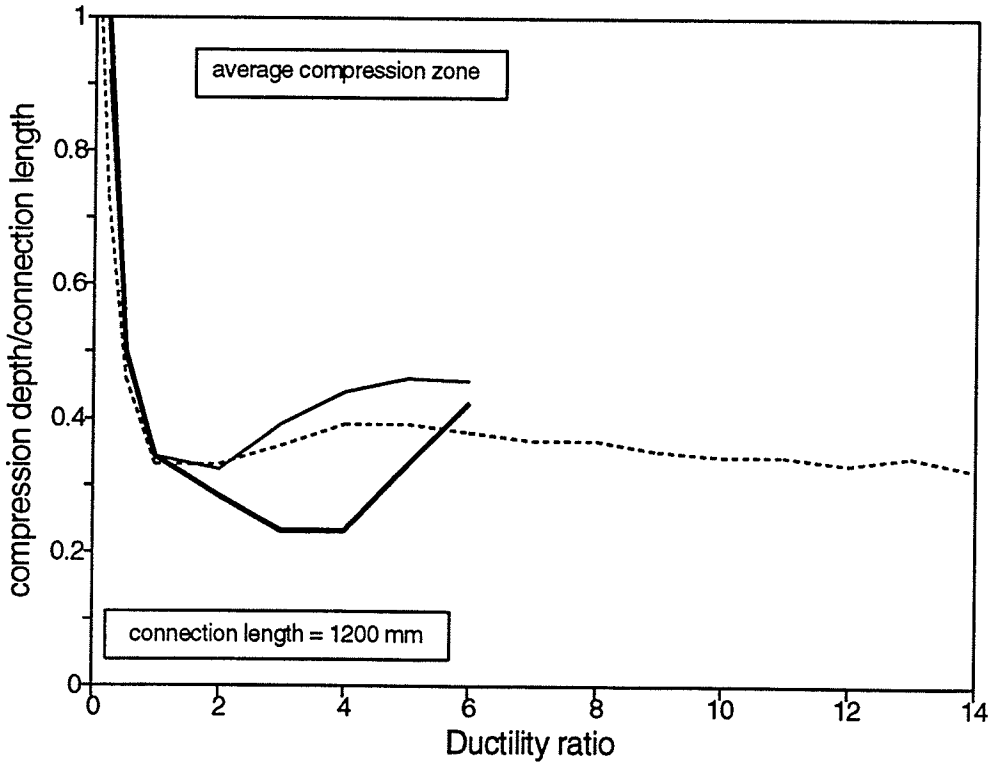

Figure 6.78(b) Comparison of normalized compression zone for prestressed specimens

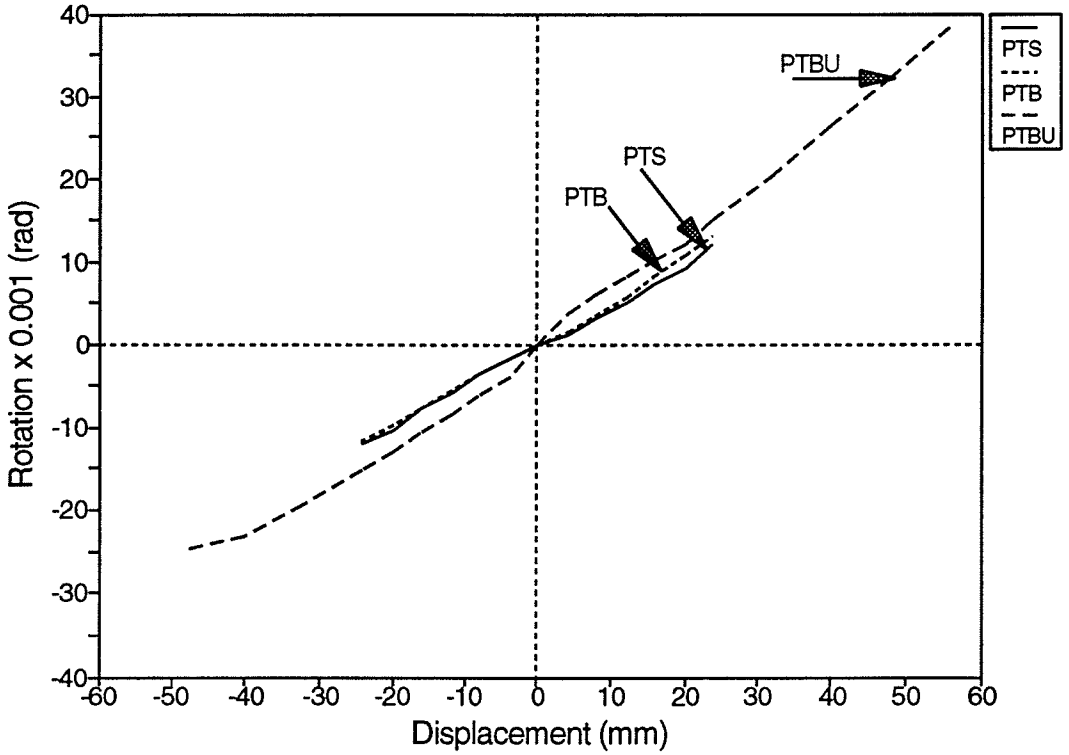

Figure 6.79(a) Rotation vs. displacement relationship for prestressed specimens

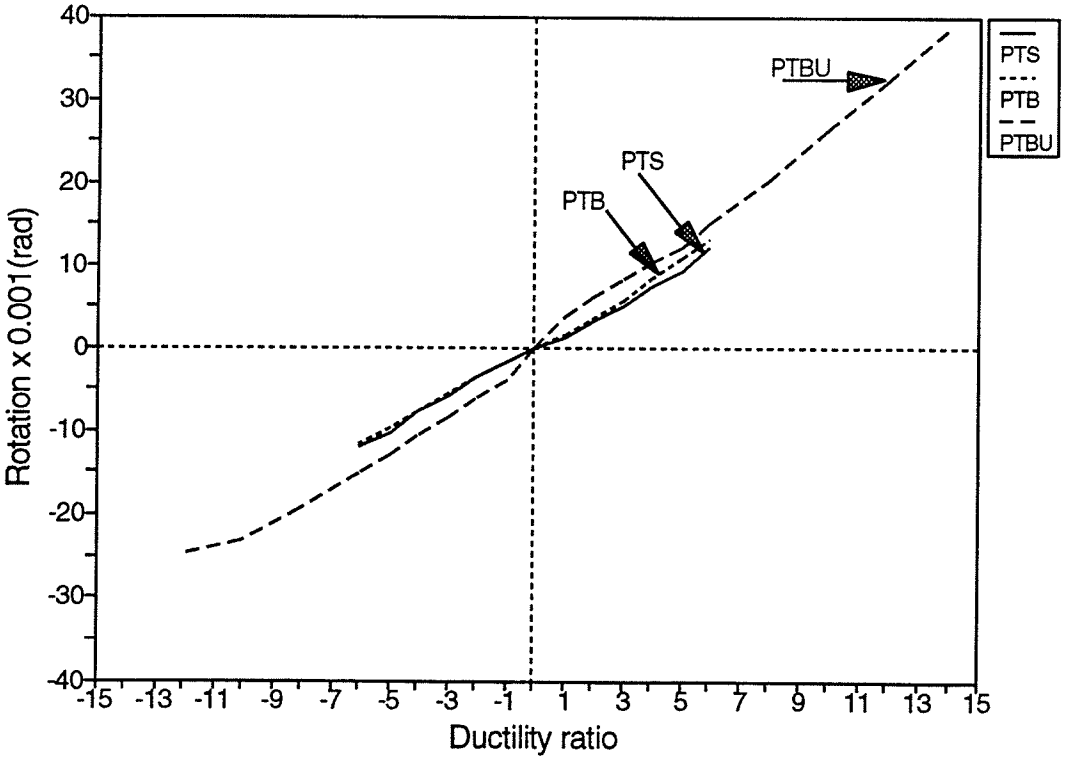

Figure 6.79(b) Rotation vs. ductility relationship for prestressed specimens

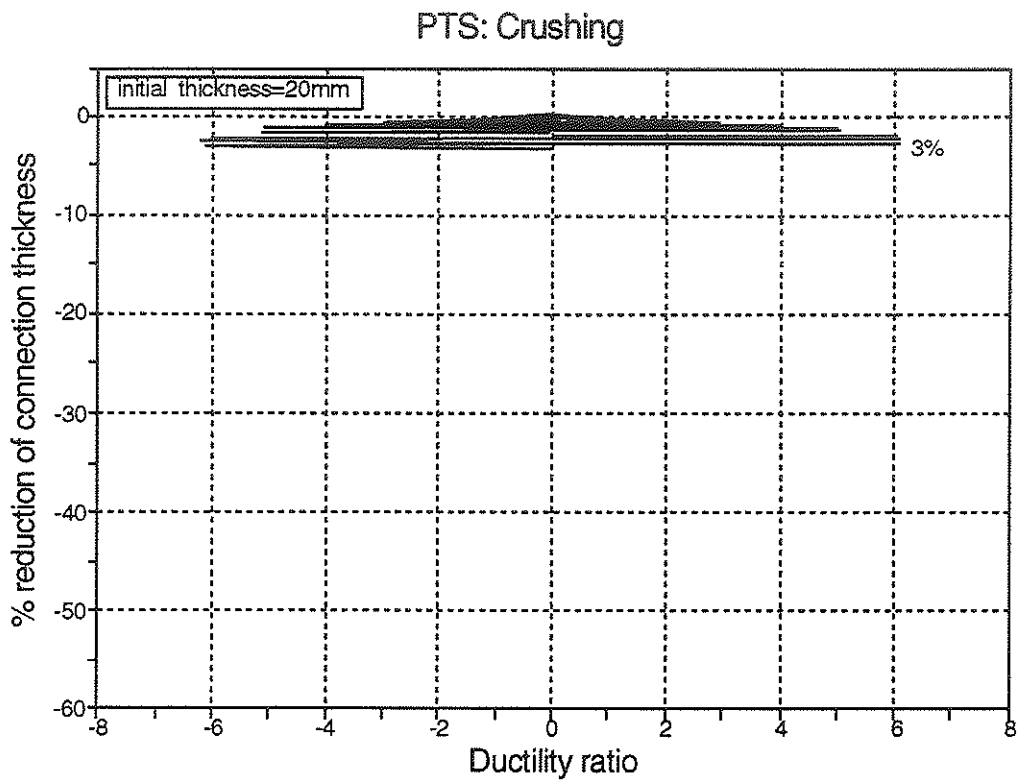

Figure 6.80 Percent reduction in connection thickness for specimen PTS

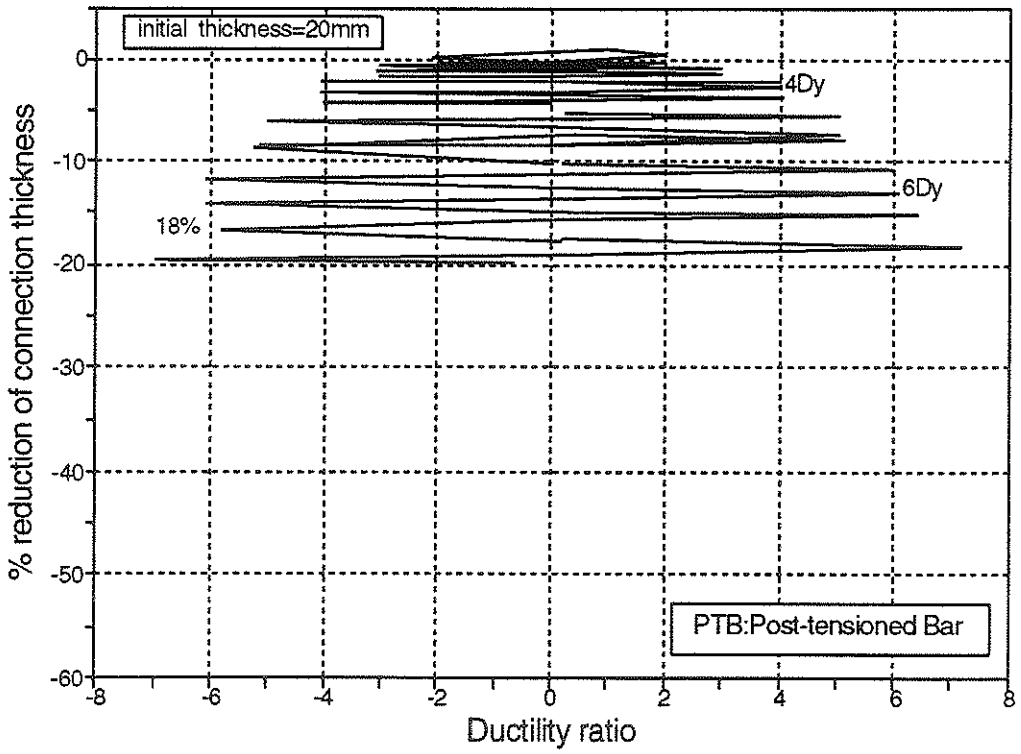

Figure 6.81 Percent reduction in connection thickness for specimen PTB

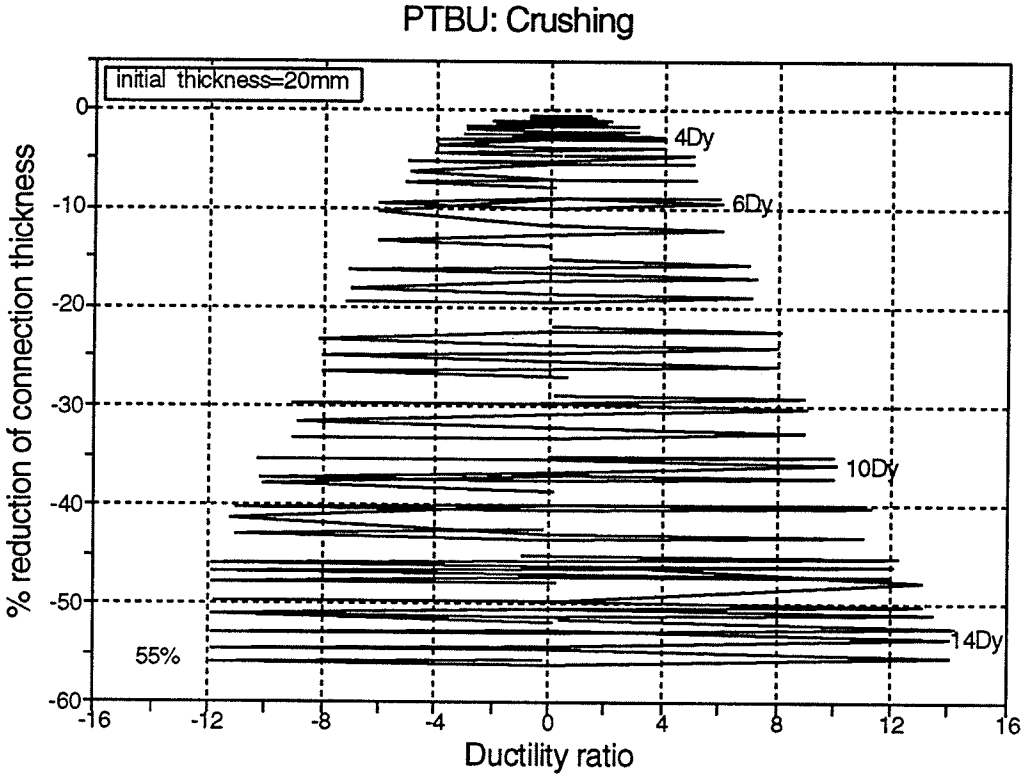

Figure 6.82 Percent reduction in connection thickness for specimen PTBU

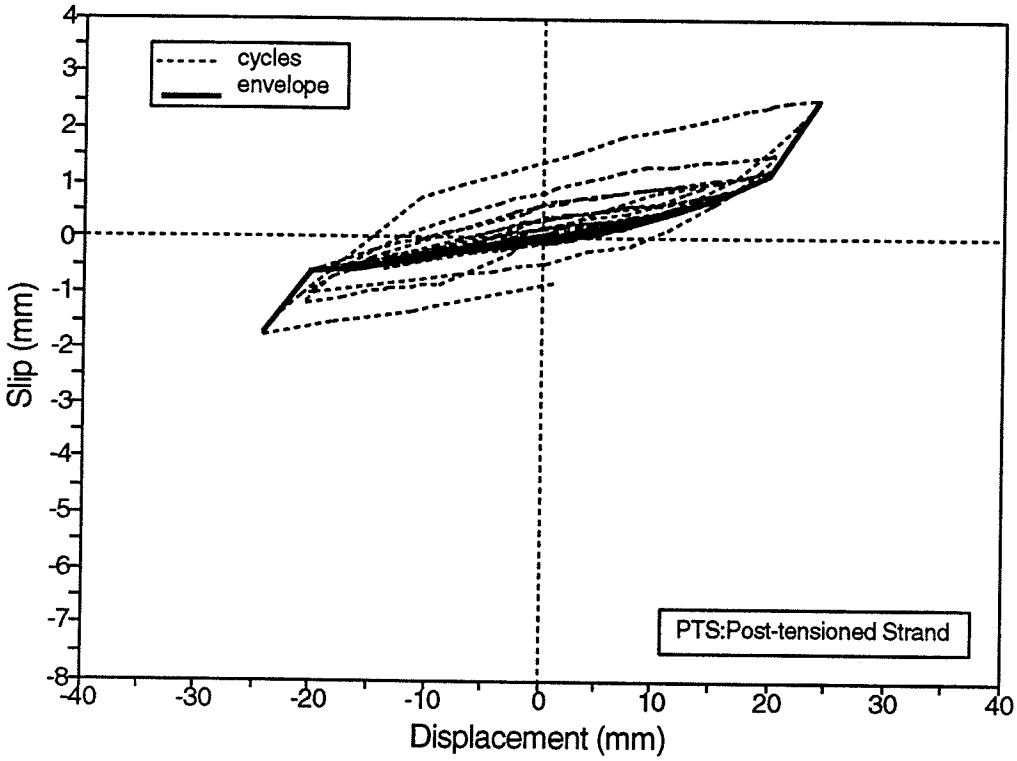

Figure 6.83 Slip-envelope for specimen PTS

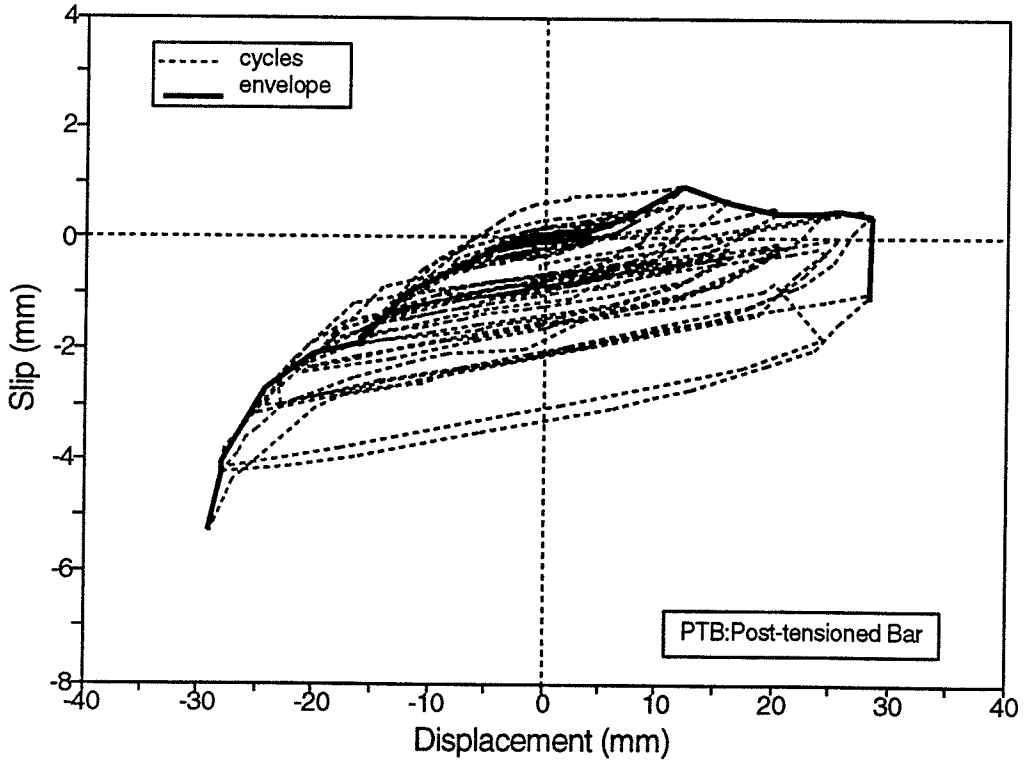

Figure 6.84 Slip-envelope for specimen PTB

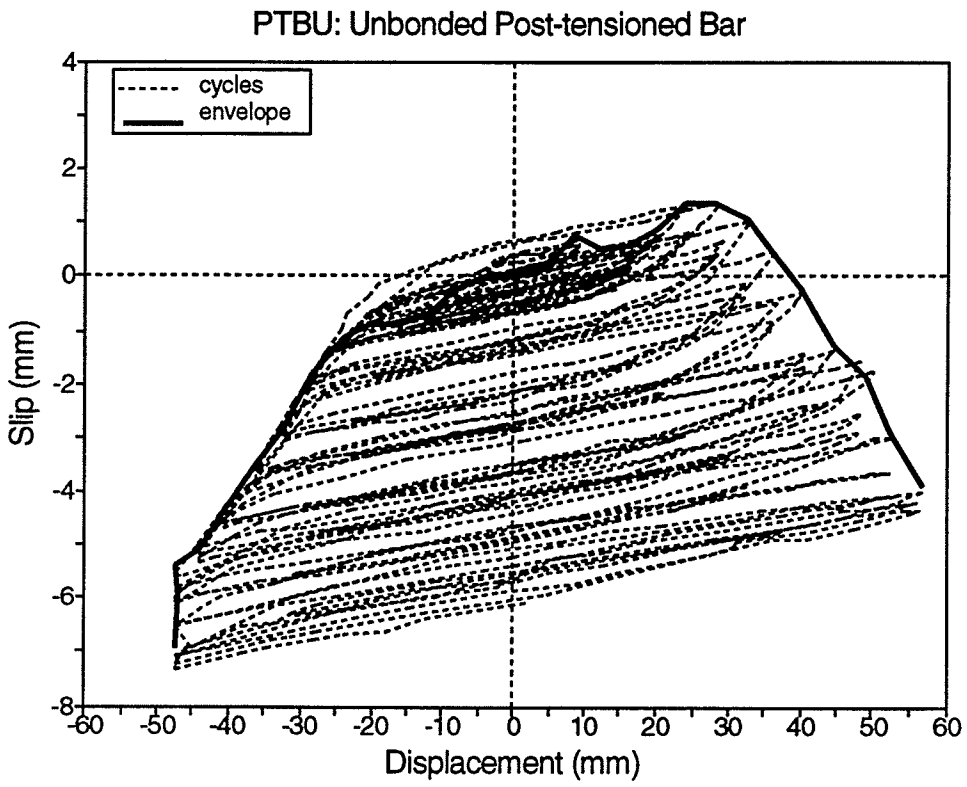

Figure 6.85 Slip-envelope for specimen PTBU

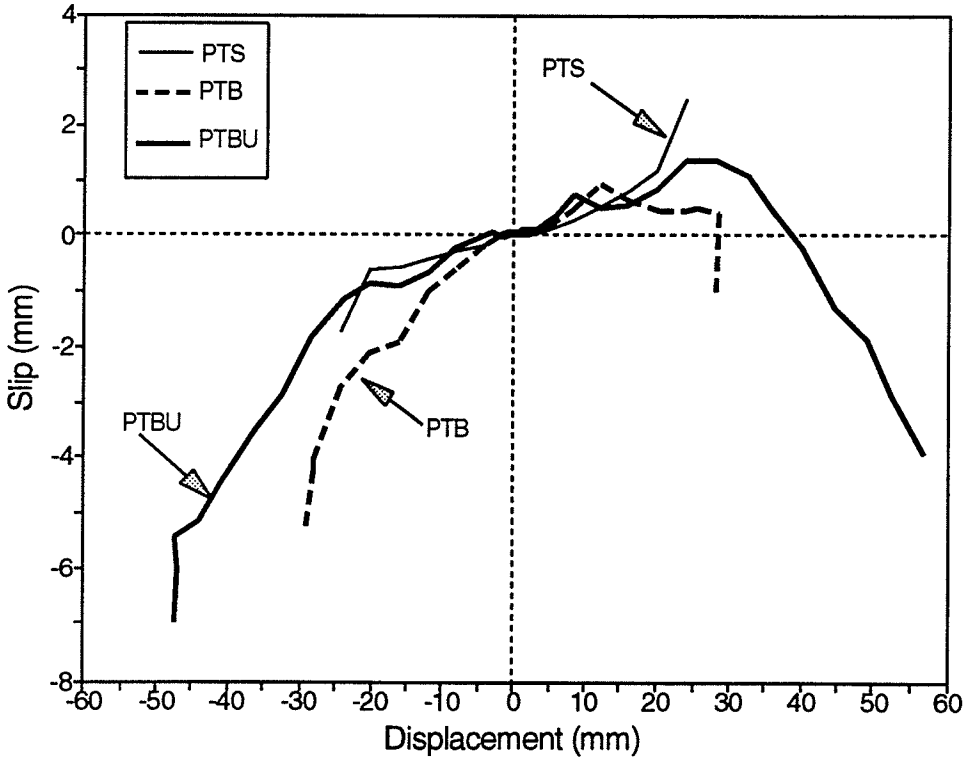

Figure 6.86 Comparison of slip envelopes for prestressed specimens

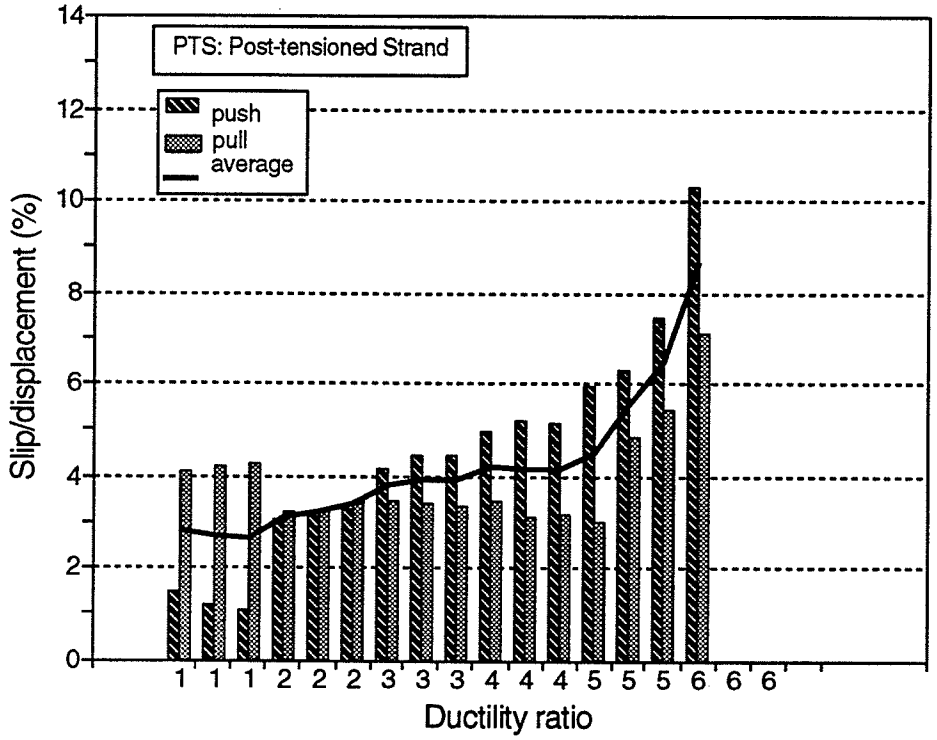

Figure 6.87 Percent slip/displacement per cycle versus ductility for specimen PTS

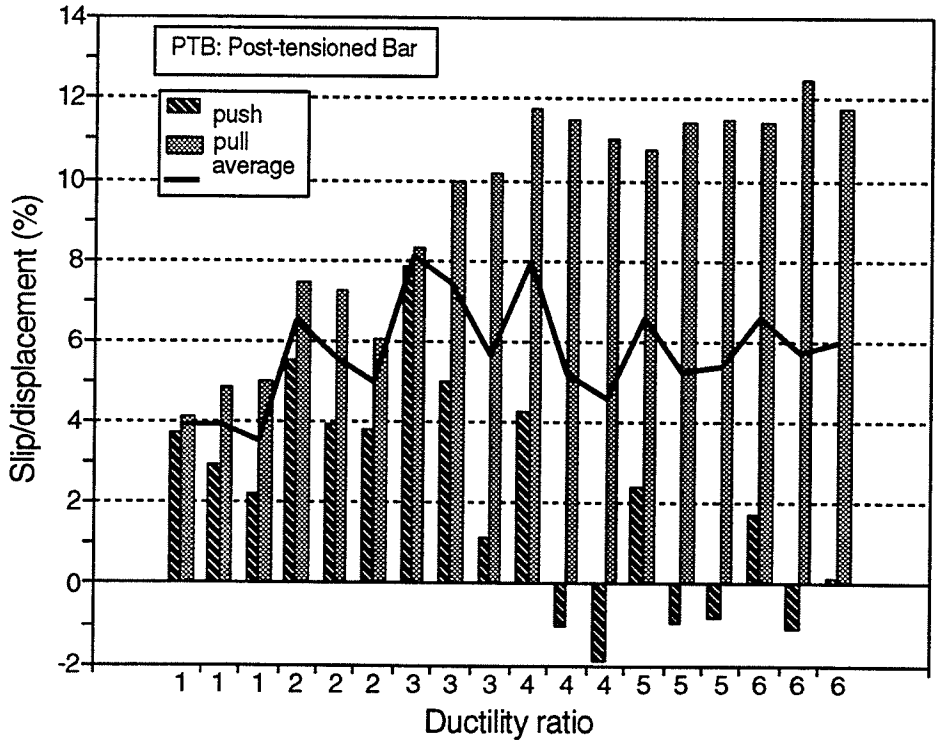

Figure 6.88 Percent slip/displacement per cycle versus ductility for specimen PTB

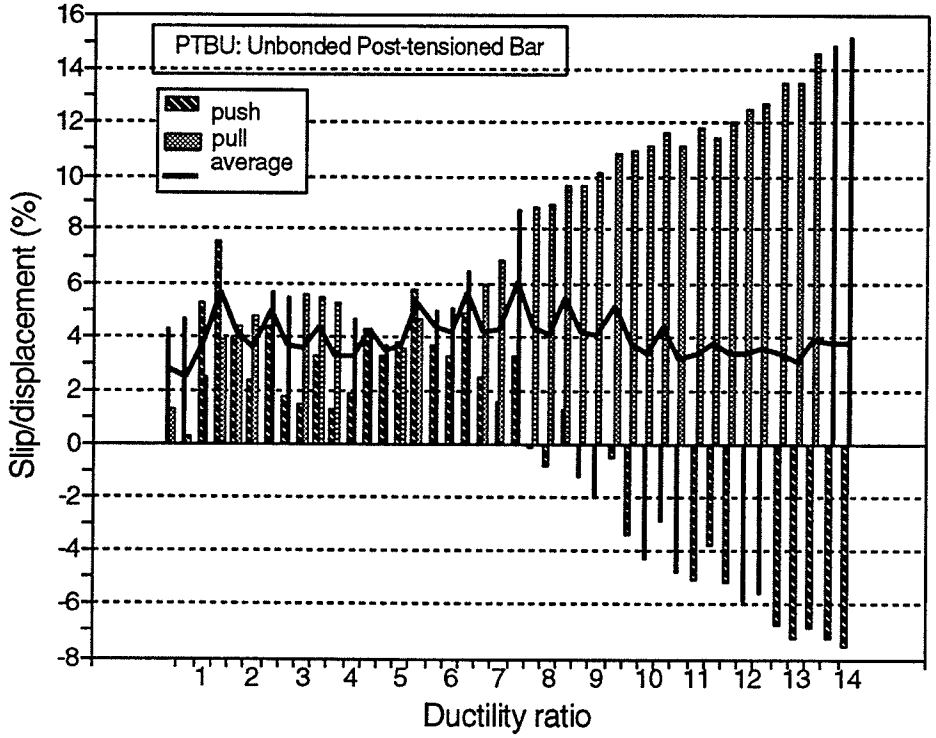

Figure 6.89 Percent slip/displacement per cycle versus ductility for specimen PTBU

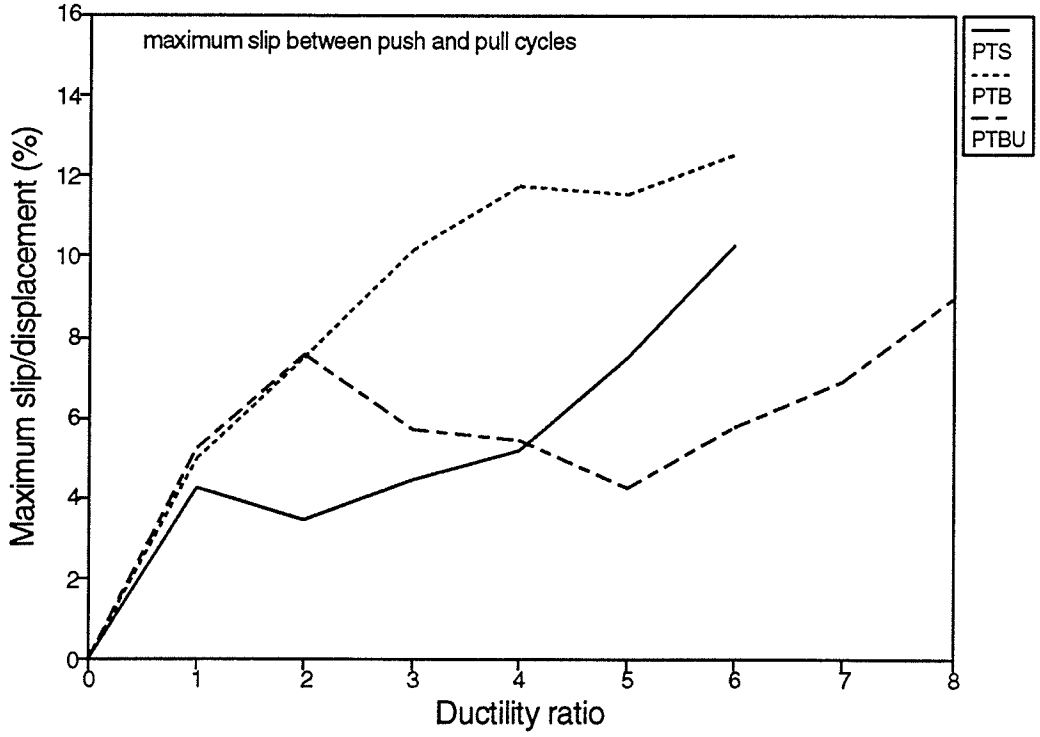

Figure 6.90 Comparison of percent slip/displacement for prestressed specimens

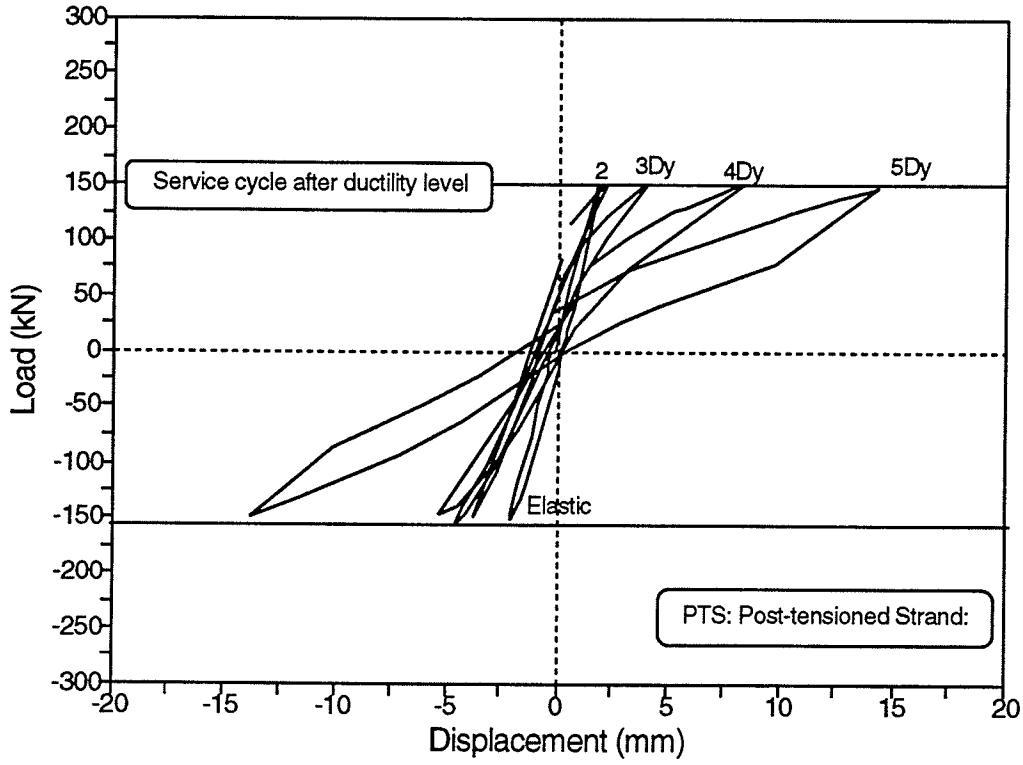

Figure 6.91 Service load-displacement cycles for specimen PTS

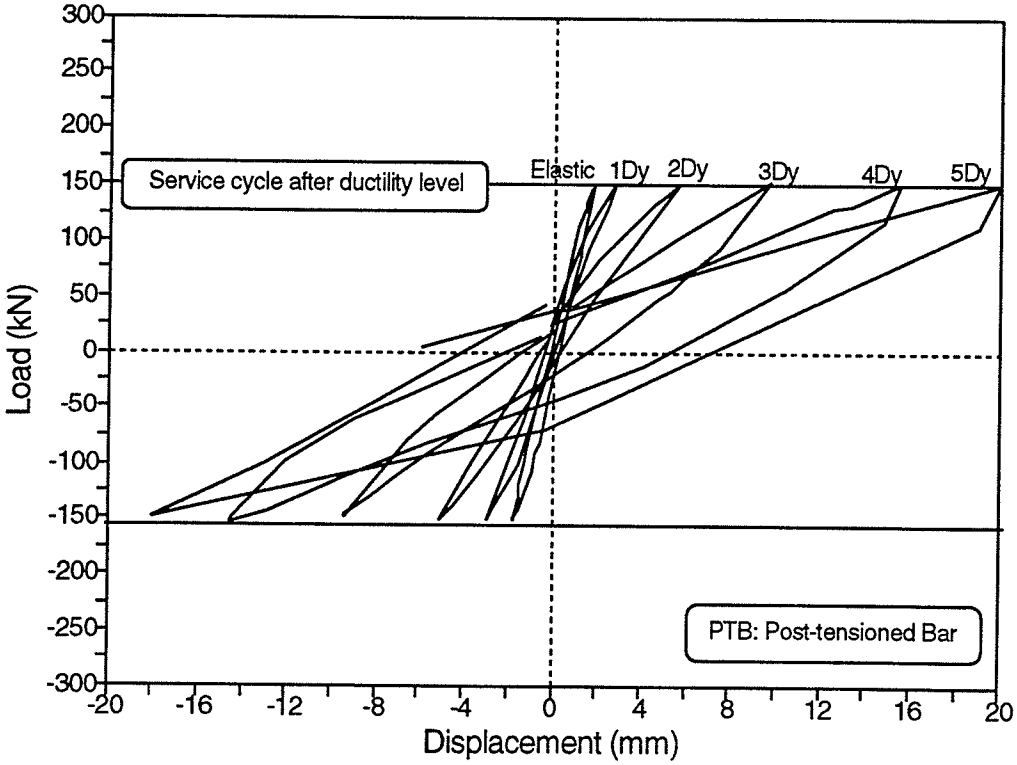

Figure 6.92 Service load-displacement cycles for specimen PTB

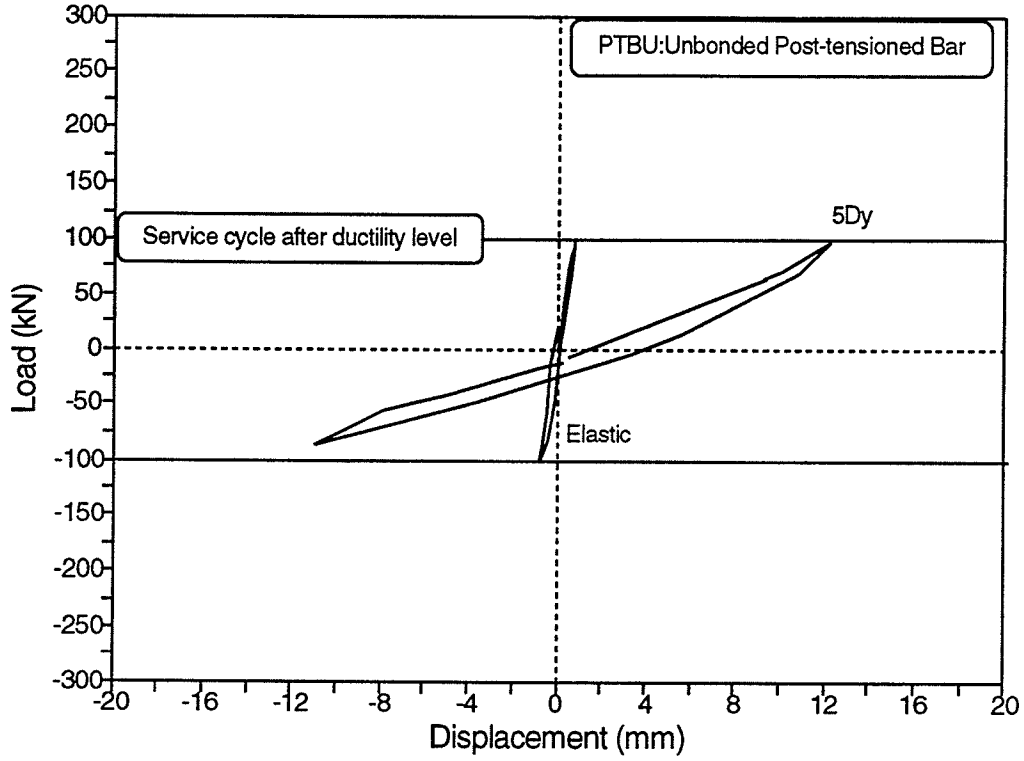

Figure 6.93(a) Service load-displacement cycle up to 5Dy for specimen PTBU

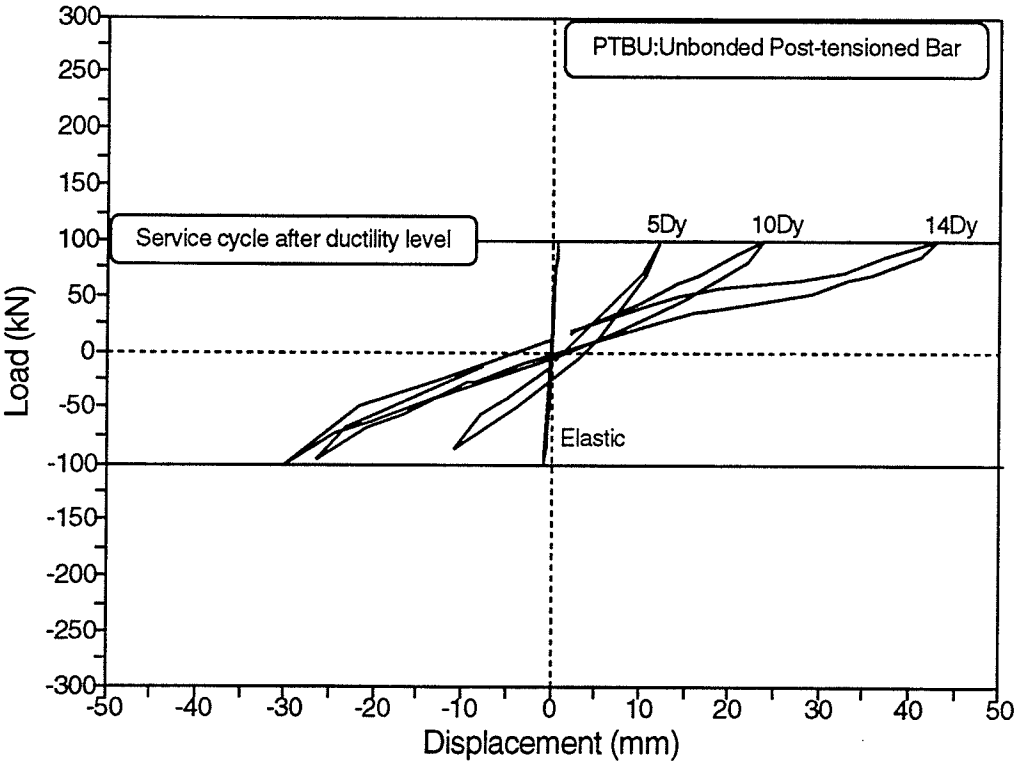

Figure 6.93(b) Service load-displacement cycles for specimen PTBU

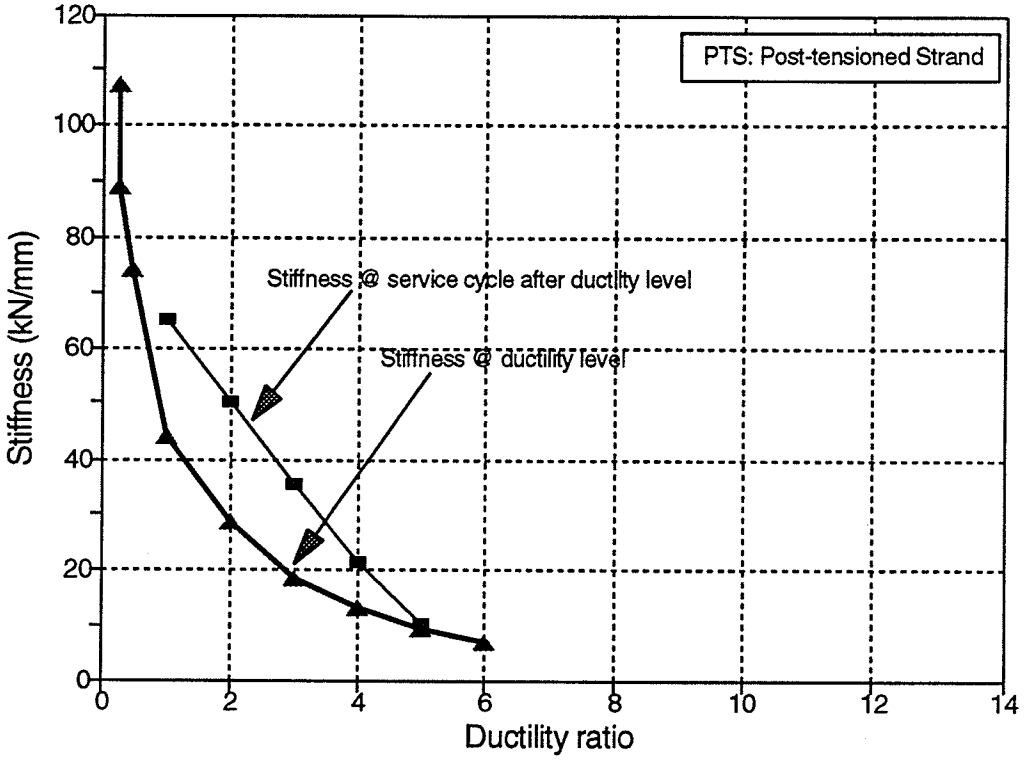

Figure 6.94 Stiffness degradation versus ductility for specimen PTS

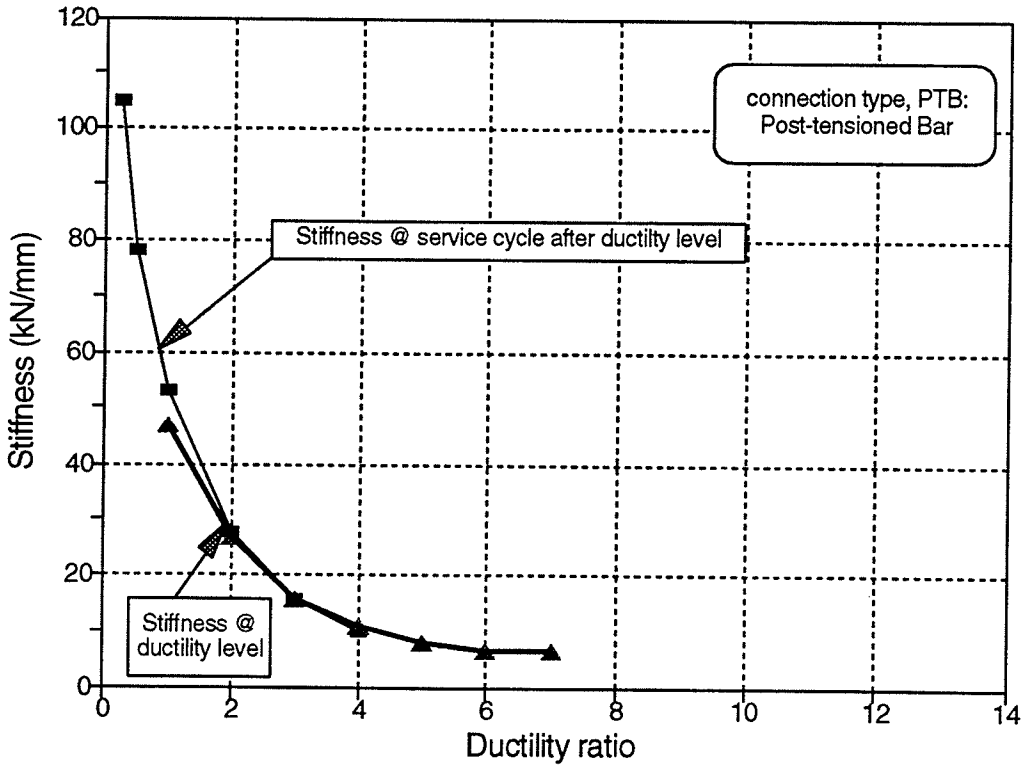

Figure 6.95 Stiffness degradation versus ductility for specimen PTB

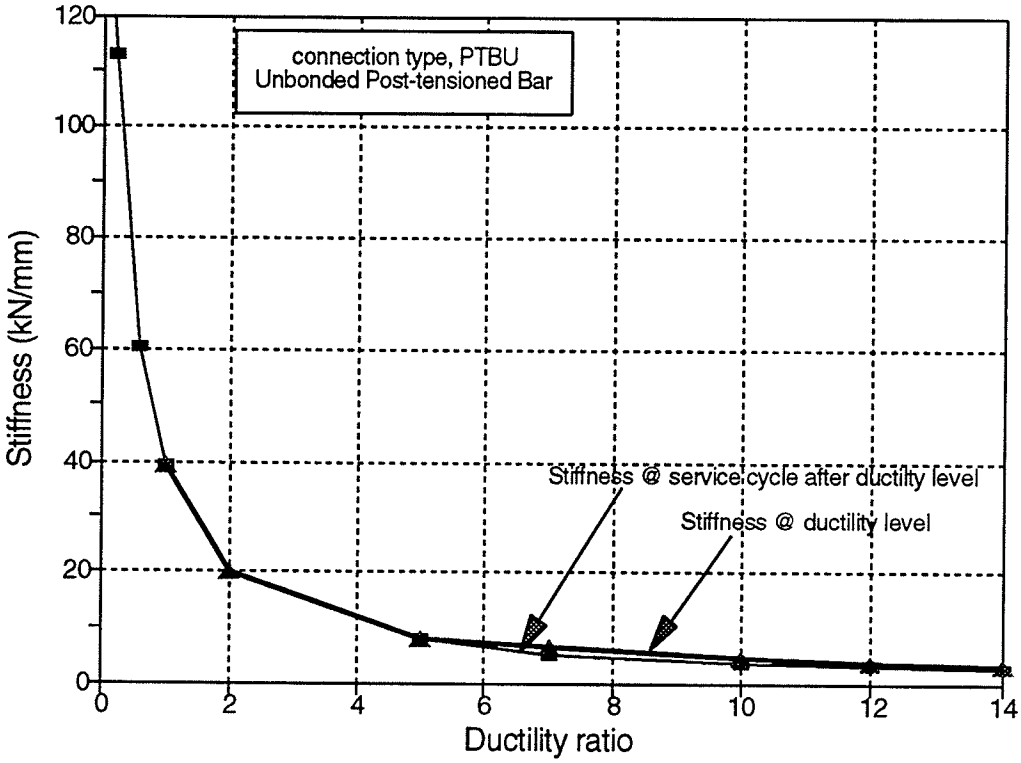

Figure 6.96 Stiffness degradation versus ductility for specimen PTBU

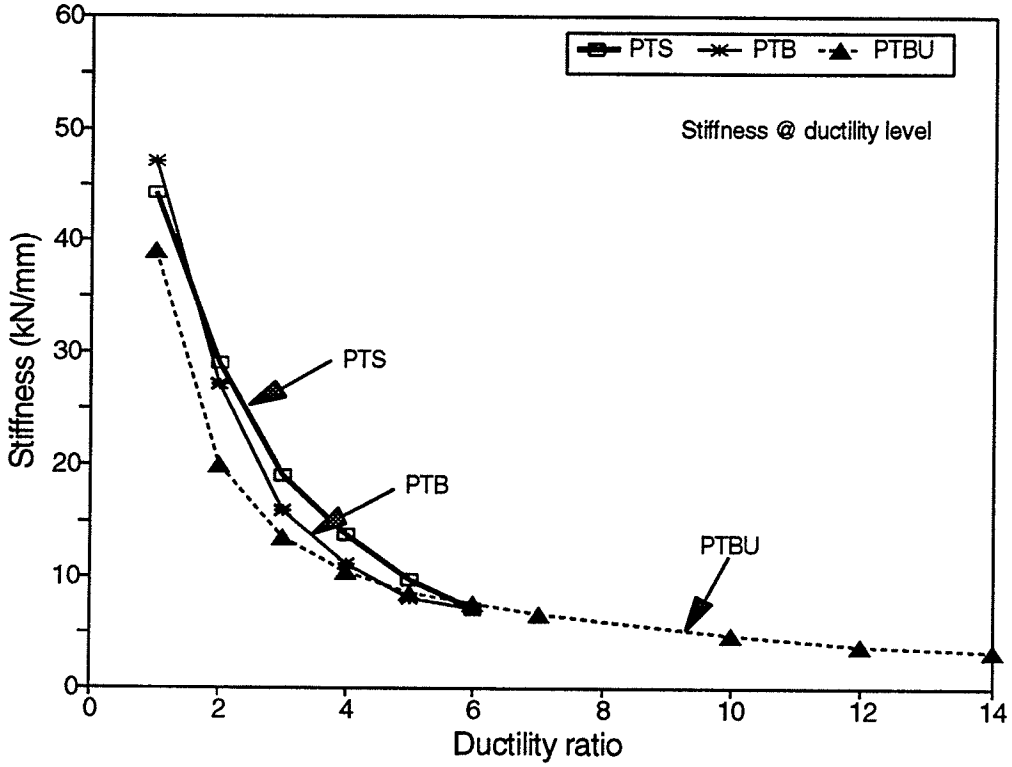

Figure 6.97(a) Comparison of stiffness degradation for prestressed specimens

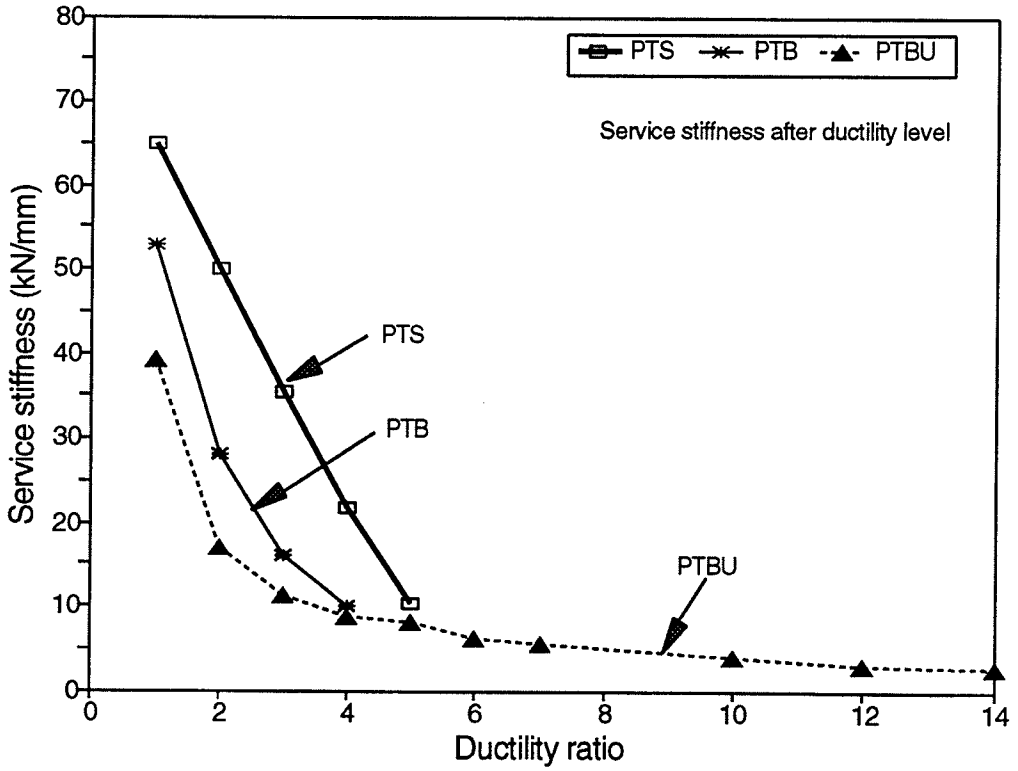

Figure 6.97(b) Comparison of service stiffness degradation for prestressed specimens

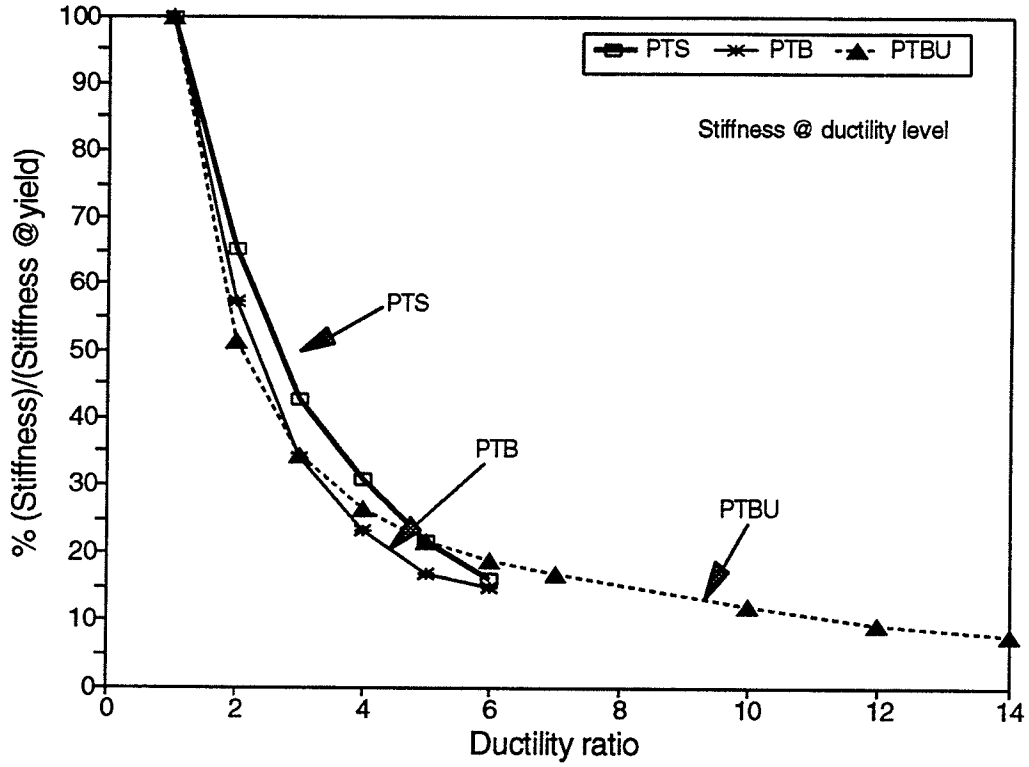

Figure 6.98(a) Comparison of % stiffness degradation for prestressed specimens

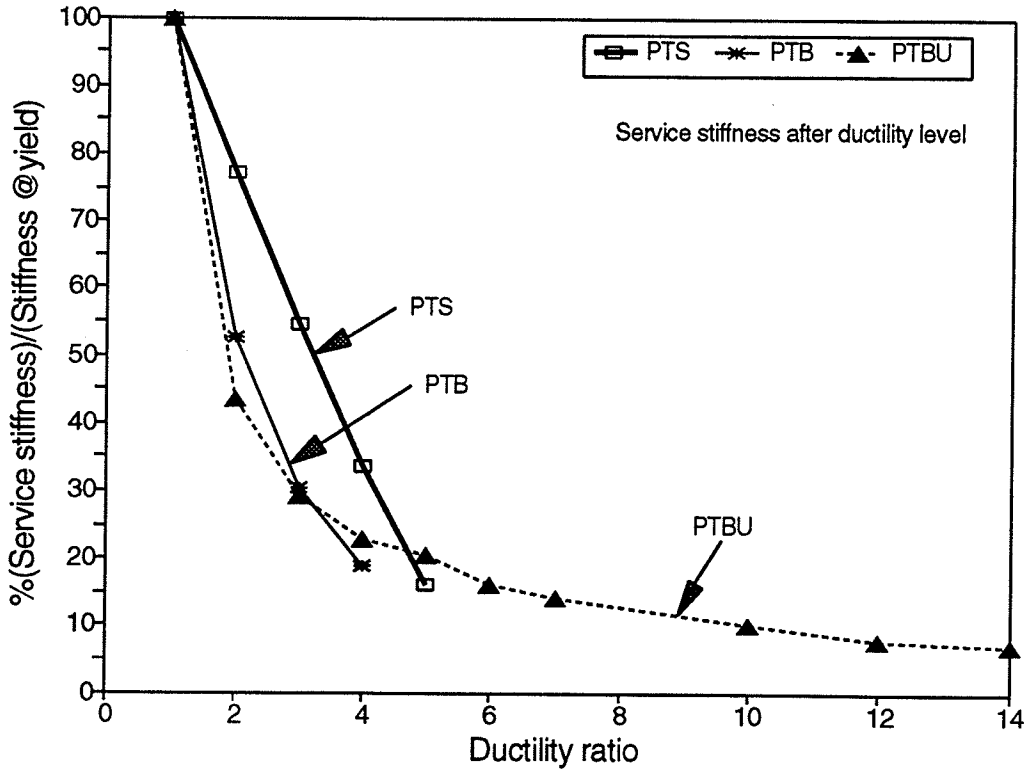

Figure 6.98(b) Comparison of % service stiffness degradation for prestressed specimen

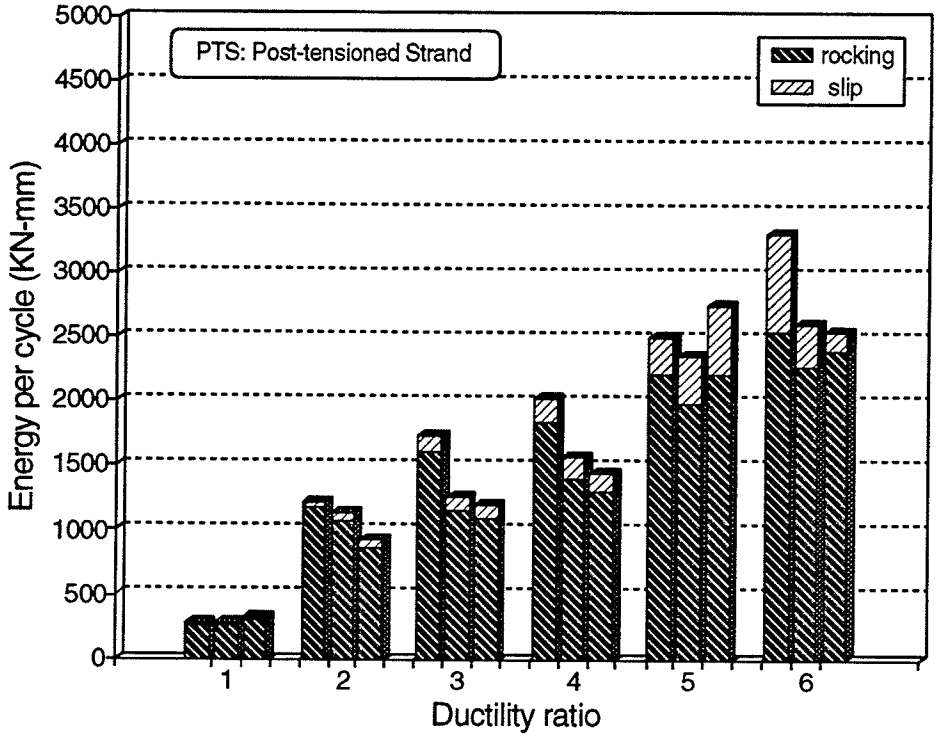

Figure 6.99(a) Per cycle energy dissipated by specimen PTS

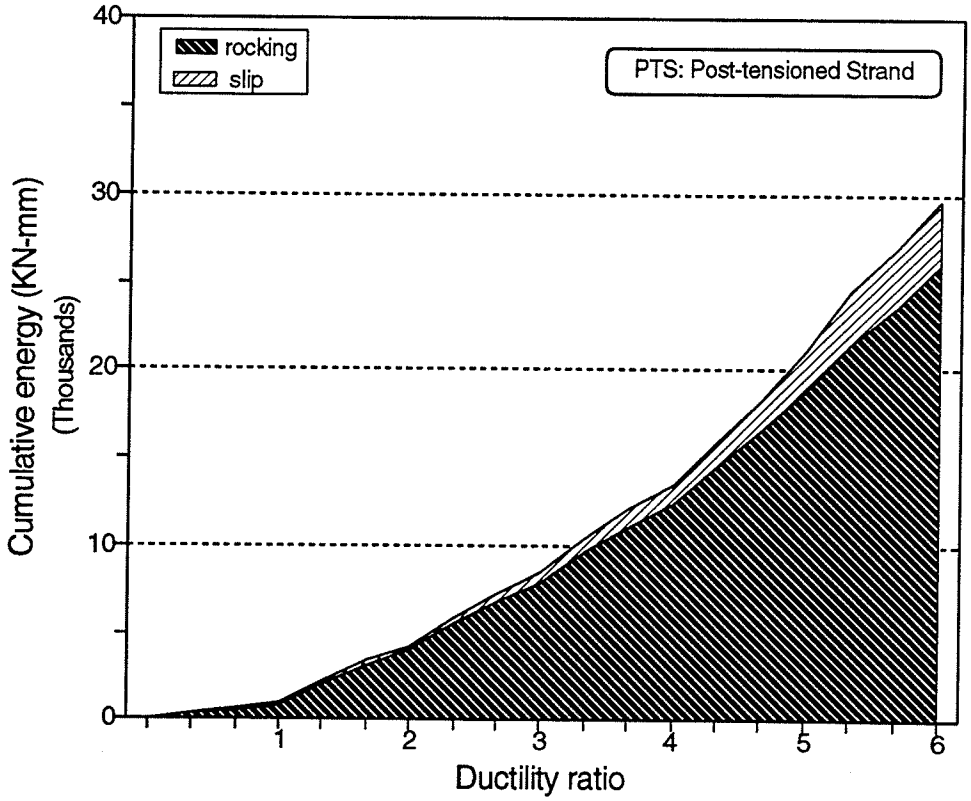

Figure 6.99(b) Cumulative energy dissipated by specimen PTS

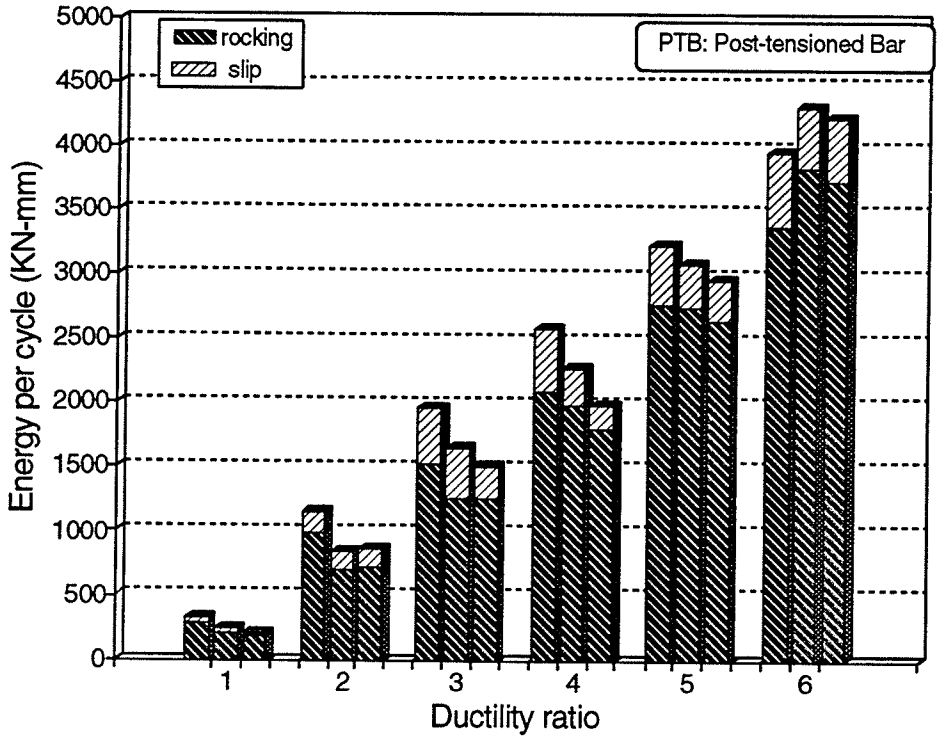

Figure 6.100(a) Per cycle energy dissipated by specimen PTB

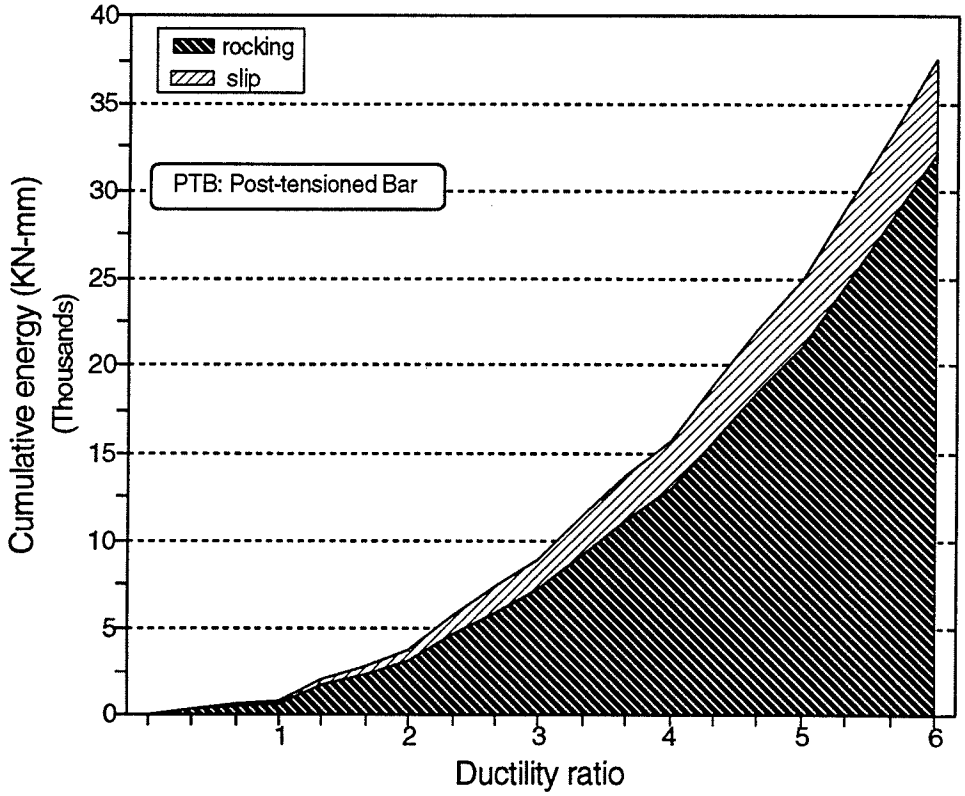

Figure 6.100(b) Cumulative energy dissipated by specimen PTB

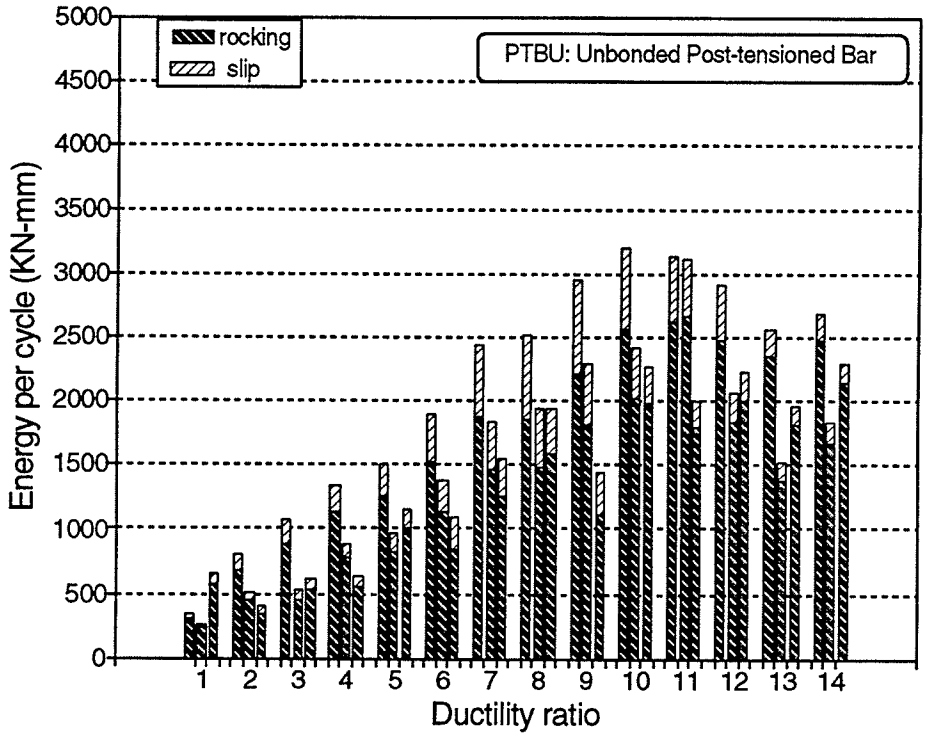

Figure 6.101(a) Per cycle energy dissipated by specimen PTBU

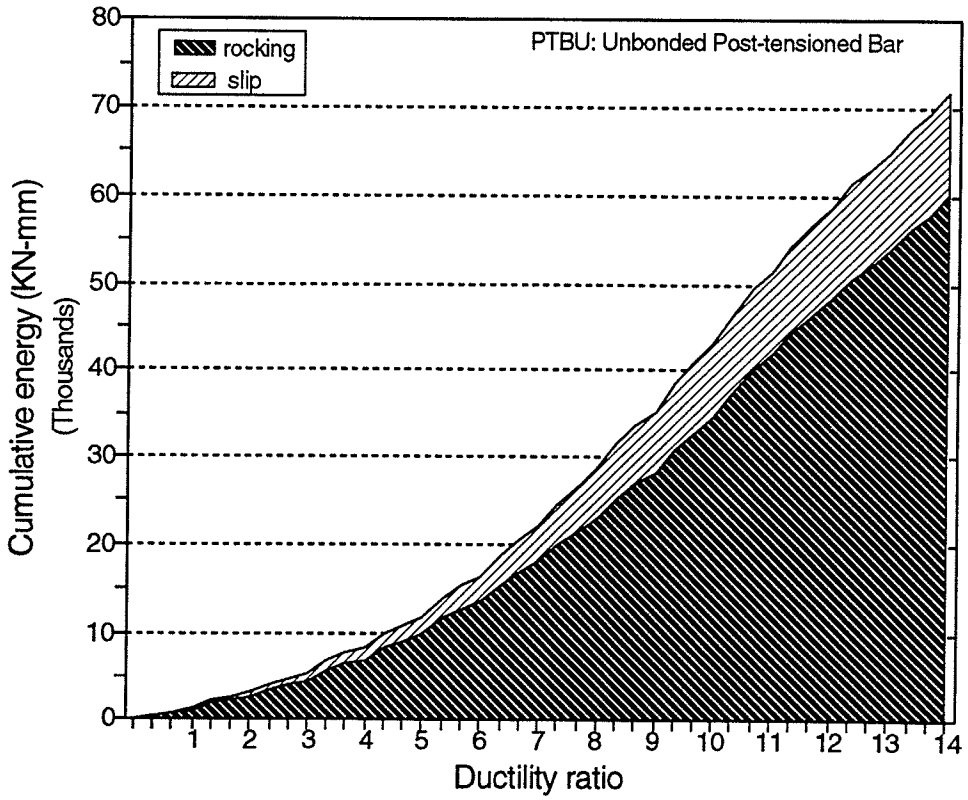

Figure 6.101(b) Cumulative energy dissipated by specimen PTBU

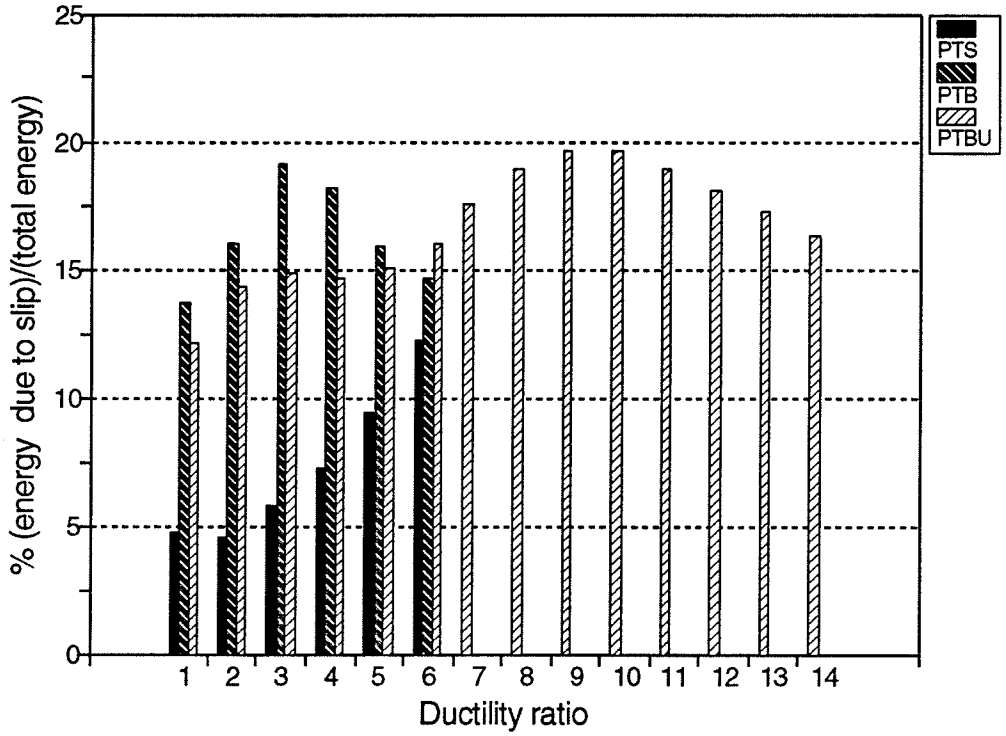

Figure 6.102 Percentage of energy due to slip to total energy for prestressed specimen

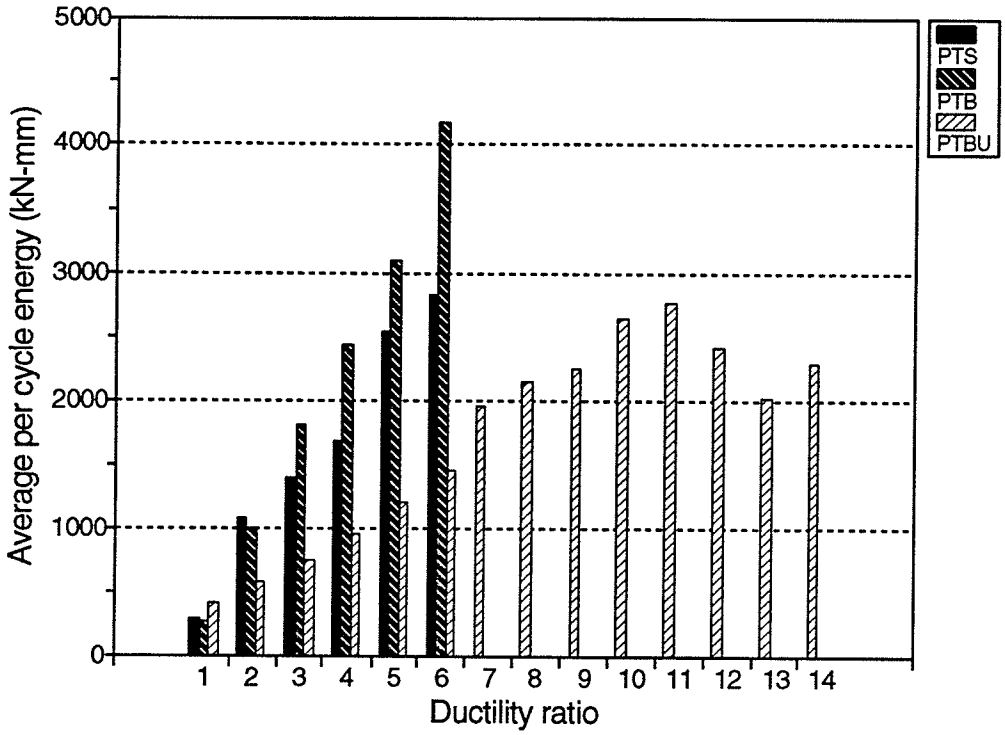

Figure 6.103 Comparison for average per cycle energy for prestressed specimen

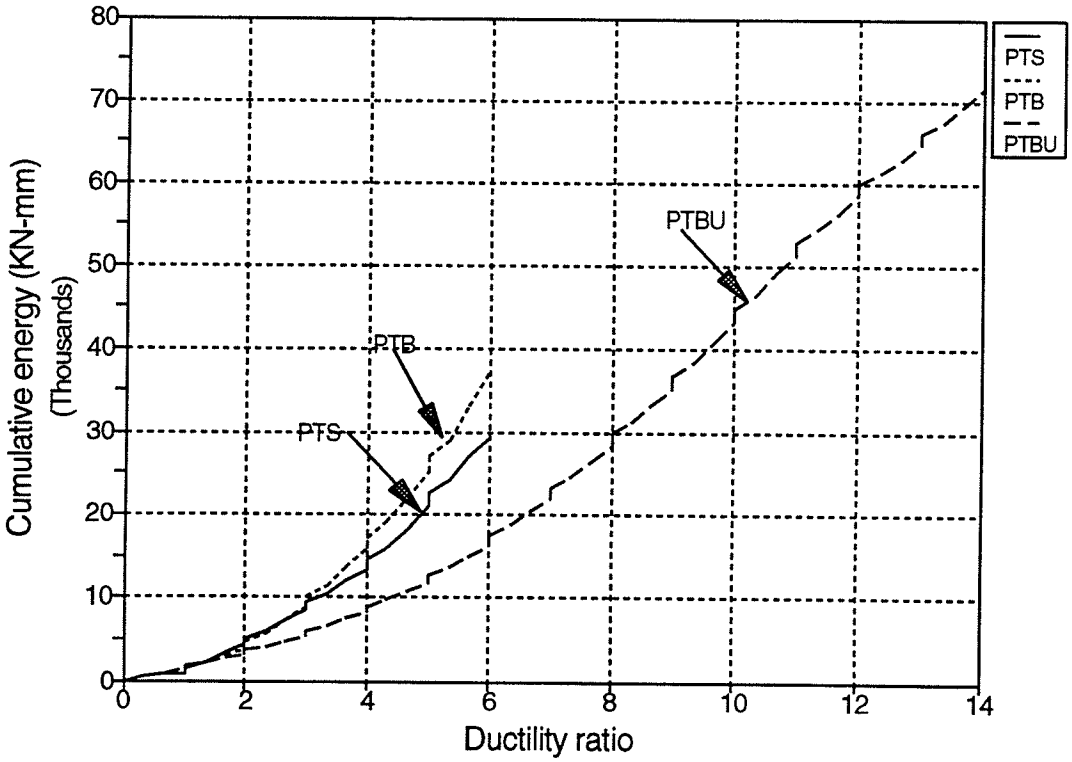

Figure 6.104 Comparison of cumulative energy dissipation for prestressed specimen

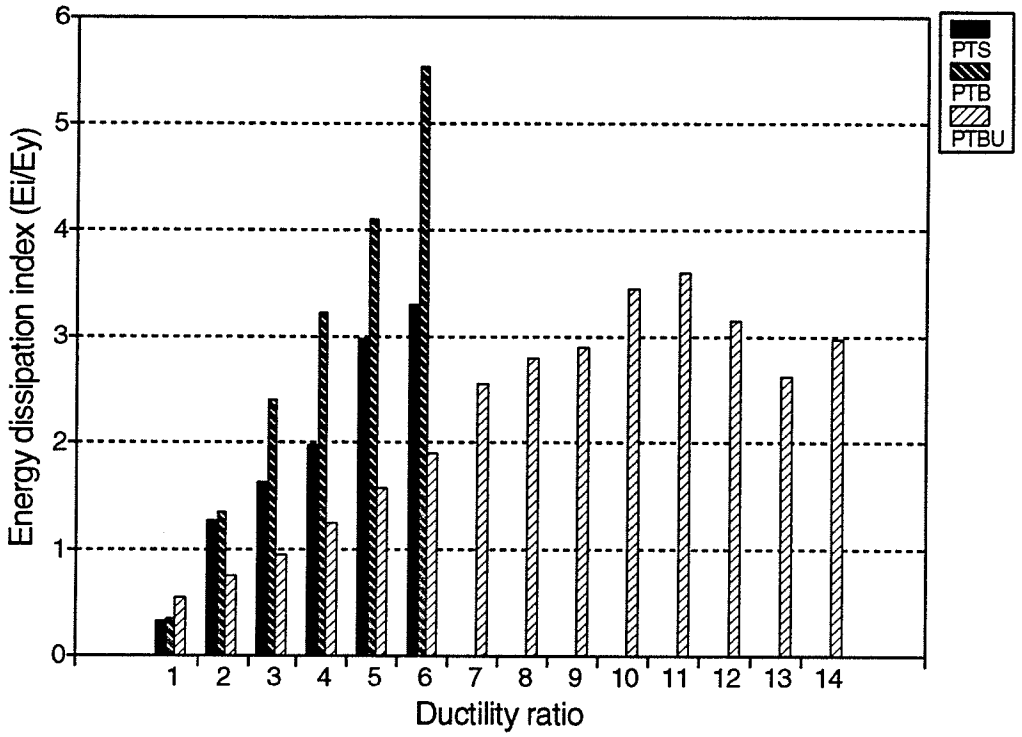

Figure 6.105 Per cycle energy dissipation index for prestressed specimen

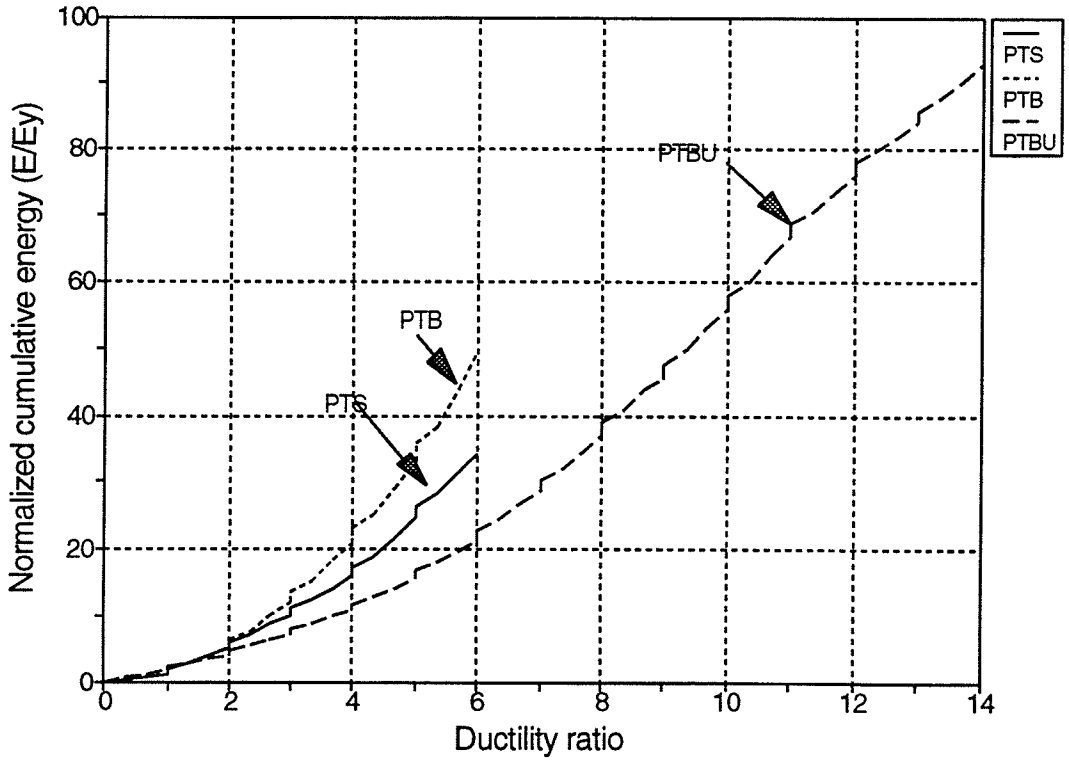

Figure 6.106 Cumulative energy dissipation Index for prestressed specimen

CHAPTER 7

RATIONALIZATION OF RESISTANCE MECHANISMS

7.1 INTRODUCTION

This chapter discusses the various response mechanisms presented in Chapters 5 and 6 for the different connection configurations considered in this experimental program. Section 7.2 characterizes the connection response in terms of the condition of loading:

(i) pure shear versus flexure/shear loading,

(ii) reversed cyclic loading,

Section 7.3 gives the effect of the different configurations on the connection response:

(i) effect of using shear keys versus plain surface,

(ii) effect of using mild steel versus prestressed reinforcement,

(iii) effect of using unbonded versus bonded reinforcement: full or partial,

(iv) effect of using welded versus sleeve connector for mild steel reinforcement,

(v) effect of using bolted to a tube versus sleeve for mild steel reinforcement,

(vi) effect of using prestressed bars versus prestressed strands

It should be noted that this investigation considered only one given condition of loading representative to the base connection of a 10-storey high building. Within the same structure, the behaviour of connections at intermediate levels may influence the overall response.

Section 7.4 presents a simplified design procedure to predict the envelope response of the connection due to reversed cyclic loading conditions. Section 7.5 gives prediction examples for the different configurations.

7.2 EFFECT OF LOADING CONDITIONS

7.2.1 Shear versus Flexure/Shear Loading

The experimental program included two different types of specimens. The first category consisted of connections subjected to pure shear loading tested by Mr. West and the author and was reported by West (1993) as summarized in Chapter 4. The second category consisted of connections subjected to flexure/shear loading as presented in Chapters 5 and 6. The shear loading was applied at the connection level and the flexural loading was selected to give a moment to shear ratio of 1.5 for the given connection length. While the geometry of the test specimens used for the two loading cases were different, the connection configuration was kept the same. This section discusses and compares three connection configurations tested for flexure/shear and shear loading conditions. These include plain surface connections connected by mild steel reinforcement, prestressed strands and prestressed bars. The flexural/shear response is compared to the shear response in terms of the load versus slip relationship and the crushing versus slip characteristic.

Figures 7.1 to 7.3 compare the envelope of load resistance-slip hysteresis response for connections with mild steel bars (RW), prestressed strands (PTS) and prestressed bars (PTB) under pure shear and combined flexure/shear loading conditions. In both cases of loading, the load-slip response was very stiff and elastic until onset of slip. The strength of the connection tested in combined loads was about 50% of the capacity for the pure shear loading condition. This behaviour was mainly due to the observed flexural failure mode without utilizing the full shear capacity of the connection. The slip magnitude at failure of the mild steel specimen RW in pure shear was very similar in magnitude to the combined flexure and shear specimen, as shown in Figure 7.1. On the other hand, slip of the connections with prestressed

reinforcement (strands or bars) subjected to combined flexure and shear was limited in comparison to identical specimens subjected to pure shear as shown in Figures 7.2 and 7.3. In general, the slip followed the load direction up to a certain level, beyond which there was permanent slip in one direction in spite of the application of reversed cyclic displacement at the top of the upper panel. This behaviour was possibly due to local shear deformation of the continuity reinforcement. The permanent slip was observed for the specimens with bars, mild steel (RW) or prestressed (PTB) and was not observed for the specimen with strands. In the pure shear specimens, slip was used to apply the loading and hence no permanent residual slip was measured.

As previously stipulated, the slip response was significantly dependent on the degree of deterioration due to drypack crushing. The more the deterioration, the higher the slip magnitude. The envelopes of crushing versus slip cyclic response for connections with mild steel bars (RW), prestressed strands (PTS) and prestressed bars (PTB) are given in Figures 7.4 to 7.6, respectively. The crushing-slip characteristic for combined flexure/shear and pure-shear specimens with mild steel reinforcement was very similar. This response was characterized by significant crushing and major slip for both loading conditions, as shown in Figure 7.4. The connection with prestressed strands subjected to cyclic combined flexure/shear versus pure shear had different response. The cyclic flexure/shear specimen had limited crushing and consequently limited slip, while the cyclic pure shear specimen had major crushing and slip as shown in Figure 7.5. The response of flexure/shear and shear specimens with prestressed bars, shown in Figure 7.6, followed the same trend as the specimen with mild steel bars. However, the crushing was major and the slip was moderate. The behaviour indicated, in general, that the response of the crushing-slip of the flexure/shear connection was lower than that of the pure shear connection.

The coefficient of friction for the connection subjected to combined flexure/shear was lower than that of the connection subjected to pure-shear loading. The lower coefficient of friction was possibly due to the difference in the normal strain distribution along the connection length between the two loading cases. In the pure-shear loading case, the normal strain was uniformly distributed along the length of the connection. In the combined flexure/shear loading, the normal strain distribution was triangular and the shear resistance was provided by the compression zone which represented a portion of the connection length. As a result, localized high strains in the compression zone caused much more severe degradation of the drypack and consequently may have reduced the coefficient of friction. The connection with mild steel reinforcement under pure shear, prior to significant degradation, had a coefficient of friction of 0.8. After severe degradation, the coefficient of friction was reduced to 0.6, which is 75% lost due to significant degradation from the cyclic loading. The same connection under combined flexure/shear had a coefficient of friction of about 0.5 mainly due to the triangular distribution. The coefficient of friction was 0.9 for the prestressed connection under pure-shear loading and 0.4 under combined flexure/shear loading. The coefficient of friction was determined in sections 6.3.4.3 and 6.4.4.4.

In conclusion, the shear resistance of the connection under combined flexure and shear loading was provided by the compression zone only and a reduced coefficient of friction. The connection under pure shear loading utilized the full connection length and hence had a higher resistance.

7.2.2 Reversed Cyclic Load

The most significant effect of the cyclic loading was the progressive deterioration of

the drypack. Drypack deterioration was obvious for all the connections tested under reversed cyclic pure shear and flexure/shear loading. In the case of pure shear specimens, the crushing was mainly due to the grinding action along the connection length. In the flexure/shear specimens, the deterioration occurred in the form of localized crushing in the compression zone due to cyclic flexural stresses followed by overall crushing along the connection length due to the grinding action. In both cases of loading, drypack crushing resulted in permanent reduction in the thickness of the drypack in the connection region.

Connection subjected to pure shear

West (1993) showed that the reversed cyclic loading did not affect the maximum shear strength of the connection subjected to pure shear loading since the measured resistance due to cyclic loading was very close to that measured in monotonic specimens. The connection under monotonic loading did not experience any reduction in the shear resistance over the same range of slip as the connection under cyclic loading. Test results suggested that the continuous grinding action of the cyclic shear load caused progressive crushing of the drypack grout and resulted in permanent thickness reduction of the connection region. As a consequence of the thickness reduction, the frictional resistance of the connection over the duration of loading was reduced. In the prestressed specimens, the thickness reduction also caused loss in the prestressing force and consequently reduced the frictional resistance.

Connection subjected to combined flexure/shear

The degree of deterioration due to cyclic loading varied depending on the type of connection configuration. All specimens with a plain-surface configuration had

moderate to major deterioration, connections with unbonded reinforcement had much more damage than connections with bonded reinforcement. The connection with shear keys had no damage since the keys remained intact at all load levels and damage concentrated at connection compression zone. No thickness reduction was noted in the shear-key configuration.

The reversed cyclic load had slight effect on the initial connection stiffness up to yielding. However, the deterioration in the drypack significantly affected the residual stiffness after cyclic load. All connection configurations had very similar stiffness degradation characteristic to cyclic load as shown in Figure 6.56 for the mild steel connections and Figure 6.97 for the prestressed connections. The degradation was characterized by a sharp decrease. The stiffness at failure was on average 20% of the stiffness at yield.

The maximum connection strength was not influenced by cyclic load. This was observed for connections with mild steel and prestressed strands or bars. Test results indicated that the response under the push and pull loading directions was slightly different and was within the range of 10%. This variation could be due to the progressive deterioration from cyclic loading between the push and pull directions.

Reversed cyclic loading significantly reduced the deformational capacity of the connection in comparison to identical connections tested under monotonic loading. For the mild steel specimens, the reduction of the ductility was from 9 to 5, as shown in Figure 6.20(e). For the prestressed connections, the deformational capacity dropped from 13 to 6 for specimens with bars as shown in Figure 6.73(c) and from 7 to 6 for specimens prestressed with strands as shown in Figure 6.73(d).

Therefore, the reversed cyclic loading introduced an additional limit state, not observed under monotonic loading conditions, in terms of severe degradation of the

drypack grout. This drypack deterioration caused a reduction in the connection deformation capacity and a degradation in the connection stiffness without significantly affecting the connection strength due to redistribution of stresses in the connection region following the severe deterioration.

7.3 EFFECT OF CONNECTION CONFIGURATION

7.3.1 Shear Keys versus Plain Surface Connection

The behaviour of the connection with shear keys was different from that of the plain surface connection. The presence of multiple shear keys across the connection significantly enhanced force-slip behaviour in comparison to plain surface connection.

According to West (1993), in the shear specimens, the maximum shear strength for the connection with shear keys was more than double the strength of the plain surface connection. This increased resistance was mainly because the shear force was transferred by direct bearing on the drypack within the shear keys. The load versus slip hysteresis loops were very narrow with the slip range limited to ±1 mm until cracking of the drypack within the keys occurred. The shear force-slip hysteresis loops for connection SK with shear keys tested under pure shear were shown in Figure 3.6. After cracking of the drypack within the shear keys, a uniform slip interface was formed along the length of the connection and the resistance was provided only by friction. The hysteresis loops, following cracking of the keys, were elasto-plastic and formed an unconfined mechanism. The ultimate resistance of the connection with shear keys was about 40% higher than that of the plain-surface connection due to the roughness of the interface surface of the cracked drypack. The increased shear resistance of the shear key connection versus the plain surface connections was mainly because of the different slip interfaces for the two connections. The interface in the

shear key connection consisted of a drypack-to-drypack region within the shear keys and a smooth concrete-to-drypack region, while the slip interface in the plain connection was a smooth concrete-to-drypack region.

For combined flexure/shear loading, the presence of shear keys prevented the extensive slip that occurred in the plain surface connections. The slip was limited at all ductility levels mainly because the shear resistance was by direct bearing on the drypack within the shear keys. The slip was limited to 6% of total deformation and the response was predominantly governed by flexural through rocking. The hysteresis loops of load versus slip were narrow and the slip was fully recoverable at zero displacement. Consequently, the hysteresis loops in the plain surface connection were wide and formed an irrecoverable mechanism.

In terms of damage, the connection with shear keys had no measurable thickness reduction along the connection length as the shear keys remained intact while crushing was concentrated at the extreme ends of the connection within the compression zone. The plain-surface connections, however, suffered overall thickness reduction due to crushing and spalling of the drypack grout along the connection length.

The initial stiffness was slightly influenced by the presence of shear keys along the connection and the stiffness degradation was similar in the two connection types.

The yield displacement of the shear key connection was slightly higher (about 5%) than that of the plain-surface connection. Also, the connection strength slightly increased due to the presence of the shear keys. However, the ultimate deformational capacity of the connection was reduced from 5Dy for the plain surface to 4Dy for the shear keys. The overall response of the two connection types was compared previously in Figure 6.20(c) in terms of strength envelope of load versus displacement.

The energy dissipation for the connection with shear keys was consistently 20% lower than the energy dissipation of the plain surface connection. This was to be expected, since the slip contribution to the energy for the shear keys connection was limited to 6% of the total energy dissipated as compared to 17% slip contribution to the energy in the plain surface connection.

In conclusion, the multiple shear key configuration was able to reduce the amount of slip without significantly affecting the overall response to cyclic loading.

7.3.2 Mild Steel versus Prestressed Reinforcement

The behaviour of connections with mild steel reinforcement was different from that of the prestressed connections. The behaviour was affected by the differences in the characteristic material properties of the mild steel versus prestressing reinforcement. However, the overall response for both types of configurations was similar.

Connection subjected to pure shear loading

For the mild steel connection subjected to pure shear, the shear resistance was transferred through a combination of Coulomb friction and dowel action of the mild steel bars. For connections prestressed by strands or bars, the resistance was provided mainly through coulomb friction. The prestressing stress increased the axial load normal to the connection and thus increased the shear resistance of the connection. The shape of the hysteresis loops varied depending on the reinforcement type. In the mild steel connection, the loops were parallelogram-shaped and the slip range was ±10 mm as shown in Figure 3.7. The connection with prestressed bar showed a similar response with slip range also at ±10 mm as shown in Figure 3.9. However, the connection with prestressing strands had elastic-perfectly plastic hysteresis loops and

the slip range was ±5 mm at onset of failure as shown in Figure 3.8. West (1993) attributed the lower slip range at failure for connections prestressed with strands to the lower ultimate strain in the material stress-strain characteristic of the strand. It was concluded that the significant drypack crushing at failure reduced the effective prestress level, causing a drop in the shear resistance.

Connection subjected to combined flexure/shear

The type of reinforcement, prestressed or mild steel, seems to have some effect on the deformational capacity of the connection. The deformational capacity was measured by the ultimate ductility. The mild steel specimen (RS) had a ductility of 5 while both prestressed specimens, with bars (PTB) or strands (PTS), had an ultimate ductility of 6. Thus, prestressing increased the ductility ratio by 20%. Figure 7.7 compares the envelope of cyclic load versus displacement hysteresis loops for these three specimens. The similarity in the overall response was very clear among mild steel specimen RS and prestressed specimens PTB and PTS.

The type of reinforcement had very little effect on the initial stiffness at yield, as seen in Figure 7.7. The stiffness was mainly dependent on the overall geometry of the connection and the material characteristic of the drypack within the connection region. The stiffness degradation was very similar for the connections with mild steel and prestressed reinforcement. Stiffness degradation was a function of the deterioration in the connection and exhibited a very sharp decrease in stiffness versus ductility.

The slip characteristic was very similar in specimens with bars, mild steel or prestressed. At failure, there was permanent slip in one direction mainly due to permanent local shear deformation of the bar at the connection level. In the specimen

prestressed by strands, no permanent slip was noted mainly because the flexibility of the strand inhibited any permanent deformation. Slip constituted a small percentage of the deformation and was limited to about 16% for the connection with mild steel bars, 12% for the connection prestressed by bars and 11% for the connection with prestressed strands.

Damage was mainly concentrated at the connection ends where the drypack was ground to powder. However, spread of damage over the entire connection length was limited. The thickness reduction of the drypack was about 5% in the mild steel specimen (RS) and 3% in prestressed specimen PTS. Thickness reduction was 16% in specimen PTB as degree of damage was more severe than the other two specimens.

The shape of the load-displacement hysteresis loops varied depending on the reinforcement type. The loops in the prestressed specimens were narrower than those in the mild steel specimens. Since the area inside the load-displacement loop represents the energy dissipated per cycle, it follows that the energy dissipation in the prestressed specimens was lower than in the mild steel specimen. This was mainly due to the inherently more ductile material characteristic of the mild steel versus the prestressing reinforcement. Figure 7.9 compares energy per cycle for the mild steel specimen and prestressed specimens with bars and strands. Figure 7.10 compares the cumulative energy dissipation of the three specimens. It was obvious that at any given ductility level, both prestressed specimens had very similar energy dissipation characteristic and that the mild steel specimen had the highest energy dissipation.

In conclusion, while prestressing could enhance ductility, the energy dissipation was significantly lower. Therefore, in using prestressed versus mild steel there is a trade-off between higher ductility and higher energy dissipation. Which system should be used depends on acceptance criteria and the designer's judgement.

7.3.3 Unbonded versus Bonded Reinforcement

Unbonding of reinforcement was a new approach for this type of connection in which the reinforcement was debonded from the surrounding concrete mainly to enhance performance characteristics for seismic zones. One mild steel specimen was partially unbonded by covering a given length of the reinforcing bar with plastic sheathing. The unbonded prestressed bar specimen was achieved by simply not grouting the ducts, thus producing fully unbonded prestressing.

The most significant observed effect of the unbonded reinforcement was the enhancement of the deformation capacity of the connection. The increased deformation capacity of the unbonded connection was given by its ability to reach higher displacement levels without significant loss in strength. For the mild steel connection, the deformational capacity almost doubled (1.8 times) with partial unbonding. In the connection prestressed with fully unbonded bars, the capacity more than doubled (2.33 times) relative to the bonded prestressed connection. It is worth noting that the yield displacement for the mild steel unbonded reinforcement was 50% higher than that for the bonded reinforcement. In the fully unbonded prestressed specimen, however, local yielding of bars did not occur and the yield displacement of the bonded prestressed specimen was used.

The strength of the connections seems to be only slightly affected by unbonding of the reinforcement. The strength of the unbonded specimens was slightly lower than that of the bonded specimens. The difference was about 5% for partially unbonded mild steel bars and 12% for fully unbonded prestressed bars. The strength reduction was mainly due to the extent of unbonding.

The stiffness at the yield of the connection with unbonded mild steel bars was 66% of that of the connection with bonded mild steel bars. Also, the initial stiffness

of the unbonded prestressed connection was 75% of the bonded one. However, the stiffness degradation of the unbonded specimens was very similar to that of the bonded specimens.

The hysteresis loops of cyclic load versus displacement were also affected by unbonding of the reinforcement. The hysteresis loops were slightly narrower in the unbonded mild steel specimen in comparison to those of the bonded specimen. For the specimen with fully unbonded prestressed bars, the loops were significantly narrower than for the bonded specimen. As a consequence of the narrow hysteresis loops, less energy was dissipated per cycle for a given displacement increment. However, since the unbonded specimens achieved higher deformational capacities, the cumulative energy dissipation was significantly higher for the unbonded specimens.

The degree of damage was much more severe in the unbonded specimens than in the bonded ones. Damage was not mainly concentrated at the connection ends as in the case of the bonded specimens, but was spread over the entire connection length of the drypack which was literally ground to powder. The thickness reduction was about 40% in the mild steel unbonded specimen (RSU) versus 6% in the bonded specimen (RS). The reduction in thickness was 60% in the unbonded prestressed specimen (PTBU) versus 16% for the bonded specimen PTB. This significant thickness reduction observed in the unbonded specimens was mainly because these connections achieved significantly higher deformations than the bonded ones.

Therefore, it seems that unbonding significantly enhances the deformational and cumulative-energy-dissipation capacities with slight reduction in the strength and stiffness quantities.

7.3.4 Mild Steel Reinforcement: Welded versus Splice Sleeve

The welded versus splice sleeve connection detail for coupling mild steel continuity reinforcement reflects typical Canadian, American and Japanese practice. Both configurations require skilled labourers to complete the connection. However, forming the splice sleeve connection requires less time than the welded detail. In the latter connection, weldable bars were used while nonweldable bars were used in the former. Both connection types showed very similar overall response characteristics in terms of stable hysteretic behaviour and ability to maintain peak resistance at large deformation levels. Failure was characterized by severe crushing of the drypack grout and was accompanied by rupture of the bar in the welded connection or bar pull out from the sleeve in the splice sleeve connection. The splice sleeve specimen (RS) failed at the third cycle of 5Dy by pull-out of the bar from the sleeve while the welded connection (RW) suffered severe drypack crushing and extensive slip with significant strength reduction at the 3rd cycle of 5Dy. Also, at this stage, local buckling of the mild steel reinforcement occurred. Therefore, both connections had the same ductility capacity of 5Dy. But the yield displacement for the welded connection (RW) was 17% higher than that of the splice sleeve connection (RS). Consequently the deformation capacity of the welded connection was 17% higher than that of the sleeve connection. The higher deformational capacity of the welded connection resulted in more severe drypack deterioration at onset of failure in comparison to the splice sleeve connection. The overall thickness reduction was moderate in the splice sleeve connection and was limited to 5% of initial thickness. While the welded connection had major thickness reduction in the order of 42% of initial thickness.

The strength of the splice sleeve connection (RS) was about 10% higher than that of the welded connection (RW). The stiffness at yield of the splice sleeve

connection (RS) was 25% higher than that of the welded connection (RW). The variation in strength and stiffness could be attributed to the characteristic material properties of the mild steel and the drypack used in the two specimens. The stiffness degradation was very similar in both connections and was characterized by a very sharp decrease versus ductility. The residual stiffness was limited to 20% of the stiffness at yield.

The slip characteristic was identical for both types of configurations. It seems that local shear deformation of the bar caused a permanent slip in one direction for both connection types. The extent of slip was in direct proportion to the degree of deterioration from cyclic loading. At 5Dy, the splice sleeve connection had a slip about 20% of the deformation while the welded connection had major slip about 40% of the deformation. This extensive slip of the RW connection was mainly because the welded angle connector was more flexible than the splice sleeve connector; hence more slip was expected. Extensive slip of the welded connection was in phase with the severe drypack deterioration which would have reduced coefficient of friction at the interface.

The energy dissipation for the welded connection was consistently 20% higher than the energy dissipation of the splice sleeve connection. This was mainly due to the higher yield displacement of the RW connection and thus the higher percent drift corresponding to a given ductility level.

Therefore, both the welded and splice sleeve connections exhibit similar behavioral characteristics and either connection could be used. The choice would depend on the availability of skilled labourers for completion of the connection type.

7.3.5 Mild Steel Reinforcement: Bolted versus Splice Sleeve

Coupling the continuity reinforcement by bolting to a hollow structural steel (HSS) tube section at the connection level was an alternative to the splice sleeve and welded connections. Such a connection would require less-skilled labour during the assembly stage. The integrity of the connection, however, significantly depends on the strength and deformation characteristic of the tube section. The tube section used in this study had a lower strength-deformation characteristic in comparison to the reinforcing bars. While the tube section was strong in tension, it was weak in compression. Also, as oriented in the specimen, the tube was weak in shear. The compression/shear resistance of the HSS tube was significantly enhanced by drypack grout inside the tube pockets which acted to confine the deformations in the tube. As soon as extensive drypack crushing occurs in the tube pockets, the tube fails in local buckling and shear deformation of its vertical walls at the connection region. This premature failure by local buckling and shear deformation was undesirable and should be prevented.

The deformational capacity of the tube connection (RT) was limited to a ductility of 4 since failure of the tube occurred at the 1st cycle of 5Dy. The splice sleeve connection had an ultimate ductility of 5Dy since failure occurred at the 3rd cycle of 5Dy due to pull-out of bar from the sleeve. The deformational capacity of the sleeve connection was 18% higher than that of the tube connection.

In both connection types, severe drypack crushing was concentrated at the extreme ends of the connection. For the tube connection, the drypack was crushed and spalled off inside the tube pocket, as well. The overall reduction in the thickness of the connection at onset of failure was limited to 5% of the initial thickness for the splice sleeve connection and 4% of the initial thickness for the connection with the tube.

The strength of the connection with the tube reached only 75% of the that of the splice sleeve connection. The lower strength was dependent on the geometry of the tube section and the characteristics of the material used. The stiffness at yield for the connection with the tube was 25% lower than that of the splice sleeve connection for the same reason.

The slip in the tube connection at onset of failure constituted about 14% of the total displacement. At this stage, the slip was symmetrical mainly because the flexibility of the tube vertical walls allowed symmetrical shear deformations at the connection region as the load was reversed. In the splice sleeve connection, permanent slip in one direction was measured due to the permanent dowel action of the bar. The maximum slip for the splice sleeve connection was also 14% of the total displacement.

The energy dissipation for the tube connection was consistently 30% lower than the energy dissipation of the splice sleeve connection. This was due mainly to the lower strength-deformation capacity associated with the tube connection. In fact, the tube connection had the lowest energy dissipation in comparison with the rest of the specimens.

Therefore, the specimen as designed with HSS tube section needs improvements to enhance its strength, deformational, and energy-dissipation capacity. As indicated above, the premature failure by local buckling and shear deformations is not desirable and should be prevented. One way to achieve this is to use thicker longitudinal walls and/or to close the tube end by a plate to enhance its shear/compression resistance.

7.3.6 Prestressed Reinforcement: Bars versus Strands

The test results indicate that the overall response of the connection with strands (PTS) was very similar to the connection with bars (PTB). Both connections had identical yield displacements. The stiffness at yield of the bar connection was nearly identical to that of the strand connection with a difference of only 6%. The deformation capacity of both connections was also the same with ultimate ductility of ratio of 6. Connection PTS maintained its peak resistance over a longer displacement range while connection PTB showed some reduction in load prior to ultimate deformation. The damage was more severe in connection PTB than connection PTS. The thickness reduction was 4% in PTS versus 16% in PTB. The significant reduction in PTB could be due to material characteristics or the lower initial prestrain in PTB versus PTS.

The strength of the connection with strands was 5% higher than that with bars. The increase in the strength could be due to the characteristic material property of the strands versus the bars.

The slip characteristic was different for the two connections. The connection with prestressed bars had a permanent slip due to local shear deformations of the bar at the connection level, while the slip followed the loading direction in the specimen prestressed with strands. The slip was in proportion to the extent of deterioration; it was 10.8% and 12.5% of displacement for connections PTS and PTB, respectively.

Connection PTB had consistently 30% higher energy dissipation per cycle relative to connection PTS mainly due to material characteristics and the higher contribution of slip to energy dissipation in the former connection.

Therefore, both connections with strands and bars exhibit similar characteristics in term of stiffness, strength, ductility and energy. While prestressed bars have higher energy dissipation, prestressed strands showed more favourable ductile behaviour.

7.4 RESPONSE PREDICTION MODELS

This section presents a simplified procedure to predict the strength and deformation behaviour of the connections for precast load-bearing shear walls based on the characteristic of the material used in the connection. The flexural strength of the connection strength was determined using conventional analysis based on equilibrium and compatibility conditions. The top deflection of the wall was estimated as the summation of slip and rocking deformation at the connection region. The slip component of the deformation was determined empirically from shear-slip test results and was expressed as a percentage of the total deformation. The rocking component of the deformation was determined based on the rotation at the connection interface.

The proposed methodology predicts the monotonic force deformation behaviour of the connection. The approach could be also used to predict the envelope curve for the hysteretic load deformation relationship with an allowance for the cyclic effect on the characteristic of the material.

7.4.1 Material Models

The horizontal connection investigated consisted of two precast concrete shear wall panels connected by a 20 mm drypacked grout region and reinforcement spaced at 900 mm on centres to provide the continuity. To be able to model the overall behaviour of the connection, proper modelling of the material is essential. The effect of reversed cyclic loading on the material characteristics should be also included to predict the behaviour of the connection under cyclic loading conditions.

7.4.1.1 Drypack

The uniaxial compression stress-strain characteristic of the drypack material was determined experimentally using 50x50x50 mm cubes. A correlation factor of 0.85 was used to determine the equivalent cylinder strength (CSA-A23.1-M90). Test results indicate that the material model for the compressive stress versus strain behaviour could follow a parabolic equation as shown in Figure 7.11:

$$f_g = f'_g \left[2\left(\frac{\varepsilon}{\varepsilon_{gu}}\right) - \left(\frac{\varepsilon}{\varepsilon_{gu}}\right)^2 \right] \qquad (7.1)$$

where f'_g = drypack compressive strength

ε_{gu} = drypack strain at maximum stress

= $2f'_g/E_g$

ε = drypack strain for a given drypack stress, f_g

Typical measured compressive cube strength of the drypack, f'_g, varies between 50 and 65 MPa. The ultimate strain, ε_{gu}, varies from 0.006 to 0.008 and the elastic modulus, E_g, varies from 8000 to 16,000 MPa.

7.4.1.2 Steel Reinforcement

Three different types of steel reinforcement were used to provide the continuity across the joint region between the two precast concrete shear wall panels. They included: 25.4 mm diameter mild steel reinforcement; 15 mm (5/8") diameter prestressing dywidag bar; and 12.7 mm (1/2") diameter prestressing strand. The tensile stress-strain characteristic of each reinforcement type was determined experimentally; the results were presented earlier in section 3.7 and are shown in Figure 7.12(a). In this section, stress-strain models based on the measured experimental data of the different

continuity reinforcement are presented.

Mild steel reinforcement

The mild steel continuity reinforcement used had a well-defined yield point and a strain-hardening region. The weldable (Grade 400W) bars had a long flat yield plateau while the non-weldable (Grade 400) bars had a very short plateau before the strain-hardening zone as shown in Figure 7.12(b). In general, the stress-strain characteristic of the mild steel reinforcement is elasto-plastic until strain hardening begins as shown in Figure 7.13. The stress-strain curve can be modelled as follows:

$$\begin{aligned} \varepsilon_s < \varepsilon_y \qquad & f_s = E_s\,\varepsilon_s \\ \varepsilon_y < \varepsilon_s < \varepsilon_{sh} \qquad & f_s = f_y \\ \varepsilon_{sh} < \varepsilon_s < \varepsilon_u \qquad & f_s = f_y[1 + A(\varepsilon_s - \varepsilon_{sh})^2 + B(\varepsilon_s - \varepsilon_{sh})] \le f_u \end{aligned} \tag{7.2}$$

where

E_s = Young's modulus

f_s = steel stress

f_y = yield stress of bar

f_u = ultimate tensile stress

ε_s = steel strain at steel stress

ε_{sh} = initial strain hardening

ε_u = ultimate strain

A,B = parameters defining the strain hardening region

Thus the stress-strain model for mild steel reinforcement can be completely defined by E_s, f_y, ε_y, ε_{sh}, f_u, ε_u, A and B. All the parameters can be determined from

the measured experimental stress-strain curve of the mild steel reinforcement. For the non-weldable bar, these properties were: E_s=200,000 MPa, f_y=400, f_u=700 MPa, ε_y =0.025, ε_{sh}= 0.005, ε_u=0.090, A=-0.078 and B=9.98. For the weldable bar, the properties were E_s=200,000 MPa, f_y=500, f_u=700 MPa, ε_y =0.025, ε_{sh}= 0.015, ε_u=0.105, A=-0.064 and B=6.64.

Prestressing Reinforcement

The stress-strain model used for the prestressed reinforcement, bars or strands, was based on a modified Ramberg-Osgood function (Mattock, 1979):

$$f_p = E_p \varepsilon_p \left\{ A + \frac{(1-A)}{[\,1 + (B\,\varepsilon_p)^C\,]^{1/C}} \right\} \leq f_{pu} \qquad (7.3)$$

where

f_p = stress in prestressing steel

E_p = Young's modulus

ε_p = strain in prestressing steel at stress f_p

f_{pu} = ultimate strength

ε_{pu}= ultimate strain

A,B,C = parameters defining the Ramberg-Osgood function

The function in equation 7.3 consists of two straight lines joined by a curve and is defined by four constants. These constants, E_p, A, B, C which can be determined from the measured stress-strain curve are illustrated in Figure 7.14. Typical measured properties of the prestressing dywidag bar were: E_p=205,000 MPa, f_{pu}=1140 MPa and ε_{pu}=0.070. The constants of the Ramberg-Osgood function were determined based on the measured stress-strain curve as A=0.024, B=0.224 and C=10. The prestressing

strand measured properties were: E_p=215,000 MPa, f_{pu}=1950 MPa and ε_{pu}=0.060. The Ramberg-Osgood constants were A=0.03, B=0.120 and C=10.

7.4.1.3 Failure Envelope for Drypack

The connection region was subjected to a multi-axial state of stress, namely, axial compressive stresses and shear stresses. The interaction between the compressive stresses and shear stresses would alter the material stress-strain characteristics of the drypack grout within the connection from the uniaxial compression case. The envelope follows the failure envelope developed by Bresler and Pister (1958) for concrete cylinders subjected to combined compression and torsion loading. The analogy between the state of stress in the test cylinders and the state of stress in the drypack within the connection region is shown in Figure 7.15. As seen in Figure 7.15, the similarity in the state of stress made it particularly possible to use their findings directly. Also, because the drypack grout and concrete were both cemenitious materials with very similar stress-strain characteristics under uniaxial compression, the behaviour of drypack under a multi-axial stress state would follow that of concrete. The results of the investigation by Bresler and Pister (1958), with the suggested failure envelope, are shown in Figure 7.16. This failure envelope represented the shear-compression interaction. It is evident that the compression strength of concrete could be greatly reduced by the presence of shear stresses. For a shear stress of about $0.2f'_c$, the concrete strength could be as low as $0.5f'_c$. The compression-shear interaction envelope used in this study is based on a parabolic envelope proposed by Llorente (1981) and provided a conservative fit for the measured data of Bresler and Pister (1958) as shown in Figure 7.16.

7.4.1.4 Cyclic Effect on Drypack

The behaviour of concrete under cyclic compressive loading was studied by Sinha, Gerstle and Tulin (1964) and by Karsan and Jirsa (1969). Their results indicated that the monotonic stress-strain curve represented the envelope of the cyclic stress-strain response as shown in Figure 7.17. Thus no modification to the stress-strain curve would be required when calculating flexural strength of concrete members subjected to stress reversals (Paulay and Priestley (1991). To date, no information has been reported on the behaviour of drypack grout under cyclic loading. However, since the drypack and concrete are both cemenitious materials and exhibit similar stress-stress characteristic under monotonic uniaxial compression, the drypack would have similar characteristic to those of concrete under cyclic loading. Thus it was assumed that the monotonic stress-strain curve could represent the envelope of the cyclic stress-strain response for the drypack grout.

7.4.1.5 Cyclic Effect on Reinforcing Steel

The stress-strain characteristic of mild steel reinforcement under cyclic reversed (tension-compression) loading is significantly affected by the loading history. The results of two different types of cyclic testing of mild steel reinforcement are shown in Figures 7.18(a) and (b) as reported by Paulay and Priestley (1991). In Figure 7.18(a), the cyclic inelastic excursions are in the tensile range, typical of a beam plastic hinge region. Figure 7.18(b) shows symmetric cyclic inelastic excursions in tension and compression, typical of columns with moderate to high axial loads. In general, once material yielding occurs in one direction, the subsequent reverse loading becomes nonlinear at a stress much lower than the initial yield stress as shown in Figure 7.18. This phenomenon is known as the Bauschinger effect. An idealization

of the reversed cyclic stress-strain response based on experimental data was proposed by Kato, Akiyama and Yamanouchi (1973). In their model, the cyclic response is determined from the monotonic curves for tension and compression as illustrated in Figure 7.19. It is evident from Figure 7.19(c) that the envelope of the cyclic response is almost identical to the monotonic curve. The only difference exists at the initial part of the curve in compression, which is curved due to the Bauschinger effect. Kato et al (1973) represented the softened part by hyperbolas. Kent and Park (1973) used Ramberg-Osgood functions to represent the softened parts of the stress-strain curve. It follows that even though the reversed stress-strain curve is different from the monotonic curve, the latter provides an envelope to the cyclic response. The reversed cyclic loading, however, limits the strain to about 50% of the measured ultimate strain of monotonic tension tests. Rupture strains in the range of 0.04 to 0.06 were measured for steel reinforcement under reversed cyclic loading compared to 0.105 obtained for the monotonic response.

Reversed cyclic loading could cause the loss of prestressing force in prestressing steel reinforcement; then the behaviour of the prestressed bar would become as for a non-prestressed bar. Thus, again it was assumed that the monotonic stress-strain curve would provide the envelope of the cyclic response.

7.4.2 Flexural Strength of the Connection

The wall subassemblage in this program can be treated as a cantilever reinforced concrete wall with a known crack location at the connection level. The wall is subjected to an axial vertical load normal to the connection and to a lateral horizontal load parallel to the connection applied eccentrically to produce a moment-to-shear ratio, M/VL, of 1.5 for the connection length, L. The connection region is subjected to shear force, bending moment, and axial load acting concurrently. The equilibrium of forces at the connection, as shown in Figure 7.20, should satisfy the following:

$$V_g + \Sigma V_s = P \tag{7.4}$$

$$C_g + C_s - T_s = N \tag{7.5}$$

$$C_g (L/2 - \beta c) + \frac{1}{2}(C_s + T_s)(d-d') = P H \tag{7.6}$$

where P = connection strength

N = applied axial load

V_g= shear resistance due to drypack grout

V_s= shear resistance due to continuity reinforcement

C_g= drypack grout compression force

C_s= compression force in steel

T_s= tension force in steel

c = depth of compression zone

β= equivalent stress block factor

d = distance from extreme compression fibre to tension steel

d′= distance from extreme compression fibre to compression steel

and d′ + d = L

Since the tested specimens were subjected to an M/VL ratio of 1.5, the strength of the connection was predominantly flexural and can be determined from the solution of equations (7.5) and (7.6) using the strain compatibility condition which would give the moment-curvature relationship at the joint region. The analysis procedure follows conventional methods and may be outlined as follows:

1. The strain in the tension steel continuity reinforcement is assumed.
2. The depth of neutral axis, c, is assumed.
3. The extreme fibre strain in the drypack and the compression steel strain are determined using compatibility relations. In case of a prestressed section, the strain increment used in compatibility is the total strain at any given time minus the initial pre-tension strain due to prestressing.
4. The total tension and compression forces acting in the section are computed.
5. If the tension and compression forces are not in equilibrium, the location of the neutral axis is adjusted until the desired axial load is reached with a specified tolerance limit (repeat steps 1-5).
6. The drypack compression stress at the extreme fibre is determined from the drypack material stress-strain relationship. For $\varepsilon_g > \varepsilon_{gu}$, the drypack stress is assumed zero, i.e., completely crushed.
7. The average shear stress in the compression zone is computed as the ratio of the applied shear load to the compression zone area.
8. The compression strength is reduced by the compression-shear interaction envelope using the shear stress.
9. Re-calculate the forces (step # 4) based on the modified extreme compression stress and reiterate (repeat steps 1-6), if necessary.

The above algorithm was implemented into a spreadsheet computer program to solve for the moment-curvature relationship at a section. The algorithm was capable of accounting for the complete stress-strain relationship for steel and the nonlinear stress-strain relationship for the drypack grout and to model the progressive drypack crushing and spalling within the compression zone, assumed to occur when the drypack strain reached its ultimate. The compression shear interaction envelope proposed earlier was also incorporated in the spreadsheet. Using this procedure, the moment and curvature at a section were determined for any given drypack strain.

Equation (7.4) gives the contribution of the different components of the connection to the shear resistance mechanism. V_d represents the contribution of the drypack through a Coulomb-type friction as a function of the coefficient of friction and the drypack compressive force. V_s represents the contribution from the steel reinforcement crossing the joint through dowel action or clamping force, which would be activated only when appreciable slip occurs.

7.4.3 Connection Deformation

Because of the inherently low stiffness of the drypacked joint compared to the precast wall panels, the top wall panel will rotate in an almost rigid-body motion about the joint interface. All the deformation will concentrate in the vicinity of the joint region and therefore the flexural and shear deformations in the panels can be neglected. The deflection at the top of the upper wall panel can be estimated as a combination of a slip and a rocking component at the joint region, as shown in Figure 7.21, as follows:

$$D = D_s + D_r \tag{7.7}$$

where

D_s = slip deformation

D_r = rocking deformation

At this stage it is difficult to quantify the magnitude of the slip deformation as reported in the pure shear experimental program (West, 1993). The test results indicated that the shear–force—shear–slip relationship was an unconfined elasto-plastic mechanism. The nature of slip deformation conformed with the findings of Mueller (1981) and Oliva (1991). Thus the slip could only be represented as a percentage of given deformation. For the current experimental program, with M/VL = 1.5, it was found that the slip varied from 6 to 20 percent of the total deformation. The variation was a function of the condition of interface and continuity reinforcement.

The flexural deformation can be determined based on the extension of the continuity reinforcement as will be discussed in the following section.

7.4.4 Flexural Deformation Based on Bar Extension

The flexural deformation, D_f can be evaluated in terms of a concentrated joint rotation as follows:

$$D_r = \theta \times H \tag{7.8}$$

where

θ = concentrated rotation at the joint interface

H = the wall height from the connection level, mm

The rotation at the joint, θ, in Figure 7.22, is significantly dependent on the extension of the continuity reinforcement in the top and bottom wall panels on either side of the soft drypacked joint. The rotation of the joint, θ, can be evaluated as:

$$\theta = \frac{\delta_s}{(d-c)} \tag{7.9}$$

where,

d = effective depth from extreme fibre of the compression zone to tension steel

c = neutral axis depth from flexural analysis

δ_s= extension of steel reinforcement in wall panels on either side of the joint

Calculation of the deformations from rotations of elements between cracks rather than from curvatures at a section was proposed by Bachman in 1970. This method is particulary suitable for the precast wall subassemblage studied due to the presence of a pre-cracked section at the joint region. The method is based on proper estimation of the bar extension in the concrete panels. The following subsection discusses evaluation of the bar extension on the basis of bond.

7.4.4.1 Extension of Reinforcement

Extension of steel reinforcement across the joint is based on the accumulation of strain along the length of the bar in the top and bottom wall panels on either side of the joint. Thus, to calculate elongation of the steel reinforcement, the bond characteristics and the stress-strain curve must be known. In general, a reinforcement bar of diameter d_b embedded in concrete over a length dx and subjected to a tension force, ΔF_s, will develop the tension force by bond as follows:

$$\Delta F_s = \frac{df_s \, \pi \, d_b^2}{4} = u \, \pi \, d_b \, dx \qquad (7.10a)$$

Therefore, length dx can be estimated as:

$$dx = \frac{df_s \, d_b}{4u} \qquad (7.10b)$$

where u = bond stress

The bond strength, u, is a function of the distance along the embedment length, dx. The elongation of the bar, ds, can be estimated as follows:

$$ds = \varepsilon_s \, dx$$

$$ds = \varepsilon_s \, \frac{df_s \, d_b}{4 \, u} \qquad (7.11)$$

The total elongation δ_s over the length of the bar is then found as:

$$\delta_s = \int ds = \frac{d_b}{4} \int \frac{\varepsilon_s \, df_s}{u} \qquad (7.12)$$

This equation indicates that the extension of the steel reinforcement is a function of the constitutive model for bond stress (u), steel stress (f_s) and strain (ε_s). Numerical procedures for the integration of equation (7.12) have been developed by several researchers; however, the computational effort involved limits their application. A simple method to determining the bar extension of mild steel reinforcement was reported by Alsiwat and Saatcioglu (1992). It was stipulated that an embedded bar in tension develops elastic and plastic regions, as shown in Figure 7.23.

The elastic region defines the limit over which the stresses in the bar are elastic. Within the elastic region the strain distribution varies linearly from zero up to the yield strain. The plastic region is the region where the bar is stressed beyond the strain-hardening range. The strain distribution in the plastic region is parabolic between the yield strain and maximum strain as given by Park and Paulay (1975). The length of the elastic or plastic region depends on the bond stress within that region.

The bond stress, u_e, of the bar in the elastic zone depends mainly on the bar size and the concrete compressive strength. The development length equations in the current ACI code for mild steel bars were derived based on assuming a steel stress of $1.25f_y$ at the critical section and the following bond equation (French, et al, 1992):

$$u_e = 16\frac{\sqrt{f'_c}}{d_b} \tag{7.13}$$

where

$f'c$ = uniaxial compressive strength of concrete, MPa

d_b = bar diameter, mm

The frictional bond stress, u_f in the plastic region, for mild steel bars in concrete has been researched extensively by Pochanart and Harmon (1989) and is

given by the following expression:

$$u_f = (5.5 - 0.07 \frac{S}{H}) \sqrt{\frac{f'_c}{28}} \quad (MPa) \tag{7.14}$$

where

S = clear spacing of lugs in the bar, mm

H = height of lugs in the bar, mm

The equations given above for the bond strength were proposed for mild steel with yield strength of 400 MPa. The same equations could be used for prestressed bars with a multiplier ($400/f_{py}$) to account for the higher yield strength of the prestressed bars as recommended by ACI (1989).

With regards to prestressing strands, Collins and Mitchell (1987) reported that the bond stress varies between 2 MPa to 5 MPa. The bond stress of the prestressed strands was taken as 3.5 MPa based on average of the two bond stress values. The frictional bond stress was also taken equal to the elastic bond stress because the bond stresses of the prestressed bars were transferred in grout and not in concrete.

Once the bond stress is found, the length of the elastic region, l_e, can be determined using equation (7.15). In this region, the stress increment, Δf_s, is set equal to the yield stress f_y. The plastic zone length, l_p, also can be determined using equation (7.15) with the incremental stress Δf_s, given as the difference between the steel stress at the current loading stage and the yield stress. Therefore, the length of the elastic (l_e) or plastic region (l_p) can be determined as follows:

$$l = \frac{\Delta f_s \, d_b}{4 \, u} \tag{7.15}$$

where

Δf_s = the steel stress increment

u = bond stress based on bond-slip tests

Once the strain distribution over the embedment length of the bar is known, the extension of the bar δ_s can be determined by integration of the strains on both sides of the connection region. The bar extension is expressed as twice the area under the strain diagram of Figure 7.23 to account for bar straining on both sides of the connection. Several cases for calculation of the bar extension are explained below.

(1) mild steel connection with fully bonded reinforcement:

$$\delta_s = 2\left\{ \frac{1}{2}\varepsilon_y l_e + \varepsilon_y l_p + \frac{1}{3}(\varepsilon_p - \varepsilon_y) l_p \right\} \qquad (7.16a)$$

(2) mild steel connection with reinforcement unbonded for a length l_u:

$$\delta_s = \varepsilon_p l_u + 2\left\{ \frac{1}{2}\varepsilon_y l_e + \varepsilon_y l_p + \frac{1}{3}(\varepsilon_p - \varepsilon_y) l_p \right\} \qquad (7.16b)$$

(3) prestressed connection with initial prestrain of ε_{pe}:

$$\delta_s = 2\left\{ \frac{1}{2}(\varepsilon_{py} - \varepsilon_{pe}) l_e + (\varepsilon_{py} - \varepsilon_{pe}) l_p + \frac{1}{3}(\varepsilon_{pu} - \varepsilon_{py}) l_p \right\} \qquad (7.16c)$$

(4) prestressed connection with reinforcement fully unbonded over length l_u and with initial prestrain of ε_{pe}:

$$\delta_s = l_u(\varepsilon_{ps} - \varepsilon_{pe}) \qquad (7.16d)$$

After determining the bar extension, the joint rotation is evaluated using equation (7.9) and the flexural deformation is the determined by equation (7.8).

7.5 PREDICTION OF TESTED CONNECTIONS

This section presents examples following the design procedure proposed in section 7.4 for prediction of the strength and deformation capacity of the connection for the precast shear wall system in this program. The examples focus only on the connections subjected to cyclic loading conditions. The connection geometry and configuration are identical to those tested in this program. The connection is 1200 mm long and 150 mm wide with a 20 mm drypacked thickness between two precast concrete wall panels. The prediction determines the movement of the upper panel relative to the lower one. The example simulates a connection at the ground level of a ten-storey-high precast building. The effect of upper storeys on the connection is simulated as an equivalent stress applied normal to the connection. The magnitude of the normal stress is 2 MPa. The horizontal load on the top panel is assumed to be applied at a height of 1800 mm above the connection region; thus achieving a moment-to-shear ratio is 1.5 for the given connection length.

The proposed methodology allows prediction of the strength and deformation capacity at different stages of connection response. The response at yield and ultimate conditions are emphasized in the example problems. The response at yield corresponds to local yielding of the continuity reinforcement at the connection level while ultimate strength corresponds to development of strain in the reinforcement equal to the ultimate strain of the material. After determining the response at yield and ultimate condition, other stages are determined and the overall predicted response is compared to the measured response for the test specimen similar to the example.

For all the examples, the connection parameters can be summarized as follows:

L = 1200 mm	connection length
b = 152 mm	connection width
t = 20 mm	connection thickness
H = 1800 mm	height of top panel from the connection region which represents the eccentricity of applied horizontal load from the connection region in the test specimen
d = 1050 mm	distance from tension steel to extreme compression fibre along the length of the connection
d′ = 150 mm	distance from compression steel to extreme compression fibre along the length of the connection
d-d′ = 900 mm o/c	spacing between continuity bars
σ_n = 2MPa	stress normal to the connection
P = variable	horizontal shear load applied at an eccentricity H, from the connection region
D = variable	horizontal deformation at the top of the upper panel (at a distance H above the connection region)

7.5.1 Connections with Mild Steel Reinforcement

For the mild steel connections tested, with the exception of specimen RT, the continuity between the two panels was provided by two 25.4 mm diameter, Grade 400 MPa, mild steel reinforcing bars spaced at 900 mm on centres.

The characteristic properties of the different materials used in the connections tested are given in section 7.4.1. The material properties used in the prediction are based on test results and are as follows:

Concrete

cylinder compressive strength, $f'_c = 48$ MPa

(based on average of 5 casts)

Drypack

cube compressive strength, $f''_g = 50$ to 60 MPa

cylinder compressive strength, $f'_g = 0.85 \times f''_g$

modulus of elasticity, $E_g = 10{,}000$ MPa

ultimate drypack strain, $\varepsilon_{gu} = 0.006$

The material characteristic of the drypack grout is parabolic as discussed in section 7.4.1.1 and given by equation 7.1.

Mild steel: 25.4 mm Grade 400 (non weldable bars)

area of one bar, $A_s = 500$ mm^2

yield strength, $f_y = 400$ MPa

yield strain, $\varepsilon_y = 0.23\%$

Young's modulus, $E_s = 200{,}000$ MPa

ultimate strength, $f_u = 700$ MPa

strain at ultimate (monotonic), $\varepsilon_u = 9\%$

(tested under monotonic loading condition)

ultimate strain (reversed cyclic), $\varepsilon_u = 3.6\%$

(due to reversed cyclic loading condition)

The measured ultimate strain of the mild steel bar in this experimental program, under reversed cyclic loading appears to be limited to about 40% of the uniaxial tension strain under monotonic loading. This is similar to the findings of Paulay and Priestley (1993) and Hawkins, Lin and Ueda (1987).

7.5.1.1 Mild steel connection with bonded reinforcement

Response at yield

For a yield strain, ε_y, of 0.23%, the procedure described in section 7.4 converged to a compression zone depth of 375 mm and horizontal load of 200 kN. The measured load for specimen RS at yield was 220 kN. The ratio of the predicted to measured was 91 percent.

The deformation at yield was determined following the procedure described in section 7.4.3. The distribution of strain along the bar was assumed to be linear and extended to a distance l_e along the bar on either side of the connection region. Length l_e was determined using equation 7.15 as follows:

$$l_e = \frac{f_y \cdot d_b}{4 \cdot u_e} = \frac{(400\ MPa) * (25.4\ mm)}{4 * (4.36\ MPa)} = 582\ mm$$

with u_e was determined using equation 7.13:

$$u_e = 16\frac{\sqrt{f'_c}}{d_b} = 16\ \frac{\sqrt{(48\ MPa)}}{(25.4\ mm)} = 4.36\ MPa$$

The extension of the bar on both sides of the connection, δ_s, was determined by integrating the strain along the bar development length on either side of the joint using equation 7.16 as follows:

$$\delta_s = 2\ \{\ \frac{1}{2}\ \varepsilon_y * l_e\ \} = 2\ \{\ \frac{1}{2}\ (0.23\%) * (582)\ \} = 1.34\ mm$$

The rotation of the joint, θ, due to the bar extension was evaluated using equation 7.9 as follows:

$$\theta = \frac{\delta_s}{(d-c)} = \frac{1.34\ mm}{(1050\ mm - 375\ mm)} = 0.002$$

The flexural deformation, D_r could be evaluated using equation 7.8 as follows:

$$D_r = \theta \times H = 0.002 \times 1800 \text{ mm} = 3.6 \text{ mm}$$

Response at ultimate

As mentioned earlier, the reversed cyclic loading limited the strain at ultimate to 40% of the ultimate strain measured in uniaxial tension test. Therefore, at ultimate strain, of 3.6%, the analysis converged to a compression zone depth of 235 mm and a horizontal load of 247 kN.

The deformation at ultimate was determined following the procedure of section 7.4.3. As shown in Figure 7.23 the bar developed elastic and plastic zones. The elastic zone extended a distance l_e in which the strain distribution was linear up to the yield strain. Distance l_e was determined as 582 mm. The length of the plastic region l_p was determined using equation 7.15 with Δf_s expressed as the difference between the ultimate strength and the yield strength. Distance l_p was based on the frictional bond stress u_f which was given in equation 7.14 as follows:

$$u_f = (5.5 - 0.07 \frac{S}{H}) \sqrt{\frac{f_c'}{28}}$$

$$= (5.5 - 0.07 \frac{8}{2}) \sqrt{\frac{48}{28}} = 6.83\ MPa$$

Distance l_p was determined using equation 7.15 as follows:

$$l_p = \frac{\Delta f_s \cdot d_b}{4 \cdot u_f} = \frac{(615MPa - 400MPa) * (25.4\ mm)}{4 * (6.83\ MPa)} = 200\ mm$$

The extension of the bar on both sides of the connection, δ_s, was determined by using equation 7.16 as follows:

$$\delta_s = 2\ \{\ 1/2\ \varepsilon_y \times l_e + \varepsilon_y \times l_p + 1/3\ (\varepsilon_u - \varepsilon_y)(l_p)\ \}$$

$$= 2\ \{\ 1/2(0.0023)(582) + (0.0023)(200) + 1/3(0.036\text{-}0.0023)(200)\ \}$$

$$= 6.75\ \text{mm}$$

The concentrated rotation of the joint, θ, was evaluated using equation 7.8 as:

$$\theta = \frac{\delta_s}{(d-c)} = \frac{6.75\ mm}{(1050\ mm - 235\ mm)} = 0.0083$$

The flexural deformation, D_r was determined as:

$$D_r = \theta \times H = 0.0083 \times (1800) = 15\ \text{mm}$$

The complete predicted strength-flexural deformation response was compared to the flexural response of specimen RS and RSK in Figures 7.24(a) and 7.24(b), respectively. The agreement between the predicted and measured response is good.

7.5.1.2 Mild steel connection with partially unbonded reinforcement

The reinforcement was unbonded for a length l_u of 600 mm above the connection region in the mild steel unbonded connection.

Response at yield

At the yield strain of 0.23%, the analysis converged at a compression zone length of 375 mm and a load of 200 kN. The measured yield strength was 210 kN, which was excellent agreement.

The extension of the bar, δ_s, was determined as follows:

$$\delta_s = 2\{\, 1/2\varepsilon_y \times l_e \,\} + (\varepsilon_y)(l_u)$$

$$= 2\{\ 1/2(0.0023)(582\text{mm})\ \} + (0.0023)(600\text{mm})$$

$$= 2.71 \text{ mm}$$

The joint rotation, θ was determined using equation 7.8 as:

$$\theta = \frac{\delta_s}{(d-c)} = \frac{2.72\ mm}{(1050\ mm - 375\ mm)} = 0.004$$

The flexural deformation, D_r was evaluated as follows:

$$D_r = \theta \times H = .0040 \times (1800) = 7.25 \text{ mm}$$

The measured flexural displacement at yield for specimen RSU was 6.0 mm. The ratio of the predicted to measured is 1.20.

Response at ultimate

The ultimate strain of 3.6% was assumed uniformly distributed over the unbonded length of the bar. For this ultimate strain, the prediction procedure converged at a compression zone length of 235 mm and a horizontal load of 247 kN.

The deformation at ultimate was determined based on the procedure of section 7.4.3. The bar strain was distributed over three regions: unbonded bar length (l_u), plastic zone (l_p) and elastic zone (l_e). The elastic and plastic zones were as previously determined: 582 mm, and 198 mm, respectively. The extension of the bar, δ_s, was determined by equation 7.16 as follows:

$$\delta_s = \varepsilon_p \times l_u + 2\{\, 1/2\ \varepsilon_y \times l_y + \varepsilon_y \times l_p + 1/3\ (\varepsilon_u - \varepsilon_y)(l_p)\ \}$$

$$=(.036)(600)+2\{1/2(.0023)(582)+(.0023)(200)+1/3(.036-.0023)(200)\}$$

$$= 28 \text{ mm}$$

The rotation of the joint, θ, was determined as:

$$\theta = \frac{\delta_s}{(d-c)} = \frac{28\ mm}{(1050\ mm - 235\ mm)} = 0.033$$

The flexural deformation, D_r was determined as follows:

$$D_r = \theta \times H = 0.033 \times (1800) = 60\ mm$$

The measured flexural displacement for the unbonded specimen RSU was 40 mm. The ratio of predicted to measured value was 1.50. This was mainly because the measured strain in specimen was 0.023 in comparison to the assumed strain of 0.036. For the later strain value of 0.023, the predicted deformation is 40 mm which agrees with the measured value. The complete predicted response was compared to envelope of the measured cyclic response for specimen RSU as shown in Figure 7.25.

7.5.2 Connections with Prestressed Bars

In the prestressed connections tested, continuity between the two panels was provided by two 15.8 mm diameter Grade 1080 dywidag bars. The measured characteristic properties of concrete and drypack were identical to those used for the mild steel connection, given in section 7.5.1. The prestressed bar had the following properties:

area of one bar,	$A_{ps} = 180\ mm^2$
equivalent yield strength,	$f_{py} = 0.80 \times f_{pu} = 900$ MPa
yield strain (ASTM),	$\varepsilon_{py} = 0.7\%$
Young's modulus,	$E_{ps} = 200{,}000$ MPa
ultimate strength,	$f_{pu} = 1137$ MPa
monotonic ultimate strain,	$\varepsilon_{pu} = 7\%$
cyclic ultimate strain,	$\varepsilon_{pu} = 3.6\%$

Unlike the mild steel reinforcement, the prestressed reinforcement had an initial pre-tension strain prior to the application of any loading. The measured effective prestressing stress in the bars, after losses, was $0.56f_{pu}$ = 600 MPa, which gave an effective pre-tension strain, ε_{pe} of 0.3% prior to loading.

7.5.2.1 Prestressed connection with bonded dywidag bars

Response at yield

The flexural strength at yield can be evaluated by assuming a strain in the dywidag bars equal to $(\varepsilon_{py}-\varepsilon_{pe})$ and using the equilibrium and compatibility approach to determine the compression zone length. Based on a strain of (0.007-0.003), the analysis converges to a compression zone of 330 mm and a compression strain in the drypack grout at the extreme fibre of 0.00185 which is less than the ultimate value of 0.006. The flexural strength at yield is 185 kN.

To determine the rotation of the connection using extension of reinforcement, the bond stress can be determined using equation (7.13) as:

$$u = 16 \frac{\sqrt{48}}{15.875} \left(\frac{400}{900}\right) = 3.10\ MPa$$

The elastic length l_e can be determined using equation (7.15) as:

$$l_e = \frac{(900\ MPa - 600\ MPa) \times (15.875\ mm)}{4 \times (3.1\ MPa)} = 385\ mm$$

Therefore, at yield, the extension of bar on both sides of connection, δ_s, can be determined by equation (7.16) as:

$$\delta_s = 2 \{ \frac{1}{2} (0.007-0.003) * (385) \} = 1.54\ mm$$

The rotation, D_y, could be evaluated using equation (7.9) as follows:

$$\theta_y = \frac{1.54\ mm}{(1050\ mm - 330\ mm)} = 0.00214$$

The flexural deformation is evaluated as follows:

$$D_y = \theta \times H = .00214 \times (1800) = 3.85\ mm$$

Response at ultimate

At ultimate the strain in the reinforcement reaches the maximum value, ε_{pu}, and the extreme fibre of the connection is greater than ε_{gu} which results in shifting of the neutral axis away from the edge of the connection due to crushing of the drypack. The reversed cyclic loading limited the strain in the bar to 50% of the ultimate monotonic strain. Based on an ultimate strain, ε_{pu}-ε_{pe}, of 0.0032, the analysis converges to a compression zone depth of 350 mm with a crushed zone of 225 mm. The drypack strain at the extreme fibre of the connection is 0.0162. The reduction of the grout compressive strength is 0.55 and the flexural strength of the connection is 160 kN-m.

To determine the rotation using extension of reinforcement, the frictional bond strength in the plastic region is determined using equation (7.14) as:

$$u_f = (5.5 - 0.07\ \frac{5}{1})\ \sqrt{\frac{48}{28}}\ \left(\frac{400}{900}\right) = 3\ MPa$$

The plastic zone l_p can be determined using equation (7.15) as:

$$l_p = \frac{(1040MPa - 900MPa) * (15.875\ mm)}{4 * (3.0\ MPa)} = 185\ mm$$

Extension of the bar, δ_s, is determined from equation (7.16) as:

$$\delta_s = 2\left\{\frac{1}{2}(0.007-0.003)(385) + (0.007-0.003)(185) + \frac{1}{3}(0.035-0.007)(185)\right\}$$

$$= 6.5mm$$

The rotation is evaluated using equation (7.9) as follows:

$$\theta_u = \frac{6.5\ mm}{(1050\ mm - 350\ mm)} = 0.0093$$

The flexural deformation, D_r could be evaluated in terms of a concentrated joint rotation as follows:

$$D_{ru} = \theta \times H = .0093 \times (1800) = 16.7\ mm$$

The measured flexural displacement was 20 mm. The ratio of predicted to measured value is 0.84, which represents good agrement.

The complete predicted response is compared to measured response of specimen PTB, with bonded prestressing bars tested under cyclic loading, as shown in Figure 7.26.

7.5.2.2 Prestressed connection with fully unbonded dywidag bars

Prediction of the response of connection prestressed by unbonded bars was different from that of the connection with bonded bars. The difference was that local yielding of the bar at the connection section does not occur, rather the strain was distributed uniformly along the length of the bar. Also, the bars in the compression zone did not resist any compression force since there was no bond between the bar and the grout; the bars were unbonded. Therefore, as soon as thickness reduction occurred, the analysis procedure was modified by setting the force in the compression bar to zero.

The analysis proceeded by assuming increments of the strain and evaluating the response accordingly using the algorithm described in section 7.4. The extension in the bar, however, was spread over the entire unbonded length, of 2600 mm between the anchorages. As an example, for a strain increment, ε_{ps} - ε_{pe}, of 0.2%, the analysis gave a compression zone depth of 479 mm and a connection strength of 192 kN. The corresponding bar extension was:

$$\delta_s = l_u \, x \, (\varepsilon_{ps} - \varepsilon_{pe})$$
$$= 2600 \text{ x } (0.2\%) = 5.2 \text{ mm}$$

The rotation at the joint was as follows:

$$\theta = \frac{\delta_s}{(d-c)} = \frac{5.2 \; mm}{(1050 \; mm - 480 \; mm)} = 0.0091$$

The flexural deformation, D_r was given as:

$$D_r = \theta \times H = 0.00910 \times (1800) = 16.4 \; mm$$

The complete predicted response was compared with the experimental response of specimen PTBU in Figure 7.27. Very good correlation was observed between the predicted and measured response. It should be noted that at a strain increment of 0.6%, the ultimate condition was reached in the prediction analysis in comparison to a measured strain increment of 0.5% at ultimate. This predicted strain increment represented the end of the elastic behaviour. At this level, the predicted deformation was 42 mm. The measured ultimate deformation, however, was 50 mm. The ratio of the predicted to measured was 84 percent.

7.5.3 Connections with Prestressed Strands

The continuity between the two panels was provided by two 12.7 mm (1/2") diameter, 7-wire strand, Grade 1860. The measured material properties of the concrete, drypack and post-tensioning grout were identical to those used for the prestressed connection with bars, given in section 7.5.2. The prestressed strand had the following properties:

area of one bar,	$A_{ps} = 99$ mm^2
yield strain (ASTM),	$\varepsilon_{py} = 1\%$
yield strength,	$f_{py} = 0.90 \times f_{pu} = 1750$ MPa
Young's modulus,	$E_{ps} = 215{,}000$ MPa
ultimate strength,	$f_{pu} = 1937$ MPa
monotonic ultimate strain,	$\varepsilon_{pu} = 5.5\%$
cyclic ultimate strain,	$\varepsilon_{pu} = 2.75\%$

The stress-strain model of prestressed strand was given by equation 7.3.

The prestressed strands had an initial pre-tension strain due to effective prestress. The applied effective prestressing stress on the strand, after losses, is $0.586 f_{pu} = 1090$ MPa, which gives an effective strain, $\varepsilon_{pe} = 0.50\%$ prior to loading.

7.5.3.1 Prestressed connection with bonded strands

Response at yield

The prestressing strand yields at a strain of 1%. Since the strand had a prestrain, ε_{pe} of 0.5%, the strand yields when the strain increment exceeds 0.5%. At this yield strain increment, the procedure converged to a compression zone depth of 331 mm and a connection strength, P, of 204 kN.

The deformation was determined following the procedure of section 7.4.3. Distance l_e was determined using equation 7.15 as follows:

$$l_e = \frac{\Delta f_s \cdot d_b}{4 \cdot u_e} = \frac{(1752\ MPa - 1090\ MPa) * (12.7\ mm)}{4 * (3.5\ MPa)} = 600\ mm$$

The extension of the bar, δ_s, was determined by using equation 7.16 as follows:

$$\delta_s = 2 \{ \frac{1}{2} \varepsilon_y * l_e \} = 2 \{ \frac{1}{2} (0.5\%) * (600) \} = 3.0\ mm$$

The rotation, θ, was determined as:

$$\theta = \frac{\delta_s}{(d-c)} = \frac{3.0\ mm}{(1050\ mm - 330\ mm)} = 0.0041$$

The flexural deformation, D_r was evaluated as:

$$D_r = \theta \times H = .0041 \times (1800) = 7.5\ mm$$

The measured flexural displacement at yield for specimen PTS was 4.0 mm. The ratio of the predicted to measured is 1.875. This difference could be due to an assumed low bond stress for the prestressed strand.

Response at ultimate

The strain increment at ultimate, ε_{pu}-ε_{pe}, was 2.75% - 0.5% = 2.25%. For this strain, the analysis converged to a compression zone of 425 mm and a strength of 180 kN.

The plastic region l_p was as follows:

$$l_p = \frac{\Delta f_s \cdot d_b}{4 \cdot u_f} = \frac{(1850MPa - 1750MPa) * (12.7\ mm)}{4 * (3.5\ MPa)} = 90\ mm$$

The extension of the bar, δ_s, was determined as follows:

$$\delta_s = 2\ \{\ 1/2\ (\varepsilon_{py} - \varepsilon_{pe}) \times l_y + (\varepsilon_{py} - \varepsilon_{pe}) \times l_p + 1/3\ (\varepsilon_{pu} - \varepsilon_{py})(l_p)\ \}$$

$$= 2\ \{\ 1/2(.005)(600) + (0.005)(90) + 1/3(.0275\text{-}.01)(90)\ \}$$

$$= 4.95 \text{ mm}$$

The concentrated joint rotation, θ, was determined using equation 7.8 as:

$$\theta = \frac{\delta_s}{(d-c)} = \frac{4.95\ mm}{(1050\ mm - 425\ mm)} = 0.008$$

The flexural deformation, D_r was evaluated as follows:

$$D_{ru} = \theta \times H = 0.008 \times (1800) = 14.40\ mm$$

The complete predicted response was compared to the measured response of specimen PTS, with bonded prestressing bars tested under cyclic loading conditions, in Figure 7.28.

Table 7.1 provides a summary of the parameters used in the prediction and gives the results of the analysis for the different connections. Values are given for parameters u_e, u_f, L_e, and L_p. Also, given are values for ε, c, δ_s, θ, D and P at yield and ultimate conditions.

Table 7.2 compares the predicted to the measured response at the yield and ultimate condition for the different connections. For all the connections in Table 7.2, with the exception of specimen PTS, the predicted response agrees well with the measured response both at yield and ultimate. The ratio of the predicted displacement to measured displacement ranged from 0.8 to 1.5 while the ratio of the predicted strength to measured strength was from 0.85 to 0.95.

Table 7.1 Summary of the results from the prediction analysis

specimen	u_e MPa	u_f MPa	L_e mm	L_p mm	ε %	ε_{pe} %	c mm	δ_s mm	θ %	D mm	P kN	condition
RS	4.36	6.83	582	200	0.23	0	375	1.34	0.2	3.6	200	yield
					3.6	0	235	6.75	0.83	16	247	ultimate
RSU	4.36	6.83	582	200	0.23	0	375	2.71	0.40	7.25	200	yield
					3.6	0	235	28	3.3	60	247	ultimate
PTB	3.10	3.0	385	185	0.7	0.3	330	1.54	0.214	3.85	185	yield
					3.5	0.3	350	6.5	0.93	16.7	160	ultimate
PTBU	-	-	-	-	0.5	0.3	479	5.2	0.9	16.4	192	elastic
PTS	3.5	3.5	600	90	1.0	0.5	331	3.0	0.41	7.5	204	yield
					3.0	0.5	425	4.95	0.8	14.4	192	ultimate

Table 7.2 Comparison of predicted vs. measured at the yield and ultimate conditions

specimen	measured		predicted		predicted/measured		condition
	Dr_{meas} mm	P_{meas} kN	Dr_{PR} mm	P_{PR} kN	$\frac{P_{PR}}{P_{meas}}$	$\frac{Dr_{PR}}{Dr_{meas}}$	
RS	4.0	220	3.6	200	0.90	0.9	yield
	20.5	230	16	247	1.07	0.8	ultimate
RSU	6.0	215	7.25	200	0.94	1.20	yield
	39.0	250	60	247	0.98	1.5	ultimate
PTB	4.0	210	3.85	185	0.88	0.96	yield
	21	163	16.7	160	0.98	0.80	ultimate
PTBU	50	202	42	190	0.94	0.84	ultimate
PTS	4.0	200	7.5	205	1.03	1.87	yield
	21.0	192	14.4	192	1.0	0.70	ultimate

D_r = rocking deformation = total deformation - slip deformation
P = horizontal load at the top of the upper panel of the specimen

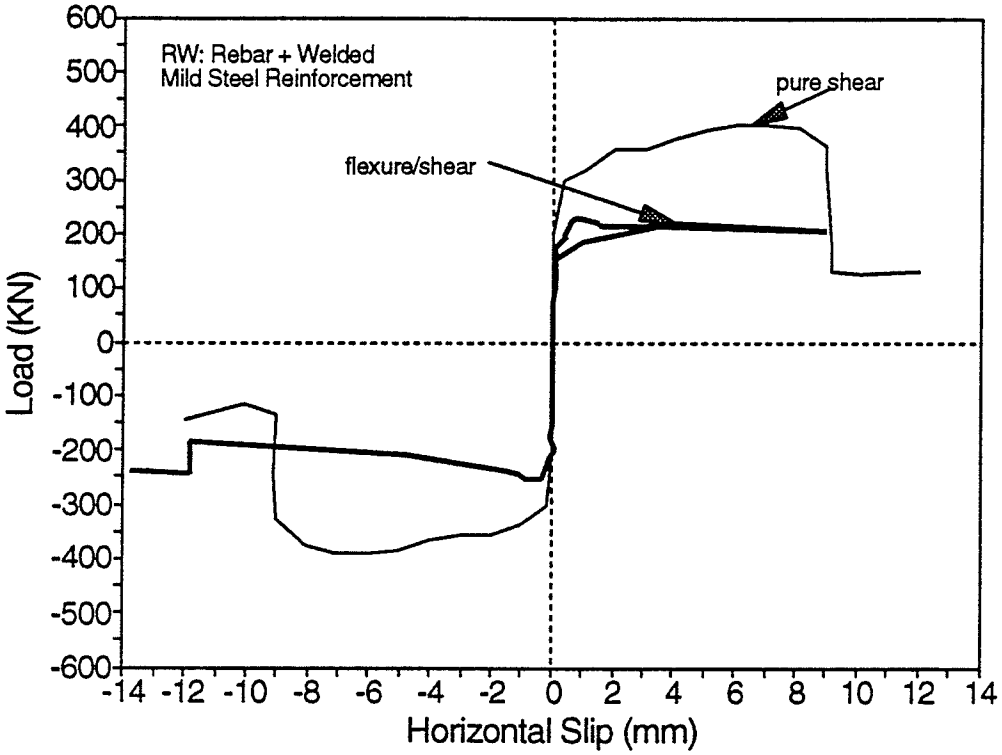

Figure 7.1 Load-slip response for connection type RW: flexure/shear versus pure shear

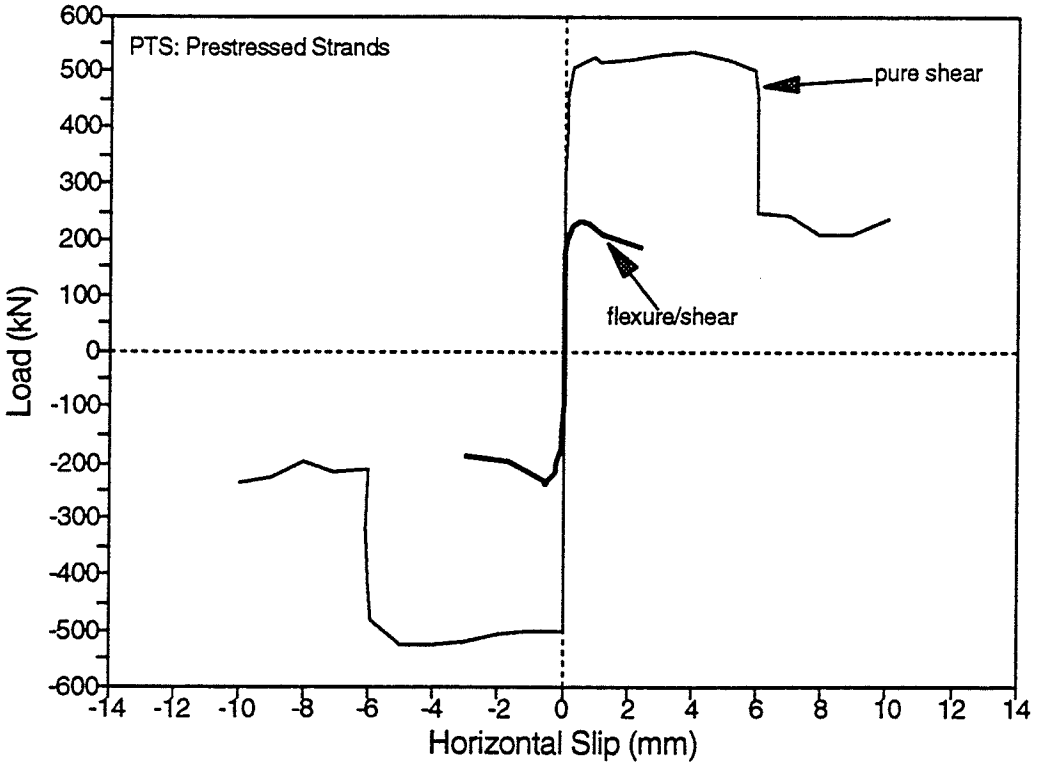

Figure 7.2 Load-slip response for connection PTS: flexure/shear versus pure shear

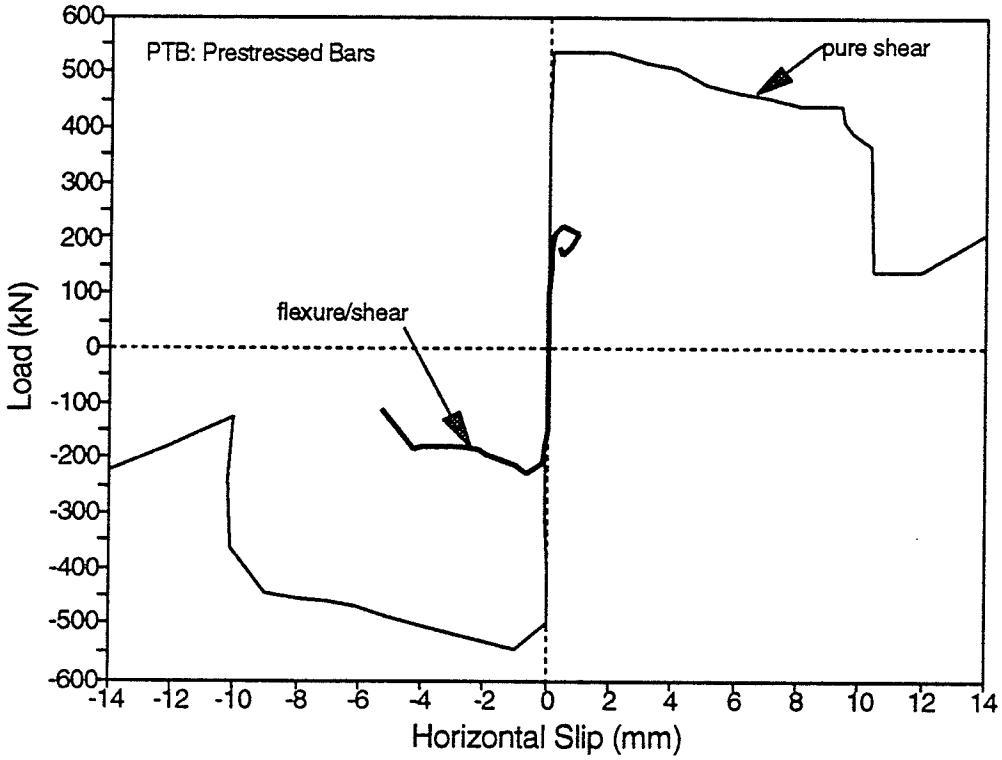

Figure 7.3 Load-slip response for connection PTB: flexure/shear versus pure shear

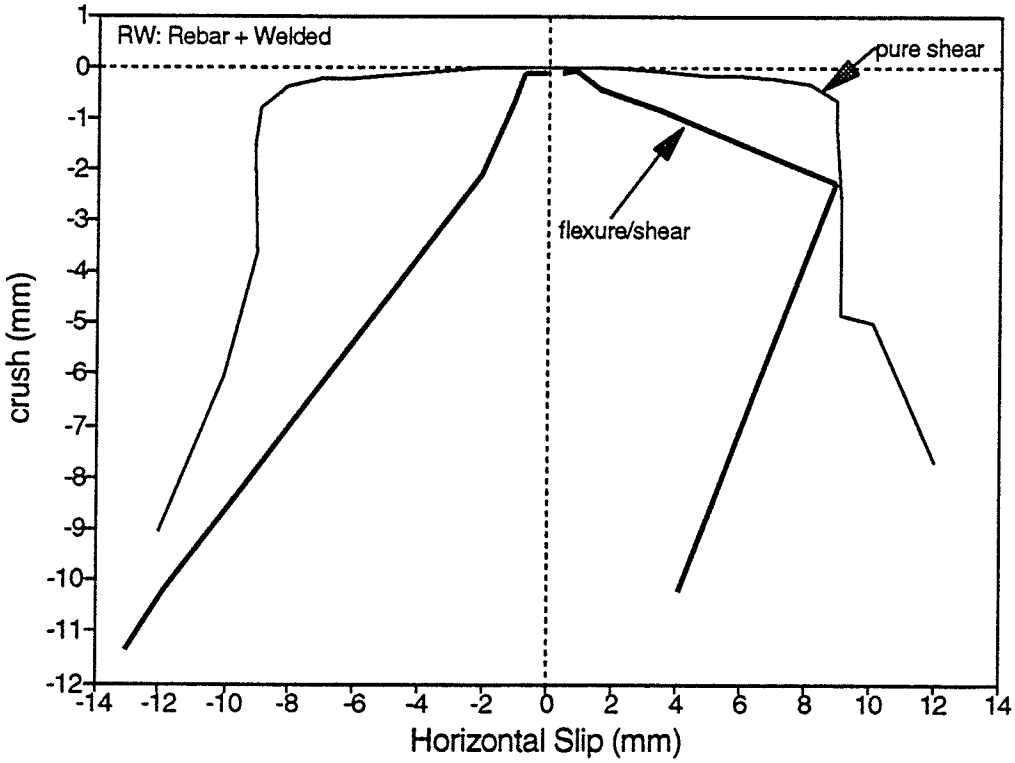

Figure 7.4 Crushing-slip response for type RW: flexure/shear versus pure shear

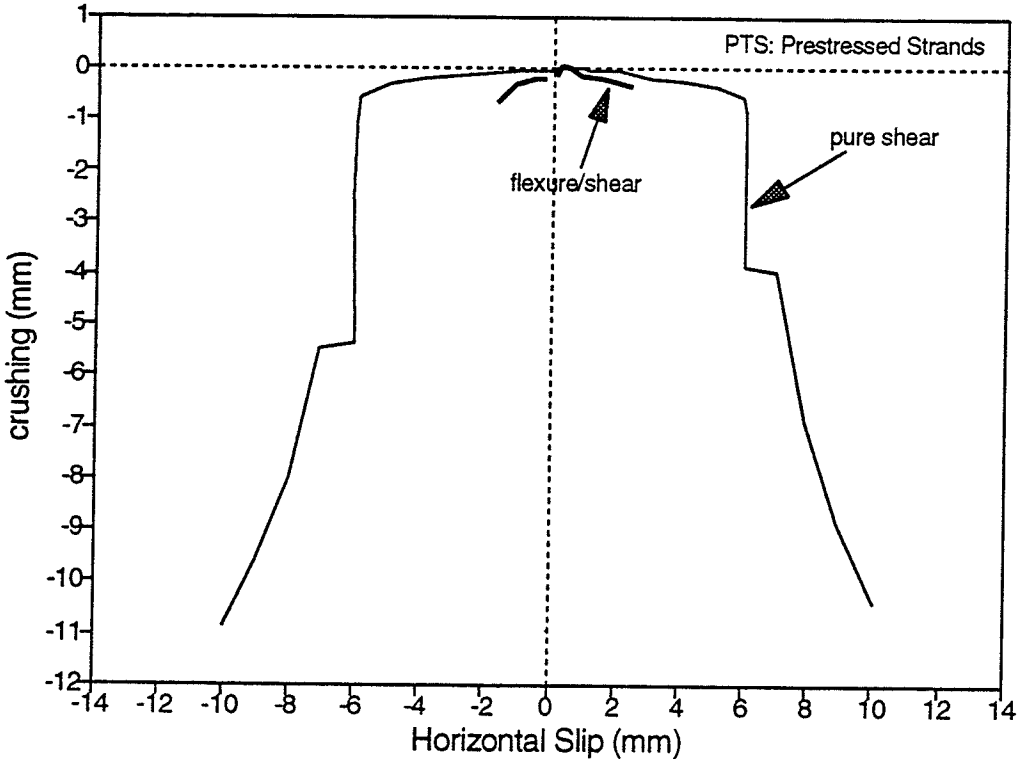

Figure 7.5 Crushing-slip response for connection PTS: flexure/shear versus pure shear

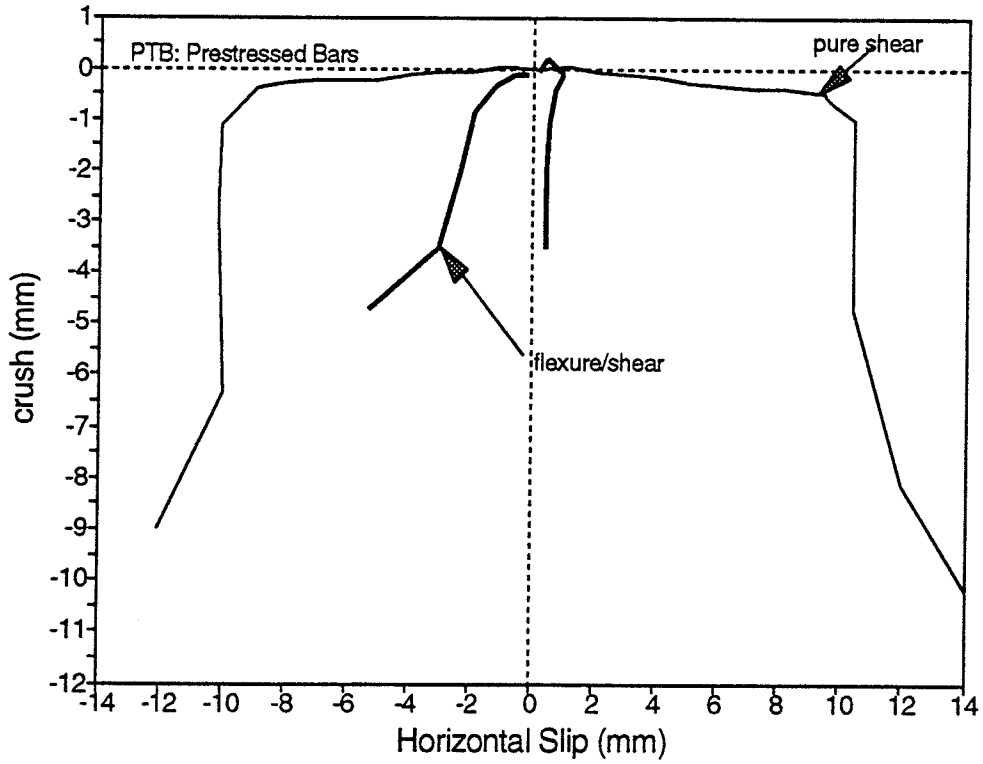

Figure 7.6 Crushing-slip response for connection PTB: flexure/shear versus pure shear

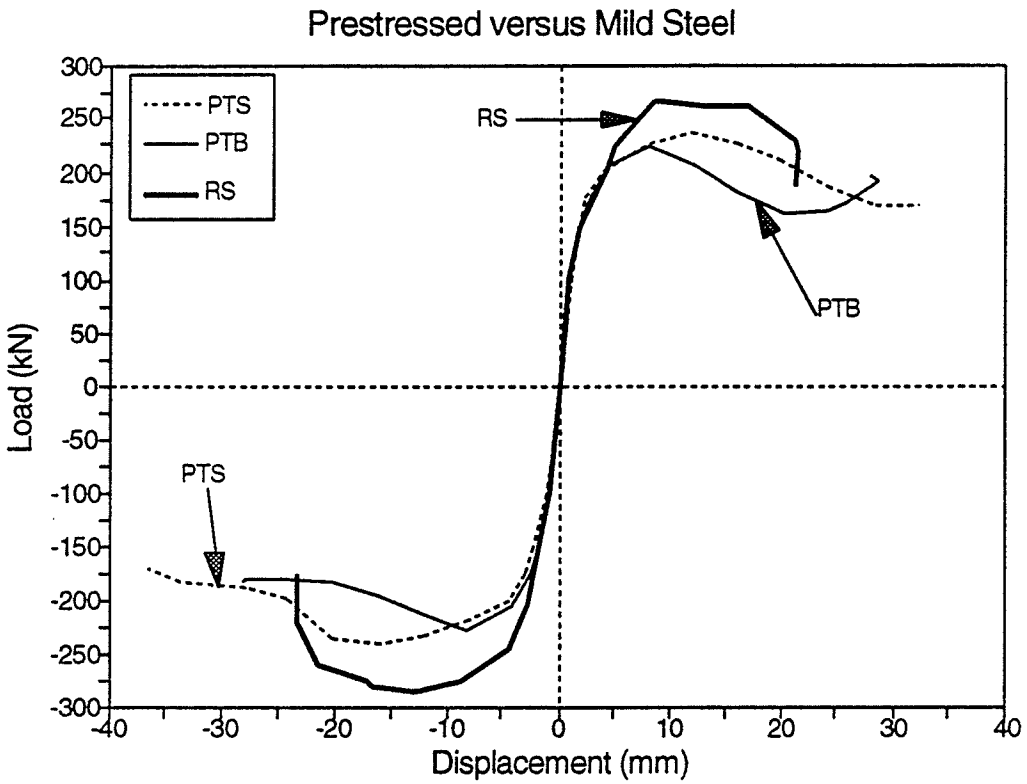

Figure 7.7 Comparison of strength envelopes for prestressed versus mild steel specimens

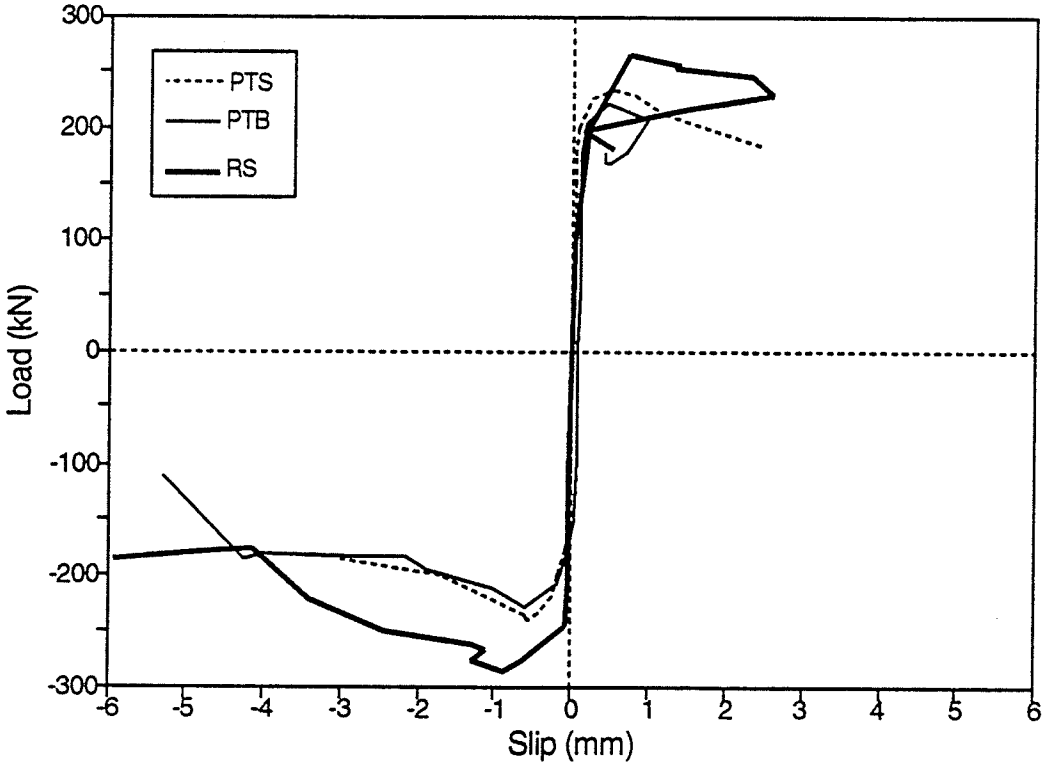

Figure 7.8 Comparison of slip envelopes for prestressed versus mild steel specimens

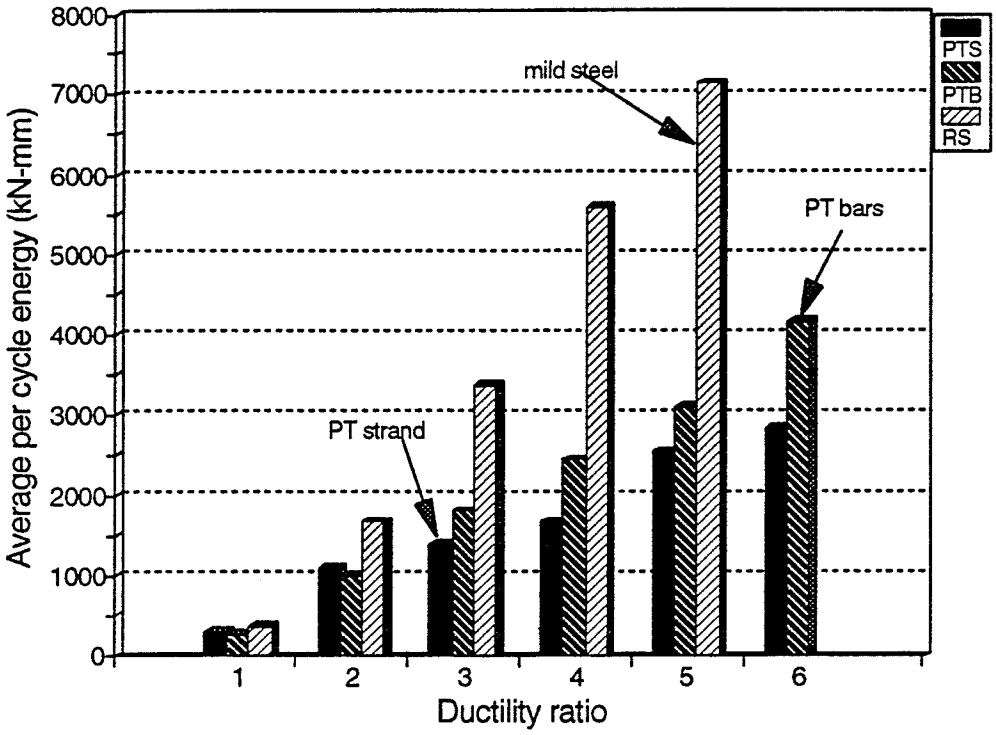

Figure 7.9 Comparison of energy per cycle for prestressed versus mild steel specimen

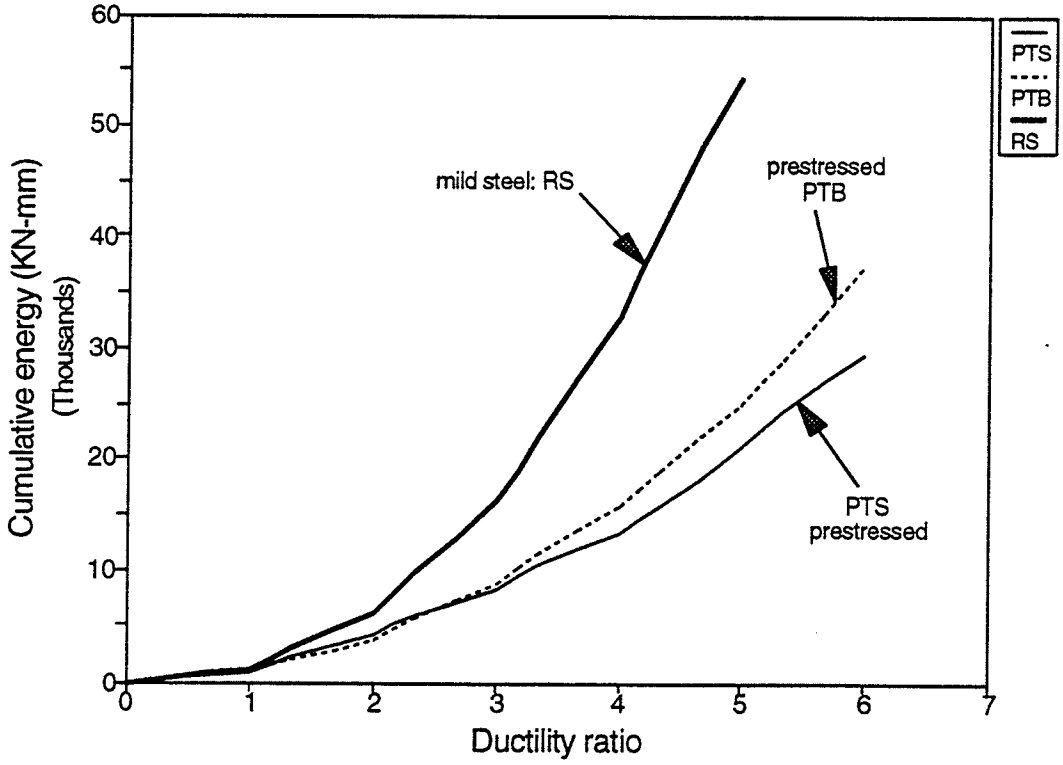

Figure 7.10 Comparison of cummulative energy for prestressed vrs. mild steel specimer

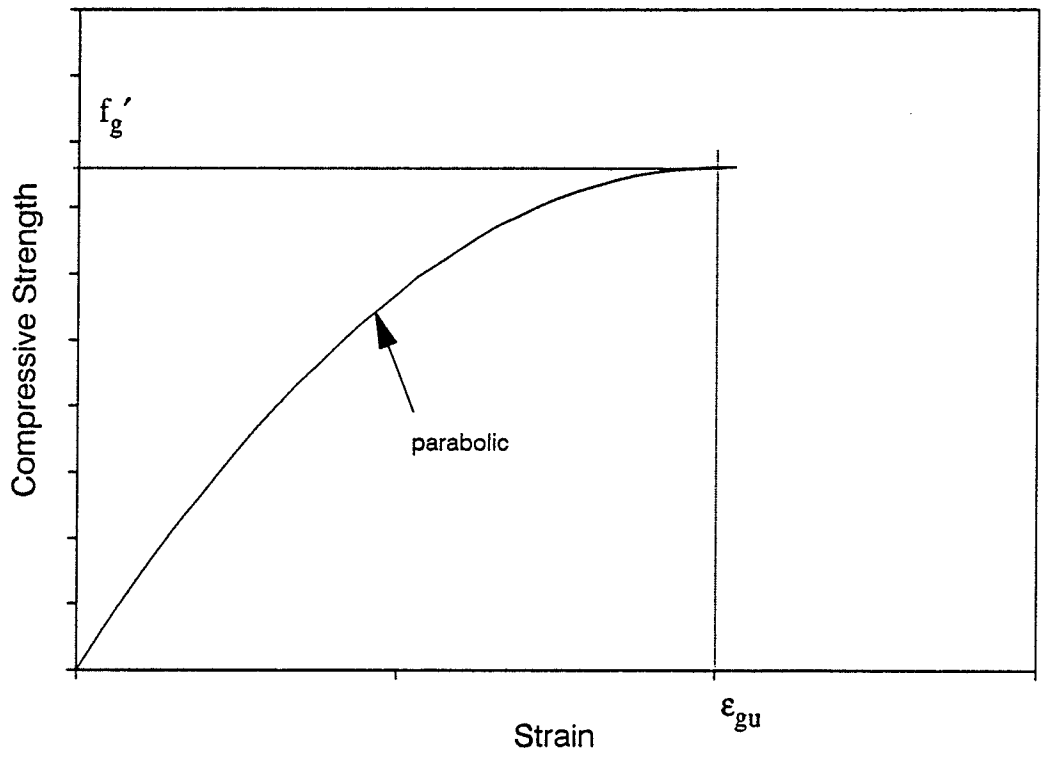

Figure 7.11 Typical stress-strain characteristic for drypack grout

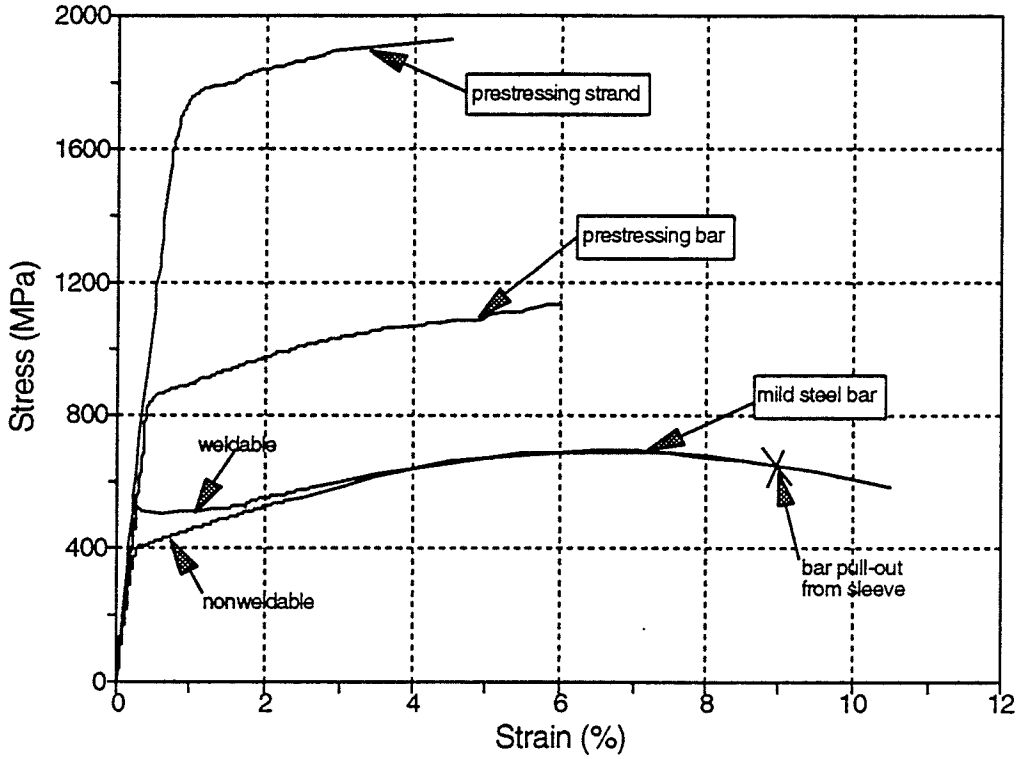

Figure 7.12(a) Measured stress strain characteristics of different types of reinforcement

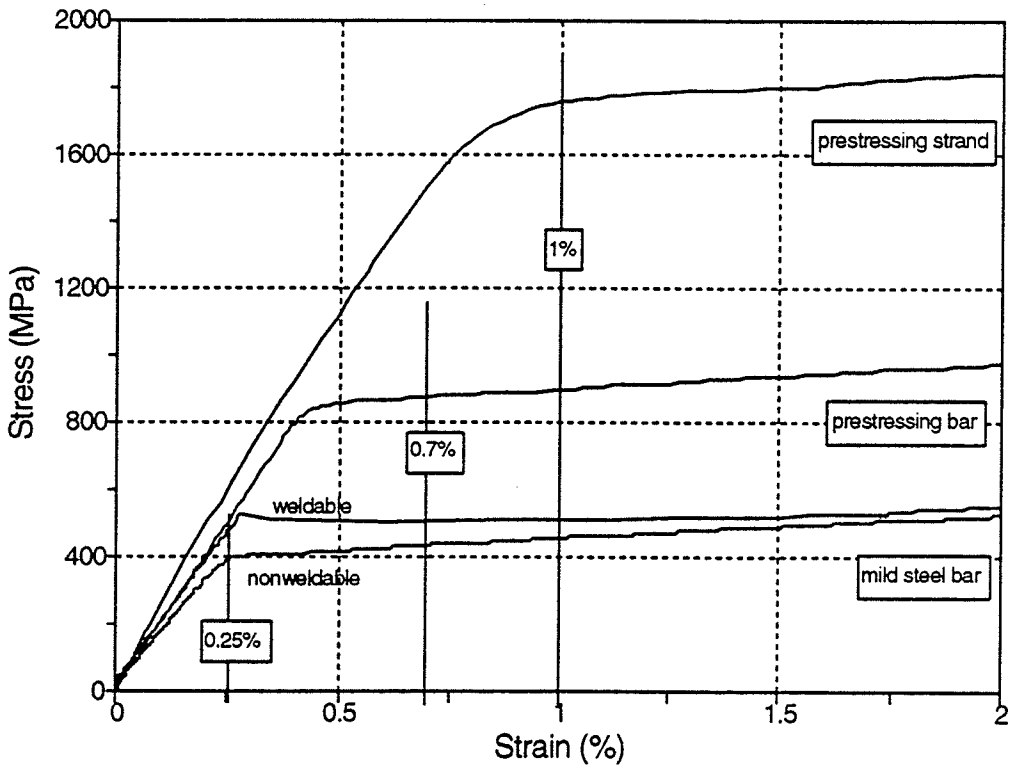

Figure 7.12(b) Magnified stress strain characteristics of different types of reinforcement

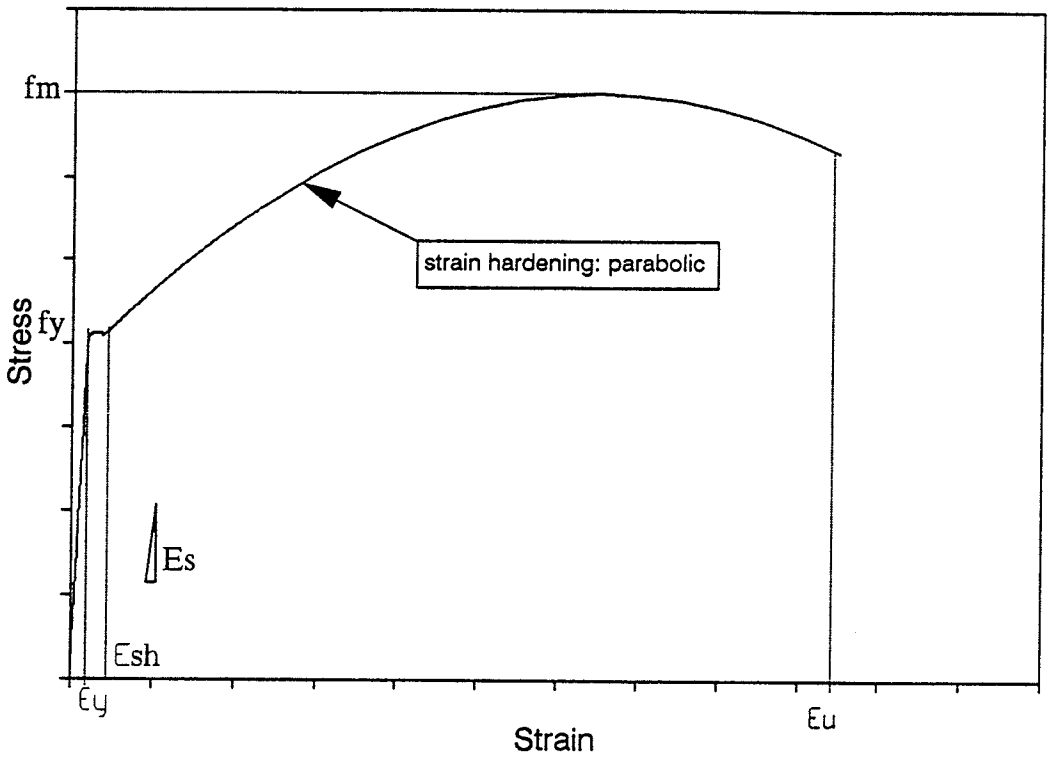

Figure 7.13 Typical stress-strain characteristic for mild steel reinforcement

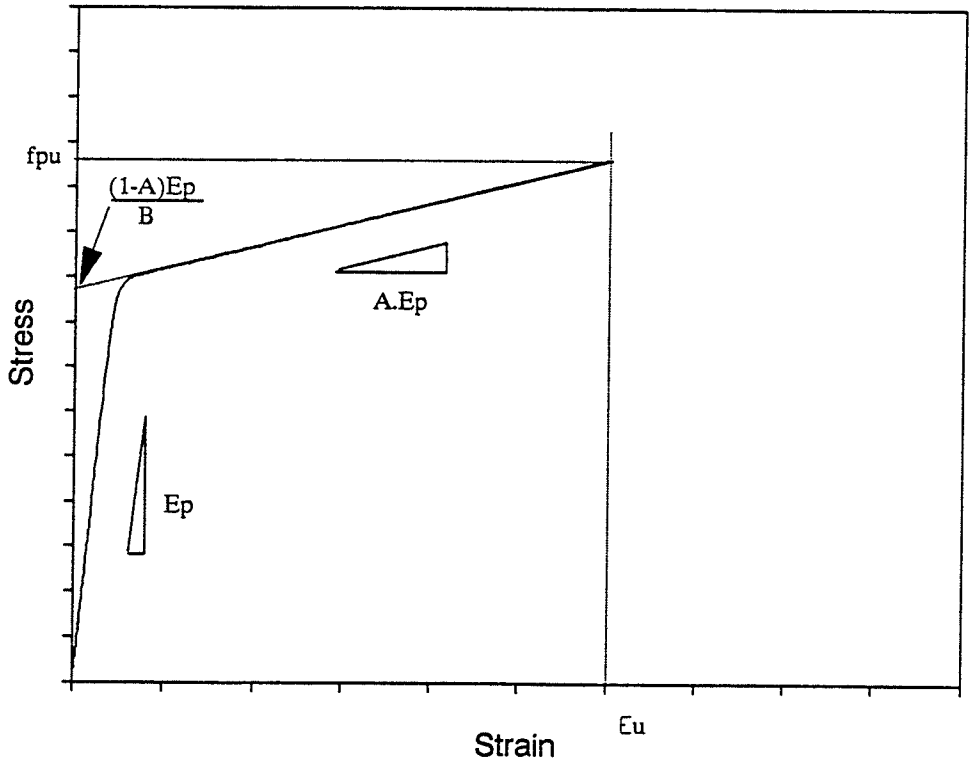

Figure 7.14 Typical stress strain characteristics for prestressing steel

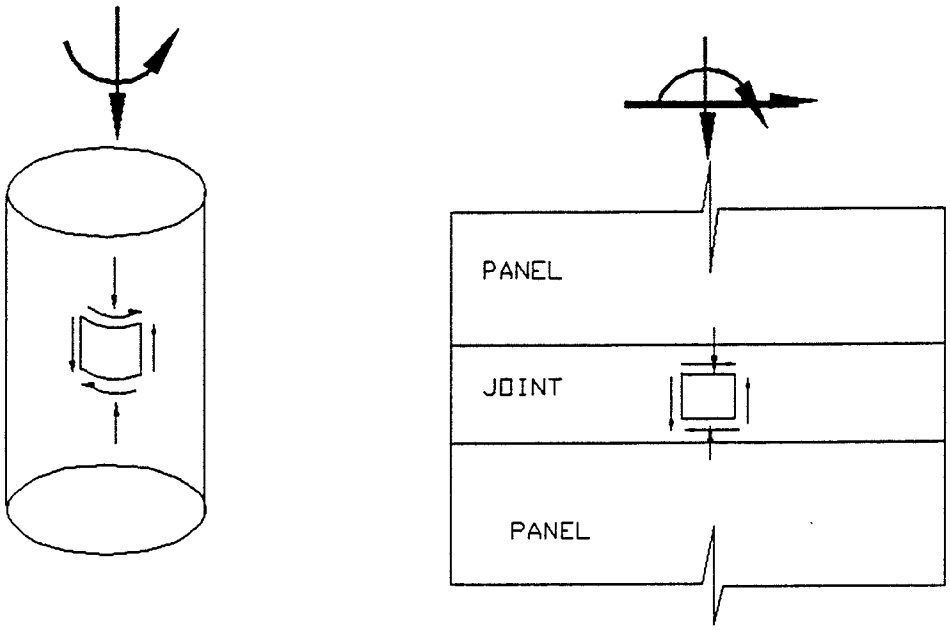

Figure 7.15 Analogy between state of stress in concrete cylinder & connection region

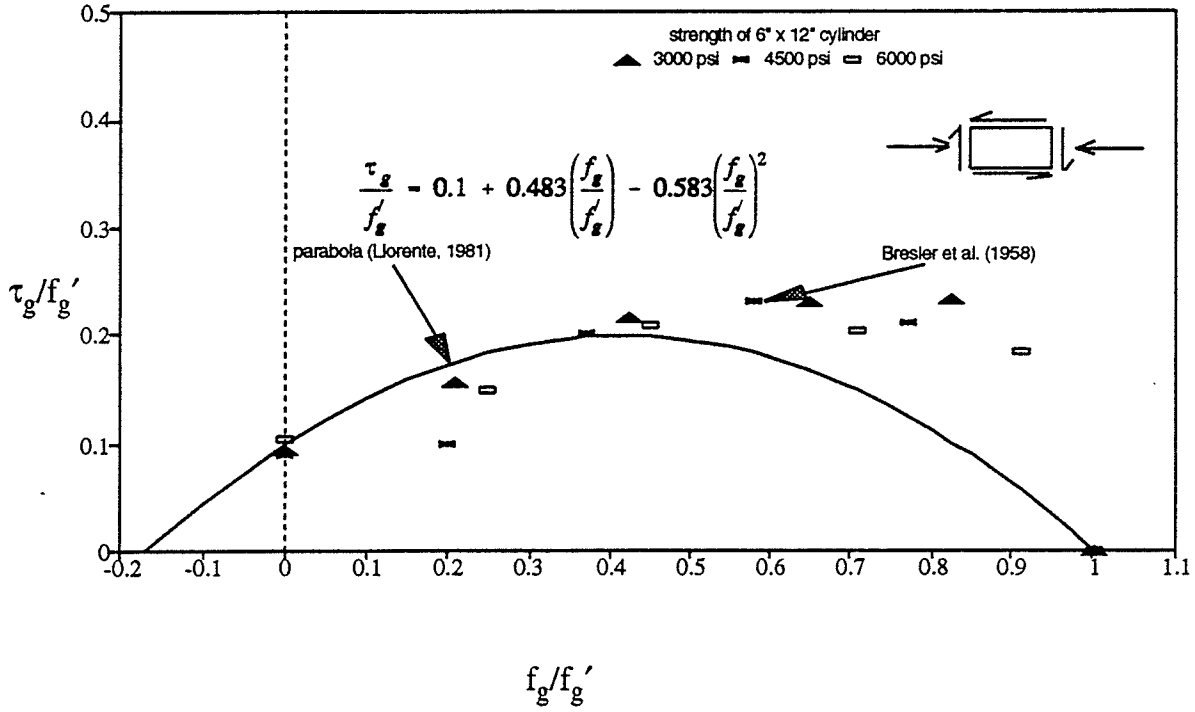

Figure 7.16 Compression-shear interaction diagram

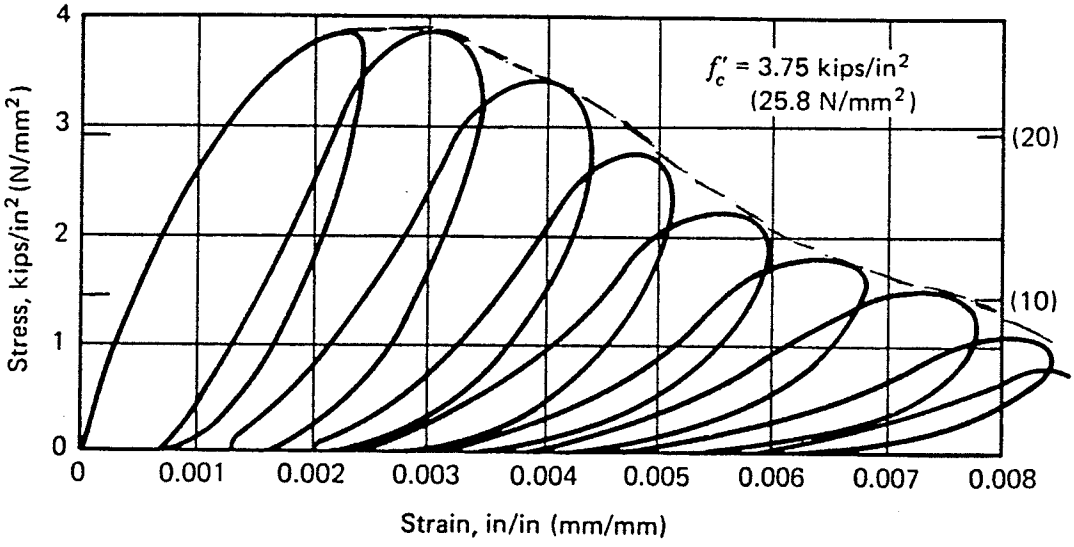

Figure 7.17 Stress-strain characteristic of concrete under repeated cyclic load (Park and Paulay, 1975)

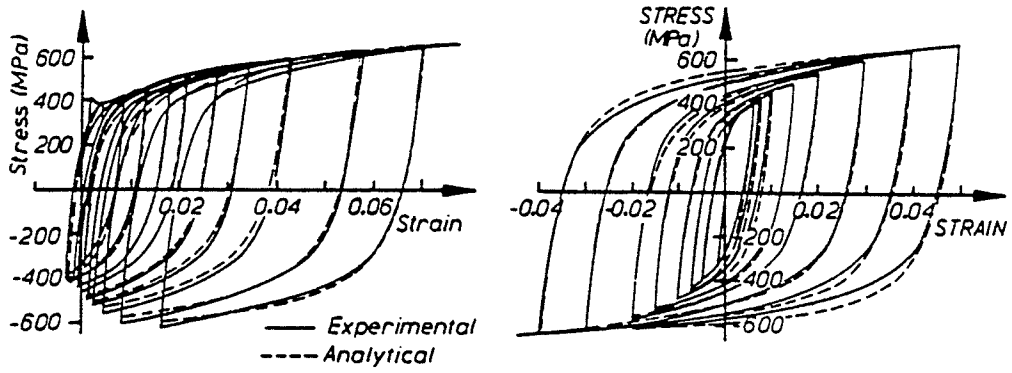

Figure 7.18 Cyclic straining of reinforced steel (Paulay and Priestley, 1992)

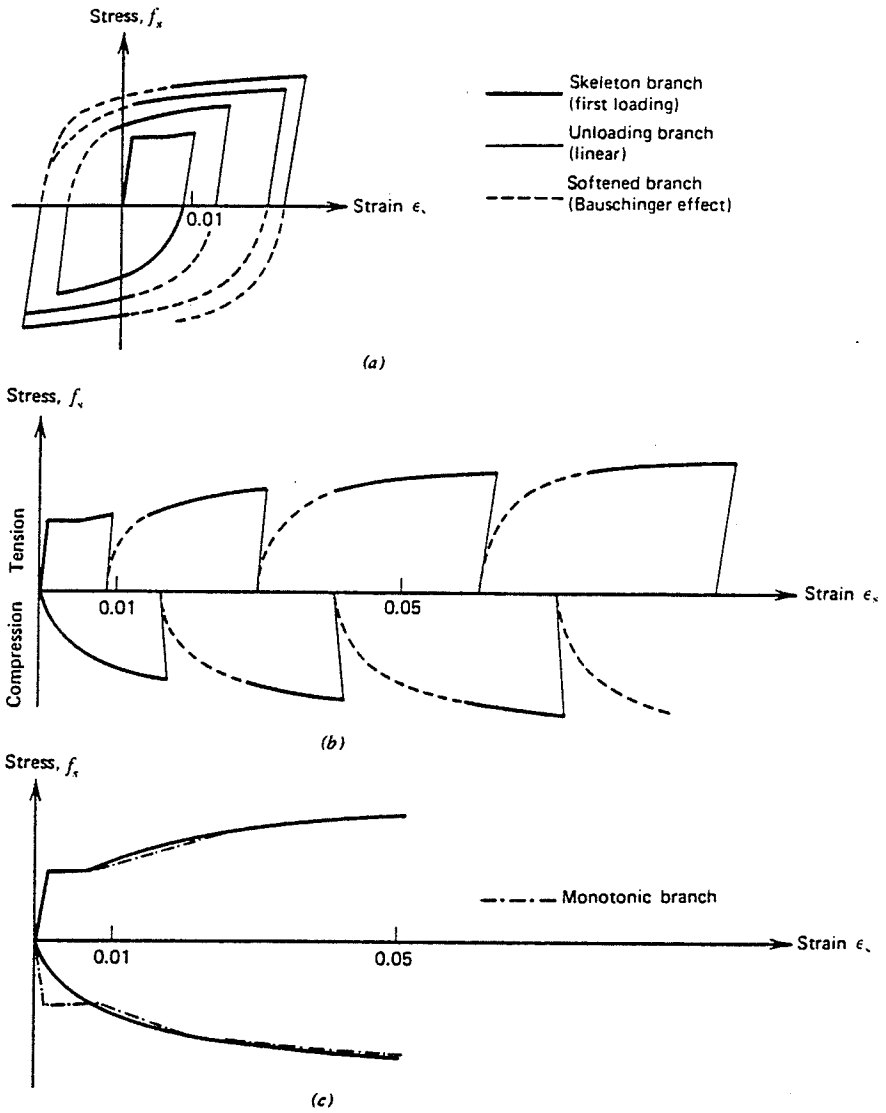

Figure 7.19 Stress strain curve for steel with reversed loading: a) reversed loading curve; b) expanded curves; c) skeleton curves (Park and Paulay, 1975)

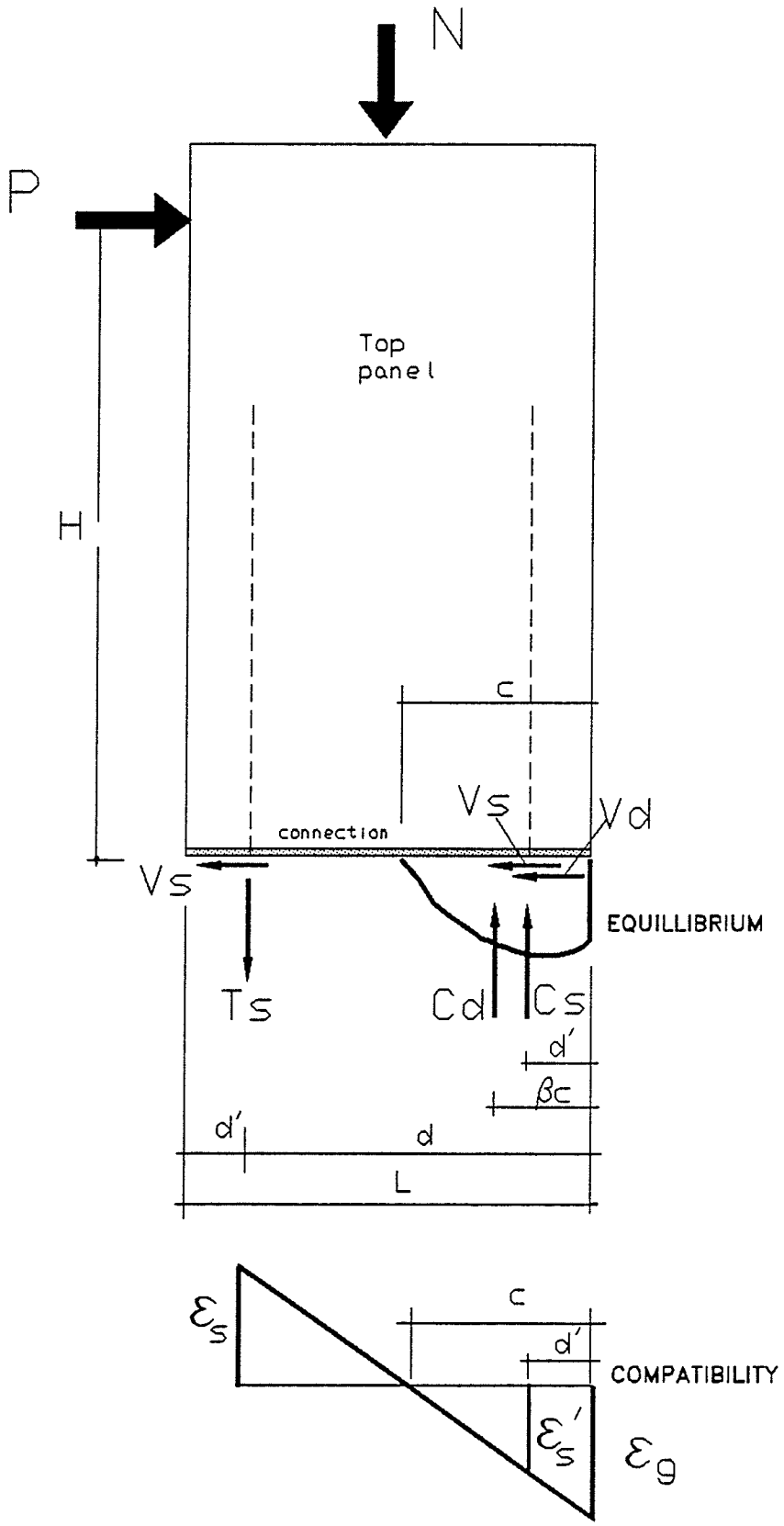

Figure 7.20 Free body diagram of connection region

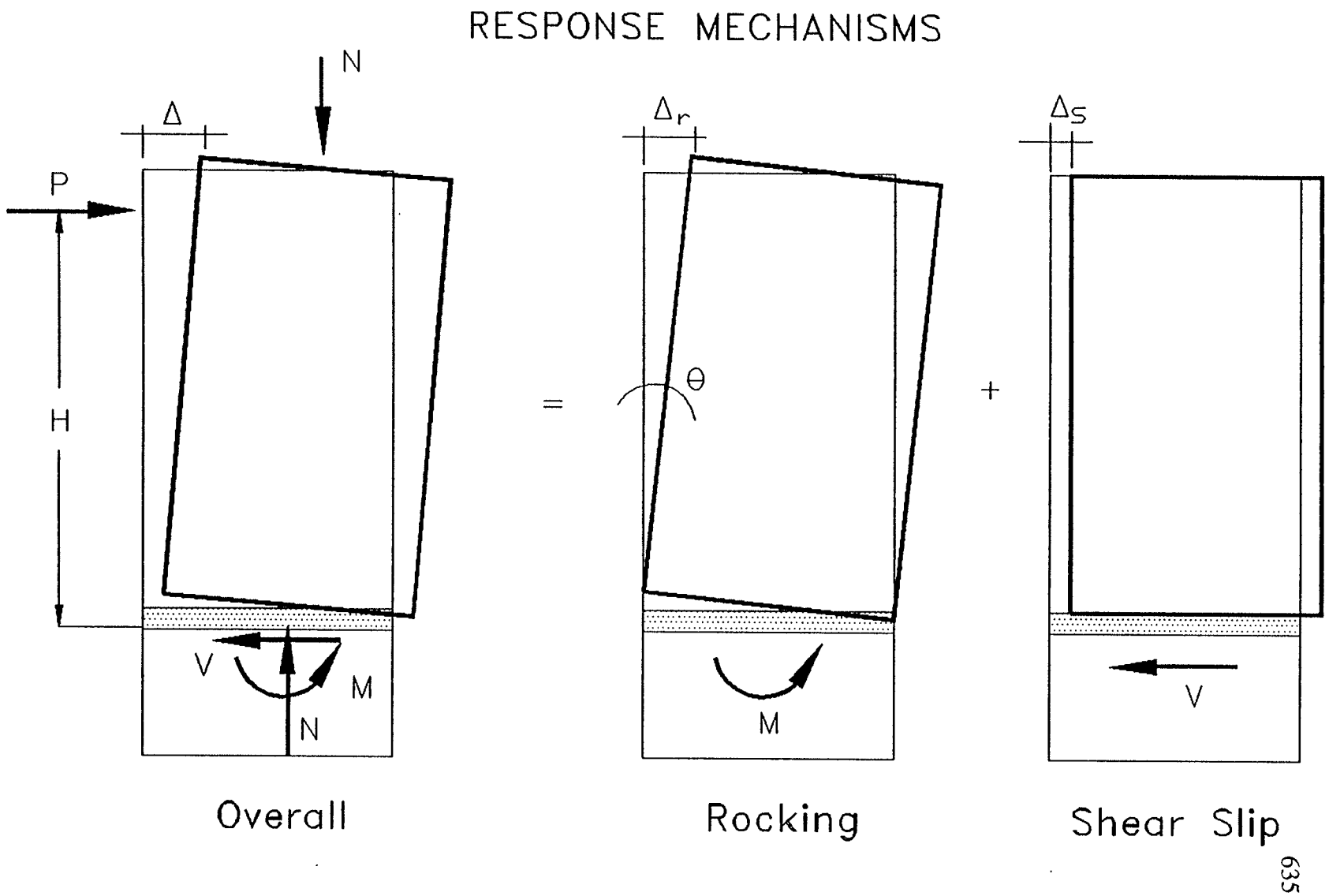

635

Figure 7.21 Components of deformation: (i) rocking and (ii) slip

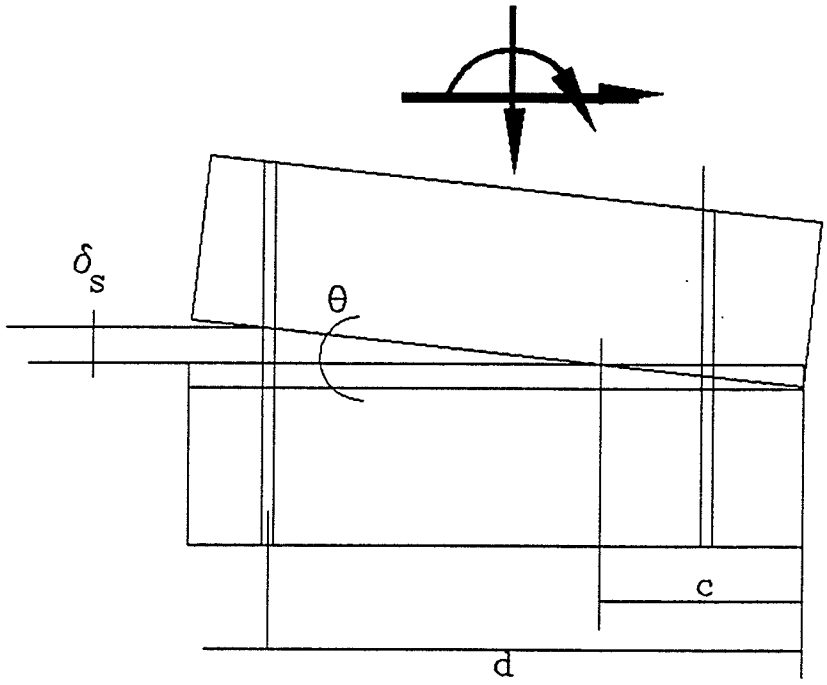

Figure 7.22 Schematic of concentrated rotation of the joint region

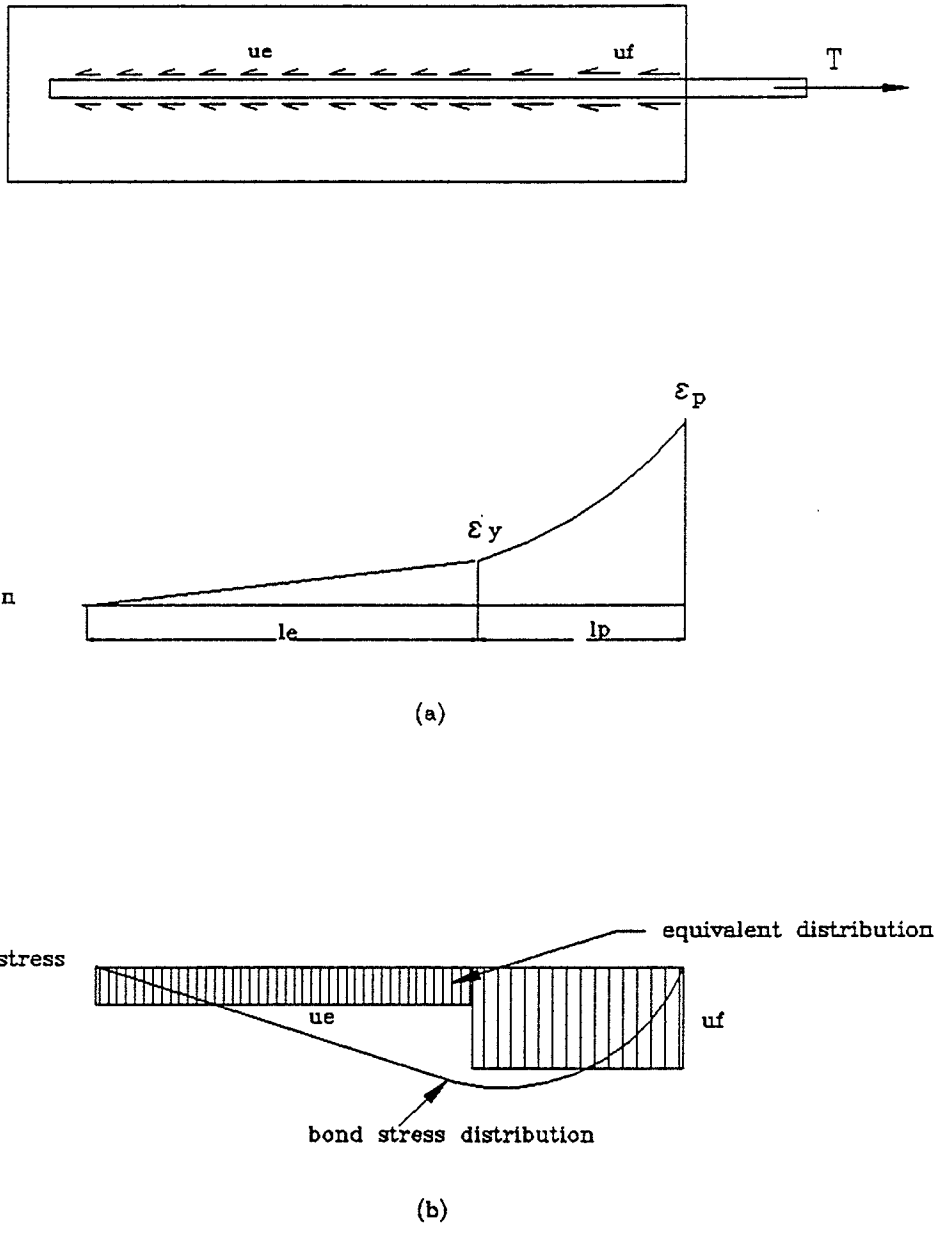

Figure 7.23 Reinforcing bar embedded in concrete: a) strain distribution; b) bond stress

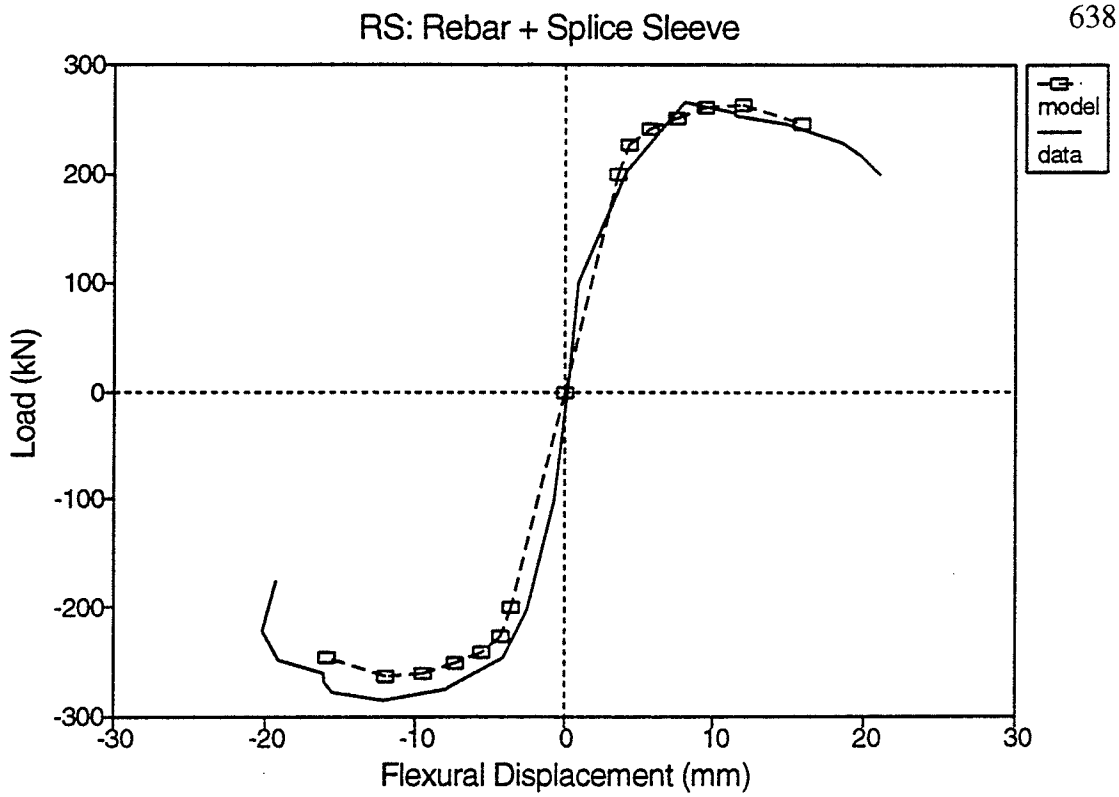

Figure 7.24 Connection RS: comparison of predicted vs. measured response

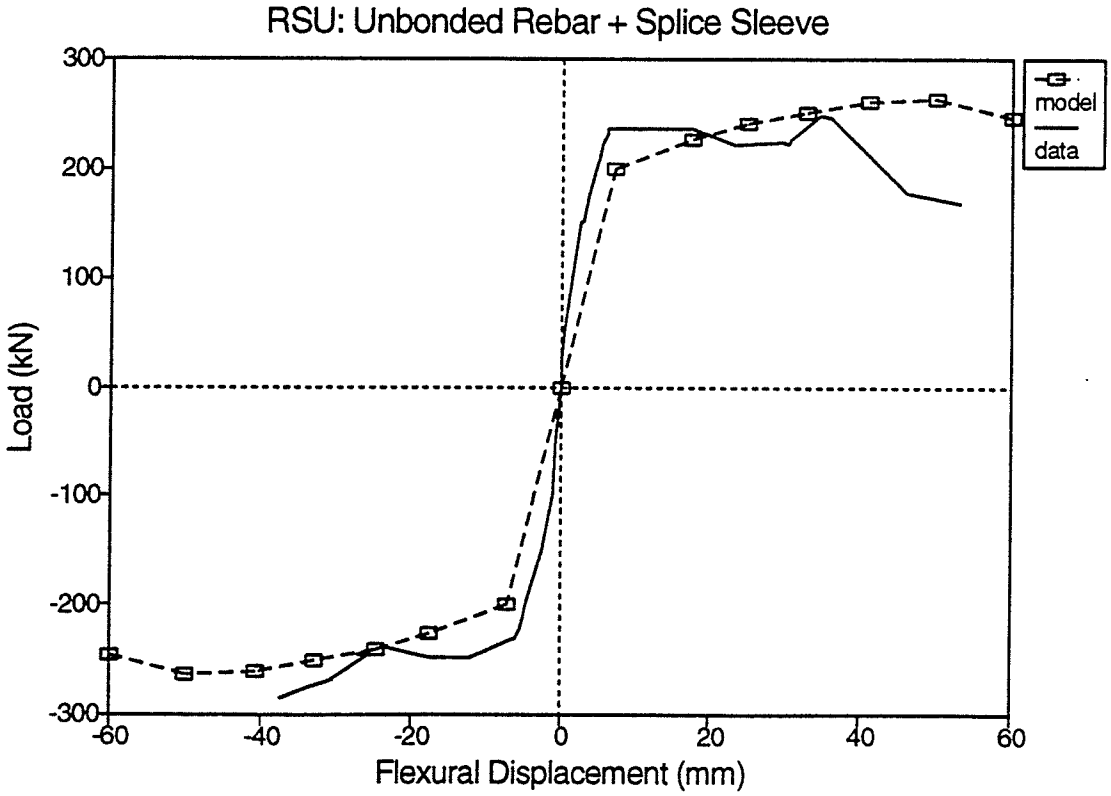

Figure 7.25 Connection RSU: comparison of predicted vs. measured response

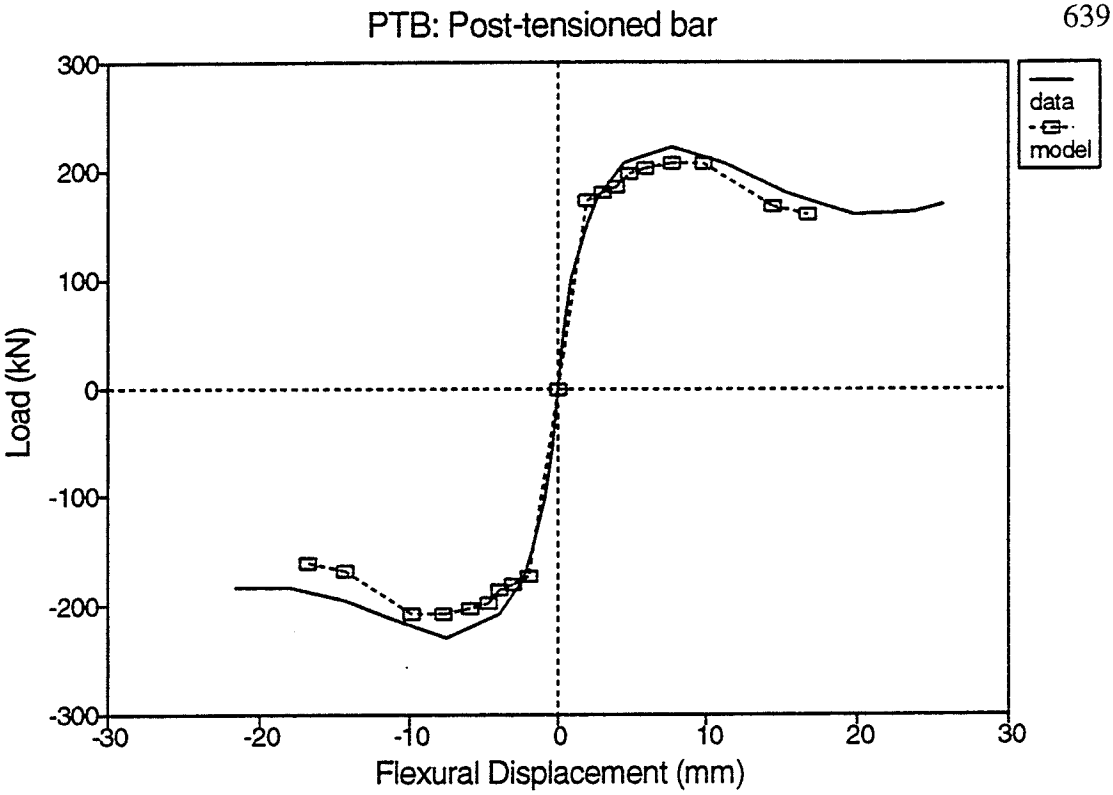

Figure 7.26 Connection PTB: comparison of predicted vs. measured response

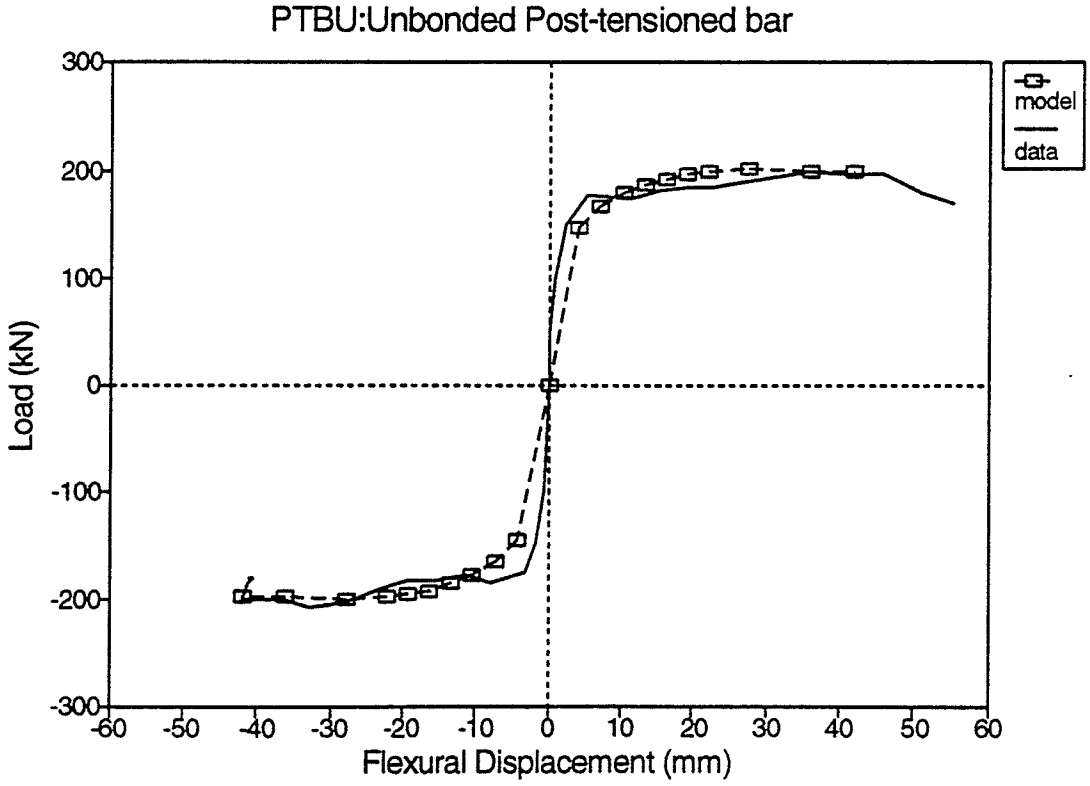

Figure 7.27 Connection PTBU: comparison of predicted vs. measured response

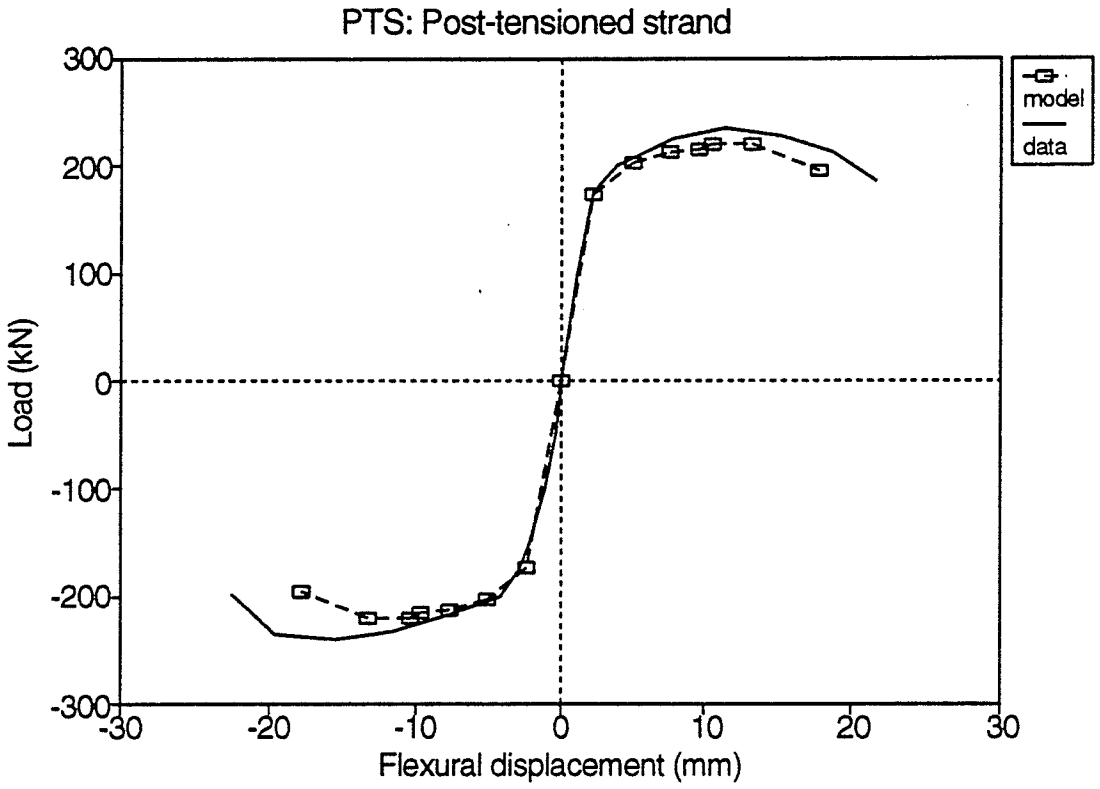

Figure 7.28 Connection PTS: comparison of predicted vs. measured response

CHAPTER 8

CONCLUSIONS AND DESIGN RECOMMENDATIONS

8.1 SUMMARY

An extensive experimental program was conducted to study the behaviour of horizontal connections for precast concrete shear wall panels subjected to large reversed cyclic deformations. The program included connection configurations currently used in practice and proposed innovative connections believed to enhance the ductility and/or energy dissipation capacity of the connections. Ten different connection configurations were investigated. The configurations studied were divided into three distinct groups:

1. D-series: Drypack connections with no reinforcement.
   - DP: Drypacked plain surface connection.
   - SK: Drypacked multiple shear keys.
2. R-series: connections with mild steel reinforcement.
   - RW: Drypack and 25M continuity rebars welded to iron angle.
   - RS: Drypack and 25M continuity rebars spliced with sleeve.
   - RSU: Drypack and partially unbonded 25M rebars spliced by a sleeve.
   - RSK: Drypack, 25M continuity rebars, splice sleeve and multiple shear keys.
   - RT: Drypack and 25M continuity rebars bolted to a tube section.
3. PT-series: Post-tensioned drypacked connections.
   - PTS: Drypack, and 13M post-tensioning strand.
   - PTB: Drypack, and 15M post-tensioning bar.
   - PTBU: Drypack, and 15M post-tensioning bar unbonded.

Seventeen full-scale specimens were tested, thirteen under reversed cyclic loading and four under monotonic loading. Each specimen consisted of full-scale shear wall panels and connection details of precast concrete shear wall buildings up to ten storeys high (low- to medium-rise structures). Two types of specimens were tested to fully examine all aspects of connection response. The first group was designed to simulate shear loading conditions and the second to simulate combined flexure and shear loading conditions. Six specimens were tested under shear alone, including currently used connection details. Eleven specimens were tested under flexure and shear loading including current and innovative configurations. All specimens were subjected to a constant stress, applied normal to the connection, to simulate effects of gravity loads typical to ten-storey structures.

The test results were used to evaluate characteristics of the connection in terms of: a) the various limit states; b) failure modes; (c) contribution of each component of the connection; (d) stiffness degradation characteristic; (e) energy absorption capacity; (f) ultimate ductility; (g) shear force-slip characteristics and coefficient of friction.

The study investigated the effects of loading conditions on the behaviour including: (1) pure shear versus flexure/shear loading, and (2) reversed cyclic loading. The effects of the connection configuration on the behaviour were also investigated and included: (1) shear keys versus plain surface, (2) mild steel versus prestressed reinforcement, (3) unbonded versus bonded reinforcement, (4) mild steel: welded versus sleeve, (5) mild steel: bolted versus sleeve, and (6) prestressed steel: bars versus strands.

A simple rational analytical procedure was proposed to predict the strength and deformation capacities at different stages of the cyclic response. The experimental results compared very well with the predicted response.

8.2 CONCLUSIONS

Based on the experimental results from the seventeen specimens tested in this program the following conclusions are drawn:

1.) The cyclic behaviour of connections can be described in three stages:

   I. Elastic stiff behaviour prior to the initiation of slip in pure shear specimens or first yield in flexure/shear specimens at the connection.

   II. Inelastic ductile behaviour after the initiation of slip in pure shear specimens or first yield in flexure/shear specimens but prior to severe deterioration of the drypack.

   III. Inelastic behaviour after significant deterioration of the drypack and reduction of the resistance (failure of the connection).

2.) All connection configurations tested under reversed cyclic loading were capable of maintaining peak resistance at very large cyclic deformations well beyond first yield. Connections with bonded mild steel reinforcement and post-tensioned connections had ductility ratios of 5 and 6, respectively. The overall behaviour for both configurations was characterized by stable hysteresis loops up to failure.

3.) Failure of all of the connection configurations tested under reversed cyclic loading conditions was due to significant crushing and spalling of the drypack. In some configurations, the crushing was accompanied by rupture of the continuity reinforcement at the connection level.

4.) Reversed cyclic loading introduced an additional limit state in terms of severe drypack deterioration beyond that which was observed for identical specimens tested under monotonic loading conditions.

5.) The cyclic loading significantly influenced the ductility capacity of the connection but had slight effect on the connection strength. In general, the ductility ratio was reduced by 50% in comparison to identical specimens tested under monotonic loads.

6.) The strength of the connection tested in combined flexure and shear was about 50% of capacity for the pure shear loading condition. This behaviour was mainly due to the observed flexural failure prior to utilizing the full shear capacity of the connection.

7.) The coefficient of friction for the specimens subjected to shear loading conditions was 0.8 for the mild steel and 0.9 for prestressed connections.

8). The coefficient of friction for the specimens under combined flexure/shear was 0.5 for mild steel and 0.4 for the prestressed connections. The lower friction coefficient in comparison to the shear specimens was possibly due to the localized high strains in the compression zone which caused more severe degradation of the drypack and reduced the coefficient of friction.

9.) The stiffness degradation was characterized by a very sharp decrease of stiffness versus ductility. This was mainly due to the severe deterioration of the drypack grout in the connection region. On average, the residual stiffness at onset of failure was about 20% of the initial stiffness at yield.

10.) The presence of shear keys significantly enhanced the shear resistance of the connection and limited slip mechanism.

11.) The use of prestressing slightly enhanced the ductility capacity but significantly reduced the energy dissipation in comparison to the specimens with mild steel reinforcement. The energy dissipation capacity of the connections with mild steel reinforcement was about twice that of connections with prestressed reinforcement. The ductility of the prestressed connections was slightly higher than that of the mild steel connections.

12.) The use of unbonded reinforcement significantly enhanced the behaviour of the connection in terms of deformation capacity and energy dissipation without significantly influencing the stiffness and strength. For partially unbonded mild steel connections, the deformation capacity was almost double (1.8 times) that for the bonded reinforcement. For fully unbonded prestressed bars configurations, the deformation capacity was 2.33 times that of the connection with bonded bars. As a result of the increased deformation capacity, more severe damage was expected in configurations with unbonded reinforcement.

13.) At a given deformation level, the energy dissipation per cycle of the unbonded connection was lower than the bonded one. The cumulative energy dissipation of the unbonded connection was higher, however, since such a connection achieved higher deformation capacity.

14.) The shear resistance for the connection tested under pure shear loading forms an elasto-plastic, unconfined mechanism with irrecoverable slip. The slip can only be recovered if the loading direction is completely reversed.

15.) The shear resistance for a connection with mild steel continuity reinforcement subjected to pure shear loading was provided by two components: 1) friction at the drypack-to-panel interface and 2) clamping of the continuity bar through dowel action. A model based on shear-friction concept was introduced and agreed well with experimental results.

16.) The shear resistance of connections with post-tensioning, strands or bars, was provided by friction at the drypack-to-panel interface. The effect of prestressing was to increase the vertical stress on the connection, in addition to the applied vertical gravity load, thus increasing the frictional resistance. A model was introduced to include the effects of prestressing and agreed well with experimental results.

17.) The strength and deformation capacity of the connections subjected to combined flexure (M) and shear (V) loading with ratio M/VL = 1.5, for the given connection length (L) can be predicted using a simple design procedure using equilibrium and compatibility relations. The procedure allowed the evaluation of the strength-deformation response at different ductility levels. The procedure was applied in design examples for different connections with mild steel reinforcement, prestressing strands and prestressed bars. The experimental results of the different connections tested compared very well with the predicted response.

18.) Seismic response up to a drift of 0.67% (ductility of three) could be resisted by all tested configurations without any apparent damage to the precast wall connection. This level represents typical seismic demand for low to moderate seismicity.

8.3 DESIGN RECOMMENDATIONS

Based on the experimental research, the following design recommendations are made:

1.) Typical precast concrete connections with mild steel or prestressing reinforcement can be used in zones of low to moderate seismicity. The tests have demonstrated that such connections possess sufficient ductility and energy dissipation capacity.

2.) The connection with unbonded reinforcement is recommended for use in high seismic area since such a connection showed significantly higher deformation and cumulative-energy-dissipation capacities with slight reduction in the strength and stiffness quantities in comparison to the conventional bonded connection.

3.) For mild steel connections, partial unbonding of the continuity reinforcement is recommended while, for prestressed connections, full unbonding of the reinforcement is recommended.

4.) For all connections, the use of multiple shear keys to limit the slip is recommended. In practical seismic applications, accumulated slip over several storeys is highly undesirable due to the resulting structural instability. The use of shear keys for limiting slip in seismic applications could enhance the overall behaviour of the structure.

5.) The use of prestressed or mild steel connections depends on the designer's judgement. In the test results, while prestressing enhanced slightly the deformational capacity, the measured energy dissipation was significantly lower in comparison to the mild steel connections.

8.4 FUTURE RESEARCH

The experimental program investigated a very wide range of connection configurations to be used in precast concrete wall systems. Both typical and new proposed configurations were tested. However, the program included only a single specimen for each connection configuration tested under cyclic loading. Clearly more tests are needed to make more definitive conclusions about the variables examined, and to include other variables. Some suggestions for future research are:

1. Additional specimens with mild steel continuity bars (RW & RS), prestressed strands (PTS) or prestressed bars (PTB) should be tested under reversed cyclic flexure and shear loading to increase the confidence in the observed behaviour.

2. Detailed investigation of unbonded specimens including different unbonded lengths of the continuity reinforcement to study the effect of unbonded length on overall behaviour of the connection.

3. The use of multiple shear keys in combination with mild steel continuity bars or post-tensioning should be investigated. The investigation should include both bonded and unbonded reinforcement, in addition to shear keys.

4. Research is needed to investigate the possible use of Fibre Reinforced Plastic (FRP) reinforcement for prestressing as an alternative to steel in precast concrete wall connections with plain surface region or with shear keys.

5. Research is needed to investigate use of different types of grout between the wall panels. Possibly the use of fibre-reinforced grouts should be investigated.

REFERENCES

ACI Committee 318, "Building Code Requirements for Reinforced Concrete," American Concrete Institute, Detroit, 1989.

Alsiwat J. and Saatcioglu M., "Reinforcement Anchorage Slip Under Monotonic Loading", *ASCE, Journal of Structural Engineering,* Vol. 118, No. 9, September, 1992.

Applied Technology Council, *Design of Prefabricated Concrete Buildings for Earthquake Loads,* ATC-8, Berkeley, California, 1981.

Applied Technology Council, *Tentative Provisions for the Development of Seismic Regular Structures for Buildings,* ATC 3-06, SEAOC, Washington, 1978.

Bachman, H., Influence of Shear and Bond on Rotational Capacity of Reinforced Concrete Beams," Publications, International Association of Bridge and Structural Engineering, Zurich, 1079 Vol. 30, Part II, pp. 11-28.

Becker, J.M., and Sheppard, D.A., "Connections for Seismic Resistant Precast Concrete Construction," Proceedings of a Workshop on Design of Prefabricated Concrete Buildings for Earthquake Loading, Applied Technology Council, 1981, 657-683.

Becker, J.M., Llorente, C., and Mueller, P., "Seismic Response of Precast Concrete Walls," *Earthquake Engineering and Structural Dynamics*, Vol. 8, Nov/Dec 1980, pp. 545-564.

Bresler, B. and Pister, K.S., "Strength of Concrete under Combined Stresses," *ACI Journal,* Vol. 55, No. 3, September 1958, pp. 321-345.

Caccesse, V. and Harris, H., "Seismic Resistance of Precast Concrete Shear Walls", *Journal on Earthquake Engineering and Structural Dynamics,* Vol.15, May, 1986, pp. 661-677.

CEB-FIP, *Draft Guide for the Design of Precast Wall Connections*, Committee European International du Beton, Bulletin d'Information No. 168, Paris, April 1985.

CEB-FIP, *Seismic Design of Concrete Structures*, Committee European International du Beton, Bulletin d'Information No. 160, Final Draft, October, 1983.

Cholewicki, A., "Loadbearing capacity and deformability of vertical joints in structural walls of large panel buildings," Building Science, Vol. 6, pp. 163-184.

Clough, D.P, *Design of Connections for Precast Prestressed Concrete Buildings for Effects of Earthquake,* Final Report, No. NSF-85-004, March 1985.

Collins M. and Mitchell D., Prestressed Concrete Structures, Prentice Hall, 1991.

CSA-A23.1-M90," Concrete Materials and Methods of Concrete Construction Methods of Test for Concrete," National Standards of Canada, 1990.

Derecho, A.T., Iqbal, M., Fintel, M. and Corley, W.G., "Loading History for Use in Quasi- static Simulated Earthquake Loading Tests", ACI Special Publication, SP 63, Reinforced Concrete Structures Subjected to Wind and Earthquake Forces, Detroit, 1980.

Dowrick, D.J. Earthquake Resistant Design for Engineers and Architects, 2nd edition, John Wiley and Sons, 1987.

Earthquake Resistant Regulations, a World List, International Association for Earthquake Engineering, Tsukuba, Japan.

Esteva, "Design: General", Chapter 3 of Design of Earthquake Resistant Structures, edited by E. Rosenblueth, John Wiley & Sons, 1980.

Fintel, M., "Performance of Precast Concrete Structures during Romanian Earthquake of March 1977," *PCI Journal*, Vol. 22, March/April 1977.

Foerster, H.R., Rizkalla S.H. and Heuvel, J.S., "Behaviour & Design of Shear Connections for Loadbearing Wall Panels," *PCI Journal*, Vol. 34, Jan/Feb. 1989, 102-119.

Fuller, G.R., " Earthquake Resistance of Prefabricated Concrete Buildings State-of-Practice in United States", Proceedings of a Workshop on Design of Prefabricated Concrete Buildings for Earthquake Loading, Applied Technology Council, 1981, 121-142.

Gaston, J.R. and Kriz, L.B., "Connections in Precast Concrete Structures-Scarf Joints," Journal of the Prestressed Concrete Institute, Vol. 9, No. 3, June 1964, pp. 37-59.

Hanson N.W., *Seismic Tests of Horizontal Joints.* Supplemental Report C. Design and Construction of Large Panel Concrete Structures, Office of Policy Development and Research, Department of Housing and Urban Development, Washington, DC, January 1979.

Harris, H. and Iyengar, S., "Full-Scale Tests on Horizontal Joints of Large Panel Precast Concrete Buildings," *PCI Journal,* March/April 1980.

Harris, H., "Shaking Table Tests on Five Story Precast Concrete Shear Walls," Seminar on Precast Concrete Construction in Seismic Zones, Tokyo, October 1986, pp. 191-206.

Harris, H., Abboud, B., and Wang, G., "Performance of Wet Horizontal Joints and Simple Shear Walls in Precast Concrete Large Panel Buildings under Earthquake Loading," Proceedings of 7th European Conference on Earthquake Engineering, Athens Greece, September 1982, pp. 123-133.

Harris, H. and Abboud B., "Cyclic Shear Behaviour of Horizontal Joints in Prefabricated Large Panel Buildings," Proceedings of a Workshop on Design of Prefabricated Concrete Buildings for Earthquake Loading, Applied Technology Council, April 1981, pp. 403-493.

Hawkins, N.M.,Lin I., and Ueda, T., "Anchorage of Reinforcing Bars for seismic forces," *ACI Journal*, September/October 1987, pp. 407-418.

Hicks, T.R. "Connections between Precast Concrete Members for Use in Seismic Zones," MSc thesis, Washington University, 1990.

Huey, S.D., Clarke, A., and Gerstle, K.H., "Shear Strength of Horizontal Wall Panel Joints," *PCI Journal*, Vol. 35, July/August 1990, pp. 84-91.

Hutchinson, R.L., Rizkalla, S.H., Lau, M. and Heuvel, S., "Horizontal Post-Tensioned Connections for Precast Concrete Load-Bearing Shear Wall Panels," *PCI Journal,* Vol. 36, November/December, 1991, pp. 64 - 76.

Jacque F.J. and Becker, J.M. "Seismic Design of Precast Wall System," Proceedings of a Workshop on Design of Prefabricated Concrete Buildings for Earthquake Loading, Applied Technology Council, April, 1981, 585-617.

Johal, L.S. and Hanson, N.W., Supplemental Report B: *Horizontal Joint Tests,"* Design and Construction of Large Panel Concrete Structures, Office of Policy Development and Research, Department of Housing and Urban Development, Washington, D.C., April 1978.

Johal, L.S. and Hanson, N.W., "Design for Vertical Load on Horizontal Connections in Large Panel Structures," *PCI Journal,* January/February 1982.

Jones, L.L., "Shear Tests on Joints Between Precast Post-tensioned Units," Magazine of Concrete Research, Vol. 11, No. 31, March 1959, pp. 25-30.

Kanouh, Y., "Review of Japanese Precast Concrete Frame Systems Used as Building Structures", Seminar on Precast Concrete Construction in Seismic Zones, Tokoyo, October, 1986, pp. 35-54.

Karsan D. and Jirsa, J.O., "Behaviour of Concrete under Compressive Loads," *Journal of the Structural Division, ASCE*, Vol 95, STE12, December, 1969, pp 2543-2563.

Kato, B., Akiyama, H. and Yamanouchi, Y., "Predictable Properties of Material Under Incremental Cyclic Loading," Symposium on Resistance and Ultimate Deformability of Structures acted on by Well-Defined Repeated Loads, *Reports of Working Commissions,* Vol. 13, International Association of Bridges and Structural Engineering, Lisbon, 1973, pp. 119-124.

Kent, D.C. and Park, R.,"Cyclic load behaviour of reinforcing steel," *Strain (Journal of the British Society for Strain Measurement)*, Vol. 9, No. 3, July 1973, pp. 98-103.

Kianoush, M.R., and Scanlon, A. *Inelastic Seismic Response of Precast Concrete Large Panel Coupled Shear Walls,* Structural Engineering Report no. 134, University of Alberta, Department of Civil Engineering, March 1985, 328 pp.

Lewicki, B., Building with Large Prefabricates, 1st edition, Elsevier Publication Co., London, 1966.

Llorente, C.A., "Inelastic Behaviour of Precast Shear Walls," M.I.T., Department of Civil Engineering, Research Report No. R81-25, Order No. 710, August 1981.

Malhas, "Seismic Response of Large Precast Panel Walls: Analytical Correlation with Shaking Table Test Results," Ph.D. Thesis, Department of Civil and Environmental Engineering, University of Wisconsin, June 1988.

Martin, L.D. and Korkosz, W.J. , *Connections For Precast Prestressed Concrete Buildings* including earthquake resistance, Prestressed Concrete Institute, Chicago, Illinois, March, 1982.

Mattock, A.H., "A Survey of Precast Wall Systems," Proceedings of a Workshop on Design of Prefabricated Concrete Buildings for Earthquake Loading, Applied Technology Council, April 1981, pp. 253-276.

Mattock, A.H., "Flexural Strength of Prestressed Concrete Sections by Programmable Calculator," *Journal of Prestressed Concrete Institute*, Vol. 24, No. 1, Jan-Feb, 1979, pp.34-54.

Mueller, P., "Experimental Investigation on the Seismic Performance of Precast Walls," 8th World Conference on Earthquake Engineering, 1988.

Mueller P., "Behavioral Characteristics of Precast Walls", Proceedings of a Workshop on Design of Prefabricated Concrete Buildings for Earthquake Loading, Applied Technology Council, April, 1981, pp. 277-308.

Mueller, P., "Hysteretic Behaviour of Precast Panel Walls," Seminar on Precast Concrete Construction in Seismic Zones, Tokyo, October 1986, pp. 127-142.

Naeim, F. Seismic Design Handbook, Structural Engineering Series, vonNostrad Reinhold Publisher, New York, 1989.

Newmark and Hall, Earthquake Spectra and Design, Earthquake Engineering and Research Center, El Cerrito, California, 1982.

NZS, Code of Practice for General Structural Design and Design loads, Standard Association of NewZealand, NZS403, Wellington, 1984.

Oliva, M.G., and Clough, R.W., *Shaking Table Tests of Large Panel Precast Concrete Building System Assemblages,* Report No. UCB/EERC-83/14, Earthquake Engineering Centre, University of California, Berkeley, May 1985.

Oliva, M., Gavrilovic, P., and Clough, R., "Seismic Testing of Large Panel Precast Walls: Comparison of Psuedostatic and Shaking Table Tests," *Earthquake Engineering and Structural Dynamics,* Vol. 19, March 1990, pp. 859-875.

Oliva, M.G., and Clough, R.W, Velkov, M., and Gavrilvoic, *Correlation of Analytical and Experimental Responses of Large Panel Precast Building Systems*, Report No. UCB/EERC-83/20, Earthquake Engineering Centre, University of California, Berkeley, May 1985.

Pall, A.S., Marsh, C., and Fazio, P., "Friction Joints for Seismic Control of Large Panel Structures," *PCI Journal,* Vol. 25, November-December 1980, pp. 38-61.

Park R., *General Earthquake Resistant Design Considerations for Prefabricated Reinforced Concrete Building Systems,* final report, UNDP Project Rep/79/015, June 1983.

Park, R., "Seismic Design Considerations for Precast Concrete in New Zealand", Seminar on Precast Concrete Construction in Seismic Zones, Tokoyo, October, 1986, 1-38.

Park, R. and Paulay, T. Reinforced Concrete Structures, John Wiley & Sons, New York, 1975.

Paulay T. and Priestley,M.J.N., Seismic Design of Reinforced Concrete and Masonry Buildings, 1991.

Pekau, O.A. and Hum, D., "Seismic Response of Friction Jointed Precast Panel Shear Walls," *PCI Journal,* Vol. 36, March April 1991, pp. 56-71.

Polyakov, S.P.V., Design of Earthquake Resistant Structures - Basic Theory of Seismic Stability, Mir Publishers, Moscow, 1985.

Pochanart, S. and Harmon, T., "Bond-slip model for generalized excitation including fatigue," *ACI Materials Journal,* Vol 86, No. 5, 1989, pp. 465-474.

Prestressed Concrete Institute, "PCI Design Handbook/ Precast and Prestressed concrete," 3nd ed., Chicago, Illinois, 1985.

Prestressed Concrete Institute, "Connections for Precast and Prestressed Concrete," 2nd ed., Chicago, Illinois, 1977.

Prestressed Concrete Institute, "PCI Manual for structural design of architectural precast concrete," 2nd ed., Chicago, Illinois, 1977.

Rosenblueth, E., Design of Earthquake Resistant Structures, John Wiley and Sons, New York, 1980.

Schultz, D.M., Johal, L.J., Derecho, A.T., and Iqbal, M., *Report 5: Special Topics*, Design and Construction of Large Panel Concrete Structures, Office of Policy Development and Research, Department of Housing and Urban Development, Washington, DC, March 1979.

Schultz, D.M., *Report 6: Design Methodology*, Design and Construction of Large Panel Concrete Structures, Office of Policy Development and Research, Department of Housing and Urban Development, Washington, DC, 1979.

SEAOC, *Recommended Lateral Force Requirements and Commentary*, Seismology Committee Structural Engineering Association of California, Sacramenta, California, 1990.

Serrette, R.L., Rizkalla, S.H., Attiogbe, E.K. and Heuvel J.S., "Multiple Shear Key Connections for Precast Shear Wall Panels," *PCI Journal*, vol. 34, March-April 1989, pp. 104-120.

Sheppard, D. and Phillips, W. Plant Cast Precast and Prestressed Concrete, McGraw Hill Publishing, New York, 1989.

Sinha, B.P., Gerstle, K.H., and Tulin, L.G., "Stress Strain Relationship for Concrete under Cyclic Loads," *ACI Journal*, vol. 61, No. 2, Fenruary, 1964, pp- 195-211.

Spencer, R., "Earthquake Resistant Connections for Low Rise Precast Concrete Buildings," Seminar on Precast Concrete Construction in Seismic Zones, Tokyo, October 1986, pp. 61-80.

Speyer, I., "Considerations for the Design of Precast Concrete Bearing Wall Buildings to Withstand Abnormal Loads," *PCI Journal,* March/April 1976.

Stanton, J.F. and Nakaki S.D., "PRESSS Industry Seismic Workshops," *PRESSS Research reports 91/01, 91/02 and 92/06,* edited by Preistley M.J., University of California San Diego.

Uniform Building Code, International Conference Building Officials, California, 1985.

Watabe, M. and Hiraishi, H., " On the Current Developments in Earthquake Resistant Design Procedures for Prefabricated Concrete Buildings in Japan", Proceedings of a Workshop on Design of Prefabricated Concrete Buildings for Earthquake Loading, Applied Technology Council, April, 1981, pp. 61-85.

West, J.S., *Behaviour of Horizontal Connections for Precast Concrete Load-Bearing Shear Wall Panels Subjected to Reversed Cyclic Loading"*, MSc. Thesis, Department of Civil Engineering, University of Manitoba, Winnipeg, Manitoba, August 1993.